CHALMERS

Crack initiation area
Crack I   Crack II

Crack initiation area
Crack III

Fatigue Analysis for Orthotropic Steel Deck Bridges

Master of Science Thesis in the Master's Programme Structural Engineering and Building Technology

ANDREA KARLSSON
CHRISTOFFER WESLEY

Fatigue Analysis for Orthotropic Steel Deck Bridges

Master of Science Thesis in the Master's Programme Structural Engineering and Building Technology

ANDREA KARLSSON
CHRISTOFFER WESLEY

Department of Civil and Environmental Engineering
Division of Steel and Timber Structures
CHALMERS UNIVERSITY OF TECHNOLOGY
Göteborg, Sweden 2014

Necessity of Advanced Fatigue Analysis for Orthotropic Steel Deck Bridges
Master of Science Thesis in the Master's Programme Structural Engineering and Building Technology

ANDREA KARLSSON
CHRISTOFFER WESLEY

Department of Civil and Environmental Engineering
Division of Structural Engineering
Steel and Timber Structures
Chalmers University of Technology
SE-412 96 Göteborg
Sweden
Telephone: + 46 (0)31-772 1000

Cover: Crack initiation areas for the three investigated crack modes in this thesis

Fatigue Analysis for Orthotropic Steel Deck Bridges

Master of Science Thesis in the Master's Programme Structural Engineering and Building Technology

ANDREA KARLSSON
CHRISTOFFER WESLEY
Department of Civil and Environmental Engineering
Division of Structural Engineering
Steel and Timber Structures
Chalmers University of Technology

ABSTRACT

The aim of the work performed in this thesis is to investigate possible profits in fatigue analysis of orthotropic bridge decks using FEM compared to hand calculations when designing an orthotropic steel deck bridge. An existing bridge, Saltsjöbron, is modelled with FEM in Brigade/PLUS. Fatigue analysis was performed using the hot-spot stress method. Conventional fatigue analysis was also performed with hand calculations based on nominal stress method.

Three cracking modes are evaluated, one crack in rib to floor beam connection and two cracks in the weld between ribs and deck plate. The comparison between the results from the two methods shows very large difference in stresses at the investigated welds.

Based on the results it is recommended to use FEM to capture the local behaviour affecting the fatigue performance of orthotropic steel decks. Guidelines for the most adverse load position regarding each crack mode is presented together with general modelling recommendations.

Key words: Orthotropic steel deck bridge, Fatigue, Welded joints, Trapezoidal ribs, Nominal stress method, Structural hot spot stress method, Finite element modelling, Shell elements, Eurocode

Utmattningsanalys av stålbroar med ortotropa däck
Examensarbete inom Structural Engineering and Building Technology
ANDREA KARLSSON, CHRISTOFFER WESLEY
Institutionen för Bygg- och miljöteknik
Avdelningen för Konstruktionsteknik
Stål- och träbyggnad
Chalmers tekniska högskola

SAMMANFATTNING

Rapporten syftar till att undersöka möjliga fördelar av att använda FEM jämfört med konventionella handberäkningar vid utmattningsanalyser av ortotropa brodäck. En verklig bro, Saltsjöbron, modelleras med hjälp av FEM i Brigade/PLUS och hot-spot spänningar. Detta jämförs med handberäkningar baserade på nominell spänningsmetod.

Tre sprickmoder undersöks, en spricka i svetsen mellan kanal och tvärbalk och två sprickor i svetsen mellan kanal och däckplåt. Jämförelsen mellan metoderna visar stora spänningsskillnader vid de aktuella svetsarna.

Baserat på resultaten rekommenderas det att använda FEM för att inkludera de lokala effekterna som påverkar utmattningsbeteendet hos de undersökta svetsarna. Riktlinjer för värsta lastplacering för respektive sprickmod presenteras tillsammans med generella modelleringsrekommendationer.

Nyckelord: Ortotropa broar med ståldäck, Utmattning, Svetsar, Trapetsformade kanaler, Nominell spänningsmetod, Hot-spot, Finit element modellering, Skalelement, Eurocode

Contents

Preface

This Master's thesis deals with fatigue evaluation of three crack modes in orthotropic steel bridge decks and a comparison between FEM and conventional hand calculations. The research has been carried out at the Division of Structural Engineering of the Department of Civil and Environmental Engineering at Chalmers University of Technology and at the structural design company ELU in Gothenburg.

The thesis work has been supervised by Erik Olsson, ELU, and Prof. Mohammad Al-Emrani, which both have given indispensable support throughout the thesis. We are very grateful for their commitment and support as well as their constructive feedback. We also like to thank Andreas Nilsson for all the help with the finite element modelling. His support has spared us many hours of work and we appreciate his time and assistance.

We like also to thank all those who have been a part in this thesis work and supported us. It has been a very interesting and motivating process.

Gothenburg, August 2014

Andrea Karlsson & Christoffer Wesely

Notations

Roman upper-case letter

A	Area
E	Elastic modulus
F_r	Axial force in rib wall
G	Self-weight
I	Moment of inertia
I_{ef}	Moment of inertia for reduced cross section
L	Span length
M	Moment
M_d	Local moment in deck plate between two ribs
M_g	Local moment in deck plate in one rib
M_p	Global moment in deck plate
M_r	Moment in rib wall
M_{Rd}	Design moment
M_y	Yield moment
N	Fatigue life (in S-N-curve)
P	Point load
Q	Distributed load
R	Reaction force
S	Stress range (in S-N-curve)
S_{nom}	Nominal stress (in notch stress equations)
S_{ar}	Completely reversed stress for a notched member
T	Temperature
V	Shear force
W	First moment of area
W_{ef}	First moment of area for reduced cross section

Roman lower-case letters

f_y	Yielding stress
k_f	Fatigue notch factor
k_s	Reduction factor of fatigue strength
k_t	Elastic stress concentration factor
q	Distributed load
t_d	Thickness of deck plate

t_{eff}	Effective thickness
t_r	Thickness of rib
z	Distance to the neutral axis
z_{ef}	Distance to the neutral axis for reduced cross section

Greek letters

α	Heat expansion coefficient
δ	Deflection
ρ	Effective notch root radius
σ	Stress
$\sigma_{\perp f}$	Stress perpendicular to the weld
σ_{ar}	Completely reversed stress for a smooth member
σ_{hs}	Hot spot stress
$\sigma_{\parallel f}$	Stress parallel to the weld
σ_{wf}	Normal stress transverse to the direction of the weld
σ_y	Yield stress
$\tau_{\perp f}$	Shear stress perpendicular to the weld
$\tau_{\parallel f}$	Shear stress parallel to the weld
τ_{wf}	Shear stress longitudinal to the direction of the weld

Glossary

Anisotropy: A material with properties in different directions.

Crack initiation phase: The phase in the fatigue life from undamaged until a macro crack has been formed.

Crack initiation: The formation of micro cracks in the material, from loads with lower amplitude than the design limit, that will grow and join together to form one macro crack.

Crack propagation phase: The phase in the fatigue life after a macro crack is formed until failure.

Crack propagation: The continued growth of the initiated crack as a result of the stresses from the repeated load applications.

Cut out: Stress reliving cut in the web of the floor beam at the intersection with the continuous rib.

Deck plate: Steel plate below the wearing surface that distributes the load to the ribs as well as act as a top flange for ribs, floor beams and main girders.

Fatigue life: The number of load cycles a component will endure before fatigue failure

Fatigue: The process of gradual crack initiation and propagation for cyclic loads below the yield limits.

Floor beam: Transversal stiffener in orthotropic decks, transfers the load from the ribs to the main girders

Inhomogeneous or heterogeneous: A material that is not uniform in consistence and/or character.

LEFM – Linear elastic fracture mechanics: A method of fatigue assessment based on crack propagation analysis.

Main girder: The main load carrying members that transfer the load from the deck to the sub-structure.

Nominal stress: The stress on a distance away from the weld where it is constant in the parent material, no stress raising effects are included in the nominal stress.

Notch effect: The increase in stress in the area near to a change in section, a notch.

Orthogonal: Two axis that are perpendicular to each other.

Orthotropic: A combination of the words orthogonal and anisotropic to describe a structure with different properties in the two orthogonal main directions.

OSD – Orthotropic steel deck: Steel deck with different properties in the two main directions due to the present of longitudinal as well as transversal stiffeners with different cross-sections and spacing.

Principal stress: The stresses in the two axles in the principal coordinate system, i.e. the system rotated to the angle in which the shear stresses are equal to zero

Residual stresses: Internal, self-balancing stresses that arises due to for example welding of the specimen.

Ribs: Longitudinal stiffeners in orthotropic ribs, can be opened or closed and transfers the load from the deck plate to the floor beams.

Slip band: Dislocations of the crystal planes due to cyclic stress and the first step of the fatigue process.

S-N-curves: The S-N-curves are the relationship between the stress range, S, and the fatigue life, N. They are detail specific relations and include many of the affecting factors for assessing fatigue life.

Stress range: The amplitude difference between the maximum and minimum stress values in one stress cycle.

Structural hot spot stress (geometrical stress): The maximum principal stress in the parent material at the weld toe calculated with linear interpolations.

Tooth of floor beam: The zone on the floor beam web between two rib walls.

Wearing surface or coating: Protective layer over the deck plate of durable material that shields the deck from wearing damage as well as distributes the loads.

1　Introduction

Bridges with orthotropic steel decks have achieved great importance in modern structural design and several of the longest bridges today are constructed with this technology. An orthotropic deck has low self-weight and slender structures, which contribute to reduction of the stresses as well as to give the bridge an aesthetically pleasing profile.

An orthotropic bridge deck is composed of a deck plate together with longitudinal and transversal stiffeners. The separate parts are welded together, creating an intricate dependency between them. As a result of the different cross-sections and spacing of the longitudinal and transversal stiffeners the deck will display different properties and behaviour in the different directions. The stiffness behaviour contributes to a complex load transfer and stress state in an orthotropic deck. Consequently, the fatigue evaluation of a deck of this type is difficult to assess, and is further complicated by the fact that for several of the joints the correct detail is not available in the present codes.

It has been shown from measurements on existing bridges that orthotropic decks suffer from higher fatigue damage than expected and accounted for in design. The increase in traffic flow has also been higher than accounted for in design for most of the orthotropic bridges in service today. Because of this many bridges with orthotropic steel decks have problems with fatigue damage. The recommendations for fatigue design of these bridges have gradually increased the dimension of several individual members to counteract the fatigue damage.

As there is no convenient way to represent an orthotropic deck with hand calculations models many simplifications have to be made. The exact consequence of each separate simplification as well as the combined effect on the behaviour is largely unknown, accordingly the correct performance of the deck is not captured. A significant part of the problem lies in the fact that the simplifications which generating large errors are unidentified. Also the fatigue assessment approaches used in hand calculations are global and do not account for the local geometrical stress raising effects in the vicinity of the joints. One possible solution is to perform the load response calculations using FE software, which give a more authentic stress picture and consequently the fatigue problem can be addresses with better results. But the use of FEA demands more effort in the design process and an awareness of the more specific behaviour of the OSDs. Also, problem can rise when extracting the correct stress results due to the difficulty in extracting the nominal stress due to stress raisers.

The transition from the Swedish bridge norm (Svenska bronormen) to Eurocode has resulted in an increase of the recommended dimensions for members in orthotropic steel deck bridges. One specific case is the fatigue recommendations for welded details in road bridges with an orthotropic steel deck.

The recommendations in existing design codes, both national and European, are at present based on experience rather than theory and give very general instructions. The general approach is to increase the dimensions to avoid performing design on a local level. The gradual increase of the recommended thickness of the deck plate from 10mm to the present 16mm can be brought forward as an illustrative example of this. If the increase in dimensions is justified is not clear, however the effects on the structure are direct with increased self-weight and higher material costs. Therefore, it

is of great interest to investigate the fatigue evaluation of orthotropic decks and the possible error sources.

1.1   Aim and scope

The principal aim of this thesis is to investigate the necessity of advanced analyse techniques when performing structural design and analysis of an orthotropic steel deck. The main focus is the fatigue assessment of critical connections. Three types of welded connections in the bridge Saltsjöbron are studied with regard to the fatigue behaviour and evaluated with different assessment methods.

From this, a comparison between hand calculations and FEA will be conducted to investigate the gaining factors of using an FE model and if the extra time and effort required is a good investment. The steps of the modelling will be commented with regard to ease of implementation in future structural design, guidelines on how to perform the model and interpret the results will be given.

The evaluation and collation between the separate approaches also aims to identify which simplifications in hand calculations that generate large errors in the results. With this as basis the current recommendations can be questioned and conclusions regarding the risk of unexpected fatigue damage can be drawn.

1.2   Methodology

To fulfil the aims of this thesis, an extensive literature study is carried out to achieve a deeper understanding of the theoretical background. The main fields of study are the structural and fatigue behaviour of orthotropic steel decks, fatigue life of welded connections and fatigue life assessment methods applicable in structural design.

To investigate the necessity of more advanced fatigue life analysis for orthotropic steel decks a structural analysis and fatigue life evaluation are conducted for an existing bridge, Saltsjöbron in Södertälje, Sweden. Saltsjöbron is representative to orthotropic bridges as it has typical cross-section, load conditions and area of use for this type of bridges. The existing hand calculations will be examined and commented, the bridge will also be modelled in Brigade/PLUS as well as structurally analysed by hand. The results from the different approaches will be compared in order to draw conclusions regarding accuracy of hand calculations and which simplifications that result in sever errors. With regard to the problem description this bridge is representative as an orthotropic steel deck bridge and the results can be applied in design and analysis for similar bridges.

Saltsjöbron is designed and constructed according to previous Swedish bridge norm BRO94. Analysis will be made according to Eurocode as well as FE analysis based on the nominal stress method and the hot-spot method. A comparison between the different design codes, assessment methods and FE-results is conducted.

1.3   Limitations

This thesis work is limited to evaluate Saltsjöbron with its given dimensions and boundary conditions. No alternative bridge is evaluated and all properties and geometric conditions are restricted to the ones stated for Saltsjöbron.

Further, the fatigue behaviour of three critical connections is evaluated and all other details are disregarded. The assessment of the fatigue life is carried out as if it would have been a design process with the present technology used by structural designers. No more advanced methods are used than the ones plausible to apply in a real project.

CHALMERS, *Civil and Environmental Engineering*, Master's Thesis 2015:14

2 Introduction to fatigue in steel members

A well-known fact is that a steel member will fail in yielding if the load exceeds the maximum capacity, and this is in general the governing design criterion for different structural components. However, damage or failures can occur for loads well below the design limits in cases where the load is cyclic. This concept is known as fatigue.

Most structures are subjected to repeated loads which give rise to cyclic stresses. Even if these stresses are below the yield limit, the material experience damage on a microscopic level. This damage accumulates over time and form a macroscopic crack that can result in failure.

When a structural component fail in yielding it usually elongate in yielding with about 25% (Gurney, 1968). For fatigue failure the stress state is much lower than the yield limit and the component may not experience any plastic deformations and the damage can be hard to detect. The fatigue crack may develop in the material for a long time without being found and progress through the whole component before the damage is discovered. This makes fatigue failure very dangerous (Gurney, 1968) and several bridge collapses has occurred directly or indirectly due to fatigue damage (Harik et.al, 1990).

2.1 The concept of fatigue

When a component is subjected to cyclic loading, a fatigue crack formation centre can arise on a microscopic scale, followed by crack growth on a macroscopic level and finally failure (Schijve, 2009). The fatigue process is divided into two different periods, the *crack initiation phase* and the *crack growth phase*, see Figure 2-1.
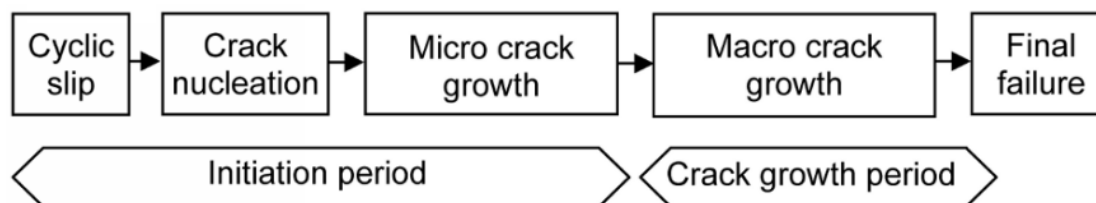
Figure 2-1 Different phases of the fatigue life (Schijve, 2009).

The separation between the two phases is a practical measure to ease the predicting of the fatigue life. The initiation phase is affected by numerous conditions that only have minor influence on the propagation phase, see Figure 2-2. Hence, a distinguishment between the two phases facilitates the fatigue prediction process.
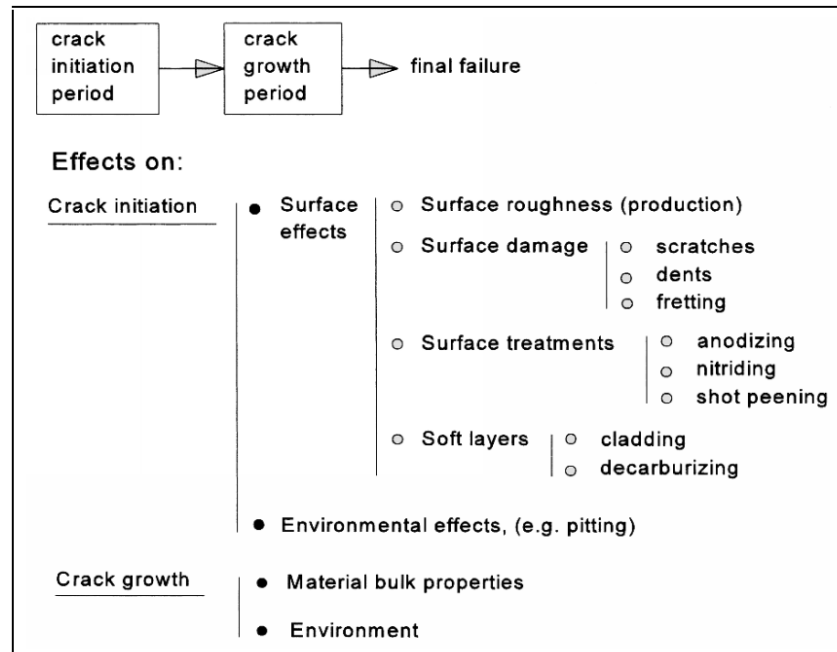
Figure 2-2 Affecting factors for the crack initiation and crack growth period (Schijve, 2009).

2.1.1   Crack initiation period

To study how fatigue damage is initiated, the material has to be examined on a microscopic level. On a sufficiently small scale all materials are anisotropic and inhomogeneous, see Figure 2-3. Steel is composed of crystalline grains arranged in planes, which makes the material both inhomogeneous and anisotropic. Inhomogeneities may also exist of particles with deviant chemical composition compared to the main material or voids of air between the grains.
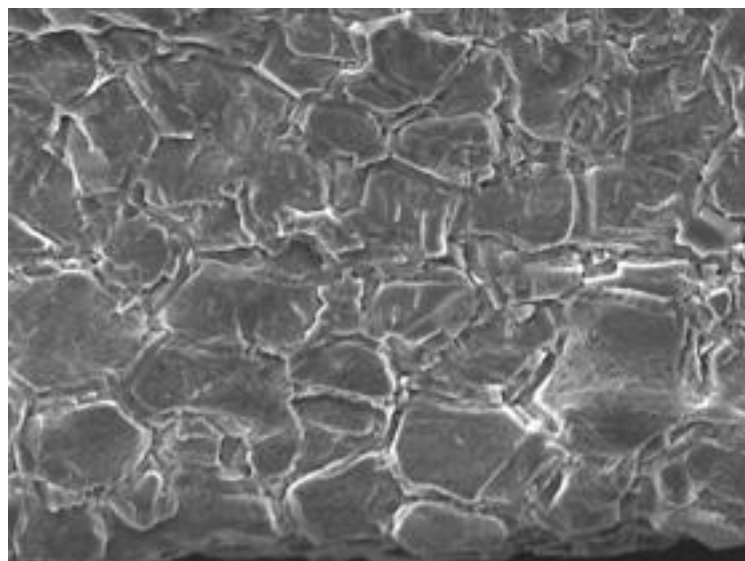
Figure 2-3 Granularity of steel seen with a scanning electron microscopy (Metallurgical Technologies, Inc., 2014)

Due to the irregularities on the micro level there will be a non-uniform stress distribution between the grains. Stress concentration points will arise at locations with a high quantity of irregularities, this is typical initiation point for a fatigue crack (Dowling, Siva Prasad & Narayanasamy, 2012).

In general fatigue cracks are initiated at the surface (Schijve, 2009). This is mainly because the slip constraint is lower at the grains located near the surface than in the sub-surfaced grains. The lower constraint at the surface results in deformations occurring at a lower stress level. Other effects that make the surface more prone to fatigue crack initiation are the presence of geometric discontinuities, surface roughness, corrosive pits and fretting fatigue.

When subjected to cyclic stresses, ductile materials such as construction steel experience stress concentration that starts to develop slip bands. Slip bands are dislocations of the crystal planes due to cyclic stress, see Figure 2-4, and are the first step of the fatigue process.
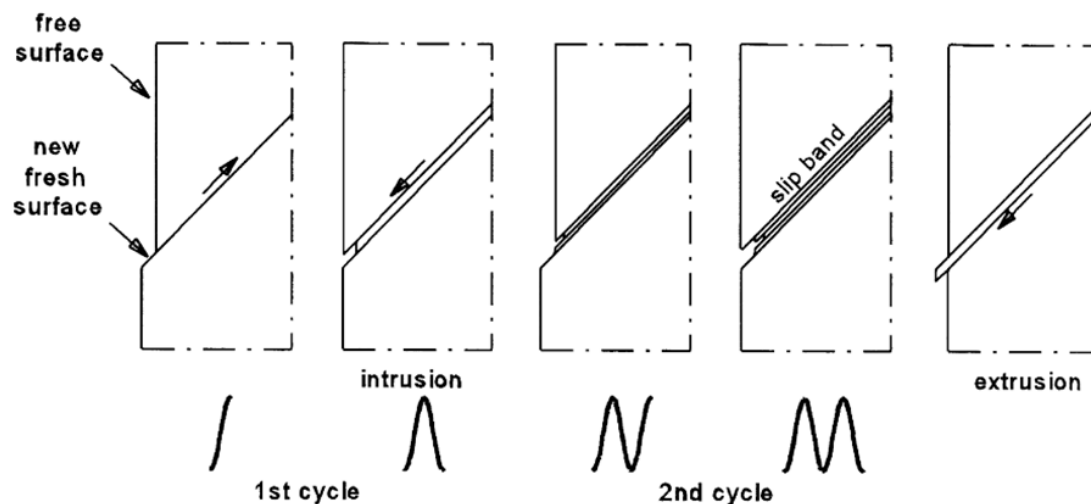
Figure 2-4 Simplified picture over the development of slip bands (Schijve, 2009).

For high-quality steel with limited ductility the fatigue crack usually starts at local defects in the material (Dowling, Siva Prasad & Narayanasamy, 2012). Even if these defects are below the surface the crack nucleus can initiate from these locations, which is uncommon for fully ductile materials (Schijve, 2009). However, the argument of low surface restraint is still valid and cracks are in general initiated at the surface.

The stress concentration starts a dislocation process near the surface that leads to plastic deformation. The dislocations are directed in a 45° angel since it is governed by shear stress. The cyclic load results in a cyclic slip that develops into a slip band (Schijve, 2009), see Figure 2-5. As the total amount of stress cycles increase so does the number of slip bands. This development continues until a saturation point is reached, after this the deformations are concentrated to a few slip bands that eventually form a micro crack inside the grain (Dowling, Siva Prasad & Narayanasamy, 2012). If enough load-cycles are applied these micro cracks will grow and spread into adjacent grains and eventually join with other micro cracks forming

an observable crack. A crack of this size is no longer governed by the surface effects but rather the crack growth resistance in the material. This marks the transition from the initial phase to the crack growth phase (Radaj, Sonsino and Fricke, 2006).
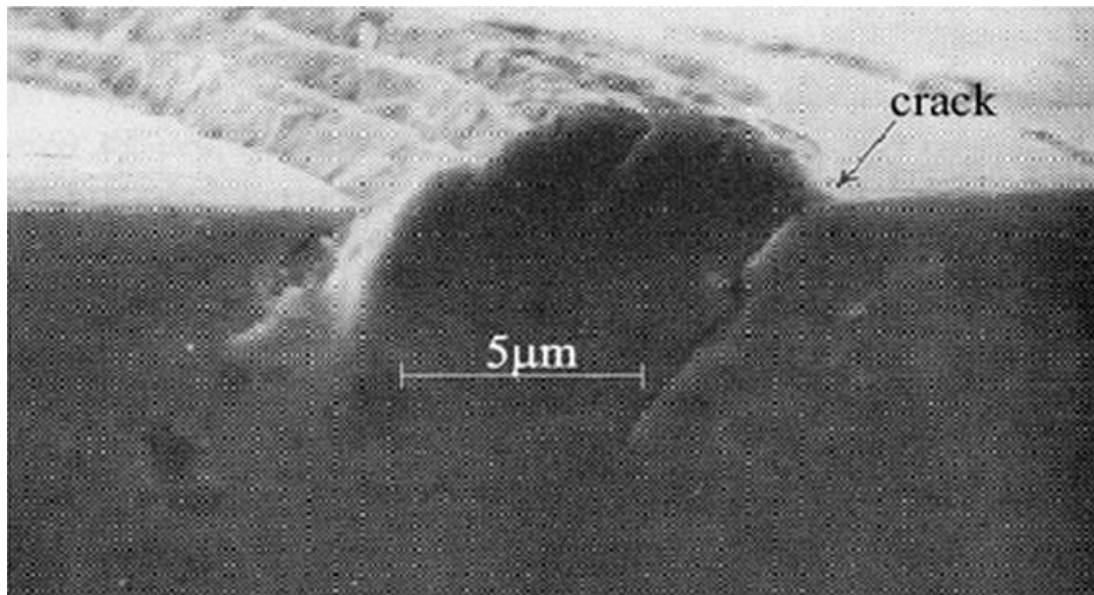
Figure 2-5 Slip bland and crack initiation point (Suresh, 1991)

2.1.2   Crack propagation period

The crack growth period starts when the growing crack is governed by the constitutive crack growth resistance and not by surface effects. When the crack grows away from the surface into adjacent grains the slip constraints increase because of the surrounding grains (Schijve, 2009). The deformations are now concentrated to a few slip bands which continue to develop into larger cracks. The growing cracks then start to deviate from the original slip plane and generally grow perpendicular to the main principle stress direction.

At first the crack growth rate is varying but when the crack front include sufficiently many grains the crack growth rate stabilize (Schijve, 2009). The final crack growth rate is determined by the crack growth resistance, which is a material property. The microscopic crack will increase with each load cycle until reaching a critical value where the structural component fails. The failure is often brittle and may cause abrupt deterioration of the structural functionality.

2.2   Fatigue in welded joints

Welding is widely used for built-up sections of metal components. One major application is found in bridges and especially in bridges with orthotropic steel decks, OSDs. In orthotropic decks the total welding length amount to tens of times the length of the bridge itself. At many locations in an OSD the welded details are intricate with crossing welds and complex stress states.

One principle difference between an unwelded joint and a welded joint is the crack initiation phase, described in Chapter 2.1.1. For an unwelded detail the main part of

the fatigue life consists of the initiation phase. For a welded detail on the other hand the initiation is significantly faster and the largest part of the fatigue life is the propagation phase.
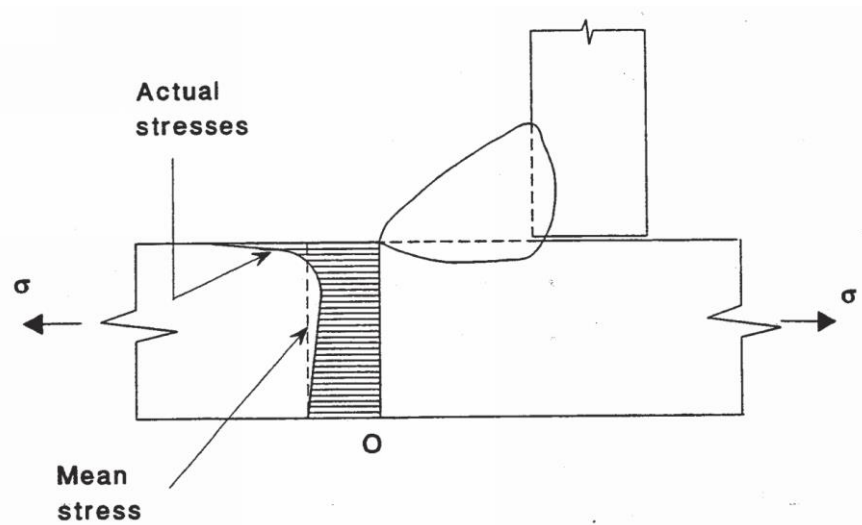
Figure 2-6 Geometric stress concentration at weld toe, (Maddox, 1991).

Welds disturb the stress flow and acts as geometric stress raiser, see Figure 2-6, which reduce the fatigue strength. Transversally loaded welds are in general more prone to fatigue than longitudinally loaded welds (Hobbacher, 2008). This is a consequence of the higher disturbance in stress flow for welds loaded transversally.

Welded joints are also known for their crack-like defects, such as lack of fusion, undercuts, porosity and lack of penetration (Mann 2006), see Figure 2-7 and Figure 2-8. Because of the many defects and the difference in welding technique quality the properties of welded joint have a considerable scatter (Schijve 2009).
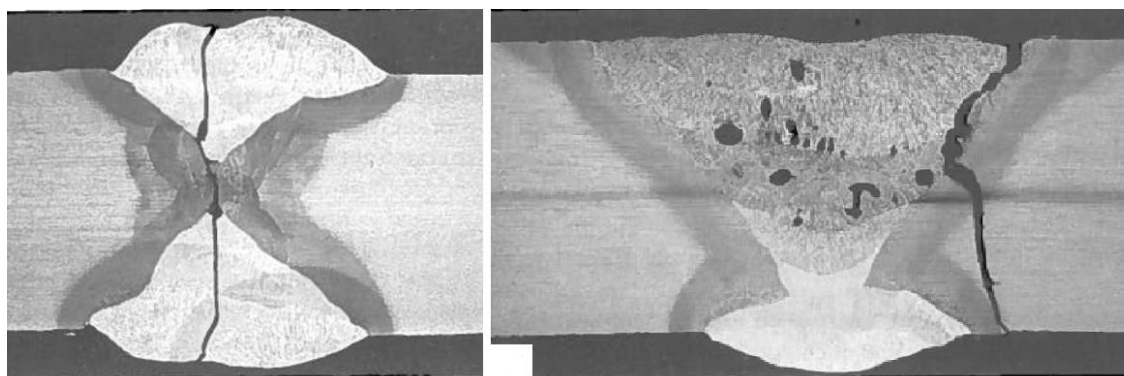
Figure 2-7 (a) Lack of penetration resulting in crack propagation through the weld; (b) Weld porosity resulting in crack propagation through the bulk material, (Gurney, 1968)
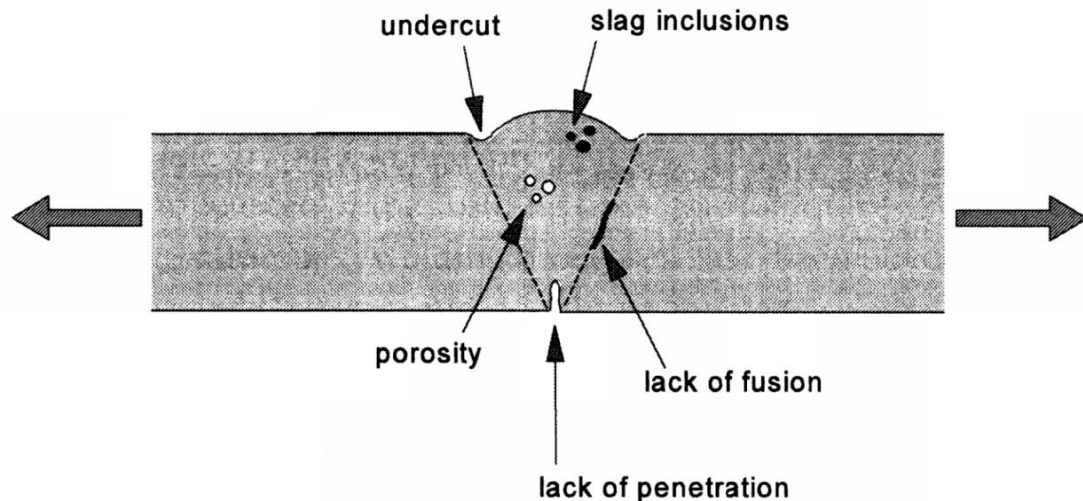
Figure 2-8 - Illustration of weld defects, (Schijve 2009)

The features of these defects are often unknown and correct stress concentration factors can be very hard to obtain (Dowling, 2013). A result of this is that most of the design codes employ an approach of S-N-curves based on the actual welded detail. The S-N-curves are the relationship between the stress range, S, and the fatigue life, N, and are developed by comprehensive experimental data of common structural components. The S-N-curves are detail specific relations and include many of the effecting factors for assessing fatigue life, but is getting more and more unsatisfactory because of the ever increasingly number of structural details and loading conditions (Al-Emrani, Bridge Fatigue Guidance – A European Research Project).

The short crack initiation phase for a welded detail is a consequence of the inherited crack like defects (Kolstein, 2007). These defects may in many cases result in that the fatigue crack already is initiated when the weld is complete and the total life of the welded joint consist only of the crack propagation. This cause shorter total life of welded connections compared to unwelded joints with the same stress range and may in some cases reduce the fatigue strength by as much as 90%. Figure 2-9 shows the difference in fatigue strength for a plain member, a notched member and a welded member. The figure clearly illustrates the strength decline for welded components.
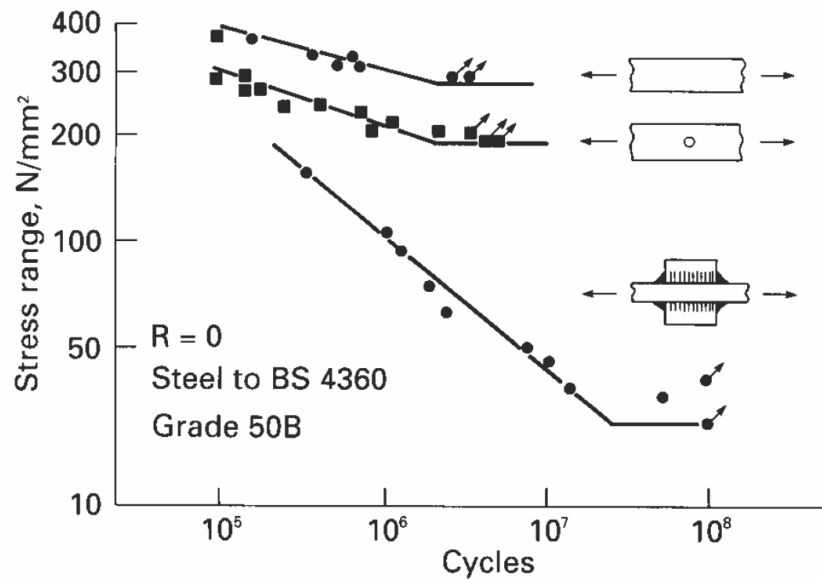
Figure 2-9 Difference in fatigue life for unwelded, notched and welded specimen (Maddox, 1991)

The crack initiation in welded joints is in almost all cases located to the root or toe of the weld because of the destructive feature of the welding process (Kolstein, 2007). During welding small crack-like defects, called intrusions, often arise at the weld toe, see Figure 2-10. These intrusions acts as starting points for micro cracks and entail the fatigue life of a welded component to be governed by the propagation phase.
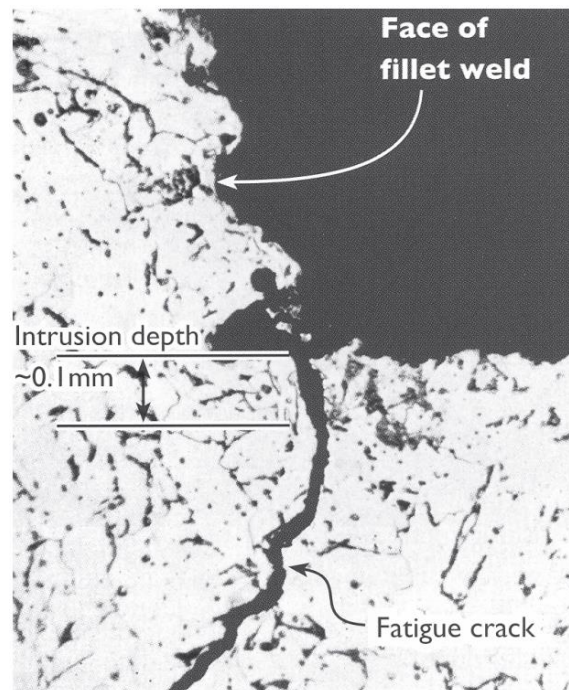
Figure 2-10 Intrusion at weld toe initiating a fatigue crack (Kolstein, 2007)

In Chapter 2.1 the fatigue crack initiation is described as a surface phenomenon. Increasing the strength of the main material will therefore also increase the initiation

period for a cyclic loaded member as stated by Maddox (1991). However, since the initiation phase of welded components are short to non-existing, increase in steel strength will have little to no effect on their fatigue life. Instead, an increase of the elastic modulus will increase the fatigue life of welded joints since this will reduce the crack propagation rate (Kolstein, 2007). The effect of ultimate strength on various members can be studied in Figure 2-11, where it can be seen that notched members, such as welded components, are less dependent of the bulk materials ultimate strength.
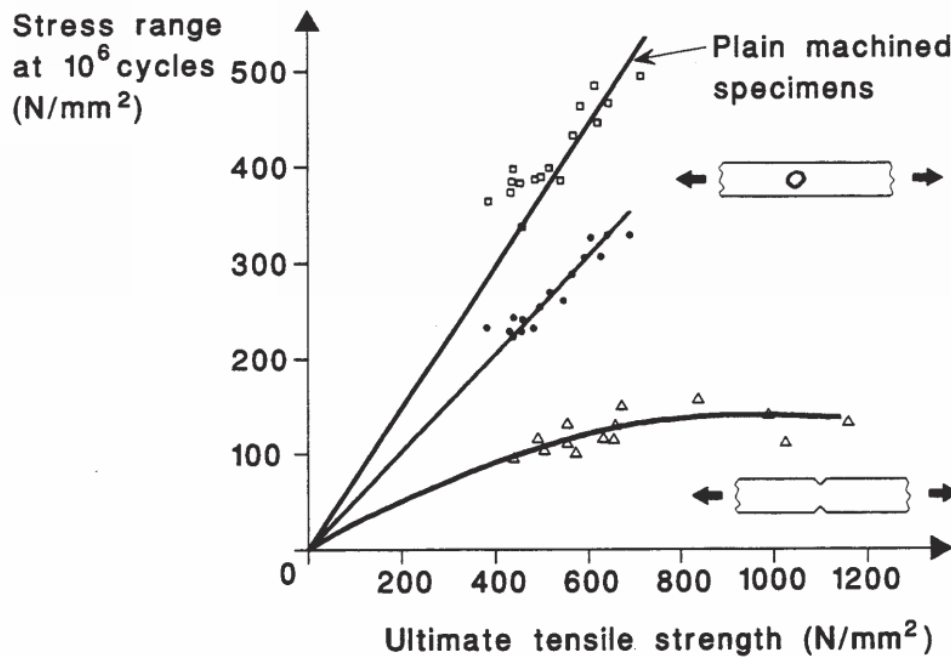
Figure 2-11 The effect of ultimate tensile strength of two types of notched speciemen (Gurney, 1968)

Another aspect that separates welded from unwelded joints is the high amount of residual stresses that rise after welding. During the welding process, liquid weld material fuses with the base material. When the weld cool down it tries to contract but is restrained by the base material. This result in considerable residual stresses that acts as an additional mean stress, (Mann, 2006). The residual stresses are always self-balancing, resulting in both tensile and compressive stresses. Tensile residual stresses can have an adverse effect on the fatigue life while compressive residual stress can significantly improve the fatigue life.

The residual stresses can sometimes be very high, even reaching the yield limit. If the residual stress is negative it can in some cases result in a negative peak stress, even if the member is loaded in tension. In this case, no fatigue crack will propagate, (Schijve, 2009). On the other hand, tensional residual stresses can cause cracks even if the member is loaded in compression (Heshmati, 2012). However, these cracks will only grow until they reach the compressive zone and then stop.

To find realistic residual stresses is extremely difficult, (Mann, 2006), and when designing with S-N-curves a conservative curve with unfavourable mean stress and residual stress are usually used (Macdonald, 2011). As previously stated, introducing

compressive residual stresses will significantly increase the fatigue life of welded members (Kolstein, 2007). Some techniques for this are shot peening, where small metallic shots pelt the surface, or thermal stress reliving treatment (Hobbacher, 2008).

Fatigue is a very localised process arising due to stress raisers. Orthotropic steel decks have many complex intersections between different structural members resulting in many local stress raisers. Orthotropic steel decks are therefore prone to fatigue damage and it is highly important to include a thorough fatigue evaluation in the design.

3 Orthotropic steel deck bridges

An OSD (Orthotropic Steel Deck) is a system built up of a steel plate with stiffeners in the two main directions. It is a structure with low self-weight, high load-carrying capacity and high stiffness. The slenderness of the deck also provides an appealing profile from an aesthetic point of view. These advantages have given the orthotropic decks high popularity, mainly in long-span bridges and moveable bridges.

The orthotropic steel deck structure is found in many of the longest-span bridges in the world today. Worth to mention is the Akashi-Kaikyo Bridge situated in Japan, connecting the main land to Awaji Island, with a main span length of 1991m (Yim, 2007), see Figure 3-1.

Figure 3-1 The Akashi-Kaikyo Bridge over the Akashi strait in Japan (Famous Wonders, 2011)

The development of the OSD began in the 1930's in Germany and continued throughout the 20th century, mainly in Europe (US Department of Transportation, 2012). In the post-war depression it became more important to save material, and with the base in this the orthotropic systems were favoured and further improved.

As the development proceeded the suitability to use the OSD systems in movable bridges became more apparent (US Department of Transportation, 2012). The lightweight structure results in less required counterweight, this generates lower encumbrance on the moving system as well as the internal forces in the rotation axles. In addition, when the bridge is in upright position, the dead weight is transferred directly to the girders from the deck plate, a much simpler mode of transfer compared to equivalent structural systems.

3.1 Typical design and mode of action for orthotropic steel deck bridges

A general OSD system is assembled from a thin deck plate, on which longitudinal stiffeners are welded, these are in turn supported by transverse floor beams and the whole deck rests on the main girders (Kolstein, 2007), see Figure 3-2. Due to interaction between the different components of the deck a complex behaviour arises. The traffic loads are distributed two-dimensionally and because of different stiffness properties and deflection induced secondary stresses the actual stress state is hard to predict.
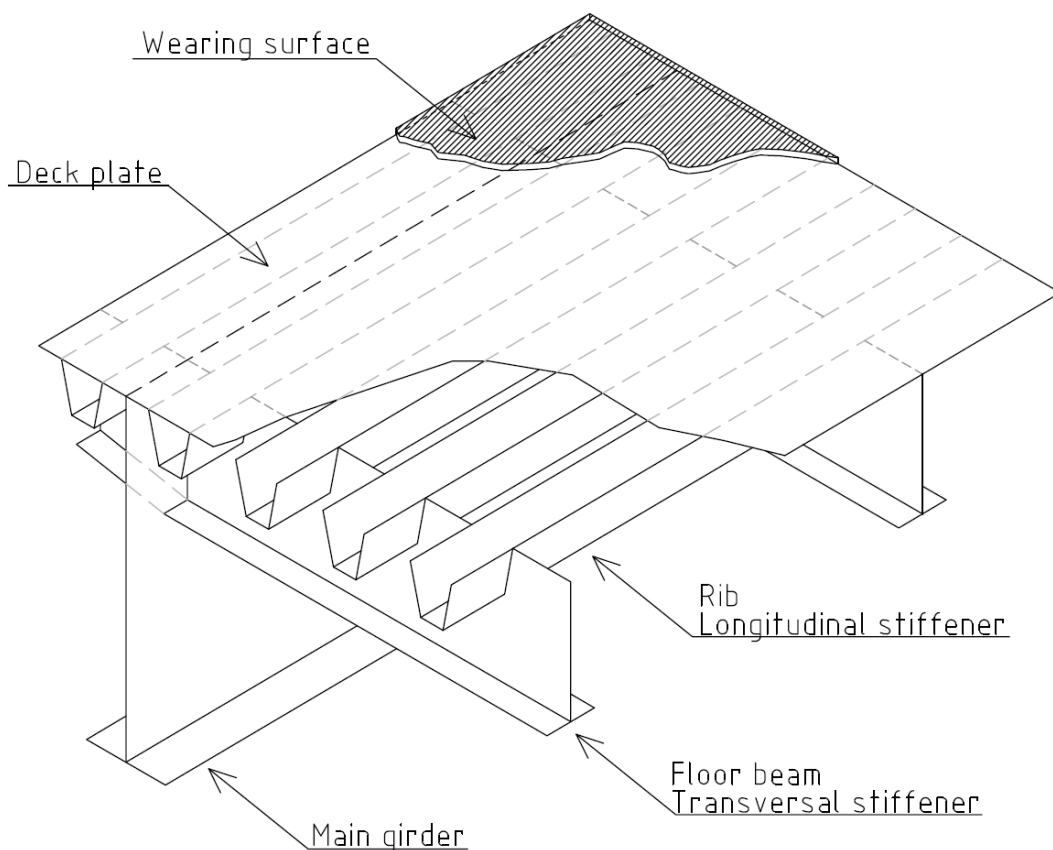
Figure 3-2 Overview of an orthotropic deck with the components of the system highlighted

Together components in an orthotropic deck form a system with anisotropic stiffness properties in the longitudinal and transversal direction since the ribs (longitudinal stiffeners) and the floor beams (transversal stiffeners) are placed perpendicular and have different structural rigidity characteristics (US Department of Transportation, 2012). In other words, it is a system with different properties in the two main directions, or an orthogonal-anisotropic system, referred to as an 'orthotropic' system.

As a result of the interaction between the components in the OSD, the deck acts as a structural unit and has to accomplish numerous functions simultaneously. Key features are the distribution of traffic loads and that the ribs, floor beams and the main girders utilize the deck panel as a top flange (US Department of Transportation, 2012), see Figure 3-2. This result in a highly effective use of material but the

interaction between the components must be regarded in design. This can be compared to the design of equivalent bridge types where the interaction is normally ignored and each component is designed separately (AISC, 1962).
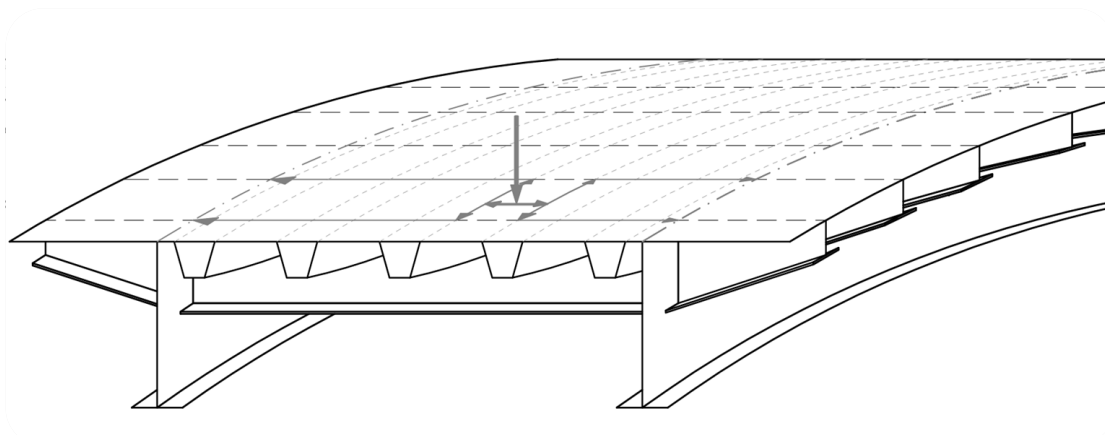
Figure 3-3 Load dispersion in an orthotropic deck, the load is applied between two rib walls and distributed in transversal direction to them, from the rib walls the load is distributed in longitudinal direction to the floor beams and then in transversal direction to the main girder

Due to the interaction in the deck, the effort required to analyse the behaviour of an OSD is higher than for equivalent bridge designs. However, a simplified method is to divide the deck in to sub-systems, see Table 3-1, which can be analysed separately and then combined by linear superposition (US Department of Transportation, 2012). This simplified method is possible to use for the limit state calculations but if a full interaction model is required the deck needs to be analysed with finite element methods.

Table 3-1 Sub-systems of an orthotropic deck

System 1 - Local deck plate deformation

System 2 - Panel deformation

System 3 - Longitudinal bending of ribs
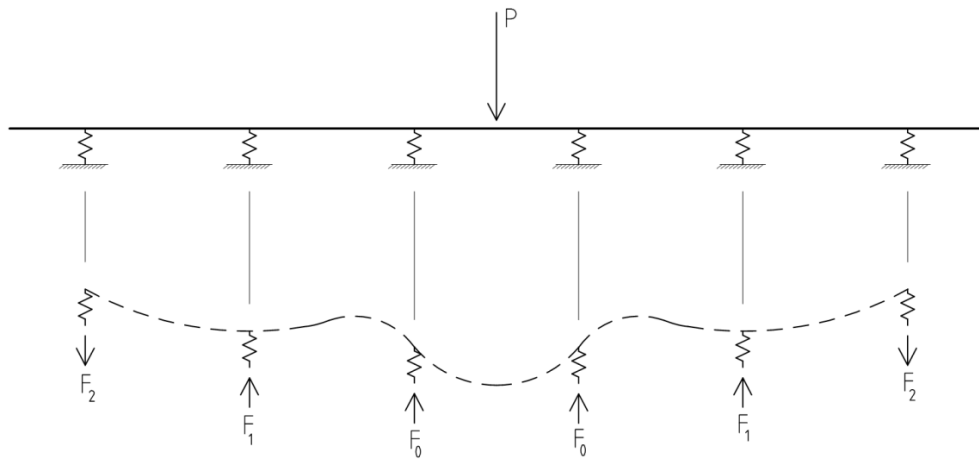
System 4 - Floor beam in-plane bending

System 5 - Floor beam distortion

Curvature of floor beam
at bottom of ribs

Curvature of floor beam
between ribs
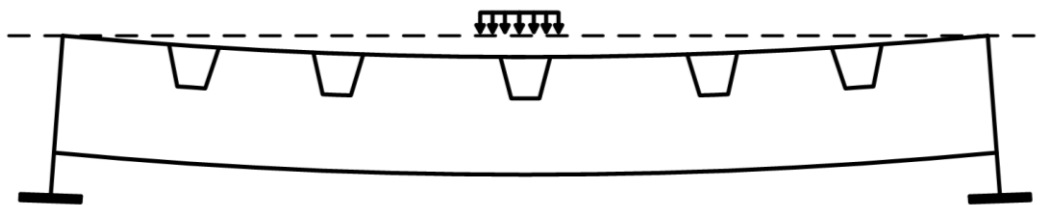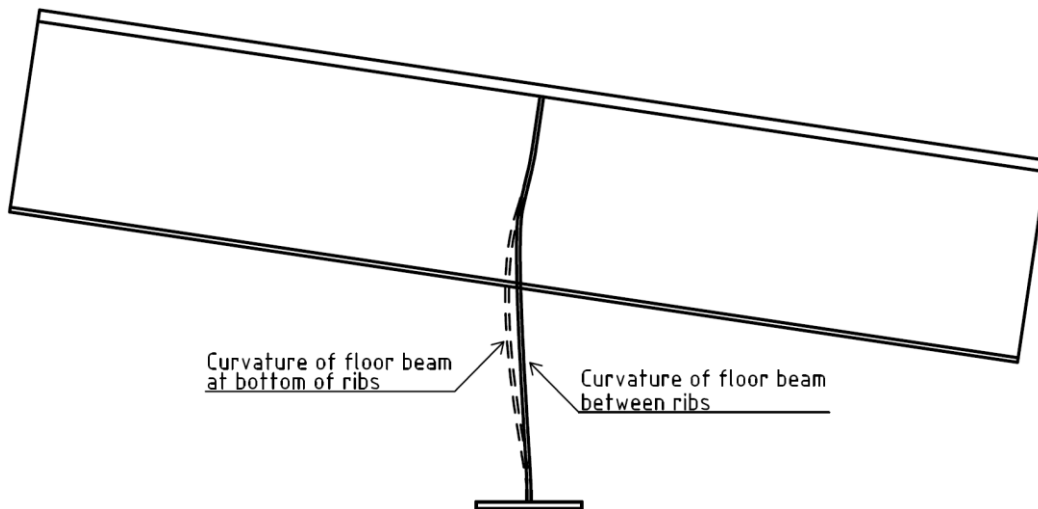
System 6 - Rib distortion
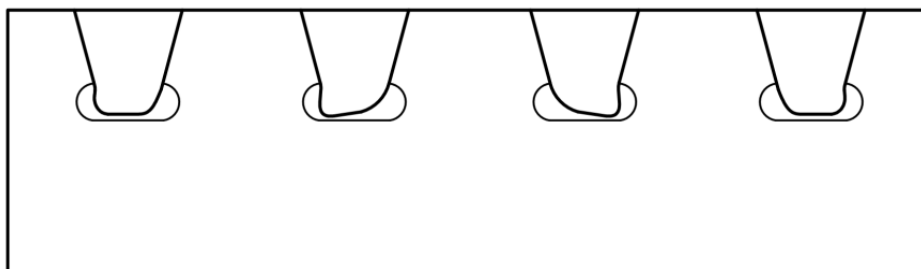
System 7 - Global
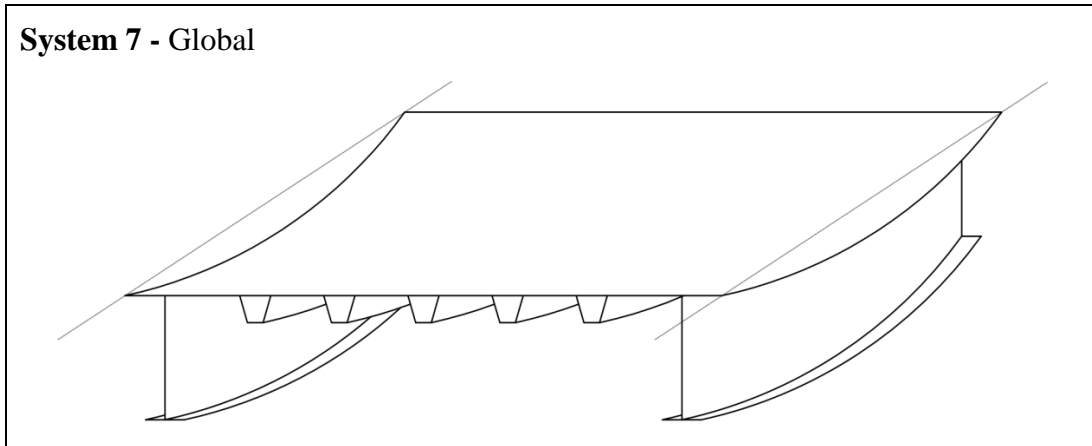
Each system has a specific behaviour that can be analysed by hand and when combined the performance of the entire deck is mirrored with acceptable accuracy. The systems will be described more thoroughly in Chapter 3.3.1.

3.1.1 Wearing surface

The wearing surface, or coating, is structurally significant in an orthotropic deck due to its multiple functions. The coating distributes the traffic loads, protect the deck plate from corrosion attacks, evens out irregularities and provide a smooth riding surface (Aygül, 2004). From this follows that the wearing surface reduces the stress levels in the steel plate, see Figure 3-4, which prolong the fatigue life. The reduced stress is a result of the load distribution the wearing surface provides to the steel plate.
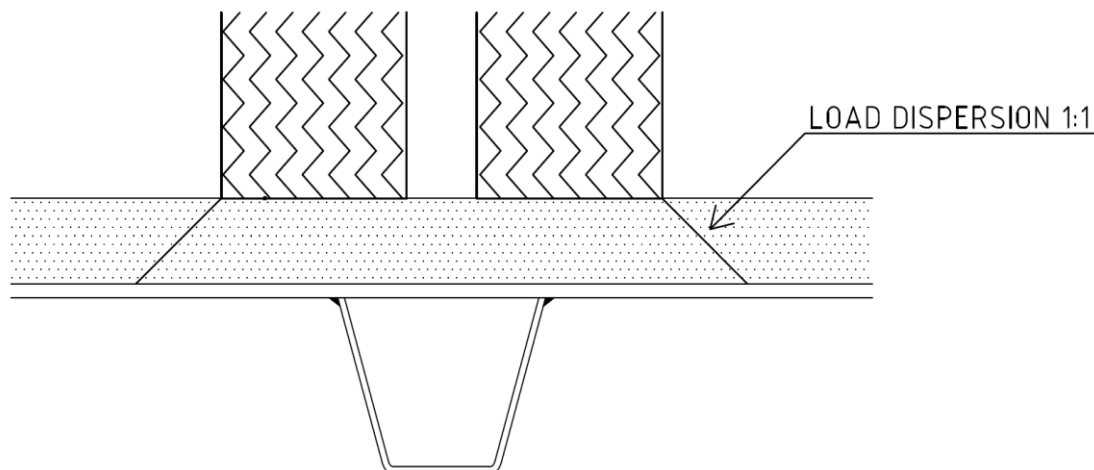
LOAD DISPERSION 1:1

Figure 3-4 Load dispersing in the wearing surface

In addition to the above mentioned effects, the wearing surface needs to be able to allow for expansion and contraction as well as bending and vibrations of the deck plate (Tourans & Okereke, 1991). It is of high importance that the coating doesn't crack, if this occurs salts will penetrate down to the deck plate and the risk for corrosion increases radically.

Ordinary wearing surface consists either of a bituminous or a polymer surface system (US Department of Transportation, 2012). A principal difference between the two systems is the thickness, the bituminous materials are in general 50mm or greater while the polymer materials are 20mm or less. However, the decisive factor for the type of surface material is in general the climate, since the bituminous system is more sensitive to temperature variations.

The wearing surface constitutes a significant part of the total weight in an orthotropic bridge and therefore has a larger structural importance for OSDs than for other types of bridges (Aygül, 2004). The weight of the coating affects the whole bridge structure and doesn't only result in a direct weight increase. Increasing the thickness of the wearing surface results in larger counterweights for moveable bridges, higher amount of steel in cables for long-span bridges and a required capacity increase for the substructures.

Other preferred characteristics of a wearing surface include stability, durability, good bonding properties, maintained stiffness over a suitable temperature range, resistance against shoving and ravelling as well as ease of affixing and maintenance (US Department of Transportation, 2012). In general the coating is rigidly bonded to the deck plate and together they act as a composite system that is subjected to both mechanical and thermal loads. Temperature loads arise due to variation in temperature and the difference in thermal properties that causes expansion and contraction at high respective low temperatures. These actions are not equal between the layers and the materials will contract or expand differently and from this stresses arise, and cracks may develop.

As mentioned earlier the wearing surface contributes to dispersion of the load and thereby lowers the stresses in the steel plate. Common practise has been to assume the angle of the dispersion to 45º in all direction, if a bituminous layer of sufficient thickness is used (US Department of Transportation, 2012). However, the material is temperature dependent, with increasing temperature the dispersion capacity decreases or completely diminishes due to that the materials softens. There is also an uncertainty of future measures, such as replacing of the wearing surface with a thinner layer. However, in design codes the dispersion in the wearing surface is in general accounted for not to underestimate the capacity of the structure.

3.1.2 Deck plate

The deck plate in OSD is a thin steel plate that forms the base for the wearing surface. Together they act as a composite system that transfers the traffic loads down to the ribs, floor beams and thereafter to the main girders. The ribs and floor beams act as longitudinal respective transverse stiffeners to the deck plate.

The interaction in the coating and deck plate system is temperature and thickness dependent (US Department of Transportation, 2012). At high temperatures the stiffness contribution from the wearing surface to the deck plate is small. However at low temperatures the contributions is substantial and will reduce the steel stress in the deck plate. Regarding the thickness of the coating, a thick wearing surface is superior concerning the distribution of loads, decreasing the stress state in the deck plate.

The presence of the wearing surface smears out the loads to act over a larger part of

the deck plate. The actual stress state in the steel deck is highly influenced by the thickness of the steel plate and also affects the fatigue life (US Department of Transportation, 2012). The thicker the plate the better stress-performance is shown both in the plate and the composite system. Although thicker deck plate means higher initial cost and heavier structure it is likely to be profitable from a life-cycle perspective due to longer fatigue life for both coating and steel plate.

The deck plate and wearing surface do not only transfer the wheel loads to the longitudinal stiffeners but also, as mentioned above, act as top flange to the ribs, floor beams and main girders. Because of this the OSD forms an intricate entity with an effective use of material.

3.1.3   Rib-system

The ribs in the OSD can either be open or closed, see Figure 3-5. The most common type is closed trapezoidal ribs (Kolstein, 2007), as was seen in Figure 3-2. The characteristics of the longitudinal ribs are used to classify the system into open-rib systems or closed-rib systems (US Department of Transportation, 2012).
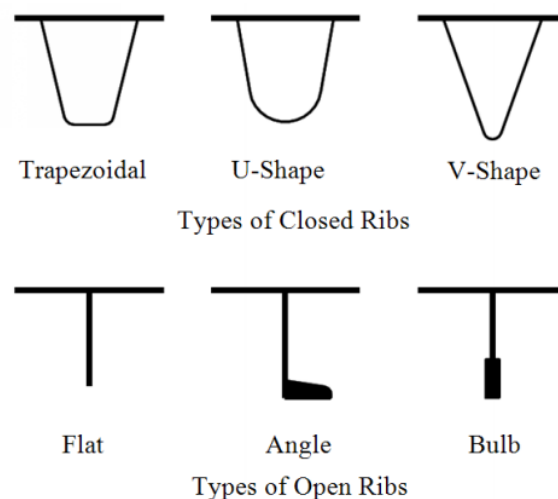
Figure 3-5 The most common types of open and closed ribs used in orthotropic systems used in bridges (US department of Transportation 2012)

Open ribs can be manufactured in different forms, either flat, angled or bulb as seen in Figure 3-5. Advantages of an open rib system are ease of production, inspections and maintenance as well as flexibility in dimensions and easy assembling with rest of the deck (US Department of Transportation, 2012). However, these benefits are in general outweighed by their low torsional and flexural stiffness, which results in an inefficient behaviour regarding the load transfer between neighbouring ribs (Aygül, 2004). This engenders the need for more ribs and tighter floor beam spacing, as a consequence more material is required. Furthermore, about twice as much welding is required in a deck with open stiffeners compared to an equivalent deck with closed ribs (US Department of Transportation, 2012), see Figure 3-6.
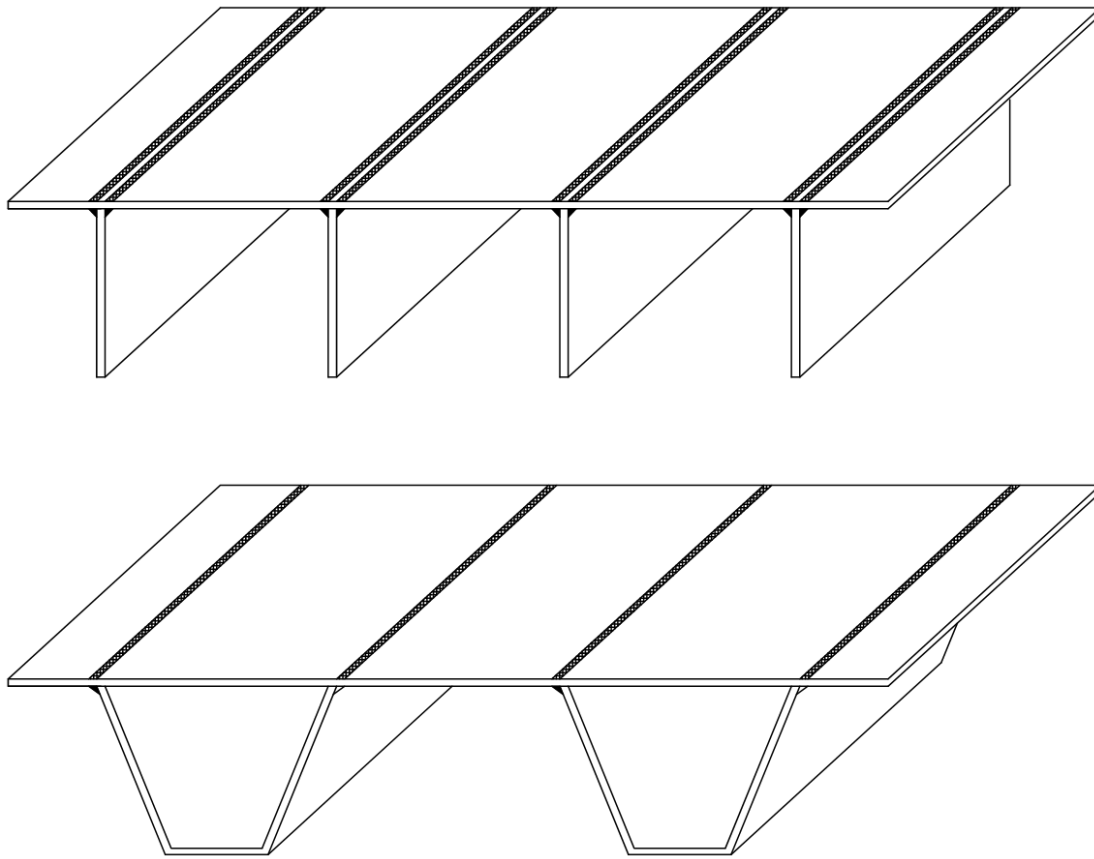
Figure 3-6 Difference between the amount of welding in open and closed ribs

An orthotropic deck with closed stiffeners has a significantly better capacity to distribute the traffic loads compared to a system with open ribs (AISC, 1962). The closed stiffeners have rectangular, trapezoidal or semi-circular cross-section, see Figure 3-5. The closed ribs give the deck elastic stability as well as increased bending capacity, hence a wider spacing compared to open ribs is possible, enabling material savings. This is due to the significantly higher flexural and torsional rigidity (Janss, 1986). The high flexural and torsional rigidity of the closed rib system makes it superior regarding erection and construction of the bridge. Also, the higher torsional rigidity results in enhanced load distribution, in particular for concentrated transverse loads, as well as to minimize the differential deflection (US Department of Transportation, 2012). This contributes to lower the stresses in the wearing surface, deck and ribs.

The possibility of larger floor beam spacing in the closed rib system is restricted by the increasing cut-out size in the floor beam webs (US Department of Transportation, 2012). The stress reliving cut-out is placed in the bottom of the rib, see Figure 3-7, and is needed to prevent excessive out-of-plane stresses in the weld, avoiding the maximum stress point. With larger cut-out the shear resistance of the floor beam is decreased and the transvers deflection increased, this may cause earlier cracking and failure of the wearing surface.
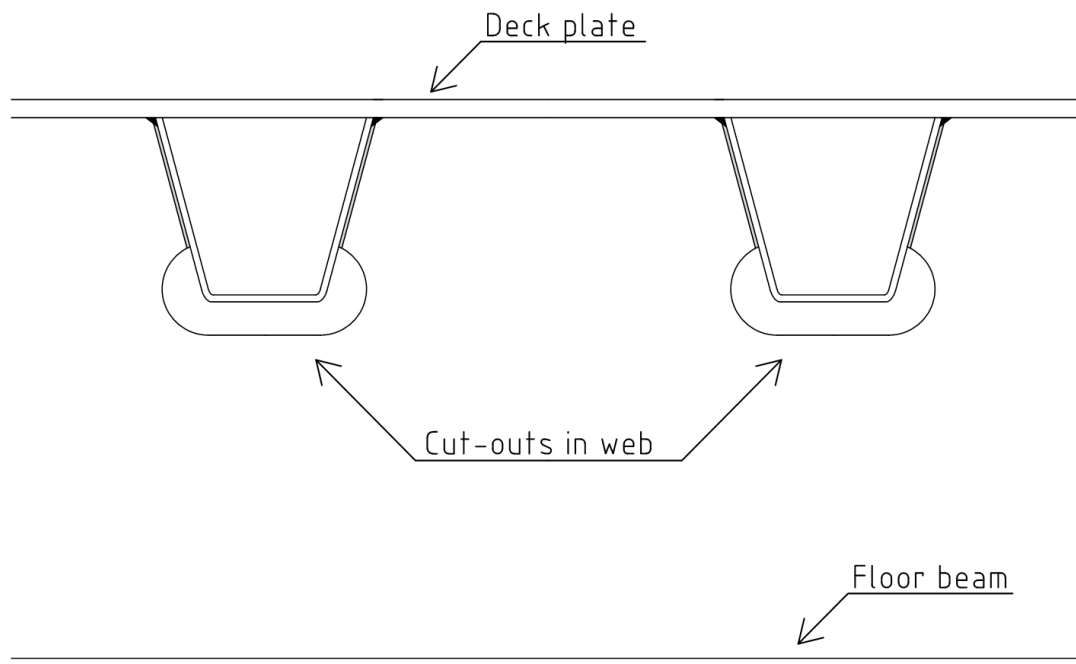
Figure 3-7 Cut-outs in transversal floor beams at the intersection with longitudinal ribs

Another advantage for closed stiffeners is the less amount of welding required compared to open stiffeners. However, the closed rib system is more difficult to fabricate and assemble with proper fit to adjacent members (AISC, 1962). Also the field splices for closed ribs are more difficult to perform than the ones for open ribs. In particular the fatigue sensitive welds between the deck plate and stiffener and between floor beam and stiffener requires high quality and care in fabrication (US Department of Transpiration, 2012).

Table 3-2 Comparison between open and closed stiffeners

	Open ribs	Closed ribs
Transfer of wheel loads		Better
Torsional stiffness		Better
Flexural stiffness		Better
Total material use in OSD		Better
Ease of manufacturing	Better	
Ease of fitting to rest of deck	Better	
Field splices	Better	
Ease of maintenance	Better	
Erection of bridge		Better

As can be seen in the comparison in Table 3-2 the closed ribs enhance the performance of the orthotropic deck while the open ribs are better with regard to fitting and maintenance.

Regardless of if the ribs are opened or closed they are normally placed in the longitudinal direction and transfer the traffic load from the deck plate to the floor beams. Ribs can be placed in the transverse direction, however this generates

problems with the durability of the wearing surface due to the washboard effect, which in addition creates discomfort for the road users (US Department of Transportation, 2012).

As mentioned, the closed ribs have several advantages, however there are some problems which needs to be regarded in design. One of the major complications is the weld between the rib and the deck plate, see Figure 3-8. This is in general a one-sided partial penetration fillet weld that needs to be performed with care due to the properties of and the load transferred in the weld. This weld is more inclined to fatigue damage than the corresponding weld for an open stiffener. This is due to the higher constraint against transversal deformations in the deck plate generated in a closed rib system compared to a system with open ribs (Liao, 2011).
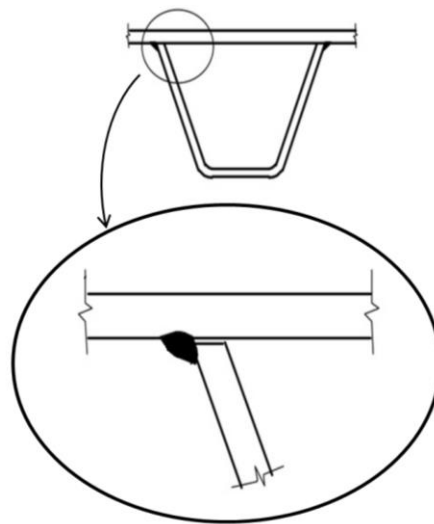
Figure 3-8 The problematic weld between deck plate and rib (Pfeil, Battista & Mergulhão, 2005)

OSDs with a closed-rib system are also amenable to fatigue damage at the weld in the intersection of floor beam and rib, see Figure 3-9. The main reason for this is the restrain from the ribs and the geometry that causes local secondary deformations and stresses (US Department of Transportation, 2012). One alternative to decrease the number of high-risk sections is to have longer spacing between the floor beams to reduce the number of intersection-points between the ribs and floor beams (US Department of Transportation, 2012). However, a larger span for the floor beam requires a larger floor beam, also the fatigue stresses in the rib-to-floor beam joint are more difficult to control for longer spans. The optimum is to have as long spans as possible without increase the stresses at the intersection with the floor beam to exceed safe levels.
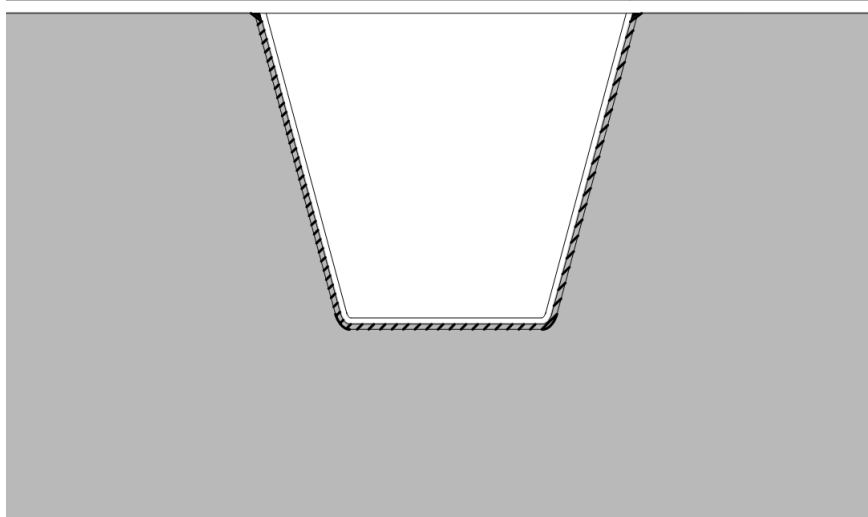
Figure 3-9 Weld at connection between rib and floor beam

3.1.4 Floor beams

The floor beam in an orthotropic deck is the transverse member supporting the ribs and deck plate and transferring the load to the main girder. The dimensions of the floor beam are in general governed by the construction and erection requirement as well as the allowed deflection (AISC, 1962).

Generally the transverse girder consists of an inverted T-section that is welded to both the deck plate and the longitudinal ribs (Tinawi & Redwood, 1976). The deck plate functions as a top flange for the floor beam. Since the floor beam is welded to both the deck plate and ribs the whole deck is interacting as one unit. The floor beams contributes to the torsional rigidity of the OSD cross-section as well as the load-carrying capacity (AISC, 1962).

To avoid stress-concentration points at the intersections between the floor beams and ribs, cut-outs can be provided (US Department of Transportation, 2012), see Figure 3-10. However, cut-outs should only be used when the depth of the floor beam is sufficient (Kolstein et al., 1996). It is of great importance that the cut-outs have smooth edges to avoid potential defects and thus fatigue cracking. Between the rib and floor beam the transferred shear force is in general low. According to this it is adequate to use one-sided welds in this connection (AISC, 1962). By doing this the shrinkage induced stresses are minimized in the floor beam web, where it's welded to the rib.
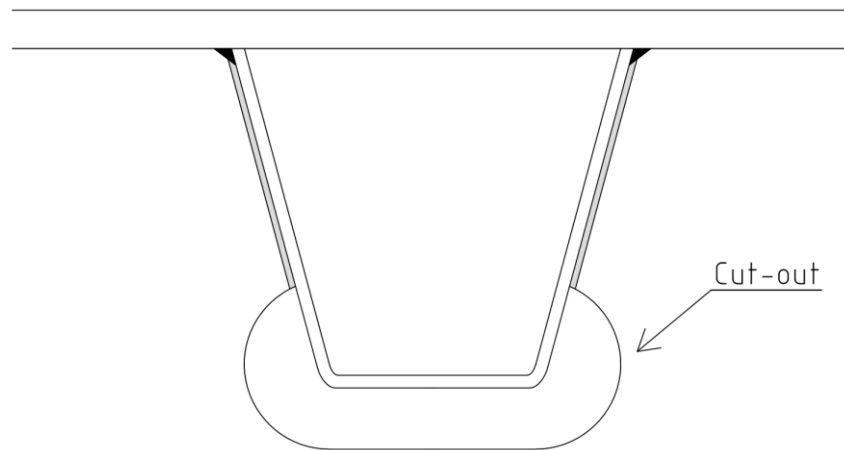
Figure 3-10 Stress-relieving cut-outs in floor beam web at intersection with ribs

Optimization of the shape and geometry of the cut-outs is an important issue to enhance the performance of OSD (US Department of Transportation, 2012). The reason for the focus on this specific detail is that a well-designed cut-out results in a decrease of the out-of-plane stresses which can be kept below 25% of the in-plane stresses if the geometry is beneficial. The decrease of out of plane stresses makes it possible to focus mainly on the in plane stresses and to thereby simplify the analysis process for orthotropic decks.

From the floor beams the load is transfer to the main girders and then via columns and supports down to the sub structure. This load path that has been described in short in the sub-chapters above is a very simplified and generalised way to observe the intricate load behaviour of a bridge with an orthotropic deck. However, for hand calculations this is the basic transfer pattern used to turn the actual bridge deck into comprehensible models from which the design can be extracted.

3.2   Economic considerations

Orthotropic steel decks have a relatively long service life, give an aesthetically pleasing profile to the structure and are economical to maintain as long as the design is properly performed (Touran & Okereke, 1991). As a consequence of the effective load distribution in an OSD less material is required in both super- and substructure and thereby money, time and effort. However, the OSDs have shown prone to fatigue and are expensive to repair if critical cracks appear and this must be taken into consideration during design and construction. Hence, they are more expensive than other types to design due to the longer time required for calculations and analysis.

There are several factors in bridge design and construction that may govern the choice of bridge type. If low self-weight, high ductility, slender section or fast construction is required an orthotropic system is an economical solution (Magnus & Sun, 200).

As mentioned earlier OSDs are frequently used in movable and long span bridges. These types of structures are in many cases technologically challenging and expensive in design and construction. Thus the self-weight and material expenses are of higher importance than for other bridges. According to this it is evident that if an economical solution is to be reached the dead weight needs to be kept at a minimum.

Consequently, an orthotropic deck is preferable to attain the optimum solution, this is also validated by the high amount of OSDs in these types of bridges around the world.

Table 3-3 Examples of beneficial economical attributes of an orthotropic deck

Beneficial attributes	Examples
Reduced structural weight	The highly efficient use of material reduces the total weight of the material required to carry the loads. The amount of material to be saved increases with the length of the spans (AISC, 1962). This results in savings on both material and total weight. When switching from a reinforced concrete deck to an orthotropic deck in a long-span bridge it is possible to reduce the dead-weight by more than 20% (Magnus & Sun, 2000). Another important effect of the lower self-weight is the improved performance for the bridge during an earthquake (Magnus and Sun, 2000). This is a result of the mechanic principle that larger mass results in greater seismic forces in the structure.
Erection efficiency	It is easier and cheaper to erect a light-weight structure and requires less man hours, decreasing the total labour costs (AISC, 1962). It is also faster than a construction with in-situ casted concrete and requires less equipment and logistic costs in total. Short construction time is in general highly valued in bridges and can mean great savings. Less scaffolding is also needed for an orthotropic deck than for composite or concrete deck.
High load-carrying capacity	The developed system of an orthotropic deck is made to carry load in the most effective way possible with as little material as possible.
Slenderness of structure	Smaller wind loads and more aesthetic structure. Also, the lower construction height results in lower approach grades. In the intersection between road and railway the structural height of the deck is of great importance (Magnus and Sun, 2000). With a slender deck large savings can be made in total to the project since high-speed trains requires minimal grades (Magnus and Sun, 2000).
Minimizing the substructure	Lower weight and less wind-load results in decreased stresses on the foundation.
Long life time	Orthotropic steel decks in general do not require replacement during the service life of the bridge structure.
Low maintenance cost	The maintenance is usually concentrated to anti corrosive painting

3.3 Structural performance, load effects and fatigue behaviour in orthotropic steel decks

The positive sides of the OSD system are many, however in several bridges built with orthotropic decks fatigue damages have been observed earlier than expected (US Department of Transportation, 2012). This is partly a consequence of the significant increase of both traffic load and intensity in the last decades and the fact that orthotropic decks chiefly were designed with regard to static load behaviour (Kolstein, 2004). A large part of the fatigue cracks, in any type of steel bridge, are initiated at weld defects and can be disastrous, see Figure 3-11.
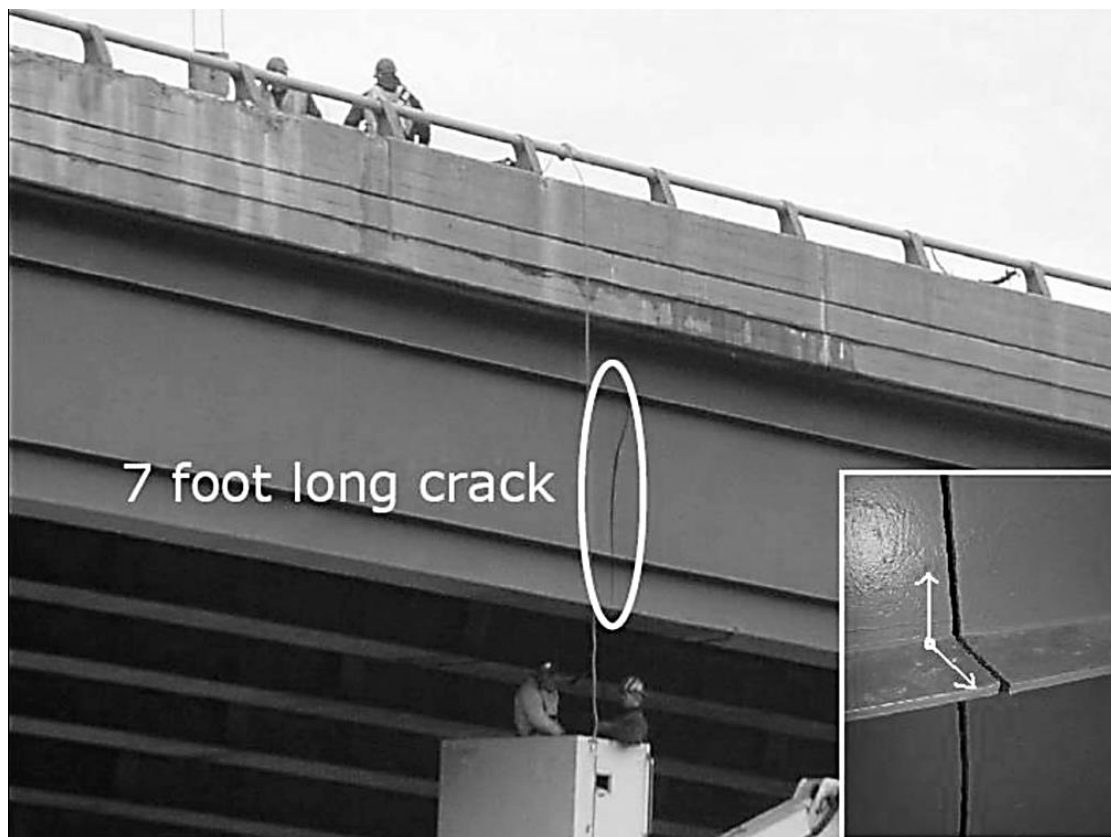
Figure 3-11 Fatigue crack in a bridge girder starting from a weld defect at an intersection point (Haghani, Al-Emrani and Heshmati, 2012). This picture shows a deck that is not orthotropic but it highlights the importance of the welds and possible fatigue defects arising

Orthotropic decks have numerous welded joints with complex structural behaviour, geometry and load situation (Aygül, Al-Emrani & Urushadze, 2011). The relative slenderness of the components and the geometric detailing make the welds in the structure vulnerable to fatigue damage from cyclic traffic loads (Pfeil, Battista & Mergulhão, 2005). Based on this, the fatigue strength of an orthotropic deck and in particular of the welded connections is complex and case specific, resulting in complicated fatigue evaluations. The main reason for this complexity is the intricate interaction between the deck plate, ribs and floor beams.

Fatigue design of an OSD, and steel bridges in general, are normally performed with the nominal stress approach using S-N curves and the related fatigue classes from the appropriate code. The nominal stress approach is explained more thoroughly in Chapter 4.1 but in short it is based on the average stress in the examined section, no local stress concentrations are accounted for and linear elastic material behaviour is assumed. Due to this simplification unrealistic results can be expected in complex structures and details, such as the welds in an orthotropic plate, hence these specific details and system should be analysed with more advanced methods to ensure the results of the fatigue calculations (Aygül, Al-Emrani & Urushadze, 2011).
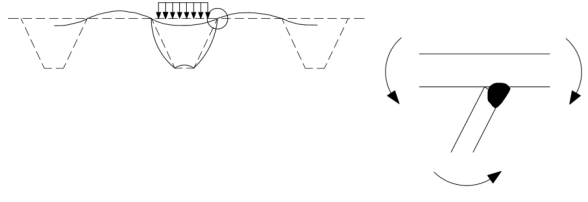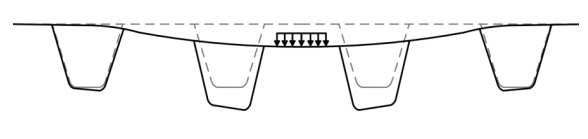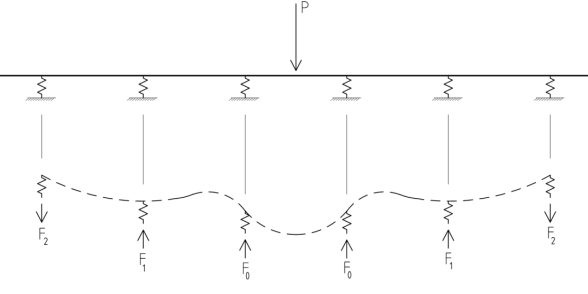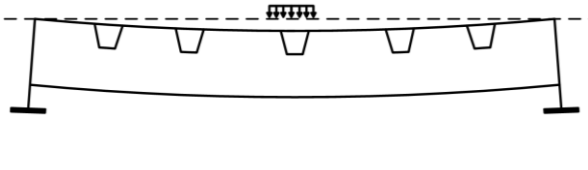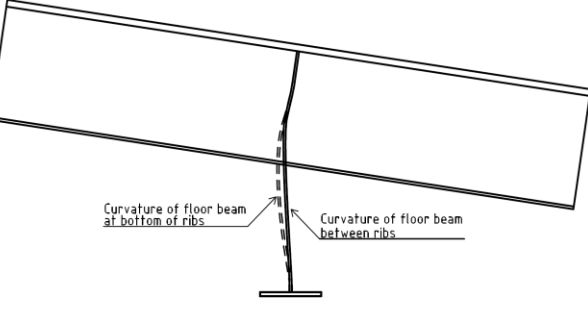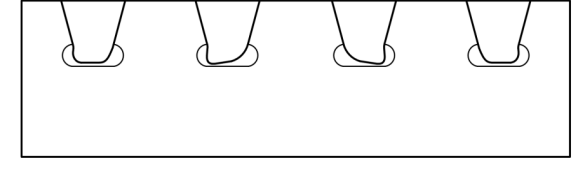
As a result of membrane stiffening an orthotropic deck have very high reserve strength for transverse loading, such as truck wheels (US Department of Transportation, 2012). This reserve strength can be beyond the yield limit but is dependent on the support conditions for the deck. As a consequence, the governing design criterion is in general the fatigue limit state at critical details with local distortional mechanisms. However, it must be taken in to consideration that in addition to global and local stresses the fatigue performance is affected by several different mechanisms which all needs to be combined in order to get a representative stress state. From this follows the necessity to divide the global behaviour into sub-systems to carry out an analysis by hand-calculations.

3.3.1 Structural sub-systems in an orthotropic deck and their behaviour

When designing and analysing an orthotropic deck with regard to load distribution there are two main focus areas to consider. Firstly, how the applied load is dispersed through the wearing surface and secondly, how the load is transferred through the deck system to the main girders. As mentioned in Chapter 3.1.1 the load dispersion in the wearing surface is difficult to determine due to the numerous uncertainties. Regarding the transfer pattern of the load from the application point to the main load carrying members of the structure it will be treated more in detail below, but in short it can be explained as the transferred from deck plate to ribs to floor beams and then to the girders.

As mentioned above, it is common in hand-calculations of orthotropic decks to divide the deck into several independent sub-systems that can be analysed separately and then combined with linear superposition to get the total response. The actual interaction between the members in the deck is partly represented but highly simplified in this way of calculating. This method is valid for application in limit state calculations only (US Department of Transportation, 2012). This differs from the conventional manner of bridge analysis where the elements are assumed to be independent and transfer the load to the next component without interaction (US Department of Transportation, 2012). However, even in other bridge types this generates conservative designs and is only used for simplified analysis. The systems will be presented more thoroughly below, a short summary and overview can be seen in Table 3-2, and at the end of the section in Table 3. 2.

Table 3.1 Assembly and description of the OSDs systems and their behaviour (US Department of Transportation, 2012)

System number and illustration	Action and result
1	**A:** Local deck plate deformation **R:** Transverse bending stress in deck plate, ribs and rib to deck plate connection
2	**A:** Panel deformation **R:** Transverse deck stress from differential displacement of ribs
3	**A:** Longitudinal bending of ribs **R:** Longitudinal bending and shear in rib acting as a continuous beam on flexible supports representing the floor beams
4	**A:** Floor beam in-plane bending **R:** Bending and shear in floor beam acting as a beam spanning between the main girders
5	**A:** Floor beam distortion **R:** Out-of-plane bending of floor beam web at rib due to rib rotation
6	**A:** Rib distortion **R:** Local bending of rib wall at floor beam cut-out
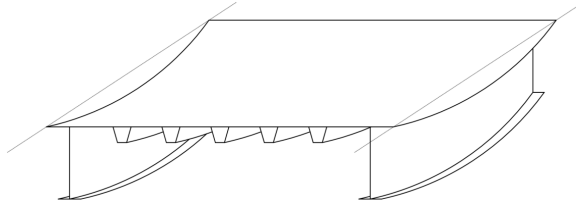
| 7 | | **A:** Global system |
| | | **R:** Axial, flexural and shear stresses from deformation of supporting main girders |

3.3.1.1 System 1 – Local deck plate deformation

The first system consists of the load transfer from the deck plate to the longitudinal ribs where the load is transmitted through deformation of the deck plate. The local deformation of the deck plate from the wheel load results in transversal flexural stress in the deck and longitudinal stiffener as well as in the weld connecting them (US Department of Transportation, 2012). The response is governed by the spacing of the ribs, transversal location of the wheel in relation to the rib as well as of the thickness of the deck plate and ribs, see Figure 3-12 (US Department of Transportation, 2012).
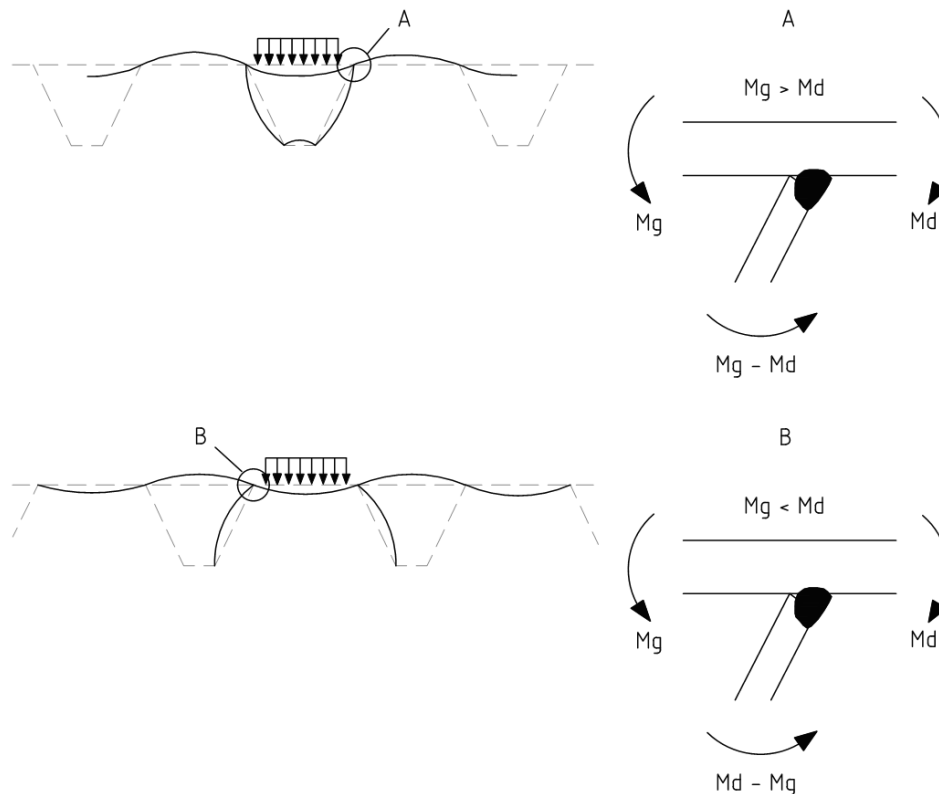
Figure 3-12 Load action and resulting flexural response in deck plate and rib. M_g is the moment in the deck plate in one rib, M_d is the moment in the deck plate between two ribs and M_r is the moment in the rib wall.

Depending on the transverse location of the load the relationship between the moment in the deck plate alters. This is due to that the rotation of the deck is more or less restricted from the ribs. A larger rotation gives a higher moment.

Another important influencing factor is the size of the wheel patch load, see Figure 3-13, and possible load dispersion in the wearing surface discussed earlier. This is a

consequence of the fact that the stresses in this system are local. The stresses generated in this stage are of great importance for the fatigue response of the rib to deck plate weld, see Figure 3-12. In general the response of this system is governed by one single tire in the front axis of a design truck.

Actual contact area

Assumed contact area at the top of the wearing surfac

Assumed loaded area at the top of the steel deck plate
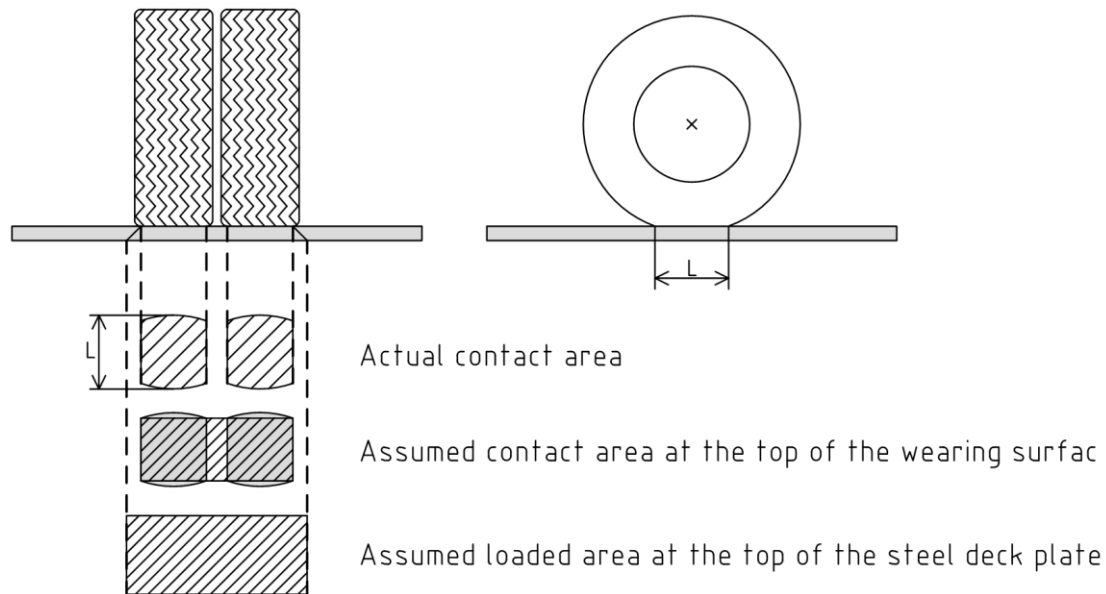
Figure 3-13 Wheel patch loading area (AISC, 1962)

For simplified analysis of System 1, a transversal strip of the deck plate and rib cross-section is studied (US Department of Transportation, 2012). The ribs are considered as either fixed or as flexible supports to the deck plate. This assumption is based on the spring stiffness of the ribs, which related to the bending stiffness of the ribs as well as their span length.

3.3.1.2   System 2 – Panel deformation

Deformation of the panel results in differential displacement of the ribs and this gives transverse stresses in the deck (US Department of Transportation, 2012). If a wheel load is applied to the deck between the ribs the load is first transmitted transversally to the adjacent ribs through the deck plate by bending and tension (AISC, 1962). The ribs cannot act independently of one another since they are connected through the steel plate, which acts a shared top flange to the ribs. Accordingly, ribs that are not subjected to direct loading will also deflect and experience stress, as can be seen in Figure 3-14.

CHALMERS, *Civil and Environmental Engineering*, Master's Thesis 2015:14
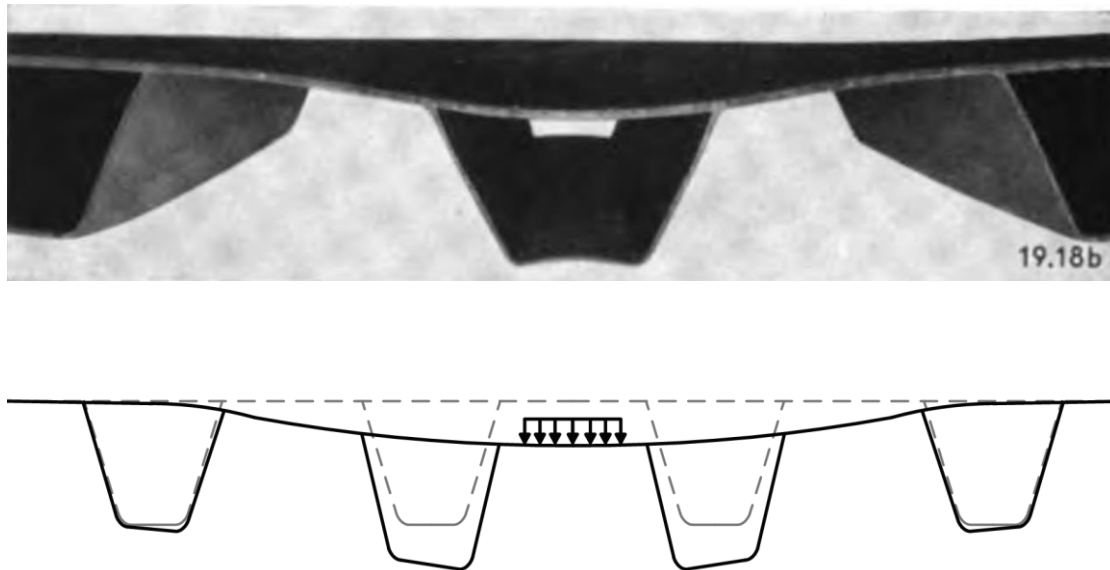
Figure 3-14 Deformation of the panel under transverse load; (a) Deflection of the panel when the load is placed directly above the middle rib (AISC, 1962); (b) Displacement of the panel when the load is placed between two ribs

The second system is the most difficult to analyse (US Department of Transportation, 2012). This is a consequence of the two-dimensional load distribution behaviour in the orthotropic deck when it is subjected to out-of-plane loading together with the anisotropic properties of the deck. Deformation of the panel under transverse load depends on the different stiffness properties, this makes it complex to predict and calculate. The same goes for the stress distribution that follows the deformation.

The deck plate experience bending stress as well as axial and shear stresses, however in this system it is the bending stress that is of interest. The bending stresses in the deck plate and wearing surface are mainly caused by a combination of bending of the deck plate between rib walls due to wheel loads, system 1 and 2, and secondary bending of the deck plate from differential deflections of the nearby ribs, system 2, (US Department of Transportation, 2012).

It has been experimentally and analytically shown that the wheel loads in general are carried by the rib closest to the load together with one adjacent rib on each side (US Department of Transportation 2012). According to this, the load accumulation on a single rib from two trucks alongside each other will be small. Hence, the rib response is governed by the single truck wheel. This of course assumes that the distance between ribs in the transversal direction of the bridge is less than half the distance between wheel loads from two neighbouring trucks.

If the behaviour in the second system is analysed by hand, numerous simplifications needs to be employed to break the system down to a graspable problem. There are a few aids, such as charts with pre-solved longitudinal moment distribution, which can be applied to facilitate the process (US Department of Transportation, 2012). The solution is based on the theory of elasticity of plates and Huber's Equation, a stress equation for elastic materials. It forms a differential equation that is dependent on the flexural rigidity in the two main directions as well as the torsional rigidity of the pate

and the location of the load, but with numerous simplifications. It is a time consuming and rather unreliable method that is rarely used.

To calculate the stresses in this system by hand different methods are applied for open and closed rib system as they display different behaviour (US Department of Transportation, 2012). For an open rib system the deck plate is regarded as several compatible beams resting on elastic foundations, representing the ribs. The concept of orthotropy is thereby discarded and the load is taken in a single rib, the global transverse rigidity is ignored and influence lines for the beams are applied. In reality this means that for a deck with open ribs System 2 is disregarded and System 3 is implemented directly after System 1.

For closed ribs the torsional rigidity of the deck plate is governed by the shear modulus for steel, the dimensions and torsional rigidity of the ribs and the transverse (bending) rigidity of the deck plate and the ribs can be ignored. Esslinger and Pelikan solved the Huber differential equation and developed charts for longitudinal moments for various loads and spans. For closed rib systems the moments are adjusted with regard to the distance between the specific rib and ta floor beam. Ribs near the floor beam displays a stiffer behaviour compared to those in the mid span, see Figure 3-15.
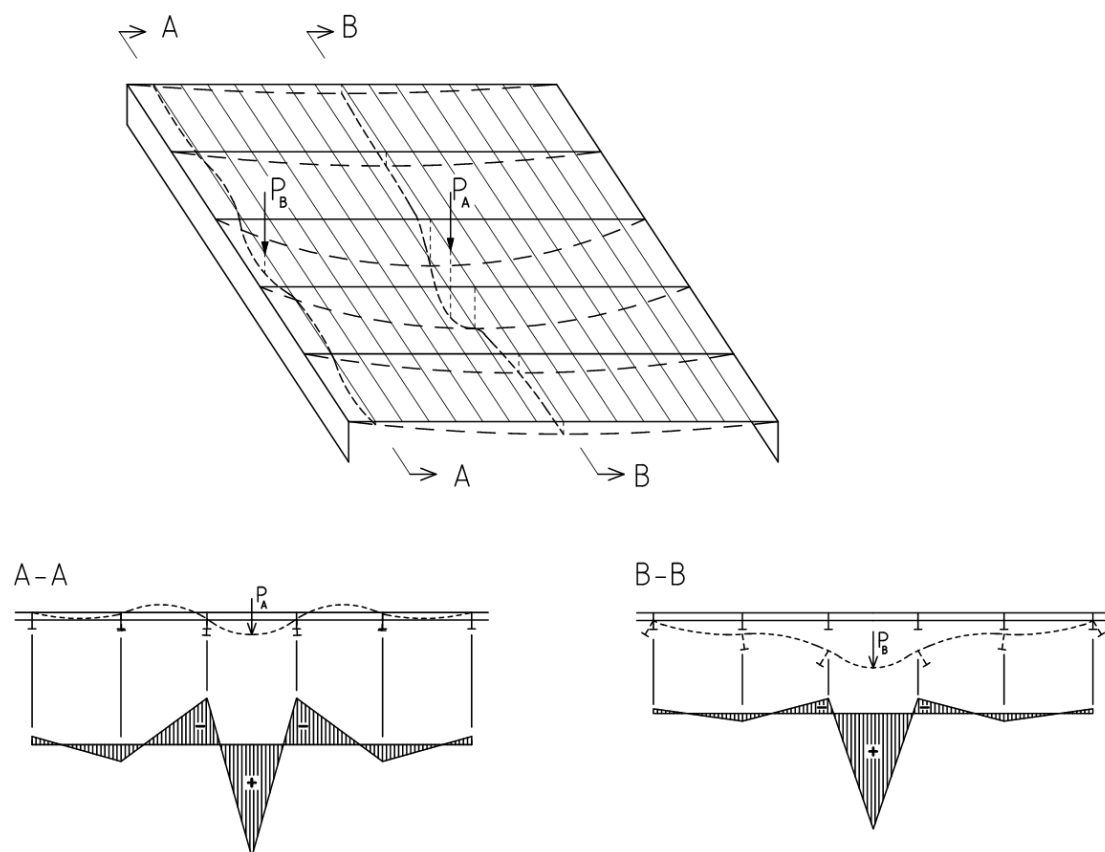
Figure 3-15 Deflection and bending moment of a longitudinal rib, and deflection and rotation of the supporting floor beam; (a) Global deflection and illustration of sections; (b) Deflection and bending moment on the rib near the main girder; (c) Deflection and bending moment in the rib near the centre line of the bridge, (AISC, 1962).

The longitudinal ribs are acting as continuous beams on flexible support, but as can be seen in Figure 3-15 closer to the main girders the effect of the flexibility of the floor

beams is decreasing and the behaviour of the rib is more similar to a member on rigid supports (AISC, 1962). This is a result of the decreasing deflection of the floor beams close to the main girders and in hand calculations the contribution of the flexibility of the floor beams closes to the main girders should be disregarded.

The primary value of this method is that it provided a direct solution technique for the orthotropic deck. The solution also reveals that the response of the orthotropic panel under System 2 is influenced primarily by the flexural and torsional stiffness of the ribs. However, the simplifications and assumptions make the method unreliable and the results only give a guide toward the actual response. If a more accurate result is required the system should be analysed with a FE model. Results from FEM have proven superior when compared to existing empirical data (US Department of Transportation, 2012).

3.3.1.3 System 3 – Rib longitudinal flexure

When the loads have been transferred transversally between ribs, System 2, the separate ribs transfer the load to the floor beams in the longitudinal direction. For a deck with closed ribs, the second system gives the torsional rib moments and shear as it would have been if the floor beams were rigid. The second system determines the load distribution in transversal direction between ribs. This action gives shear stresses in the ribs which cause bending together with torsional moment as well as wrapping stresses in System 3.

The third system consists of the longitudinal section of rib. The ribs act as continuous beams resting on the floor beams, which are represented by discrete flexible supports. The transversal floor beams are seen as flexible supports to the longitudinal ribs since they deflect in proportion to the load and with regard to their bending stiffness properties (AISC, 1962), see Figure 3-16. In Figure 3-17 below the difference between System 2 and System 3 is visualised. Bending of the rib causes longitudinal flexure and shear in the same (US Department of Transportation, 2012).
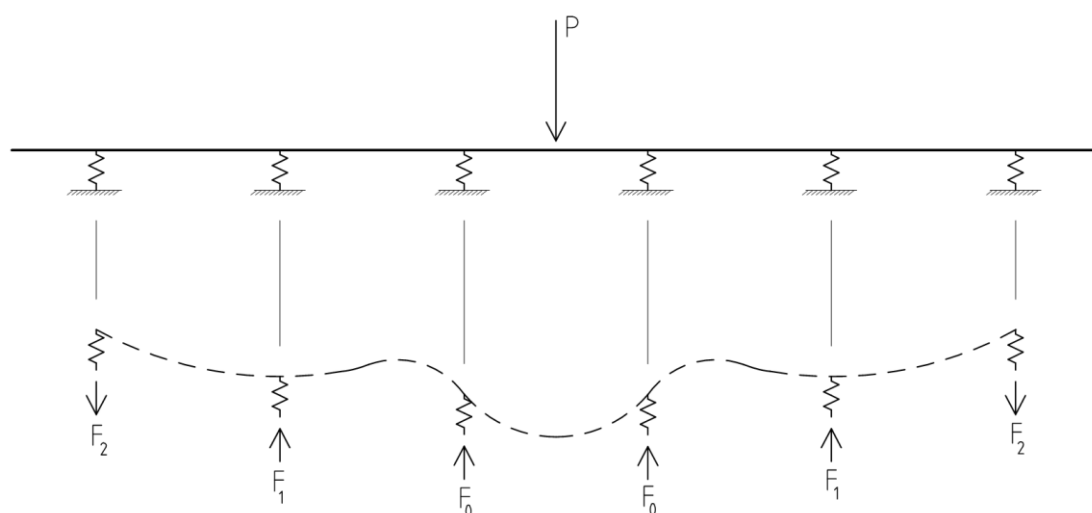
Figure 3-16 The deflection of the longitudinal rib and the arising forces in the floor beams (AISC, 1962)
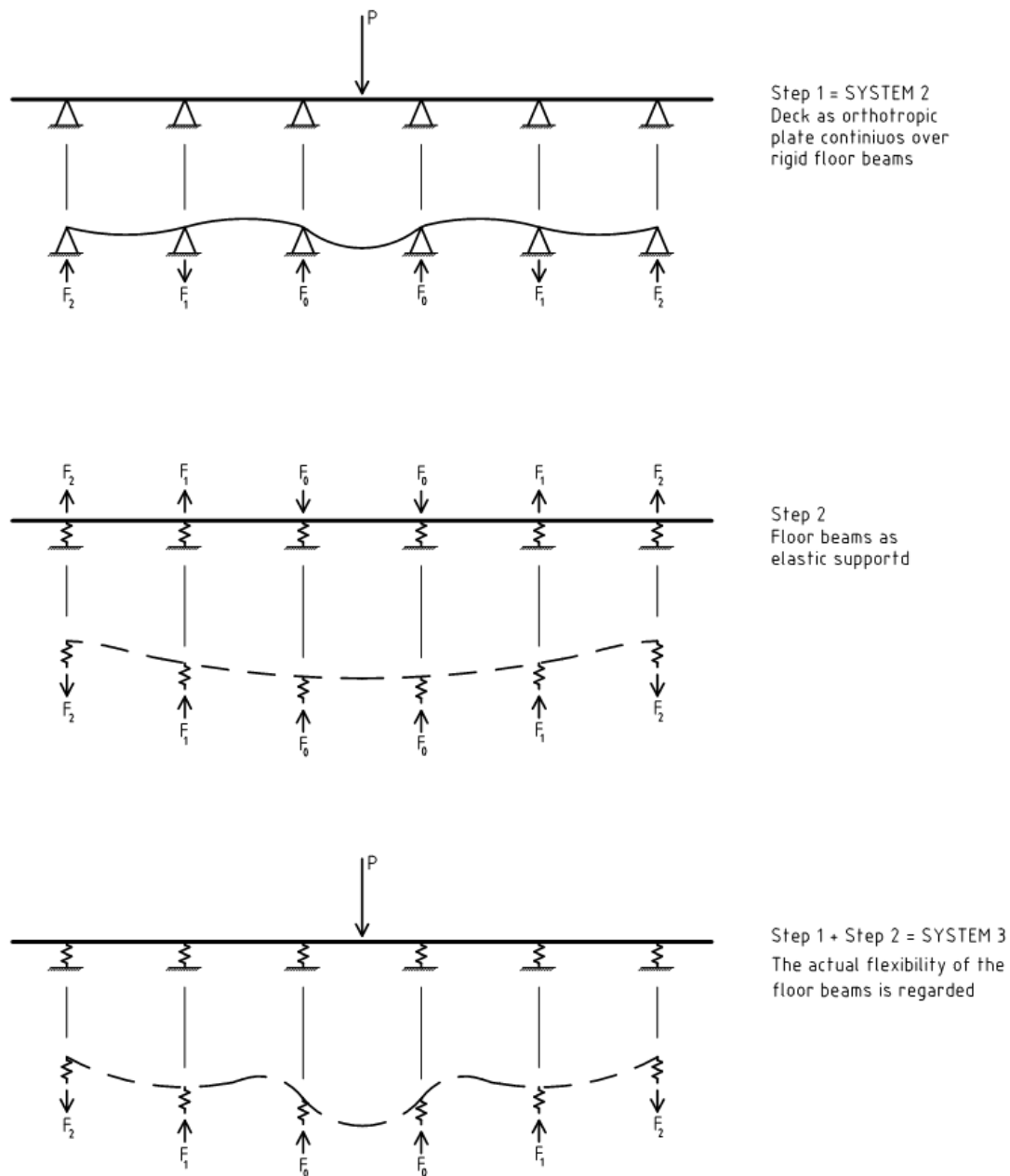
Figure 3-17 The Pelikan-Esslinger design method represents system 1 and 2 and explains the behaviour of the different systems (AISC, 1962)

The flexibility of the floor beams give rise to an increase of positive rib moments and a decrease of positive floor beam moments (US Department of Transportation, 2012). However, the fact that the individual ribs are continuous over the floor beams and the interaction between ribs and the flexible floor beams makes also this system difficult to calculate by simplified analysis.

3.3.1.4 System 4 – In-plane flexure of floor beam

After that the load has been transferred between and along the ribs, i.e. transversally and longitudinally in System 2 respective 3, it is transmitted from the ribs to the main

girders through the floor beams, see Figure 3-18. The floor beam acts as a beam supported on rigid supports representing the main girders.
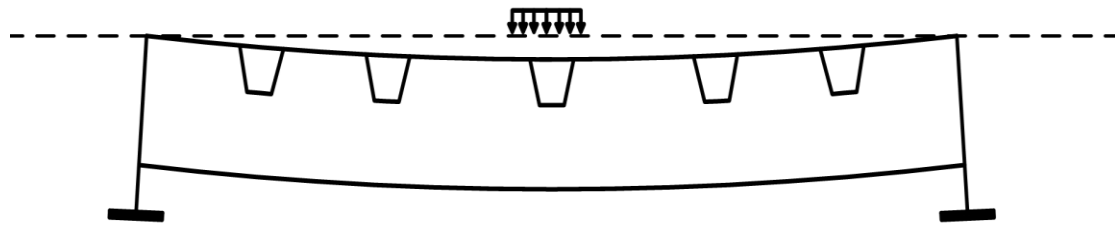
Figure 3-18 Load is transmitted from the ribs to the main girders through the floor beams (US Department of Transportation, 2012)

The floor beams experience in-plane flexure from bending of the ribs generating in-plane flexure stresses and shear stresses in the floor beam. The complete stress state in the floor beam in this system is a combination between these in-plane stresses with out-of-plane stresses resulting from rotation of the ribs.

The stress state in the floor beams is three-dimensional and thereby difficult to analyse. The "reaction forces" from the ribs generates in-plane flexure stresses and shear stresses in the floor beams. The bending deflection of the ribs and the associated end rotation subjects the floor beam to out-of-plane forces which causes local distortions of the floor beam web as well as twisting of the whole floor beam. The local out-of-plane responses are accounted for in System 5 while System 4 regards the in-plane moment and shear. The response of the floor beam when interacting with the ribs is three-dimensional and includes twisting.

There is a simplified two-dimensional model for analysis of the floor beam, which provides the shear force in the direction of the floor beam in each tooth, see Figure 3-19, the web of the floor beam between ribs (US Department of Transportation, 2012). The floor beam is divided into an upper and lower part. The upper part consist of the web area between the deck plate down to the lowest point of the cut-out, the tooth, and the lower is the remaining, undisturbed, web area together with the lower flange. To improve the response of this model it is possible to combine it by a FE analysis of the tooth.
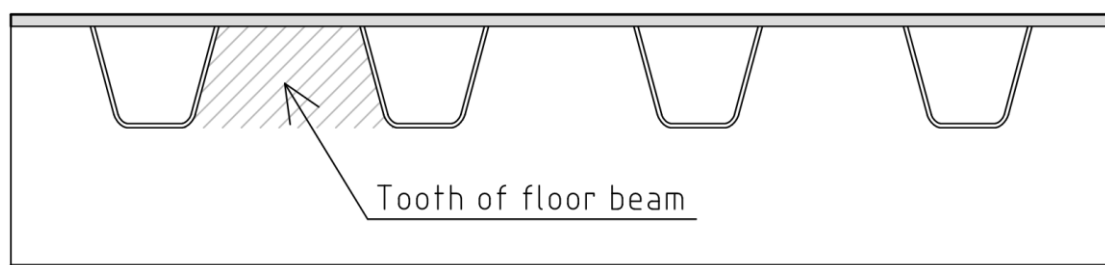
Figure 3-19 Tooth of floor beam between ribs
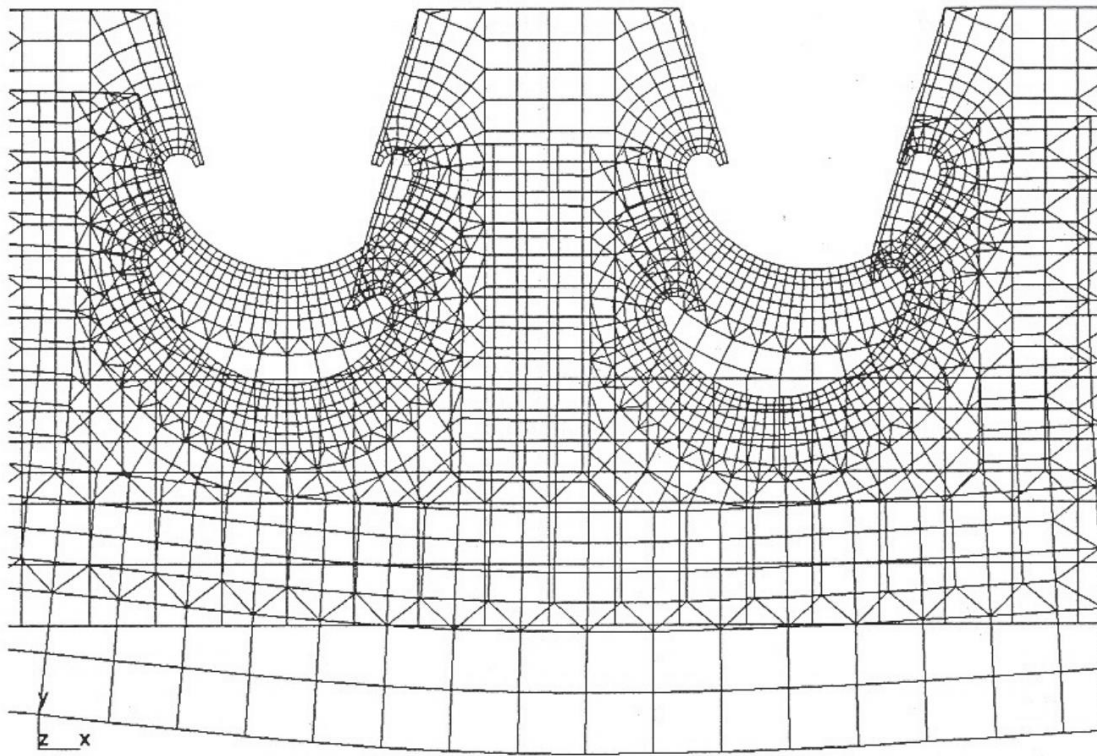
Figure 3-20 Deformation of floor beam web tooth when left rib is loaded with a point load directly above the right wall (Kolstein, 2007)

This is a straightforward model when analysing the in-plane performance of the floor beam (US Department of Transportation, 2012). However, the liability and accuracy is limited at the cut-out and free edge and no stress assessment at the termination point at the cut-out is received. As can be seen in Figure 3-20 the deformation and thereby stresses at the cut-out area are intricate. Since this is a section highly prone to fatigue it is better to perform an FE analyse of the whole floor beam to receive proper stress information.

3.3.1.5   System 5 – Floor beam distortion

Distortion of the floor beam is caused by rotation of ribs and engenders out-of-plane flexure at the floor beam web at the intersection with ribs (US Department of Transportation, 2012), see Figure 3-21.
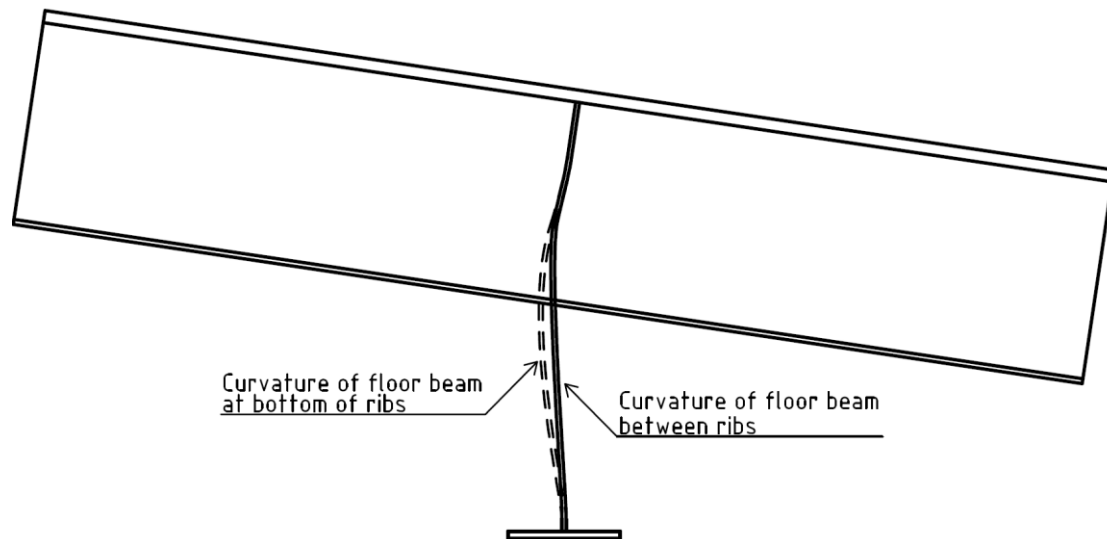
Figure 3-21 Distortion of floor beam due to rotation of rib

In system 1 to 4 the behaviour of the deck and load transfer to the ribs and floor beams have been described. The general load response of an OSD is orthogonal in two directions and includes distortion of the floor beam, as discusses above. However, directly beneath the wheel load stresses will arise in three orthogonal directions (US Department of Transportation, 2012).

The effects, stresses and service life of the rib-to-floor beam connection have been comprehendingly studied the last decade, resulting in a better understanding of the complex performance. Laboratory tests and FE-analysis have explained the effects along the floor beam and the intricate interaction between the floor beam and deck plate. The results have shown that the rigidity of the two components, floor beams and deck plate, often counteract. As an example can be mentioned that an increase of the floor beam web thickness can reduce the stress effect at the weld between rib and deck plate at the floor beam intersection, but the stress range at the cut-out or at the weld around the rib will at the same time be increased.

The rib to floor beam details is influenced by three local effects (US Department of Transportation, 2012):

- Out-of-plane distortion of the floor beam from rib rotation
- In-plane distortion of the floor beam from horizontal shear
- In-plane distortion from vertical displacement of the tooth

The out-of-plane distortion caused by the rib rotation is illustrated in Figure 3-22. From the same figure it can be recognised that the stresses will be high at the weld at the termination of the cut-out as well as at the curvature of the cut-out. If no cut-out is present the peak stress will occur at the base of the rib, following the same discussion.
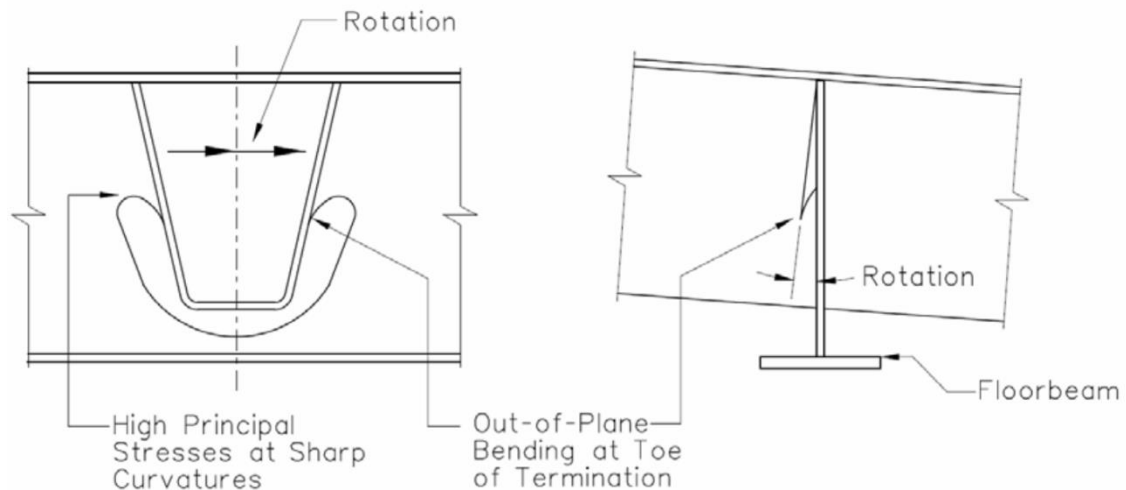
Figure 3-22 Out-of-plane distortion of floor beam due to rotation of rib at support (US Department of Transportation, 2012)

For the in-plane distortion caused by horizontal shear the basic principle is presented in Figure 3-23. For all members in bending with shear forces transversally to the axis of the member, shear effects in the longitudinal direction arise internally. The distortion is a result of the shear stress per unit thickness. The shear mechanism is a failure mode associated with high shear forces and the formation of plastic hinges in the sections connected to the intersection with the ribs (Demirdjian, 1999). This behaviour is in particular pronounced for members with shallow sections and long welds as well as short floor beams since the shear action here is governing. The sections connected to the opening must carry the shear force together with the primary and secondary moments and the size of the opening is directly related to the amplitude of these.
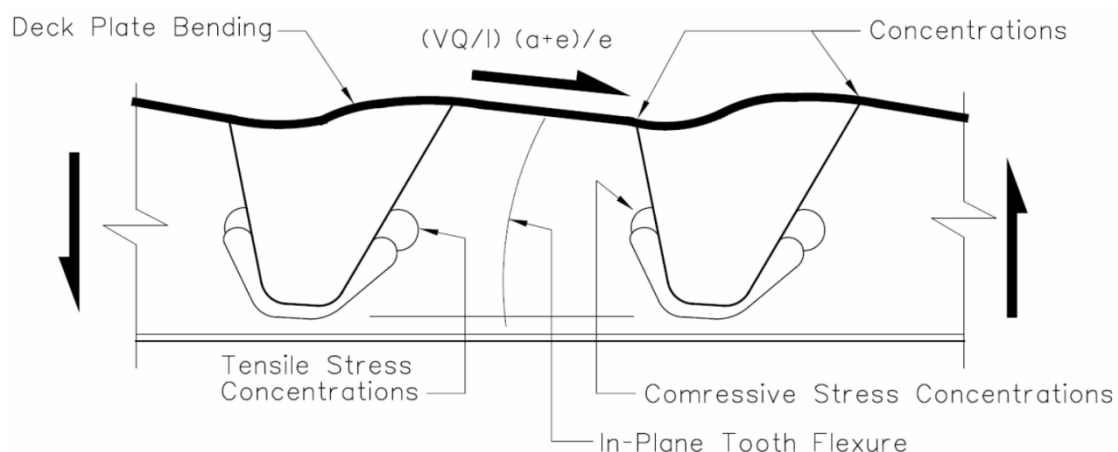
Figure 3-23 Deformation to the deck, floor beam and rib as a result of the shear on the floor beam tooth (US Department of Transportation, 2012)

The floor beam web is reduced where the ribs intersect, causing the adjacent parts to carry higher load. The larger the opening in the web, the larger the additional force that the surrounding structure have to carry (Tsavdaridis & D'Mello, 2012).

CHALMERS, *Civil and Environmental Engineering*, Master's Thesis 2015:14

Moreover, if a cut-out is used the stress state will be more severe since the web is debilitated even more. Another aspect regarding cut-outs is how the cut-out height affect the stress state. A large cut-out height result in lowering the stress around the rib edge, but increase the bending stress in the deck plate in the transversal direction of the bridge (US Department of Transportation, 2012). Accordingly, many different factors have to be considered when determining the geometry and dimensions of the cut-out. The shear force compels the section to deform, causing in-plane bending of the tooth that in turn results in stress concentrations at the termination of the cut-out, or if no cut-out exist at the base of the rib and in the deck plate.

In-plane distortion from vertical displacement of the tooth is illustrated in Figure 3-24. When a wheel load is applied to an OSD the teeth of the floor beams will be subjected to bending and compression that causes them to displace (US Department of Transportation, 2012). These displacements influence the stresses in the deck plate at the intersections with the ribs and floor beams. There are some measures to take to control the displacements. The dimensions of the teeth can be increased, the same goes for the thickness of the floor beam and the cut-outs should be minimised.
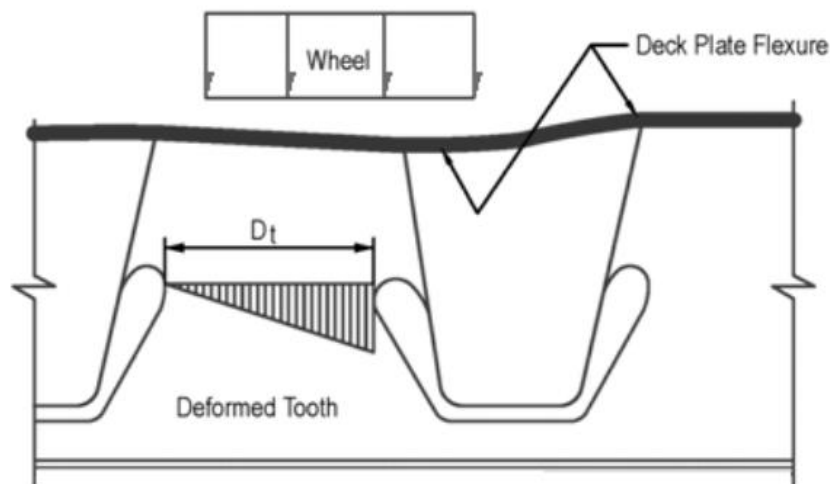
Figure 3-24 The vertical displacement of the tooth due to flexure and compression from wheel load (US Department of Transportation, 2012)

3.3.1.6   System 6 – Rib distortion

Distortion of the ribs engenders local flexure of the rib walls as a result of the cut-out in the floor beams, see Figure 3-25, (US Department of Transportation, 2012). The distortion of the ribs is a result of the wheel load when placed at mid span between floor beams and with an eccentricity to the axis of rotation of the rib in question. The ribs rotate around the axis causing lateral displacement. The distortion is at its maximum in the mid span between floor beams and decreases when approaching the floor beam, which represents a fixed boundary. However, if a cut-out is present the boundary is seen as partially fixed and the ribs can deform out-of-plane, generating high stresses at the cut-out termination and thereby exacerbate the fatigue situation. For decks without cut-outs the ribs will be fixed at the intersections with floor beams and higher stresses will arise at the bottom of the ribs.
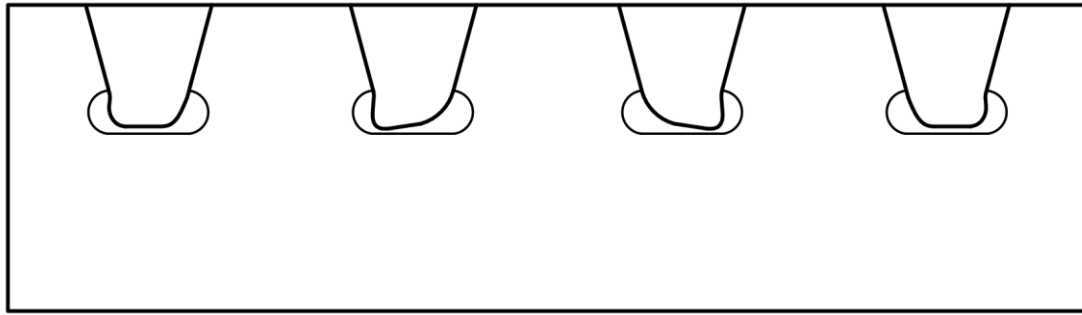
Figure 3-25 Rib distortion at cut-outs at intersections with floor beams

It is of great importance to observe the difference in behaviour between decks with and without cut-outs in the floor beams, see Figure 3-26. The deformation of the floor beam web, and thereby the stresses in the same, is highly dependent on the design of this area and it needs to be considered in calculations.
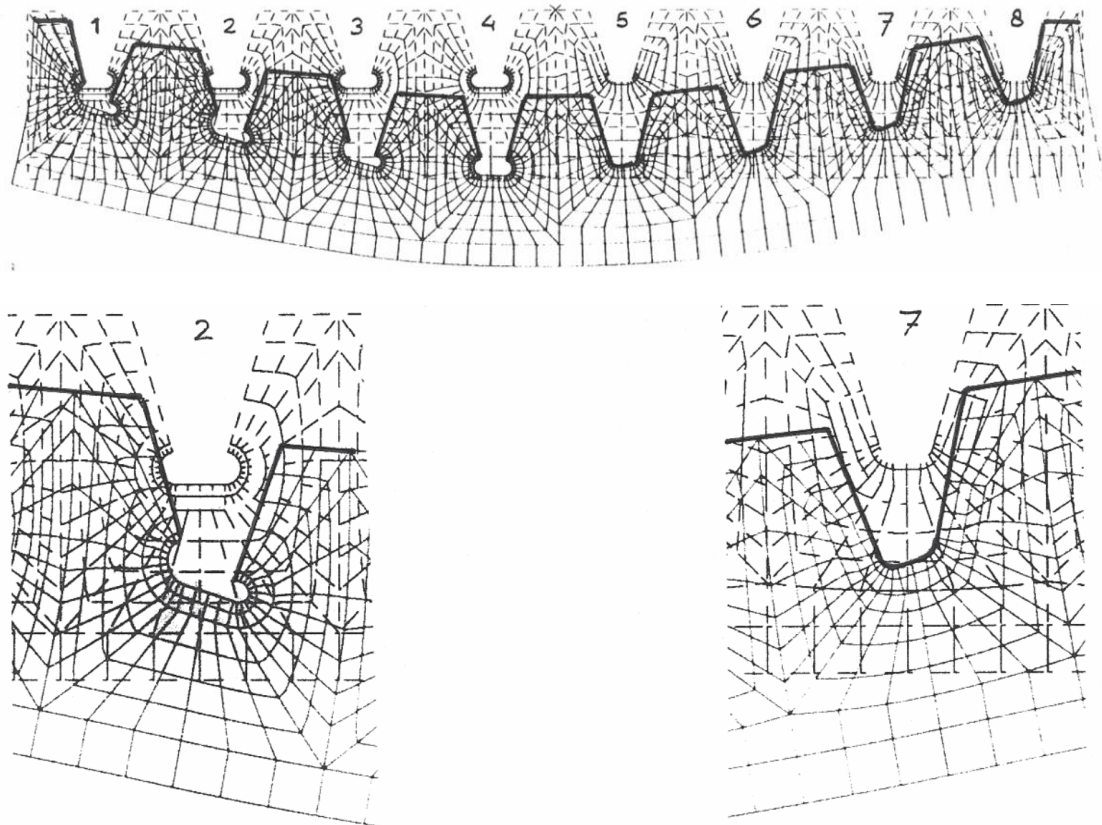
Figure 3-26 Difference in distortion behaviour between ribs (a) With cut-outs; (b) Without cut-outs (Kolstein, 2007)

In Figure 3-27 it can be observed that the geometry of the cut-out at the termination is of great importance, a low grade cut-out results in inferior effects at the termination. The stresses around the base of the rib are both longitudinal and vertical. The distortion generates tension on the outside on one of the rib walls, and compression on the other. This in turn, results in reversed stresses at the inside of the rib walls (US Department of Transportation, 2012).
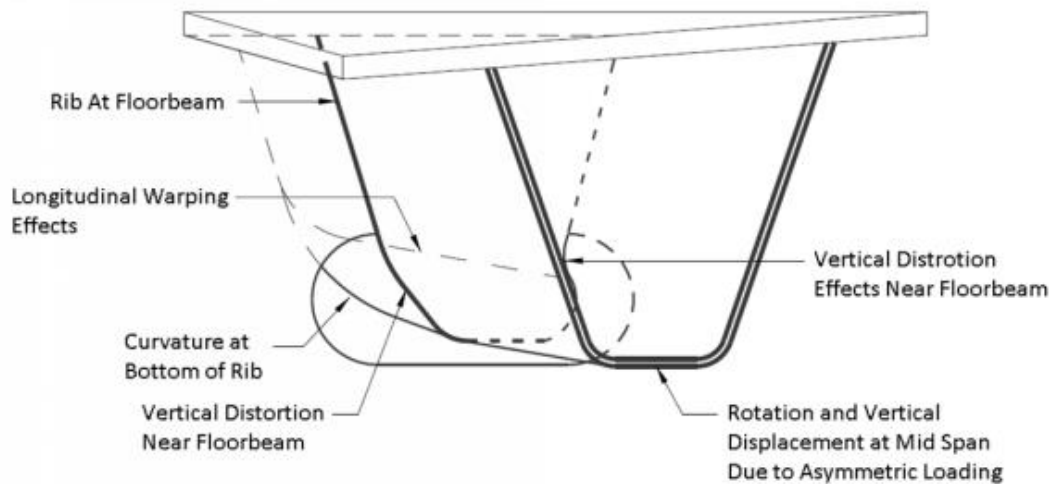
Figure 3-27 Rib distortion in the rib-to-floor beam intersection with cut-out

3.3.1.7 System 7 – Global

In the global system the orthotropic deck and main girders acts as a unit, see Figure 3-28, supported on the bridge supports, columns or abutments (US Department of Transportation, 2012). The unit is subjected to the traffic load causing deformation and displacement of the panel and girders that result in axial, flexural and shear stresses. These stresses can be evaluated by hand with global structural analysis.
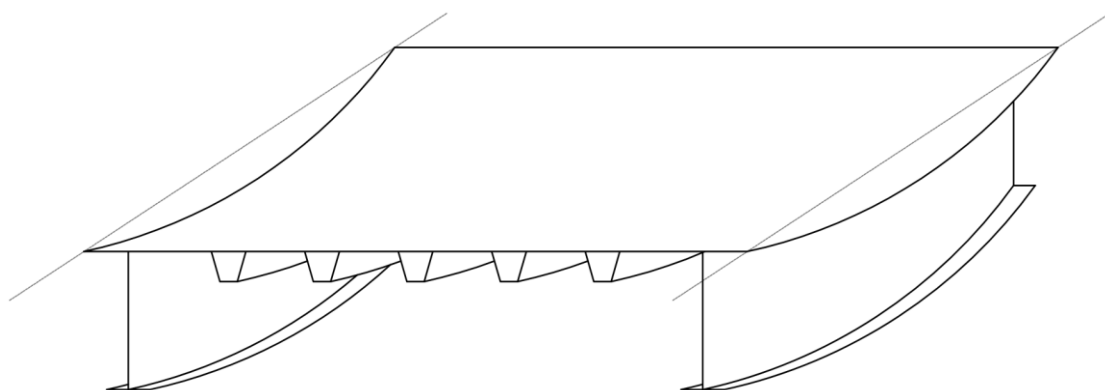
Figure 3-28 Global system and deformation

3.3.1.8 Summary of the systems

A wheel load applied somewhere on the central parts of the deck will be transferred and dispersed through the wearing surface to the deck plate and to the nearby longitudinal ribs by flexure of the plate. The floor beams give an elastic support to the ribs and load is transferred through longitudinal bending of the ribs to the floor beams. The load is transmitted from the floor beams to the main girder by flexure. The whole OSD transmit the load to the global supports in bending.

As a result of the flexible support conditions and that the deck plate acts as a shared upper flange to the ribs they cannot act independently of each other, causing unloaded ribs to react in flexure as well.

Earlier, a larger focus was placed in the load transfer between neighbouring ribs and the rib moments. At present the most important characteristic of an orthotropic deck is considered the effects at the rib-to-floor beam intersection, how these effects influence the local in-plane stresses in the floor beam and the fatigue behaviour in these sections (US Department of Transportation, 2012).

Table 3. 2 Overview of the different system and their behaviour

System	Behaviour and action
1	The deck plate transfers load down to the longitudinal ribs. Local deformation of the deck plate results in transversal flexural stress in the deck and longitudinal stiffener as well as in the welds between them.
2	Deformation of the panel results in differential displacement of the ribs and this gives transverse stresses in the deck. A concentrated load applied to the deck is transmitted to adjacent ribs through the deck plate by bending and tension.
	Stresses in the deck plate and wearing surface results from the combination of bending of the deck plate between rib walls and secondary bending of the deck plate.
	The second system gives the rib moment and shear as it would have been if the floor beams were rigid, the ideal case.
3	The ribs act as continuous beams on flexible supports. Bending of the rib causes longitudinal flexure and shear in the same and transferring the load to the floor beams.
	The third system regards the flexure of the floor beams and gives the moments and shear in the rib that is the outcome of the flexibility of the floor beams.
4	The load is transmitted from the ribs to the main girders through the floor beams. The floor beam acts as a beam supported on the rigid main girders.
	The floor beams experience a combination of in-plane flexure and shear with out-of-plane twisting.

5	The distortion of the floor beam is caused by the rotation of ribs and engenders out-of-plane flexure at the web of the floor beam at the rib.
6	Distortion of the ribs results in local flexure of the rib walls due to the cut-out. The distortion of the ribs is a result of the wheel load when placed at mid span and with an eccentricity to the axis of rotation. The ribs rotate around the axis causing lateral displacement.
7	The orthotropic deck and main girders acts as a unit supported on the bridge supports. The unit is subjected to traffic loads, the following displacements generates axial, flexural and shear stresses.

3.3.2 Fatigue behaviour and associated load effects in an orthotropic steel deck bridge

A bridge is subjected to a constant succession of vehicles that influence the structure differently depending on velocity, location, mass, temperature, tyre pressure and several other factors. As a consequence of the complex welded joints and the relative slenderness of the members of an orthotropic deck, see Figure 3-29, they are rather vulnerable to fatigue, in particular in long span bridges (Pfeil, Battista & Mergulhão, 2005). There are several known cases of fatigue damage and failure of orthotropic bridge structures since the 1960s and today fatigue is one of the most important aspects when designing an orthotropic steel deck. To achieve an economical and secure design solution of an orthotropic deck the detailing has a great influence on the efficiency of the whole structure. The reason for this is the fact that fatigue generally is the governing design criteria for OSDs and fatigue is a highly localized phenomenon (US Department of Transportation, 2012).
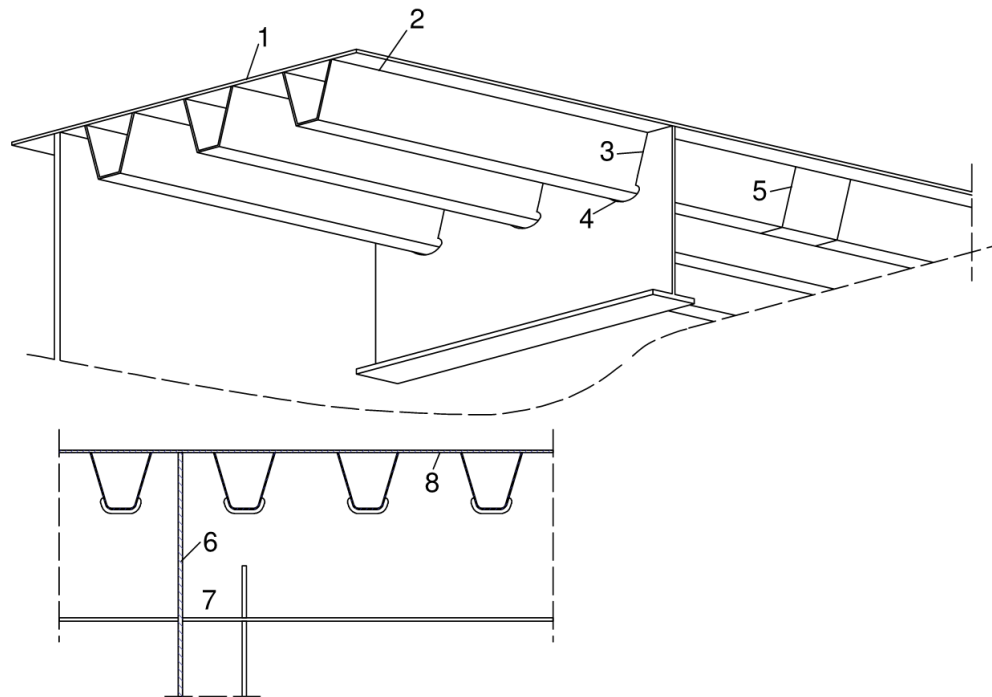
1	*Deck plate*	*5*	*Slice of longitudinal rib*
2	*Welded connection of longitudinal rib to deck plate*	*6*	*Splice of floor beam*
3	*Welded connection of longitudinal rib to web of transversal floor beam*	*7*	*Welded connection of floor beam to main girder*
4	*Cut-out in web of floor beam*	*8*	*Welded connection of web of floor beam to deck plate*

Figure 3-29 Detail over members and welded connections in an orthotropic steel deck (SS-EN 1993-2:2006)

The passing of a vehicle over an orthotropic plate causes variation of the flexural stresses, see Figure 3-30. The fatigue life is closely connected to the flow of vehicles and in an orthotropic deck there are some specific details that have displayed a special proneness to fatigue. Several of these details are related to the longitudinal connection between the rib and deck plate and these will be more closely discussed below.
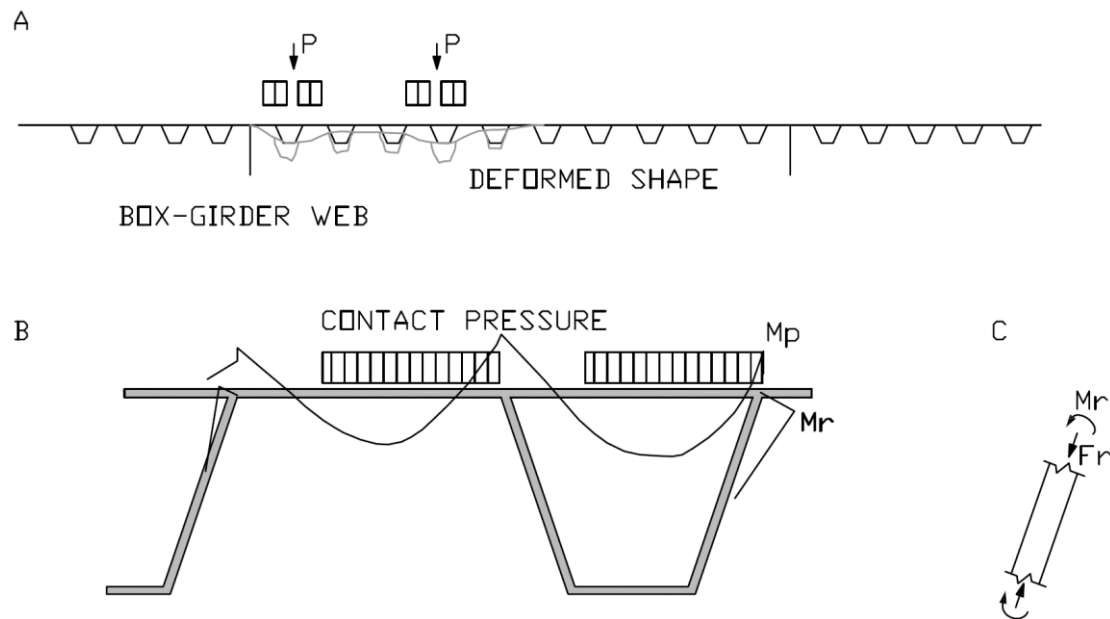
Figure 3-30 Load effect on an OSD from traffic induced load; (a) Local transversal deformation beneath load application point; (b) Transverse bending moment inflicted by the showed tyre location, M$_p$ it the moment in the plate and M$_r$ the moment in the rib; (c) Internal forces in the rib web.

Figure 3-30 shows the result from a numerical model performed by Pfeil, Battista and Mergulhão (2005) in which the localised effects on deck plate and ribs from wheel loads at a specific location are studied. The transverse bending stresses are governed by the load of the passing axel, air pressure and radius of the tyres, the softness and irregularities of the wearing surface as well as the transverse location of wheels in relation to the placing of the ribs. Hence, these stresses are elaborate to determine with required accuracy. In a flexible deck, as an OSD is, these flexural stresses will be considerable and the fatigue life will be determined by the induced stress magnitude and frequency from an individual wheel (Cullimore & Smith, 1981).

At the present there is no simple method to determine the stress in the separate members of an orthotropic deck. As a consequence of this the fatigue assessment for an orthotropic deck is rather time consuming if it is to be done realistically, or if simplifications are used there are numerous potential sources of errors. Predominantly the nominal stress approach using S-N curves and appropriate fatigue class according to current standards is used for fatigue life prediction for steel bridges (Aygül, Al-Emrani & Urushadze, 2011), this is discussed more thoroughly in Chapter 4.1. This method gives unreliable results for orthotropic decks as a consequence of the complexity of the OSDs. The procedure of fatigue life prediction would be aided if more classifications well adapted to orthotropic decks were available (Kolstein et al., 1996). Another, more time-consuming, solution is to use FE models to determine a more accurate stress (Aygül, Al-Emrani & Urushadze, 2011) but even here it is difficult to fully understand and interpret the behaviour.

In an experiment performed by Tinawi and Redwood (1976) the deflection of an OSD have been evaluated when the rib spacing increases at the same time as the dimensions of plate and rib are increased to keep the relative thickness constant. The experiment data and results can be viewed in Figure 3-31 and Figure 3-32.
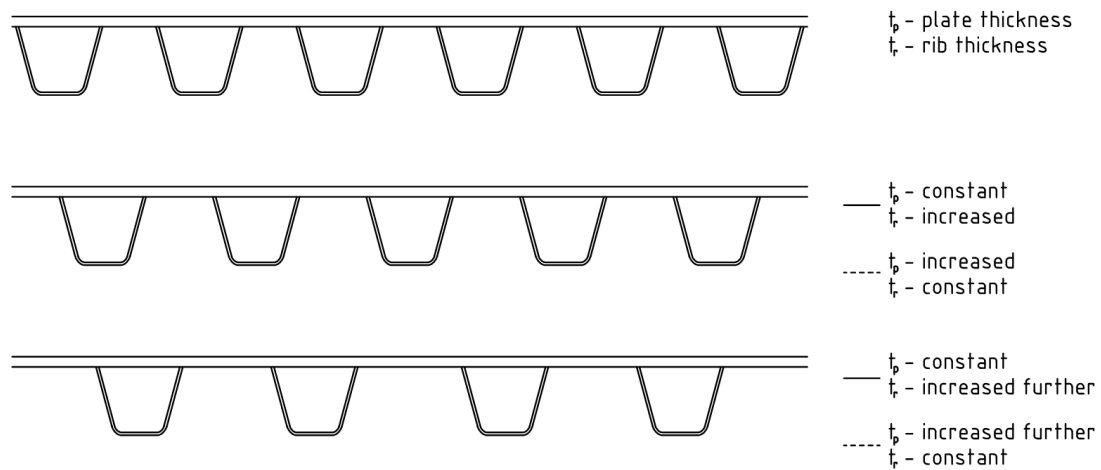
Figure 3-31 The three different decks, spacing of the ribs as well as the and thickness of the deck plate, t_p, and ribs, t_r, are altered respectively to keep the relative thickness constant (Tinawi & Redwood, 1976).
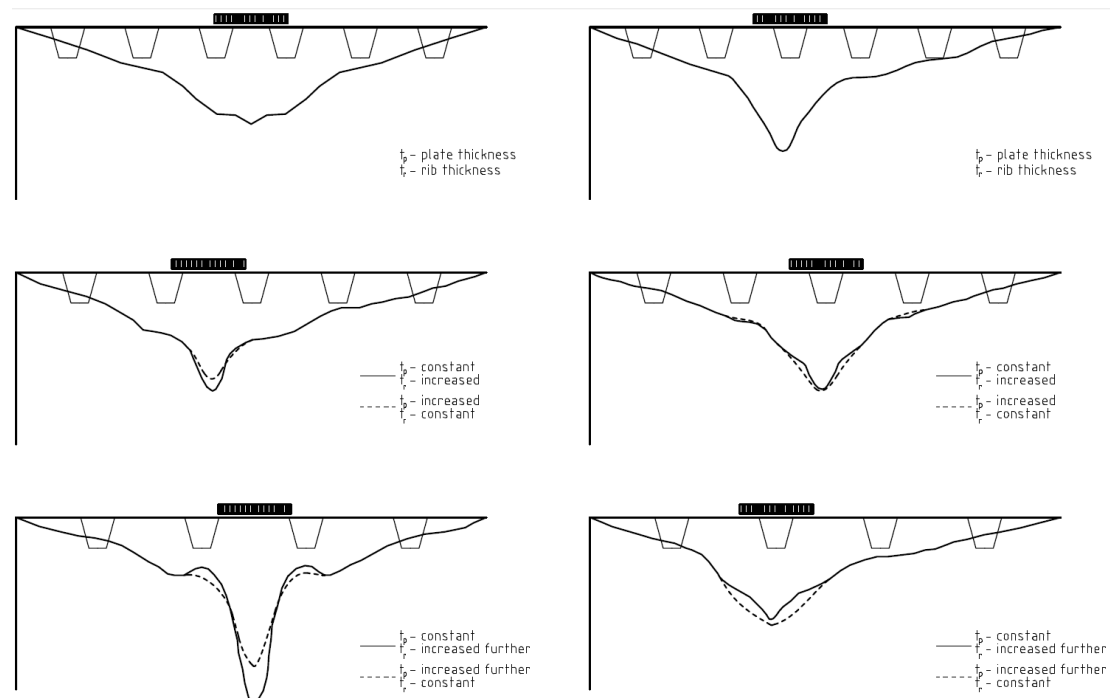
Figure 3-32 Deflection of an orthotropic deck with the load placed (a) Between two longitudinal stiffeners; (b) Over one longitudinal stiffener.

When the wheel load is applied between two ribs, see Figure 3-32 (a), the deflection increases with increasing spacing. However, if the wheel load is placed directly above one rib the deflection will decrease when the spacing is increased and the relative thickness is constant, Figure 3-32 (b). From this follows the realisation of how complex the behaviour of an orthotropic plate is and how the alteration of one variable results in different fallouts depending on the specific situation.

Some of the factors influencing the fatigue behaviour of an OSD are specific stress concentration points, corrosion induced steel degradation and the stress variation over the life time (Kolstein, 2007). From the intricacy of the load distribution and geometry of an orthotropic deck follows that the appropriate fatigue strength is particularly

difficult to predict. An orthotropic deck is directly subjected to the effect of traffic loads that results in the highest stress range. This, together with the fact that the OSDs also are subjected to a large number of loading cycles during the lifetime makes them highly prone to fatigue.

One important factor in the fatigue behaviour of an orthotropic deck is the interaction between the wearing surface and deck plate and the load dispersion resulting from this. However, as mentioned above the contribution is uncertain and difficult to predict due to several influencing factors on the performance such as the temperature and loading frequency. To be on the safe side the reducing effect on the stress range from the wearing surface should not be accounted for in design, but will contribute greatly to prolong the fatigue life never the less (Kolstein, 2007). However, the dispersion in the wearing surface is in general included in the design codes not to underestimate the resistance.

High risk locations for the initiation of a fatigue crack are at points with a change in section due to the local stress raising this causes, as a rule of thumb "the sharper the notch the shorter the fatigue life" (Kolstein, 2007). Since orthotropic decks have a great number of sharp section changes it has as many sections that are prone to fatigue and have to be designed and constructed with care. However, with the progress of technology, increasing experience and understanding as well as the development of the FEA programs the issue of fatigue in OSDs have gradually improved, although there is still much work to be done (US Department of Transportation, 2012).

To investigate the fatigue behaviour of an orthotropic deck the possible cracks can be subdivided into categories after where they initiate. As mentioned above the focus in his report will be directed at the fatigue cracks in relation with the longitudinal rib, which each will be evaluated more thoroughly below

The principal crack modes associated with the closed ribs are:

- Cracks in the longitudinal rib-to-deck plate connection in the span between floor beams.
- Crack in the joint of rib-to-floor-beam.
- Cracks in the longitudinal rib-to-deck plate connection at the intersection with the floor beam.

3.3.2.1 Load response and fatigue performance of the rib-to-deck plate connection

In this sub-chapter the rib-to-deck plate connection for orthotropic decks with closed trapezoidal stiffeners will be evaluated. Here the focus is directed to the fatigue behaviour of this specific connection in the span between floor beams. The welded connection is shown in Figure 3-33 and Figure 3-34
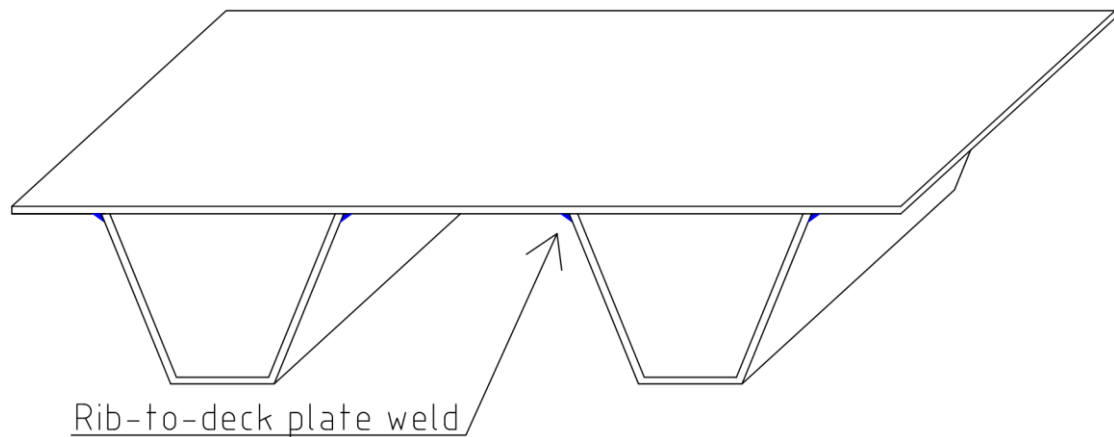
Figure 3-33 Weld at the rib-to-deck plate connection
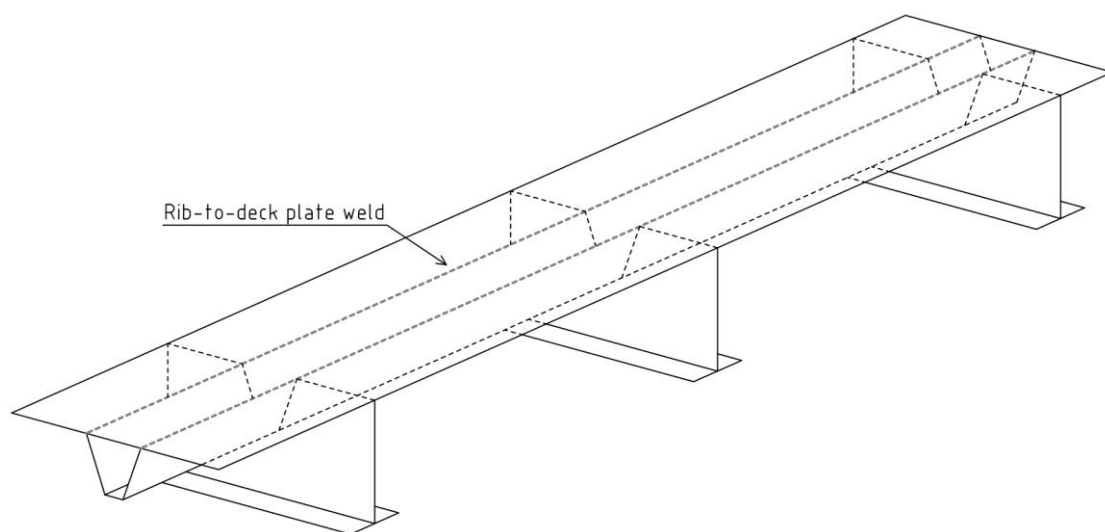
Figure 3-34 The weld in the connection of rib and deck plate seen from above

In an OSD the deck plate is supported by the rib walls and as a wheel load is placed on the plate it will deflect and force the rib walls to deflect as well while the nearby deck plate deflect in the upward direction, see Figure 3-35. The ribs represent elastic supports to the deck plate and the stiffness of these elastic supports depends on the spacing of the floor beams (Jong, 2004). As a consequence of the elastic behaviour the maximum deflection will be found directly beneath the loading point. The deformations generate bending moments in the deck plate and the rib webs which in turns causes stresses in the longitudinal weld. It is these stresses that provoke the fatigue cracks in the weld between the rib and deck plate.
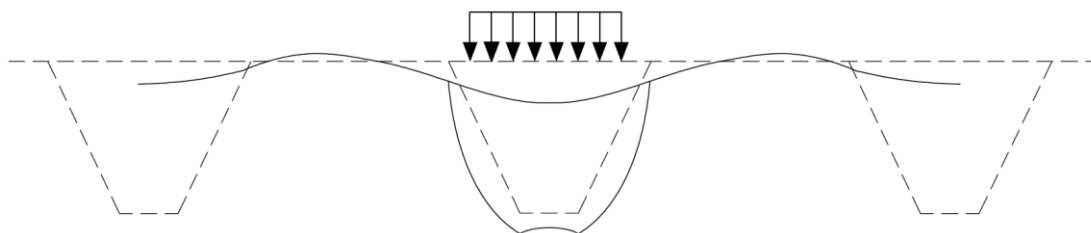
Figure 3-35 Behaviour of rib and deck plate under the influence of a wheel load direct above the rib

The total length of the welds in the connections between longitudinal ribs and the deck plate amounts to many times the length of the bridge deck itself (US Department of Transportation, 2012). Accordingly it is of great importance that an economical solution that suits production and attachment as well as the in-place performance is achieved. As a result of the mere amount of this weld the risk of defects is high and thereby the risk of fatigue cracks increases, due to for example the increased risk of stop-start defects. Together with the complex and varying stress situation this connection experience severe fatigue behaviour.

The welding of a closed stiffener is only possible from the outside of the rib, as a consequence of this it is a higher risk for errors in execution. Defects in the weld are a possible initiation position for fatigue cracks, and to reduce the risk, fabrication specifications are stated. However, as the requirements become more specific the production cost increases and thereby the economic advantage of closed ribs before open decreases (Kolstein, 2004). The weld in this joint is mainly a fillet weld which will not penetrate the whole rib web but leave a gap which represents a stress raiser at the root of the weld. To improve the performance of this connection it is necessary to minimize the weld defects. Therefore the recommended welding procedure is automatic welding with the rib pressed to the deck plate during welding. This excludes human errors such as stop-start defects.

There are several reported fatigue failures in the connection between the longitudinal stiffener and deck plate (Kolstein, 2004). It is difficult to estimate the stress at this intersection since it is affected by several variable factors such as the temperature of the wearing surface, multiple vehicles in different lanes and sections as well as transversal forces from vehicles changing lanes contributes to the stress state (US Department of Transportation, 2012). The stresses are also governed by the dimensions and geometry of the members of the structure as well as the distribution area of the load (Liao, 2011). The transverse location of the wheel load is important for where the maximum stress will appear. If the wheel is positioned direct above the rib wall the highest stress will be found in the deck, if the wheel on the other hand is placed between the ribs the maximum stress will occur in the rib.

In the orthotropic deck the longitudinal rib acts as a continuous beam on supports consisting of the floor beams. At the location of the supports the ribs will be subjected to negative flexural moments from the traffic load generating compressive stresses in the base of the rib (Wolchuk & Ostapenko, 1991). As a result of lateral load distribution in the orthotropic deck the ribs will experience local out-of-plane deformation causing traverse flexural stresses in the walls of the ribs.

The response of the connection between the deck plate and rib is governed by individual wheel loads (US Department of Transportation, 2012). The global effects only have small influence on this section compared to the local effects as well as they

chiefly generates stresses parallel to the weld and thereby poses less risk of initiating a fatigue crack.

The stress cycles from the single axis wheel load can be observed in Figure 3-36, the response shown is in the perpendicular direction to the weld and for the deck plate and rib respectively. The five individual wheel-axes are represented by the distinct peaks in the diagram. From this follows that it is the single axel load that governs the behaviour of this detail.

Figure 3-36 Response of the rib and deck plate from a five axis truck (Connor & Fisher, 2001)

Another distinction that can be made is that the full behaviour and response of the stress range cycle is a result of several vehicles in sequence as well as the location of

the vehicle in relation to the rib, see Figure 3-37. The data seen represents the response in the rib wall perpendicular to the weld. If compression or tension arises in the given rib is governed by the transverse location of the wheel load (Conner & Fisher, 2001). If the vehicle passes directly above the rib, the rib and weld will experience compression otherwise tension. This can be observed in Figure 3-37 where the first truck is located to the side in transverse direction and the second truck is directly above. For the second truck it is also possible to distinguish the individual axel loads clearly.
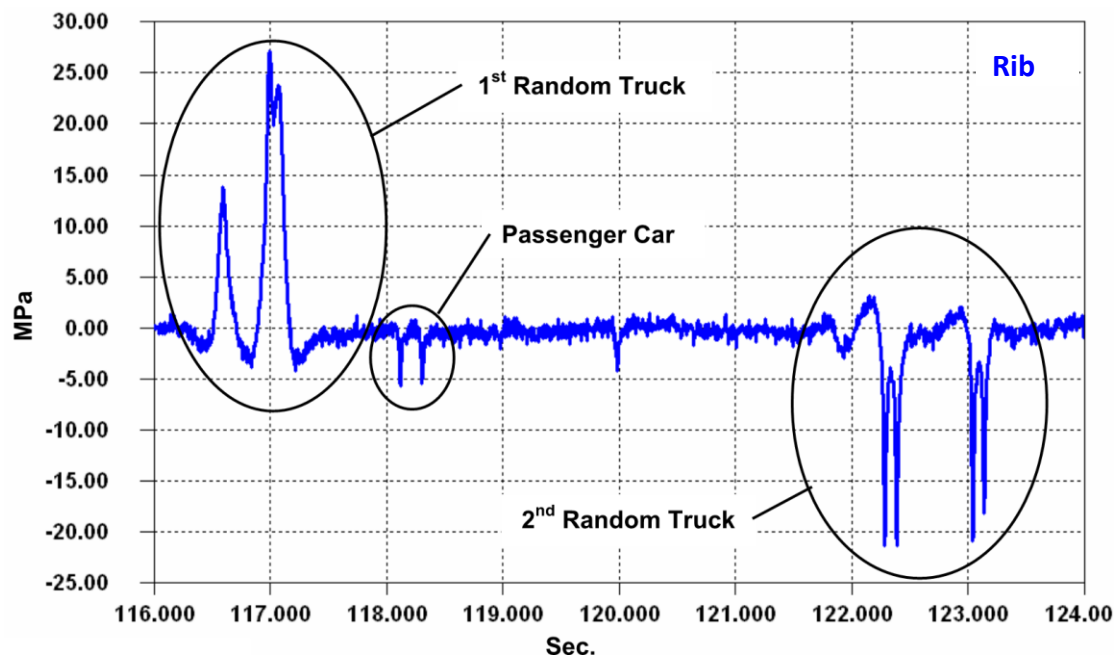
Figure 3-37 Response of the rib causes by two trucks and a passenger car (Connor & Fisher, 2001)

In Figure 3-37 the first and second truck generates stresses of approximately the same magnitude in the rib web and thereby in the weld. However, since fatigue is evaluated with regard to the stress range and thus the maximum and minimum stresses will be added and the total is considerably higher than if only the passing of one vehicle is considered (Connor & Fisher, 2001). This response behaviour is very important to consider in the fatigue design of the connection between the longitudinal stiffeners and deck plate.
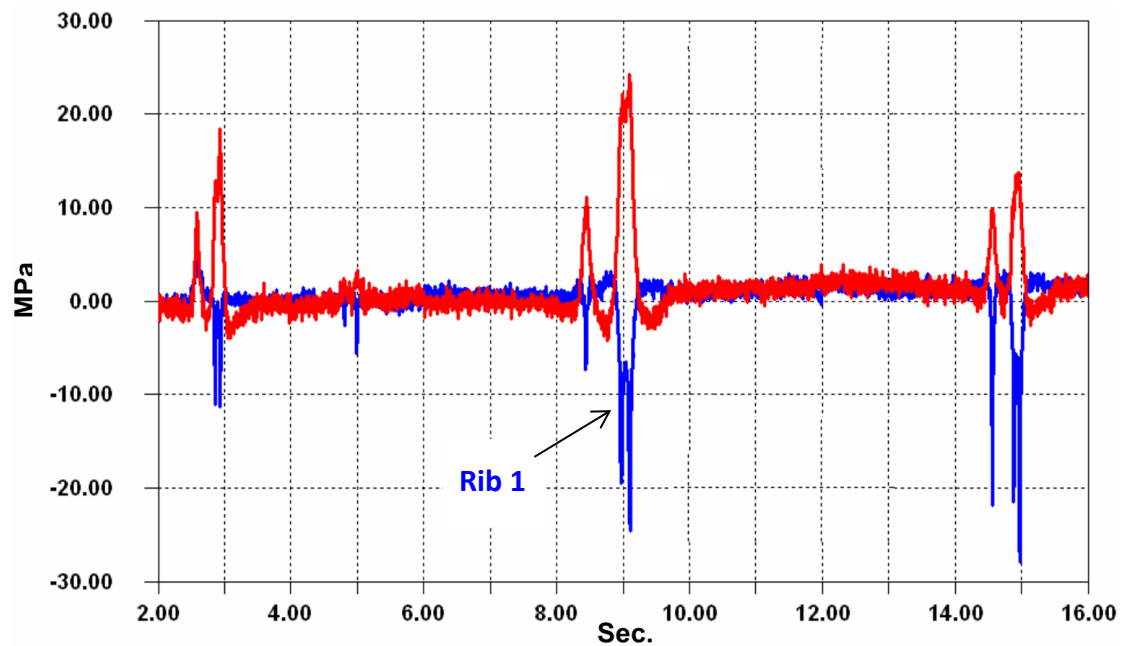
Figure 3-38 Response in the two rib walls of one rib for the same loading (Conner & Fisher, 2001)

In Figure 3-38 the response from the passing of random trucks, the same sequence as in Figure 3-37, in both the rib webs of one rib are displayed. It can clearly be seen that the responses are opposite, one are in compression and the other in tension simultaneously.

In general this connection experience high stresses, this together with weld defects results in the tendency for fatigue (Kolstein, 2004). The stress range in the weld between the rib and deck plate is highly influenced by the thickness of the deck plate and the type and thickness of the wearing surface, as mentioned above. The local effects experienced by the rib-to-deck connection from wheel load can be seen in Figure 3-39.
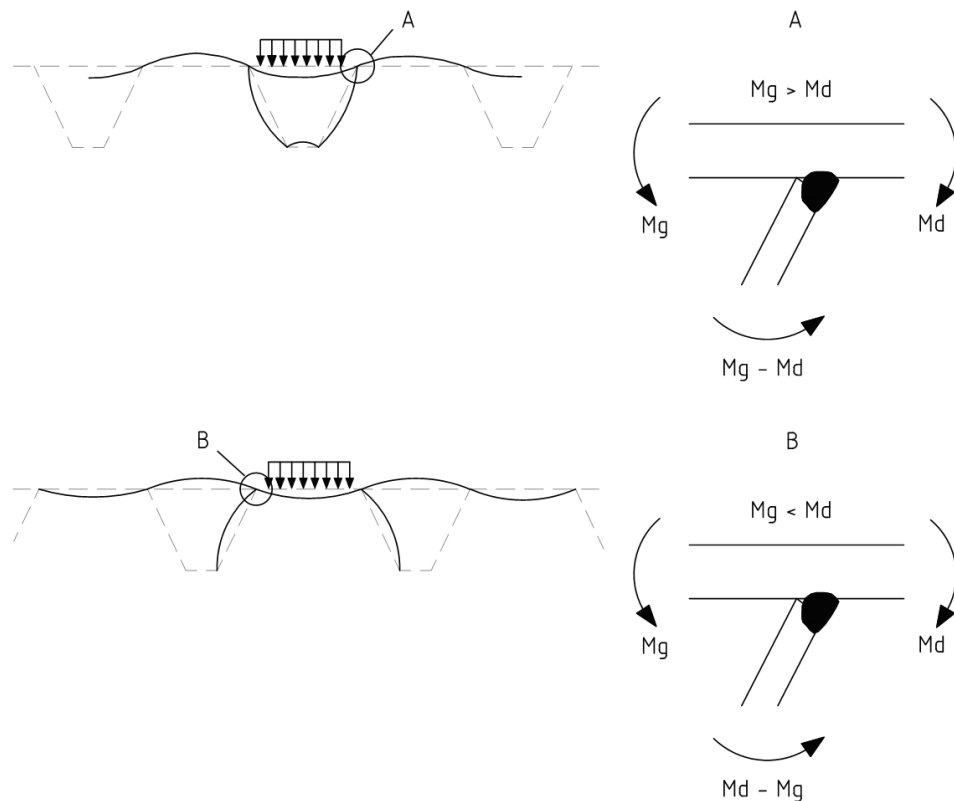
Figure 3-39 Local effects on connection between deck plate and longitudinal rib from wheel loading.

When the deck plate deforms beneath the wheel load it will deflect downwards directly under the load application point, the adjacent spans will deflect in the opposite direction, upwards (Liao, 2011). As a consequence of the rigid connection between rib and deck this action will generate a bending moment in the webs of the ribs, see Figure 3-39. Fatigue is in general originated from flexure in the deck plate as a result of wheel load, see Figure 3-39 and Figure 3-40, (SS EN 1993, 2006). Fatigue cracks can arise in the welded connections between the ribs and deck plate, see Figure 3-41 and Figure 3-42.

C = Compression

T = Tension
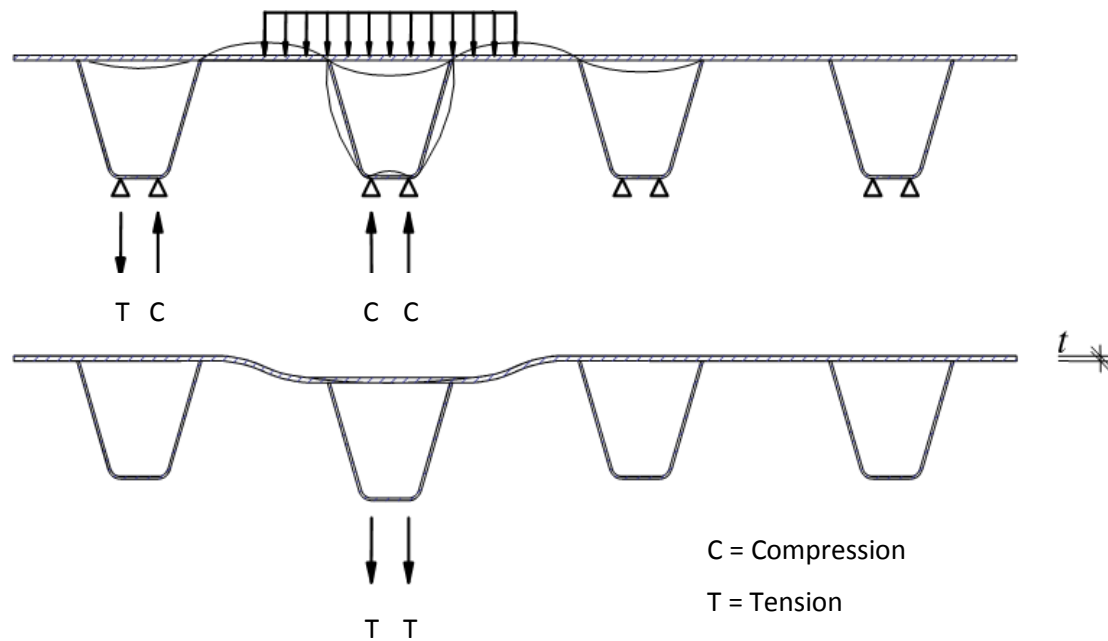
Figure 3-40 Resulting action in the deck plate and ribs from wheel load; (a) The bending profile as it would appear if the stiffeners will not deflect; (b) The effect of differential deflections of the ribs (SS EN 1993, 2006).

The deck plate will not only deform in the wave like manner seen Figure 3-39 and Figure 3-40(a) but will at the same time experience a vertical deflection, Figure 3-40(b), an effect of the bending of the longitudinal ribs between the floor beams (Liao, 2011). As a result additional bending moment will be induced in the rib web. This deflection is governed by the spacing and stiffness of the floor beams as well as the rib stiffness. The point of maximum deflection will be located directly beneath the wheel, this applies for both the deflection described in Figure 3-40(a) and Figure 3-40(b).

a) crack initiation starting at weld root inside the stiffeners

b) crack initiation starting at weld toe outside the stiffeners
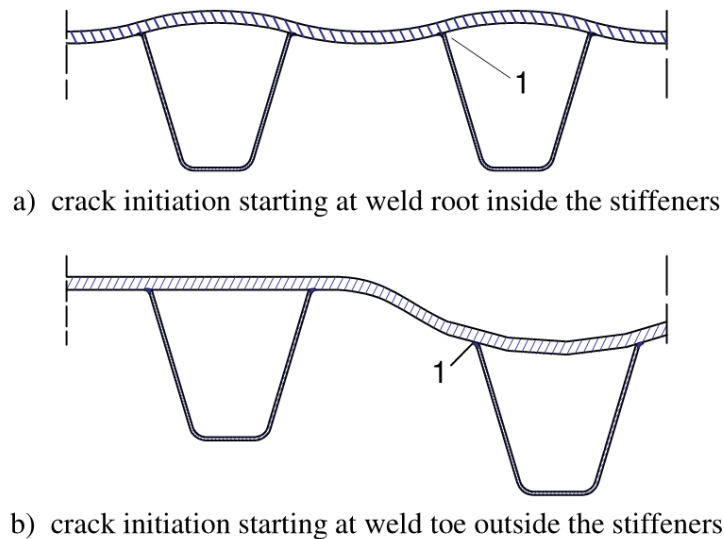
1   crack initiation

Figure 3-41 Fatigue cracks in the deck plate; (a) Cracks initiated at the weld root are a consequence of the bending of the deck plate; (b) Cracks initiated at the weld toe are imitated as a result of the differential defections of the ribs

Regarding the fatigue behaviour of the weld in the longitudinal rib-to-deck plate connection there are numerous factors influencing the performance. Among these are the thickness of the plate and stiffener, the load distribution through the wearing surface, any splices in the deck plate and possible weld defects and stress raisers in and near the weld. However, the combination of the several different stress states occurring at the same time in this location is one of the most important aspects. When the deck plate deforms the ribs will experience bending and stresses are induced in the welds, when shear forces arises in the stiffeners they are transmitted through the welds, the same goes for longitudinal stresses from bending moments and axial forces (SS EN 1993, 2006). The production and assembly of the separate members into a unit is also of great importance as errors in the connections may result in poor fatigue strength. However, there is no apt way to include this in the design more than to give recommendations.

If a fatigue crack arises in this connection it is either from the toe of the weld into the parent material in rib web or deck plate, or from the root of the weld and then either into the deck plate or into the weld itself, see Figure 3-42. If the crack is initiated at the toe the stiffness relation between the deck plate and rib wall decides in which of the members the crack will arise (US Department of Transportation, 2012). As a consequence of the unsatisfying penetration cracks can also be commenced at the weld root.
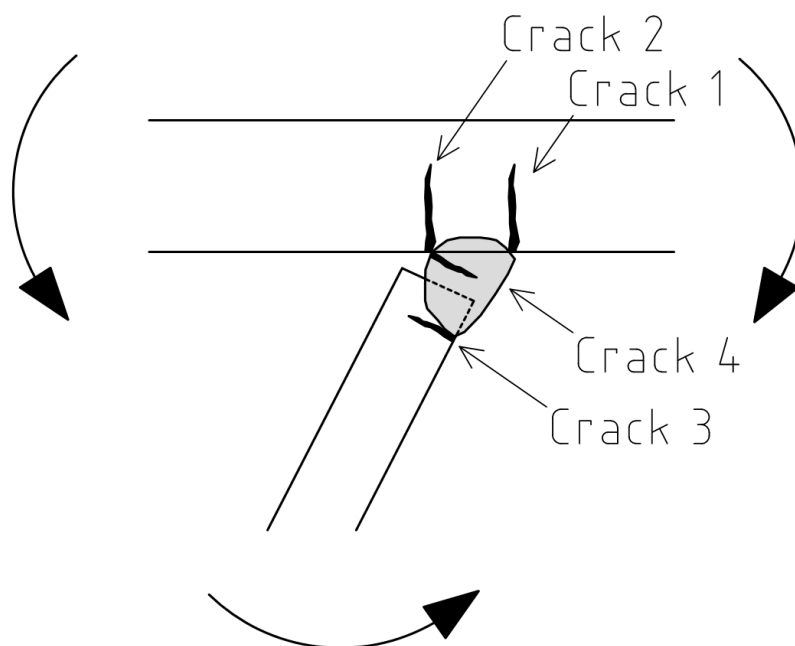
Figure 3-42 Potential crack positions in the rib-to-deck plate connection

As seen in Figure 3-42 there are four principal crack modes for the detail of the connection between the deck plate and longitudinal trapezoidal stiffener.

Crack 1   Toe crack in the deck plate above the weld, either in the field between floor beams or above the cross-connection with longitudinal rib and transversal floor beam, see Figure 3-43 (a)

Crack 2   Root crack in the deck plate above the connection weld to the longitudinal rib, either in the field between floor beams or above the cross-connection with longitudinal rib and floor beam, Figure 3-43 (b)

Crack 3   Toe crack in the rib wall

Crack 4   Root crack weld in the field between floor beams, see Figure 3-46
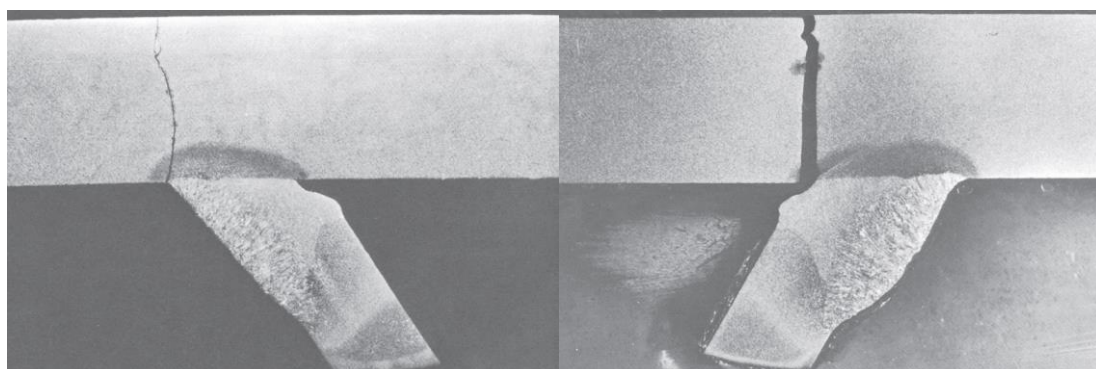
Figure 3-43 Cracks in deck plate at the welded connection with a rib, the cracks arises either in the field or at the intersection with a floor beam; (a) Crack 1; (b) Crack 2, (Kolstein, 2007)
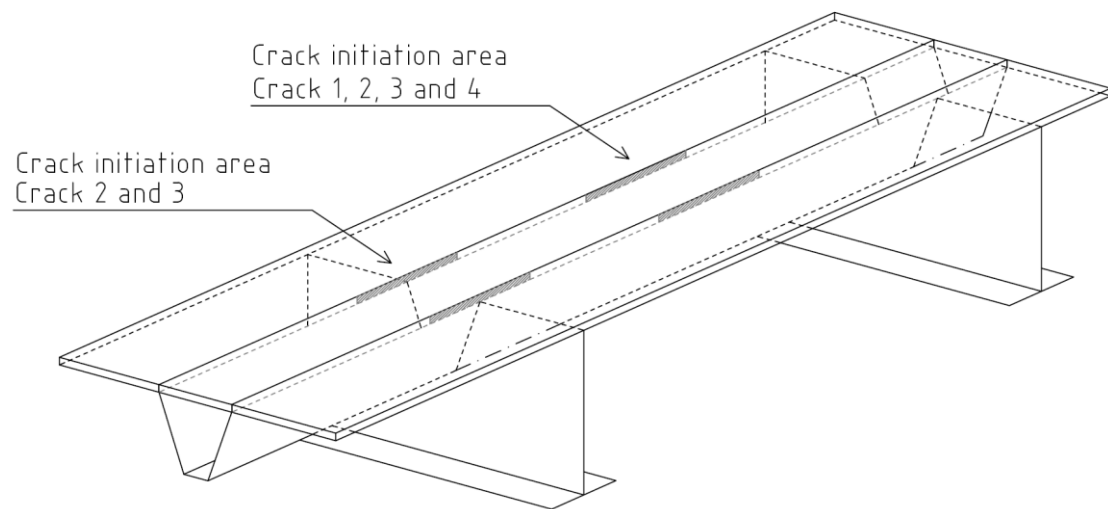
Figure 3-44 Cracks in deck plate at the rib-to-deck weld

A crack in the longitudinal weld propagating in the deck plate can either arise above the intersection with the floor beam or in the field between the floor beams. These types of cracks are initiated either in the weld toe or root, depending on the highest stress concentration (Liao, 2011). A crack in the deck plate grows from the initiation point to the upper surface of the steel plate and affects the wearing surface negatively and can cause spalling of the wearing surface, (Jong, 2004) see Figure 3-45. These types of cracks are generally not detected until they surface and deteriorate the wearing surface.

A crack located above the intersection of rib and floor beam grows vertically from the lower surface of the deck plate to the upper, after this the crack starts to propagate further in the longitudinal direction (Jong, 2004). A crack in the deck plate located in the span between the floor beams grows in the vertical and longitudinal direction simultaneously, which makes them harder to detect before they are rather long. The cracks in the deck plate are initiated in the same manner but have different behaviour while propagating.
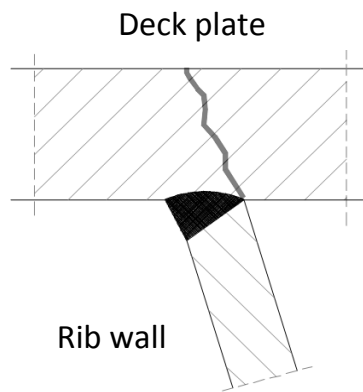
Figure 3-45 (a) Crack in deck plate at the connection to the longitudinal rib; (b) Spalling of wearing surface from cracks in the deck plate (Jong, 2004)

The deck plate is supported by the floor beams between the ribs, but between the rib walls the floor beam do not give any support to the plate (Jong, 2004). If a wheel load is applied directly above the rib the deck plate and rib walls will deform and the section will experience high transversal bending moments (Janss, 1986), as could be seen in Figure 3-39. Since the rib walls at the floor beam and deck plate between the floor beams are welded to the transversal floor beam a clamping moment will arise in the deck plate with high stress concentrations in the same causing the fatigue cracks described above (Jong, 2004).
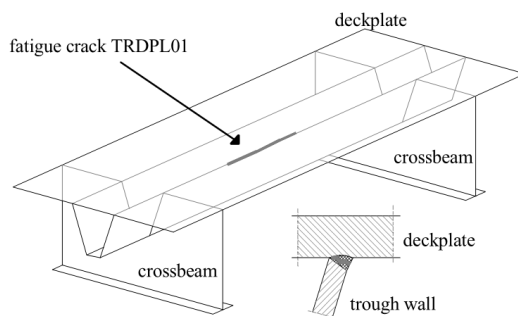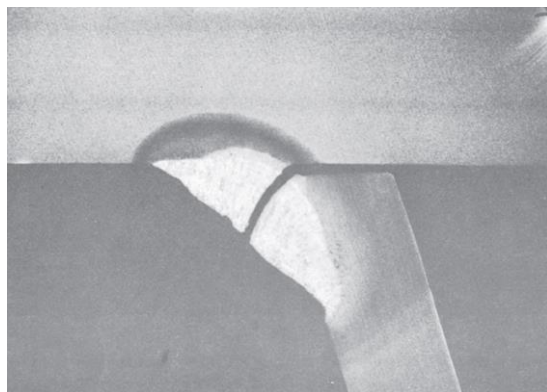
Figure 3-46 Crack in the weld root at the rib-to-deck plate connection; (a) Section of a typical fatigue crack at the weld root (Kolstein, 2007); (b) Overview of where root cracks arises (Jong, 2004)

An important factor with regard to these fatigue-cracking modes is the influence of the gap between the rib web and deck plate. It is possible to prevent these crack modes if full, or sufficient, penetration of the weld is achieved (Kolstein, 2007). Cracks in the weld itself or in the web of the rib are chiefly a result of transversal bending moment in the rib web (Liao, 2011). This flexural moment arises as a result

of the forced deformation of the rib when the deck plate is deformed under wheel load. However, even if longitudinal crack in the weld arises the deck plate can redistributes the loads and thereby the crack only poses a relatively small risk (Jong, 2004).

As a result of the defects and partial penetration this crack in general initiate at the weld root, between the web of the rib and the deck plate (Jong, 2004). It grows through the weld from the root to the toe and after this it starts to propagate in the longitudinal direction along the weld. The initiation point for this type of crack can be anywhere in longitudinal direction along the weld except at the intersection with the floor beam where this behaviour is restrained and the stress range in the weld root is decreased.

3.3.2.2 Load response and fatigue performance of the rib-to-floor beam connection

The connection between the rib and floor beam can be composed either with a stress relieving cut-out or by fitting the rib closely in the floor beam, the latter is shown in Figure 3-47. The fatigue resistance is highly dependent of the type of detail and welding technique (US Department of Transportation, 2012). The joint can be manufactured with either full penetration butt welds or double side fillet welds. The butt weld is in general superior with regard to fatigue but have higher production costs. The shape of the closed rib is also of importance, a V-shaped rib is more prone to fatigue than a U-shaped, trapezoidal, rib (Kolstein, 1996).
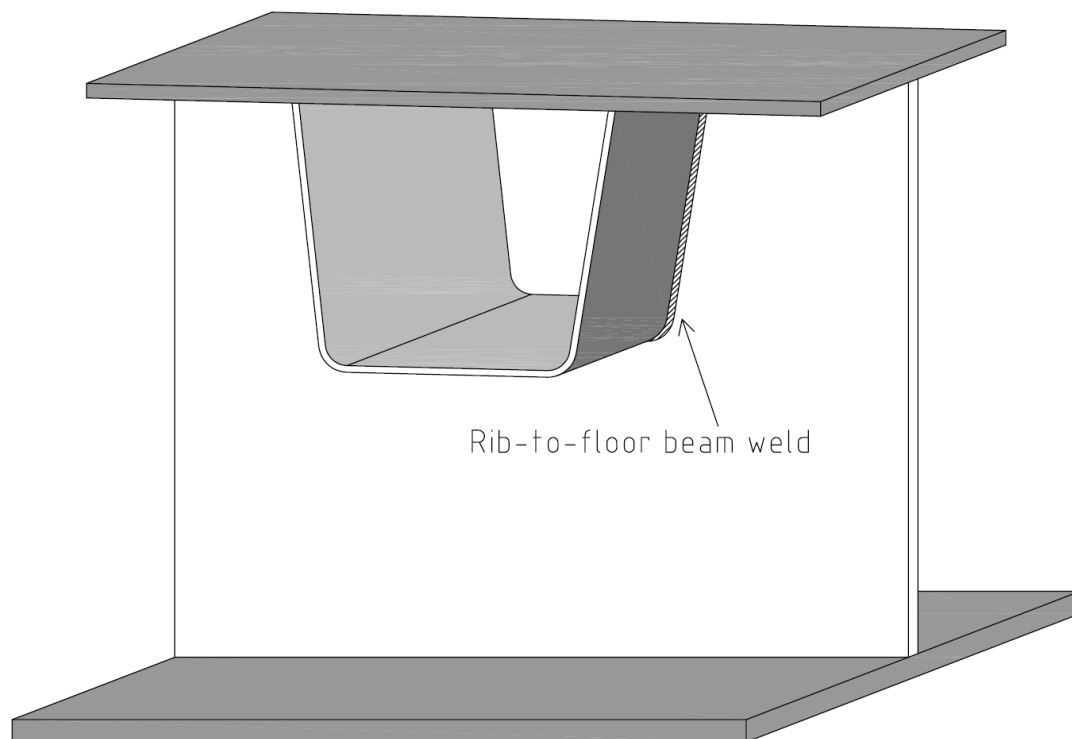
Figure 3-47 Illustration of the rib-to-floor beam weld

In general the rib is continuous through the floor beam. The reason for this is the lower stress experienced by the connecting weld, compared to discontinuous ribs over the floor beams. When the rib is passing through the floor beam the load in the rib is effectively distributed to adjacent ribs without stressing the weld (Kolstein, 2007).

The floor beam is subjected to both local and global shear stresses from wheel loads, these stresses can be significant depending on the spacing of the floor beams (Kolstein et al., 1996). The floor beam is also exposed to out-of-plane bending that can generate stress concentration points at the floor beam weld toe causing fatigue cracks. At the intersection with ribs the floor beam web has a loss in cross-section and is thereby weaker here.

In field studies performed by Connor and Fisher (2001) the floor beams unique stress cycle with a combination of in-plane stresses and out-of-plane stresses is presented, see Figure 3-48. This combination of stresses is derived back to systems 4 and 5 described in Chapter 3.3.1.

In Figure 3-48 the green line represents the out-of-plane stresses in the floor beam on the right side of the rib, seen in section in the direction of the traffic, and the red is represented by the out-of-plane stresses in the left side. The blue line represents the in-plane stresses in the floor beam.
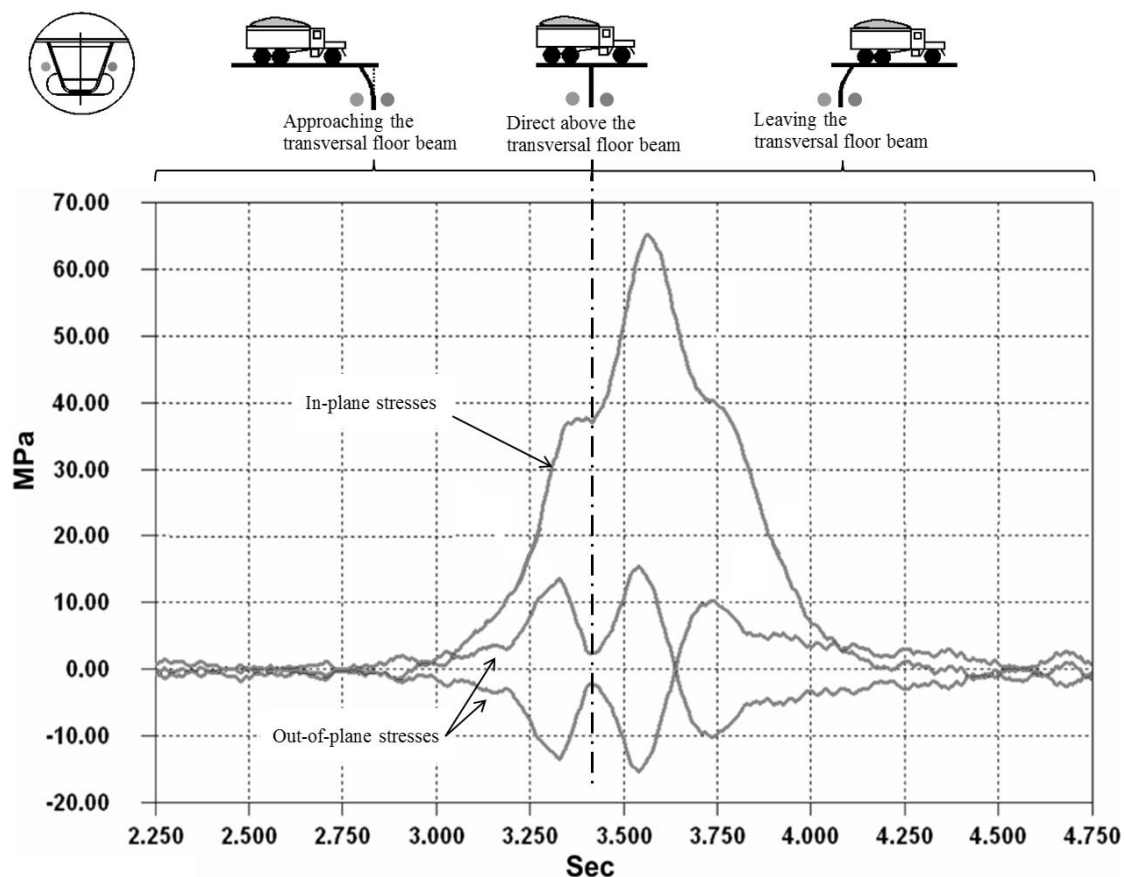
Figure 3-48 Comparison of in-plane-stresses and out-of-plane stresses in the tooth of the floor beam close to a cut-out (Connor & Fisher, 2004)

As can be seen in Figure 3-48 the in-plane stresses dominate the behaviour, and this is the most common situation (Connor & Fisher, 2004). In some cases the out-of-plane stresses will govern the behaviour, in particular in decks with large spacing between either ribs or floor beams. This results in increased out-of-plane stresses that may exceed the in-plane stresses in some ribs, depending on the transversal location and the loading point relation to the rib in question.

The rotation of the rib ends (i.e. at connection to the floor beams) governs the proportion of the out-of-plane stress in the floor beam (Connor & Fisher, 2004). Since the ribs have basically the same boundary conditions and stiffness regardless of the transverse location and thereby experience the same quantity of rotation when subjected to the same load. As a consequence the magnitude of the out-of-plane stress range will be almost the same in the different ribs when subjected to wheel load. However the contribution to the total stress range cycle will vary since the in-plane stress range is not the same for the different ribs (US Department of Transportation, 2012).

From the same in-situ tests by Connor and Fisher (2004), it was concluded that trucks driving in a sequence will generate a single stress cycle but with larger peak stress range. The test results, Figure 3-49, showed that two trucks following each other resulted in an increased peak stress magnitude of 40-50% compared to the single truck event.
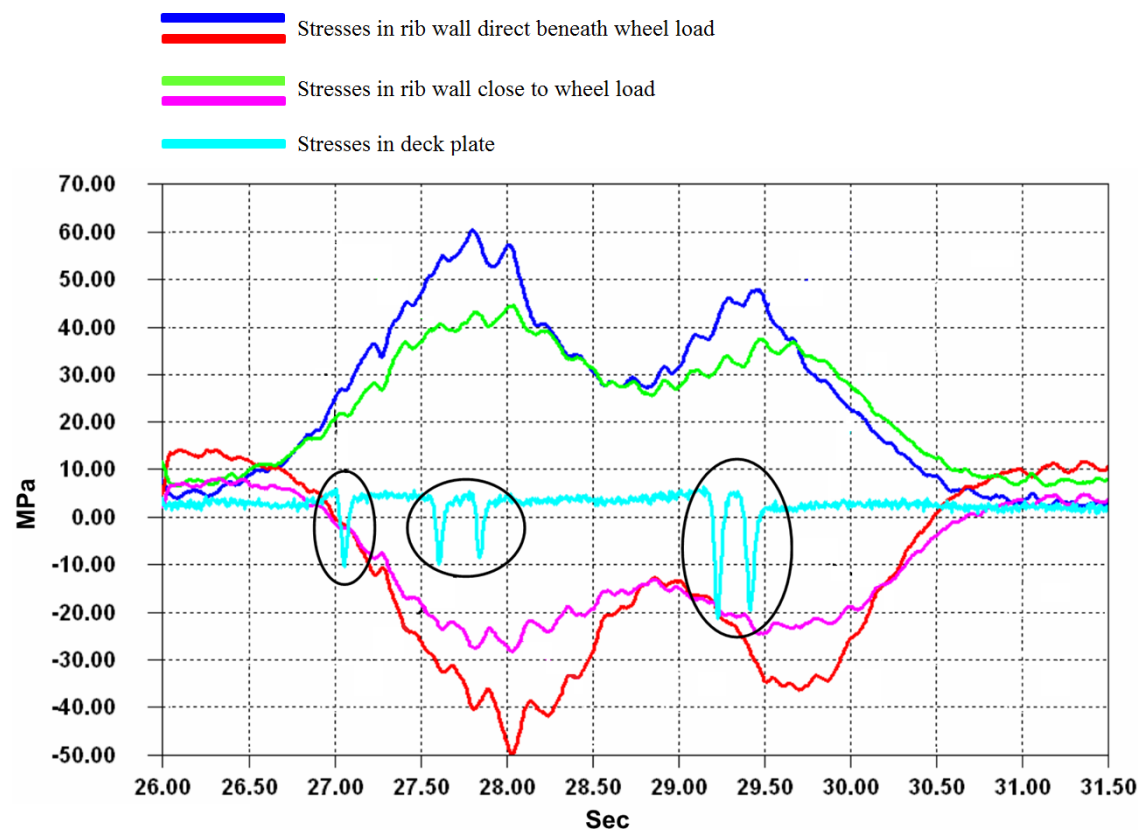
Figure 3-49 Response of floor beam tooth from a five-axle truck. Circled stress peaks in deck plate represents passing of axis (Connor & Fisher, 2004).

One stress cycle in the floor beams and ribs is produced from the passing of a truck with several axes (Connor & Fisher, 2004). Nevertheless in the rib-to-deck plate connection as well as in the deck plate itself each individual axis produces a separate stress cycle. This can be observed in Figure 3-49, which shows stresses in the deck plate close to the floor beam and stresses in two individual ribs at the intersection with the floor beam. For the deck plate the passing of the five separate axes are clearly visible as peaks in the stress diagram. For the ribs however, independently of the distance from the application point of the load, the individual effects from the respective axes are highly reduced and only one primary stress cycle appears. A secondary cycle with smaller magnitude exists but the contribution from this to the fatigue behaviour is negligible (US Department of Transportation, 2012).

The test also shows that the floor beam response from a multi-axel vehicle best is represented by a single stress cycle and that this cycle is governed by a single axis or close-spaced axes. As a result of this the peak stress range in the tooth of the floor beam is governed by the maximum axle pressure rather than by the total weight of the truck (Connor & Fisher, 2004). The general assumption made is that each passing truck only generates a single primary stress cycle in the rib-to-floor beam connection, regardless if a cut-out is present or not.

When the bottom side of the rib is subjected to compressive bending stresses at the intersection with the floor beam Poisson's expansion will take place in the transverse direction, see Figure 3-50 (Wolchuk & Ostapenko, 1991). Poisson's expansion is caused by compression in one direction that leads to expansion in the other direction. Between the floor beams this type of expansion is not restrained and as a consequence no stresses arise. However, in the crossing between rib and floor beam this expansion is prevented and thereby local out-of-plane stresses arise. If a cut-out in the floor beam is present the bottom of the rib will still be unstressed, but the expansion of the rib webs are prevented resulting in stresses in the rib walls. The repressed expansion, causing out-of-plane stress, together with the interaction between rib and floor beam, which is subjected to high in-plane bending stresses, results in a stress situation that must be resisted by shear in the welds.
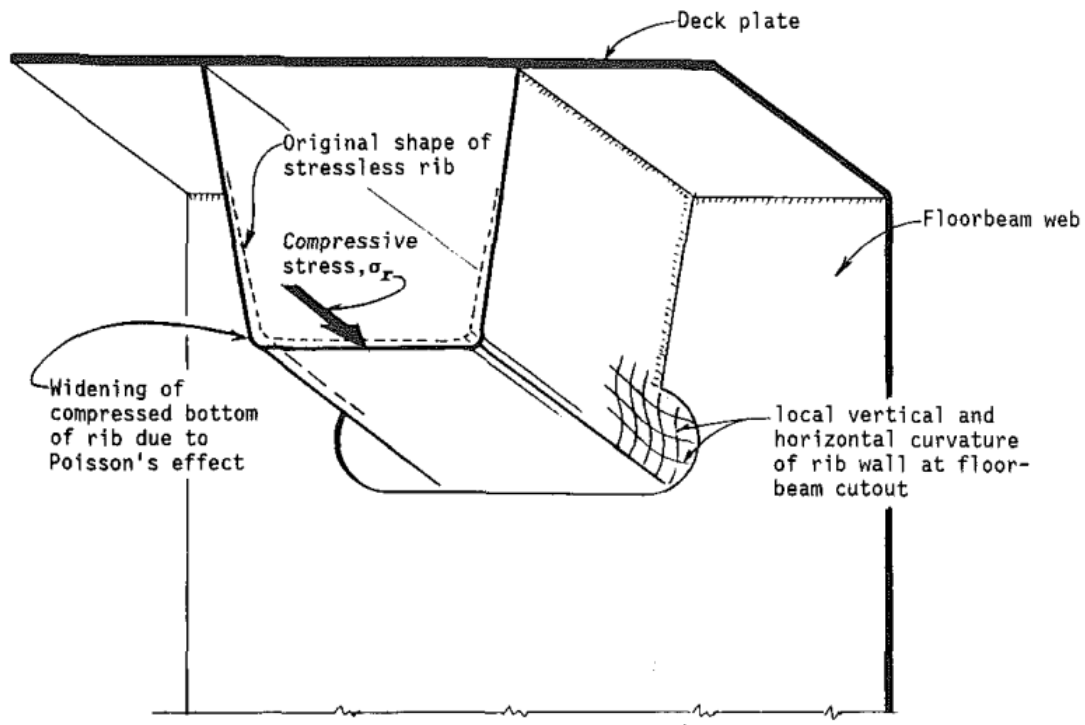
Figure 3-50 Deformations of rib from compressive flexural stresses (Wolchuk & Ostapenko, 1991)

However, it is important to mention that the cracks arising in the rib-to-floor beam connection are in general not a threat to the traffic safety (Jong, 2004). This is a consequence of the capacity to redistribute the load as long as the dimensions of the cracks are limited. Another important factor in this is that the observed cracks at this connection are an outcome of pore weld quality. These cracks are generated by secondary stresses that arise in the floor beam web due to its out of plane stiffness that restrains the rotation of rib ends. When the cracks propagate, a reduction of the local stiffness of the web of the floor beam will be obtained and the stresses will be relived. In other words this is a deformation-controlled cracking with crack propagation decreasing with increase crack length. However, it is important to emphasize, that once the cracks have initiated, they may continue growing due to other load effects than distortion out-of-plane, for example shear stresses in the floor beam web.

If no cut-outs are used, the ribs are fitted to the floor beams and welded all around both sides with fillet welds. For this type of connection there are three general fatigue crack modes to consider (Kolstein, 2007).

- Crack starting at the weld root and propagate to the weld toe, weld throat failure, see Figure 3-51 (a).
- Crack starting at the weld toe and propagating in the rib.
- Crack starting at the weld toe and propagating in the floor beam, see Figure 3-51 (b).

Figure 3-51 (a) Weld throat failure at the rib-to-floor beam connection; (b) Fatigue crack at the weld toe progressing into the floor beam due to longitudinal stresses in the rib (Kolstein, 2007)

The fatigue crack initiated in the weld root, Figure 3-51 (a), is in general a consequence of the insufficient fusion between floor beam web and rib at the weld root and the crack-like defect this region. This together with high in-plane stresses makes this a high-risk area for fatigue crack initiation (US Department of Transportation, 2012). However, root cracking is avoided by prescribing sufficient penetration of the weld and therefore the governing cracking mode is toe cracking.

Longitudinal bending moment in the rib together with the out-of-plane bending of the floor beam causes a longitudinal stress in the rib. This stress is the inducing force for crack in the weld toe at the curvature of the base of the rib, same as in Figure 3-51 (b), this is the point where cracks are most likely to arise in this type of detail (Kolstein, 2007). Shear and out-of-plane bending will drive the crack to propagate in the floor beam.

If this intersection between rib and floor beam instead is constructed with a stress reliving cut-out there will be no welds in the highly stressed region around the base of the rib and this decreases the risk of cracks at the weld toe (Kolstein, 2007). However, with the cut-outs the floor beam loses rigidity. This together with the distortion of the floor beam, described in System 5 in Chapter 3.3.1.5, causes high stresses to arise in the termination of the welds and the fatigue resistance becomes more critical (Aygül, Al-Emrani & Urushadze, 2011). For this detail there are three principal cracking modes:

- Crack starting at the weld toe and propagate vertically in the rib.
- Crack starting at the weld toe at the weld end and propagating up longitudinally in the rib, Figure 3-52 (a).
- Crack staring at the weld toe at the weld end and propagating in the web of the floor beam, Figure 3-52 (b).

Figure 3-52 (a) Longitudinal fatigue crack in the rib at the termination of the weld at the cut-out; (b) Fatigue crack in the floor beam at the termination of the weld at the cut-out (Kolstein, 2007)

When the intersection is designed with a cut-out the shear stresses in the floor beam increases and this induces a higher risk for fatigue cracking in the floor beam (Kolstein, 2007). When calculating the fatigue resistance for this connection the type of weld used is of high importance and as mentioned above if a fillet weld is used the fatigue strength will be lower but the production costs will be lower.

Cracking in the rib starting in the weld toe is generally initiated from longitudinal bending stress (US Department of Transportation, 2012). The fatigue cracks initiated at the termination of the weld and propagating in the rib is a reaction from the rib distortion, taking place in the cut-out where the rib is free to move. This type of fatigue crack is predominantly initiated at the weld toe, this is generally the case even if weld improving techniques have been used to reduce the defects (US Department of Transportation, 2012). The distortion of the rib creates local transverse bending stresses that is combined with the global longitudinal bending stresses. For the cracks initiated at the termination of the weld at the weld toe and propagating in the floor beam the driving stresses are in-plane as well as out-of-plane and are thereby difficult to assess correctly.

3.3.2.3 Load response and fatigue performance of the rib-to-deck plate connection at the floor beam joint

As a result of the geometry and stiffens that the closed ribs provides, the connection between rib and deck is subjected to local secondary deformations and stresses. In particular at the intersection with the floor beams the proneness to fatigue is high (US Department of Transportation, 2012). This is a complex detail in the orthotropic deck and the one with highest uncertainties related to it. The stress state related to the fatigue behaviour in this detail is influenced from several factors which are difficult to analyse analytically.

It is known that the stress and fatigue behaviour is controlled by the pressure of a single axis rather than the total weight of the passing vehicle, as for the details discussed above. It has also been observed that the thickness of the deck plate is of major importance for the fatigue strength in this joint (US Department of

Transportation, 2012). The thinner the deck plate, the higher the risk for fatigue in this detail.

The distortional stress in the connection can cause tension stresses in the weld root and this is believed to be the governing factor with regard to the fatigue performance (US Department of Transportation, 2012). This is a result of the rigid support the floor beams represents in these sections together with the distortion in the deck plate from in-plane bending. In other sections of the rib-to-floor beam connection the root cracking can be controlled by limiting the gap tolerance in production. In the intersection with the floor beams however the tensile stresses in the weld root are considerably larger and fatigue cracks may be initiated anyway.

3.3.3 Critical cracks chosen for subsequent analysis

With regard to the layout of an orthotropic deck and the localised fatigue behaviour three specific cracks are chosen to be the base of the following investigations and analysis.

The studied cracks are:

- Crack initiated at the weld toe in the rib-to-deck plate weld, the crack propagates in the deck plate and is referred to as R-DP Crack I, see Figure 7-1 (a).
- Crack initiated at the weld toe in the rib-to-deck plate weld, the crack propagates in the rib wall and is referred to as R-DP Crack II, see Figure 7-1 (a).
- Crack initiated at the weld toe at the radii in the rib-to-floor beam weld, the crack propagates in the floor beam web and is referred to as R-FB Crack III, see Figure 7-1 (b).
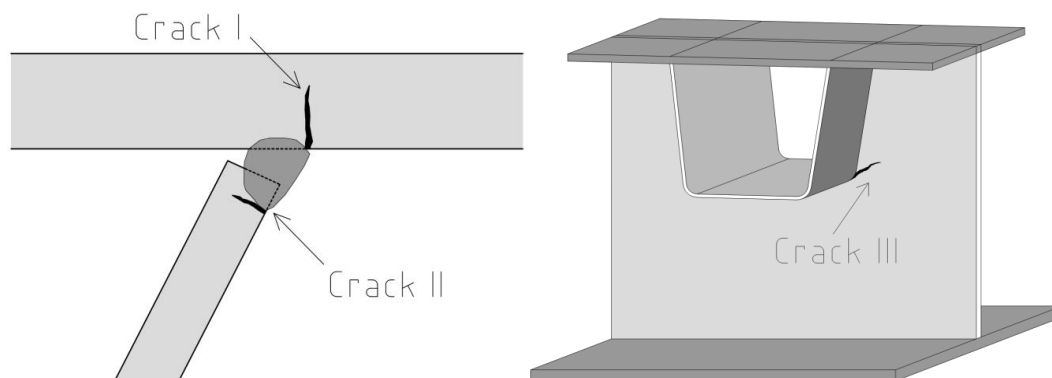
Figure 3-53 The three investigated cracks (a) Crack I and II at the rib-to-deck plate weld; (b) Crack III at the radii of the rib-to-floor beam weld.

4 Description of fatigue life assessment methods in design and analysis

Fatigue failure of structural members is an extremely localized process including crack initiation and propagation as well as fracture. The importance of representing the local parameters regarding geometry, loading and material is therefore of great importance (Radaj, Sonsino, Fricke, 2006). On the other hand these local effects are only treated schematically in design rules for fatigue assessments. The design is usually based mainly on the nominal stress approach, which is a global approach. For structures with difficulties to determining the nominal stress, such as an OSD, the design codes are unsatisfactory (Radaj, Sonsino, Fricke, 2006).

Generally the fatigue assessment methods are divided into two main subcategories based on their detail level, global and local approaches. The most common method in design is the nominal stress approach, which is a global method. If more detailed results are required local approaches need to be used. The hot sport method is the easiest design approach on local level but other methods are available for more accurate investigations. These are *global approaches,* such as the nominal stress method, and *local approaches*, such as the effective notch stress method. The more detailed a method is the more complicated it is to execute, hence the global approaches are best suited for rough estimates and the local approaches for more exact studies. Different stress concepts and distribution in the vicinity of a weld can be seen in Figure 4-1.
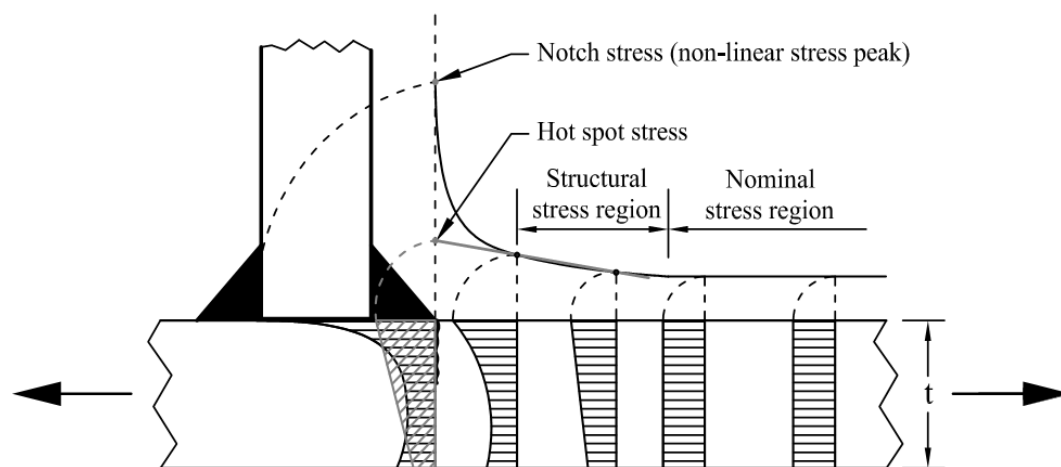
Figure 4-1 Stress distribution through the plate and along the surface close to the weld, with some stress concepts presented (Heshmati, 2012)

In the global approaches stresses based on derivations from global loads and continuum theories, mainly elasticity and plasticity theory, are used (Radaj, Sonsino, Fricke, 2006). The end of the critical fatigue life of a specimen is a global phenomenon, such as the total fracture or fully plastic yielding, and is corresponding to the critical nominal stress (Radaj, Sonsino, Fricke, 2006). The global approaches were the first to be used in fatigue evaluations and are still the most used in bridge design, mainly due to its simplicity and the restricted amount of work effort needed. A significant disadvantage with this approach is the fact that it doesn't include localized

phenomena, such as stress raising effect. The fatigue process is complex and a highly localized event, as described earlier in the report, and this is not well represented in a global fatigue approach. Another disadvantage is that the fatigue strength is decided by comparison by S-N curves that are empirically developed for specific details. This result in difficulties to predict the fatigue life for unique details not included in the design codes.

The need for an improved understanding and description of the fatigue behaviour has led to the development of several localized fatigue approaches. Two examples are the effective notch stress method and linear elastic fracture mechanics method (LEFM), which are more commonly used in manufacturing industry than in structural design. These local approaches are based on the behaviour in the vicinity of the crack initiation point (Heshmati, 2012).

In the localized methods it is possible to consider the different fatigue phases, the methods thereby represent the actual behaviour in a better manner compared to the global approach. A disadvantage of the localized methods is the increasing work effort, as concluded by Marquis and Samuelsson (2005), see Figure 4-2, and the importance of correct modelling when using FEM. The hot spot method can be seen as a method somewhere between a global and local approach since it consider the inhomogeneous stress in the vicinity of the weld but not the local notch effect (Yuan, 2011).
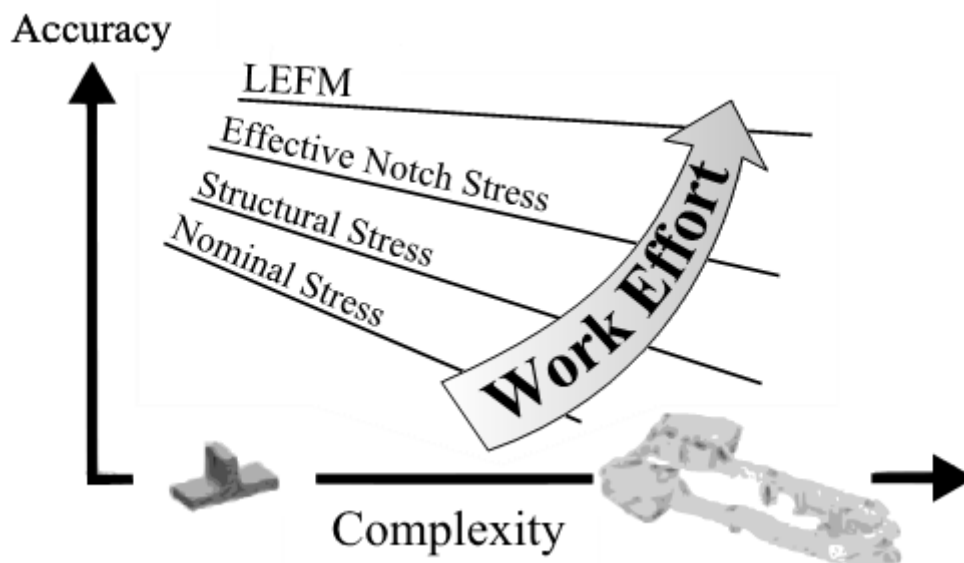
Figure 4-2 Work effort, complexity and accuracy for four fatigue assessment methods (Marquis and Samuelsson 2005)

The build-up of defects caused by the welding process results in that the fatigue life for a welded detail almost exclusively is governed by the crack propagation phase. If this is to be described in a model for fatigue life prediction a crack propagation analysis, a LEFM, gives the closest reflection of the real behaviour (Mann, 2006). However, this is a time demanding and difficult approach requiring a large amount of input information, such as the initial crack length and shape, to be known in advance. Therefore, the crack propagation model cannot substitute the nominal and structural

approaches used in design codes (Radaj, Sonsino, Fricke, 2006) but is rather a tool for researchers and in detail developing. Fracture mechanics and the crack propagation method will not be discussed further in this report.

A short comparison between the global nominal stress approach and the loach structural hot spot and effective notch stress approaches are conducted in Table 4-1. This together with Figure 4-2 gives a good picture of the required input and effort as well as implementation methods used.

Table 4-1 Overview of the three most common fatigue assessment methods

Analyse approach	Load and geometry	Implementation method
Nominal stress	Simplified assumptions	Hand calculations, structural analysis
Structural hot spot stress	Global	Finite element modelling with partitioned mesh
Effective notch stress	Global and local	Finite element modelling with special considerations

The three models uses stresses retracted at different locations in relation to the investigated weld, see Figure 4-3. The used stress is a reflection of the chosen method and how this specifically addresses the problem and which geometrical properties are accounted for as well as how accurate the approach is.
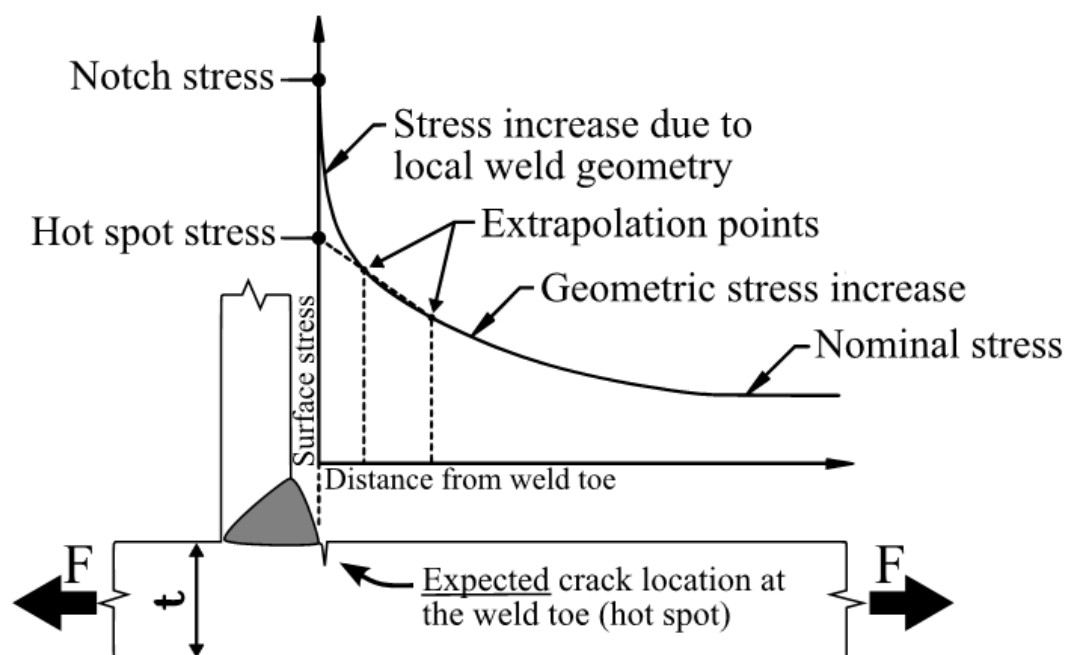
Figure 4-3 Schematic stress diagram in a welded detail (Heshmati, 2012)

As a consequense of the different stresses used as well as the level of complexity of the model, there are diffrents alternatives to be applied when usinge a FE softwere to evaluate the fatigue life. A short overview is given in Table 4-2, the adventages and disadventages of each approach will be discussed more elaborately in Chapter 4.1, 0 and 4.3 respectivly.

Table 4-2 Possible FEA models for the different fatigue life assessment methods for welded structures (Martinsson 2005).

Approach	FEA model	Mesh size	Accuracy
Nominal stress	Part structure	Coarse	Weak
	Assembled structure	Coarse	Weak
	Assembled structure with sub-model	Coarse/fine	Weak
Hot spot	Part structure	Coarse	Weak
		Fine	Average
	Assembled structure	Coarse	Weak
		Fine	Average
	Assembled structure with sub-model	Coarse/fine	Average
Effective notch	Part structure	Fine	Good
	Assembled structure	Fine	Good
	Assembled structure with sub-model	Coarse/fine	Good
LEFM	Part structure	Fine	Good
	Assembled structure	Fine	Good
	Assembled structure with sub-model	Coarse/fine	Good

4.1   Nominal stress approach

The nominal stress approach is the most common fatigue evaluation method in structural design (Aygul, Al-Emrani, Urushade, 2011). This has its reason in the simplicity of the approach itself as well as in determining the stresses (Fricke, 2013). The stresses are calculated with Navier's formula, see Equation 4-1, and all local stress raisers from structural discontinuity or local weld profile are disregarded.

$$\sigma = \frac{N}{A} + \frac{M}{I}z$$ **Equation 4-1**

The stress can also be obtained by the use of FEA as long as stress-raising effects are excluded (Heshmati, 2012). With a general FE model the stress in direct vicinity of the weld is the local notch stress. This stress is the non-linear peak stress in a region with high strain gradient resulting in a stress singularity. When applying the nominal stress method it is not the peak stress that should be used, but the stress away from the weld where it is unaffected of the local notch effect, see Figure 4-4. The obtained

nominal stress is then compared to the allowable value for the corresponding structural detail represented in design codes.
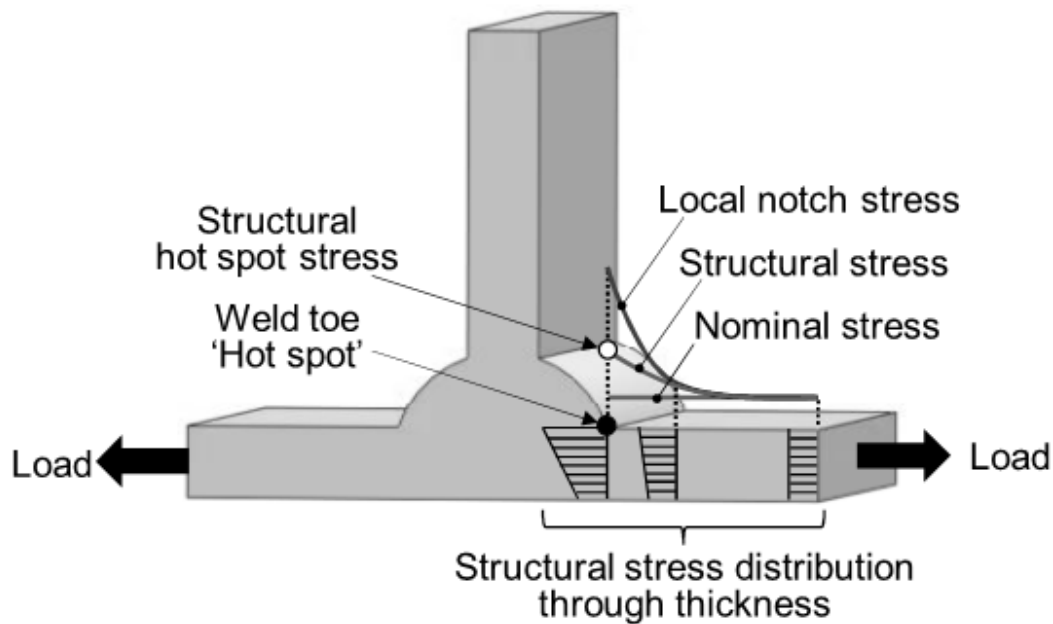
Figure 4-4 Representation of different stresses defined at the weld toe (Takeda and Papalambros, 2012)

Stress raising effects are not included in the nominal stress calculation if they exist due to the structural discontinuity or local weld profile, or effects originating from the same. However, if an abrupt geometrical change occurs near the weld, the nominal stress needs to be modified with regard to this, see Figure 4-5.
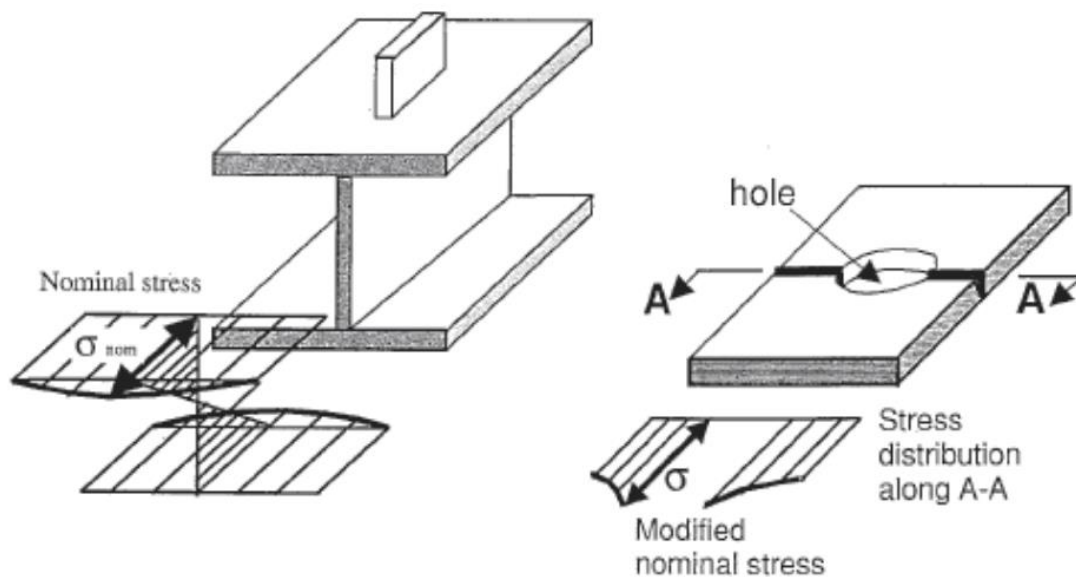
Figure 4-5 (a) Nominal stress distribution in an I-beam with flange attachment; (b) Modified nominal stress in a detail combining butt weld and hole. (Liao, 2011)

The stress raising effect from the weld is not considered when determining the stress, as mention above, instead the effects are considered in the S-N curves (Fricke 2013). The S-N curves are empirically determined, mainly in the 1970th by Maddox, and since they are based on experiments on real welded specimens they naturally include defects and stress raisers of the weld. In Eurocode, fatigue design classes, also called detail classes or FAT, represent common welded details. For each detail the allowed nominal stress range at $2 \cdot 10^6$ load cycles is specified with a survival probability of 95% (EN-1993-1-9). A clarification of the concept of FAT can be studied in Figure 4-6 where the butt weld has a FAT 80, meaning that with a probability of 95% the weld will survive $2 \cdot 10^6$ load cycles with a stress range of 80MPa.
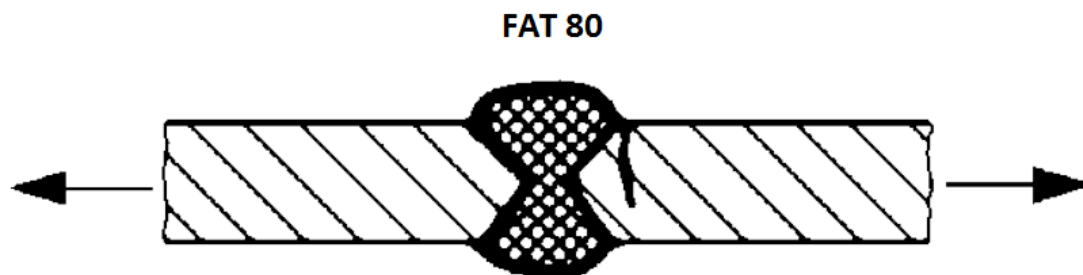
Figure 4-6 Two-sided transverse butt weld with FAT 80 according to structural detail 213 in IIW (2008).

Other influence factors, such as size effect and misalignment effect, are only vaguely treated in the nominal stress approach (Fricke, 2013). These effects are included to a certain degree due to the fact that the S-N curves are based on experiments. However, these experiments are performed on laboratory specimens and not actual structural members. From this follows an uncertainty of to how large degree the defects are accounted for. The specimen used to establish the S-N curves had generally a thickness in the range 10-30mm (Heshmati, 2012). Bridge details can have considerably larger plate thickness resulting in the need to consider the effect due to increased thickness, see Figure 4-7 (a). For plates with a thickness greater than 25mm a strength reduction should be applied (EN 1993-1-9:2005).
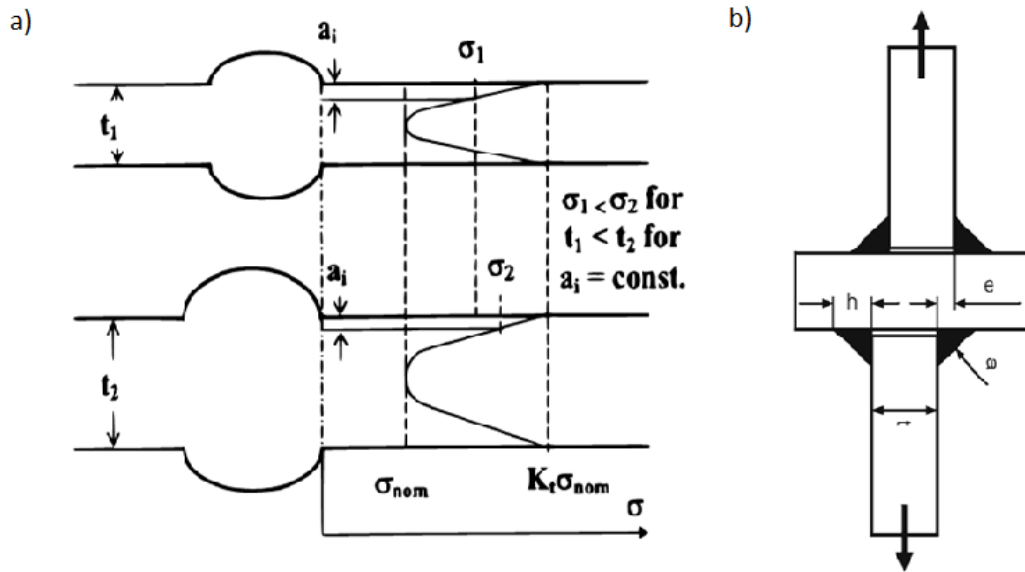
Figure 4-7 (a) Simplified model for description of the geometrical thickness effect for fatigue failures developing from the weld toe, (Berge, 1985); (b) Axial misalignment of a cruciform joint (Fricke, 2013)

Axially loaded welded joints misalignment give rise to secondary bending stresses in the weld, see Figure 4-7 (b). To some extent this is included in the S-N curves because of the natural misalignment in the specimen. Although on components with large misalignment it is recommended to use a reduction factor, k_s see **Equation 4-2**, on the fatigue strength (EN 1993-1-9:2005). Other effects, such as weld throat bending, are not treated in the nominal method, according to this the nominal stress method should only be used when the design case is well represented by one of the detail categories in the code (Fricke, 2013).

$$k_s = \left(\frac{25}{t}\right)^{0.2} \qquad t\ [mm] \geq 25mm \qquad \textbf{Equation 4-2}$$

An OSD has a complex geometry including many stress raisers, from this follows that the welds used in an orthotropic deck are not always well represented in the design codes. The complexity of the deck results in many stress raising effects and difficulty to determine the nominal stress as well as intricate details, as discussed in Chapter 3, which are not well represented in the design codes (Aygul, Al-Emrani and Urushade, 2011). As a consequence the nominal stress approach is not a good fatigue life evaluation method for an OSD since the results are unreliable. More advanced local methods that include the stress raising effects, such as the hot sport or effective notch stress methods, are required together with refined finite element stress analysis to obtain representative fatigue assessments of orthotropic steel decks.

4.2   FE-analysis using structural hot spot stress method

The structural hot spot approach reflects the reality more correctly compared to the nominal stress approach. The hot spot method is a compromise between a global and local approach and accordingly it still contains global simplifications but also considers local effects. In the hot spot method structural stress at a crack initiation

point is determined and used in the fatigue evaluation. The stress amplitude in the detail is compared to the corresponding structural S-N curve to assess the fatigue life of the studied detail.

Hot spots are local areas with risk of fatigue crack initiation. The name 'hot spot' relates to local temperature increase, produced by cyclic plastic deformation prior to the crack initiation (Radaj, Sonsino, Fricke, 2006). The structural hot spot method is only applicable when the fatigue crack initiate from the weld toe (Maddox, 2001). If the failure initiate from the root, the nominal stress approach provided that the correct nominal stress is obtained, otherwise fully locally approaches such as notch stress or notch strain methods are required. In Figure 4-8 principal joints are shown and divided according to if they can be assessed by the hot spot approach or not.
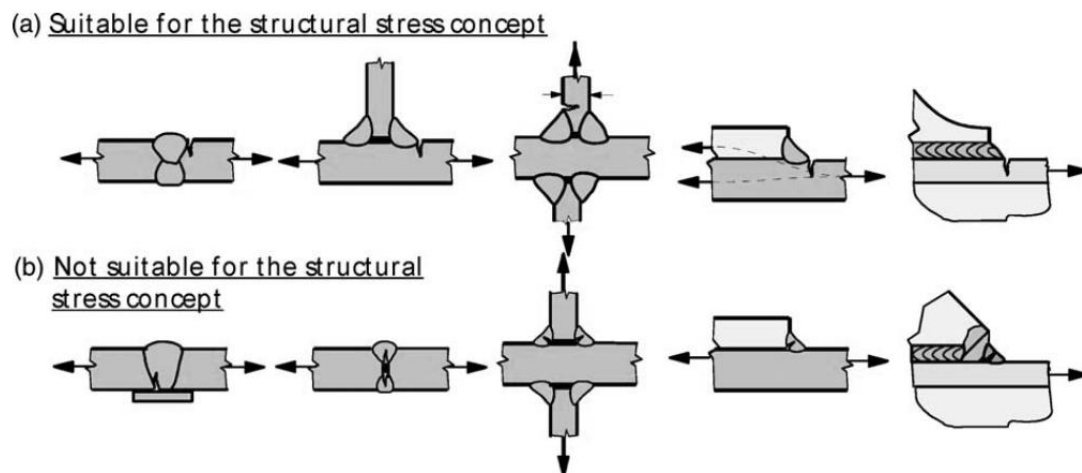
Figure 4-8 The suitability of some welded joints for use of structural hot spot stress in fatigue assessments (Morgenstern, 2005).

The hot spot approach was invented in the 1960s, and developed further in the 1970s, mainly to enable the fatigue assessment of tubular joints in offshore structures (Fricke, 2002). These types of joints experience high local stresses as a result of local bending and superimposed notch effects (Radaj, Sonsino, Fricke, 2006). Also, the nominal stress for this type of details is very hard to obtain. Instead the stress evaluation is performed at a reference point and extrapolated at a given distance from the weld, depending on the thickness making the hot-spot stress a fictitious value (Fricke, 2002).

In complex welded structures, such as orthotropic decks, it can be an important part in the fatigue evaluation to identify all the potential hot spots (Radaj, Sonsino, Fricke, 2006).

The structural stress is either measured in-situ with strain gauges or calculated either with engineering formulas or FEA (Radaj, Sonsino, Fricke, 2006). In the design phase of a bridge the stresses cannot be measured, accordingly the potential methods for finding the structural stress are restricted to calculations or analysis with an FE-model. As mentioned above, the structural hot spot method can be seen as a link between a global approach and a local approach since it includes all stress raising effects except those arising as a consequence of the geometry at the weld toe (Maddox, 2001).

Accordingly, the non-linear peak stress caused by the local notch, the weld toe, is excluded from the structural hot spot stress.

Three possible fatigue critical areas exist in welded joints for plate-type structures and can be seen in Figure 4-9. These are:

a) Weld toe on plate surface at the end attachment
b) Weld toe on plate edge at the end attachment
c) Weld toe on plate surface amid the weld along the attachment

Type a) and c) are depending on plate thickness while type b), edge cracking from weld toe or end, is usually not. Therefore the methods generally used to evaluate type a) and c) failures are not suitable for type b) failures. Since type b) cracks rarely arises in orthotropic deck they will not be discussed further in this report.
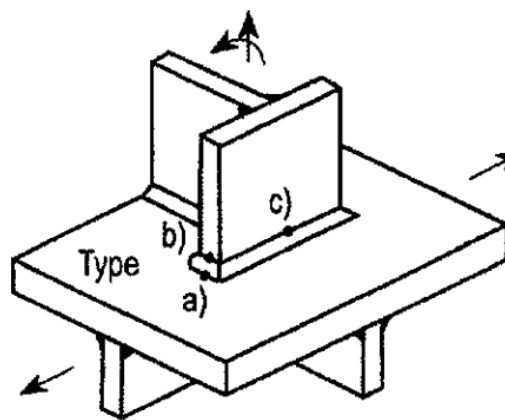
Figure 4-9 Three types of fatigue-critical weld toes in plate-type structures (Maddox, 2001)

The structural stress is in fact a fictitious value, extrapolated from reference points or calculated at a certain distance from the weld toe (Fricke, 2002). Determination of the structural stress eliminates the non-linear peak stress in vicinity to the weld toe. Only extrapolation of the surface stress will be treated further in the report.

The structural stress is calculated by determine the stress level at two or three reference points at given distances from the weld toe in the stress direction (IIW, 2006). Close to the weld, the stress will have a non-linear peak value, referred to as notch stress, see Figure 4-10, due to the influence of the local notch created by the weld toe. As a consequence of this the closest reference point has to be located away from the weld toe, avoiding this stress raising effect. According to the IIW (2006) recommendations this distance is 0.4t from the weld toe, where t is the plate thickness, see Figure 4-11.
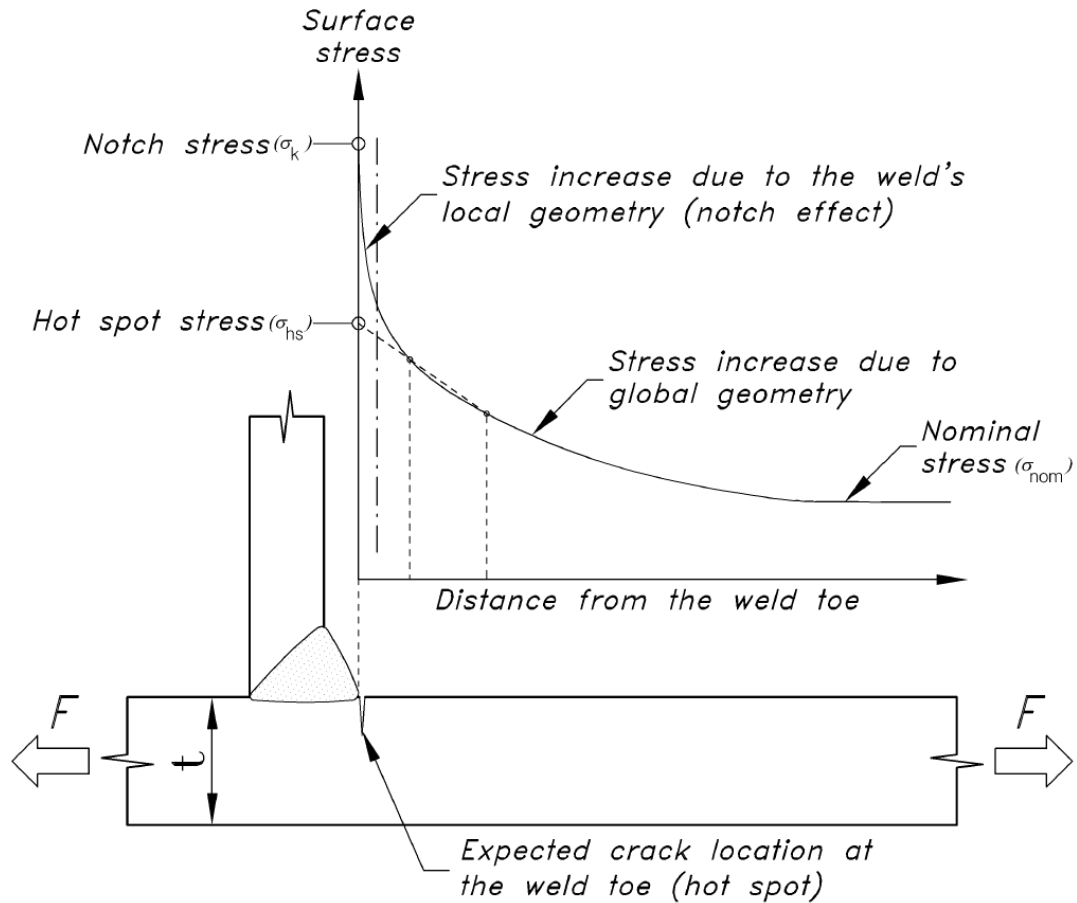
Figure 4-10 Stress state at a transversally loaded fillet weld toe and definitions of different stress concepts (Akhlaghi, 2009)
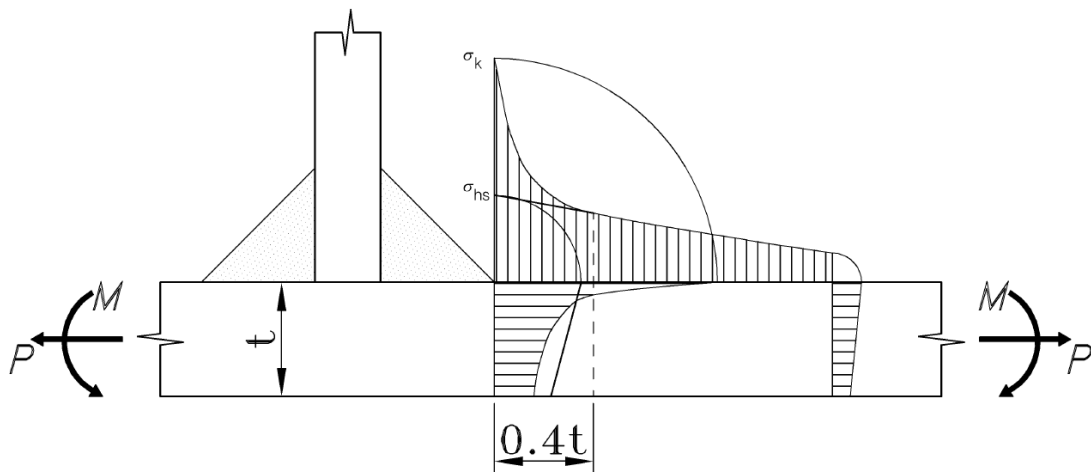
Figure 4-11 Illustration of the stresses in the hot-spot area (Akhlaghi, 2009).

The hot spot method has several advantages when it comes to OSDs. However, when FEM is used the results are heavily influenced by the mesh density and the element properties, such as element length and type (IIW, 2006). According to IIW (2006), if FEM is used and a mesh with element size less than 0.4t at the hot spot must be used.

The hot spot stress can be obtained by use of **Equation 4-3**, where $\sigma_{0.4 \cdot t}$ is the stress at distance 0.4t from the hot-spot.

$$\sigma_{hs} = 1.67 \cdot \sigma_{0.4 \cdot t} - 0.67 \cdot \sigma_{1.0 \cdot t} \qquad \text{Equation 4-3}$$

As for the nominal stress approach the fatigue resistance should be reduced for specimens with a thickness exceeding 25mm when using the structural hot spot method. The resistance is reduced by multiplication of the fatigue strength with a reduction factor, k_s, see Equation 4-4. The thickness correction exponent, n, is determined according to Table 4-3, and the effective thickness is determined according to Figure 4-12 below.

$$k_s = \left(\frac{t_{ref}}{t_{eff}}\right)^n \qquad t_{ref} = 25mm \qquad \text{Equation 4-4}$$

Table 4-3 Thickness correction exponent (IIW, 2008)

Joint category	Condition	n
Cruciform joints, transverse attachments, ends of longitudinal stiffeners	As welded	0.3
Cruciform joints, transverse attachments, ends of longitudinal stiffeners	Toe grounded	0.2
Transverse butt welds	As welded	0.2
Butt welds ground flush, base material, longitudinal welds or attachments	Any	0.1

if $\quad \dfrac{L}{t} > 2 \qquad$ then $\quad t_{eff} = t$

if $\quad \dfrac{L}{t} \leq 2 \qquad$ then $\quad t_{eff} = \max(0.5 \cdot L, t_{ref})$
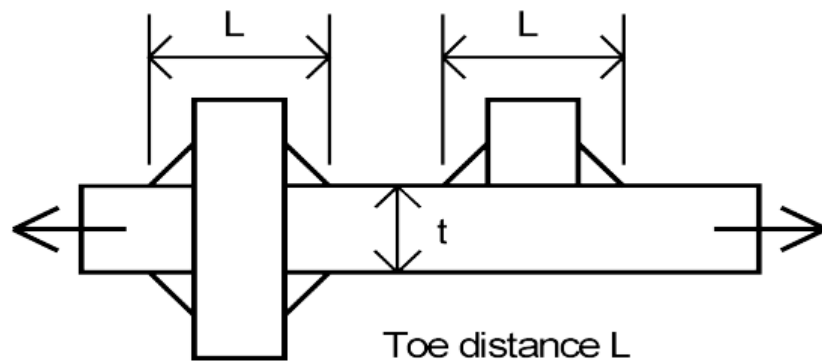
Figure 4-12 Definition of toe distance (IIW, 2006)

The structural hot spot approach is, as mentioned, superior to the nominal stress method. Although it requires somewhat more calculations as well as initial assumptions or input data the working effort and complexity is reasonable. The hot spot approach is a good alternative for structural design if more realistic results are required and used for this purpose in similar industries. However, the hot spot method does not take account for all effects and if even more credible values are needed other approaches should be considered. Though, this is more applicable in the detail manufacturing industry rather than in structural design.

4.3   FE-analysis using effective notch stress method

For modelling the behaviour in the welded member closer to the real behaviour the effective notch stress approach is a possible option. This method is more time demanding and computational heavy as well as requiring more input parameters than the hot spot approach. However, the results reflect the reality closer since they account for the stress raising effects the weld inflict on the member.

The effective notch stress is the highest elastic stress and is found at the crack initiation point, at the weld toe or root, see Figure 4-13. The real weld contour is replaced by an effective one to account for the statistical nature and scatter of the weld shape parameters (Martinsson, 2005). The effective notch root radius, ρ, has been proposed by Radaj et.al (2006) to $\rho = 1$ mm for thick walled members, $t \geq 5mm$, and is included in the IIW design recommendations against fatigue.
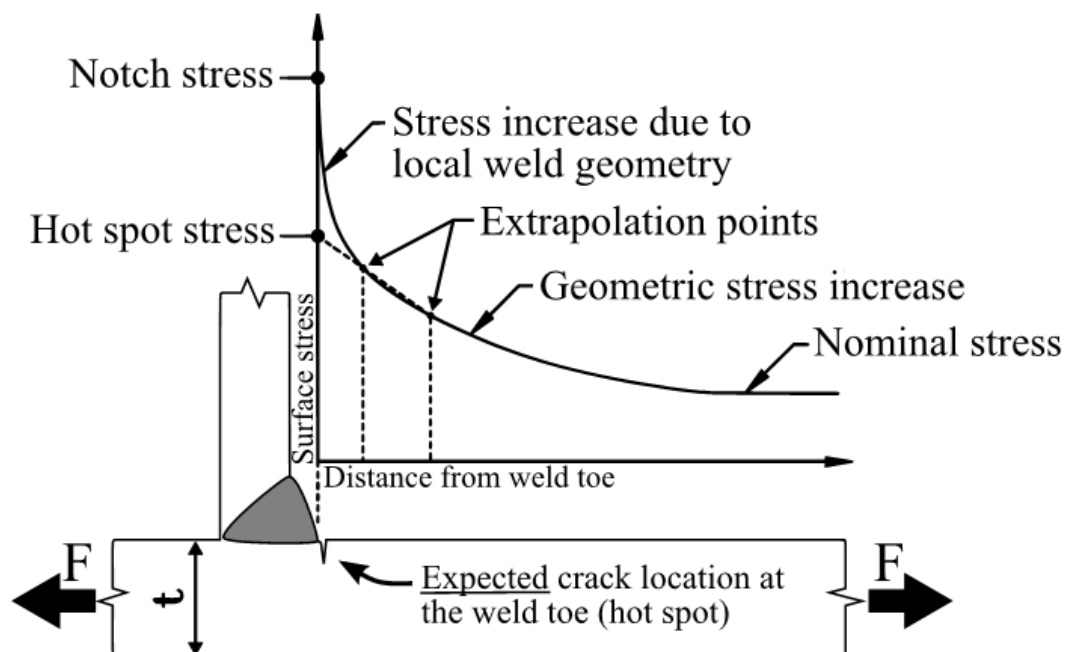
Figure 4-13 - The surface stress in the vicinity of a tensioned fillet weld and some stress concepts (Hesmathi, 2012).

Another variant of the notch stress method is used for thin-walled welded joints, with plate thickness <5mm, where the reference radius is set to $\rho=0.05$ mm (Sonsino et.al, 2010). This variant mainly used in the automotive industry and is not practical in structural design due to the, in general, thick plates required. Other reference radius have been suggested, however only a limited number. The inadequate amount of reference radius has been questioned by Schijve (2010), who instead propose a reference ratio, ρ/h, between the notch radius and a weld dimension, h. A ratio between the notch radius and the geometric properties of the weld would result in a continuous interval depending on the weld dimensions. Although the studies on this subject are not substantial enough to endorse this approach at present. For big as-welded structures the members are usually classified as thick-walled and the reference radius is set to $\rho=1$ mm.

The fatigue strength of a member is highly affected by its "notch effect". The notch effect includes the stress concentration as well as the strength reduction related to notched members (Radaj, Sonsino, Fricke, 2006). The elastic stress concentration factor k_t, see **Equation** 4-5, is the ratio between the local notch stress, σ, and the nominal stress, S_{nom}, based on the assumption of linear elastic material behaviour, and can be used to determine the severity of a notch (Dowling, 2012).

$$\sigma = k_t \cdot S_{nom}$$

Equation 4-5

In high cycle fatigue the elastic stress concentration factor actually have a lower influence on the fatigue life than proposed by the k_t-factor, this is showed by experiments performed by MacGregor (1952). Instead another reduction factor should be used in high cycle fatigue, the fatigue notch factor denoted k_f, see Equation 4-4, (Radaj, Sonsino, Fricke, 2006). The fatigue notch factor is always smaller than the elastic stress concentration factor, $k_f < k_t$, with higher discrepancy for smaller notch radii.

$$k_f = \frac{\sigma_{ar}}{S_{ar}}$$

Equation 4-6

σ_{ar} = Completely reversed stress for a smooth member

S_{ar} = Completely reversed stress for a notched member

The fatigue notch factor is derived from the elastic stress concentration factor together with a 'microstructural notch support' hypothesis (Radaj, Sonsino, Fricke, 2006). The 'microstructural notch support' hypothesis says that a material is not sensitive to the peak stress occurring at the notch but rather the average stress that acts in a small, but final, region in close vicinity of the notch (Dowling, 2012). The active region where the mean stress is calculated over is generally referred to as the process zone. Several hypotheses can be used, e.g. the 'stress averaging approach' by Neuber.

The basic theory is the same for the different alterations of the effective notch stress method but the following theory and implementation differs a great deal. Accordingly the choice of method has to be conducted with regard to applicable conditions and available information. The effective notch stress method is not used in structural design as a consequence of the high computational effort required and will not be evaluated further in this report. However, it is an important tool in detail analysis and may be implemented in design procedures in the future.

5 Design calculation and structural performance of orthotropic bridge decks with conventional methods

Conventional methods used in bridge design today are usually based on the global behaviour of the bridge and do not account for the numerous local behaviours described in Chapter 0. The design process disregards several effects, some of which are essential for an accurate and sound design of orthotropic bridge decks.

In this chapter an introduction to the conventional design method is presented. This is later, in Chapter 7.4, used as a basis for the comparison between the simplified hand calculations and the advanced FEM analysis. To get a better understanding of the overall behaviour the first subchapter, Chapter 5.1, present the structural design of the different components in an OSD from a global perspective. The load is calculated from the top of the structure to the ground and each component is designed to resist the load separately. The second subchapter, Chapter 5.2, focus on the fatigue design process, where the welds are evaluated separately with the corresponding stress level and fatigue class. In the second subchapter it is also include a short summary of the load model recommended by Eurocode.

In the following chapter all statements and assumptions referred to are an appraisal of thorough studies of design of the bridge Saltsjöbron. The bridge Saltsjöbron is an existing bridge located in Södertälje. It is a movable steel bridge with two bascule parts and an orthotropic deck which was designed according to the standard BRO94.

5.1 Global structural analysis

The conventional design process seen from a global point of view evaluates each structural component separately with regard to its load situation and structural capacity. In an OSD the global behaviour can be simplified into a load path where the load is transferred from the wearing surface → deck plate → ribs → floor beams → main girder, see Figure 5-1.
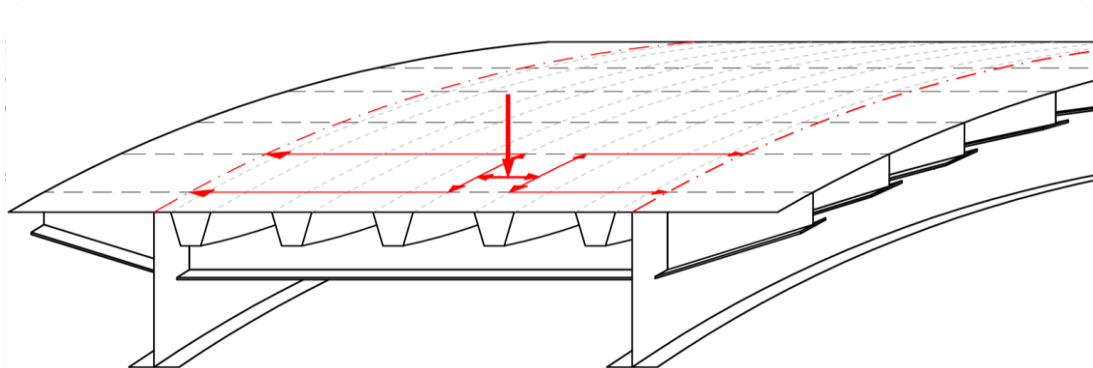
Figure 5-1 Load path in an orthotropic steel deck bridge

The separate parts are evaluated with regard to their structural behaviour. The different parts are described briefly with the loads acting on them and their behaviour.

Structural models of the separate sub-systems are presented as well as general comments.

5.1.1 Deck plate

The deck plate transmits the load to the ribs and also acts as a top flange for the ribs, floor beams and main girders. The deck plate also interacts with the wearing surface in distributing wheel loads.

The governing load for the deck plate is the concentrated wheel load. The main component of the wheel load will be the vertical load due to the weight of a truck. Other components of the wheel load rising from trucks changing lanes or break are disregarded due to the high horizontal stiffness of the deck plate, resulting in small load effects in comparison with the vertical component of the wheel load. The wheel load is distributed through the wearing surface to the deck plate, resulting in a larger load distribution area and lower stress. This can be seen in Figure 5-2 below. The figure is a principal illustration of a wheel load on the deck plate and dispersion through the wearing surface is shown. The dashed lines are the walls of the ribs. The inner rectangle is the actual loading size applied as wheel pressure on the wearing surface. The outer rectangle, with given dimensions, is the loading size on the deck plate after dispersion through the wearing surface.
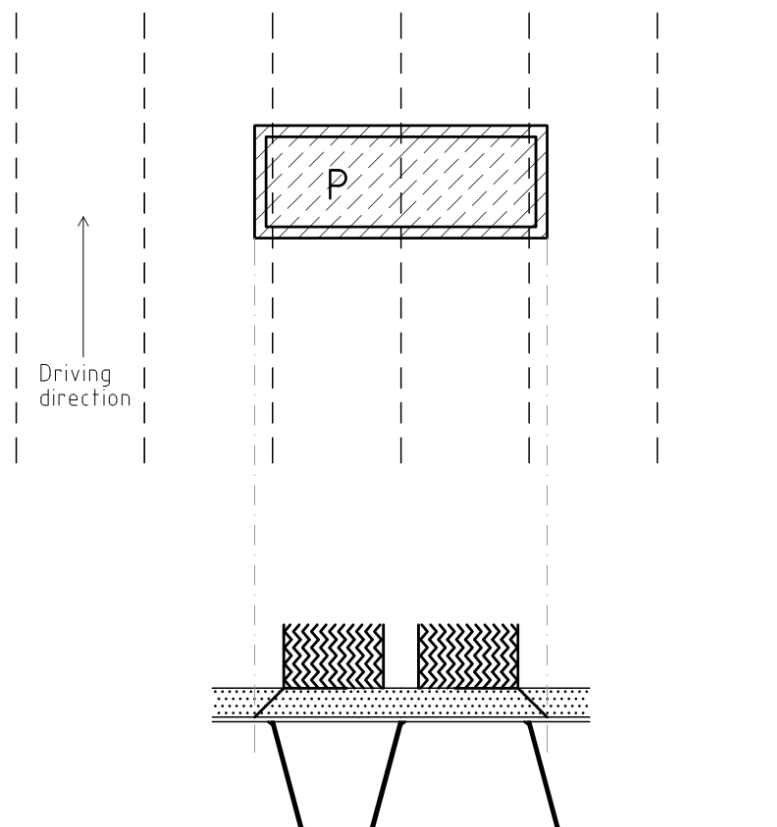
Figure 5-2 Structural system for deck plate and load dispersion in the wearing surface

The load is assumed to distribute through the wearing surface with a dispersion of 1:1. This is not always the case, e.g. when the surface layer is worn down or at high temperatures there is almost no dispersion. If seen over the whole service life this is an assumption on the unsafe side but if no load distribution would have been assumed it would have been very conservative.

The load is distributed over the wheel pressure area and converted into a transversal line load. The model used to calculate the moment forces in the deck plate is a continuous beam with two spans, see Figure 5-3 below. The load acting outside of the outer rib walls are disregarded in the model. This simplification is on the unsafe side.
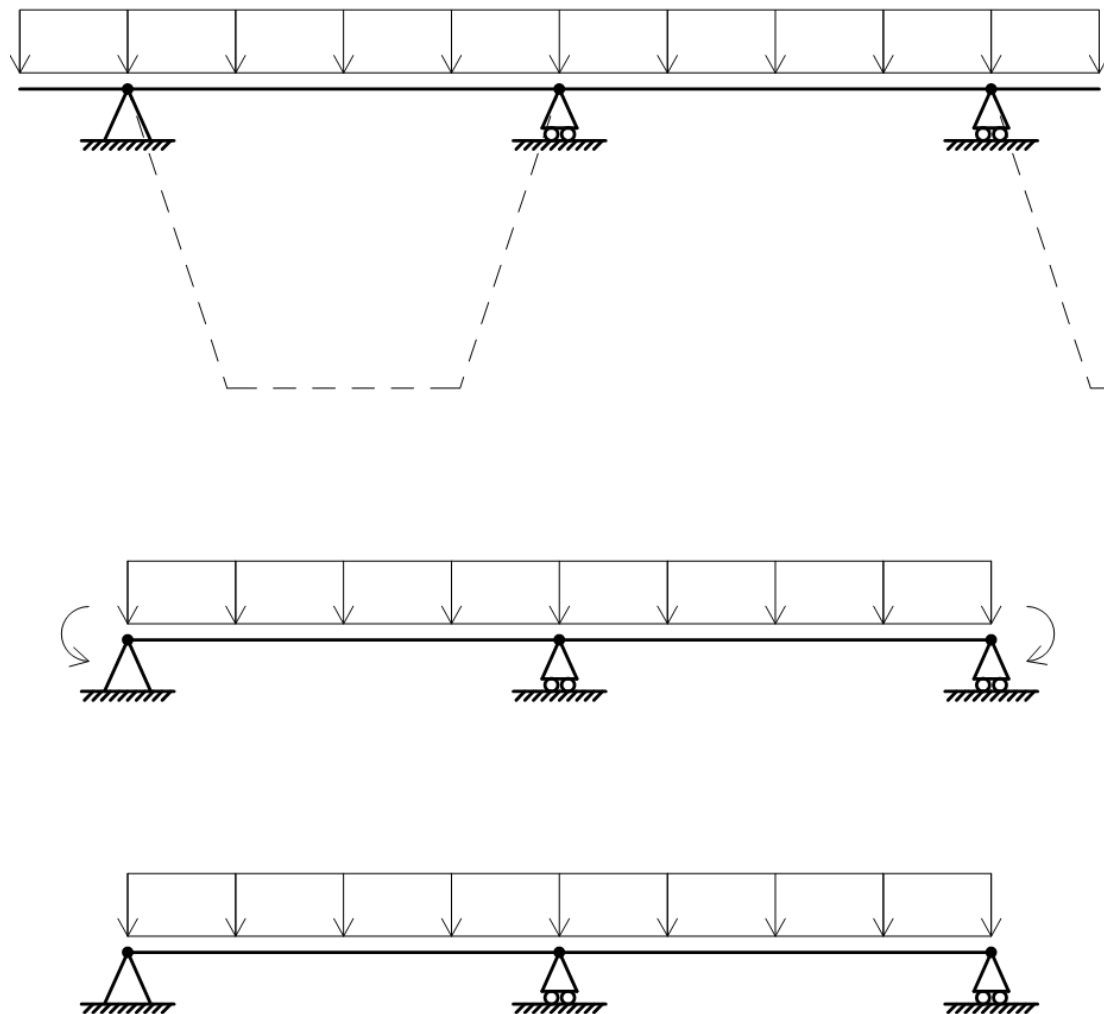
Figure 5-3 Different models to describe the wheel load over the rib walls; (a) The actual model of the load on the deck plate over ribs; (b) Shortened model of deck plate with added moments; (c) The third model disregard the moments at the supports and this is the one used in hand calculations.

The load is mainly distributed to the ribs, in the transversal direction, and only a small part is distributed directly to the floor beams, longitudinal direction. As a result of this, together with the fact that the plate is very stiff in the longitudinal direction the analysis is mainly focused on the transversal behaviour.

The deck plate is analysed in transversal direction with the structural model as can be seen in Figure 5-4. The rib walls are seen as stiff supports and the load considered is

the one in the spans between these rib walls and not the part of the load on the other side, as described in Figure 5-3. The acting wheel load is converted to a line load and the deck plate is analysed as a beam with the same thickness as the deck plate and the width is set as the width of a wheel, referred to as *b* below.
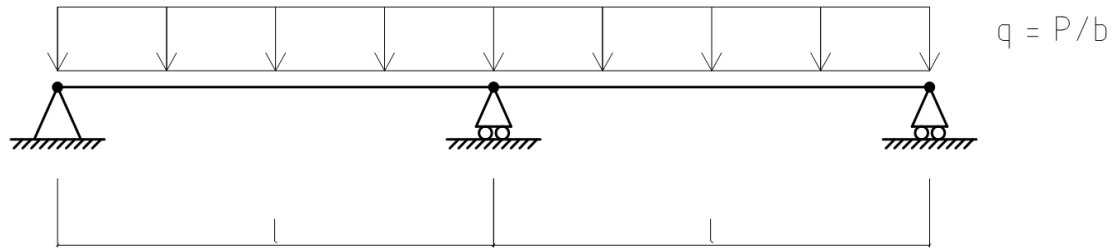
Figure 5-4 Structural model for the deck plate

$$M_{mid-support} = \frac{ql^2}{8}$$

<div align="right">**Equation 5-1**</div>

The maximum moment is found at the mid-support, according to Equation 5-1, and is compared to the moment resistance, see Equation 5-2, Equation 5-3, Equation 5-4 and Equation 5-5. The check is for yielding in Ultimate Limit State, ULS. The load carrying width of the plate is calculated by the use of Pusher diagram to account for longitudinal load distribution, see Figure 5-5.
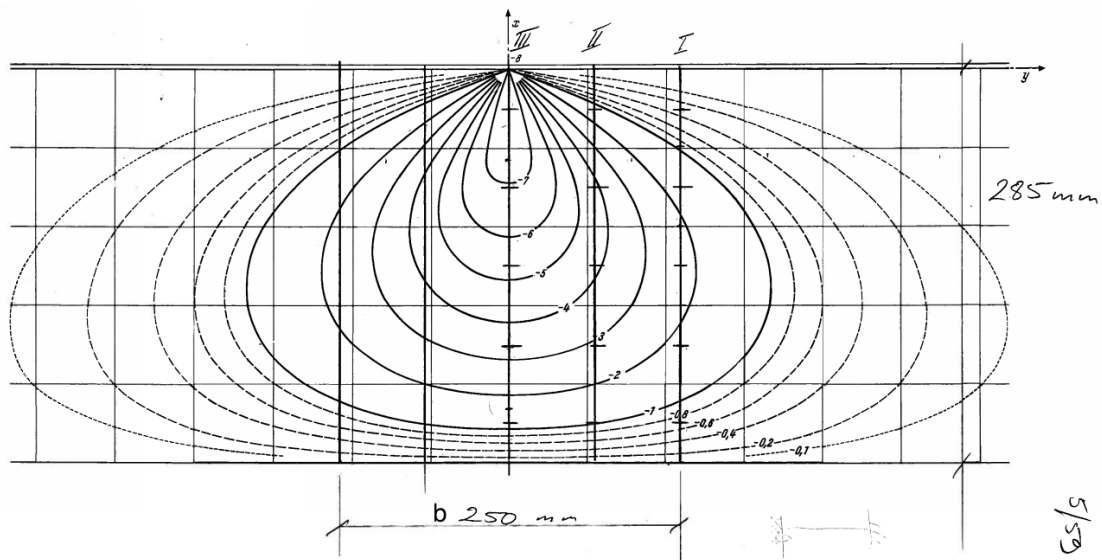
Figure 5-5 Pusher diagram used in calculations of the load distribution in deck plate in the Saltsjö Bridge

$$\sigma \leq \sigma_y = f_y$$

<div align="right">**Equation 5-2**</div>

$$f_y = \sigma_y = \frac{M_y}{W} = \frac{M_{Rd}}{W} \qquad \qquad \textbf{Equation 5-3}$$

$$W = \frac{b \cdot t^2}{6} \qquad \qquad \textbf{Equation 5-4}$$

$$M_{max} \leq M_{Rd} = f_y * W \qquad \qquad \textbf{Equation 5-5}$$

5.1.2 Longitudinal stiffeners – Ribs

The rib acts as a beam with a box section, with an effective part of the deck plate acting as top flange. The ribs are modelled as a continuous box beam, with the effective part of the deck plate as the top flange, see Figure 5-6 below.
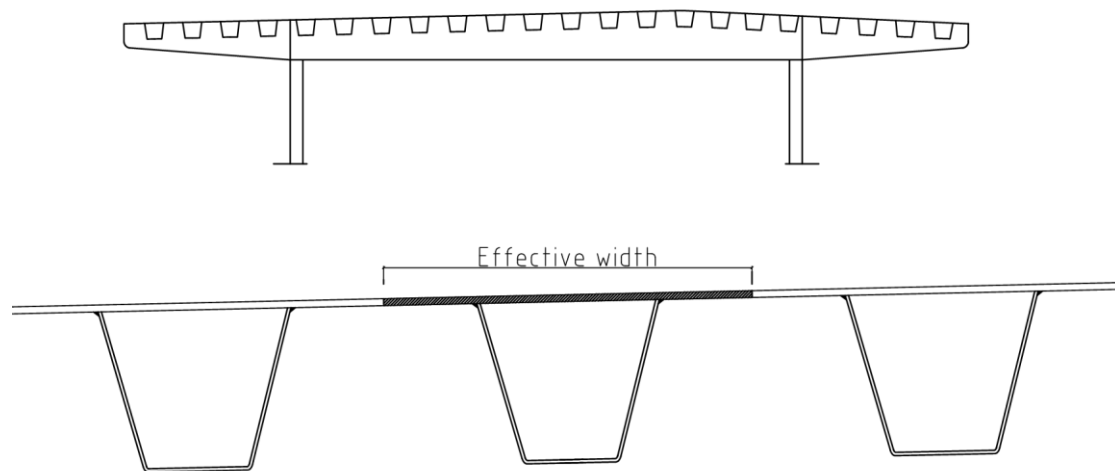
Figure 5-6 Structural model and effective width for the trapezoidal ribs

The ribs receive load from the deck plate and transfer it to the floor beams. The acting loads are the traffic load together with self-weights of the members and temperature load in the deck. The governing load for traffic is the load from a single truck wheel, the same load that governs the deck plate.

In the analysis conducted to retrieve the design moment the wheel is usually placed centrically above the rib, see Figure 5-8.
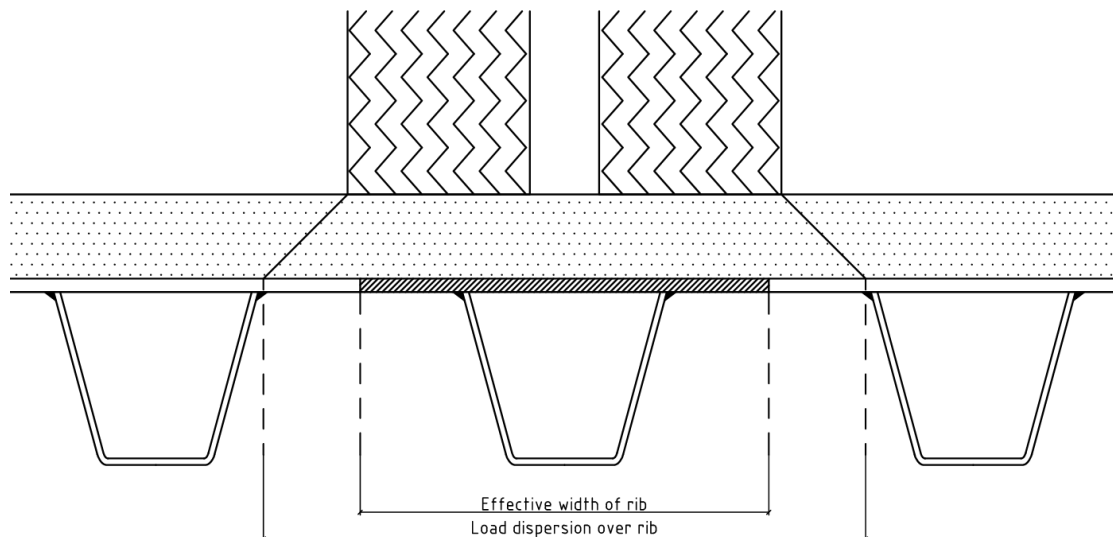
Figure 5-7 Effective width of the rib-beam and the actual length the load is acting over

The ribs are modelled as a continuous beam over the floor beam. The floor beams can be seen in Figure 5-8. When modelling the floor beams as support for the ribs, two different models are used. In model 1, see Figure 5-9, the floor beams are represented by stiff supports and in Model 2, see Figure 5-10, by spring supports. The highest shear and moments from the two models are compared and the governing (maximum) is used in the design of the ribs. All the ribs are design according to the worst case scenario, disregarding many influence factors such as varying deflection between floor beams, and varying moment distribution over the bridge.
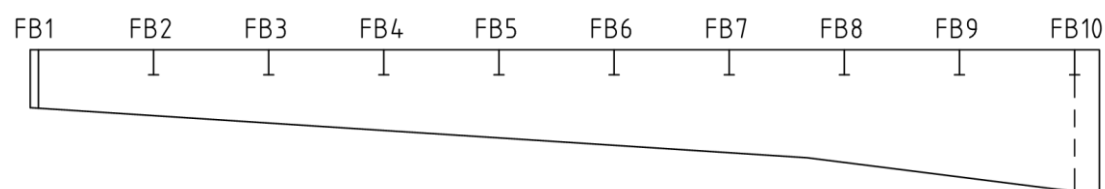
Figure 5-8 Section of floor beam location in the main girder

Model 1: The floor beams are represented with (one) pinned and roller supports (Figure 5-9).

Model 2: The floor beams are represented with elastic springs. The spring stiffness is represented by corresponding floor beam deflection (Figure 5-10).

Figure 5-9 Model 1
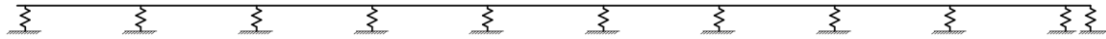
Figure 5-10 Model 2

The ribs are analysed as a separate box beam. The wheel load will distribute to adjacent ribs, but this interaction is disregarded and only the load carried by the examined rib is included. This simplification is on the safe side.

The spring stiffness representing the support from the floor beams to the rib in Model 2 is calculated by the corresponding floor beam deflection in the middle of the span between the main girders, see Figure 5-11 and Equation 5-6. In this simplification all ribs are assumed to have the same stiffness, the lowest stiffness, regardless of the location in relation to the girders. In reality the ribs closer to the main girder will deflect significantly less and therefore have a higher stiffness. However, this is disregarded and only the worst case for the span moment is studied. The calculation and model for the spring stiffness can be seen below.
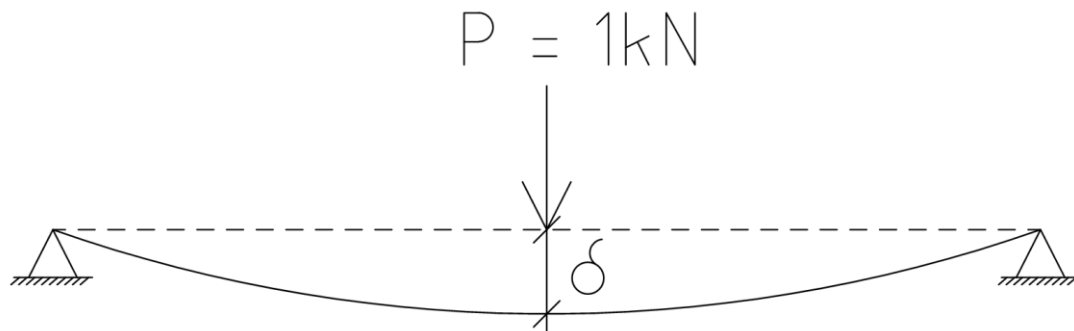
Figure 5-11 Model used for calculation of the spring constants

$$F = \delta = \frac{Pl^3}{48EI}$$

Equation 5-6

Another simplification made is the negligence of the cantilever part in the floor beam deflection calculations. The cantilever part would give a restraint moment, lifting the deflection curve. Instead the end of the floor beams are represented by pinned support allowing free rotation, see Figure 5-12. This result in larger deflections than in reality, and therefore smaller stiffness's for the springs. When considering the span moment this is on the safe side, however if the support moments are considered a fixed support generates higher support moments. Here the span moment is assumed to governing and the first assumption is the one proceeded with.
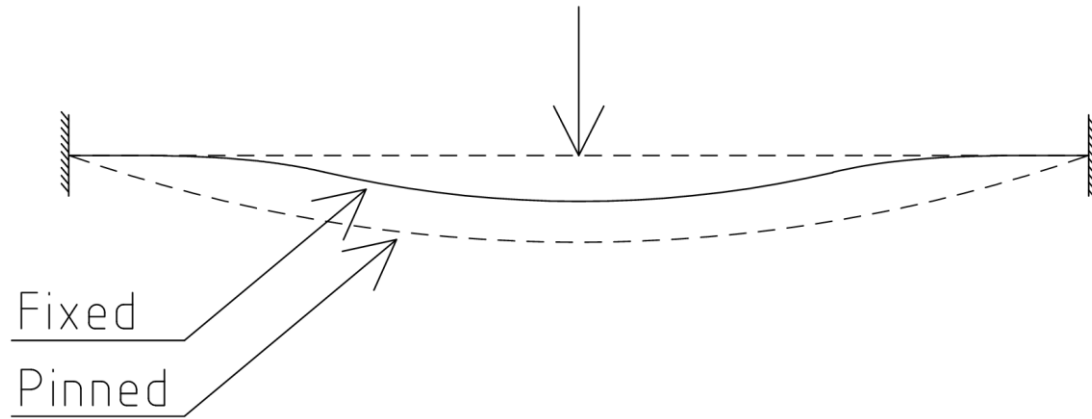
Figure 5-12 Difference between the pinned model, the used one, and a fixed model, the real behaviour is somewhere in-between

Model 2 gives the highest moment force. The field moments are higher, but also the support moment due to the stiff K-Joint that is represented by the single pinned support, see Figure 5-13. The highest shear force is obtained in Model 1 with pinned support.
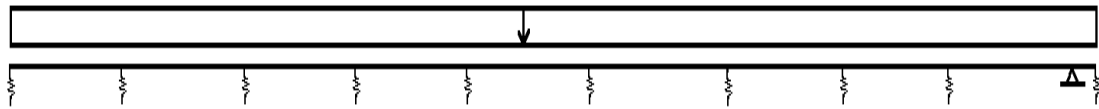
Figure 5-13 Model 2 with the K-joint represented by an unyielding pinned support

The moment and shear force are compared with the moment resistance, M_{Rd}, and the shear resistance, V_{Rd} and also the interaction between these. These resistances are calculated with effective cross sections according to recommendations regarding cross sectional classes.

$$\sigma \leq \sigma_y = f_y \qquad \text{Equation 5-7}$$

$$f_y = \sigma_y = \frac{M_y}{I_{ef}} \cdot z_{ef} = \frac{M_{Rd}}{I_{ef}} \cdot z_{ef} \qquad \text{Equation 5-8}$$

$$M_{max} \leq M_{Rd} = f_y \cdot \frac{I_{ef}}{z_{ef}} \qquad \text{Equation 5-9}$$

The reaction forces at the floor beam supports in the models are transferred from the ribs to floor beams through the welds in the connection. Mainly the vertical welds transfer this reaction. The stresses in the weld between the rib and floor beam caries

the reaction force from the rib corresponding to τ. Accordingly, the parallel stress in the weld is calculated using the reaction forces from the models, see Equation 5-10, and compared to the detail category.

$$\tau_{\parallel,weld} = \frac{\Delta R_{fatigue}}{A_{weld} \cdot n_{welds}}$$

<div align="right">**Equation 5-10**</div>

5.1.3 Transversal stiffeners – Floor beams

The transversal floor beams main function is to transfer the acting loads from the ribs to the main girders. The main loads on the floor beams are reaction forces from the ribs. However, load applied on the deck plate close to the floor beams will be transferred direct without passing through the ribs.

In the bridge Saltsjöbron there are in total 10 floor beams in each of the bascules, see Figure 5-14. Floor beam 1 and 10 have a significantly higher stiffness than the intermediate located floor beams 2 to 9 and are therefore not the governing in design. Floor beam 2-9 are identically designed and the cross-section of the bridge and one of these floor beams can be seen in cross section in Figure 5-15
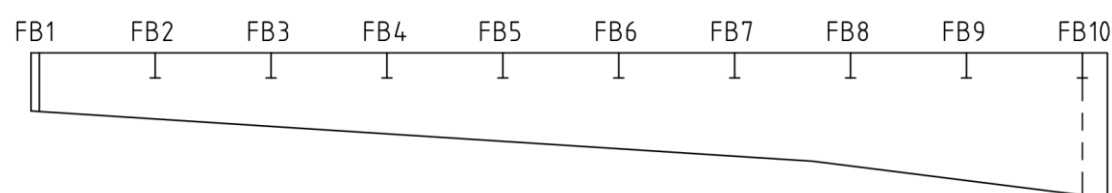
Figure 5-14 The location of the floor beams in one of the leafs of the bridge. TV1 and TV10 have reinforced cross-sections and are thereby stiffer than floor beam 2 to 9. The distance between floor beams can also be seen.
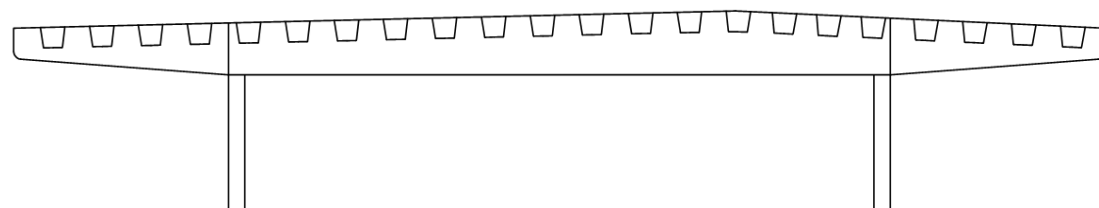
Figure 5-15 Cross-section of floor beam 2 to 9

The floor beams are supported by the main girders resulting in both an internal part and two cantilever parts. An important aspect is the loss of cross section where the ribs pass through the floor beams, see Figure 5-16. The recess at the web of the floor beam results in complex and local stresses as well as local reduction of the stiffness. The width of the resisting top flange is determined based on the concept of effective width. The cross-section of the floor beam at the rib intersection can be seen in the Figure 5-16.
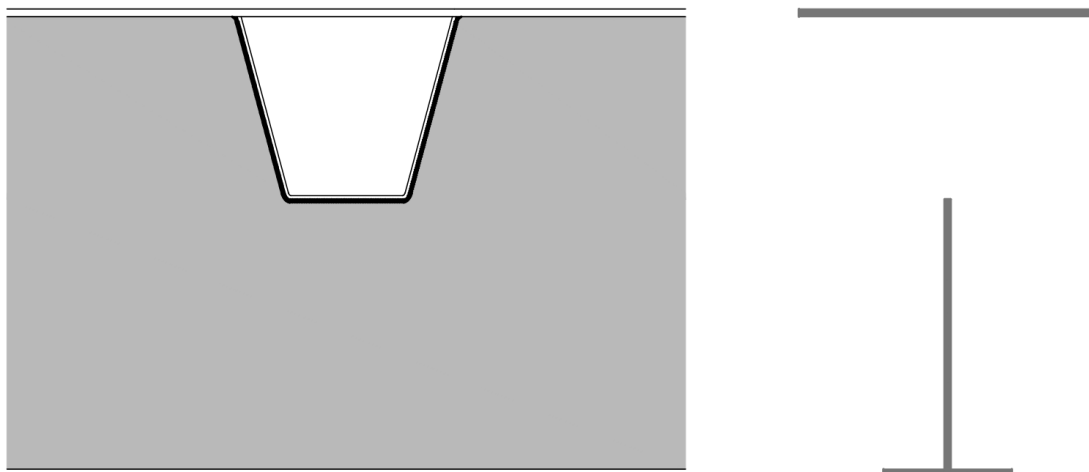
Figure 5-16 Effective cross-section of floor beam at intersection with longitudinal rib for a floor beam without cut-out in the web at intersection with the rib

The studied bridge has no cut-outs in the floor beam web where the ribs connect, see Figure 5-16. The main reason for this choice is to simplify the buckling calculations according to codes, not for a structural reason related to performance. Without cut-outs the region in the vicinity of the horizontal weld usually experiences a severe stress state and is very prone to fatigue.

Several different loads act on the floor beams. The main loads can be seen in Figure 5-17 below. The traffic load includes both distributed load and wheel loads. The wind load acts horizontally on the traffic on the bridge as well as on the height of the bridge itself. The wind load component on the floor beams is represented by two point loads, one from the reaction of the wind on the traffic and one from the reaction on the structural height of the bridge. The component from the wind load acting on the bridge is mainly taken in the deck plate due to the high horizontal stiffness. The wind load acting on the traffic is applied in the centre of a standard truck. According to this both the components will have an eccentricity to the neutral axis of the floor beam and an additional moment will arise.
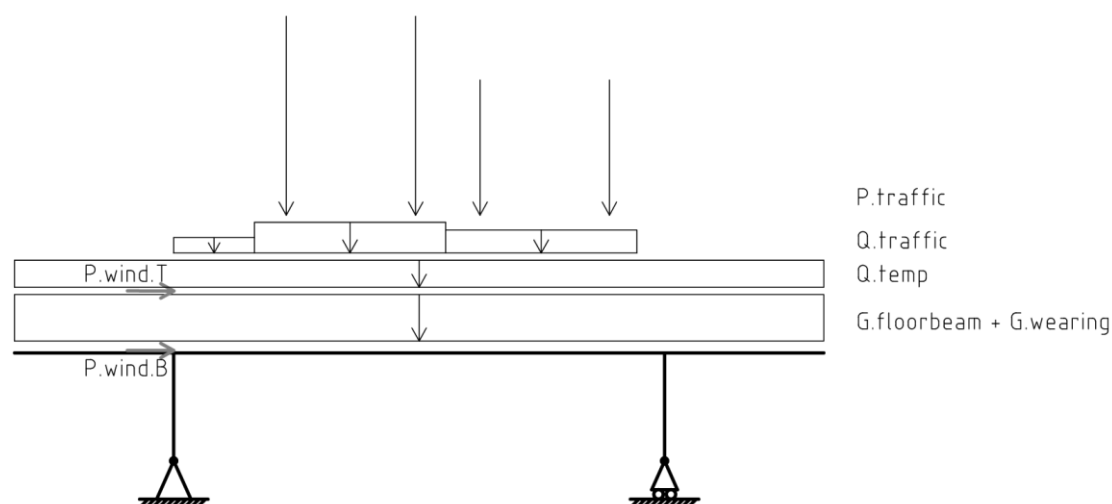
Figure 5-17 Structural load situation for floor beams

The floor beam is studied in two different models, the internal part between the main girders and the cantilever parts, outside of the main girders. The cantilever part is modelled as a cantilever beam fixed at the main girder connection. This is a simplification on the safe side.

The model used to analyse the internal part of the floor beam is modelled as a frame where the top beam represents the floor beam and the two frame legs representing the main girders. The boundary conditions are set to one pinned and one roller supports at the end of the frame legs. However, the behaviour of the main girder would be more realistically represented if a horizontal spring was included to restrain the horizontal translation to include the stiffness of the main girders.
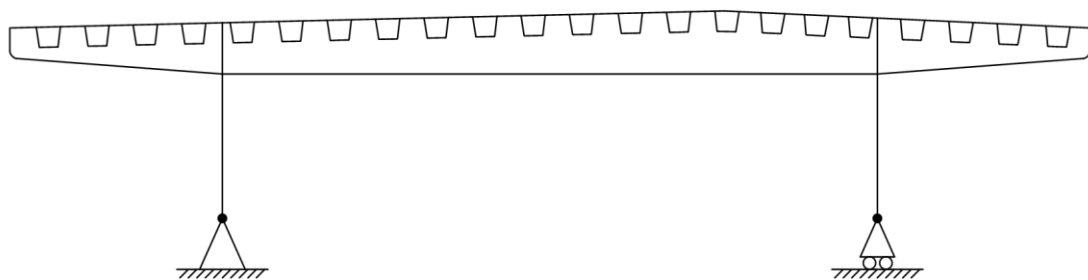
Figure 5-18 Boundary conditions for the structural model for the middle part of the floor beam
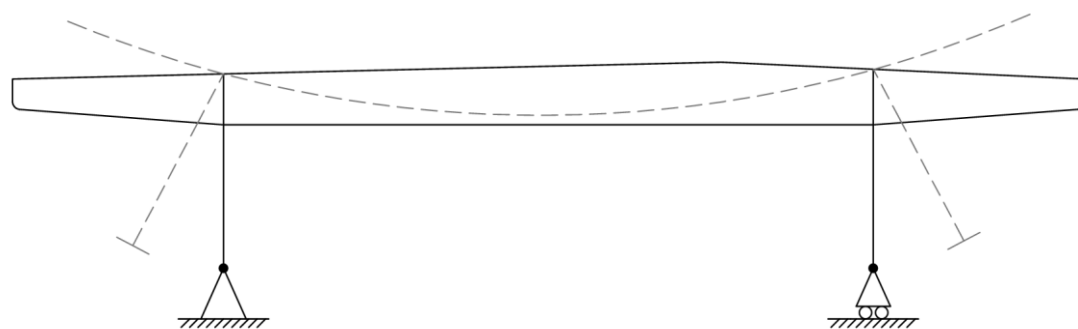
Figure 5-19 Structural model for the middle part of the floor beams and the bending behaviour

The highest shear force is found close to the main girder and the highest moment is found in the middle region. The shear force and moment are compared to the cross-sectional resistance based on the effective cross section with the rib cut-out excluded. Also instability and interaction between shear and moment are checked.

The floor beams will experience a multi-axial stress state. The floor beams bend transversally and the main global system bend longitudinally, see Figure 5-20. At the intersection with the main girders the floor beams are forced to bend longitudinally giving them a multi-axial stress state which has to be regarded in the design.
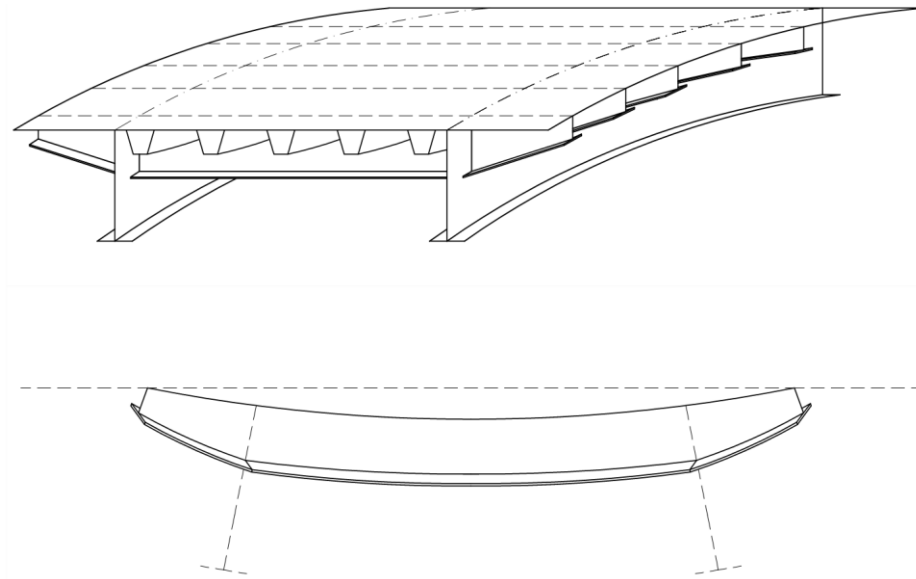
Figure 5-20 (a) Bending of bridge in the longitudinal direction of the main girders; (b) Bending of floor beam in the longitudinal direction of the floor beam
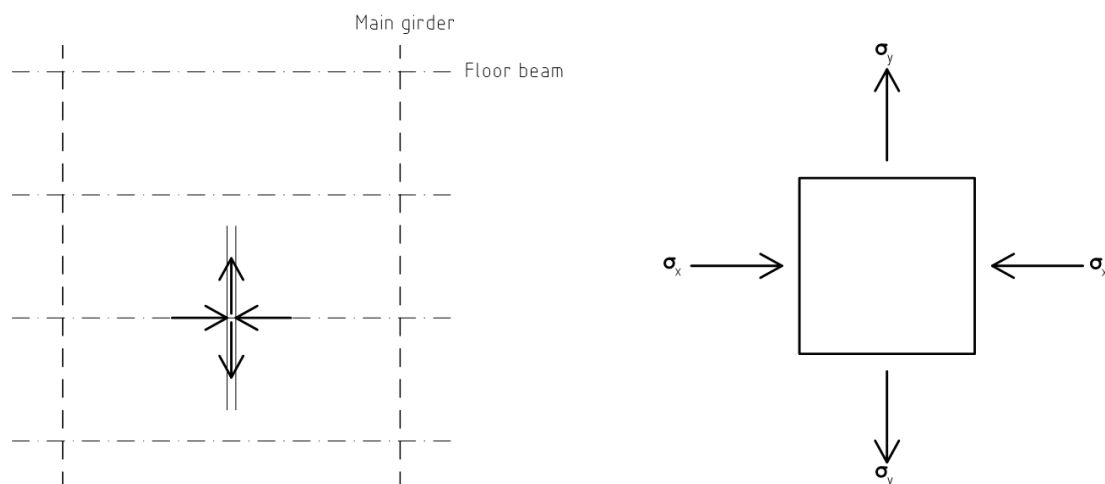
Figure 5-21 Multi-axial stress state in floor beams given from bending according to Figure 5-20a respective b

The deck plate experience a multi-axial stress state since it is exposed to bending around the y-axis for the global system as well as bending around the x-axis in the floor beam system, as can be seen in Figure 5-20. The stress state can be seen in Figure 5-21 below and the stress state is evaluated according to Equation 5-11 below from BSK2007:3:412. The tensile component is derived with Navier's formula for the moment in the rib system. The compressive component is derived in the same manner for the floor beam system and the shear component is minimal due to the two-dimensional behaviour of the plate and therefore disregarded.

$$\sqrt{\sigma_x{}^2 + \sigma_y{}^2 - \sigma_x\sigma_y + 3\tau^2} \leq 1.1 \cdot f_{yd} \qquad \text{Equation 5-11}$$

At the connection between rib and floor beam in the middle of the span, the buckling resistance of the deck plate is controlled. At the intersection with the rib, the deck plate is unsupported between the rib walls, see Figure 5-22. Since the deck plate acts as a top flange for the floor beams, the deck plate is compressed making it possible to buckle. The compression capacity is therefore checked according to code.
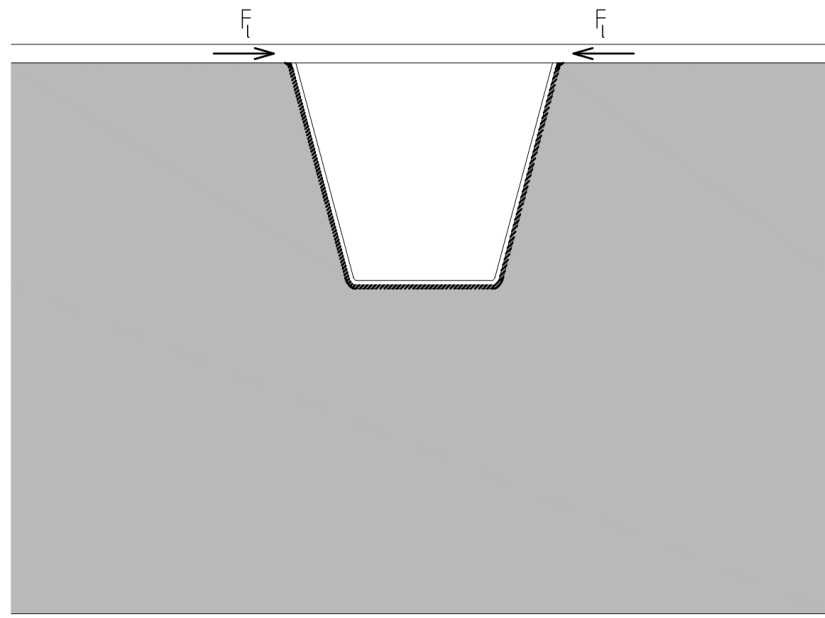
Figure 5-22 Compression of top flange of floor beam at the intersection with ribs where the flange is unsupported

5.1.4 Main girders

The main girder transfer all load acting on the bridge to the substructure and can be seen in Figure 5-23 below. The main girders are modelled as a continuous beam over two supports with a large cantilever part. The girders are checked for moment and shear capacity as well as for stability, weld strength, stiffeners and the local stress state at specific details.
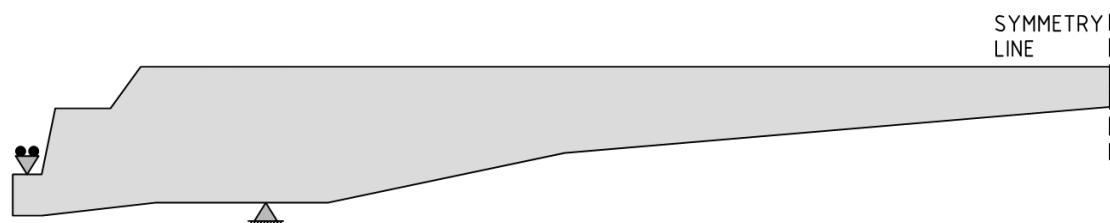
Figure 5-23 Overview of the main girders

All of the loads acting on the bridge deck are transferred through the main girders. The loads are placed in the super-system and are resisted by the main girders with the deck plate acting as the top flange. The main loads acting on the main girders are:

- Self-weight main girders

CHALMERS, *Civil and Environmental Engineering*, Master's Thesis 2015:14

- Vertical distributed load from the self-weight of ribs, floor beams, wearing surface and counterweight
- Traffic loads
- Breaking force (force couple in x-direction)
- Temperature loads – two cases, described below
- Wind loads

The cross-section of the main girders is varying, as seen in Figure 5-23. Consequently, the self-weight is dependent on which section is considered in the calculations and determined accordingly.

For the case with uneven temperature difference the temperature variation over the cross section should be considered. If the temperature is higher in the bridge deck than in the lower part of the bridge, the uneven temperature distribution have the same effect as a distributed vertical load. This is due to the restriction in expansion of the bridge deck.

The breaking force from vehicles acts as a horizontal load on the deck. Due to the high horizontal stiffness of the deck plate the breaking force is assumed to distribute equally to the two girders. This results in the resisting symmetrical and horizontal force pair in the main girders.

Regarding the wind load it act on both the traffic as well as on the height of the bridge. Wind load on the bridge generate a bending moment around the vertical z-axle. This moment is resisted by a force-couple in the main girders. The wind load therefore results in a normal force contribution in the main girders, see Figure 5-24. The wind load acting on the trucks in traffic generate a bending moment around the longitudinal axel of the bridge, x-axis. This moment results in a vertical force couple in the main girders. This wind loads thereby result in contributing compression or tension in the main girder, see Figure 5-25.
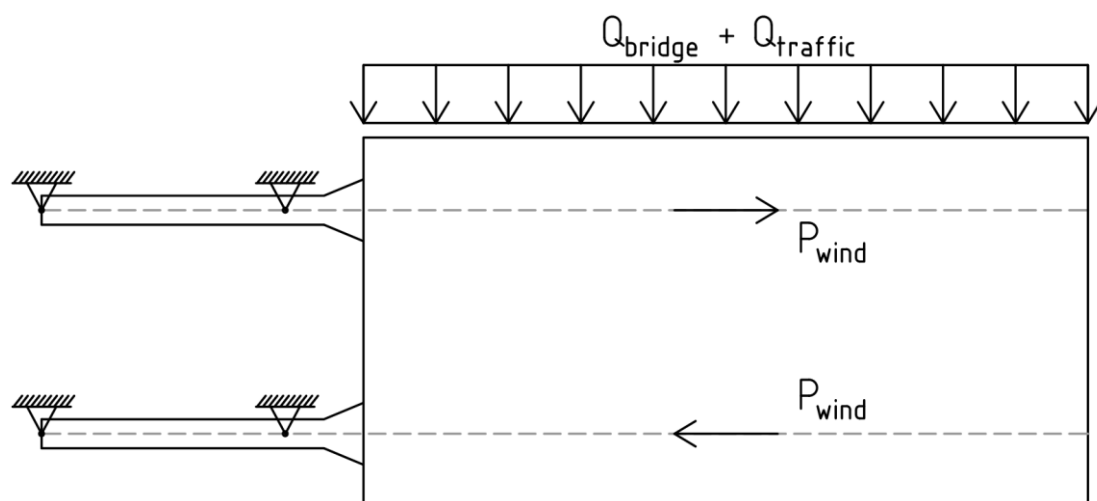
Figure 5-24 Model of reaction from the wind load in the main girders
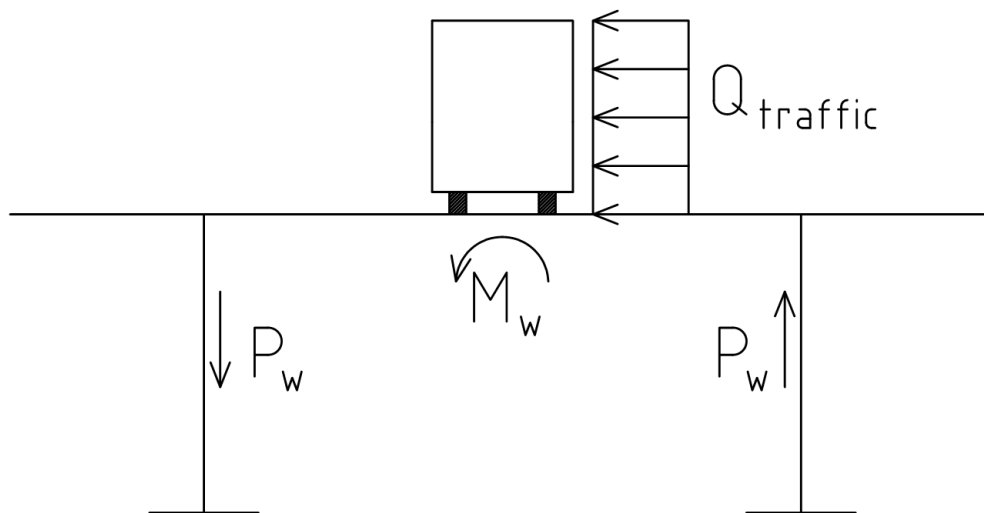
Figure 5-25 Model for the action from the wind load in the traffic

Most of the traffic load and the deck self-weight are transferred to the main girders via the floor beams. The reaction forces from the floor beams can applied as point loads when analysing the main girder. But also, the original loads can be used directly applied on the main girder for isolated analysis. When doing this simplification the point loads from the floor beams are smeared out as a distributed load instead. The right graph in Figure 5-26 below compare the difference between uniformly distributed load and load acting in ten point loads. As can be seen the curves are almost identical and therefore the use of the original loads are applicable.
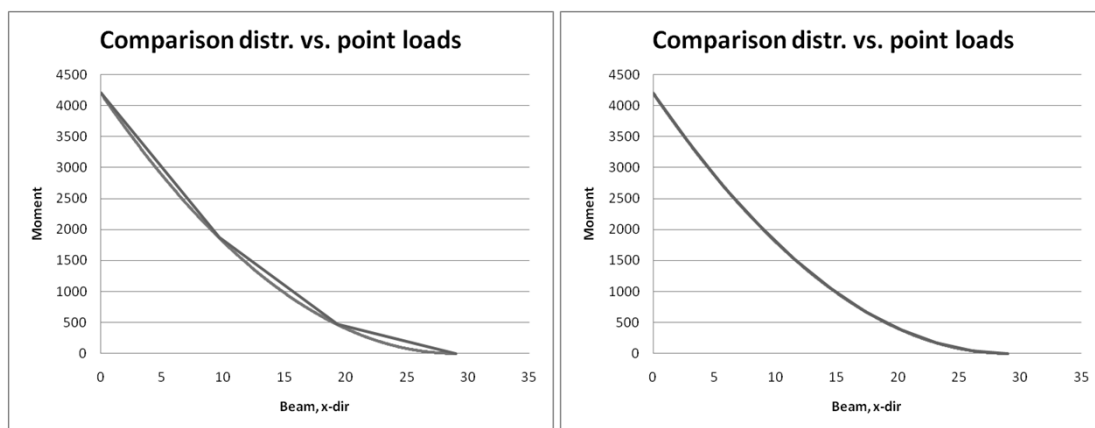
Figure 5-26 - Moment distribution for a cantilever beam, with a comparison between uniform distributed load and point loads. Left figure has 3 point loads and right figure has 10 point loads. In the right figure the difference in moment distribution is so small that only one curve can be seen.

The main girders are modelled as a continuous beam over two supports followed by a cantilever part ending with support transferring only shear, see Figure 5-27. The bascules are seen as symmetric and only one of them is studied.
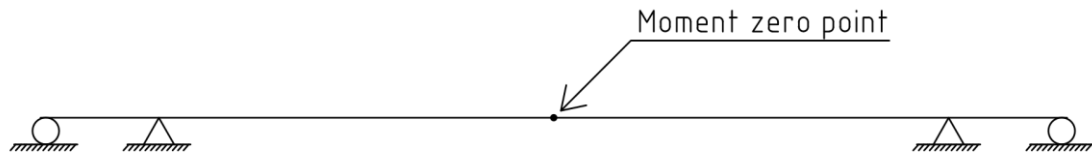
Figure 5-27 Structural model for the main girders

The bascule cross-section consists of two main girders with the deck plate acting as top flanges. Half of the internal part of the deck plate acts as top flange for each main girder, see Figure 5-28. With these dimensions the effective cross sections are calculated and used to determine the moment and shear capacities, see Equation 5-12, Equation 5-13, Equation 5-14 and Equation 5-15.
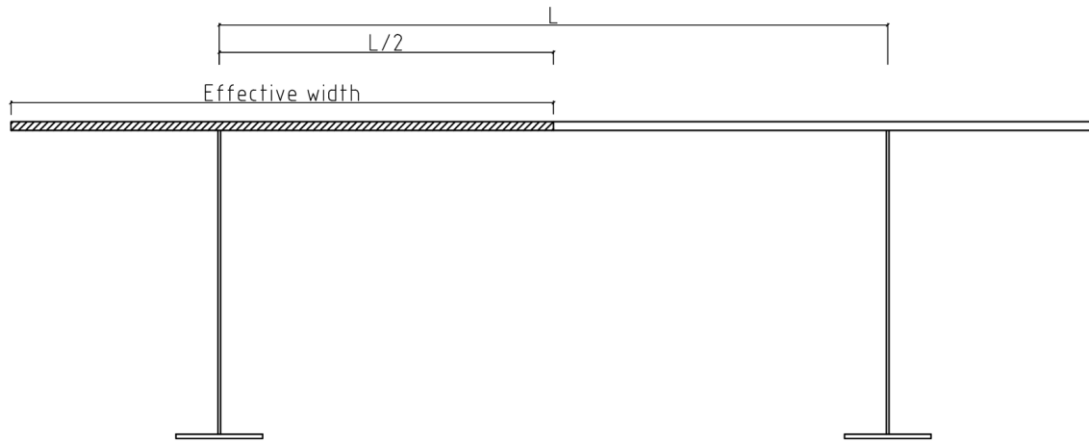
Figure 5-28 Cross-section of the main girders, with effective flange width marked for the left main girder.

Moment:
$$f_y = \sigma_y = \frac{M_y}{I_{ef}} \cdot z_{ef} = \frac{M_{Rd}}{I_{ef}} \cdot z_{ef}$$
Equation 5-12

$$M_{max} \leq M_{Rd} = f_y \cdot \frac{I_{ef}}{z_{ef}}$$
Equation 5-13

Shear:
$$\frac{f_{yd}}{\sqrt{3}} = \tau_{Rd} = \frac{V_{Rd} \cdot S}{I \cdot t}$$
Equation 5-14

$$V_{max} < V_{Rd} = \frac{f_{yd}}{\sqrt{3}} \cdot \frac{I \cdot t}{S}$$
Equation 5-15

5.2 Fatigue analysis

The fatigue analysis is performed for a weld respective the parenting material but not for the individual crack modes. The welds have fatigue strength, FAT, stated in several standards and these are compared to the stresses in the welds. The stresses are calculated from global moments and shear forces in effective cross sections of the model stated for the worst load case. If the stresses are lower than the fatigue strength, including partial factors for safety, the weld is regarded as safe. The first subchapter, Chapter 5.2.1, give a short description of the fatigue load model and some other fatigue concepts according to Eurocode, EN-1993-1-9, while the second subchapter describe the method for fatigue analysis by conventional method. The results from that method are later compared to the results given by the FE-analysis.

5.2.1 Fatigue load model according to Eurocode

With regard to fatigue design there are five load models in Eurocode.

Fatigue Load Model 1 is used to establish the minimum and maximum stress generated from the different load arrangements on the deck. Model 1 is applied to check if the fatigue life of a member is infinite for a constant amplitude stress, this is appropriate for steel members but can be unsuitable for other materials. In general model 1 is conservative, here multi-lane effects are covered automatically.

Fatigue Load Model 2 is used to establish the minimum and maximum stress generated from the different load arrangements on the deck. Compared to fatigue load Model 1, Model 2 is more accurate if it is possible to neglect the simultaneous passing of multiple lorries. Otherwise, model 2 should only be applied if additional data is available.

Fatigue Load Model 3 is used to establish the minimum and maximum stress generated from the different load arrangements on the deck. Model 3 is applied to check the fatigue life together with fatigue strength curves. Also, this model can be used to confirm the design using simplified methods.

Fatigue Load Model 4 is used to establish the stress range generated from the passing lorries on the deck. Model 4 is applied to check the fatigue life together with fatigue strength curves, never to determine if the fatigue life is unlimited. Compared to fatigue load model 3, model 4 is more accurate if it is possible to neglect the simultaneous passing of multiple lorries. Otherwise, model 4 should only be applied if additional data is available.

Fatigue Load Model 5 is used to establish the stress range generated from the passing of lorries on the deck. Model 5 is applied to check the fatigue life together with fatigue strength curves, never to determine if the fatigue life is unlimited. Fatigue load model 5 uses the actual traffic data and is the most general of the models, but can only be accurately applied when correct data is available.

According to available data and preferred application fatigue load model 3 will be used in the design performed in this thesis and will be the only one further explained.

For all fatigue verifications a traffic category should be determined with regard to the number of slow lanes on the deck and the number of heavy vehicles on the bridge per year and slow lane, see Table 5-1.

Table 5-1 Indicative number of heavy vehicles expected per year and slow lane, (EN 1991-2)

	Traffic categories	N_{obs} per year and per slow lane
1	Roads and motorways with 2 or more lanes per direction with high flow rates of lorries	2.0×10^6
2	Roads and motorways with medium flow rate of lorries	0.5×10^6
3	Main roads with low flow of lorries	0.125×10^6
4	Local roads with low flow rates of lorries	0.05×10^6

The fatigue load should be placed in the centre of the lanes defined according to the rules above for assessment of general actions effects, for example in the main girders.

With regard to local action effects, such as the actions in the deck, the load should be placed in the centre on theoretical lanes which are assumed to be positioned anywhere on the deck. Important to emphasize is the significance of the transverse location for orthotropic decks which needs to be taken into account with a statistical distribution, see Figure 5-29.
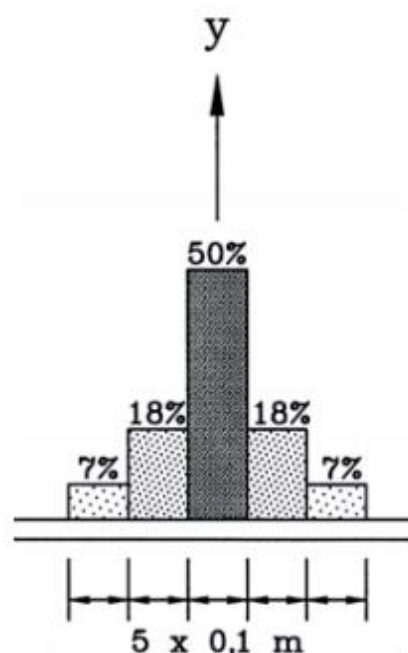
Figure 5-29 Frequency distribution of transverse location of centre line of vehicle [EN 1991-2]

Concentrated loads, related to local verifications, should be applied over their whole contact area as a uniformly distributed load. The contribution from dispersion through the wearing surface should be considered with a slope of 1:1, see Figure 5-30

Figure 5-30 Dispersal of concentrated loads through pavement and orthotropic decks [EN 1991-2]

Fatigue load model 3 (single vehicle model)

Model 3 represents a single vehicle with four axes with identical wheels, see Figure 5-31. Each axis has a weight of 120 kN that is placed on a square contact surface. It is possible to place two vehicles in the same lane, if this generates larger stresses. The geometry of the second vehicle is the same as for the first but the weight is reduced to 36 kN for each axis. However, this is valid only if the distance between the centre points of the vehicles is 40m or less.

Figure 5-31 Fatigue load model 3 according to Eurocode (EN 1991-2), w_1 = Lane width, X = Bridge longitudinal axis

The fatigue assessment in Eurocode is chosen to be either a damage tolerant method or a safe life method by the designer. The damage tolerant method is used if the structure is redundant and with the reservation that inspections and maintenance will be performed throughout the design life. The safe life method is applied for structures for which regular fatigue damage inspections will not be held

or if a local fatigue crack can lead to rapid failure of either an element or the entire structure.

For the damage tolerant method it is important to select the correct detail, material and stress levels with the intention to keep a low crack propagation rate as well as a long critical crack length in case of the development of a fatigue crack. For the safe-life method on the other hand it is important to select a detail and stress level providing an unlimited fatigue life at the end of the service life.

The stresses used in the fatigue evaluation should be calculated in the serviceability limit state and at the position of the potential fatigue initiation. If the exact detail is not provided in the code a stress concentration factor should be used to modify the nominal stress. The relevant stresses for details in the parent materials are the nominal direct stress and the nominal shear stress or the combination of both. The relevant stresses in the welds are the nominal stress transverse to the axis of the weld, σ_{wf}, as well as the one longitudinal to the axis, τ_{wf}, see Equation 5-16, Equation 5-17 and Figure 5-32.

$$\sigma_{wf} = \sqrt{\sigma_{\perp f}^2 + \tau_{\perp f}^2}$$ **Equation 5-16**

$$\tau_{wf} = \tau_{II f}$$ **Equation 5-17**
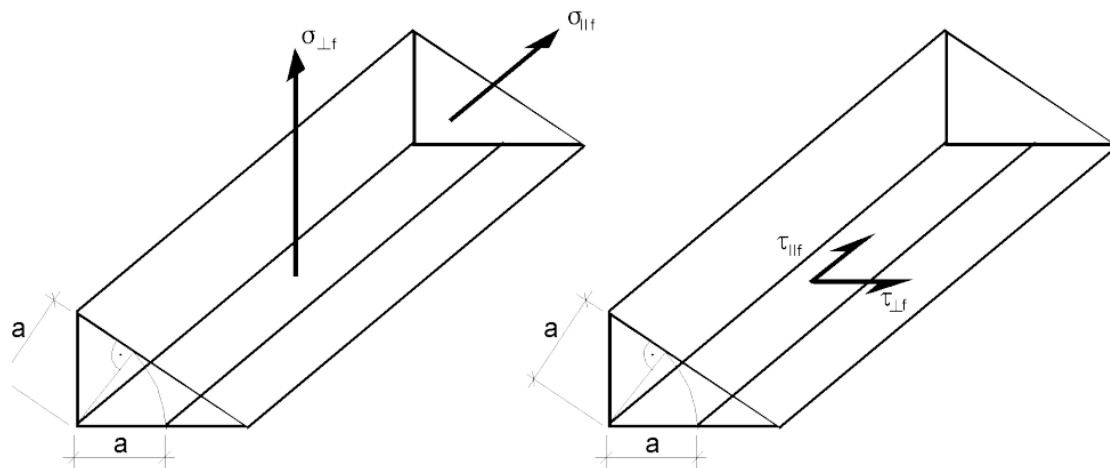
Figure 5-32 Relevant stresses in fillet welds; Left: Relevant normal stresses; Right: Relevant shear stresses. (EN1993-1-9)

Regarding the stress range, the design values to be used should correspond the two million loading cycles when the simplified lambda-method is used. In this method the stress range is an equivalent stress range, i.e. it is not really two million cycles of real traffic load but two million cycles of an equivalent stress range. For the nominal stress range the fatigue strength is represented by S-N curves corresponding to specific detail categories, see Figure 5-33 and Figure 5-34 respectively. Each detail category is assigned a reference value [N/mm2] which represents the fatigue strength at 2 million load cycles.
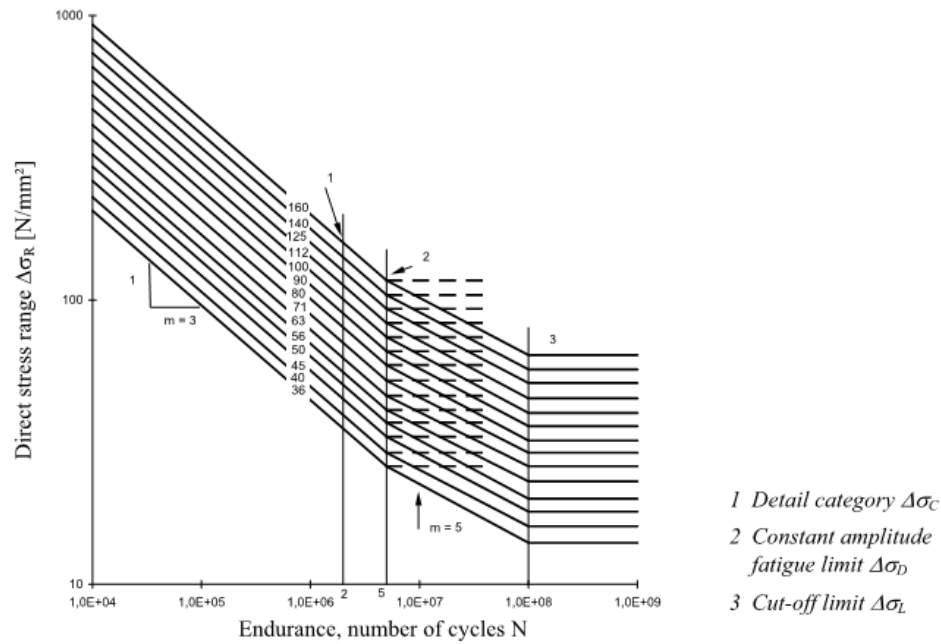
Figure 5-33 Fatigue strength curves for direct stress ranges. (EN1993-1-9)
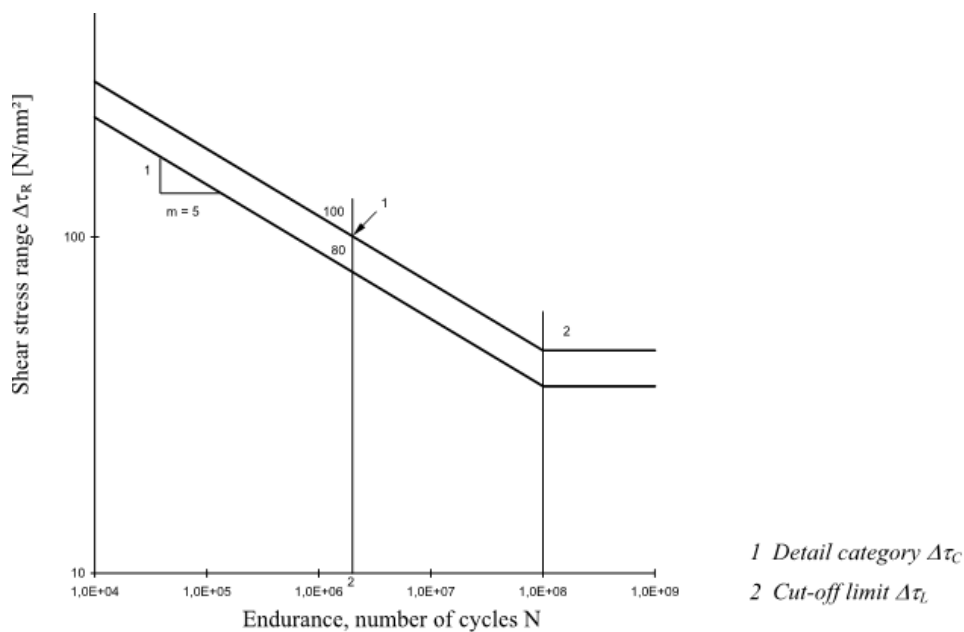
Figure 5-34 Fatigue strength curves for shear stress ranges (EN1993-1-9)

The effect of thickness or other size effect is regarded with a size effects factor and the fatigue strength is reduced with a factor, k_s.

5.2.2 Conventional fatigue analysis

The approach of performing a fatigue design of an OSD according to conventional methods is based on the global behaviour described in Chapter 5.1. The three cracks, according to Chapter 3.3.3, are investigated by investigate the welds where the cracks

are initiated. Crack I and crack II initiate at the weld between the rib and the deck plate. These two cracks are therefore analysed in a combined way by the analysis of rib-deck plate-weld. Crack III is analysed by investigation of the weld between the floor beam and the ribs.

The conventional fatigue analysis of one weld includes

- Definition of an appropriate global model
- Definition of an appropriate load model
- Calculation of global sectional forces (moment and shear force)
- Definition of the effective cross section that will carry the load
- Calculation of stresses in the section
- Comparison between the calculated stresses at the welds location in the section and its fatigue resistance, FAT

The fatigue assessment of the weld is made according to a safe life method according to EN 1993-1-9, with a high consequence of failure, see Table 5-2.

Table 5-2 Partial factors for fatigue strength according to EN-1993-1-9

Assessment method	Consequence of failure	
	Low consequence	High consequence
Damage tolerant	1,00	1,15
Safe life	1,15	1,35

5.2.2.1   Conventional fatigue analysis of weld between rib and deck plate

To determine the stress in the weld between the rib and deck plate an appropriate global model must be defined. Two models where described in Chapter 5.1.2 and it is these that define the global system for the ribs. One rib is studied with an effective part of the deck plate acting as a top flange, see Figure 5-35. Effective cross section for the rib itself is also controlled with regard to buckling.
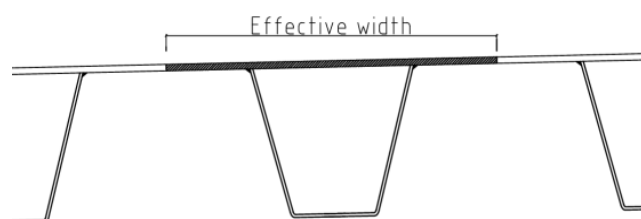
Figure 5-35 Section of a rib with effective part of the deck plate acting as top flange

When using both models with stiff support and spring support the rib in the middle of the bridge will experience the highest stresses and is therefore the only rib that is controlled, see Figure 5-36.
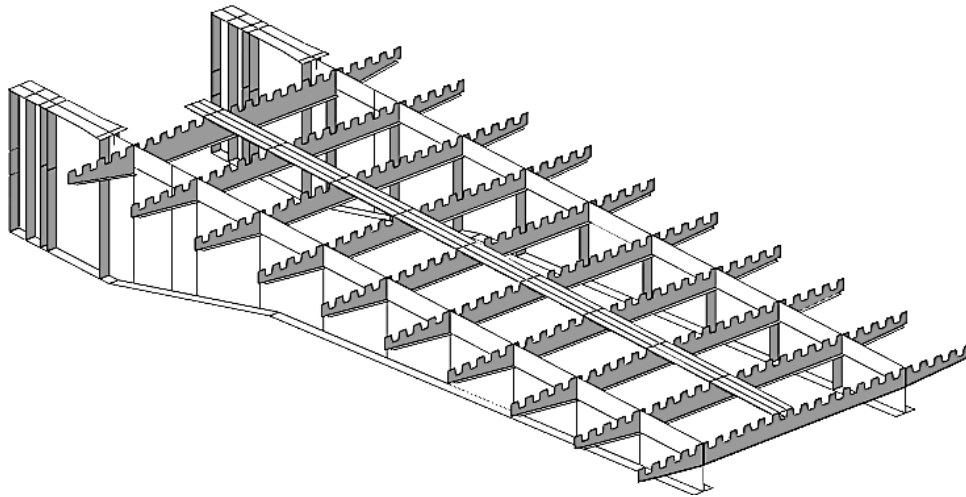
Figure 5-36 The studied rib, located in the middle of the bridge

The floor beams are modelled both as stiff supports - model 1, see Figure 5-9 and as spring supports – model 2, see Figure 5-10. The load model that results in the highest stresses is the response from a single wheel. This is modelled as a single point load, see Figure 5-37.
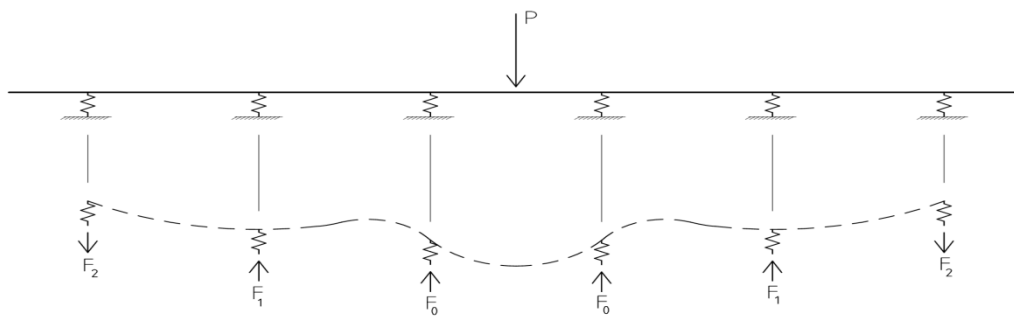
Figure 5-37 Load model for conventional fatigue analysis of weld between rib and deck plate

In the bridge Saltsjöbron there are mainly four different types of floor beams resulting in 4 different springs for the model. The floor beams spring stiffness is described in Chapter 5.1.2 using Equation 5-6. In the spring stiffness calculations the effective cross sections of each floor beam are used, with $b_{eff} = 10 \cdot t_{flange}$ according to BRO94. This result in four types of springs with different spring stiffness, see Figure 5-38.

Figure 5-38 Spring model of one rib on springs with different stiffness; (a) Main girder seen from the side; (b) Structural model with springs representing the floor beams

The two models are analysed to get the highest global moment and shear force along the rib. The highest sectional forces are used to calculate the stresses in the section at the weld according to Navier's formula for normal stress and Jourawski's formula for shear stress. The effective cross sections used in the stress calculations can be reviewed in Appendix IV.

The experienced stress in the weld results in an equivalent stress and is compared to the FAT of the weld according to Equation 5-18. The FAT of the weld between rib and deck plate is determined according to detail 8 in table 8.8 in EN-1993-1-9, see Figure 5-39.

Figure 5-39 Detail category used to determine FAT of the weld between rib and deck plate according to EN-1993-1-9

$$\frac{\gamma_{Ff} \cdot \Delta\sigma}{\dfrac{FAT}{\gamma_{Mf}}} < 1$$

Equation 5-18

5.2.2.2 Conventional fatigue analysis of weld between floor beam and rib

To determine the stress in the weld between the floor beam and ribs, see Figure 5-40 an appropriate global model must be defined. The stresses in the weld are determined

by the behaviour of the floor beam. An appropriate model is therefore the floor beam supported by the two main girders. The cantilever parts of the floor beam are disregarded and the system is modelled as a simply supported beam on two stiff supports.
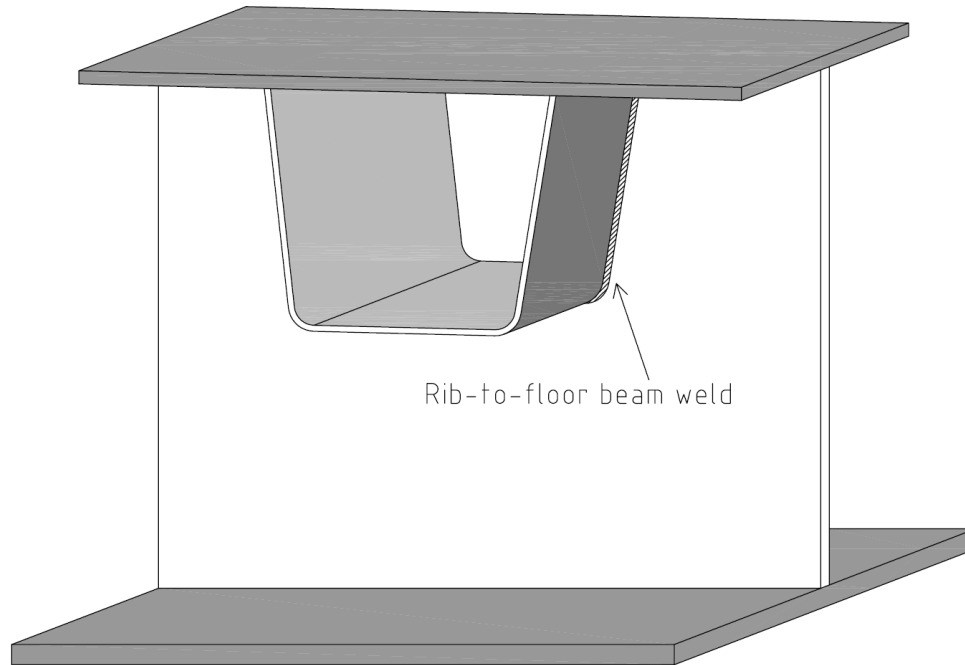
Figure 5-40 Illustration of rib-to-floor beam weld

Two load models are used, one for highest moment and one for highest shear force, see Figure 5-41 and Figure 5-42. The fatigue load model is used with the two point loads representing the wheel loads. The point loads are increased to 150% to include the second axle loads effect on the floor beam. In Saltsjöbron, the 2nd load axle place itself in the middle between two floor beams and therefore the contribution is chosen to 50%.
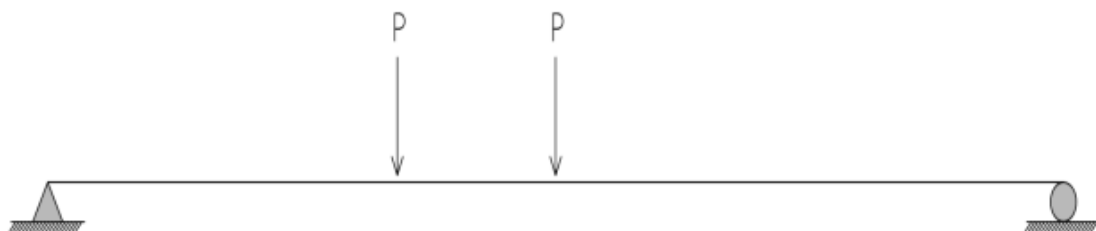
Figure 5-41 Load model giving highest moment in the floor beam for fatigue evaluation of weld between floor beam and rib

Figure 5-42 Load model giving highest shear force in the floor beam for fatigue evaluation of weld between floor beam and rib

The two load models are used to calculate the global moment and shear forces along the floor beam as can be seen in Figure 5-43 and Figure 5-44.
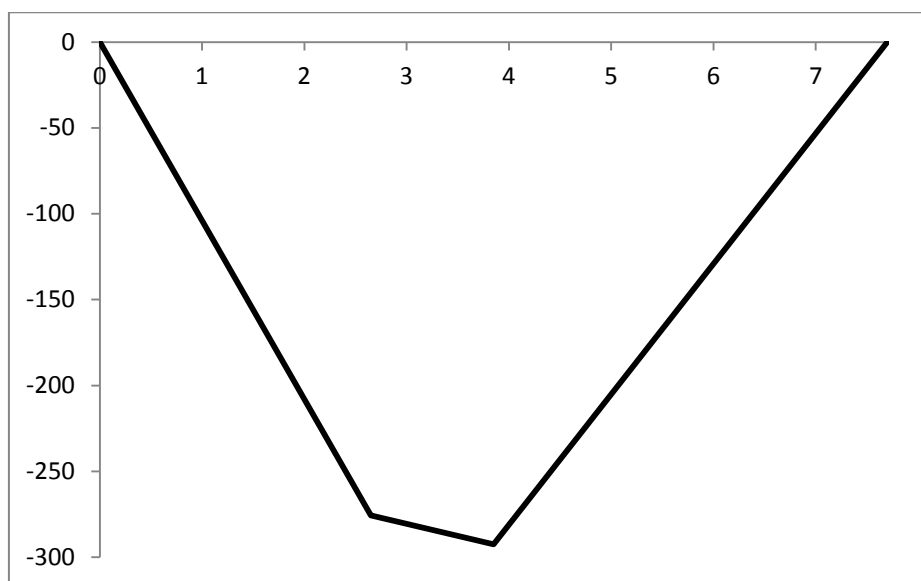
Figure 5-43 Moment distribution along the floor beam according to the model shown in Figure 5-41
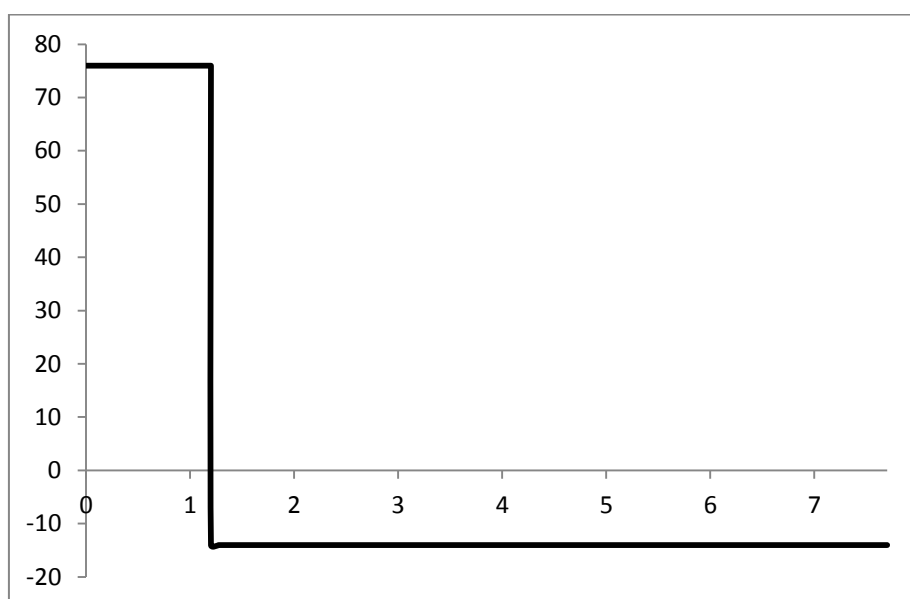
Figure 5-44 Shear force distribution along the floor beam according to the model shown in Figure 5-42

The highest moment and shear force obtained are used to calculate the stresses in the section of the floor beam. The effective cross section of the floor beam include an effective part of the deck plate acting as a top flange for the floor beam and also the loss of web area where the rib intersect the floor beam web, see Figure 5-45.
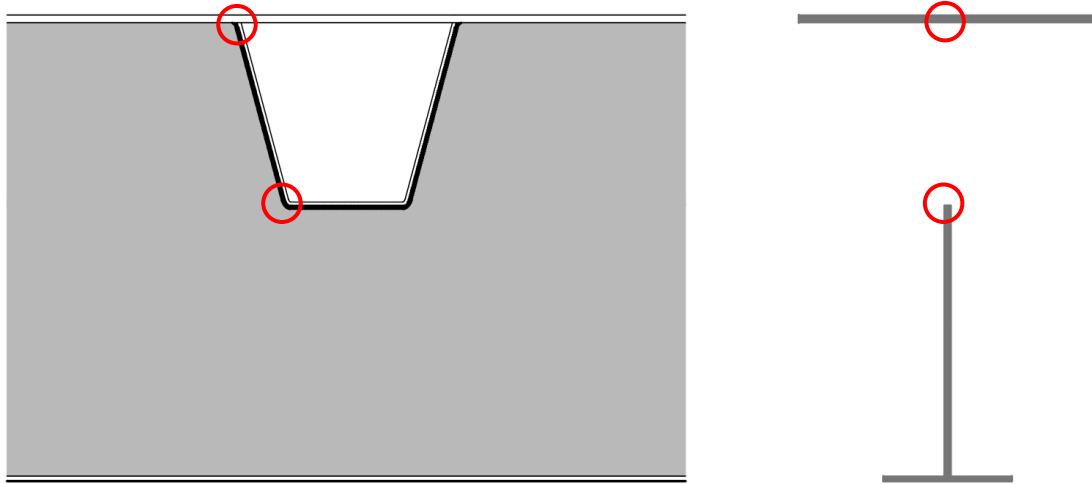
Figure 5-45 Effective cross-section of floor beam at intersection with longitudinal rib

The stresses are calculated at two locations in the section, at the rib radius and at the deck plate connection, these locations are highlighted in Figure 5-44. The stress calculations are made according to Navier's formula for normal stress and Jourawski's formula for shear stress, with effective cross sections, see Appendix IV.

The experienced stress in the floor beam at the weld location results in an equivalent stress and is compared to the FAT of the weld according to Equation 5-18. The FAT of the weld is determined according to detail 2 in table 8.8 in EN-1993-1-9, see Figure 5-46. In the fatigue evaluation at the top of the section the fatigue strength is lowered one step due to the intersecting weld between rib and deck plate (BSK07 6.522).
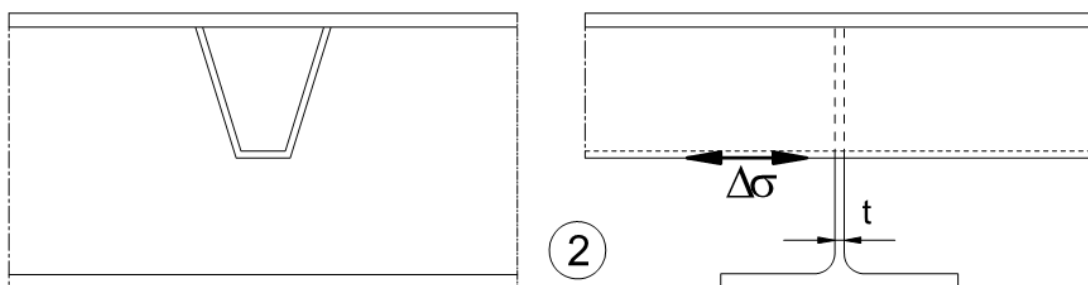
Figure 5-46 Detail category used to determine FAT of the weld between floor beam and rib according to EN-1993-1-9

6 Advanced fatigue analysis using finite element method

Finite element analysis has proven to be a powerful tool in numerous different fields. With FE analysis of an OSD the engineer can include aspects of local behaviour that ordinarily are excluded in conventional hand-calculations. As described in the previous chapters, the local effects are very important when evaluating the fatigue performance of an orthotropic deck since they result in high local stresses. However, the use of FEM is also connected with some difficulties. If understanding of the structural behaviour of the deck or of the software is insufficient the obtained results or interpretation of these results may be faulty. In this chapter a guideline on how to model an orthotropic deck in FE software is presented and explained.

The model is based on the existing bridge Saltsjöbron and three cracks are studied. The studied cracks are:

- Crack initiated at the weld toe in the rib-to-deck plate weld, the crack propagates in the deck plate and is referred to as R-DP Crack I, see Figure 6-1(a).
- Crack initiated at the weld toe in the rib-to-deck plate weld, the crack propagates in the rib wall and is referred to as R-DP Crack II, see Figure 6-1(a).
- Crack initiated at the weld toe at the radii in the rib-to-floor beam weld, the crack propagates in the floor beam web and is referred to as R-FB Crack III, see Figure 6-1(b).
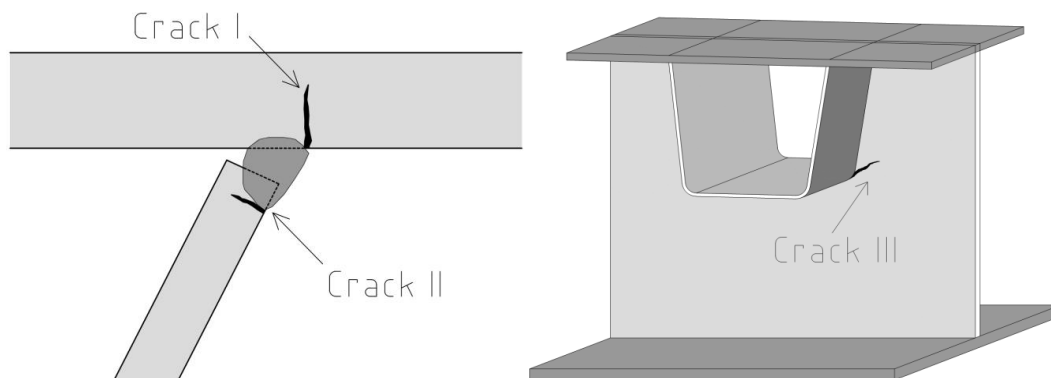
Figure 6-1 The three investigated cracks (a) Crack I and II at the rib-to-deck plate weld; (b) Crack III at the radii of the rib-to-floor beam weld.

6.1 Important issues when using FEM

You can use FEM to evaluate any type of cracking, even the root cracks, there are some techniques that allow for evaluation of root cracks. However, these methods are rather difficult to implement and here only cracks initiated at the weld toe are investigated. A possible measure to take to prevent the root cracks is to ensure sufficient penetration of the weld as well as to minimize the gap between the rib and deck plate.

When using FEM it is important to choose the correct stress output to the fatigue evaluation. The investigated crack will grow perpendicular to the highest principle stress direction. The principle stress directions do not need to correspond to the chosen global coordinate systems, see Figure 6-2, and therefore the use of stress output related to the global coordinate system is discouraged, and the use of principle stresses advised.
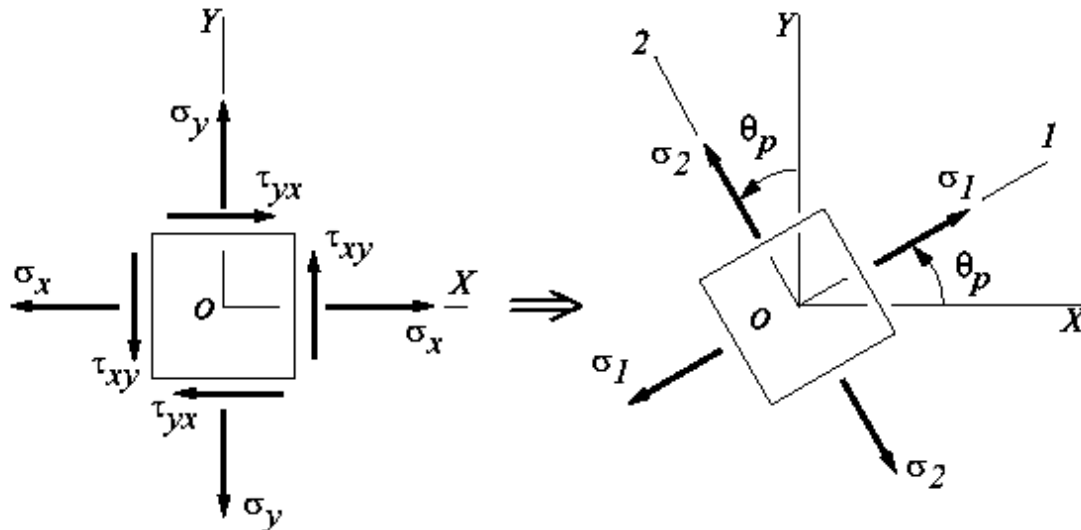
Figure 6-2 Definition of principal stresses (a) Stresses given in the coordinate system; (b) Principal stresses.

$$\sigma_{1,2} = \frac{\sigma_x + \sigma_y}{2} \pm \sqrt{\left(\frac{\sigma_x + \sigma_y}{2}\right)^2 + \tau_{xy}^2}$$

Equation 6.1

Another important aspect with the stress output in the model is to take the stresses in nodes and not in elements. This is a consequence of how the stresses in the elements are calculated. The stress stated for one element is in fact the average stress of all the nodes connected to the elements which can give a very misleading value if high stress peaks occur in vicinity of the element.

Moreover, it is important not to read the node values at the exact location of the weld since this section will experience singularities and the results are unrealistic. Also, these points are connected to several planes and will give one stress for each plane. To avoid these problems the stresses can be extracted by the structural hot spot stress method.

Since shell elements are used in the model the extraction of stresses must be performed at the correct side of each separate member (i.e. to include bending effects in addition to membrane effects). In this specific model bottom values are to be used for both deck plate and longitudinal ribs since these represent the stresses at the side to which the weld is connected. Since the floor beam has a weld at both side of the shell element the side with the highest stress should be used.

If trustworthy stress values are required, e.g. in fatigue evaluation and not only for comparison, the hot spot method should be used. However, it must be noted and taken into consideration that the nodal values are highly dependent on the mesh quality and

size. It is of great significance to use a suitable mesh for the hotspot in the investigated areas.

One other thing to consider in FEM-analysis is how the loads are applied to the model. In global models where only the global behaviour is of interest the load from e.g. a wheel can be modelled as a point load. But if the load is modelled with a point load the local behaviour of the structure will be very unrealistic. The load will create a singularity with very high stress values in the region close to the load. For the global behaviour it does not matter, but as stated previously the fatigue process is a very localized process. Therefore the need of correct load modelling is crucial for a successful fatigue evaluation using FEM.

The need of a correct load modelling is even more important in analysis of an OSD. This is due to the intricate behaviour of the different structural components. If the wheel load is modelled as a point load placed in the middle of a rib, the rib will deform according to Figure 6-3 a). The rib walls will show a high deformation and the local stresses due to the behaviour of the rib will be very high. If the load on the other hand is modelled as a distributed load over the area of the wheel, the OSD will deform according to Figure 6-3 b). This results in lower stress values and a more correct modelling of the real load case.
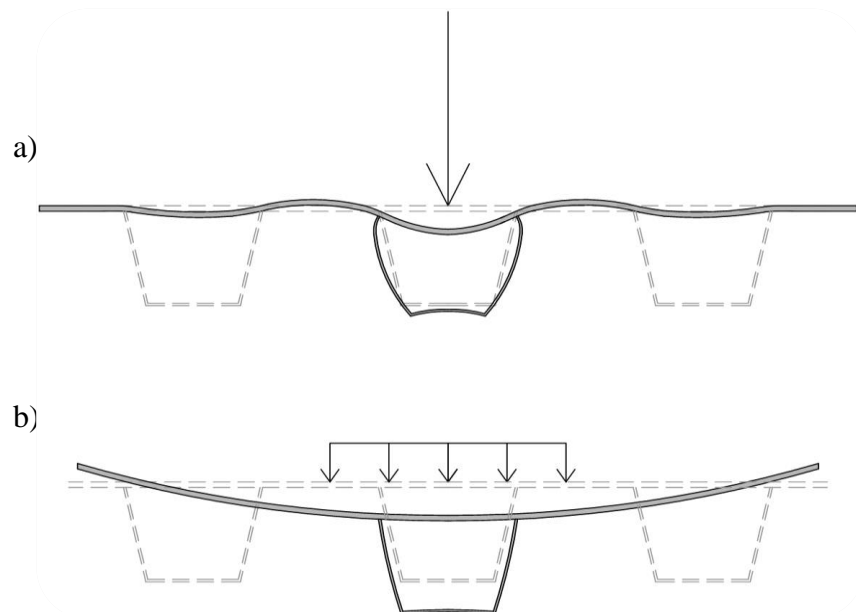
Figure 6-3 Difference in behaviour of an OSD when exposed to a point load compared to a distributed load

6.2 Modelling of the studied bridge

In this subchapter the modelling procedure for the case-study bridge is described, the assumptions and simplifications made in this specific case are presented and commented. The bridge is modelled in Brigade/Plus version 5.1-4. Only one of the two leafs is modelled, to take the interaction from the other leaf into account spring supports are modelled at the end of the cantilever. All parts except a K-joint are modelled with shell elements. The K-joint is modelled with beam elements.

6.2.1 The part module

When constructing the bridge in Brigade, some parts are modelled individually and later assembled together to the final bridge. The model procedure is explained below.

6.2.1.1 Modelling Part 1

The first part in the model consists of the deck plate, ribs, endplates, floor beam and top part of the main girder web. The part is modelled from one floor beam to the next floor beam and will later be copied in a linear pattern along the bridge.

To minimize the amount of work effort, an AutoCAD drawing of the section is imported and modified in the sketch module and then extruded to a 3D part. In the real bridge there is an inclination in the longitudinal direction of the bridge between the abutments and the nose opening. This is disregarded in the model since the effect on the behaviour is judged to be very limited.
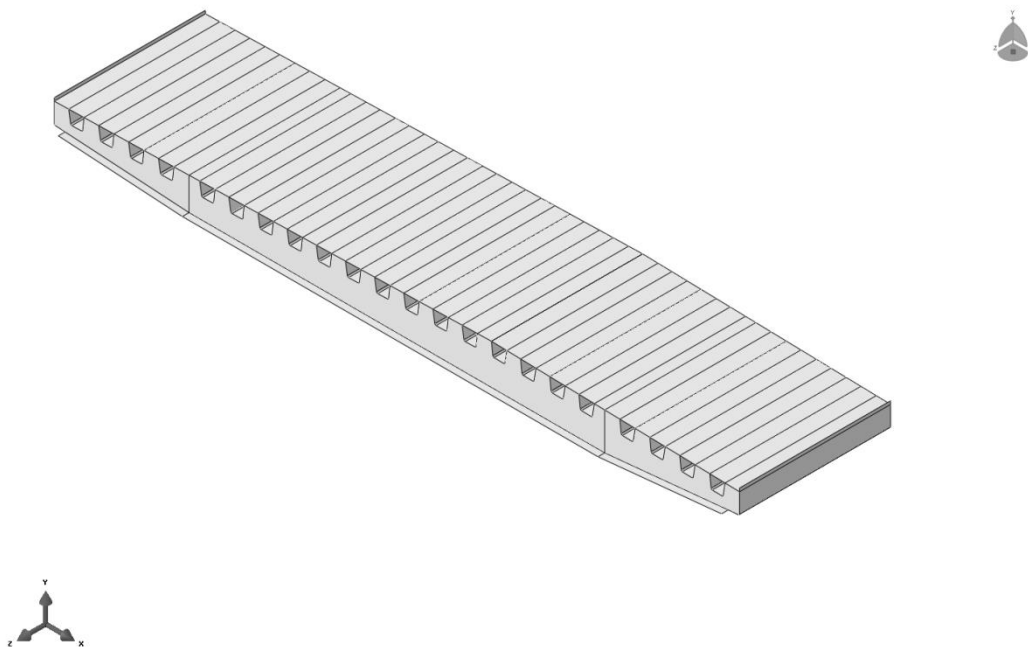
Figure 6-4 Part 1 seen from above
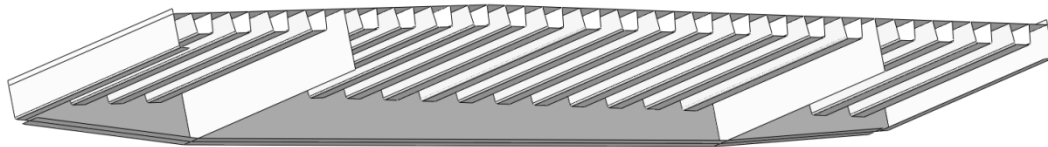
Figure 6-5 Part 1 seen from below

6.2.1.2   Modelling Part 2

The second part modelled the part representing the main girders. Only one of the main girders is modelled and is later mirrored to represent the other main girder. The mirroring is done in a manner so the stiffeners along the beam are located at the face directed to the middle of the bridge-section.

The top parts of the main girders are already modelled in part 1 and are therefore not included in part 2. This can be seen in Figure 6-6 at the drastic change of web height to the left in the figure.

The two supports modelled are the support beam and a fixed support, these are highlighted in Figure 6-6. The roller support is modelled as the top flange of the support beam since this is the part transferring the main part of the load in reality. The fixed support is explained more thorough below.
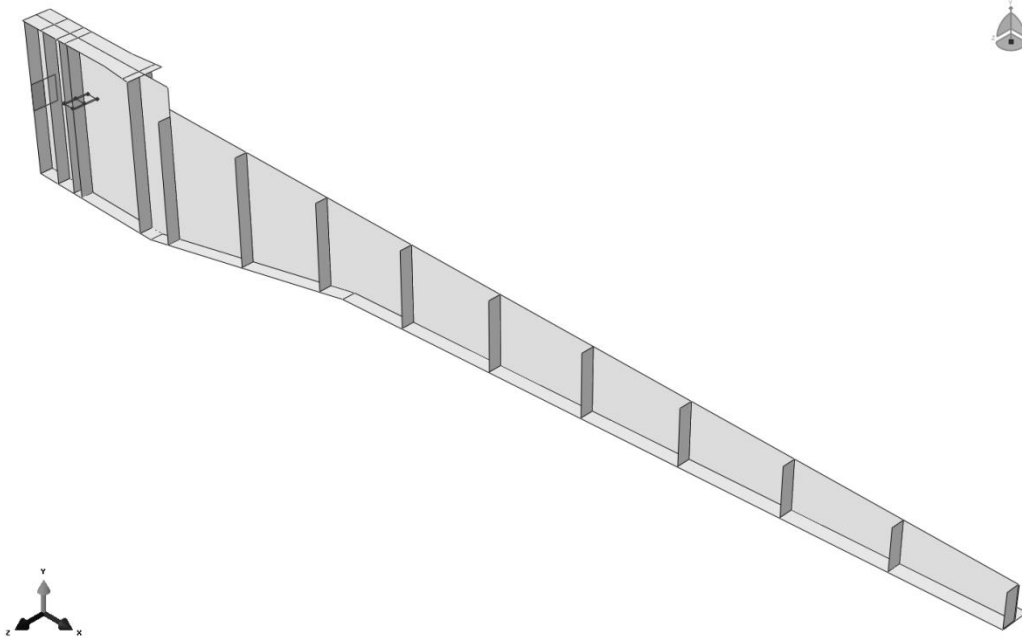
Figure 6-6 Part 2

6.2.1.2.1 Modelling simplification regarding the main girders

A relatively large part of the real main girder is not included in the model. The part not modelled are geometrically intricate with several stiffeners and varying cross-section. The main girders are modelled only from the bridge rotational axis and out to the nose opening. This simplification is justified by the time savings in modelling procedure and the small effect this part has on the local behaviour at the crack initiation areas.

The regions of interest are the ribs and their intersecting parts. It is therefore of great importance that the simplification made do not influence the global behaviour of the bridge and thereby the behaviour of the ribs.

To represent the global behaviour in a good way the main girders are made fully fixed at the rotational axis. This is a relatively large simplification that may affect the global behaviour of the bridge. But since the fatigue behaviour is very local, the significance of this simplification is low and therefore justified.

6.2.1.3 Modelling part 3

The third part modelled is floor beam 1, the floor beam closest to the nose opening, see Figure 6-7. In part 3 the closing of the ribs are also included.
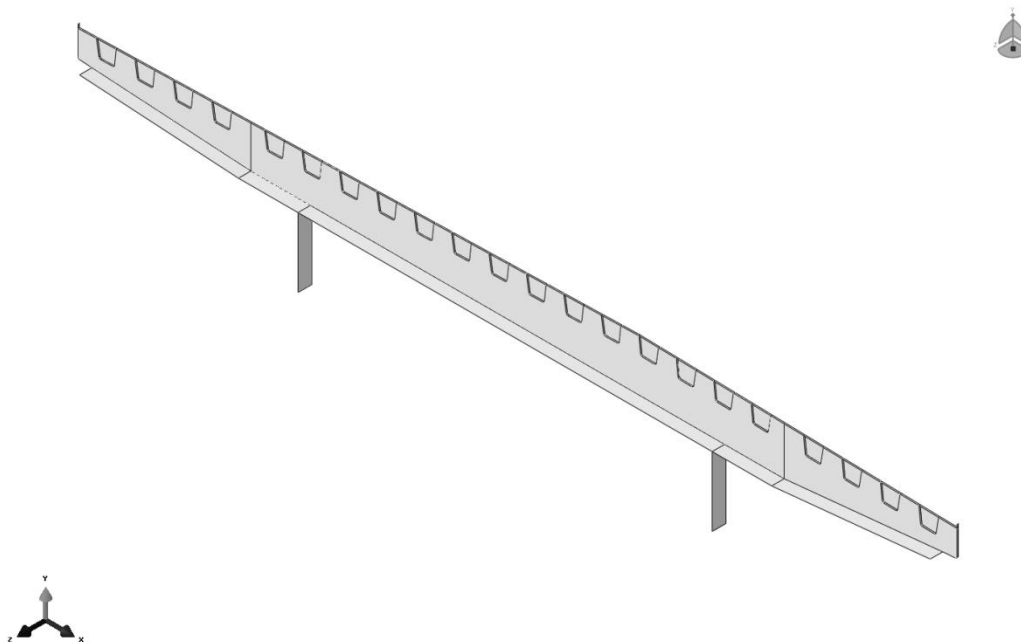
Figure 6-7 Part 3

6.2.1.4 Modelling part 4

In part 4, floor beam 10 is modelled together with a part of the bridge deck, see Figure 6-8. This is the floor beam closest to the abutments and has an increased web height compared to the other floor beams. Floor beam 10 is also connected to a K-joint, which makes this bridge section very stiff. The K-joint is described further in Chapter 6.2.2.6.
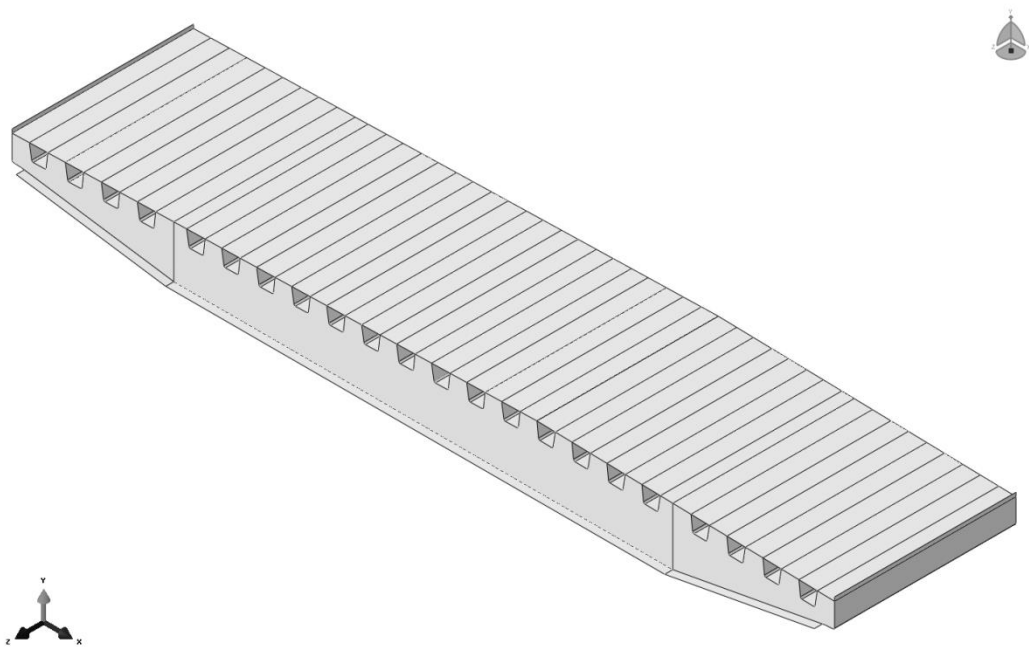
Figure 6-8 Part 4

6.2.1.5 Modelling part 5

Part 5 is the last part that is modelled separately and consists of the abutment endplate and the bridge deck towards the floor beam 10, see Figure 6-9. In reality the end plate have an inclination of 45 degrees which is disregarded in the modelling process. The end plate is instead modelled as vertical.
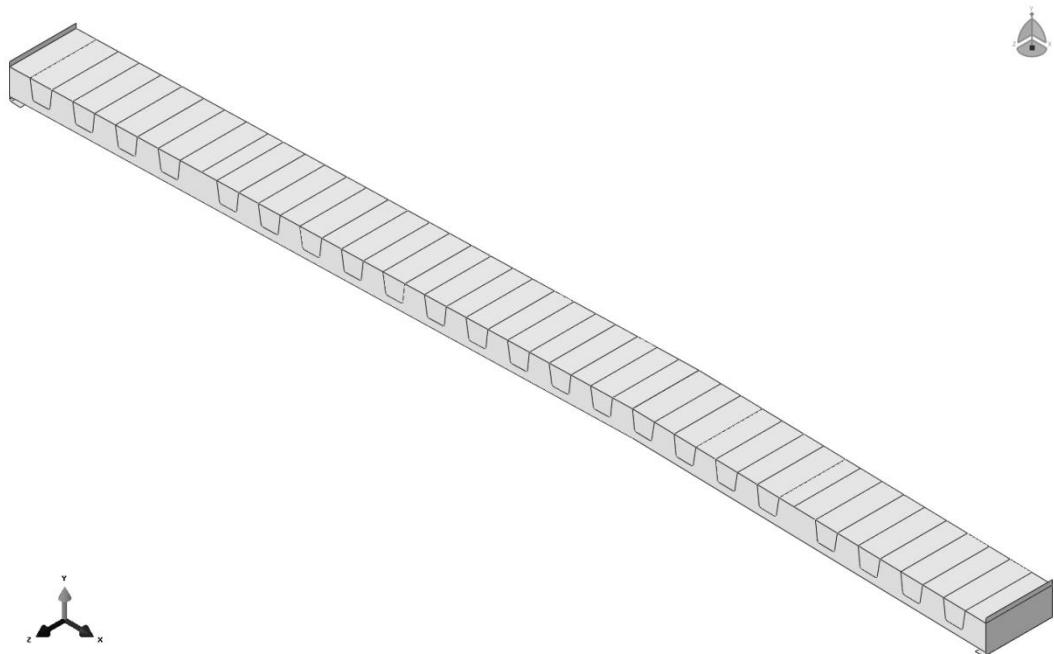
Figure 6-9 Part 5

6.2.2   Assembly module

The main parts of the bridge are now modelled separately and assembled together in the assembly module. At the bridge section were floor beam 10 is located a K-joint is modelled. This is done in the sketch module into the assembled model and is described in this chapter.

6.2.2.1   Assembling main girders and part 1

The main girders are assembled with a spacing of 7.7m and part 1 is assembled on top of the main girders, see Figure 6-10. Part 1 represent floor beam 2-9 and are therefore assembled at the section for floor beam 9.
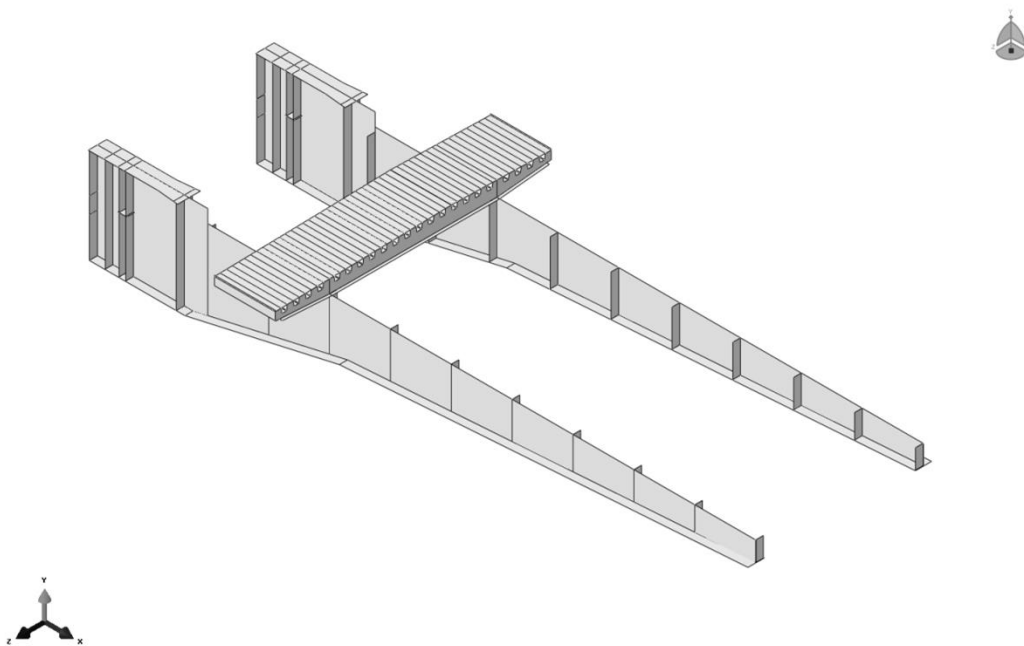
Figure 6-10 Assembly of part 1 and 2

6.2.2.2   Assembling linear pattern of part 1

Part 1 is copied in a linear pattern containing 8 parts along the main girders, see Figure 6-11. These parts represents floor beam 2 – 9 with the associated bridge deck.

CHALMERS, *Civil and Environmental Engineering*, Master's Thesis 2015:14
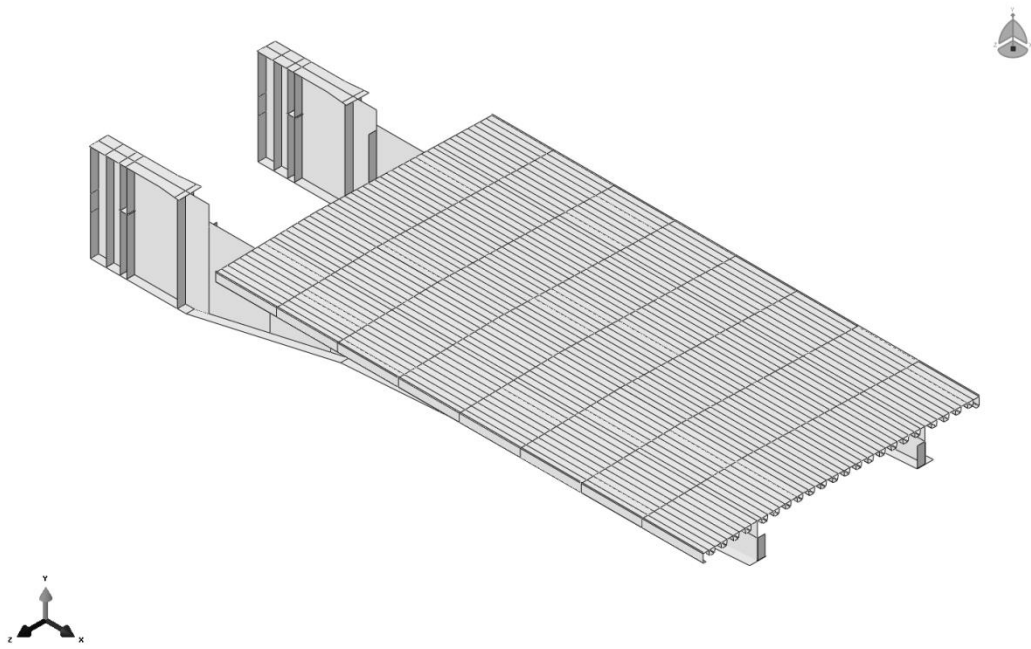
Figure 6-11 Assembly of part 1 (in a linear pattern) and part 2

6.2.2.3   Assembling floor beam 10

Floor beam 10 with associated bridge deck is assembled into the model, see Figure 6-12.
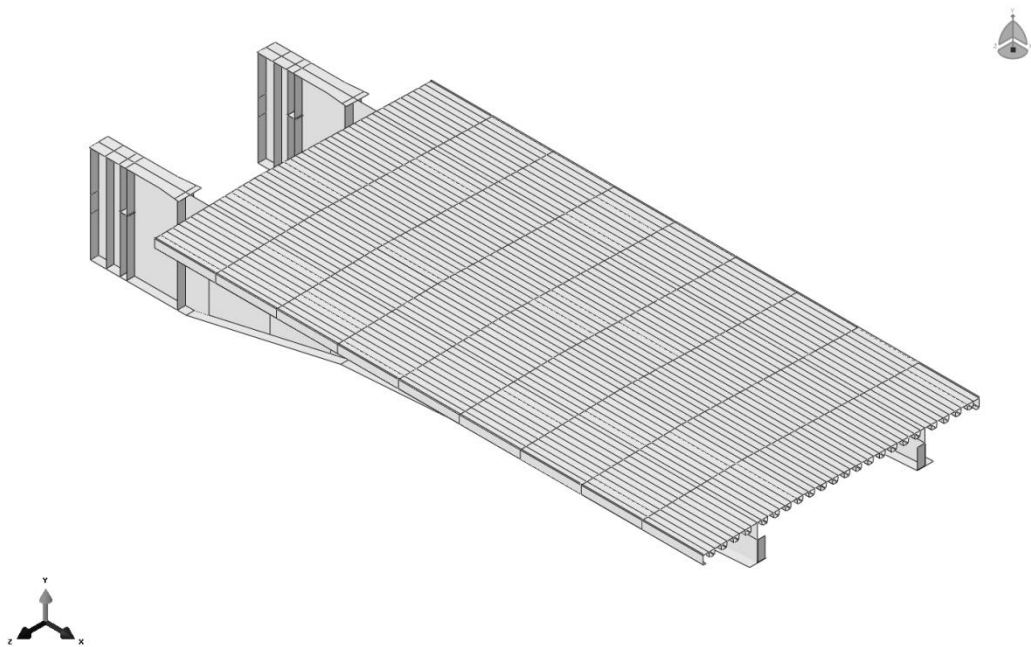
Figure 6-12 Assembly with floor beam 10

6.2.2.4 Assembling abutment endplate

The abutment endplate with associated bridge deck is assembled into the model, see Figure 6-13.
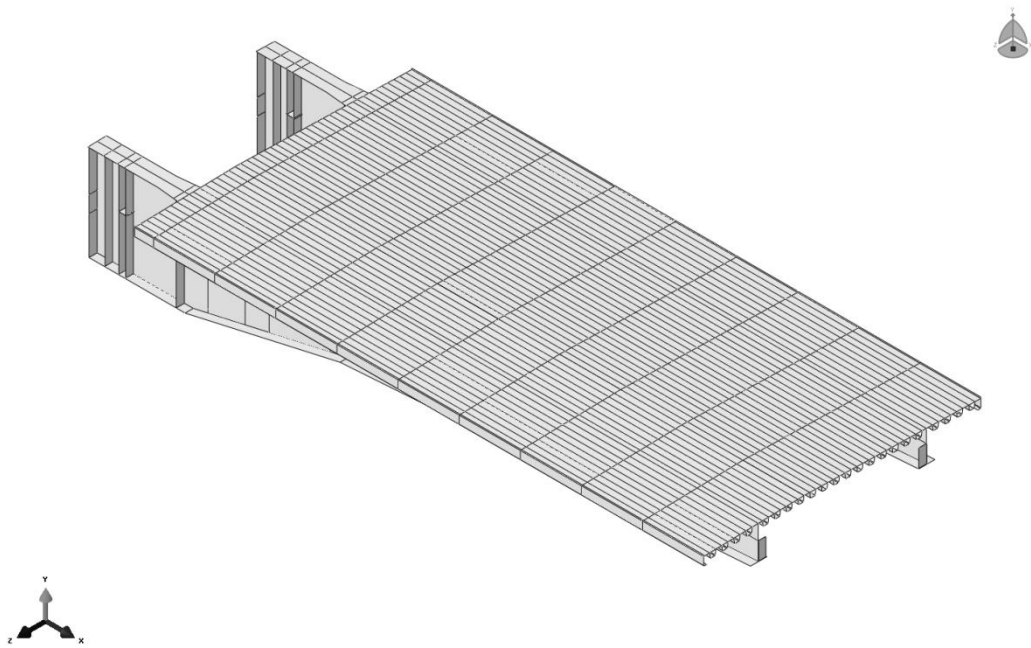
Figure 6-13 Assembly with abutment endplate

6.2.2.5 Assembling end plate at nose opening

The endplate at the nose opening is assembled into the model, see Figure 6-14. The box for the locking mechanism is also included in the model to better simulate the sectional stiffness at the bridge end section. The plates for the locking mechanism are added in the sketch module.
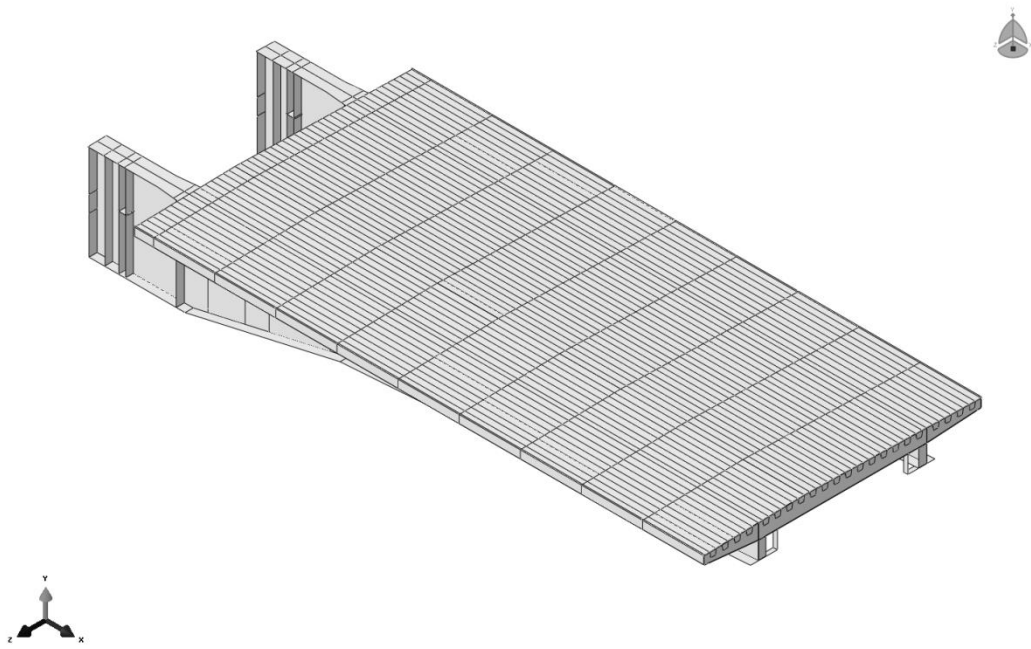
Figure 6-14 Assembly with nose endplate

6.2.2.6 Modelling the K-joint

In the section at floor beam 10 there is a K-joint. This K-joint consists of steel box beams which are welded to connection plates at the floor beam and the main girder stiffeners.

The K-joint, see Figure 6-15, is modelled with wires which will be assigned beam sections later on. The connecting plates are disregarded and are replaced with stiff couplings. This simplification results in higher local stresses at the connection points for the coupling, but do not influence the global behaviour of the bridge or the local behaviour at the crack initiation areas.
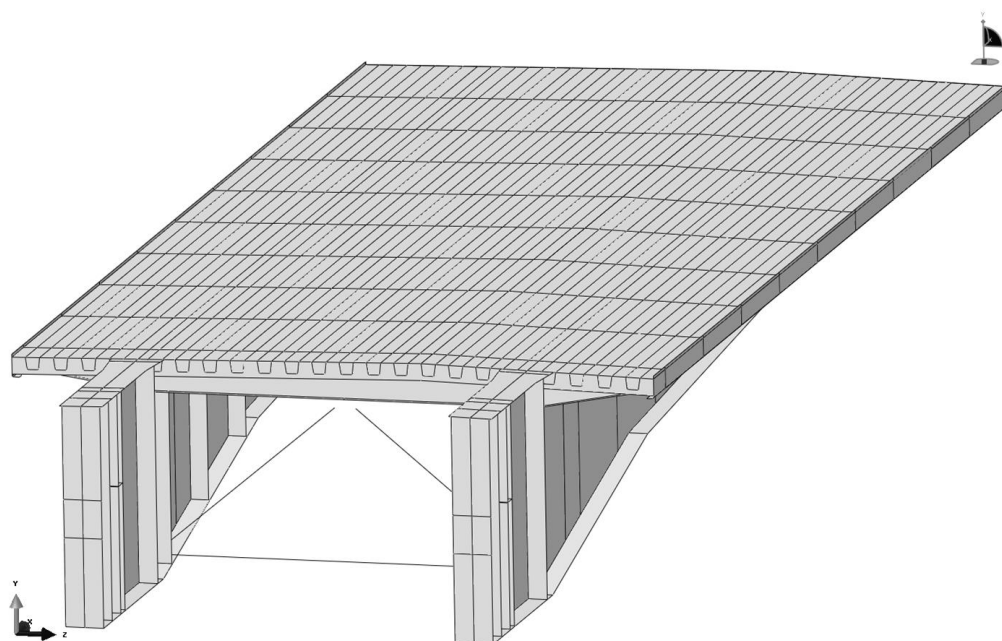
Figure 6-15 Assembly with the K-joint

6.2.2.7 Final geometry of the bridge modelled

All parts of the bridge are assembled together to the bridge-model, see Figure 6-16.
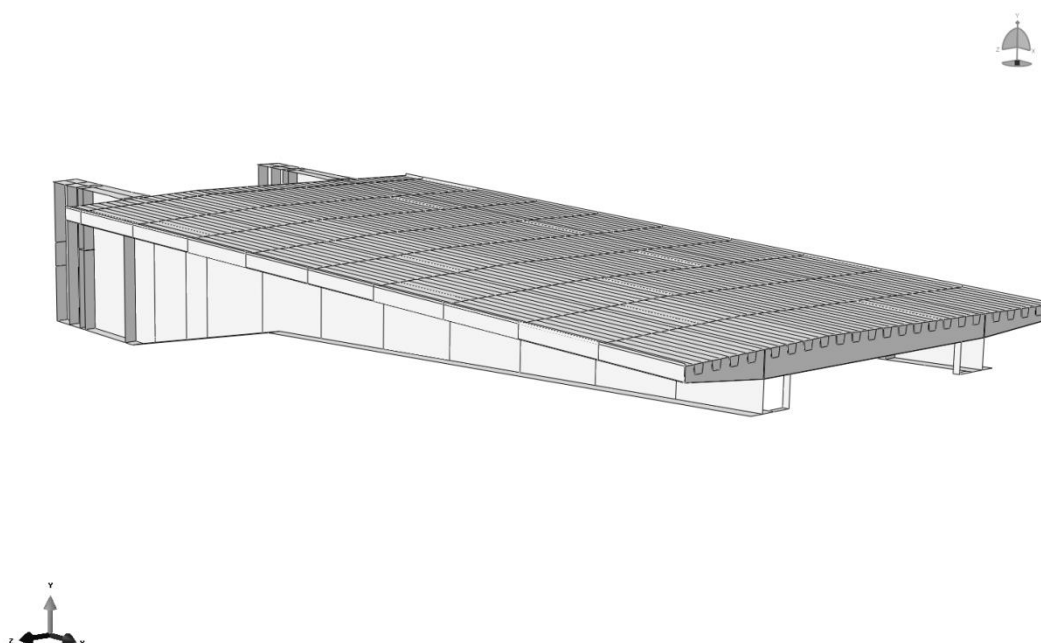
Figure 6-16 Final geometry of the bridge modelled.

6.2.3 Property module

In the property module materials are defined and assigned to the parts. Material orientation and element normal are defined. Sections with thickness and thickness orientations are created and assigned to the parts.

6.2.3.1 Materials

In this specific bridge three different steel grades are used. The three steel materials are defined with density of 7800 kg/m^3, Young's modulus of 210 GPa and a Poisson's ratio of 0.3. The plastic yield stresses are also defined, but is not necessary for this type of analysis since only a linear analysis is performed.

The different members are divided into sets to make the modelling process easier and to be more precise in the analysis and result extraction.

Table 6-1 Different sets and corresponding material

No.	Member	Material
a	Deck plate	S420
b	Rib	S420
c	End plate	S275
d	Main girder web	S420
e	Main girder flange	S420
f	Floor beam web	S355
g	Floor beam bottom flange	S355
h	Stiffeners	S355
i	Support plate	S420
j	Lock plates	S355
k	K-joint beams	S355

6.2.3.2 Element normal

The element normal directions are defined for the different members according to Figure 6-17 and Figure 6-18. The brown areas have a normal direction positive outwards and the purple a negative normal direction outwards. The element normal defines the direction for thickness offset direction for the shell element.
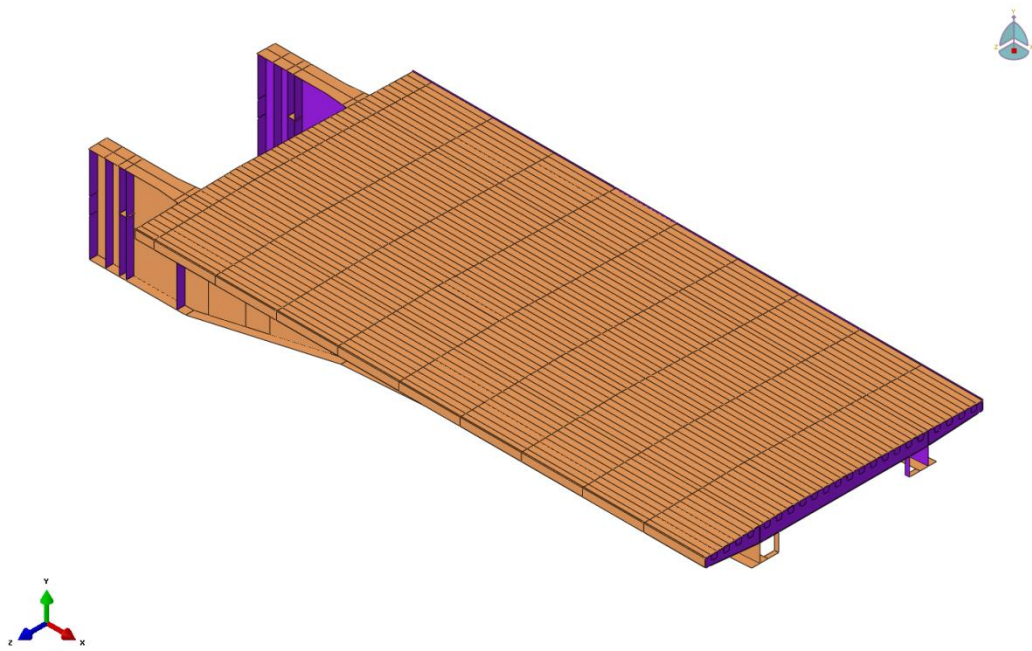
Figure 6-17 Definition of element normal direction, (brown = positive upwards)
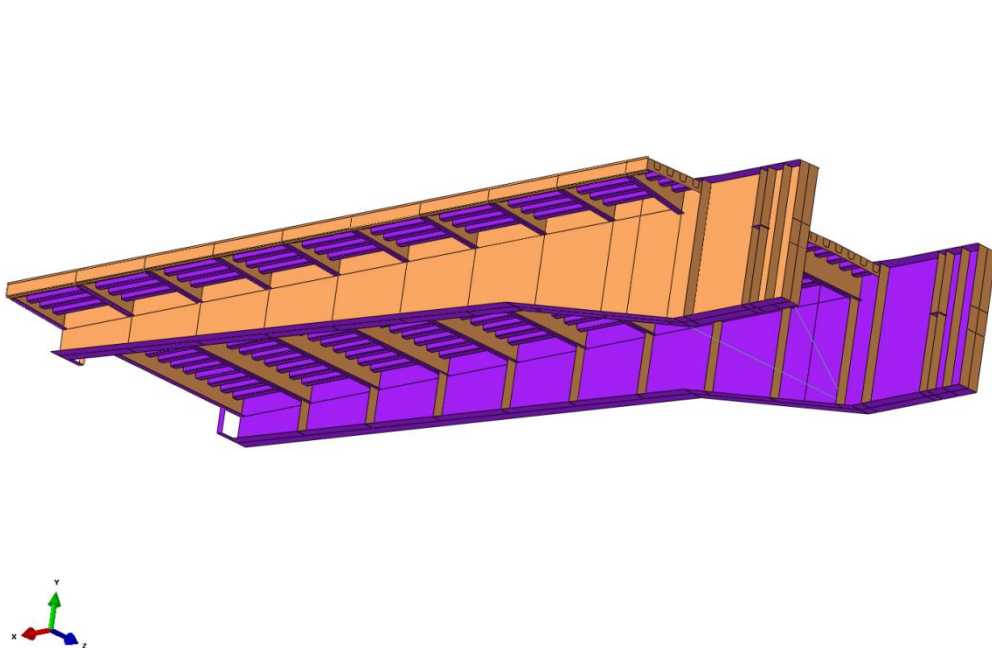
Figure 6-18 Definition of element normal direction, (brown = positive upwards)

6.2.3.3 Material orientations

Material orientations are assigned to all parts. This defines the material directions. Since the bridge model is made entirely of steel, which is an isotropic material, the material orientation assignment need only consider that the definition of the material orientation is three-dimensional. The material direction for the ribs can be seen in Figure 6-19 below.

CHALMERS, *Civil and Environmental Engineering*, Master's Thesis 2015:14
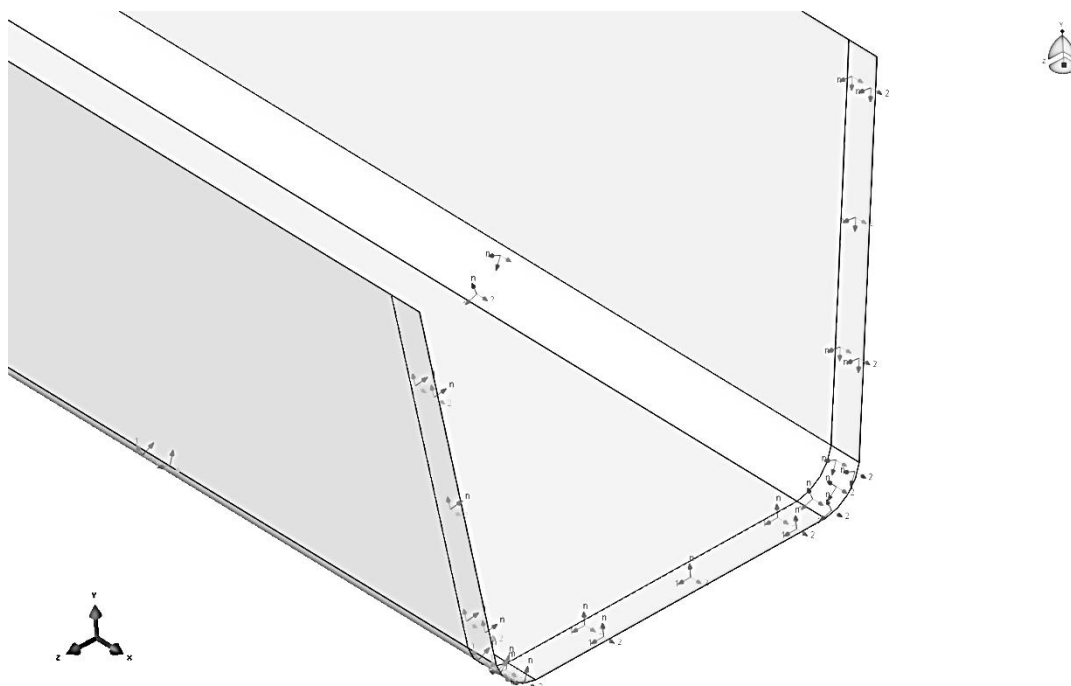
Figure 6-19 - Material orientation in the ribs

6.2.3.4 Sections

All parts of the model need to be assigned a section. Sections are created and assigned to the different parts. The sections primary defines the shell thickness and the material, but also the number of integration point in the thickness direction. All sections, except the K-joint, are created as homogenous shells and a summary of the varying material and thickness assignment can be seen in the table below. The K-joint is created as constant beam elements. All sections are defined with five integration points in the thickness direction.

Table 6-2 Thickness and material of different members

No.	Member	Thickness	Material
a	Deck plate	14 mm	S420
b	Rib	6 mm	S420
c	End plate	12 mm	S275
d	Main girder web	20 mm	S420
		25 mm	
e	Main girder flange	40 mm	S420
f	Floor beam web	10 mm	S355
g	Floor beam bottom flange	20 mm	S355
h	Stiffeners	10 mm	S355
		15 mm	
i	Support plate	50 mm	S420
j	Lock plates	20 mm	S355
k	K-joint beams	10 mm	S355

Table 6-3 After this the sections are assigned according to definitions below:

No.	Member	Shell offset from
a	Deck plate	Bottom
b	Rib	Mid
c	End plate	Bottom
d	Main girder web	Mid
e	Main girder bottom flange	Top
f	Floor beam web	Mid
g	Floor beam bottom flange	Top
h	Stiffeners	Mid
i	Support plate	Mid
j	Lock plates – Horizontal	Top
	Lock plates – Vertical	Mid
k	K-joint beams	Mid

The K-joint is modelled with beam sections. The profiles can be seen in Figure 6-20 and Figure 6-21 below. The horizontal beam has a quadratic profile RK120x120x10 and the inclined beams have a rectangular profile RK120x200x10.
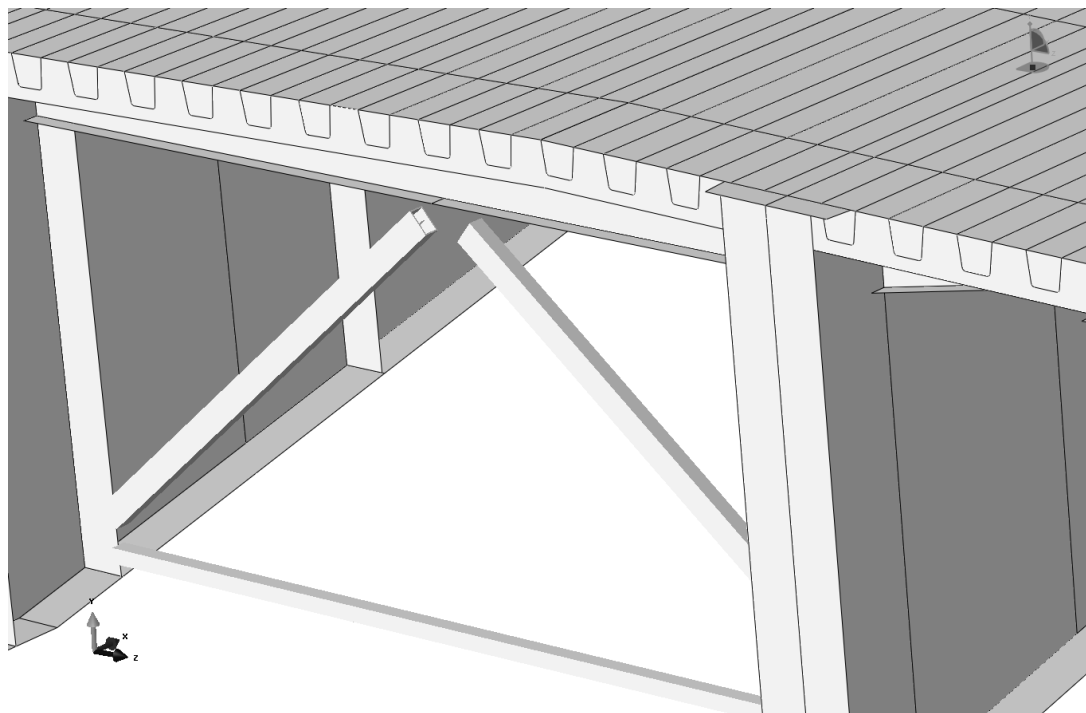
Figure 6-20 K-joint with rendered profiles
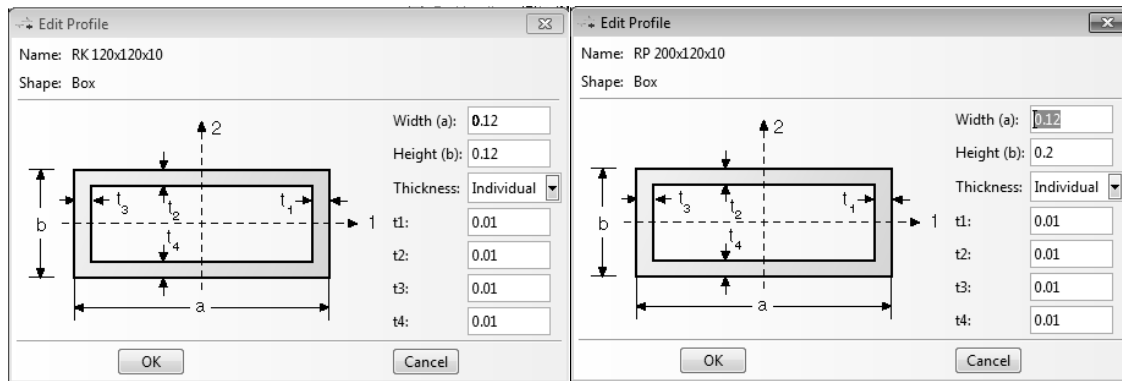
Figure 6-21 Beam cross sections for the K-joint. The left figure shows the cross section for the horizontal beam. The right figure shows the cross section for the inclined beams.

6.2.3.4.1 Interesting details regarding the thickness rendering using shell elements

When using shell elements it is important to be aware of in which direction the shell thickness rendering be generated. In many cases the most convenient way of modelling a structure is by model the shells in the separate components mid-line. But this way is not always the most representative way of modelling the structure and specific regard should be taken to this problem. One example is the endplates seen in Figure 6-22, where the shell is modelled at the connection with the floor beam web and then the thickness of the endplates is rendered outwards. This method excludes unnecessary overlap or loss of area.

Despite the careful considerations regarding the thickness rendering, using shell element will always result in small areas with overlap or loss of material. Some of these areas from the modelled bridge are presented below.
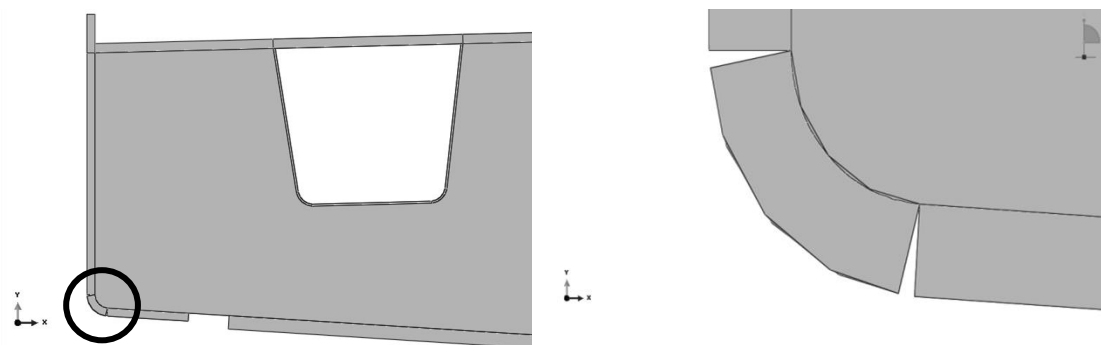
Figure 6-22 End plate thickness rendering

Inclination of rib walls resulting in overlap of area, see Figure 6-23:
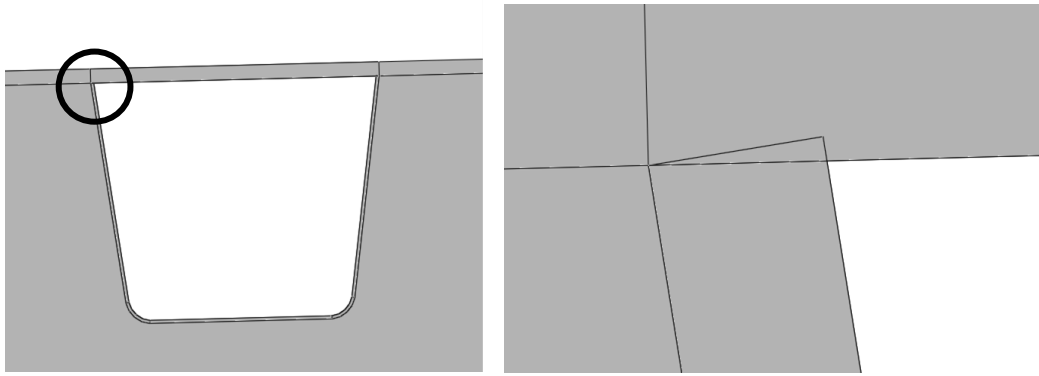
Figure 6-23 Overlap of areas at intersection between rib wall and deck plate

Inclination of floor beam flange resulting in loss of area, see Figure 6-24:
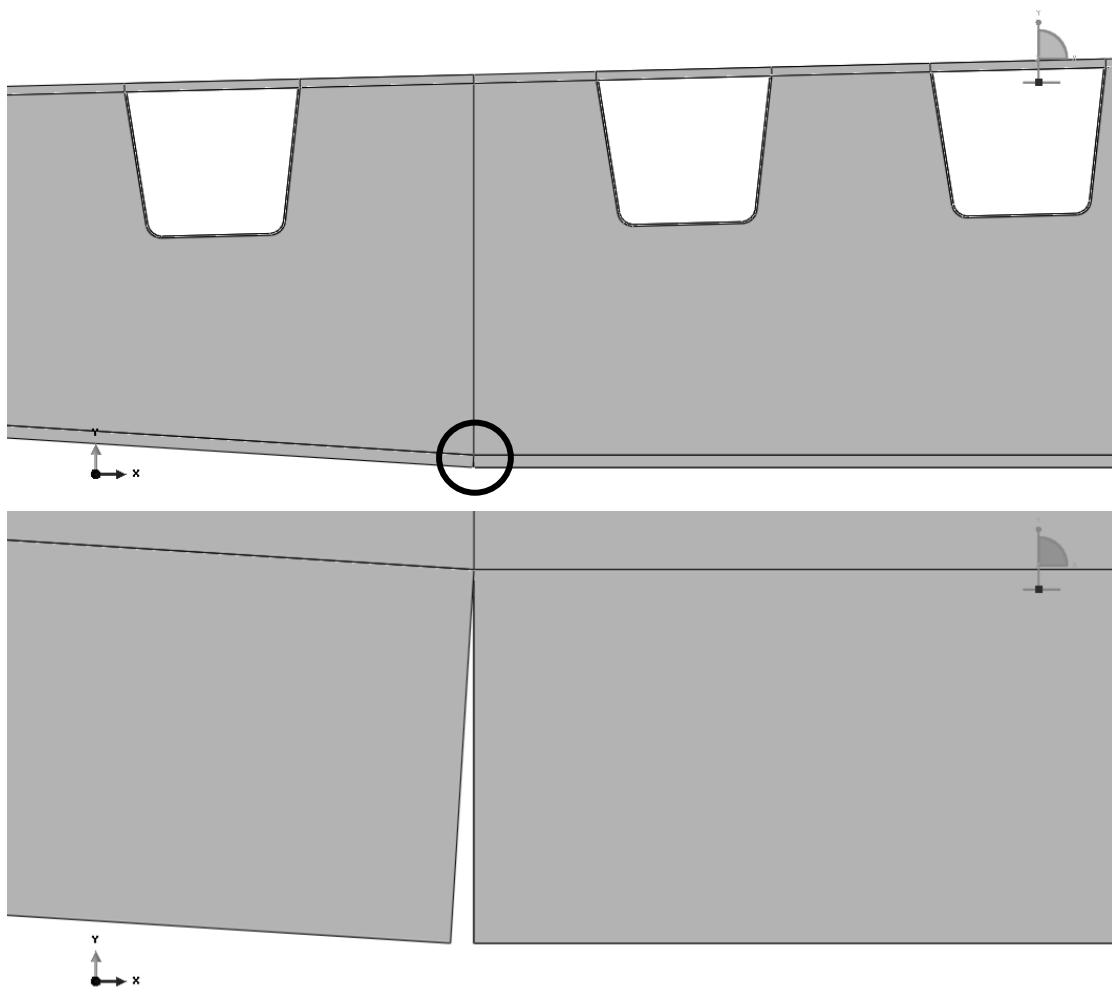
Figure 6-24 Inclination of floor beam web results in gap between floor beam bottom falange

Deck plate crown point resulting in loss of area, see Figure 6-25:

CHALMERS, *Civil and Environmental Engineering*, Master's Thesis 2015:14
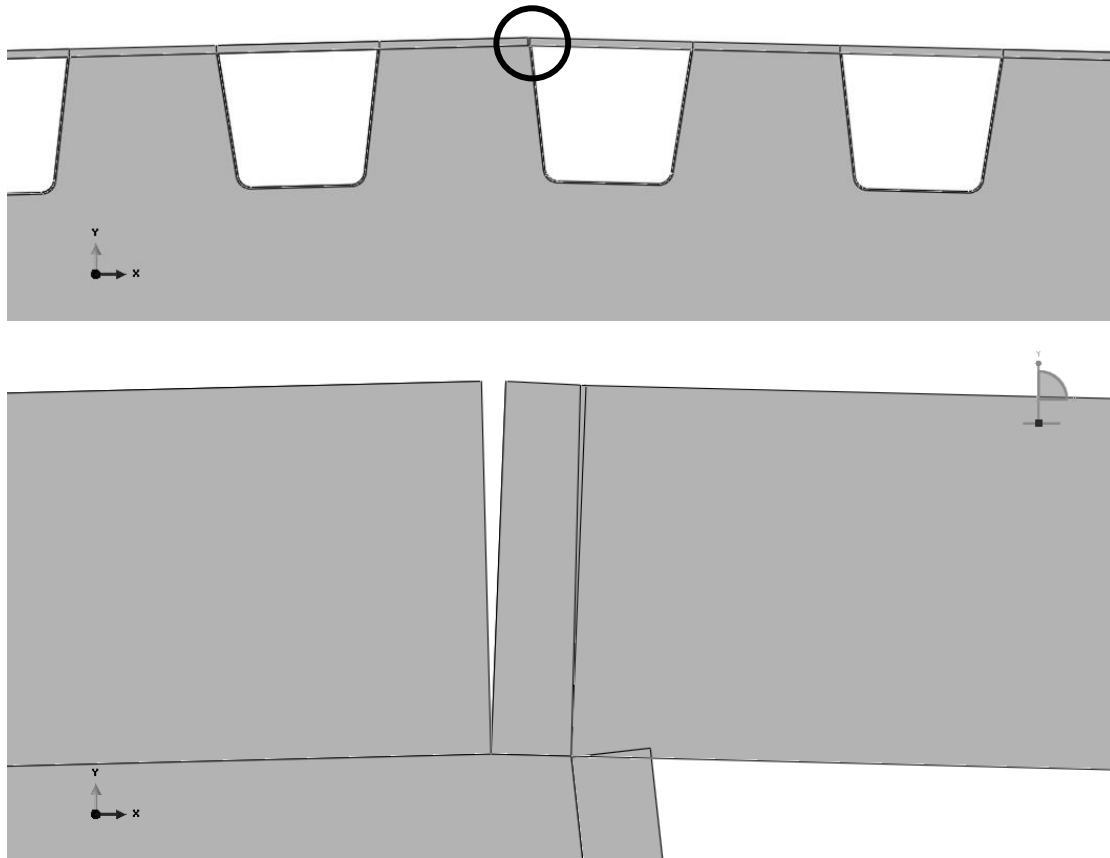
Figure 6-25 Crown point results in gap at deck plate

The close capture of the crown, see Figure 6-25, also shows a division of elements where the first rib wall connects to the deck plate. The part from the crown to the connected rib wall seems to have a different inclination than the rest of the DP. This was investigated and ruled out.

6.2.4   Interaction module

The K-joint is modelled as wires with beam sections, as previously noted. In the interaction module, these beams are constrained to the main structure with coupling constrains, see Figure 6-26. The connected nodes are constrained in all translation and rotational degrees of freedom to each other.
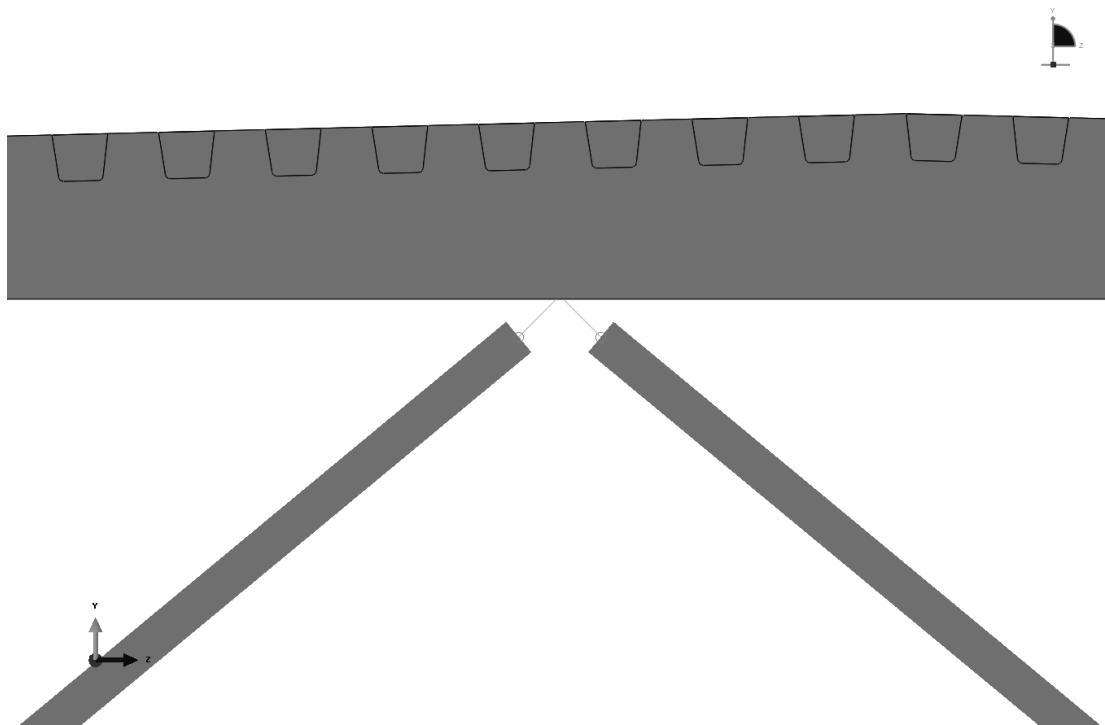
Figure 6-26 - Coupling constraint between beams and floor beam flange

In the interaction module the springs representing the resistance of the second leaf of the bridge deck are modelled. The springs are modelled as elastic spring in the connector builder in the interaction module. The springs only transfer vertical force. The spring stiffness is calculated using a unit force, P, placed above each main girder in the FE-model, with no other loads present. The deflection is measured at the intersection between main girder and floor beam flange. The spring stiffness is calculated with Hooke's law, see Equation 6-2.

$$K = \frac{P}{\delta}$$

Equation 6-2

The location of the loads straight above the main girder results in that almost the whole load is taken by the main girders directly below the respective load. Therefore the two loads can be placed simultaneously without disturbing interaction and the deflections are not affected by distortion or rotation of one side of the bridge which would have been the case if only one side was loaded. On the other hand the total deflection will be slightly larger resulting in lower spring stiffness. The lower spring stiffness the more similar the behaviour is to cantilever action. In this investigation when the behaviour in vicinity of the ribs are of interest, this is on the safe side. Both methods are checked and the difference is less than 2.5%

Table 6-4 - Spring constants for spring at bridge nose

	Deflection for P=1kN, [mm]	**Spring stiffness, K, [MN/m]**
Left side spring	0,231	4,326
Right side spring	0,222	4,505

There is a small difference in the spring stiffness for the studied bridge. This is due to the fact that the bridge is not symmetric along the longitudinal axis. The crown on the deck is not placed in the middle, but instead towards one of the main girders.

6.2.5   Step module

In the step module analysis steps are defined and loads are assigned to their respective step. If several load positions is to be investigated in the same analysis, the number of steps is the same as the number of load positions. The type of step suitable for this kind of analysis is static general.

One important topic to consider when large jobs are analysed is the output requests. In the step module there exist two different output requests, Field output and History output. To perform a fatigue analysis it is only necessary to request the stress, S, in field output. The history output can be suppressed and thereby saving much computational time and storage memory. The analysis can be further refined by only requiring field output in the specific region of interest. This is done by creating a set of the desired region in the part module, and in the field output only request output on this set. By doing these two tasks, the amount of data that needs to be processes is decreased significantly. This results in faster analysis time and smaller result files.

6.2.6   Load module

Loads and boundary conditions are defined in the load module. The boundary conditions are created in the initial step and propagated through the whole process since they are constant in the whole analysis. For this model two boundary conditions in addition to the springs at the cantilever side of the leaf are introduced, as described above and shown in Figure 6-27. The boundary condition at the vertical edge is modelled as a fixed support with full restrains in all translation and rotational degrees of freedom. The boundary condition at the horizontal plate is modelled as a pinned support and fully restrained in the vertical translation degree of freedom.
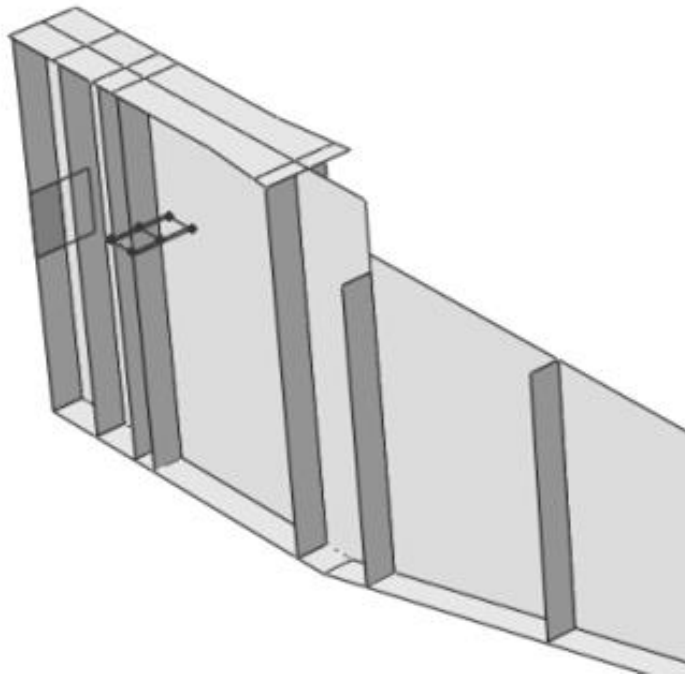
Figure 6-28 Illustration of location of the boundary conations

The modelling of loads is done by creating a load in an active step. The load is modelled as pressure and applied to predetermined surfaces. These surfaces can be created in the part module in a similar way as the sets. In this case with regard to the fatigue damage the most severe load positions for each crack mood must be known in beforehand. The load for the respective crack investigated is to be placed at this position.

6.2.7 Live load module

In Brigade/PLUS there is an additional module called the Live load module. In this module loads can be modelled as moving loads. However, for fatigue this tool is not recommended. The main reason for this is that the live load applies the wheel loads as point loads and moves in steps in the longitudinal direction. By doing this the local load response of the OSD becomes very different compared to applied area loads, see Chapter 6.1. Another reason against the use of the live load module is the uncertain local load position in longitudinal direction, since the load is applied with a defined interval along a load line. The local effects in longitudinal direction will affect the local stresses at the crack initiation areas and will therefore differ depending on the exact location. A third reason against the live load module is the excessively amount of processing power needed for this analysis and the size of the result files. This is usually not a problem in global analysis because of the lower mesh density required, but in fatigue analysis the mesh is much denser resulting in large files reaching up to 100 gigabytes.

6.2.8 Mesh module

In the mesh module the part, or the assembly, is meshed and nodes and elements are defined. For global analysis it may often be sufficient to use a global seed for the whole structure. In fatigue analysis the local behaviour is very important and therefore the mesh usually needs to be denser. Therefore a global seed is not applicable in these situations since the immense amount of elements thus generated would require unnecessary processing power. Instead a local seed with high mesh density should be used in the area of interest and the remaining part of the structure is to be assigned a global seed.

Before meshing of the model is implemented the location of the crack initiation must be known since this is the area that is to be meshed with higher density.

When the worst load location and the investigated crack initiation area are known, the structure can be meshed. It is recommended to use the hot spot stress method for extracting the stresses at the crack initiation areas. This is easily done by partition the face along paths where the hot spot stress should be extracted. By doing this it is guaranteed that nodes will be placed along the partitioning line. Thereby assuring that the stresses can be extracted at the relevant distances from the connection according to the hot spot stress method, this is described in Chapter 4.2.

It is recommended by the authors to place partitions at 0.4t and 1t distance from the investigated crack initiation point, where t is the thickness of the member investigated, see Figure 6-29. By including these partitions it simplifies the stress extrapolation needed in the structural hot spot method. It is also recommended to place a partition at 2t to simplify the transition from the very small local mesh to a larger global mesh. A recommendation is that the mesh should be structured in the area of interest. Therefore the areas close to the crack initiation should be assign structured element type and remaining structure can be modelled with free element type, see Figure 6-34. To simplify the transition between the areas with high density mesh to the areas with lower mesh density it is recommended to use the single bias tool in the local seed. This concentrates the number of element to one side of the edge and gradually smoothen the transition to larger element size. When the structure is meshed it should also be verified in the mesh module and the number of poor elements should be kept at a minimum.
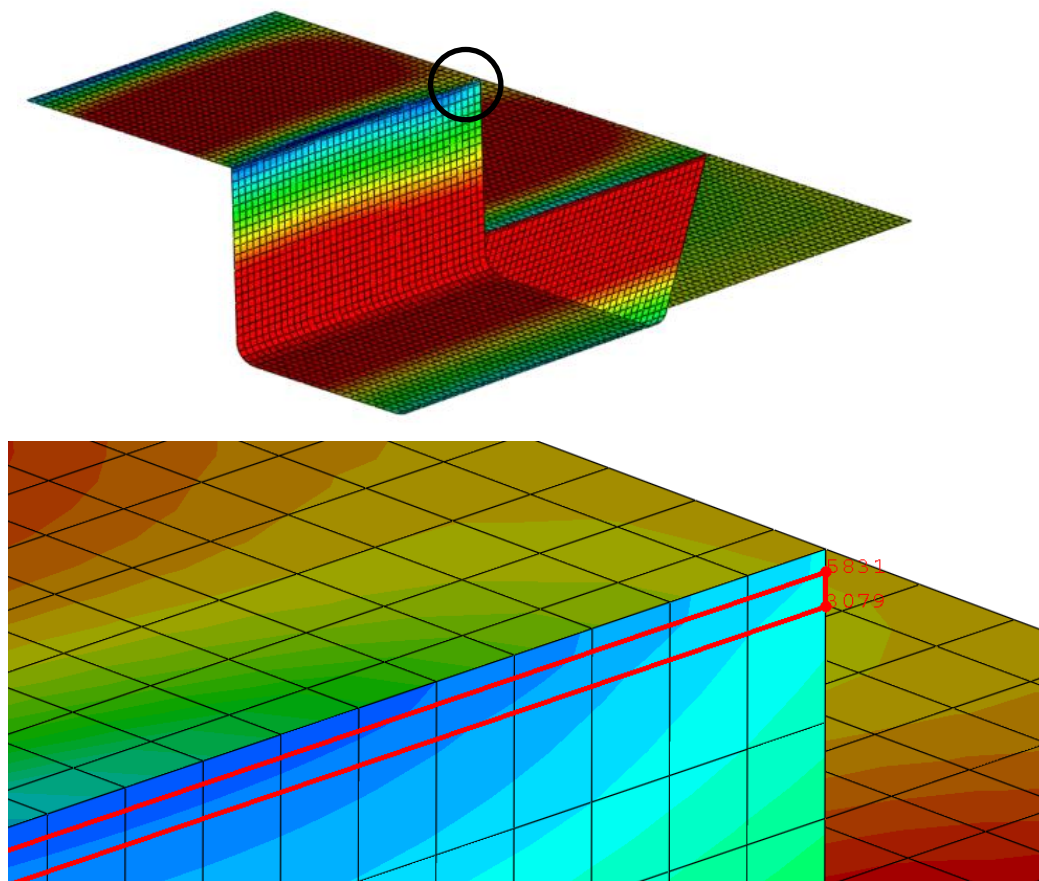
Figure 6-29 (a) Stress concentration in rib and deck plate; (b) Illustration of hot spot partitioning lines

6.2.8.1 Meshing technique when using hot spot stress method

The mesh quality is of large significance for the stress extraction. Therefore an example is presented below with some recommendations regarding the mesh technique for hot-spot stresses.

Crack II, crack at weld between deck plate and rib wall, propagating in the rib wall, will be investigated for fatigue. The hot spot stress in mid span is needed for the fatigue evaluation. The centre part of the rib can be seen highlighted in Figure 6-30. The hot spot stress should therefore be extracted for the worst region in the rib wall, at distances defined from the connection to the deck plate.
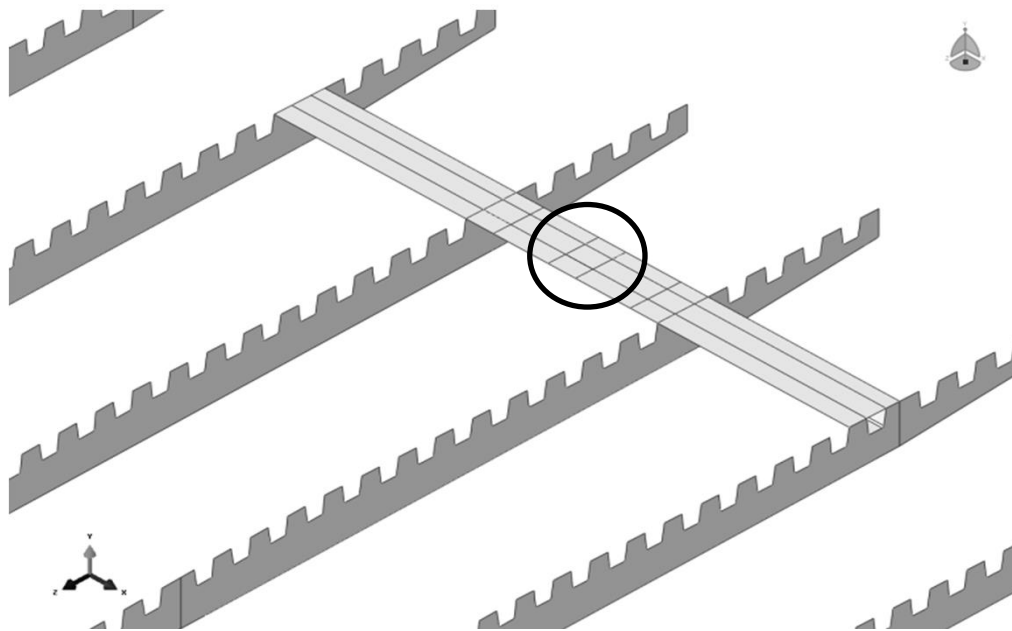
Figure 6-30 Investigated region for Crack II

1. Define partitions where the stresses should be extracted.

Partitions are made in the rib wall at distances 0.4t and 1.0t from the intersecting deck plate. These are done in the part module by creating datum planes and define partitions with the datum planes. The closest partitions are highlighted in Figure 6-31.
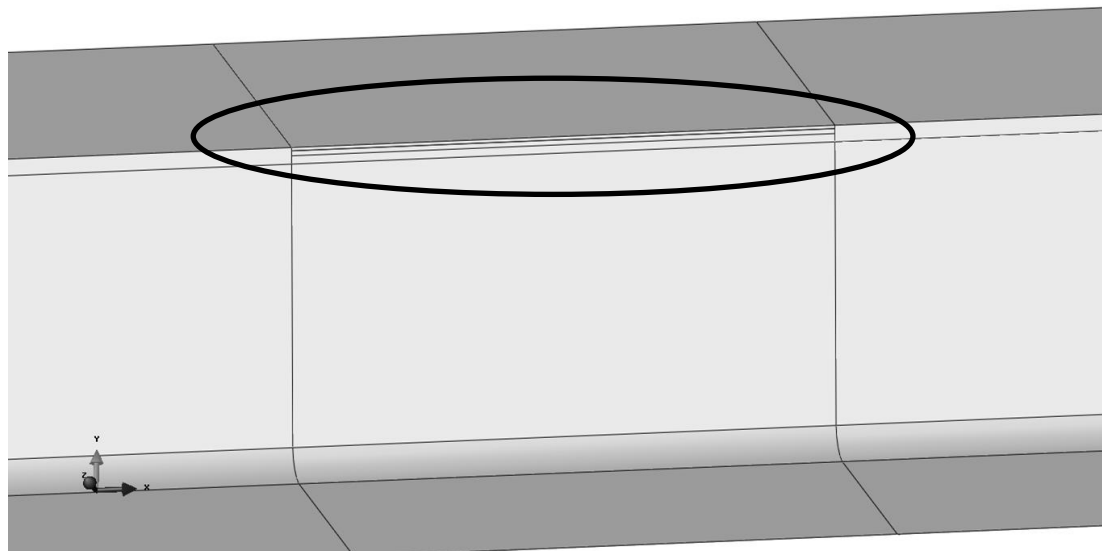
Figure 6-31 Hot spot partitions in the rib wall

2. Assign structured element meshing technique to the region of interest

In the mesh module, start by define the meshing technique in the region of interest to structured. This area will be coloured green, this is shown by the darker shaded area in Figure 6-32.
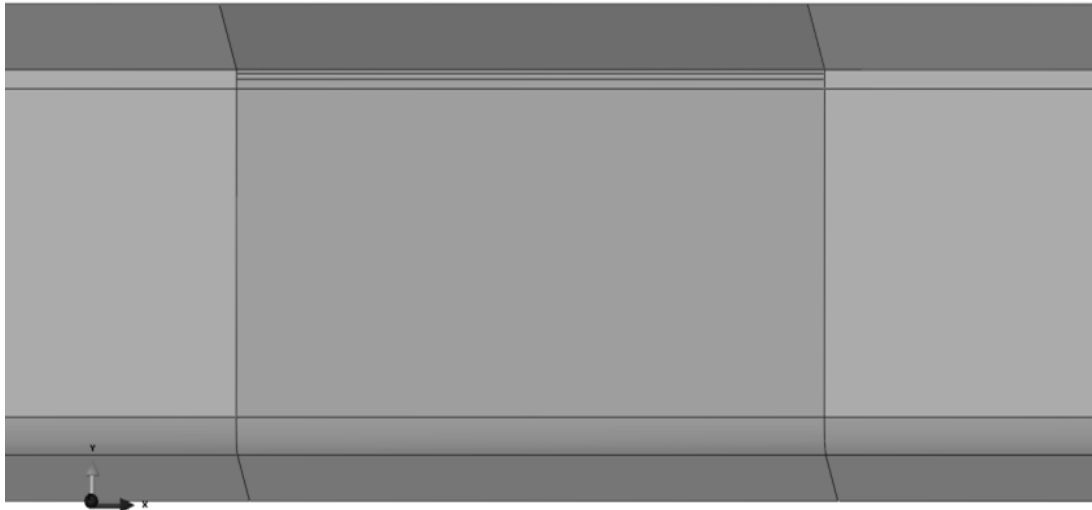
Figure 6-32 Different element meshing technique, dark shade represent structured mesh and lighter shade represent free meshing technique

3. Define global seed to the whole model

Start by defining a global seed to the entire model. Approximate global size is put to 0.2.

4. Define the local seed

The local seed is assigned. Recommended is to use previously defined set and assign local seed to these. Start with the region close to the stress extraction point. Define a seed in such a way that 2 elements fit inside the interval 0t to 0.4t and also between 0.4t and 1.0t, see Figure 6-33. In the model used this seeding corresponds to an element size of approximately 0.002m. The recommended element type to use is the S8R, which is a 8-node doubly curved shell element. This can be edited in the element type window by choosing quadratic as the geometric order of the element.
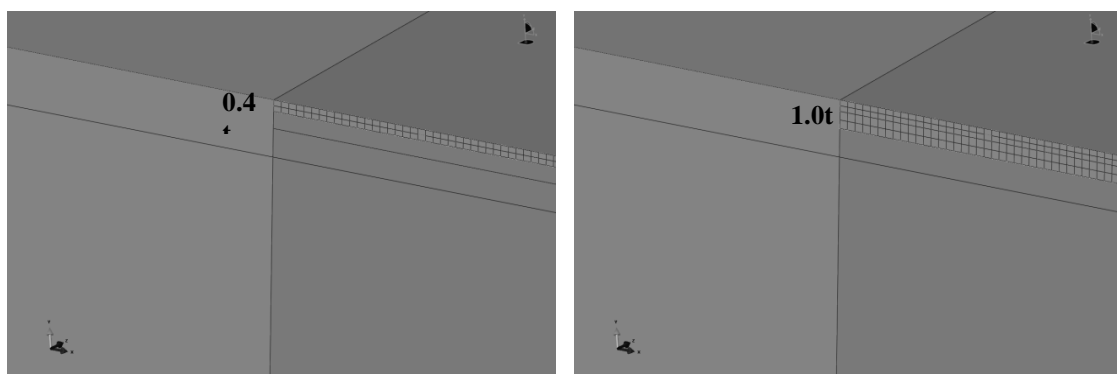
Figure 6-33 Mesh in the hot spot area

Everything needed to extract the hot spot stress is now defined. But if the analyst tries to mesh the whole structure with only this local seed and the global seed it will in

many cases fail, or at least create an unsatisfactory mesh with malfunctioning elements that will disturb the stresses in the region of interest.

To improve the mesh quality further local seeds should be defined. Start from the region seen in the figure above and work away from the investigated area by gradually increase the element size. This can effectively be done by use of the single bias in the local seed toolbox, see Figure 6-34. The figure below defines the seeding along an edge so the minimum size is 0.004 and gradually increase the element size to 0.025. The arrow along the edge shows what side of the edge that will have the densest mesh.
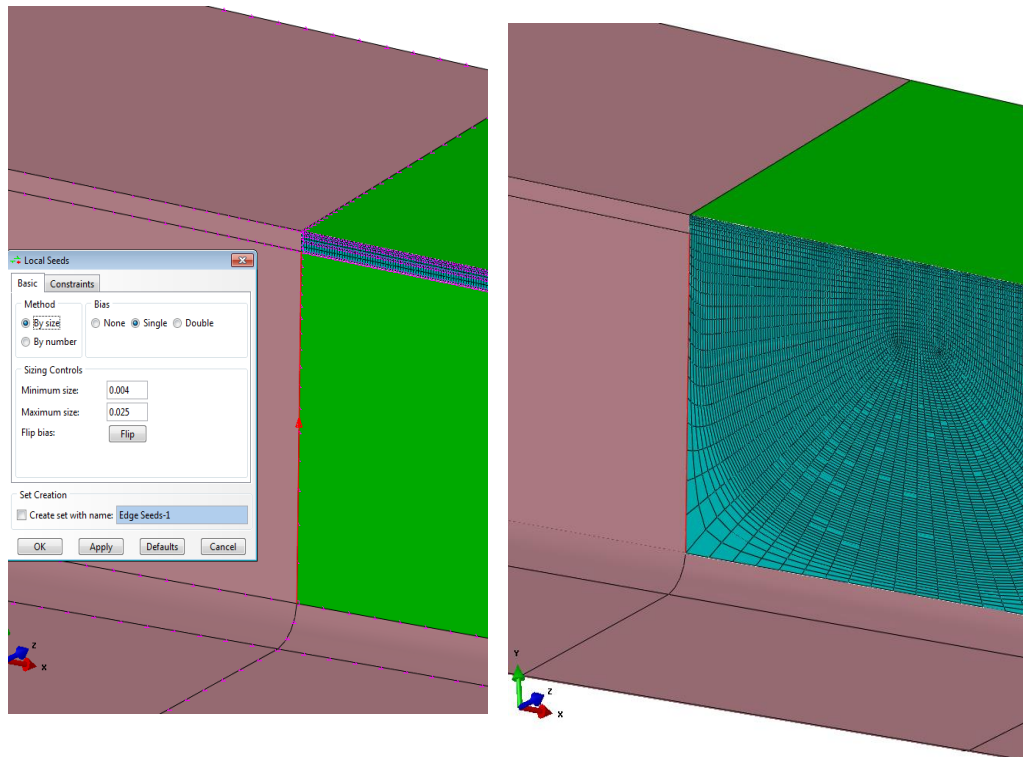
Figure 6-34 Mesh at the Hot spot region and the transition towards the global mesh

By using structured meshing technique and the bias tool, there is a good chance of getting a good mesh. The mesh quality can be verified in the mesh module with the tool Verify mesh.

The final mesh can be seen in Figure 6-35 below. As can be seen it has a smooth transitions from small elements to larger elements. The mesh quality is also verified in the mesh module which states that the worst angle for Quad elements is 25 degrees and for Triangular elements 16 degrees.
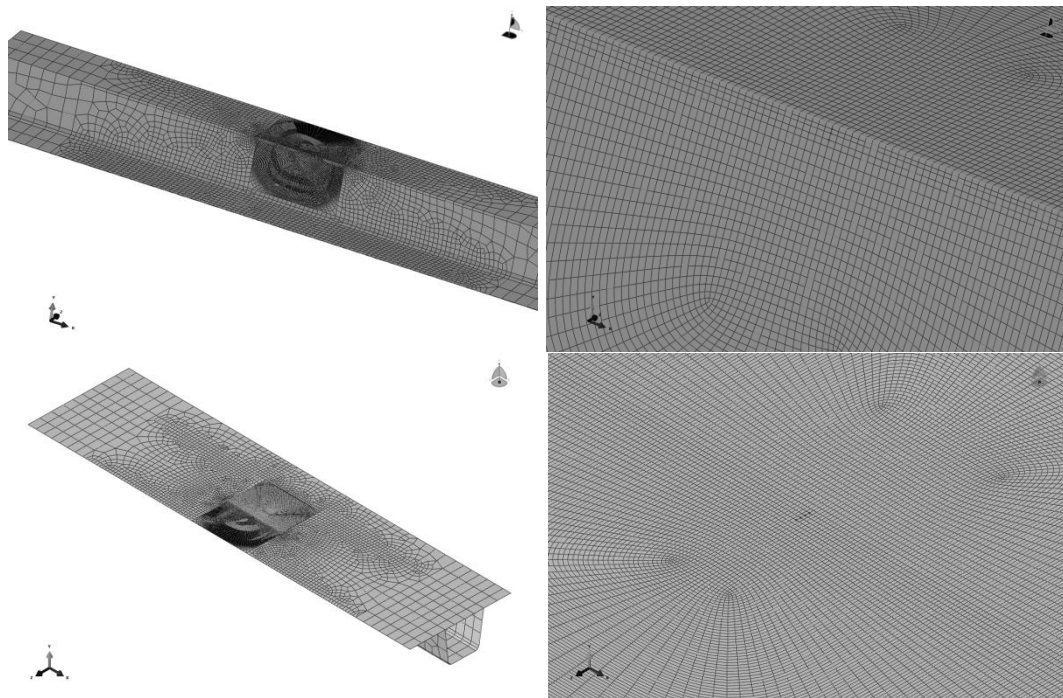
Figure 6-35 Transition from high density mesh to low density mesh; (a) Rib wall and deck plate seen from below; (b) Deck plate seen from above

6.2.9   Job module

In the job module the job is created and the submitted for analysis. The result files will be created in the defined work directory.

6.2.10 Visualization module

When the job is complete the results can be seen in the visualization module. The stresses used in the fatigue evaluation are principal stresses perpendicular to the weld. It is also necessary to pick the correct stress value in the thickness direction when using shell elements. Shell elements have several integration points in the thickness direction and the stresses showed in Brigade/PLUS are by default the bottom values. That means that the stress showed is the stress at the defined bottom of the shell element. To change the stress results to show the shell top values go to Results → Section points → choose top or bottom. It should also be controlled which side of the shell the stresses should be extracted from and if that side corresponds to the top or bottom values.

The stresses used to control the fatigue performance are principal stresses perpendicular to the weld. The direction of the principal stresses can be seen by choosing to display the stresses as vectors. According to IIW (2008) all principal stresses with a principal direction within 60 degrees of the normal direction of the weld is seen as perpendicular stresses. All principal stresses with a principal direction differing more than this is seen as parallel to the weld and should be disregarded.

6.3   Verification of model

It is important to verify that the FE-model have a realistic behaviour. In the model used for this thesis the verification is performed by comparing the deflection of the bridge in the FE-software with hand calculations. The deflection is calculated for one of the main girders with effective width of the bridge deck according to Eurocode 3 (EN 1993-1-5). The model used in hand calculations can be seen in Figure 6-36, the stiffness distribution along the beam in Figure 6-37, the cross section of the beam in Figure 6-38. The calculations are found in Appendix II.
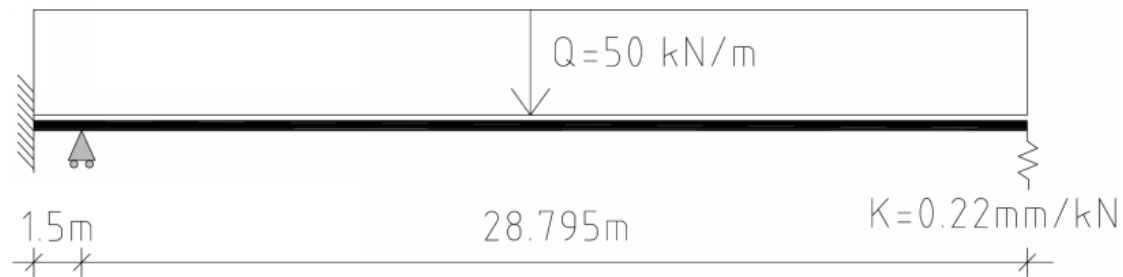
Figure 6-36 System used in deflection calculations by hand
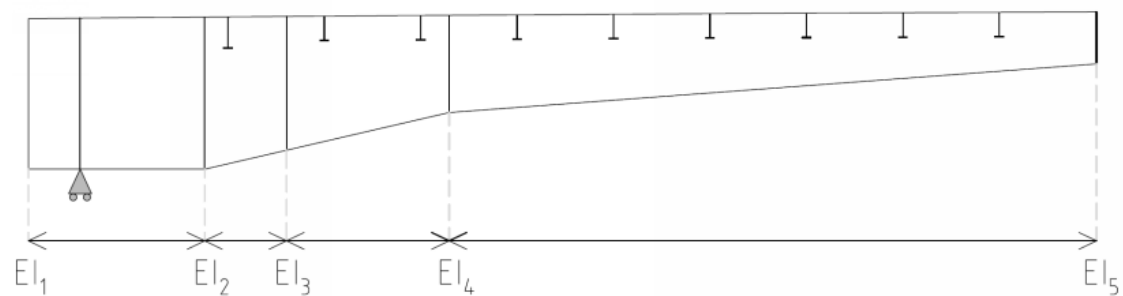
Figure 6-37 Stiffness distribution used in deflection calculations by hand
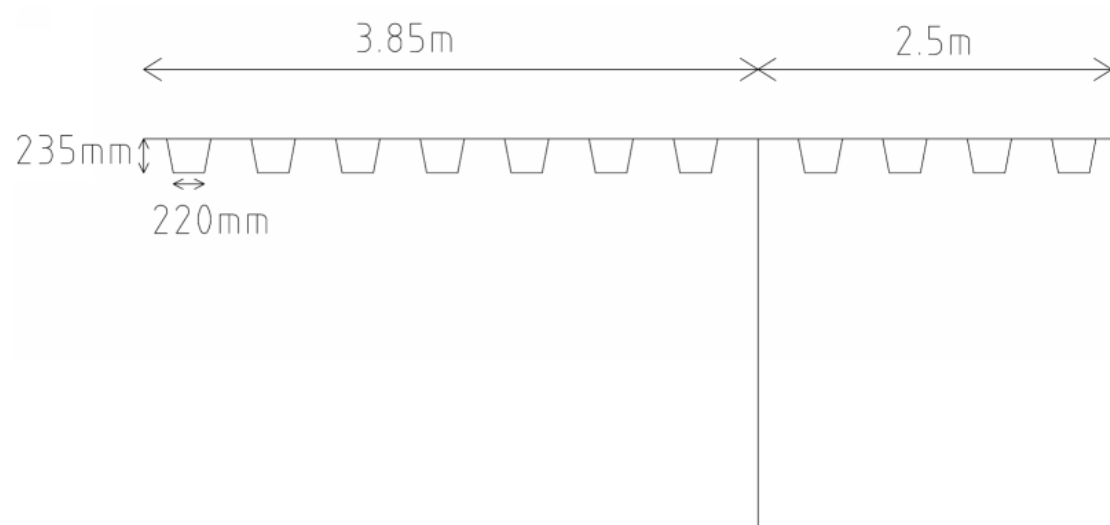
Figure 6-38 Cross section of the main girder used in deflection calculations by hand

The deflection from hand calculations is compared to the deflection in the FE-model and can be seen below in Table 6-5. The deflections are calculated at the nose opening and correspond very well. The FE-model is realistic and is determined to be verified. For full calculations see Appendix II.

Table 6-5 Deflection results from hand calculations and FEM

	Hand calculations	FEM-Model
Deflection	41.7 mm	42.1 mm
Error	1.06%	

7 Results and comparison of analysis techniques

In an orthotropic deck there are several positions where cracks can initiate with different modes and propagation paths. Several of these cracks have been found to appear with high frequency in OSD bridges. Part of the reason for this is believed to be the difficulty to determine the stresses at these areas and that the fatigue evaluations are performed with inaccurate models for calculating the governing stresses. Three of the frequently reported cracks have been chosen for investigation. In this chapter the most adverse load location for these three crack and their initiation positions will be investigated through an iterative process in Brigade/PLUS. Also the stresses with the load placed in these locations and the fatigue life of the members will be evaluated. This will be compared to the fatigue life calculated with conventional methods with the load placed according to hand-calculations models.

The studied cracks are:

- Crack initiated at the weld toe in the rib-to-deck plate weld, the crack propagates in the deck plate and is referred to as R-DP Crack I, see Figure 7-1 (a).
- Crack initiated at the weld toe in the rib-to-deck plate weld, the crack propagates in the rib wall and is referred to as R-DP Crack II, see Figure 7-1 (a).
- Crack initiated at the weld toe at the radii in the rib-to-floor beam weld, the crack propagates in the floor beam web and is referred to as R-FB Crack III, see Figure 7-1 (b).
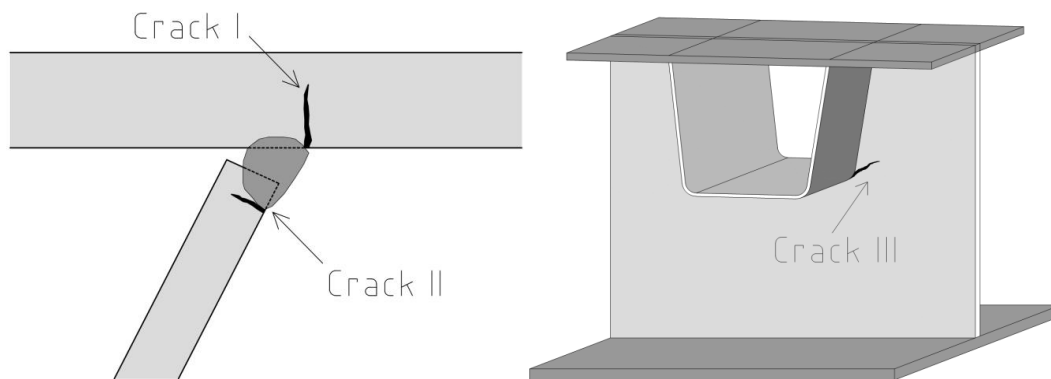
Figure 7-1 The three investigated cracks (a) Crack I and II at the rib-to-deck plate weld; (b) Crack III at the radii of the rib-to-floor beam weld.

7.1 The process of determine the most adverse load position in the deck

To determine the fatigue stress range for the three critical crack initiation areas it is important to find the most adverse load position for the response in each region separately. This is done through an iterative process in which stresses at interesting sections for different load cases are calculated and compared.

First, a lighter investigation with a coarser mesh and more general approach to study the behaviour of the interesting areas is performed. From the first analysis and the

results, general conclusions regarding overall responses and load positions are drawn, also a better understanding of the behaviour of the deck and load transfer are obtained. This gives an understanding of the performance of the deck and a foundation for later assumptions. With the base in these conclusions new investigations regarding more local and detailed response are performed. For these analyses more dense mesh and improved stress reading will be used to assure more reliable interpretations. The conclusions drawn here will be evaluated and used in the final part of process that is to determine the most adverse load position with regard to the three interesting crack modes.

With the basis in these investigation recommendations regarding modelling, meshing, stress reading, hot spot calculations and load positions will be given. The last part of the study will be performed with the objective to be able to find general and practical recommendations. As one of the main purposes of the thesis is to produce general guidelines that can be used in design of similar bridge decks only positions that can be generalized and translated to other bridges will be analysed.

All performed analyses are based on Fatigue load model 3 in Eurocode, described in Chapter 5.2.2, and the recommendations given will therefore be in line with the requirements of the current codes.

7.2 Assumptions based on the initial analysis

In the initial analysis the general behaviour of the OSD is studied. From the results of these tests conclusions regarding how to proceed and which aspects are important to consider are drawn. The studied subjects for the initial analysis are:

- Load application with regard to distribution area
- Relevance of the second wheel on the load axle
- Influence of the two rear axles in the fatigue vehicle
- Relevance of the longitudinal position in an orthotropic deck
- Influence of self-weight

7.2.1 Load application with regard to distribution area

In conventional design loads are in general applied as point loads. When this is translated to FEA it is a proper method for global design, but with regard to the localized methods appropriated for fatigue design it generates problems. In Figure 7-2 a principle comparison between the local behaviour of the deck and rib when the load is applied in one point and distributed over an area. The initiation of cracks I and II, at the intersection between deck plate and rib wall, is governed by the moment in the respective member and this moment is driven by the rotation of the respective element. When the load is applied in one point the distribution effect in the deck is significantly larger as can be seen in Figure 7-2 and accordingly the moments will be unrealistically high.
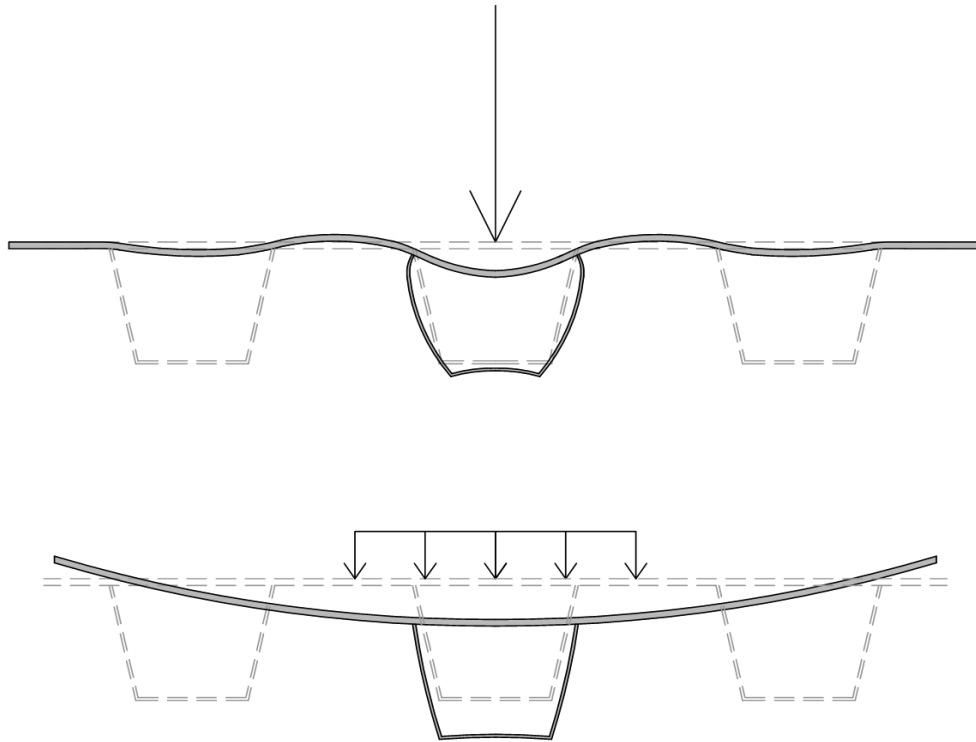
Figure 7-2 Behaviour of deck and rib walls when the wheel load is applied as (a) A point load; (b) An area load

For load placed between the rib walls in the span between floor beams, the behaviour is quite different depending on the width of the load. When applying a point load in the centre, as in Figure 7-2 (a), the response in rib-to-deck plate weld is very sever. All loads will be taken by the rib walls which also will suffer local distortion. When instead applying the load distributed over an area, as in Figure 7-2 (b), the load will distribute over several rib walls and balance the section, resulting in lower amount of local distortion. The distortion will be more of a global phenomenon and the stresses transferred through the weld decrease.

As a result of the localized behaviour governing the fatigue cracks it is of high importance to mirror the actual behaviour as close as possible. One step in this is to model the load over the wheel pressure area and not as a point load.

7.2.2   Relevance of the second wheel on the load axle

In hand-calculations of crack modes I and II it is general practise to only look at the effect generated by one wheel of the axis when evaluating the fatigue performance. Using the argument of the localized response with regard to fatigue crack initiation together with the fact that the most severe response is expected directly beneath the wheel load it is of interest to examine the importance of the second wheel on the load axle in a FE model.

When adding the second wheel of the axle larger load will be carried by the deck in total and higher load effects with respect to global bending and shear is expected in the span in which the load axle is applied. This load will, as described in Chapter 0, mainly be transferred to the floor beam and through the crack initiation area for Crack III but not be transferred in the transversal direction to pass the investigated section of

Crack I and II. One wheel load over the studied rib is taken directly by this rib to the floor beams. Load shedding in the transversal direction to the neighbouring rib is very limited. If the second wheel is located on the second neighbouring rib or further away, its effect on crack mode I and II can be neglected. This applies for cases with standard deck configurations usually seen in orthotropic decks. However, due to the intricate behaviour when additional load is applied in the same span this must be investigated more thoroughly for each separate crack. This will be done in the final analysis which is presented in Chapter 7.3 below.

7.2.3 Influence of the two rear axles in the fatigue vehicle

The stresses distribution pattern in an OSD ensures that loads applied between two floor beams to great extent are carried in that span, transferred to the two floor beams and through them directly to the main girders. In theory the ribs behave as continuous beams, as explained in Chapter 3.1. This will be tested by checking the stresses in at the longitudinal connections between the deck plate and rib when first only the two front axles and thereafter all four axles. The loads are applied over the wheel pressure area and the results can be seen in Figure 7-3 and Figure 7-4.
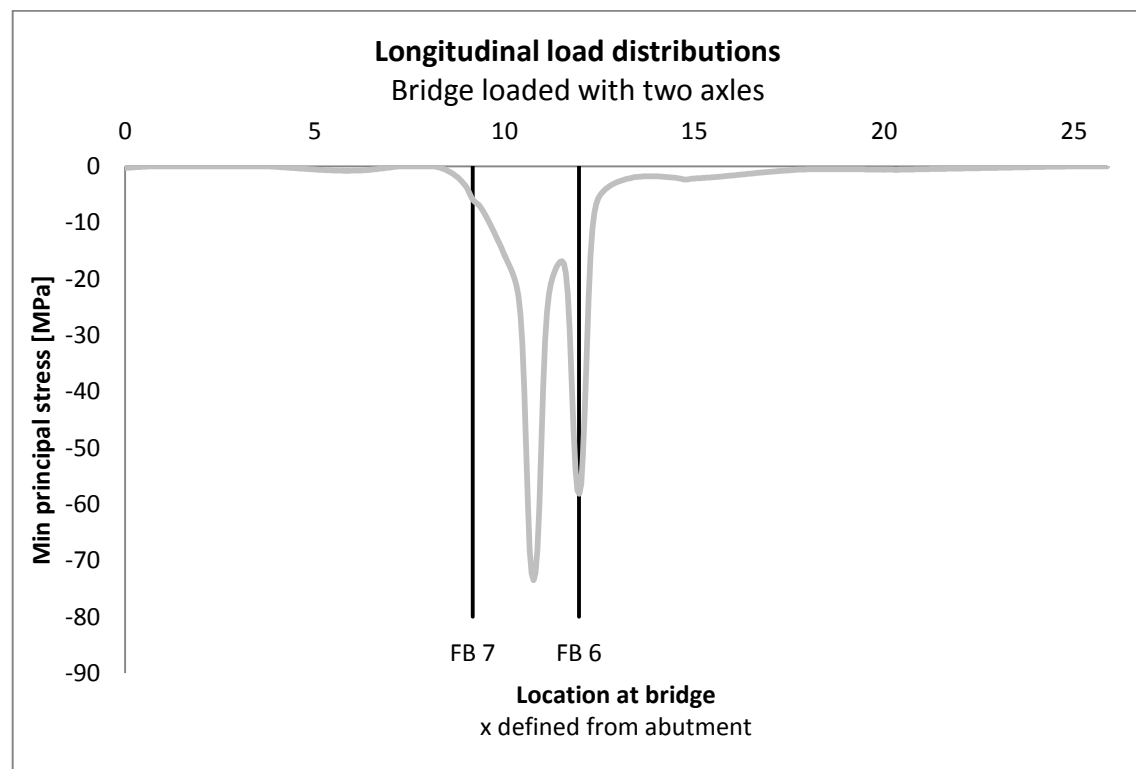
Figure 7-3 Bottom values of the minimum principal stresses in the deck plate one node away from the intersection with the rib for two axles.
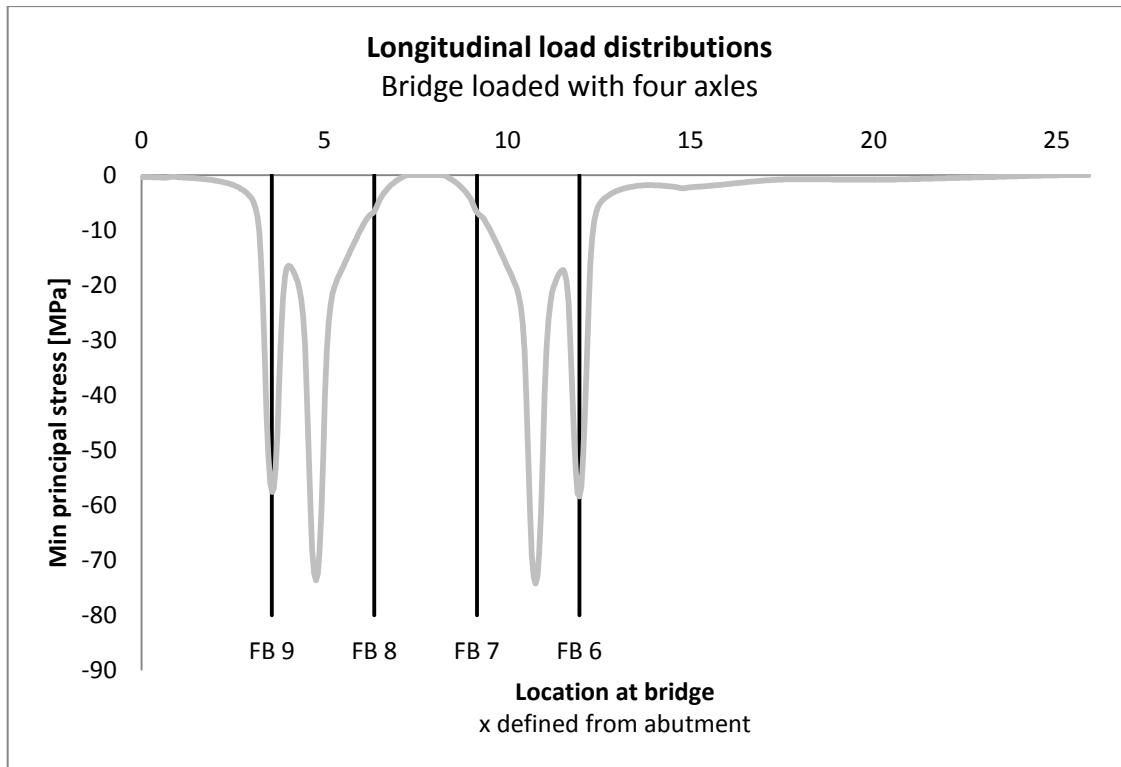
Figure 7-4 Bottom values of the minimum principal stresses in the deck plate one node away from the intersection with the rib for four axles.

Table 7-1 Comparison between the stress amplitude of the minimum values for two respective four load axles.

Minimum values in span between floor beam 6 and 7		
Two axles [MPa]	Four axles [MPa]	Difference [%]
-73.5	-74.2	0,97

The values in Table 7-1 are the minimum values of the principal stress in the deck for the given load cases. When comparing the longitudinal position for the respective case represented in Table 7-1 it is found that these are retrieved from the same x-coordinate which entails that the position of the most adverse response is unchanged. This is expected since the response is predicted to be worst just below the load application point.

As can be seen in the graphs over the stress distribution in the deck and in the table, there is only a very low part of the stresses that is distributed in the longitudinal direction over floor beams. Accordingly the two rear axles can be disregarded in the model and analysis for fatigue behaviour. This is true for the studied bridge and bridges with similar construction. The distance between floor beams is less than the distance between the rear bogy axles. Position of front axles giving maximum stress in the deck (mid-span of the ribs) results in the rear axles being positioned two spans away from the critical point.

7.2.4 Relevance of the longitudinal position of the fatigue load

From the investigation with regard to the effect of the rear axles of the fatigue vehicle it can be seen that the longitudinal position of the load seem to be of minor importance for the stress in the mid span between main girders. In Table 7-2 it can be seen that the stresses in the two different spans are very similar with a difference of less than 1% and accordingly the longitudinal position is here irrelevant.

Table 7-2 Comparison between the stress amplitude of the minimum values in two different spans in the deck

Minimum values of principal stresses for load applied in span		
FB6 - FB7 [MPa]	FB8 – FB9 [MPa]	Difference [%]
-74.2	-73.7	0,78

However, it is of interest to look at the influence of the longitudinal position over the entire deck and not just at two spans. To get an influence line this is done by using the moving traffic load option in Brigade/PLUS. Here this can be accepted since the values are only to be compared to each other and to give an indication of the behaviour and they are not to be used in any calculations or other analysis. The load set-up can be seen in Figure 7-5 and the results can be seen in Figure 7-6 and Figure 7-7 below.
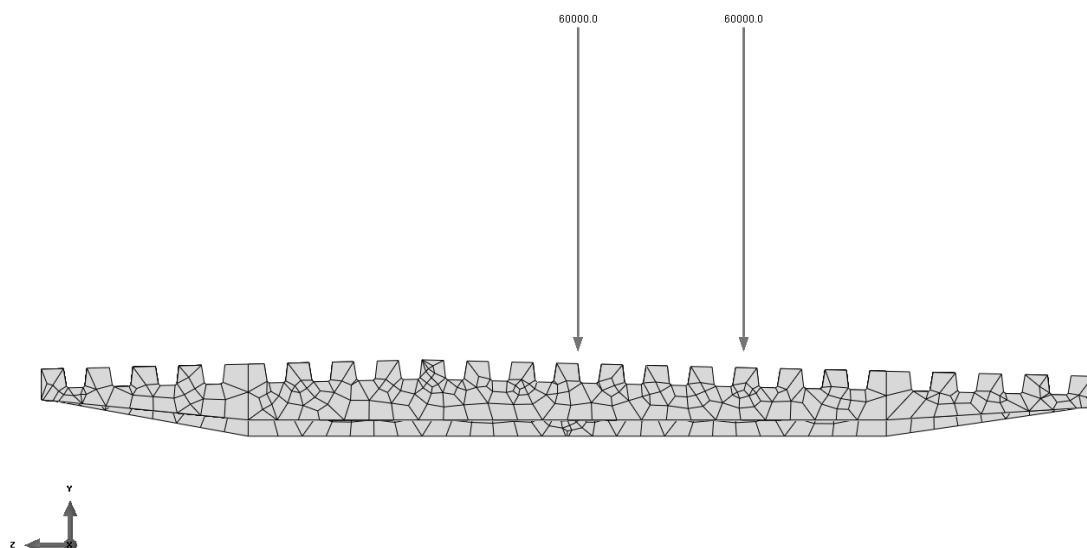
Figure 7-5 Illustration of placement of the traffic load line so that one wheel is placed directly above rib wall 7.2
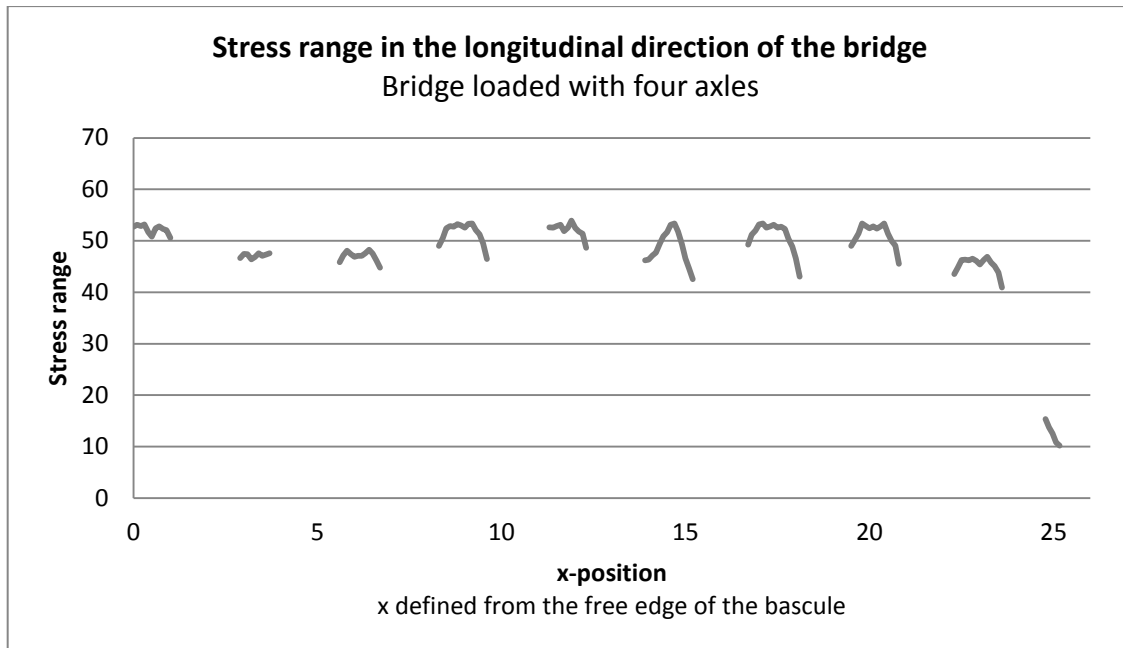
Figure 7-6 Stress range in rib wall from moving traffic load in the span between floor beams in the longitudinal direction of the bridge. The stresses above the floor beams are removed to emphasise the similarity of the stresses in spans between floor beams.

It can be seen in Figure 7-6 that the stress range differs between the longitudinal positions in the bridge. However, this can be explained with the differing dimension of floor beams and thereby the changing stiffness of the deck. If a section of the bridge deck with the same dimension of floor beams is selected, as in Figure 7-7 below, it can clearly be seen that the response is much more similar between the different spans.
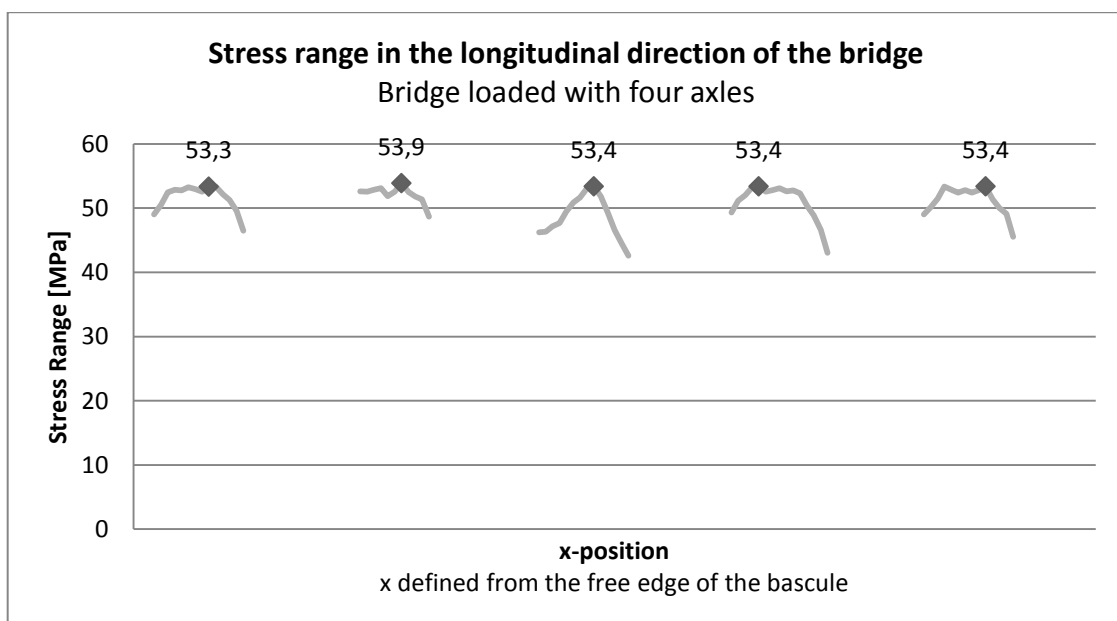
Figure 7-7 Stress range in rib wall from moving traffic load in the span between floor beams in the longitudinal direction of the bridge with almost constant stiffness in the deck. The stresses above the floor beams are removed to emphasise the similarity of the stresses in spans between floor beams.

In Figure 7-7 above the stiffness along the investigated part of the bridge deck is almost constant and it can also be seen that the peak values are very similar. The difference between them depends on the exact x-position with regard to the distance to the corresponding floor beams. Accordingly, the location of the load in longitudinal direction is irrelevant as long as the stiffness and dimensions of the members are constant in the deck.

7.2.5   Influence of self-weight

In fatigue evaluation the stress range is the affecting factor. The stress range is only affected by the difference in the stress amplitude this is unaffected by the self-weight of the deck. The self-weight can therefore be neglected in fatigue analysis to shorten the computational time for the FE-model.

7.2.6   Summary of assumptions from the initial analysis

From the initial investigations the following conclusions are drawn:

- Load should be applied as area loads, distributed over the wheel pressure area
- The relevance of the second wheel on the load axle with regard to additional loads in the same span between two floor beams must be checked for each specific crack case
- The influence of the two rear axles in the fatigue vehicle can be disregarded for this type of bridge
- The longitudinal position in an orthotropic deck is insignificant for the stress range in the rib wall as long as the stiffness of the deck is constant
- Self-weight can be neglected

The conclusions from the initial analysis are used to base the following investigations regarding the more local and detailed response on. These analyses will generate more reliable results and interpretations of the behaviour of the deck and stress distribution with regard to fatigue design and analysis. A denser mesh that is better suited for evaluations of crack initiation areas will be used and the stresses retrieved will be more adequate.

7.3   Final analysis

In the final analysis each crack initiation area for the three cracks will be investigated separately to find the most critical load position for each specific crack, see Figure 7-8. The stresses in relation to each crack will be calculated using the structural hot spot method. A comparison between the results from the FEA and conventional hand-calculations will be made to investigate possible error sources.
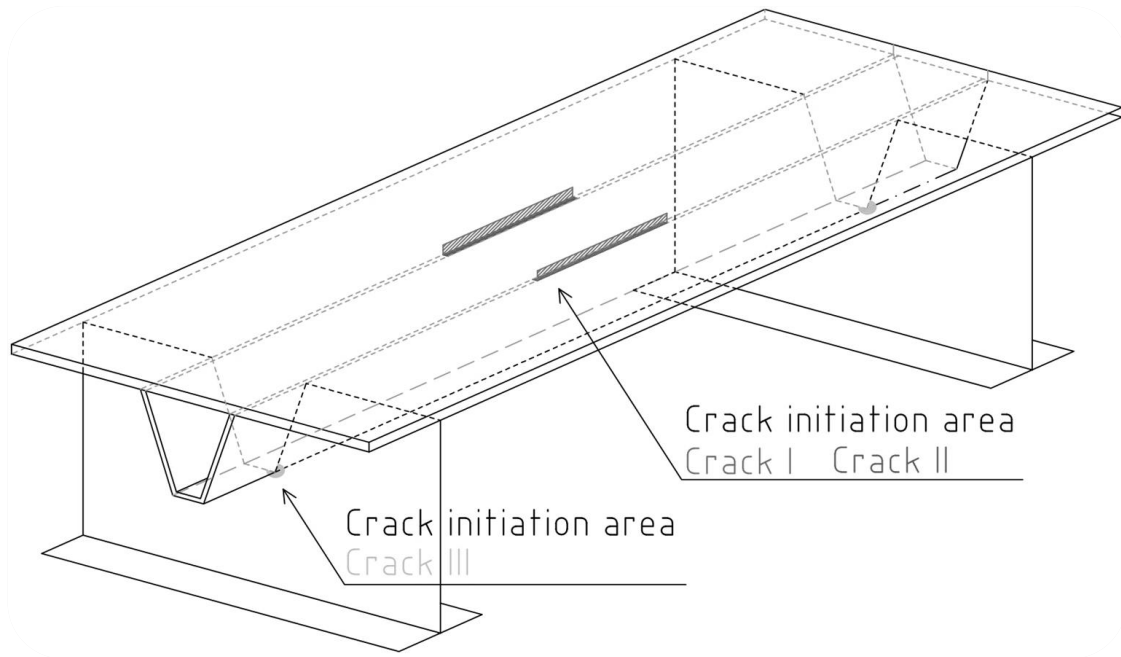
Figure 7-8 Crack initiation areas for the three investigated cracks

The first part of the final analysis aims to find the most critical load positions for each separate crack. The steps followed in this phase of the analysis are:

1. Determination of most unfavourable local transversal location, in relation to the rib walls
2. Determination of most unfavourable global transversal location, between main girders
3. Determination of most unfavourable local longitudinal location, in one span between floor beams

When these steps are completed the final load positions are found. However, all steps will be performed with the aim to find general and usable recommendation. Accordingly, only positions that comply with these demands will be included.

7.3.1 Description of the method used

For the three investigated cracks the most sever load position will be derived. To simplify this process a general approach was developed and used on all cracks. Also, only positions which can be generalised and translated to other similar decks are included in the method. The four main steps are explained below.

The stresses in all following analysis are either extracted one node away from the intersection or calculated as hot spot stresses according to Equation 7.1. As a consequence of this it is necessary to use a proper mesh with nodes in the specific positions where the stresses are read. This is secured by modelling partitions at the interesting distances.

$$\sigma_{hs} = 1.67 \cdot \sigma_{0.4t} - 0.67 \cdot \sigma_{1.0t}$$ **Equation 7.1**

The perpendicular hot spot stresses in the deck plate are extracted from the FE-analysis with principal stresses from nodal values in a path. To find the governing

stress, bending or membrane stress, both top and bottom values in the shell element is extracted and the membrane stress is calculated. From this the pure bending stress can be calculate.

7.3.1.1 Local transverse load location

The first step is to find the most adverse local position in transverse direction in relation to the rib walls. Four different positions are analysed and the response is examined in the crack initiation area, see Figure 7-9. To avoid disturbance from the boundary conditions, the main girders, this analysis is performed in the mid span between the girders.
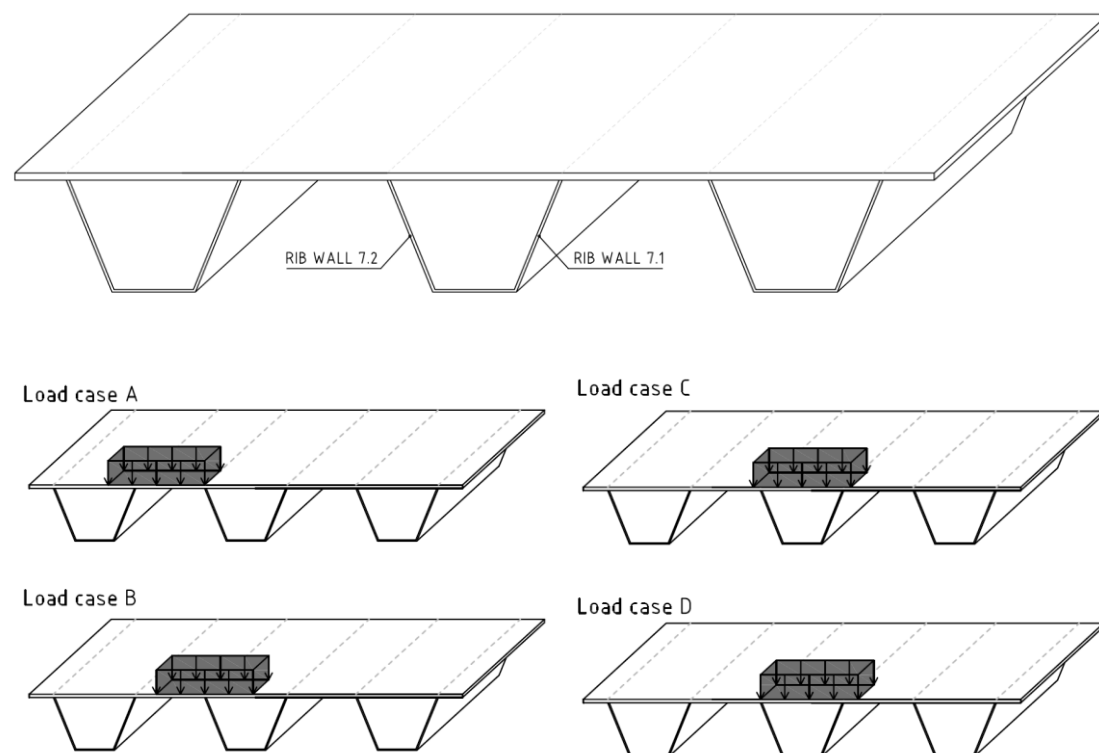
Figure 7-9 The four different load positions related to rib wall 7.1 respective 7.2 used in the local transversal analysis

Load case A: The load is placed with the start above the rib wall closest to the centre of the span and positioned towards the adjacent rib.

Load case B: The load is centred above the rib wall closest to the centre of the span.

Load case C: The load is positioned in the centre of the rib.

Load case D: The load is with the start above the rib wall closes to the centre of the span and positioned towards the other rib wall in the same rib. Accordingly, the main part of the load is carried in one rib and that most of this load is taken in one of the rib walls.

Only one axle is included in this analysis for simplicity and this is justified by the fact that the investigation is local and further studies will be performed later. The axis is place in two positions, in the middle of the span or directly above a floor beam, to capture the behaviour of the crack initiation areas.

7.3.1.2 Global transverse load location

When the local position in relation to the rib wall is found for each crack, the global transversal position is investigated. In this analysis the results from the previous analysis is used and the load axle is positioned according to the found results. The worst local load position is used to place loads above all ribs in the bridge. The stresses are extracted for each rib and compared to each other, see Figure 7-10. Also, for this analysis the importance of the second wheel on the load axis is controlled by performing the analysis for both one and two wheels and comparing the results for the three cracks.
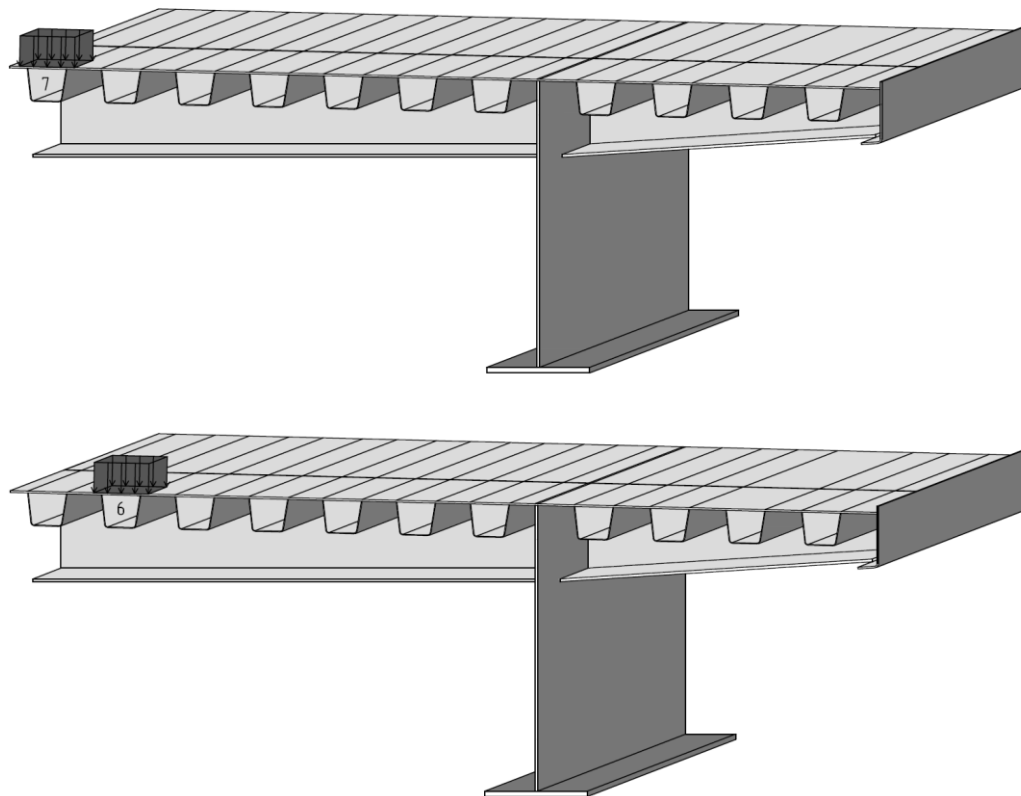
Figure 7-10 Overview load application positions used in the global transversal analysis

7.3.1.3 Local longitudinal load location

When the worst transversal load location is found, the load is placed at three different locations in longitudinal direction in relations to the floor beam to find the most adverse local longitudinal positions for each crack, see Figure 7-11. Here the results from the two previous steps will be used for each crack. Also the importance of the second axle in the span will be investigated for the three cracks to see if the responses

are so local that the other axle in the same span can be disregarded to simplify the modelling and computational time.
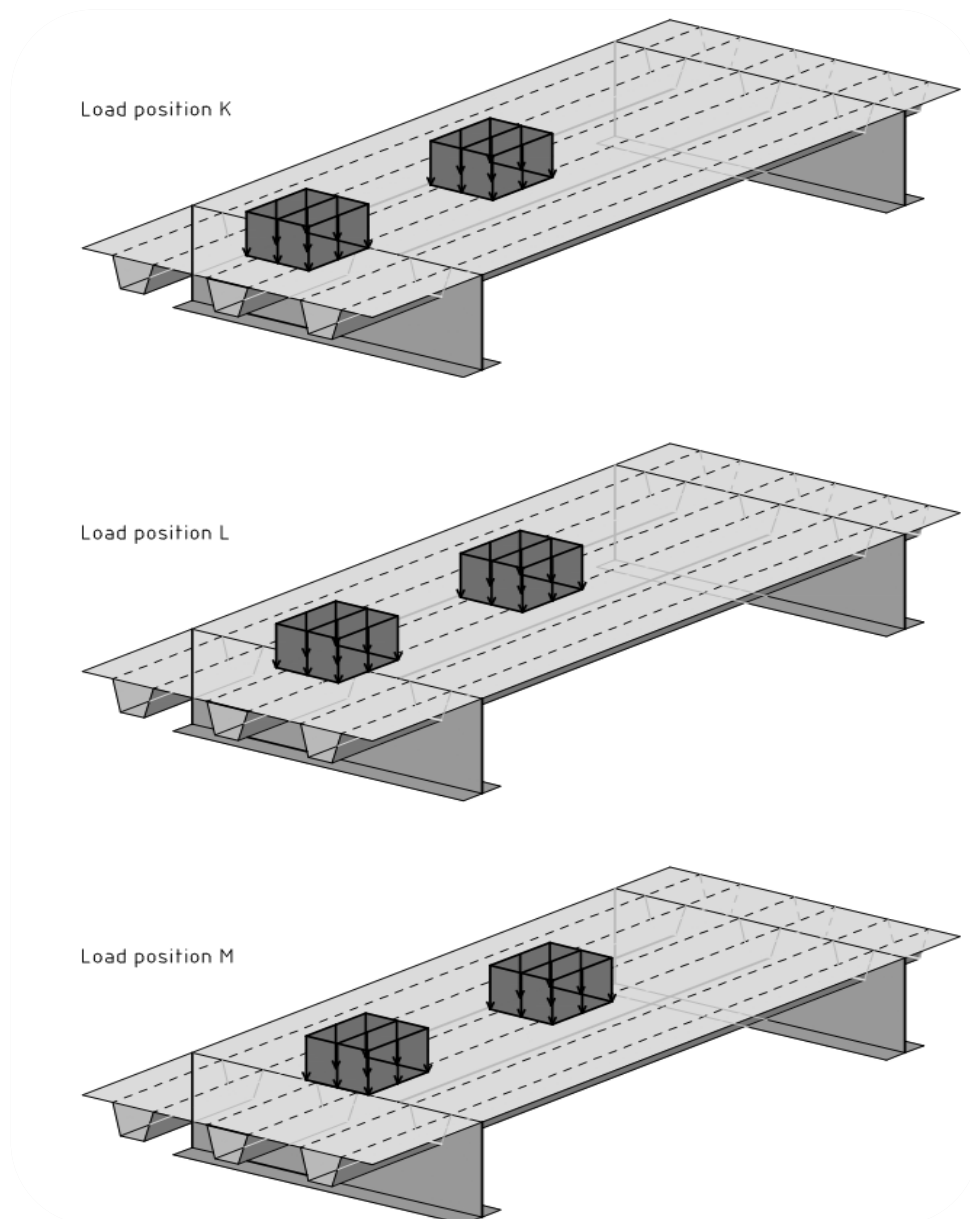
Figure 7-11 The three load positions used in the local longitudinal analysis

Load position K: The first load axle is aligned with the floor beam and out to the span and the second axle is placed in the span on the other side of the floor beam.

Load position L: The first load axle is placed centred above the floor beam and the second load axle is placed in the span.

Load position M: The first load axle is placed in the centre of the span between floor beams and the second towards either floor beam. In this bridge this coincides with that the first axle aligns with the floor beam and out to the span and the second axle is placed in the same span.

7.3.2 Crack I – Determination of most critical load position

Crack I is a toe crack propagating longitudinally in the deck plate with the bending moment in the deck plate as the driving force. The crack in the deck plate at the connection to the longitudinal rib, crack I, can be seen in Figure 7-12. For this crack the load situation is very local and the worst response is expected directly below the load.
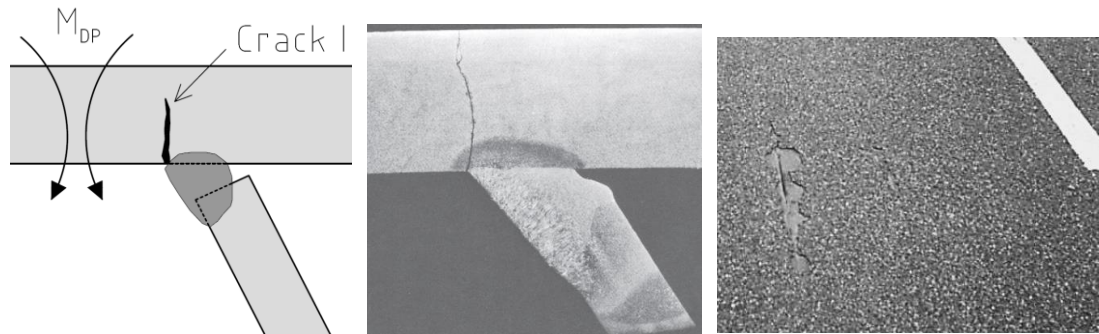
Figure 7-12 Crack I in the deck plate at the connection to the longitudinal rib (a) Structural overview; (b) Section Crack I from an experiment (Kolstein, 2007); (c) Possible consequences that can arise from this crack (Kolstein, 2007)

For Crack I it is the bottom values in the deck plate that should be used since they corresponds to the stresses in the lower part of the deck plate, this applies for this specific model.

7.3.2.1 Local transverse load location
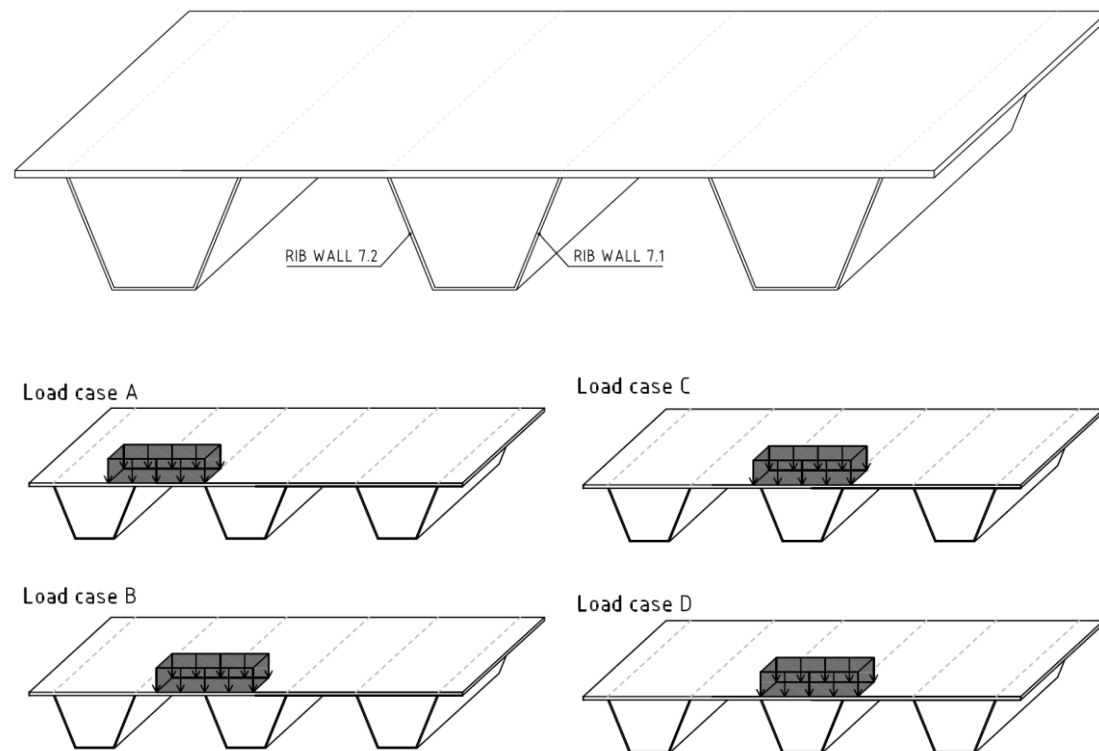
Figure 7-13 The four different load positions related to rib wall 7.1 respective 7.2 used in the local transversal analysis

For Crack I all loads are placed in the span. When the loads are placed above floor beam no effect is shown and this is not investigated further. First is the load response checked in rib wall 7.1, toward the main girder, and then the load response is checked for rib wall 7.2, toward the middle of the bridge.
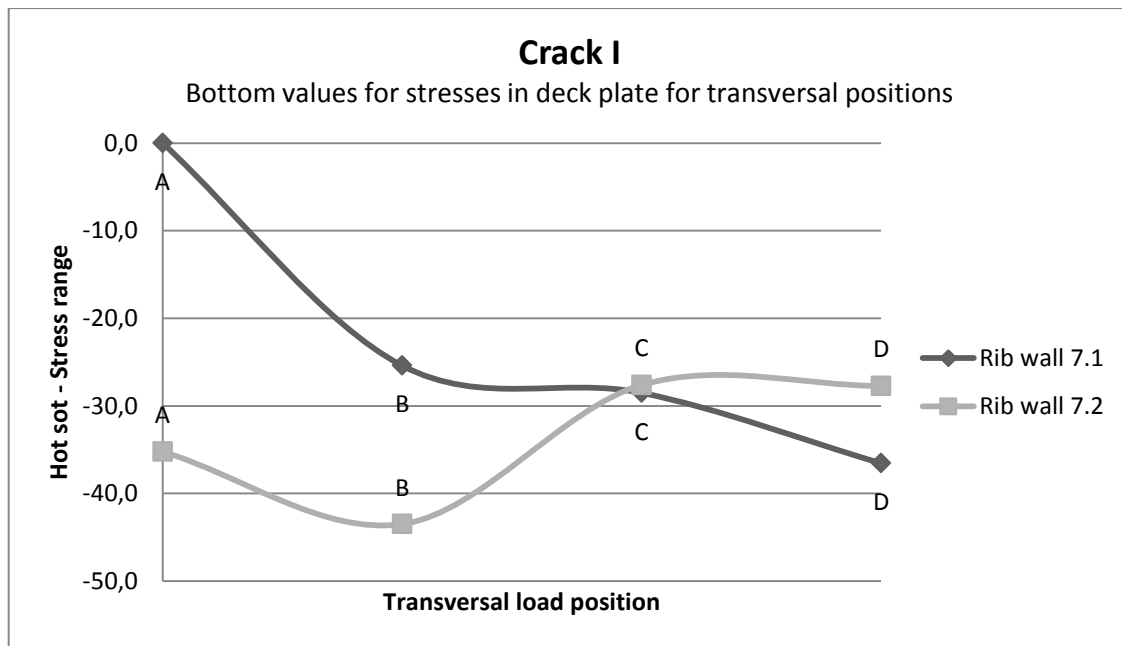
Figure 7-14 Comparison of the response in the two rib walls for the four load positions

In Figure 7-14 it can be seen that the most adverse response is found in the deck plate at the intersection with the rib wall closest to the middle of the span between main girders at position B. It can be seen that the stress in the deck plate above rib wall 7.1 increases continuously as the load approaches and a larger part of the load is carried by this rib wall. A conclusion that can be drawn from this is that the effect of distortion is not of high influence for Crack I. However, it gives a small effect as can be seen when load case C and D for rib wall 7.2 is compared. In load case D less of the load, compared to case C, is carried in rib wall 7.2 but the stresses in the deck are higher. This depends on the bending experienced and shows that the deformation induced stresses have a small influence on the behaviour for Crack I.

To get a better overview of the response governing Crack I, an influence line is created, see Figure 7-15.
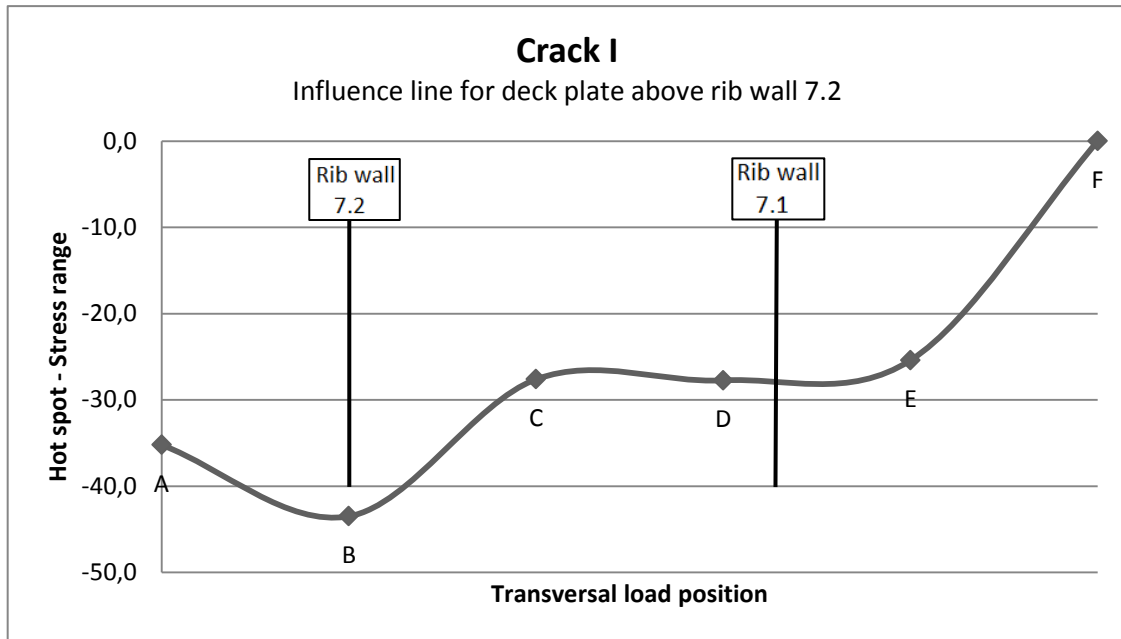
Figure 7-15 Influence line of the response in rib wall 7.2, closes to the centre in the span between main girders for Crack I, (Point E and F correspond to the stress values in rib wall 7.2 when the load is placed in load case C and D relative to rib wall 6.2, and is thereby an continuation of the load moving away from rib wall 7.2.)

From the influence line it can clearly be seen that the response in the deck plate is most adverse when the load is positioned directly above the rib wall (position B). For this position the load is concentrated in the deck plate to one of the rib walls. This also reinforces the discussion regarding influence of deformation induced effects for Crack I.
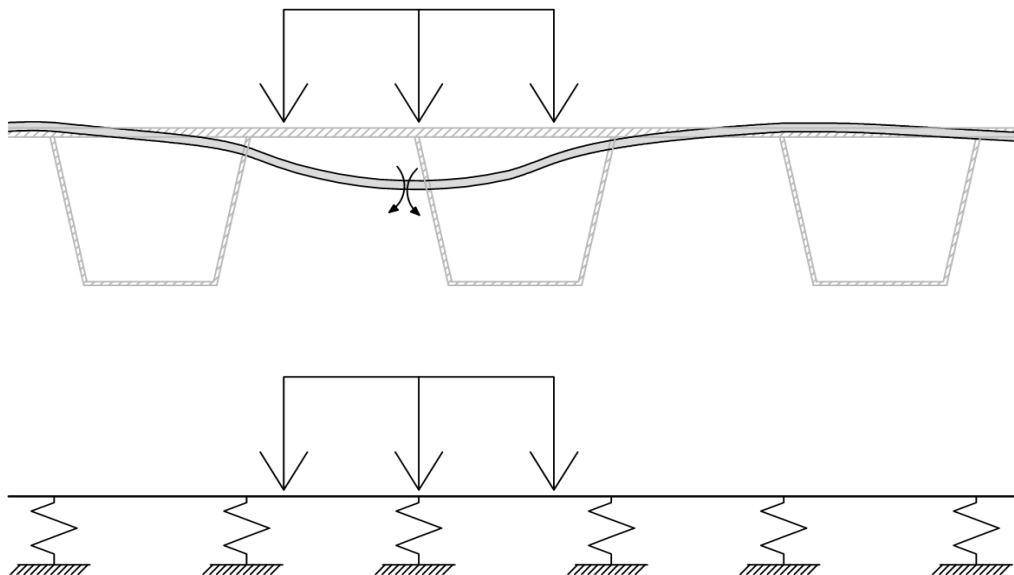
Figure 7-16 Principal model of governing moment for Crack I

The deck plate can be seen as a beam resting on spring supports representing the rib walls in the transversal direction. For this model the highest moment will be found when the load is placed in the centre of the span and this is why we find the highest stresses for these cases. The stresses in the vicinity of the weld will peak when as much load as possible is transmitted to one weld and thereby is concentrated in a small area in the deck plate. This also results in larger local bending of the deck plate giving significantly higher local moments, consequently the local transversal position is highly important for the stresses in the plate. This is also seen if the stress at the B position is compared to the lowest stresses generated, here that is found when the load is positioned at C, see Table 7-3.

Table 7-3 Comparison between the response in the deck plate above the rib wall closest to the centre of the span between the main girders for the load positioned in B respective C

Comparison between response in B and C	
x-position	**Bottom stresses**
B	-43,5
C	-27,6
Difference:	58%
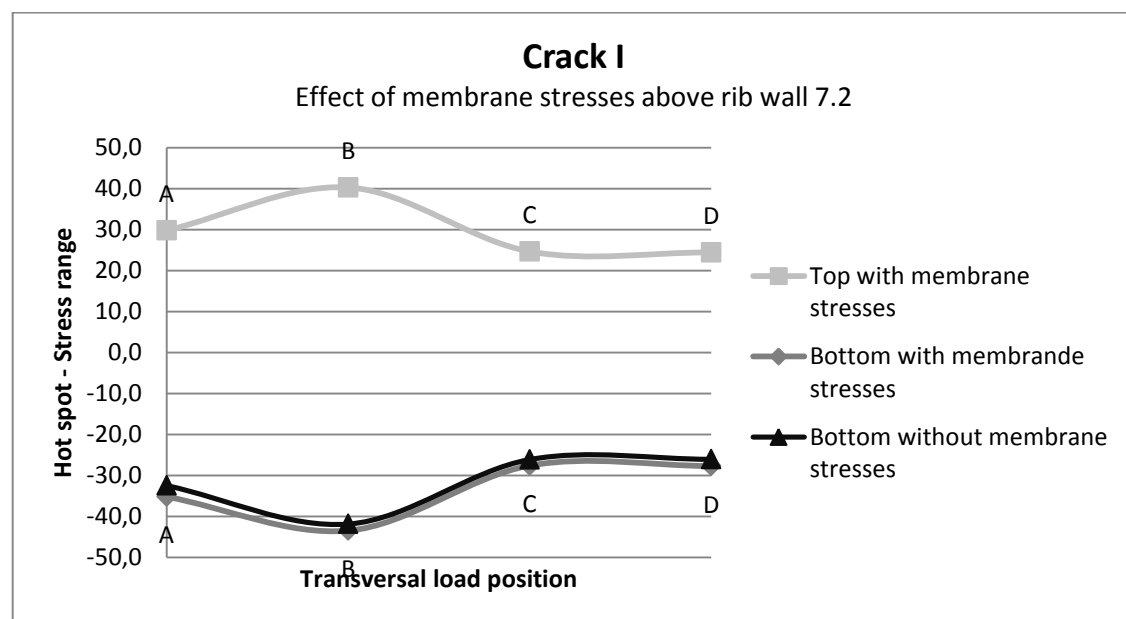
Figure 7-17 Effect of membrane stresses in the deck

In Figure 7-17 it can be seen that the membrane stresses are very small in comparison to the bending stresses in the deck plate. This is expected since the theory states that the governing stress for initiation and propagation of Crack I is the bending in the deck plate at the intersection to the longitudinal rib.

For Crack I the most adverse load response is experienced when the load is placed directly above the rib wall closest to the middle of the span between main girders. For

this load situation the main part of the load is transferred through the deck plate to only one rib wall instead of to a higher extent being distributed to other rib walls. Accordingly high moments arise in the deck plate close to the connection. Hence, for Crack I the load case that the following analysis will be based is B.

7.3.2.2 Global transverse load location

The load is placed at position B for rib 1 to rib 7. The stress in the deck plate at the connection to the rib wall towards the centre of the span between the main girders is extracted. Also the influence on the load response from the second wheel on the axle is investigated. The results can be seen in Table 7-4 and Figure 7-18. The stresses in this analysis are minimum principal stresses and the bottom values for the shell element representing the deck plate. They are extracted one node away from the intersection with the rib to avoid singularities and nodes with two stress values.

Table 7-4 Principal stresses in the deck plate for different transversal locations of the load

Minimum principal stresses in deck plate above rib wall

Rib wall	σ_{min} for one wheel	σ_{min} for two wheels	Difference
7.2	-31,04	-31,69	2,0%
6.2	-31,06	-31,65	2,0%
5.2	-31,03	-31,48	1,7%
4.2	-30,95	-31,07	0,9%
3.2	-30,79		
2.2	-30,62		
1.2	-30,06		

The stresses are very similar for all the ribs and confirm that the load response is determined by the local wheel load. A slight increase of stresses can be seen in the ribs located in mid-span, where rib 7 experiences the highest stress. As can be seen the second wheel does not influence the stress by more than 2% and can therefore be disregarded. This confirms the highly local behaviour for crack I.
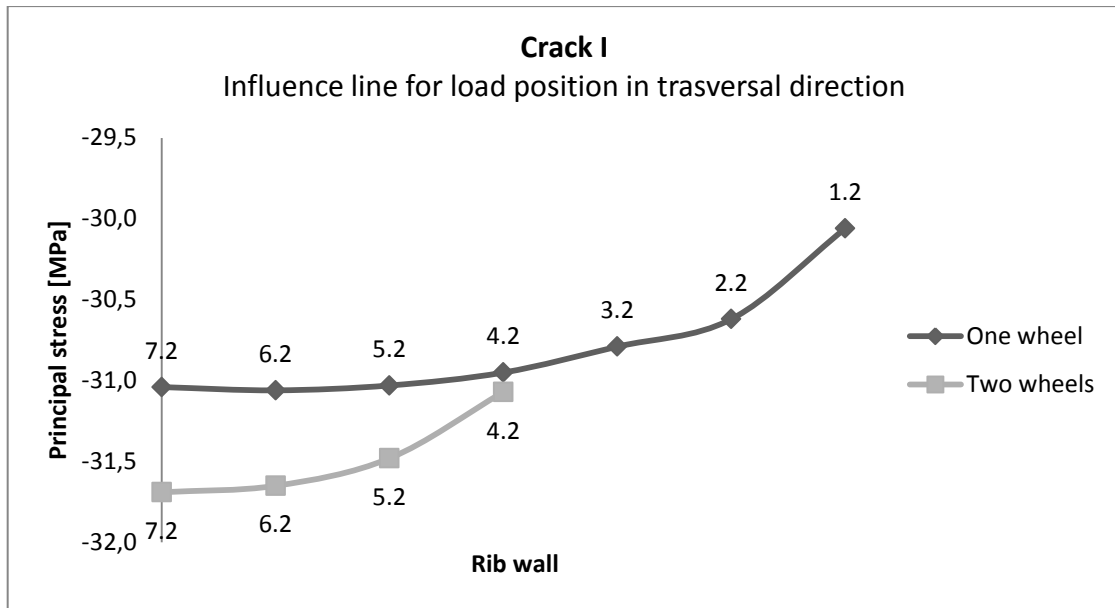
Figure 7-18 Influence line for stresses in the deck plate for load placed in transversal location above different rib walls

The difference in stresses between one and two wheels increases the further toward the middle of the span between the main girders the load is positioned. Accordingly, the global deflection has an influence on the stress state for Crack I, although small. Second wheel causes bending stresses in the rib wall and in the deck plate due to continuity effects. Also, the membrane stresses increases when the second wheel is applied compared to when only one wheel is used.

The response in the deck plate is most adverse when the load is placed in the middle of the span between the main girders. However, it is very similar along the transversal direction. The influence of the second wheel on the load axle can be neglected due to highly localized response for Crack I.

7.3.2.3   Local longitudinal load location

The worst principal stresses rise directly below the wheel load as showed from the two previous analysis steps. If the system is modelled as a beam on springs the worst response will be found when the load is placed in the middle of the span or in the vicinity of this region. Consequently, only load position M is investigated, when the first axle is placed in the middle of the span and the second in the same span and aligned with the floor beam. In this analysis the stresses presented are hot spot stresses, calculated as described in Equation 7.1, from the bottom values of the shell element representing the deck plate.

The influence of the second load axle is investigated and the principal stresses in the deck plate are presented in Table 7-8. This shows that the second axle increase the stress by 7% and should therefore be included in a load analysis. However, important to observe is that when the second axis is applied the stresses in the deck plate decreases, this behaviour is not expected and it should be further investigated in future work.

Table 7-5 Minimum principal stresses in deck plate for local longitudinal load position

Minimum principal stresses in deck plate for longitudinal load position M			
Longitudinal position	One load axle One wheel	Two load axles One wheel/axle	Difference
M	-42,9 MPa	-40,1 MPa	-6,6%

To capture the behaviour of the deck that is of importance for this crack mood the second axle should be included in the analysis if it is in the same span as the first. However this should be further investigated to find the proper relation.

7.3.2.4   Summary - Final load position

With regard to fatigue analysis of Crack I the load should be placed as in Figure 7-19 below.
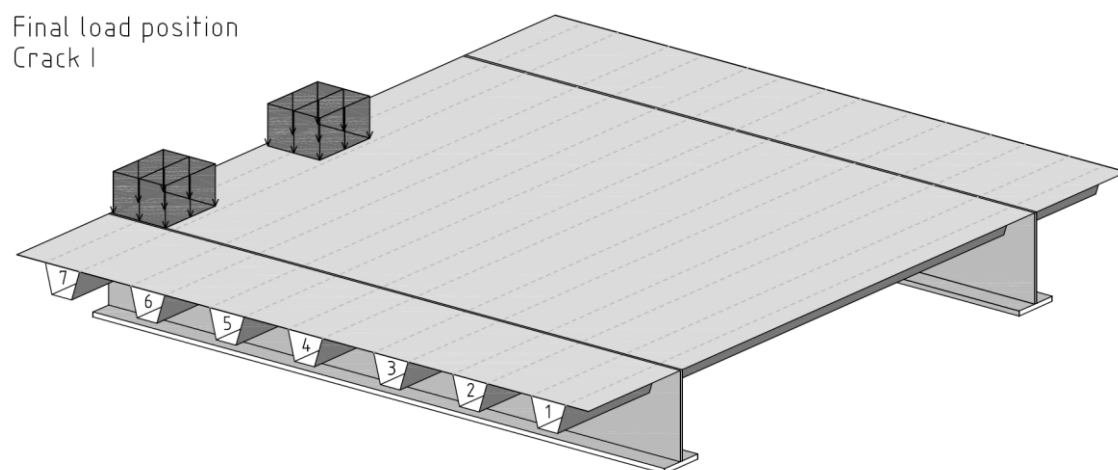
Figure 7-19 Final load position for Crack I

- Local transversal location: The load should be centre above the rib wall closest to the centre of the span between main girders, load case B.
- Global transversal positions: The load should be placed above the rib in the centre between the main girders, rib 7.
- Local longitudinal position: The first axle should be placed in the middle of the span between floor beams and the second axle should be included if it is in the same span, load case M.

The deck plate can be seen as a beam resting on spring supports representing the floor beams in longitudinal direction and ribs in the transversal direction. For this model the highest moment will be found when the load is placed in the centre of the span and this is why we find the highest stresses for these cases.

The stresses in the vicinity of the weld will peak when as much load as possible is transmitted to one weld and thereby is concentrated in a small area in the deck plate. This also results in larger local bending of the deck plate giving significantly higher local moments, consequently the local transversal position is highly important for the stresses in the plate.

The second wheel on the load axle can be excluded from the analysis. If the second load axle of the fatigue vehicle is in the same span as the first it should be included, with one wheel.

7.3.3 Crack II – Determination of most critical load position

Crack II is a toe crack propagating longitudinally in the rib wall driven by the distortion in the rib which creates a bending stress in the rib wall, see Figure 7-20. For this crack the load situation is very local and the worst response is expected directly below the load.
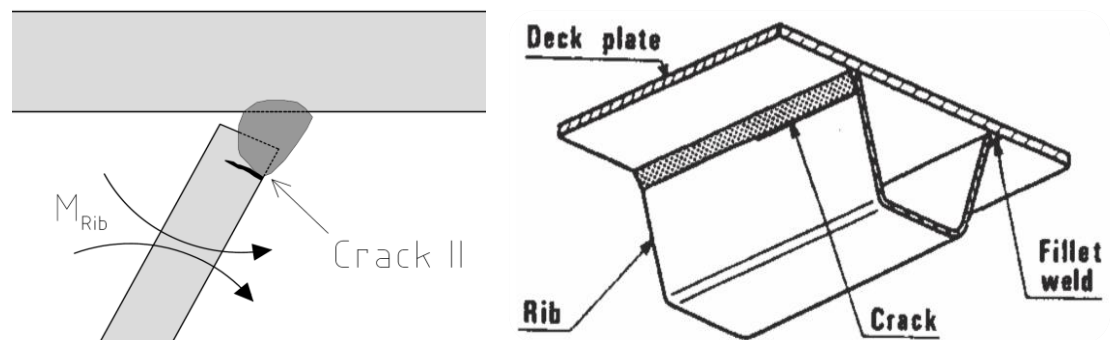
Figure 7-20 Crack II in the rib wall at the connection to the deck plate (a) Sectional overview; (b) Structural overview

For Crack II it is the bottom values in the rib wall that should be used since they correspond to the stresses in the outside part of the wall, this applies for this specific model.

7.3.3.1 Local transverse load location
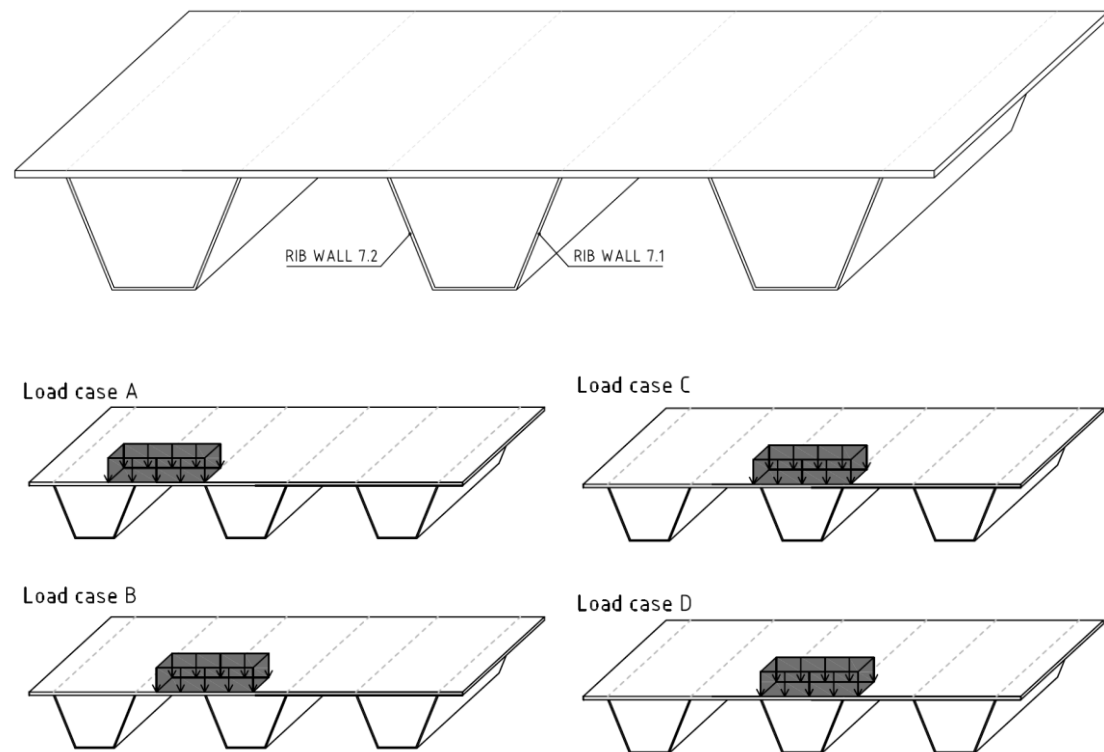
Figure 7-21 The four different load positions related to rib wall 7.1 respective 7.2 used in the local transversal analysis

For this crack all loads are placed in the span. When the loads are placed above floor beam no effect is shown and this is not investigated further. The load response is checked in rib wall 7.1, toward the main girder, and for rib wall 7.2, toward the middle of the bridge.

Crack II

Bottom values for stresses in rib walls for transversal positions
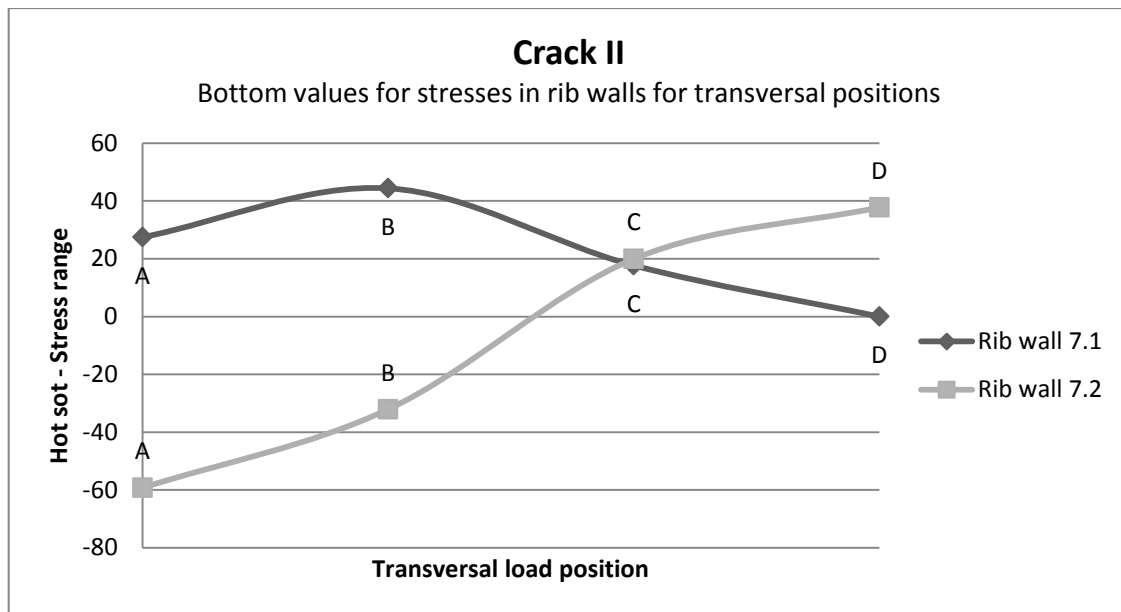
Figure 7-22 Comparison of the response in the two rib walls for the four load positions

In Figure 7-22 it can be seen that the most critical position for Crack II is found in the rib wall 7.2 when the load is placed in position A. From this can be concluded that for this crack mode the local distortion of the rib has greater influence than for Crack I. This is in accordance with the behaviour described in System 5, see Chapter 3.3.1.5 since Crack II arises in the rib wall and the local distortion affects the stresses locally.
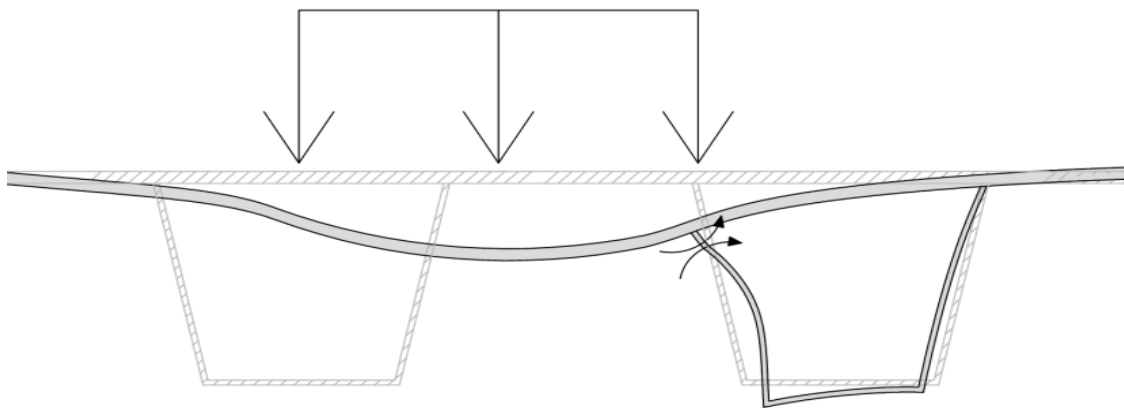
Figure 7-23 Driving moment for Crack II with load positioned in A

In load case A only a small part of the load is transferred through rib wall 7.2, the largest part of the load is taken in rib wall 8.1. This indicated that the distortion and deformation induced stress in the ribs are of higher importance than the direct reaction from the load, this can be studied in Figure 7-23. This is emphasised by the fact that the stresses in rib wall 7.2 decreases as the load is placed more centred, load case B and C, and increases again when the distortion increases for load case D. The same behaviour is found in rib wall 7.1 which experienced the most adverse response for load case B which also results in the largest distortion.

When performing a hand-calculation, the load is usually centralized above the rib wall. If this position were to be used in an FEA this simplification results in 197% lower stresses than if the load is placed at load location A, see Table 7-3. This shows that it is of very high importance that the load is placed in this position when FE modelling is used for fatigue analysis.

Table 7-6 Comparison between the responses in the rib wall closest to the centre of the span between the main girders for the load positioned in A respective C

Comparison between response in A and C	
x-position	**Stress range**
A	59,3
C	20,0
Difference:	197%

To get a better view of the response governing Crack II a influence line is created, see Figure 7-24. From the influence line it can be seen that the response in the rib wall is most adverse when the load is aligned with the rib wall and placed out towards the free span between ribs, position A.
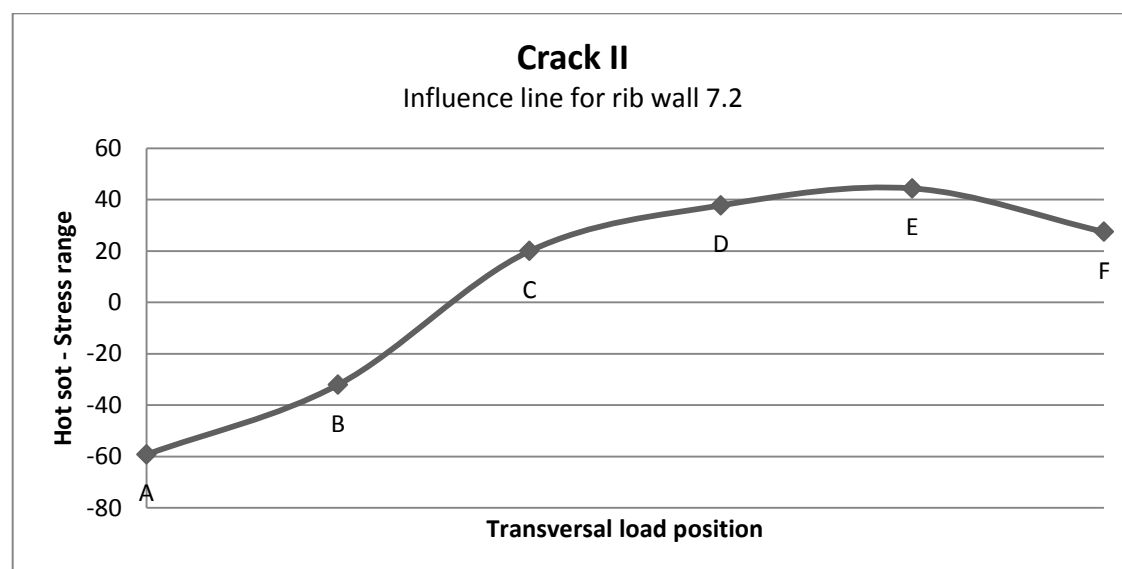
Figure 7-24 Influence line of the response in the rib wall closes to the centre in the span between main girders for Crack I, E and F are the corresponding values for the rib wall closest to the main girder in position B respective A

To investigate the amount om membrane stresses and bending stresses in the rib wall the top values for the shell element representing the rib wall vas extracted and the membrane stresses calculated. In Figure 7-25 it can be seen that the membrane stresses are larger here than for Crack I but still small in comparison to the bending stresses in the deck plate. This is expected since the theory states that the governing stress for initiation and propagation of Crack II is he bending in the rib wall from out-of-plane distortion of the rib.
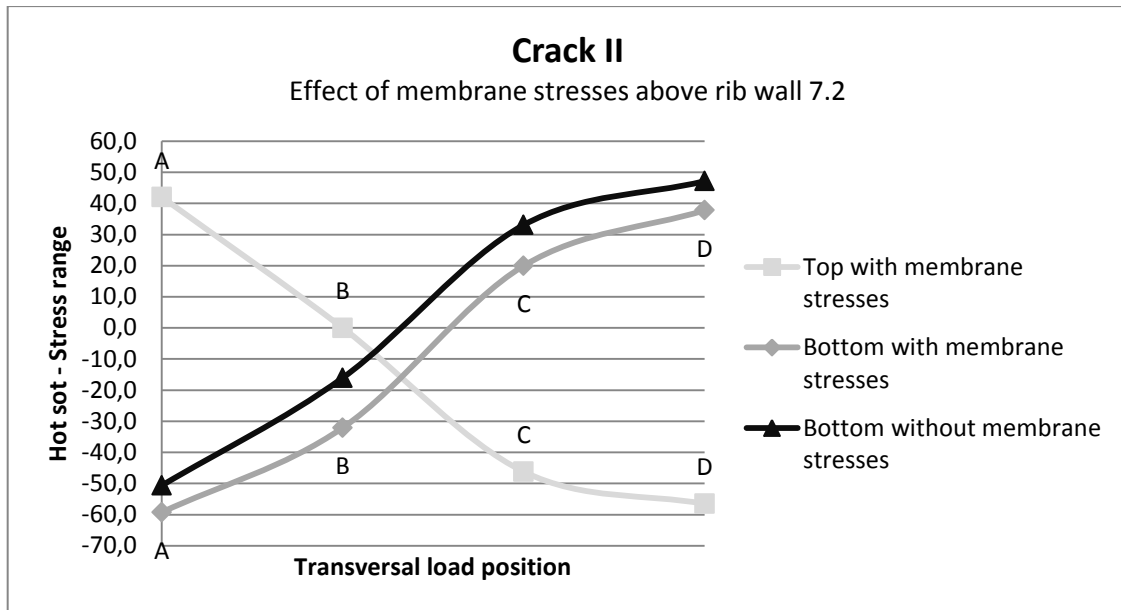
Figure 7-25 Effect of membrane stresses in the rib wall

The worst load position for Crack II is when the load is placed aligned with the rib wall and out to the span between ribs. This result in a large distortion of the rib wall and from this high bending stresses arises. For Crack II the load case on which the following studies will be based on is load case A, and the rib wall to be investigated is the one closest to the centre of the bridge.

7.3.3.2 Global transverse load location

The load is placed at position A for rib 1 to rib 7. The stress in the rib wall towards the centre of the span between the man girders at the connection to the deck plate is extracted. Also the influence on the load response from the second wheel on the axle is investigated. The results can be seen in Table 7-7 and Figure 7-26. The stresses in this analysis are minimum principal stresses and the bottom values for the shell element representing the rib wall. They are extracted one node away from the intersection to avoid singularities and nodes with two stress values.

Table 7-7 Principal stresses in the deck plate for different transversal locations of the load

Minimum principal stresses in rib wall

Rib wall	σ_{min} for one wheel	σ_{min} for two wheels	Difference
7.2	-56,06	-54,76	-2,3%
6.2	-56,32	-55,28	-1,8%
5.2	-56,59	-55,84	-1,3%
4.2	-56,90	-58,54	2,9%
3.2	-57,21	-59,13	3,4%
2.2	-57,48	-59,63	3,7%
1.2	-59,49	-61,70	3,7%

For rib 1, 2, 3 and 4 the second wheel is placed towards the span. For rib 5, 6 and 7 the second wheel is placed towards the main girder.
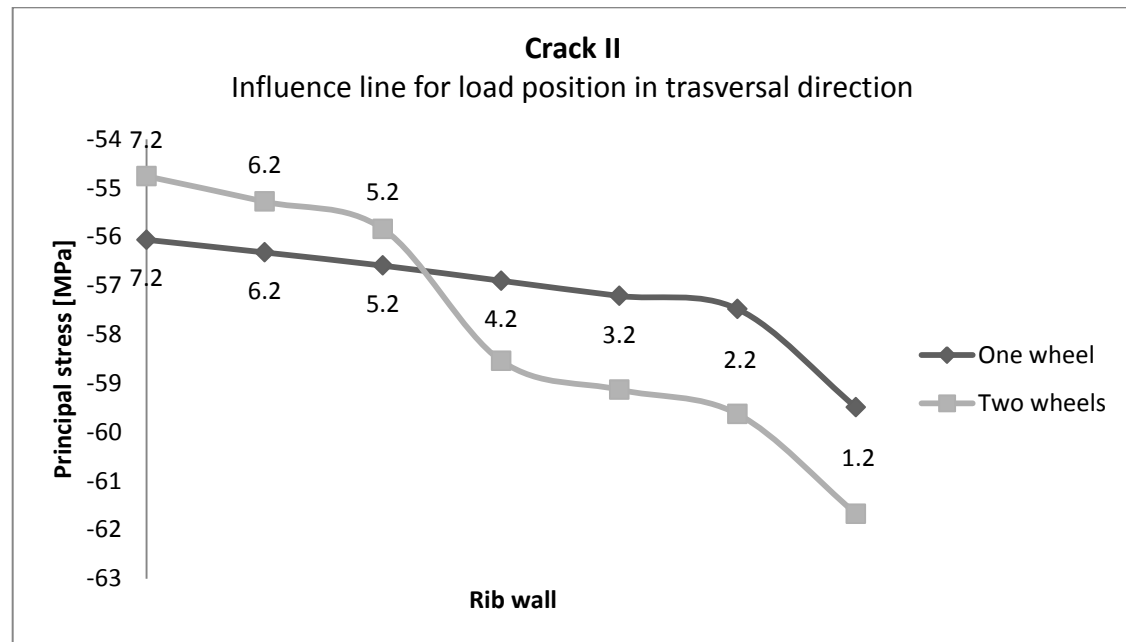
Figure 7-26 Influence line for stresses in the deck plate for load placed in transversal location above different rib walls

The influence from the second wheel is less than 4% and can be neglected in models for Crack II. The difference in stresses between one and two wheels increases the further toward the main girder the load is positioned. Accordingly, the global deflection has an influence on the stress state for Crack II.

The stresses in the rib wall display the most adverse response when the load is placed at the rib closest to the main girder. This is a consequence of the increased rotational stiffness the deck have closer to the main girder and a restraint is created, see Figure 7-27. This restraint increases the moment experienced by the rib wall. Important to point out is that this behaviour is highly affected by the relation between the stiffness of the rib walls in relation to the moment of inertia of the deck. Accordingly, this is very specific to this bridge but for orthotropic decks with similar dimensions this is applicable.
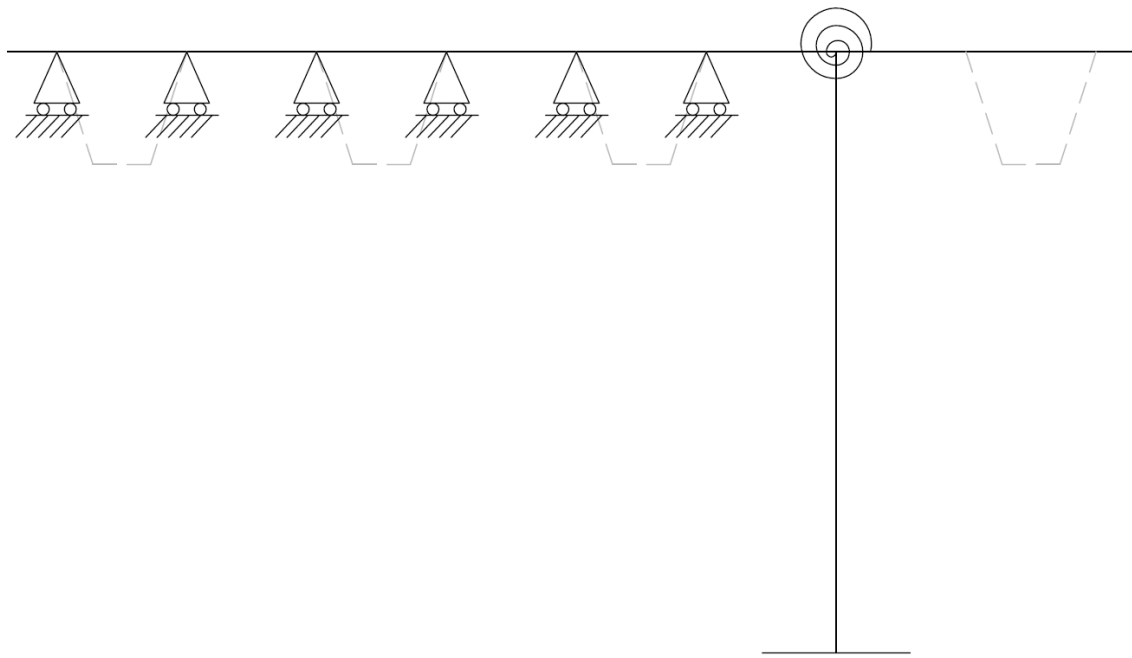
Figure 7-27 Structural model of the deck and the increased rotational stiffness from the main girder

Since the highest stresses are found in rib wall 1.2 it is of interest to investigate the response in rib wall 1.1. Due to the dimensions of the deck and distance between rib wall 1.1 to the main girder the load would either be placed so that a large part would be carried directly by the main girder or similar to load case D. If the load is placed so that parts of the load distribution area is connected to the main girder the main part of the load will be transferred directly to the main girder due to higher stiffness and only low stresses arises in rib wall 1.1 If the load is placed as in load case D and the stresses are checked for rib wall 1.1 they will be lower since the distortion of the rib wall is smaller for load case D than for load case A according to Chapter 7.3.3.1 Hence, rib wall 1.1 is for this bridge not of interest.

For Crack II the load is to be placed above the rib closest to the main girder in the following investigations, at the rib wall towards the middle of the floor beam.

7.3.3.3 Local longitudinal load location

For Crack II the response is highly local and the highest stress is directly beneath the wheel load. Here the same principal as for Crack I with the system is modelled as a beam on springs can be used and the worst response will be found when the load is placed in the middle of the span. As for Crack I only load position M is investigated, when the first axis is placed in the middle of the span and the second in the same span and aligned with the floor beam. In this analysis the stresses presented are hot spot stresses, calculated as described in Equation 7.1, from the bottom values of the shell element representing the rib wall.

The influence of the second load axle is investigated and the stresses in the rib wall for one and two load axles are presented in Table 7-8. This shows that the second axle increase the stress by 11% and should therefore be included in a load analysis.

Minimum principal stresses in deck plate for longitudinal load position M			
Longitudinal position	**One load axle** One wheel	**Two load axles** One wheel/axle	**Difference**
M	-64,4 MPa	-71,3 MPa	10,8%

7.3.3.4 Summary - Final load position

Crack II is driven by the distortion of the rib creating a bending stress in combination with a normal force in the rib wall. This distortion is a consequence from bending of the deck plate. When the load is applied, the deck deflects and the rib wall distorts, as was shown in Figure 7-23This is a result of the stiff, welded, connection between the deck and the rib making the rib subordinated to the behaviour of the deck for this local effect.

The effect is highly localized and the highest stress will rise in the rib below the wheel load. The distortion of the rib wall is highest when the load is placed as in load case A, and the most adverse stress state arises when the load is placed in the A-position at the rib closest to the main girder in the span between floor beams. The transversal position of the load is of high importance since the lever arm of the load to the rib wall effects the rotation angel of the deck plate at the connection and thereby the rib wall distortion.

With regard to fatigue analysis of Crack II the load should be placed as in Figure 7-28 below.
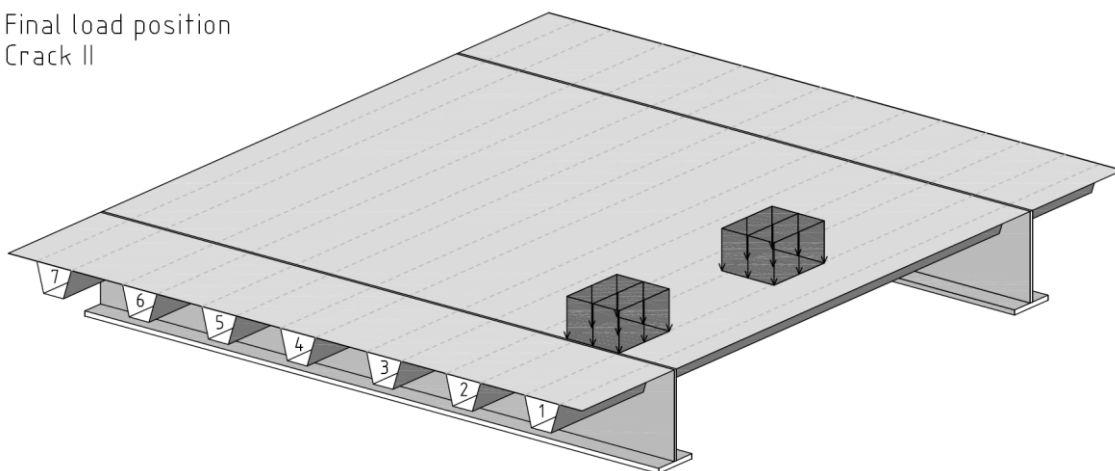
Figure 7-28 Final load position for Crack II

- Local transversal location: The load should be aligned with the rib wall towards the span between main girders and positioned towards the free span between ribs, load case A.
- Global transversal positions: The load should be placed above the rib closest to the main girder, rib 1.

- Local longitudinal position: The first axle should be placed in the middle of the span between floor beams and the second axle should be included if it is in the same span, load case M.

The second wheel on the load axle can be excluded from the analysis. If the second load axle of the fatigue vehicle is in the same span as the first it should be included, with one wheel.

7.3.4 Crack III – Determination of most critical load position

Crack III is a toe crack initiating at the radii of the rib at the intersection with the floor beam and propagating in the floor beam web. The crack propagation direction is perpendicular to the main direction of the highest principal stress. As a simplification it is in this investigation assumed that the crack propagates from the middle of the rib radius and with an inclination of 45 degrees. The stresses are therefore extracted in a perpendicular direction to this, see Figure 7-29 b). Hot spot stresses in the floor beam are extracted from the FE-analysis with principal stresses from nodal values of this path.
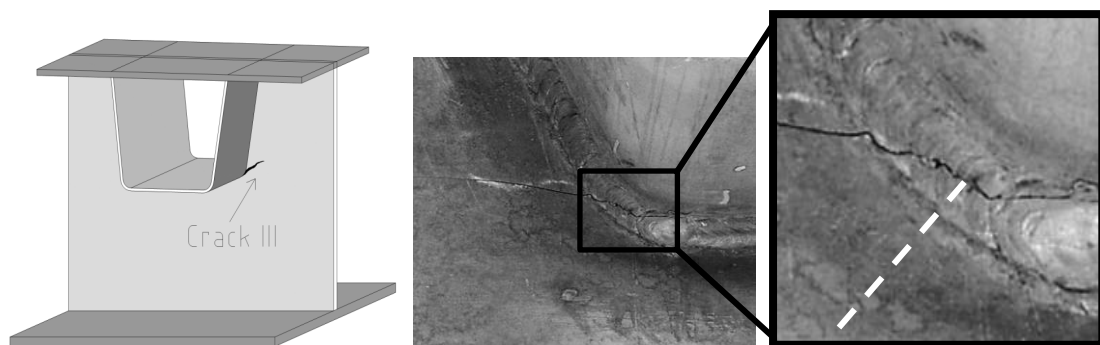
Figure 7-29 Crack initiation angle at radii of rib, the stress are extracted along the withe dashed line; (a) Structural illustration of Crack III; (b) Photograph of a crack classified as Crack III (Kolstein, 2007)

Crack III can arise on either side of the floor beam since there is a weld on both sides, as a consequence of this both top and bottom values of the stresses in the floor beam web must be checked and the largest is the governing.

7.3.4.1 Local transverse load location

Cack III is located in the floor beam web at the intersection with a rib. For the 'local' transversal investigation the loads will be placed centred above the floor beam, according to load case L described in Chapter 7.3.1.3 for the four load position in transversal direction to find the most critical load effects. The load response is checked in the floor beam web at rib wall 7.1, toward the main girder, and at rib wall 7.2, towards the middle of the bridge.
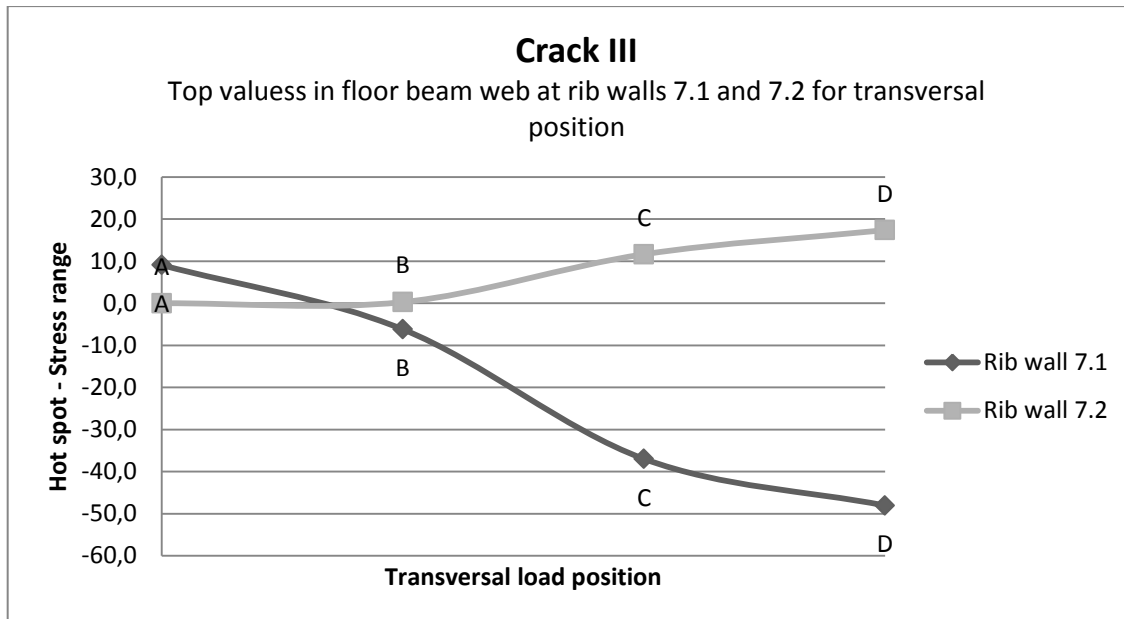
Figure 7-30 Comparison of the response in radii in the floor beam web at the two rib walls for the four load positions

The worst load position is when the load is placed in position D which generates the highest principal stresses in the floor beam web at the rib wall towards the main girder. For this load case the whole load is carried by one rib and the main part by the rib wall closest to the main girder. The stresses arise due to bending of the floor beam.

When performing a hand-calculation, the load is usually placed centrally above the rib wall. If this position was to be used in an FEA this simplification results in 30% lower stresses than if the load is placed at load location D, see **Error! Reference source not found.**. The positioning in local transversal direction is of large importance for Crack III, but the influence is not as large as for Crack I and II.

Table 7-9 Comparison between the response in the rib wall closest the main girder for the load positioned in D respective C

Comparison between response in D and C

x-position	Stress range
D	48,1
C	37,0
Difference:	30%

To get a better overview of the response governing Crack III an influence line is created, see **Error! Reference source not found.**. From the influence line it can clearly be seen that the response in the floor beam web is most adverse when the load positioned in D, aligned with the rib wall to the centre of the span and directed to the main girder. Important to point out is that the error can be extremely high if the load is positioned in other locations. For example can be mentioned that if the load is placed in position B the stresses are 675% lower compared if the load is poisoned in D.
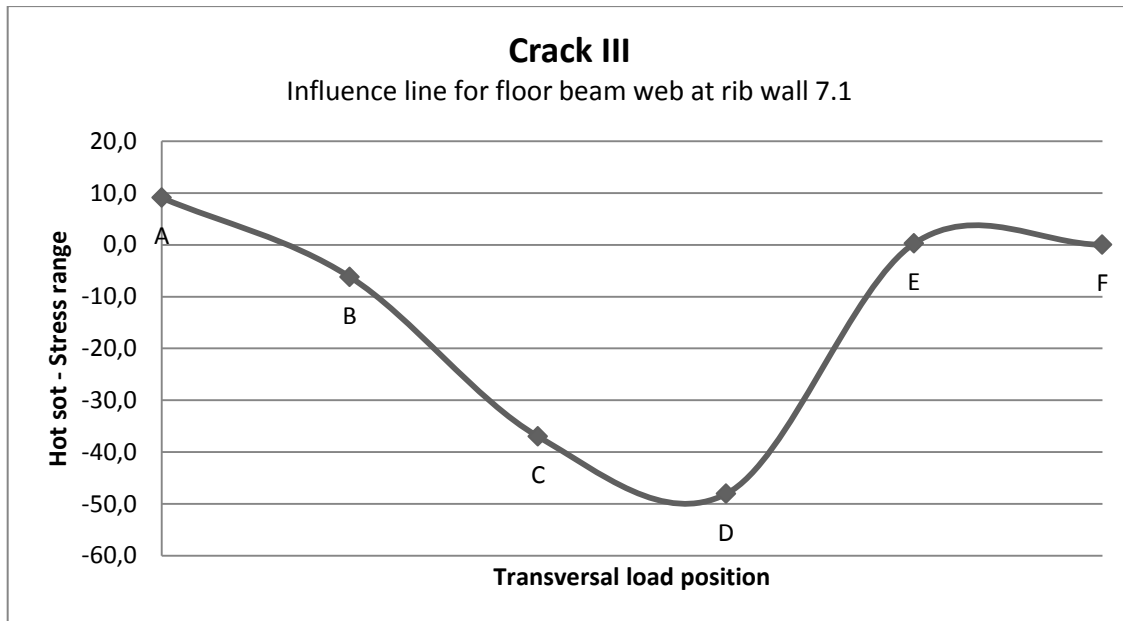
Figure 7-31 Influence line of the response in the floor beam wed at the rib wall closes to the centre in the span between main girders for Crack I, E and F are the corresponding values for the rib wall closest to the main girder in position B respective A

The amount of membrane stresses and bending stresses in the floor beam web is investigated, see **Error! Reference source not found.**. For Crack III the membrane stresses are significantly higher than for Crack I and II. This is expected since the stresses in the floor beam web to a higher extent is affected by mechanisms that are not related to bending. This is also seen in the figure below, where it can be seen that the membrane stresses is about half of the total stress state for load position D.
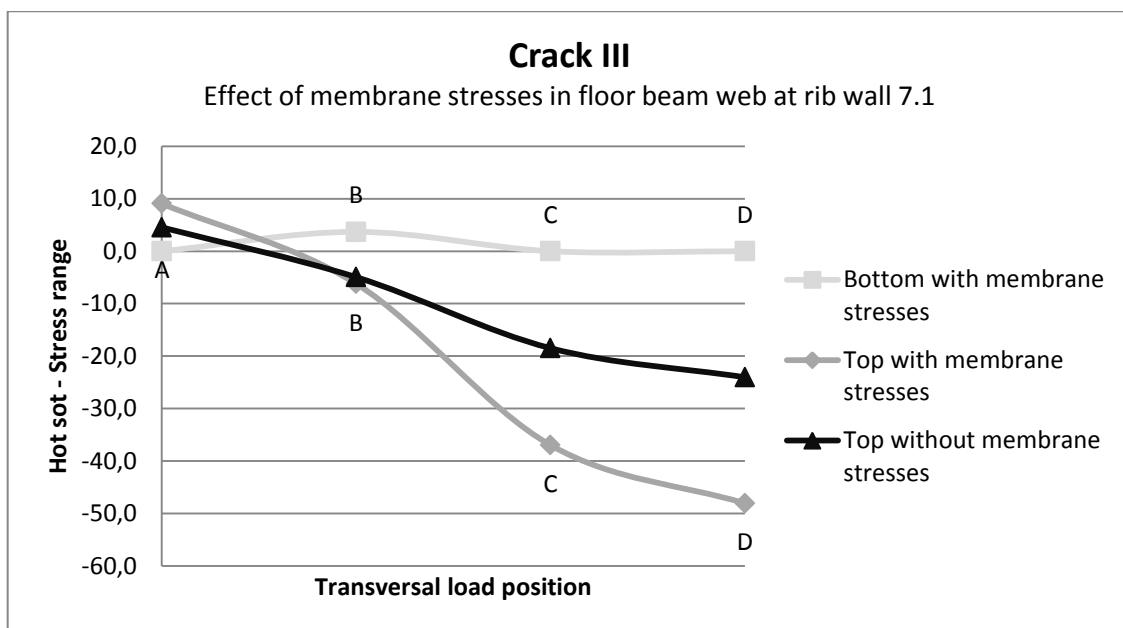
Figure 7-32 Effect of membrane stresses in the floor beam web at rib wall 7.1

The worst load position for Crack III is when the load is placed aligned with the rib wall and to the inner span between the rib walls. For Crack II the load case on which the following studies will be based on is D, for the rib wall closest to the main girder.

7.3.4.2 Global transverse load location

The load is placed at position D for rib 1 to rib 7 and the stress in the floor beam web at the rib wall towards the main girder is extracted. The influence on the load response from the second wheel on the axle is investigated. The results can be seen in Table 7-10 and Figure 7-33. The stresses in this analysis are minimum principal stresses and the bottom values for the shell element representing the floor beam web. They are extracted one node away from the intersection to avoid singularities and nodes with weighted stress values for connecting plates. The reason not to use structural hot spot stresses in this evaluation is because the magnitude of the stress is not relevant, but only the response from different load positions.

Table 7-10 Principal stresses in the deck plate for different transversal locations of the load

Minimum principal stresses in floor beam web

Rib wall	σ_{min} for one wheel	σ_{min} for two wheels	Difference
7.1	-30,80	-42,25	37,2%
6.1	-26,18	-33,95	29,7%
5.1	-22,96	-26,76	16,6%
4.1	-19,07		
3.1	-14,62		
2.1	-11,49		
1.1	-16,91		
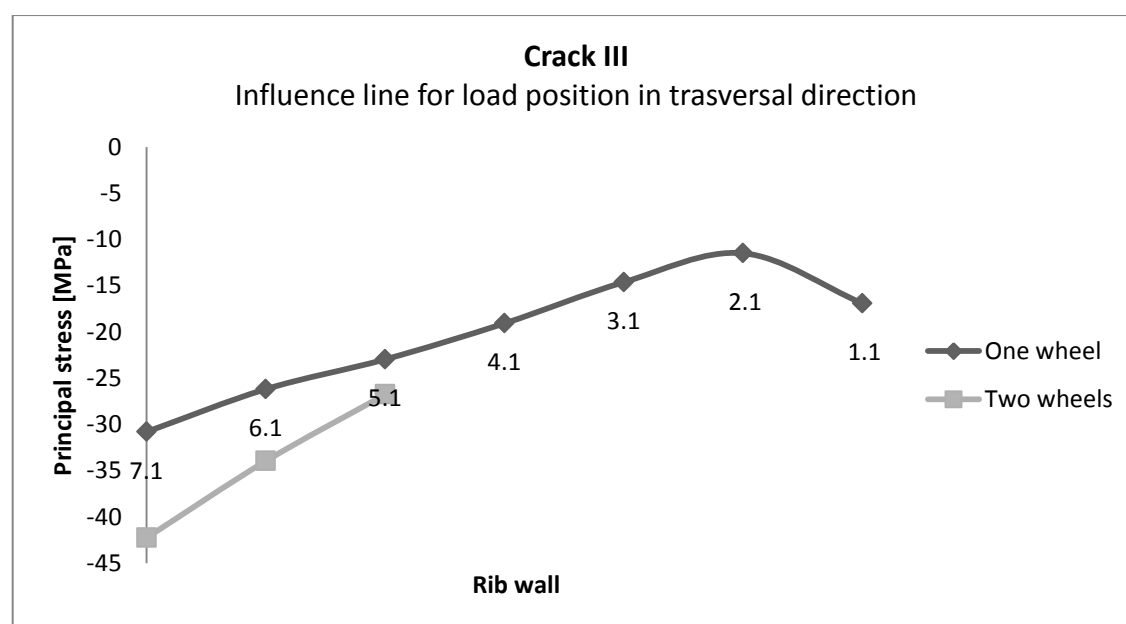
Figure 7-33 Influence line for stresses in the deck plate for load placed in transversal location above different rib walls

The stress state is clearly highest when the load is placed in the centre of the span between main girders. This indicates that the global bending of the floor beam is of large importance for the stresses, which is expected. This is also consolidated with the fact that the stresses are increased when the second wheel is added, a second wheel effects the global bending but not local effects, which govern the load effects for Crack I and II. The stresses increases with 37% in the middle rib when the second wheel is added, this indicates that the second wheel must be considered in analysis. From this discussion it is clear that Crack III is more global than Crack I and II and the global effects must be considered here to a higher extent and both wheels in the load axle must be accounted for.

An increase of the stresses can be seen at the rib connection closest to the main girder. This is a consequence of the high shear stress that arises in the floor beam at this position. However, the shear arising when the load is located as in Figure 7-34 is still lower than the bending moment that arises form when the load is located as in Figure 7-35. From this is clear that the stresses governing Crack III is a combination of shear and in-plane flexure of the floor beam.

Figure 7-34 Model of floor beam for highest shear force
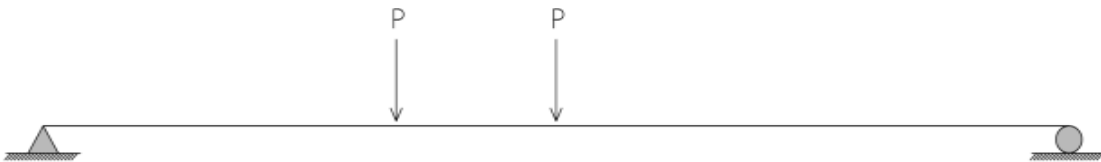
Figure 7-35 Model of floor beam for highest moment

7.3.4.3   Local longitudinal load location

When investigating the local longitudinal positions it is seen in Table 7-11 that the stresses are rather similar for all three positions, of much larger importance is to consider the second axle. If only one axle is included, the stresses are highest when the load is placed in L, centred above the floor beam due to that the highest pressure stress in the floor beam web arises for this position. When both front axles are included in the analysis the highest stresses in the floor beam web arises for position M, the load is aligned with the floor beam and the positioned to the span and the second axle is placed in the same span. This can be explained by the stresses in the floor beam at the radii of the rib connection also are highly influenced by the out-of-plane distortion of the floor beam web caused by rotation of the ribs, see Figure 7-36.

Table 7-11 Minimum principal stresses in deck plate for local longitudinal load position

Minimum principal stresses in deck plate for longitudinal load position M

Longitudinal position	One load axle Two wheels	Two load axles Two wheels/axle	Difference
K	-48,0	-90,5	88,3%
L	-55,4	-88,7	60,1%
M	-41,5	-92,8	123,7%
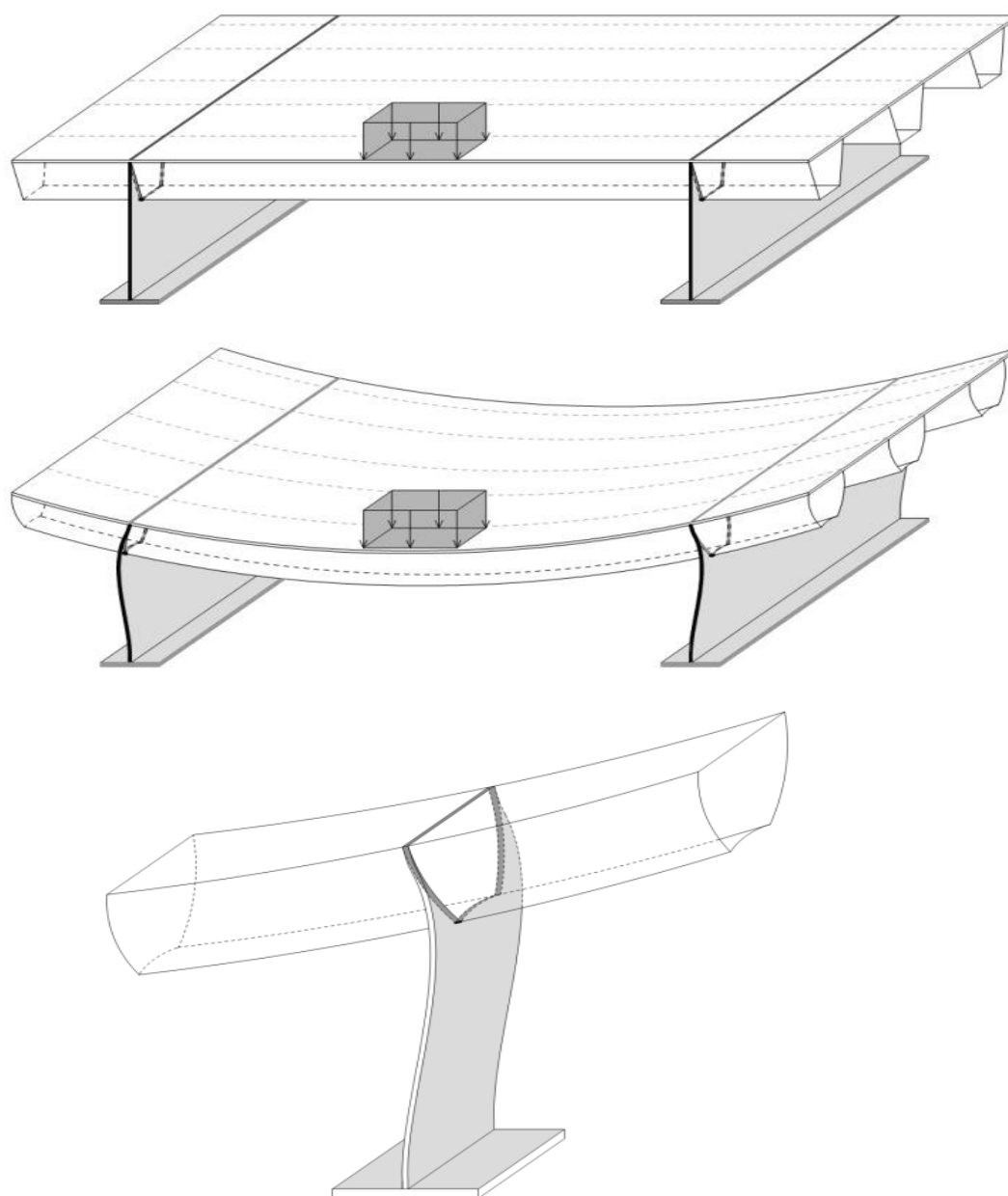
Figure 7-36 The out-of-plane bending governed by the rib rotation

When a load is placed in the centre of the span between floor beams the ribs will deflect forcing the floor beam web to translate out-of-plane. Since the web and bottom flange of the floor beam are welded to the main girders the translation will be restrained and an out-of-plane moment will arise in the floor beam web. This is the reason for the large influence of the second axle for the stresses governing Crack III.

7.3.4.4 Summary - Final load position

Crack III is driven by bending and shear stresses in the floor beam web. The bending stress is a combination of in-plane and out-of-plane flexure that arises as a result of global bending of the floor beam respective local distortion of the floor beam web from rotation of the rib in the longitudinal direction.

The load should be placed so that the main part of the load is carried in one rib and that most of this load is taken in one of the rib walls, this is represented by load case D. The highest global bending of the floor beam arises when the first load axle is placed in connection to the floor beam and the second in the span, load case M. This also generated the largest rotation of the ribs due to that the load is placed with as much lever arm as possible to the floor beam in the longitudinal direction. Both front axles must be included in the analysis and both wheels shall be included on each axle.

With regard to fatigue analysis of Crack III the load should be placed as in Figure 7-28 below.
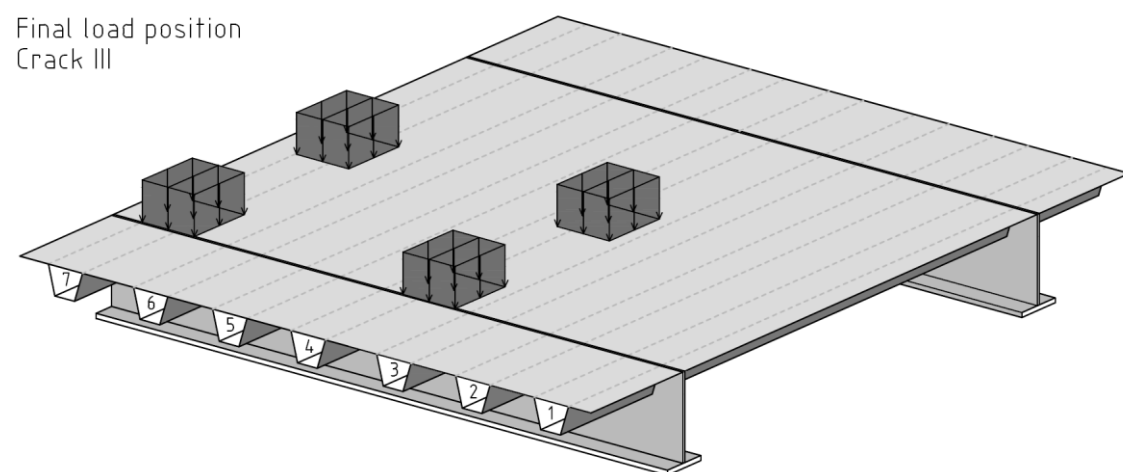
Figure 7-37 Final load position for Crack III

- Local transversal location: The load should be aligned with the rib wall towards the span between main girders and positioned inwards to the other rib wall of the same rib, load case D.
- Global transversal positions: The load should be placed above the rib in the centre of the span between the main girders, rib 7.
- Local longitudinal position: The first axle should be placed aligned with the floor beam and the second axle in the same span, load case M.

The second wheel and the axle and the second axle must be included in the model for fatigue analysis.

7.3.5 Summary of the local position in transversal direction

In Table 7-12 a summary over the final load positions to be used in fatigue analysis of Crack I, II and III is presented. Important to point out is that this applied for this specific bridge and can be used for orthotropic decks with similar dimensions.

Table 7-12 Summary of the final load positions for the three cracks

Summary of most adverse load position for the three cracks

Crack	Local trans. position	Global trans. position	Local long. position	Second wheel	Second axle
I	B	Rib 7	M	Neglect	Include
II	A	Rib 1	M	Neglect	Include
III	D	Rib 7	M	Include	Include

7.4 Comparison of response from hand-calculations and FEM

To single out the simplifications generating major errors in conventional design a comparative analysis between hand-calculations and FEA is performed. The FEA is executed in Brigade/PLUS and the hand-calculations in MathCAD and GoBeam, see Appendix VI. The stresses at the positions of the welds are calculated and compared between the different methods.

In Brigade/PLUS the loads are modelled as four wheel loads distributed over the square pressure area with the side of 0.4m, according to the two front axles in Eurocode fatigue load model 3. This is done in the same model as used for previous analysis. This model, is as described above, a simulation of an existing bridge with the actual dimensions and three-dimensional connections between members.

In the hand-calculations one single rib is analysed for two different load situations. The first is when the wheel loads are represented by point loads and the second when they are modelled as line loads. In both cases only two wheels are included, one wheel from each of the two front axles since the hand-calculation model represent only one rib. This rib is seen as a beam which rests on supports representing the floor beams. The load used in calculations is the worst possible which can be reached in one point in the rib, this is assumed as one and a half wheel load. When the load distribution between ribs, in transversal direction, is neglected in the hand-calculations the investigated rib is carrying a significantly higher load and this simplification is on the safe side.

Conventional analysis includes defining of a simplified model and dividing this global model into separate sub-systems that are analysed individually. With regard to fatigue evaluation in orthotropic decks, in general two welds are of primary interest, the longitudinal weld between rid and deck plate and the weld at the intersection between rib and floor beam. In this chapter the stresses received from hand-calculation are compared to the stresses calculated with FEM and from this, conclusions according the simplifications made in the hand-calculations can be drawn.

7.4.1   Result evaluation of rib-to-deck plate weld

In the following the loads will in all cases be placed in the same positions for both the conventional hand-calculations and the FE-analysis. The hand calculation method is described in Chapter **Error! Reference source not found.** and the actual hand calculation in Appendix VI.

For the rib-to-deck plate weld the rib located in the centre of the span between main girders is studied in the hand-calculations since this rib experience the largest global deflections. As a simplification, the rib is seen as a box girder with the effective with of the deck plate as the top flange. The girder is resting on spring supports, representing the floor beams, and has no restriction or boundary conditions in the transversal direction and accordingly no load distribution in the transversal direction can occur. From this system the global moments and shear forces in the rib-girder is retrieved and the stresses in the welds are calculated and the fatigue evaluation with detail categories is executed.

The first load axis will be placed in the centre of the span between floor beam 6 and 7 and the second axis 1.2m toward floor beam 7, see Figure 7-38. The stresses presented below represents the values in the centre of the span between floor beam 6 and 7.
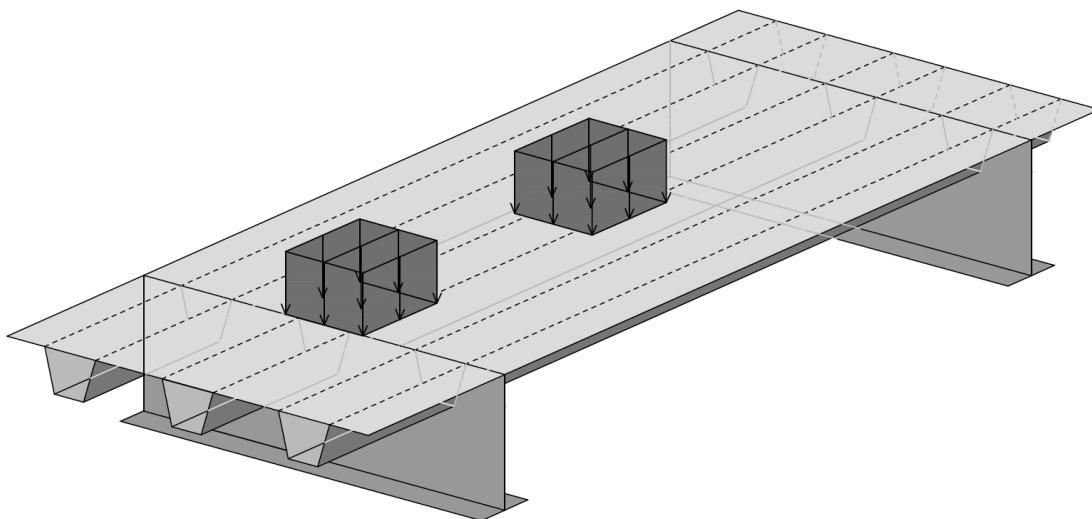
Figure 7-38 First load axle placed in the centre of span between floor beams and the second 1.2m towards the floor beam 7

The stresses in the top and bottom flange of the cross-section are printed in Table 7-13 and from these figures it can be seen that the stresses differs. This is expected due to

the simplifications made in the hand-calculations. However, if the simplifications are realistic the proportion between the stresses in the top and bottom flange for the two models should correspond, this is checked in Figure 7-39 below.

Table 7-13 Stresses in the cross-section according to Brigade/PLUS respective calculated in from the moments from GoBeam

| | **From Brigade** | **From GoBeam** | |
	Wheel loads	*Point loads*	*Line loads*
Moment in section [kNm]:	-	31,9	29,1
Stresses in top flange [MPa]:	-12,1	-21,6	-19,7
Stresses in bottom flange [MPa]:	58,3	60,5	55,2

The stress distribution in the rib cross-section is assumed to be linear for both the hand-calculations and the FE-analysis. According to this the neutral axis is found at the height where the stresses equal zero. If the behaviour would be the same in the simplified method and the FE-method the neutral axis would be the same even if the magnitude of the stresses differed. As can be seen in the figure above, see Figure 7-39, this is not the case. The neutral axis is placed closer to the deck plate in the FE-model compared to in the simplified model. From this can be concluded that the structural behaviour differs in the two models and the assumptions made in the hand-calculations do not account for all effects in the member. For the simplified beam model described in Chapter 5.2.2.1 the top flange represented by the deck plate does not include axial force that comes from that the deck plate also acts as top flange for the main girders.
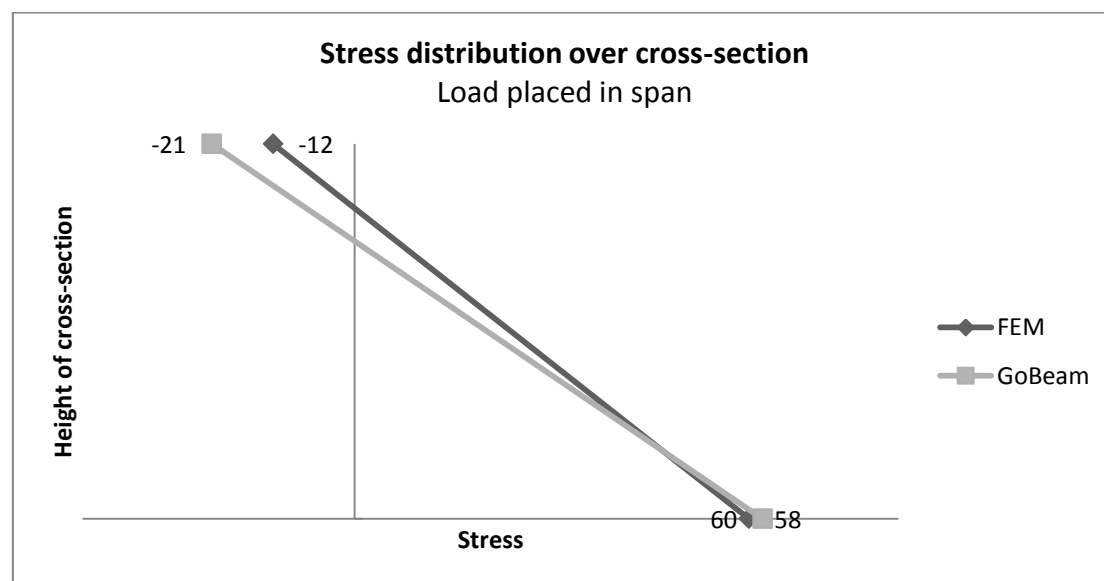
Figure 7-39 Comparison between assumed stress distribution in the cross-section for hand-calculations and FEM analysis

7.4.1.1   Shear lag effect

The reason for the difference in position of the neutral axis for the two models depends on the shear lag effect. The shear lag accounted for in the FE-analysis can be visualised if the stresses in over the cross-section in transversal direction for the top and bottom flange of the rib system are plotted.

Stresses in top flange over the effective width
Load placed in span
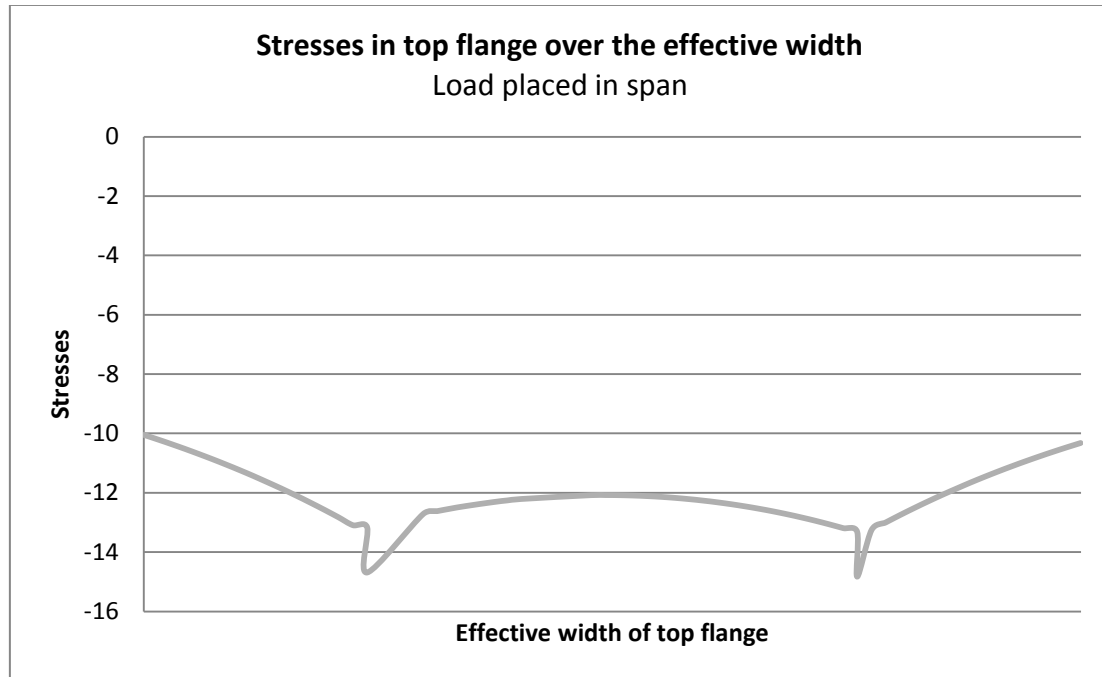
Figure 7-40 Stress distribution over the top flange of the rib system with stresses read from a path in the centre of the span in Brigade/PLUS

In Figure 7-40 it can clearly be seen that there is a significant shear lag effect in the top flange. Due to the shear lag the normal stress will not be evenly distributed. The peaks in the graph represent the location where the deck plate is connected with the rib walls This location experience higher stresses due to the shear lag effect, which can be seen in Figure 7-41.
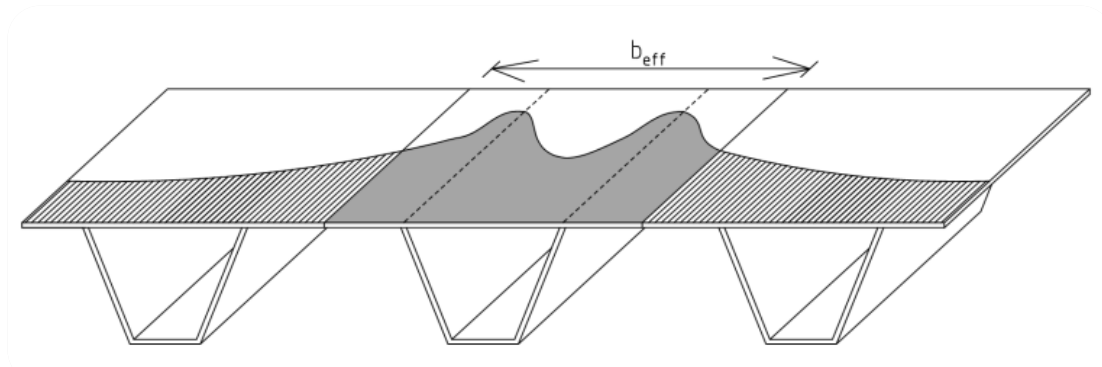
Figure 7-41 Structural overview of the stresses in the deck plate and the shear lag effect at the connection between deck plate and rib walls

During hand calculations the shear lag effect is considered by the use of effective width. The effective width average the total stress over the effective width as can be seen in **Error! Reference source not found.** (left) below. The local stress peak at the intersection is therefore not considered in hand calculations.
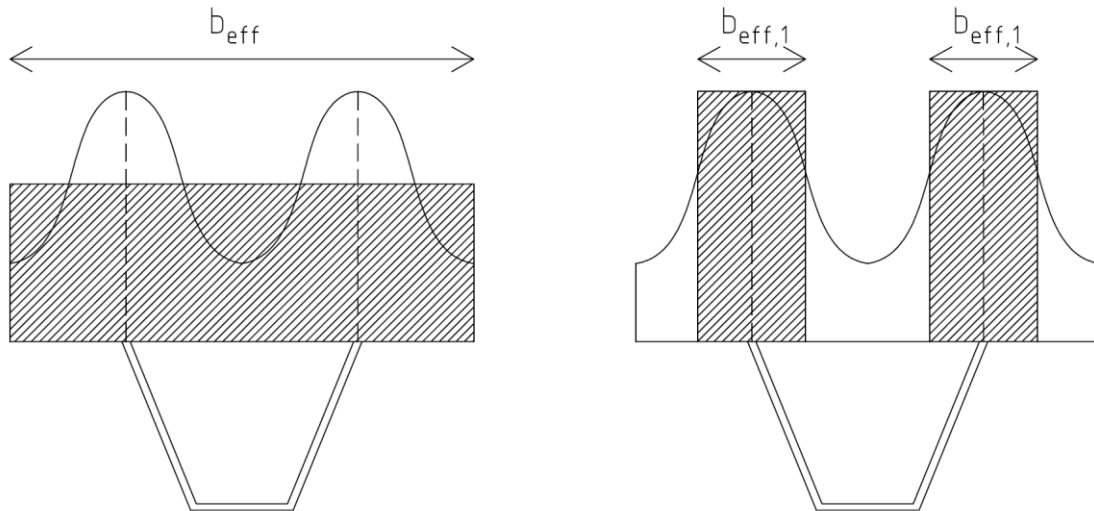
Figure 7-42 Adjusting of the effective width to account for the shear lag effect at the intersection between deck plate and rib wall

7.4.1.2   Transversal load distribution

As can be seen in Figure 7-40 the stresses at the end of the effective width are not zero. Hence, the rib distributes the stresses via the deck plate in the transversal direction to the adjacent ribs. This transversal distribution is not included in hand-calculations. To investigate the proportion of stresses that are distributed to the nearby ribs a separate investigation in Brigade is performed with only one wheel and the stress effect over several ribs are studied. The results from this study are presented below in Figure 7-43.
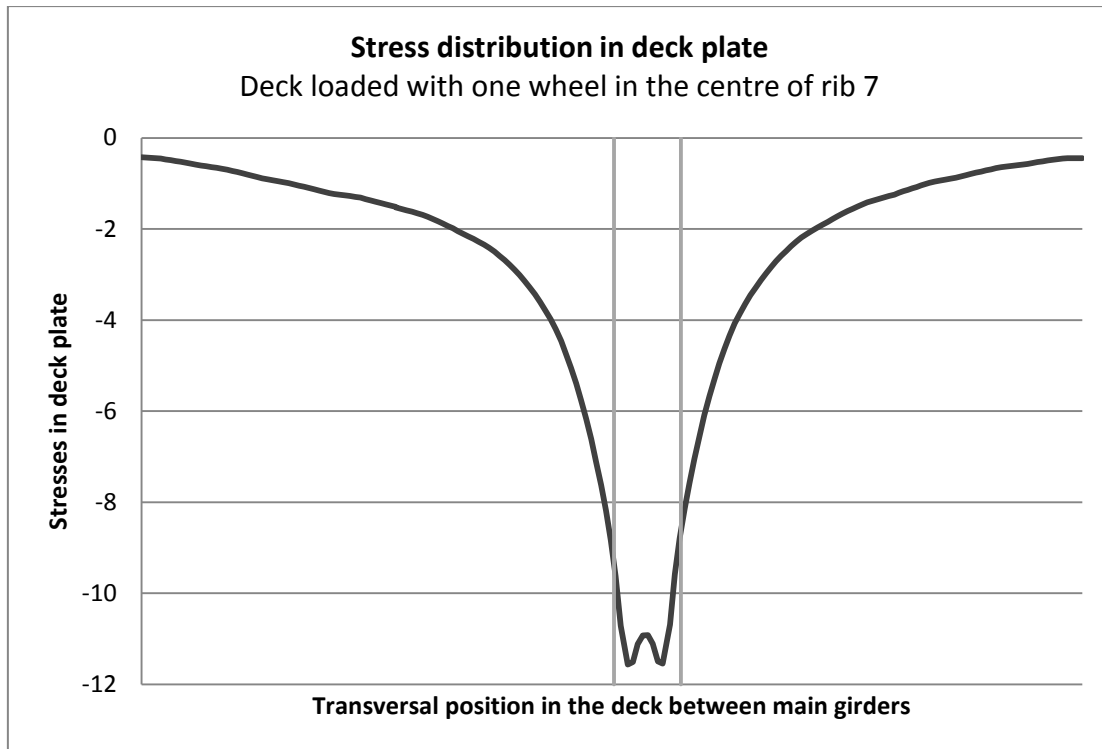
Figure 7-43 Stress distribution in the deck plate seen in transversal direction when the deck is loaded with one load axle placed above rib 7, in the span between floor beam 6 and 7. The effective witdh of the rib model used in ch. Error! Reference source not found. **is presented by the two vertical lines.**

The effective width of the loaded rib used in the hand calculations is marked out in the graph and it can clearly be seen that the load is distributed over a significantly larger width than only the investigated rib. Therefore it can be concluded that the second wheel on the axle contribute to the stress state at the investigated section, even though it is applied two meters away. One important observation from Figure 7-43 is the behaviour at the position of the load where it is visible that no extreme peak value is received. This is a result of that the load is located symmetrically above the rib, if the load instead would have been placed with the centre above one of the rib walls the peak value in this wall would be significantly higher. This can be observed in Figure 7-44 which shows the stress distribution in the deck when two wheels are applied and the second wheel (right in the figure) is placed closer to one rib wall.
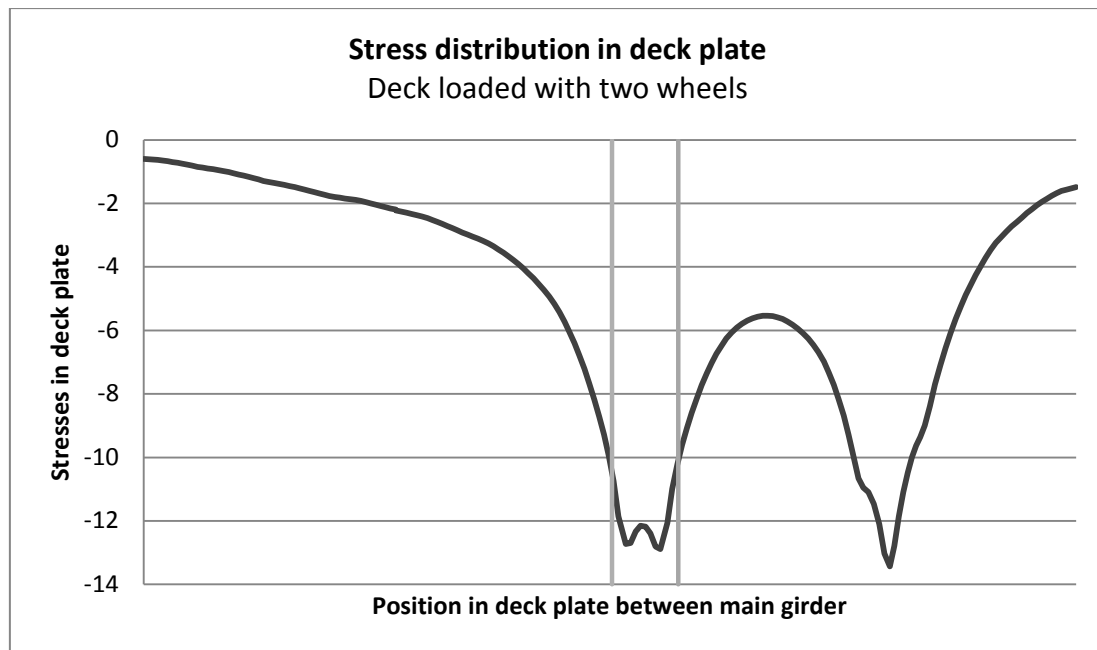
Figure 7-44 Stress distribution in the deck plate seen in transversal direction when the deck is loaded with two load axles, the first placed above rib 7 and the second 2 m to the side.

When comparing the two graphs, Figure 7-43 and Figure 7-44 it is observed that the stress at the investigated rib increases when the second wheel is included in the analysis. In Figure 7-43 it can be seen that the stresses at the loaded rib do not exceed 12 MPa but in Figure 7-44 the stresses approaches 13 MPa. From this is clearly concluded that the second wheel increases the stresses in the deck plate but the increase is rather small. The maximum stress is higher at the location of the second wheel. This is not because of the global effects are worse at this location compared to the centre of the span between the main girders. This is explained by the local effect of the wheel load. The first wheel is symmetrically placed above the rib while the second wheel is unsymmetrically placed resulting in higher peak stress.

For the stress in the bottom flange, Figure 7-45 (a), it is seen that the shear lag effect is considerably smaller than for the top flange but still present. The shear lag effect is clearly visible in the zoomed in graph in Figure 7-45 (b).
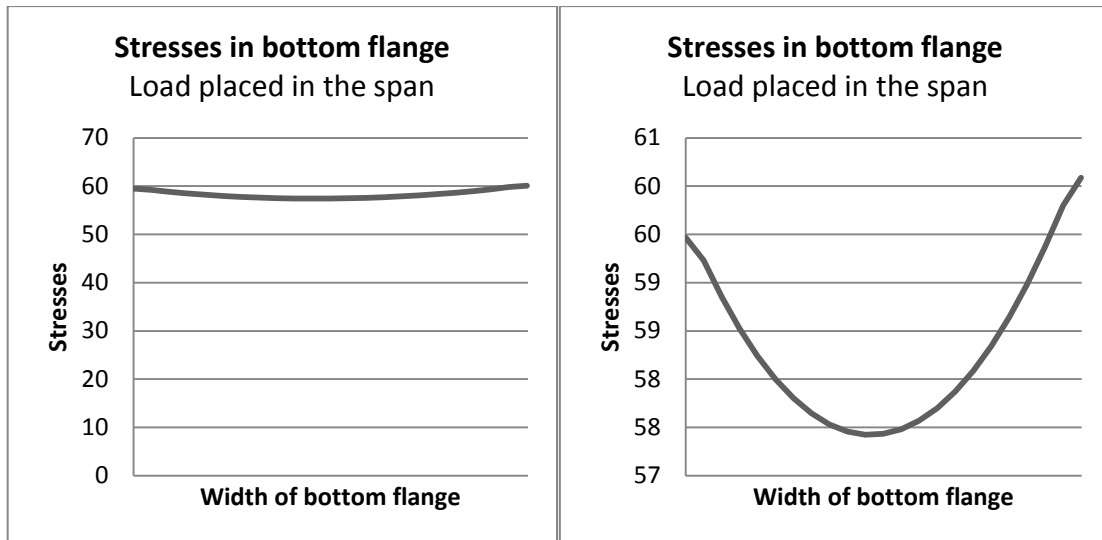
Figure 7-45 Stresses in the bottom flange of the investigated rib; (a) Overview; (b) Zoomed-in view showing the shear lag effect in the bottom flange

7.4.1.3 Longitudinal stress distribution

Another aspect to consider in the analysis is the longitudinal stress distribution in the rib. In the FE model the load is distributed from the application point via the deck plate to the ribs and then to the nearest floor beams which transfer the load to the main girders. Accordingly, all load response is mainly found in only one span. In the hand-calculation model on the other hand the load is distributed over several spans and the moment will display a different behaviour, as can be seen in Figure 7-46.
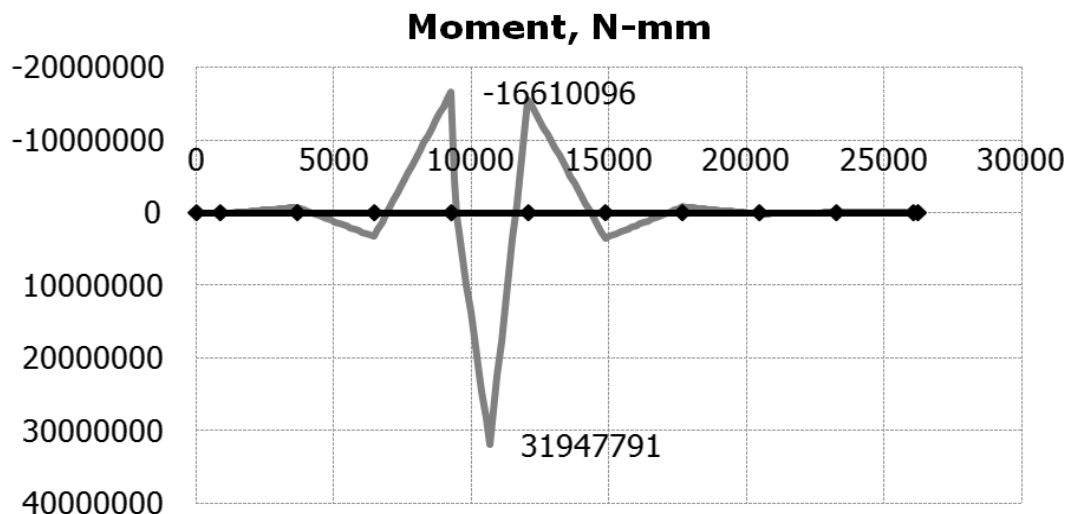
Figure 7-46 Moment distribution (y-axis) along the longitudinal direction of the bridge for one rib (x-axis), when loaded by two load axles located between floor beam 6 and 7

In the hand-calculations no interaction between members in transversal direction is accounted for and as a result all load is distributed in the longitudinal direction. As can be seen in Figure 7-46 the moment in the hand-calculations is distributed over

several spans in the longitudinal direction. This can be compared to the longitudinal stress distribution from the FE-analysis seen in Figure 7-47 below.
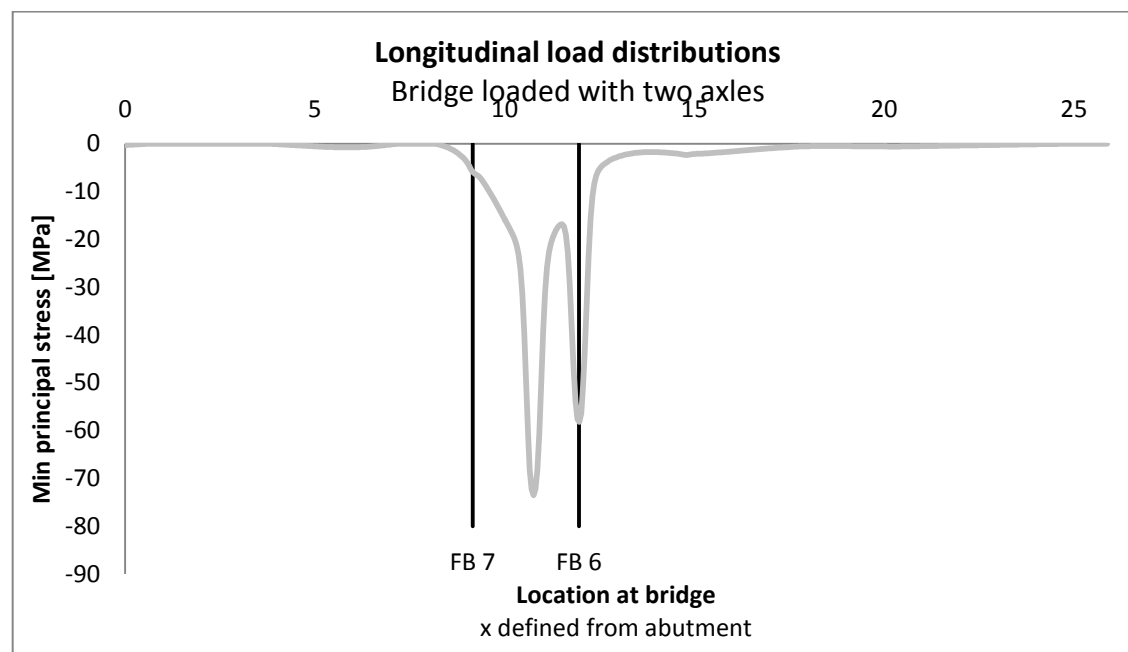
Figure 7-47 Longitudinal stress distribution in the deck plate when the bridge is loaded by two load axles located between floor beam 6 and

In the hand-calculation model the spring supports representing the floor beams, do not include the load distribution in the transversal direction to the main girders. The moment is instead distributed only in longitudinal direction. As can be seen in the graph of the stress distribution in longitudinal direction for the FE model there is only a negligible part of the stress that is distributed longitudinally since the main part is transferred from the floor beams directly to the girders. This is a simplification in hand calculations that results in lower stresses than experienced in reality.

There is a third effect that is over looked in the hand-calculations and that is that normal stresses in compression are not accounted for. This also gives lower stresses than the real behaviour, stresses are neglected. Other local effects are also neglected such as bending of the deck plate, distortion of the rib wall and out-of-plane bending in the floor beam web. However, the stresses from the hand-calculations are higher than the stresses from the FEA. Accordingly, the simplifications on the unsafe side are compensated by the ones on the safe side, see Table 7-14.

Table 7-14 Comparison between stresses for rib in mid-span between main girders from FEA and hand-calculations

Stress comparison for load placed in span for rib placed in mid span between main girders		
	From Brigade *Wheel loads*	**From GoBeam** *Point loads*
Stresses in top flange [MPa]:	-12,1	-21,6
Stresses in bottom flange [MPa]:	58,3	60,5

The effects on the unsafe side from the hand-calculations are:

- Load distribution in transversal direction is not accounted for
- Normal stresses in compression from global action are not accounted for
- The local stress raising effect from shear lag effect is not accounted for

The effects on the safe side from the hand-calculations are:

- Neglecting load distribution in transversal direction, which increase the stress in mid-span at the rib-deck plate intersection

As can be seen if the stresses from the FE-analysis and the hand-calculations with GoBeam are compared the differences are reasonable. Accordingly, it can be concluded that the simplifications used in the hand-calculations are reasonable with regard to stress calculations since the final result is on the safe side and rather realistic. However, this only applies for orthotropic decks with similar proportions between members as the investigated.

Although, with regard to fatigue, the local effects are of major importance and when the stresses are translated into fatigue life a significant difference is seen, Table 7-15. For the hand-calculations the fatigue evaluation is performed with the use of detail categories and S-N curves. The fatigue evaluation for the FE analysis on the other hand is executed according to the hot spot method since the stresses are hot spot stresses and different detail categories are here appropriate.

Table 7-15 Comparison between fatigue utilization ration from hand-calculations and FEM

Fatigue utilization ratio		
	Crack I	**Crack II**
FEM (hot spot)	64%	107%
Hand-calculation	53%	53%

7.4.2 Result evaluation of rib-to-floor beam weld

In the weld at the rib-to-floor beam intersection the floor beam with an effective part of the deck plate acting as top flange is studied. The floor beam is connected to the main girders, which are represented by pinned supports. For a system of a beam on pinned supports there is one load position when the load is placed in the middle of the span that gives the highest moment, Figure 7-48 (a) and Figure 7-49 (a), and another load position with the load placed at the support giving the highest shear force, Figure 7-48 (b) and Figure 7-49 (b).
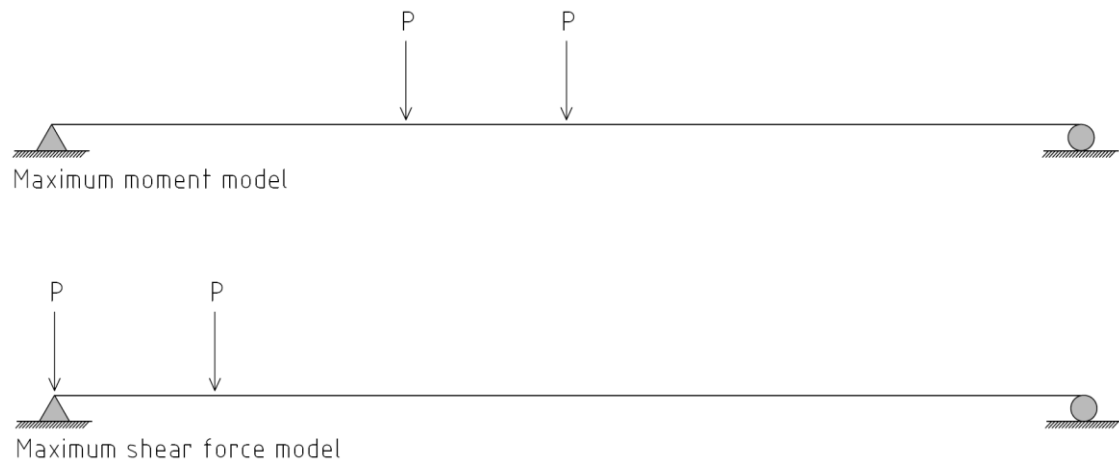
Figure 7-48 Transversal overview of the floor beam models used in hand-calculations; (a) Maximum moment model; (b) Maximum shear force model
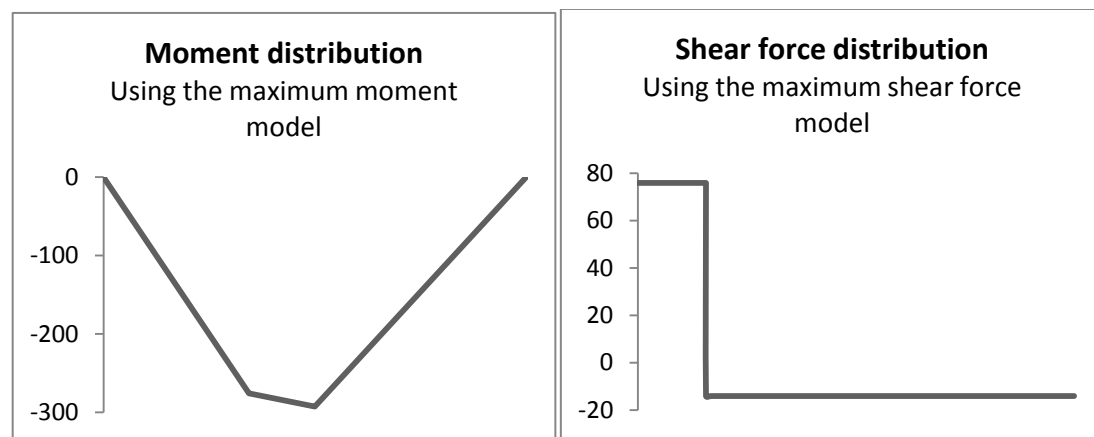
Figure 7-49 Principle distribution in the floor beam using the models above; (a) Moment distribution; (b) Shear force distribution

The floor beam is loaded with two axles both with two wheels, the first placed directly above the floor beam and the second axle 1.2m out in the span, see Figure 7-50. In the hand-calculations the second load axle is simplified to distribute half its load to the present floor beam.
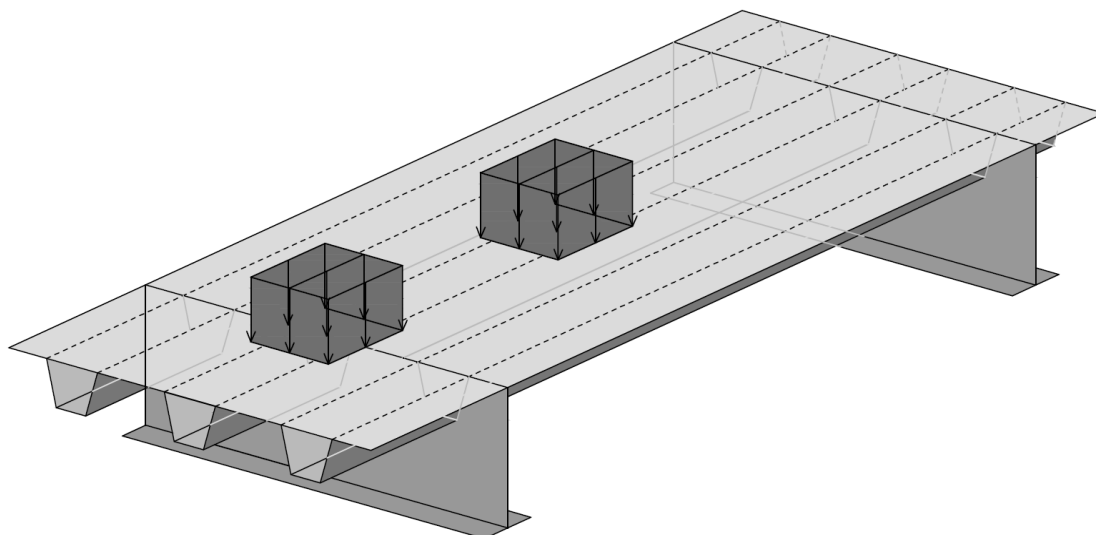
Figure 7-50 Longitudinal overview of the placement of the two load axle in relation to the floor beam

At the intersection between floor beam and rib the floor beam cross-section is reduced by the rib. To account for this an effective cross-section is calculated and used, see Figure 7-51.
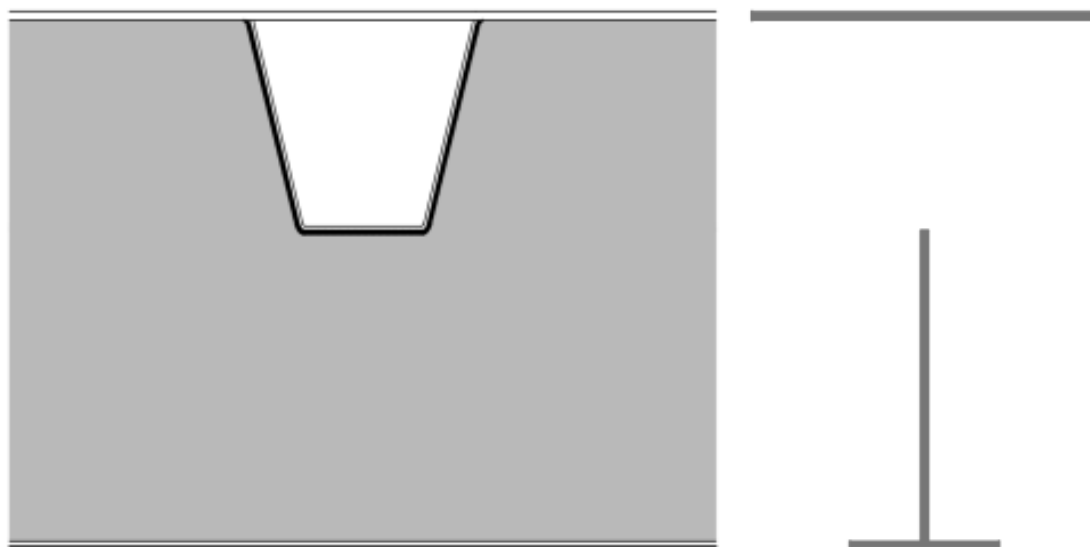
Figure 7-51 Effective cross-section of floor beam at intersection with rib; (a) Transversal view of the floor beam at the intersection with rib; (b) Effective floor beam cross-section.

With the models above the stresses in the effective cross-sections are calculated and thereafter the stresses in the welds. From theses stresses the fatigue evaluation is performed and can be compared to the fatigue evaluation from the FE-analysis which is conducted as described earlier. The comparison can be seen in Table 7-16 and as for Crack I and II it is a significant overestimation of the fatigue strength from the hand-calculations depending on the neglected local effects. Differing from Crack I and II is that also the stresses in the floor beam web at the rib radii are considerably

lower according to hand-calculations compared to FE-analysis. Accordingly, the calculation models for this specific area shall be used with caution.

Table 7-16 Comparison between fatigue utilization ration from hand-calculations and FEM

Comparison between result from hand-calculations and FEM		
	Stress range	Fatigue utilization ratio
FEM (hot spot)	92,8 MPa	125%
Hand-calculation	15,2 MPa	26%

7.4.3   Summary of comparison between hand-calculations and FEM

The hand-calculation models are representative for global analysis and global stresses but for local fatigue analyse the stress-raising effects that are disregarded in the hand-calculations results in large errors. The fatigue strength is highly overestimated which can lead to premature fatigue damage. To get realistic results the local effects must be included, either in hand-calculations (if possible) or by the use of FE modelling.

8   Conclusions

Orthotropic decks are very complex structures with stresses that are difficult to calculate by simple hand-calculation models. The main intention of this thesis work was to investigate the benefits of advanced analyse techniques when evaluating the fatigue performance of an orthotropic deck. Three crack moods were examined with conventional hand calculations and FE-analysis and the result from the different methods compared.

8.1   Concluding remarks

The primary conclusion from this thesis work is that when design is governed by local effects, such as fatigue design, accurate models that are capable of capturing these local affects should be used to ensure the accuracy of the results. This can generally be achieved when finite element models are used. Accordingly, there is a large risk that orthotropic decks constructed according to conventional simplified hand calculation models overestimate the fatigue strength to those proportions that premature cracking may take place. However, in all calculations safety factors are applied and account for results on the safe side. Also, in the executed investigation in this thesis the loads and application points for each of the three crack modes considered are chosen as the most adverse with regard to fatigue. This generates more extreme results than the real life situation accounts for.

During the investigations the time required for FE-modelling and calculations were judged to be rather similar to the time required for hand calculations. A problem with the FEA is the large computer space it requires and when shell elements are used, as in this case, the number of elements and thereby steps for each analyse are immense. It is possible to reduce the number of elements in the model for fatigue evaluation since the interesting areas are known. But if the bridge is to be designed using FE software the full model must be submitted to analyse and these will require large amount of memory as well as computational time. Consequently, the conclusion is that if only the fatigue evaluation is of interest the additional time required compared to hand calculations are indifferent. Regarding a full design of an orthotropic deck using FEM further investigations must be undertaken before any conclusions regarding this is drawn.

8.1.1   Conclusions regarding the finite element modelling

The model structure and the result extraction are of great importance when it comes to FEA. The general conclusion with respect to this and as a guide on how to construct a finite element model for fatigue evaluation the aspects below can be presented.

- In Brigade/PLUS the traffic load is modelled as point loads that are shifted forward step by step. This is not a suitable model for fatigue evaluation of the deck since the local behaviour is highly sensitive to the singularities of this approach. It is possible to make own loading areas that distribute the load and move this area along the lane. This is recommended if a moving load is required.

- It is of importance to extract the results from nodes and not from elements. The node in question shall not be a node in an intersection between two planes.
- The result should be extracted according to the hot spot method if reliable values are to be retrieved.
- With regard to stresses and fatigue evaluation it is the principal stresses in the nodes that are to be used for calculations. The crack is driven of the principal stresses perpendicular to the weld. The principal stresses must be within the range of 60 degrees from the weld of interest.
- Shell elements are defined with a thickness and the stresses will differ between the top and bottom part of the element. Accordingly, the stresses must be extracted at the same side of the element as the weld. It is therefore important to know what side of the shell that is defined as top side respective bottom side.

8.1.1.1 Guidelines on how to perform a hot spot analysis

- Choose the area to be investigated
- Define partitions where the stresses are to be extracted, in this specific case: at 0.4t and 1t distance from the weld
- Assign structured element meshing technique to the region of interest
- Define global seed to the whole model
- Define local seed
- In the visualisations module, extract the principal stresses at the partitions at the correct side of the shell, top or bottom depending on the position of the weld
- Calculate the hot spot stress according to Equation 4-3

More thorough guidance on how to perform a hot spot analysis is given in Chapter 6.2.8.1.

8.1.2 Conclusions regarding load applications for the crack moods

To find the highest stresses related to the three investigated cracks the load application rules and positions given below can be used. These recommendations include the necessary local and global effects and will give a very realistic stress picture. If these simple guidelines are used in the fatigue evaluation the modelling time required for an FE-analysis decrease significantly. This will motivate the use of FEM in the fatigue evaluation of orthotropic steel decks and result in more accurate fatigue estimations.

- The loads should be applied as area loads, distributed over the wheel pressure area.
- The relevance of the second wheel on the load axle must be checked for each specific crack case.
- The influence of the two rear axles in the fatigue vehicle can be disregarded.
- The longitudinal position in an orthotropic deck is insignificant as long as the stiffness of the deck is constant.
- Self-weight can be neglected.

In Table 8-1 a summary over the most adverse load positions with regard to fatigue analysis of Crack I, II and III. Important to point out is that this applied for this specific bridge and can be used for orthotropic decks with similar dimensions.

Table 8-1 Summary of the most adverse load positions for the three cracks according to investigations in this report

Summary of most adverse load position for the three cracks

Crack	Local trans. position	Global trans. position	Local long. position	Second wheel	Second axle
I	B	Rib 7	M	Neglect	Include
II	A	Rib 1	M	Neglect	Include
III	D	Rib 7	M	Include	Include

8.1.2.1 Crack I

- Local transversal location: The load should be centre above the rib wall closest to the centre of the span between main girders, load case B.
- Global transversal positions: The load should be placed above the rib in the centre between the main girders, rib 7.
- Local longitudinal position: The first axle should be placed in the middle of the span between floor beams and the second axle should be included if it is in the same span, load case M.
- The second wheel on the load axle can be excluded from the analysis
- If the second load axle of the fatigue vehicle is in the same span as the first it should be included, with one wheel.

8.1.2.2 Crack II

- Local transversal location: The load should be aligned with the rib wall towards the span between main girders and positioned towards the free span between ribs, load case A.
- Global transversal positions: The load should be placed above the rib closest to the main girder, rib 1.
- Local longitudinal position: The first axle should be placed in the middle of the span between floor beams and the second axle should be included if it is in the same span, load case M.
- The second wheel on the load axle can be excluded from the analysis.
- If the second load axle of the fatigue vehicle is in the same span as the first it should be included, with one wheel.

8.1.2.3 Crack III

- Local transversal location: The load should be aligned with the rib wall towards the span between main girders and positioned inwards to the other rib wall of the same rib, load case D.
- Global transversal positions: The load should be placed above the rib in the centre of the span between the main girders, rib 7.
- Local longitudinal position: The first axle should be placed aligned with the floor beam and the second axle in the same span, load case M.
- The second wheel on the load axle should be included in the analysis
- The second load axle of the fatigue vehicle should be included, with two wheels.

8.1.3 Conclusions regarding conventional hand-calculation

The following conclusions are regarding the revised calculations on Saltsjöbron. However, these calculations are according to general practise and design codes and the conclusion can therefore be viewed in a more general way.

The effects on the unsafe side from the hand-calculations are:

- Load distribution in transversal direction is not accounted for
- Normal stresses in compression from global action (i.e. the deck acting as a flange to the main girders) are not accounted for
- Shear lag effect is not accounted for

The effects in the safe side from the hand-calculations are:

- Neglecting load distribution in transversal direction

8.2 Future work

This thesis work is limited to the evaluation of one bridge with an orthotropic deck, Saltsjöbron, with its given dimensions and boundary conditions. To consolidate the results similar investigations should be performed on other orthotropic deck and the conclusions compared to the one given in this thesis.

The fatigue behaviour of three critical crack moods is evaluated and all other details and crack patterns are disregarded. It would be of interest to investigate other critical details.

To assess the required time more properly this type of investigation should be performed for a full design of a bridge with an orthotropic deck. Is it possible to use shell elements in this case or is there an alternative method that meet both the requirement for global and local analyses?

9 References

AISC (1962): *Design Manual for Orthotropic Steel Plate Deck Bridges.* American Institute of Steel Construction, New York, USA, 1963

Akhlaghi, F. Z. (2009): *Fatigue life assessment of welded bridge details using structural hot spot stress method - A numerical and experimental case study*. MSc thesis. Chalmers University of Technology, Publication no.2009:104, Göteborg, Sweden, 2009.

Al-Emrani M., Nilsson M. and Lukić: *Bridge Fatigue Guidance – A European Research Project.* Article from www.sib.se, 2014-02-03

Aygül M. (2004): *Fatigue Strength of Welded Details in Steel Bridges with Orthotropic Plates* (Utmattningshållfasthet hos svetsade detaljer I stålbroar med ortotopa plattor, in Swedish). Master's thesis. Department of Structural Engineering, Chalmers University of Technology, Publication no.2004:10, Göteborg, Sweden, 2004.

Aygül M., Al-Emrani M. and Urushadze S. (2011): *Modelling and Fatigue Life Assessment of Orthotropic Bridge Deck Details Using FEM.* International journal of fatigue 40, 2012, pp. 129-142

Aygül, M. (2012). *Fatigue Analysis of Welded Structures Using the Finite Element Method.* Licentiate thesis, Department of Structural Engineering, Chalmers University of Technology, Göteborg, Sweden, 2012.

Berge, S. (1985): *On the effect of plate thickness in fatigue of welds*. Engineering Fracture Mechanics, Vol. 21, No. 2, 1985, pp. 423-435

Connor R. J. and Fisher J. W (2001): *Results of field measurement on the Wiliamsburg Bridge orthotropic deck, Final report on phase III.* ATLSS Reports. Paper 10 2001

Cullimore M. S. G. and Smith J. W (1981): *Local Stresses in Orthotropic Steel Bridge Decks Caused by Wheel Loads.* Journal of Constructional Steel Research, Vol. 1, No. 2, January 1981

De Jong F.B.P (2004): *Overview Fatigue Phenomenon in Orthotropic Bridge Decks in the Netherlands.* Orthotropic Bridge Conference, Sacramento, California, USA, August 2004. Article from www.ferroplan.com, 2014-02-03

Demirdjian, S. (1999); Stability of Castellated Beam Webs. Ms.S Thesis. Department of Civil Engineering and Applied Mechanics, McGill University, Montreal, Canada, 1999

Dowling N. E., Prasad K. S. and Narayanasamy, R. (2012). *Mechanical Behaviour of Materials: Engineering Methods for Deformation, Fracture, and Fatigue.* 4th ed., International ed. Harlow: Pearson Education

Eriksson K. (2009): *Fatigue of Steel Structures According to Eurocode 3* (Utmattning av stålkonstruktioner enligt Eurocode 3). Nyheter om Stålbyggnad nr 2, Sweden, 2009, pp 46-50

Famous Wonders (2011): *Akashi Kaikyō Bridge.* www.famouswonders.com. http://famouswonders.com/akashi-kaikyo-suspension-bridge/ (2014-04-01)

Fricke W. (2003): *Fatigue Analysis of Welded Joints: State of Development*, Marine Structures 16, 2003, pp. 185-200.

Frýba L. and Urushadze Sh. (2011): *Improvement of Fatigue Properties of Orthotropic Decks.* Engineering Structures 33, 2011, pp. 1166-1169

Gurney, T.R. (1968): *Fatigue of welded structures.* Cambridge University Press, Cambridge, UK, 1968

Harik, I., Shaaban, A., Gesund, H., Valli, G., and Wang, S. (1990): *United States Bridge Failures, 1951–1988.* Journal of Performance of Constructed Facilities, vol 4(4), 1990 pp. 272–277.

Heshmati M. (2012): *Fatigue Life Assessment of Bridge Details Using Finite Element Method.* Master's thesis. Department of Structural Engineering, Chalmers University of Technology, Publication no.2012:3, Göteborg, Sweden, 2012.

Hobbacher A. (2008): *Recommendations for fatigue design of welded joints and components.* IIW document IIW-1823-07, 2008

International Conference on Bridge Maintenance, Safety and Management, Biondini F. and Frangopol D. M. (2012 [2012]). *Bridge Maintenance, Safety, Management, Resilience and Sustainability: Proceedings of the Sixth International Conference on Bridge Maintenance, Safety and Management,* Stresa, Lake Maggiore, Italy, 8-12 July 2012, 638 pp.

Janss J. (1986) *Fatigue of Welds in Orthotropic Bridge Deck Panels with Trapezoidal Stiffeners.* Journal of Constructional Steel Research 9 (1988) CRIF, Liège, Belgium pp. 147-154

Kolstein M. H. (2004): *European Research Project on the Improvement of the Fatigue Resistance and Design of Steel Orthotropic Bridge Decks.* Orthotropic Bridge Conference, California, USA, 2004

Kolstein M. H. (2007): *Fatigue Classification of Welded Joints in Orthotropic Steel Bridge Decks.* Ph. D. Thesis. Department of Design and Construction, Delft University of Technology, the Netherlands 2007

Liao J. (2011): *Fatigue Damage in the Orthotropic Steel Deck with Respect to the Trough-to-Deck Plate Joint in between the Crossbeams.* Master's thesis. Department of Design and Construction, Delft University of Technology, the Netherlands, 2011

MacGregor C.W., Grossman N. (1952): *Effects of cyclic loading on mechanical behavior of 24S-T4 and 75S-T6 Aluminum alloys and SAE 4130 Steel.* National Advisory Committee for Aeronautics, Washington, US, 1952

Maddox S. J. (1991): *Fatigue Strength of Welded Structures.* Cambridge: Abington, UK. 1991

Maddox S. J. (2001): *Recommended Hot-Spot Stress Design S-N Curves for Fatigue Assessment of FPSOs.* International Society of Offshore and Polar Engineers, 2001, pp. 97-104

Maddox S. J. and Razmjoo G. R. (2001): *Interim Fatigue Design Recommendations for Fillet Welded Joins Under Complex Loading.* TWI Limited, Cambridge, UK. 2001

Maddox, S.J. (1991): *Fatigue strength of welded structures, 2nd edition*. Woodhead publishing Ltd, Abington, UK, 1991

Marquis G. and Samuelsson J. (2005): *Modelling and fatigue life assessment of complex structures*. Materialwissenschaft und Werkstofftechnik, 36(11):678–684, November 2005

Martinsson J. (2005). *Fatigue Assessment of Complex Welded Steel Structures*. Ph.D. Thesis, Stockholm, Royal Institute of Technology, 2005

Metallurgical Technologies Inc.: Corrosion Assisted Fatigue Cracking Of A 316l Stainless Steel Nozzle Sleeve From A Chemical Processing Vessel. *http://www.met-tech.com/* . (2014-03-28)

Pfeil M., Battista R. and Mergulhão A. (2005): *Stress Concentration in Steel Bridge Orthotropic Decks*. Journal of Constructional Steel Research, 61. 2005

Qian Z.H. and Abruzzese D.: *Fatigue Failure of Welded Connections at Orthotropic Bridges*. University of Rome, Italy

Radaj D., Sonsino C. M. and Fricke W. (2006): *Fatigue Assessment of Welded Joints by Local Approaches. 2nd ed.* Woodhead publishing limited, Cambridge, England, 2006

Radaj D., Sonsino C. M. and Fricke W. (2008): *Recent developments in local concepts of fatigue assessment of welded joints*. International Journal of Fatigue 31, 2009, pp 2-11.

Schijve J. (2009): *Fatigue of Structures and Materials*. Springer Science and Business media, B.V. Delft, The Netherlands, 2009

Schijve J. (2012): *Fatigue predictions of welded joints and the effective notch stress concept*. International Journal of Fatigue vol. 45, 2012, pp 31-38.

Sonsino C.M., Fricke W., de Bruyne F., Hoppe A., Ahmadi A., Zhang G. (2010): *Notch stress concepts for the fatigue assessment of welded joints – Background and applications*. International Journal of Fatigue vol. 34, 2012, pp 2-16.

Suresh, S. (1998): *Fatigue of materials*. 2nd ed. Cambridge: Cambridge Univ. Press, UK, 1998

Takeada N. and Papalambros P. (2012): *Optimization of Welded Structures with Hot Spot Stress Consistent Finite Element Meshing*. International Conference in Engineering Optimization, Rio de Janeiro, Brazil, 2012

Tinawi R. and Redwood R. G. (1976): *Orthotropic Bridge Decks with Closed Stiffeners – Analysis and Behaviour*. Computers & Structures, Vol. 7, Pergamon Press, Great Brittan 1977, pp. 683-699

Touran A. and Okereke A. (1991): *Performance of Orthotropic Bridge Decks*. Journal of Performance of Constructed Facilities, vol. 5 No. 2 1991

US Department of Transportation (2012): *Manual for Design, Construction, and Maintenance of Orthotropic Steel Deck Bridge*. US Department of Transportation, Federal Highway Administration, Publication no. FHWA-IF-12-027. USA February 2012.

Wheelabrator Corporation, Mishawaka, Ind (1946). *Shot Peening*. Mishawaka: Wheelabrator Corporation, Mishawaka, Ind 1946

Wolchuk R. and Ostapenko A. (1992): *Secondary Stresses on Closed Orthotropic Deck Ribs at Floor Beams.* Journal of Structural Engineering, Vol. 118, No. 2, February 1992, pp. 582-595

Xiao Z.-G., Yamada K., Ya S. and Zhao X.-L. (2007): *Stress Analyses and Fatigue Evaluation of Rib-to-Deck Joints in Steel Orthotropic Decks.* International Journal of Fatigue 30, 2008, pp 1387–1397.

Ya S., Yamada K. and Ishikawa T. (2011): *Fatigue Evaluation of Rib-to-Dekc Welded Joints of Orthotropic Steel Bridge Deck.* American Society of Civil Engineers, 2011

Yim W. T. (2007): *The Bridge Engineering 2 Conference Akashi Bridge.* Proceedings of Bridge Engineering 2 Conference, University of Bath, Bath, UK (2007)

Yuan, H. (2011): *Optimization of rib-to-deck welds for steel orthotropic bridge decks*. MSc thesis. Virginia Polytechnic Institute and State University. Blacksburg, VA, USA, 2011

Appendix

Appendix I

How to model the spring at the bascule in Brigade/Plus

The calculation of the spring stiffness is made using an unit force, P, placed above each main girder. No other loads are present. The deflection is measured at the intersection between main girder and floor beam flange. The spring stiffness is calculated with Hooke's law.

Comment about the load placement:

The location of the loads straight above the support (main girder) result in that (almost) the whole load is taken by the support directly below the respective load. Therefore the two loads can be placed simultaniously without disturbing interaction and the deflections are not affected by distortion or rotation of one side of the bridge which would have been the case if ony one side was loaded. On the other hand the total deflection will be slightly larger resulting in lower spring stiffness. The lower spring stiffness the more similar the behaviour is to cantilever action. In this investigation when the behaviour in vicinity of the ribs are of interest, this is on the safe side. Both methods are checked and the difference is less than 2.5%

P =   1000 N

	Deflection x:	k:	k*1e6 :	
Right girder:	-0,000221954	4505438,064	4,50543806	N/m
Left girder:	-0,000231139	4326400,997	4,326401	

1. Calculations of deflection with spring according to:
Interaction -> Special -> Spring

Left girder	Top	-0,0326862
	Bottom	-0,0327245
Right girder	Top	-0,0469292
	Bottom	-0,0469861

2.Calculations of deflection with spring according to:
Interaction -> Connector builder - (with beam)

Left girder	Top	-0,0336898
	Bottom	-0,0336511
Right girder	Top	-0,038471
	Bottom	-0,0383974

3. Calculations of deflection with spring according to:
Interaction -> Connector builder - (without beam)

Left girder	Top	-0,0327136
	Bottom	-0,0327245
Right girder	Top	-0,0469693
	Bottom	-0,0469861

Difference spring1 - spring2

		Spring1	Spring2	Diff (mm)
Left girder	Top	-0,0326862	-0,0336898	1,0036
	Bottom	-0,0327245	-0,0336511	0,9266
Right girder	Top	-0,0469292	-0,038471	-8,4582
	Bottom	-0,0469861	-0,0383974	-8,5887

Difference spring1 - spring3

Left girder	Top	-0,0326862	-0,0327136	0,027400
	Bottom	-0,0327245	-0,0327245	0,000000
Right girder	Top	-0,0469292	-0,0469693	0,040100
	Bottom	-0,0469861	-0,0469861	0,000000

Comments:

We choose to modell the nose with a spring accordingly to alternative 3. The spring is modelled in the interaction module, connector builder as an elastic spring with stiffness according to calculations above. The spring only acts in vertical direction.

Appendix II

Verification of the FE-model, by use of hand calculation.

Hand calculation of the main girder deflection according to EC. The result will be compared to the result from FE model to verify the model.
The deflection is calculated for one main girder with effective width of the bridge deck.

System:
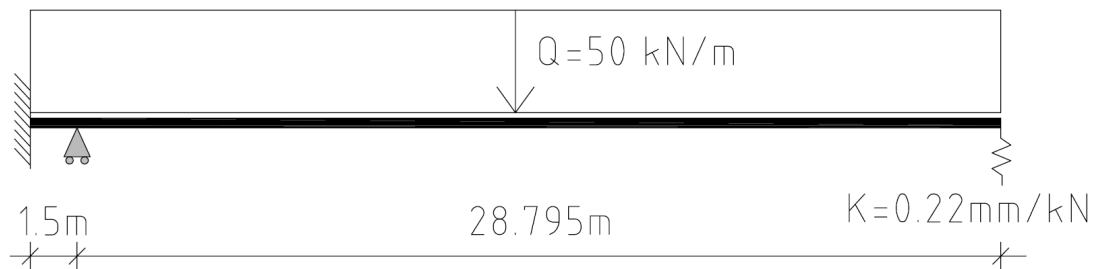
Stiffness distribution:
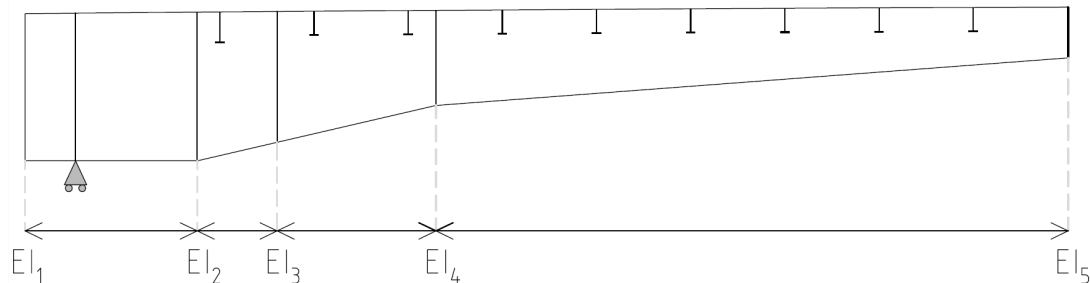
The regions are defined according to the figure above.
Section 1a is the start of the modeled main girder and also where the fixed support is located.
Section 1b is the location of the pinned support.
Section 2 is the start of the bridge deck.
Section 3 is the location of the change in web thickness for the main girder.
Section 4 is the location of the change in inclination for the main girders bottom flange.
Section 5 is the end section of the bridge, the nose opening where the modeled spring is located.

Effective width of bridge deck:

The bridge deck acts as a top flange for the main girders. The effective width of the top flange is calculated according to EN1993-1-5.3.2.1

Effective width of the bridge deck, according to EN1993-1-5.3.2.1:

$L_1 := 28.795 m$ Length of bridge from roller support to nose opening.

Effective length, L_e, is simplified for the whole bridge according to figure 3.1 in EC1993-1-5:3.2.1. This simplify the spring support as a pinned support.

$L_e := 0.85 \cdot L_1 = 24.476 \, m$

$b_{0.mid} := 3.85 m$ $b_{0.cant} := 2.5 m$

$t_{rib} := 6 mm$ $t_{dp} := 14 mm$

$A_{sl.i} := (2 \cdot 0.235m + 0.220m) \cdot t_{rib} = 4.14 \times 10^{-3} \, m^2$ Area of one rib

$n_{rib.mid} := 7$ $n_{rib.cant} := 4$

$A_{sl.mid} := n_{rib.mid} \cdot A_{sl.i} = 0.029 \, m^2$ $A_{sl.cant} := n_{rib.cant} \cdot A_{sl.i} = 0.017 \, m^2$

$$\alpha_{0.mid} := \sqrt{1 + \frac{A_{sl.mid}}{b_{0.mid} \cdot t_{dp}}} = 1.24 \qquad\qquad \alpha_{0.cant} := \sqrt{1 + \frac{A_{sl.cant}}{b_{0.cant} \cdot t_{dp}}} = 1.214$$

$$\kappa_{mid} := \frac{\alpha_{0.mid} \cdot b_{0.mid}}{L_e} = 0.195 \qquad\qquad \kappa_{cant} := \frac{\alpha_{0.cant} \cdot b_{0.cant}}{L_e} = 0.124$$

$$\beta_{mid} := \frac{1}{1 + 6.4 \cdot \kappa_{mid}^2} = 0.804 \qquad\qquad \beta_{cant} := \frac{1}{1 + 6.4 \cdot \kappa_{cant}^2} = 0.91$$

Effective width:

$$b_{eff.mid} := \beta_{mid} \cdot b_{0.mid} = 3.096\,m \qquad\qquad b_{eff.cant} := \beta_{cant} \cdot b_{0.cant} = 2.276\,m$$

==> 5,5 ribs   ==> 4 ribs

$$b_{eff} := b_{eff.mid} + b_{eff.cant} = 5.372\,m$$

$$n_{rib.tot} := 5 + 4 = 9$$

Number of ribs included in the total effective width of the top flange. In the mid-span the included width end in the 6th rib, but the area from this rib is disregarded.

Calculation of moment of inertia, I, for the main girder with effective part of the bridge deck as top flange:

I varies along bridges longitudinal direction due to variation of web thickness and height, and the effective width of the top flange. The variation of effective width of the top flange is disregarded.

The bridge is divided into 4 parts with different I. 6 sectional moment of inertia needs to be calculated and the parts will be appointed the mean value over their length.

$$E := 210\,GPa$$

$$t_{bf} := 40\,mm \qquad\qquad \text{Thickness bottom flange, main girder.}$$

$$b_{bf} := 750\,mm \qquad\qquad \text{Width bottom flange, main girder.}$$

$$A_{bf} := t_{bf} \cdot b_{bf} = 0.03\,m^2$$

$$t_{wI} := 25\,mm$$

$$t_{wII} := 20\,mm$$

$$t_{tf.I} := 40\,mm \qquad\qquad \text{Thickness top flange in sections without bridge deck.}$$

$$b_{tf.I} := 850\,mm$$

$h_{w1} := 4.417 \text{m}$

$h_{w2} := 4.417 \text{m}$

$h_{w3} := 3.882 \text{m}$

$h_{w4} := 2.817 \text{m}$

$h_{w5} := 1.497 \text{m}$

$A_{rib} := n_{rib.tot} \cdot A_{sl.i} = 0.037 \text{ m}^2$

$h_{rib} := 235 \text{mm}$

$b_{rib} := 220 \text{mm}$

$$z_{rib} := \frac{2 \cdot \left(t_{rib} \cdot \frac{h_{rib}^2}{2} \right) + b_{rib} \cdot t_{rib} \cdot h_{rib}}{t_{rib} \cdot \left(2 \cdot h_{rib} + b_{rib} \right)} = 0.155 \text{ m}$$

Neutral axis for rib itself, defined from top of rib.

$$I_{rib} := \frac{b_{rib} \cdot \left(2 \cdot h_{rib} \right)^3}{12} = 1.903 \times 10^{-3} \text{ m}^4$$

Section 1 - Main girder fixed end:

$A_1 := t_{tf.I} \cdot b_{tf.I} + t_{wI} \cdot h_{w1} + A_{bf} = 0.174 \text{ m}^2$

$$z_{tp1} := \frac{t_{tf.I} \cdot b_{tf.I} \left(t_{bf} + h_{w1} + \frac{t_{tf.I}}{2} \right) + t_{wI} \cdot h_{w1} \cdot \left(\frac{h_{w1}}{2} + t_{bf} \right) + b_{bf} \cdot \frac{t_{bf}^2}{2}}{A_1} = 2.3 \text{ m}$$

$$I_1 := \frac{b_{tf.I} \cdot t_{tf.I}^3}{12} + b_{tf.I} \cdot t_{tf.I} \cdot \left(z_{tp1} - \frac{t_{tf.I}}{2} - h_{w1} - t_{bf} \right)^2 + \frac{t_{wI} \cdot h_{w1}^3}{12} \dots \qquad = 0.497 \text{ m}^4$$
$$+ t_{wI} \cdot h_{w1} \cdot \left(z_{tp1} - \frac{h_{w1}}{2} - t_{bf} \right)^2 + \frac{b_{bf} \cdot t_{bf}^3}{12} + b_{bf} \cdot t_{bf} \cdot \left(z_{tp1} - \frac{t_{bf}}{2} \right)^2$$

Section 2 - Bridge deck starts:

$$A_2 := t_{dp} \cdot b_{eff} + A_{rib} + t_{wI} \cdot h_{w2} + A_{bf} = 0.253\,\text{m}^2$$

$$z_{tp2} := \frac{t_{dp} \cdot b_{eff} \cdot \left(t_{bf} + h_{w2} + \dfrac{t_{dp}}{2}\right) + A_{rib} \cdot \left(t_{bf} + h_{w2} - z_{rib}\right) + t_{wI} \cdot h_{w2} \cdot \left(\dfrac{h_{w2}}{2} + t_{bf}\right) + b_{bf} \cdot \dfrac{t_{bf}}{2}^2}{A_2}$$

$$z_{tp2} = 2.946\,\text{m}$$

$$I_2 := \frac{b_{eff} \cdot t_{dp}^3}{12} + b_{eff} \cdot t_{dp} \cdot \left[z_{tp2} - \left(t_{bf} + h_{w2} + \frac{t_{dp}}{2}\right)\right]^2 + I_{rib} \,\ldots \qquad = 0.734\,\text{m}^4$$

$$+ A_{rib} \cdot \left[z_{tp2} - \left(t_{bf} + h_{w2} - z_{rib}\right)\right]^2 + \frac{t_{wI} \cdot h_{w2}^3}{12} \,\ldots$$

$$+ t_{wI} \cdot h_{w2} \cdot \left[z_{tp2} - \left(t_{bf} + \frac{h_{w2}}{2}\right)\right]^2 + \frac{b_{bf} \cdot t_{bf}^3}{12} + b_{bf} \cdot t_{bf} \cdot \left(z_{tp2} - \frac{t_{bf}}{2}\right)^2$$

Section 3_left - Change of web thickness:

$$A_3 := t_{dp} \cdot b_{eff} + A_{rib} + t_{wI} \cdot h_{w3} + A_{bf} = 0.24\,\text{m}^2$$

$$z_{tp3} := \frac{t_{dp} \cdot b_{eff} \cdot \left(t_{bf} + h_{w3} + \dfrac{t_{dp}}{2}\right) + A_{rib} \cdot \left(t_{bf} + h_{w3} - z_{rib}\right) + t_{wI} \cdot h_{w3} \cdot \left(\dfrac{h_{w3}}{2} + t_{bf}\right) + b_{bf} \cdot \dfrac{t_{bf}}{2}^2}{A_3}$$

$$z_{tp3} = 2.625\,\text{m}$$

$$I_3 := \frac{b_{eff} \cdot t_{dp}^3}{12} + b_{eff} \cdot t_{dp} \cdot \left[z_{tp3} - \left(t_{bf} + h_{w3} + \frac{t_{dp}}{2}\right)\right]^2 \,\ldots \qquad = 0.544\,\text{m}^4$$

$$+ I_{rib} + A_{rib} \cdot \left[z_{tp3} - \left(t_{bf} + h_{w3} - z_{rib}\right)\right]^2 + \frac{t_{wI} \cdot h_{w3}^3}{12} \,\ldots$$

$$+ t_{wI} \cdot h_{w3} \cdot \left[z_{tp3} - \left(t_{bf} + \frac{h_{w3}}{2}\right)\right]^2 + \frac{b_{bf} \cdot t_{bf}^3}{12} + b_{bf} \cdot t_{bf} \cdot \left(z_{tp3} - \frac{t_{bf}}{2}\right)^2$$

Section 3_right - Change of web thickness:

$$A_{3R} := t_{dp} \cdot b_{eff} + A_{rib} + t_{wII} \cdot h_{w3} + A_{bf} = 0.22 \, m^2$$

$$z_{3R} := \frac{t_{dp} \cdot b_{eff} \cdot \left(t_{bf} + h_{w3} + \frac{t_{dp}}{2} \right) + A_{rib} \cdot \left(t_{bf} + h_{w3} - z_{rib} \right) + t_{wII} \cdot h_{w3} \cdot \left(\frac{h_{w3}}{2} + t_{bf} \right) + b_{bf} \cdot \frac{t_{bf}^2}{2}}{A_{3R}}$$

$$z_{3R} = 2.682 \, m$$

$$I_{3R} := \frac{b_{eff} \cdot t_{dp}^3}{12} + b_{eff} \cdot t_{dp} \cdot \left[z_{3R} - \left(t_{bf} + h_{w3} + \frac{t_{dp}}{2} \right) \right]^2 \dots \qquad\qquad = 0.511 \, m^4$$
$$+ I_{rib} + A_{rib} \cdot \left[z_{3R} - \left(t_{bf} + h_{w3} - z_{rib} \right) \right]^2 + \frac{t_{wII} \cdot h_{w3}^3}{12} \dots$$
$$+ t_{wII} \cdot h_{w3} \cdot \left[z_{3R} - \left(t_{bf} + \frac{h_{w3}}{2} \right) \right]^2 + \frac{b_{bf} \cdot t_{bf}^3}{12} + b_{bf} \cdot t_{bf} \cdot \left(z_{3R} - \frac{t_{bf}}{2} \right)^2$$

Section 4 - Change of inclination:

$$A_4 := t_{dp} \cdot b_{eff} + A_{rib} + t_{wII} \cdot h_{w4} + A_{bf} = 0.199 \, m^2$$

$$z_{tp4} := \frac{t_{dp} \cdot b_{eff} \cdot \left(t_{bf} + h_{w4} + \frac{t_{dp}}{2} \right) + A_{rib} \cdot \left(t_{bf} + h_{w4} - z_{rib} \right) + t_{wII} \cdot h_{w4} \cdot \left(\frac{h_{w4}}{2} + t_{bf} \right) + b_{bf} \cdot \frac{t_{bf}^2}{2}}{A_4}$$

$$z_{tp4} = 2.003 \, m$$

$$I_4 := \frac{b_{eff} \cdot t_{dp}^3}{12} + b_{eff} \cdot t_{dp} \cdot \left[z_{tp4} - \left(t_{bf} + h_{w4} + \frac{t_{dp}}{2} \right) \right]^2 \dots \qquad\qquad = 0.248 \, m^4$$
$$+ I_{rib} + A_{rib} \cdot \left[z_{tp4} - \left(t_{bf} + h_{w4} - z_{rib} \right) \right]^2 + \frac{t_{wII} \cdot h_{w4}^3}{12} \dots$$
$$+ t_{wII} \cdot h_{w4} \cdot \left[z_{tp4} - \left(t_{bf} + \frac{h_{w4}}{2} \right) \right]^2 + \frac{b_{bf} \cdot t_{bf}^3}{12} + b_{bf} \cdot t_{bf} \cdot \left(z_{tp4} - \frac{t_{bf}}{2} \right)^2$$

Section 5 - Spring support, end of bridge:

$$A_5 := t_{dp} \cdot b_{eff} + A_{rib} + t_{wII} \cdot h_{w5} + A_{bf} = 0.172 \, m^2$$

$$z_{tp5} := \frac{t_{dp} \cdot b_{eff} \cdot \left(t_{bf} + h_{w5} + \frac{t_{dp}}{2}\right) + A_{rib} \cdot \left(t_{bf} + h_{w5} - z_{rib}\right) + t_{wII} \cdot h_{w5} \cdot \left(\frac{h_{w5}}{2} + t_{bf}\right) + b_{bf} \cdot \frac{t_{bf}^2}{2}}{A_5}$$

$$z_{tp5} = 1.113 \, m$$

$$\begin{aligned} I_5 := & \frac{b_{eff} \cdot t_{dp}^3}{12} + b_{eff} \cdot t_{dp} \cdot \left[z_{tp5} - \left(t_{bf} + h_{w5} + \frac{t_{dp}}{2}\right)\right]^2 \dots && = 0.063 \, m^4 \\ & + I_{rib} + A_{rib} \cdot \left[z_{tp5} - \left(t_{bf} + h_{w5} - z_{rib}\right)\right]^2 + \frac{t_{wII} \cdot h_{w5}^3}{12} \dots \\ & + t_{wII} \cdot h_{w5} \cdot \left[z_{tp5} - \left(t_{bf} + \frac{h_{w5}}{2}\right)\right]^2 + \frac{b_{bf} \cdot t_{bf}^3}{12} + b_{bf} \cdot t_{bf} \cdot \left(z_{tp5} - \frac{t_{bf}}{2}\right)^2 \end{aligned}$$

Stiffness of the different sections:

$I_1 = 0.497 \, m^4$ $\qquad\qquad$ $EI_1 := E \cdot I_1 = 1.044 \times 10^{11} \cdot N \cdot m^2$

$I_2 = 0.734 \, m^4$ $\qquad\qquad$ $EI_2 := E \cdot I_2 = 1.541 \times 10^{11} \cdot N \cdot m^2$

$I_3 = 0.544 \, m^4$ $\qquad\qquad$ $EI_3 := E \cdot I_3 = 1.143 \times 10^{11} \cdot N \cdot m^2$

$I_{3R} = 0.511 \, m^4$ $\qquad\qquad$ $EI_{3R} := E \cdot I_{3R} = 1.073 \times 10^{11} \cdot N \cdot m^2$

$I_4 = 0.248 \, m^4$ $\qquad\qquad$ $EI_4 := E \cdot I_4 = 5.217 \times 10^{10} \cdot N \cdot m^2$

$I_5 = 0.063 \, m^4$ $\qquad\qquad$ $EI_5 := E \cdot I_5 = 1.326 \times 10^{10} \cdot N \cdot m^2$

Stiffness of the regions:

Part 1:
$$I_1 = 4.969 \times 10^{11} \cdot \text{mm}^4$$

$$EI_{11} := E \cdot I_1 = 1.044 \times 10^{11} \cdot \text{N} \cdot \text{m}^2$$

Part 2:
$$I_{22} := \frac{I_2 + I_3}{2} = 6.39 \times 10^{11} \cdot \text{mm}^4$$

$$EI_{22} := E \cdot \frac{I_2 + I_3}{2} = 1.342 \times 10^{11} \cdot \text{N} \cdot \text{m}^2$$

Part 3:
$$I_{33} := \frac{I_{3R} + I_4}{2} = 3.797 \times 10^{11} \cdot \text{mm}^4$$

$$EI_{33} := E \cdot \frac{I_{3R} + I_4}{2} = 7.974 \times 10^{10} \cdot \text{N} \cdot \text{m}^2$$

Part 4:
$$I_{44} := \frac{I_4 + I_5}{2} = 1.558 \times 10^{11} \cdot \text{mm}^4$$

$$EI_{44} := E \cdot \frac{I_4 + I_5}{2} = 3.272 \times 10^{10} \cdot \text{N} \cdot \text{m}^2$$

Deflection according to hand calculations:

The stiffness values calculated above is used in the Microsoft Excel macro *GO-Beam* resulting in a deflection of close to 42mm mm. This deflection corresponds to the line load 50kN/m.

$$\delta_{hand} := 41.66 \text{mm} \qquad \text{for} \qquad q_{line} := 50 \frac{kN}{m}$$

Deflection according to FE-model:

An analysis is made for the FE-model with the line load smeared as a pressure over the whole bridge-deck. The deflection is presented below.

$$b_{dp} := 7.7\text{m} + 2 \cdot 2.5\text{m} = 12.7\,\text{m} \qquad \text{Total width of the bridge deck.}$$

$$Q_{dp} := \frac{q_{line}}{\dfrac{b_{dp}}{2}} = 7.874 \cdot \frac{kN}{m^2} \qquad \text{Distributed load on the bridge deck. Half the load is taken by each main girder.}$$

$$\delta_{FEM} := 42.1\text{mm}$$

Comparissson of the deflection according to FEM and hand calculations:

$$error_{FE} := \frac{\left| \delta_{hand} - \delta_{FEM} \right|}{\delta_{hand}} = 1.056 \cdot \%$$

Engineer: Andrea Karlsson
Christoffer Wesley

Date: 09-May-14

Verification calculations of FE-model

Modulus of elasticity, E

Beam: 210000 MPa

Span №	3	4	5	6	5
Length, m	1,5	2,9	2,375	4,725	18,795
Moment of Inertia, m⁴	0,497	0,497	0,639	0,380	0,156

Support №	1	4	5	6	7	6
Support coordinate, m	0	1,5	4,4	6,775	11,5	30,295
Vertical spring constant, N/m	0		0	0	0	4505000
Support type or hinge		Roller	Roller	Roller	Roller	Roller

Positive loads: ↑ ↻	Load case:	DL			
Comment	Load	WA	WB	LA	LB
	Type	N or N/m	N/m	m	m
	Linear	-50000	-50000	0	30,295

Deflections, mm
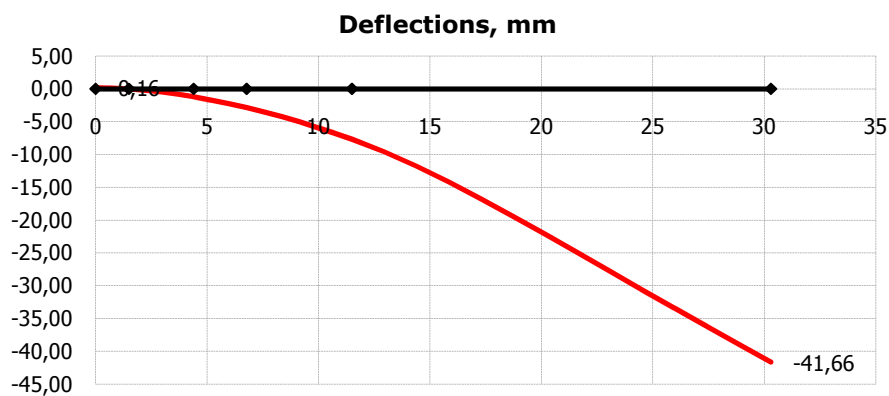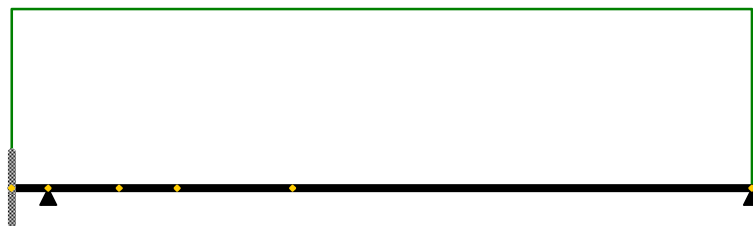
Appendix III

Influence of second axle and the two rear axles

Bridge seen from above with all 4 axle loads present. The first load axle is placed above floor beam 6.
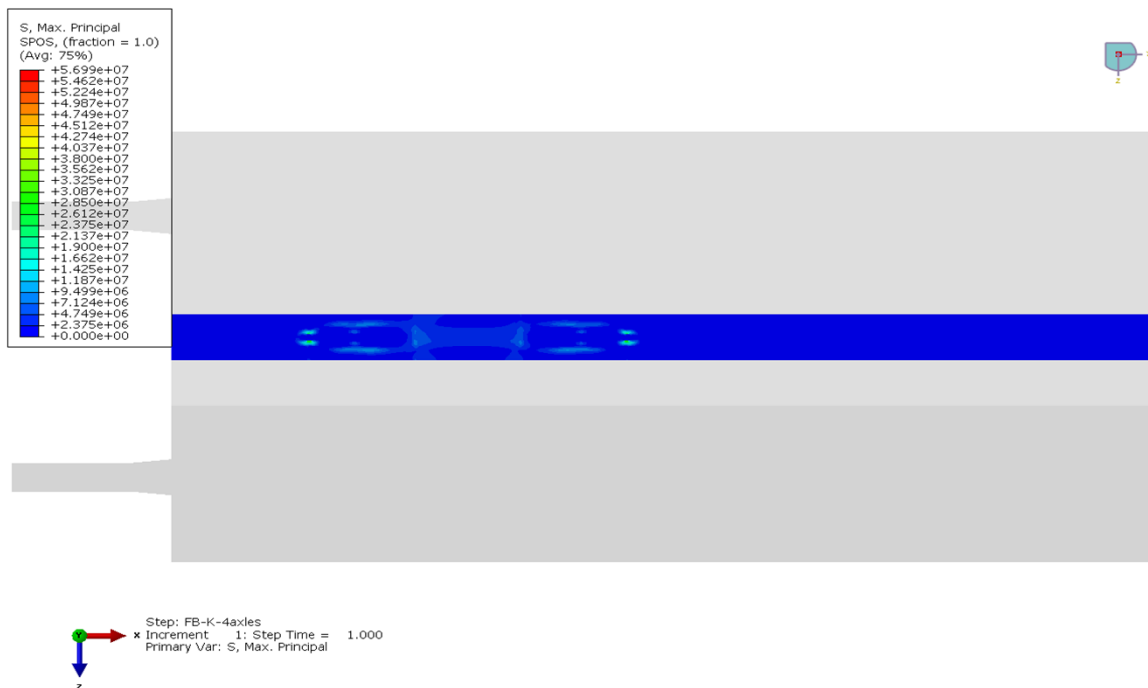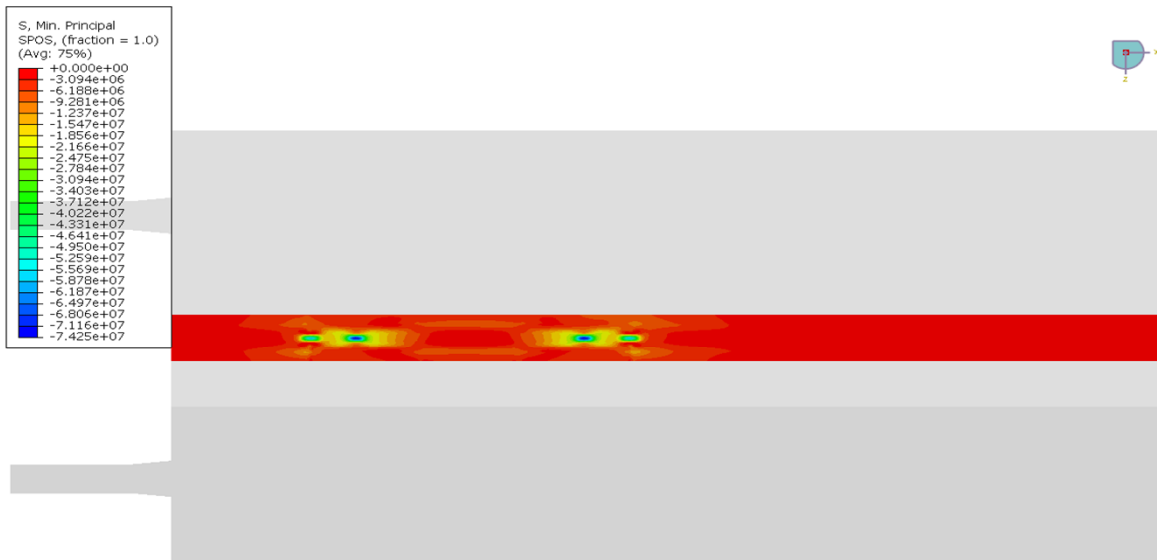
Bridge loaded with two axles

Minimum principla stress in the longitudinal direction

Longitudinal load distributions
Bridge loaded with two axles

Min principal stress [MPa]

FB 7   FB 6

Location at bridge
x defined from abutment

Maximum principla stress in the longitudinal direction

Longitudinal load distributions
Bridge loaded with two axles

Max principal stress [MPa]

FB 7   FB 6

Location at bridge
x defined from abutment
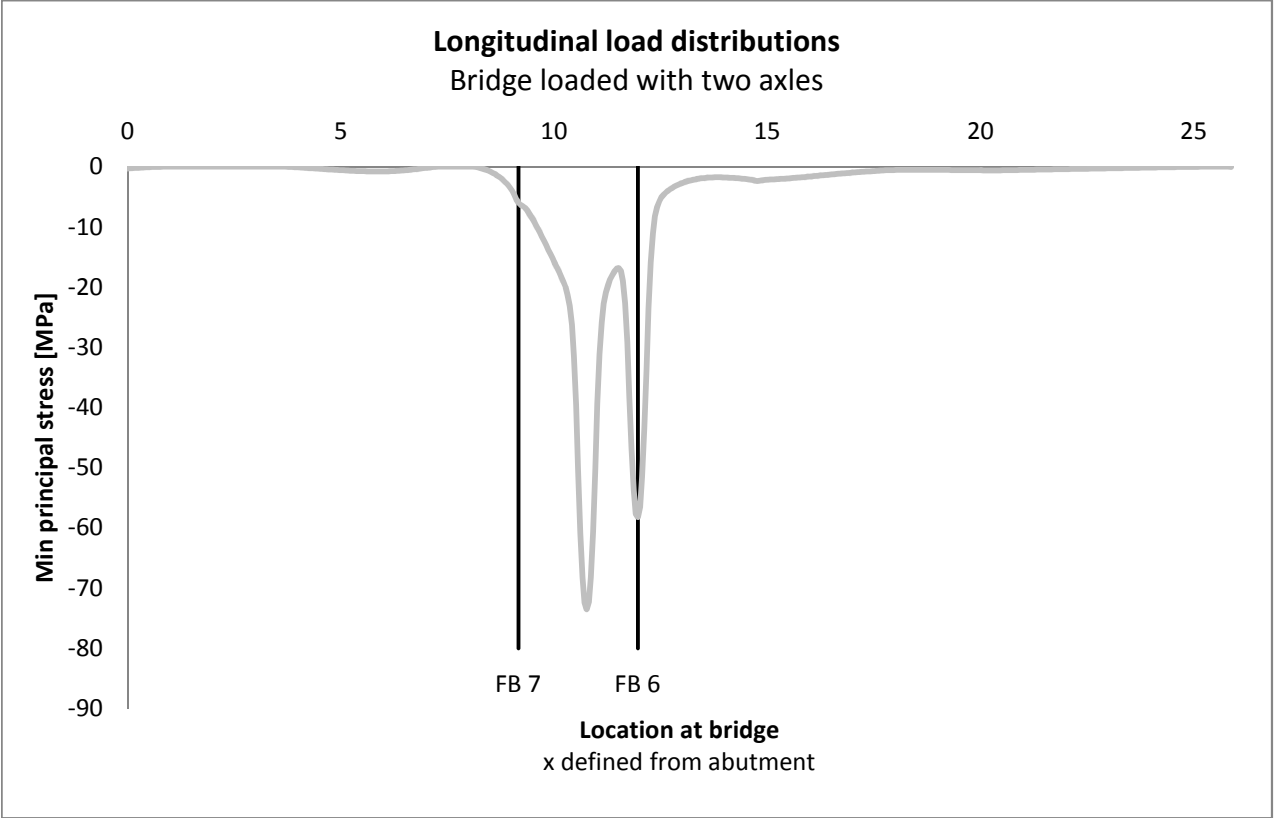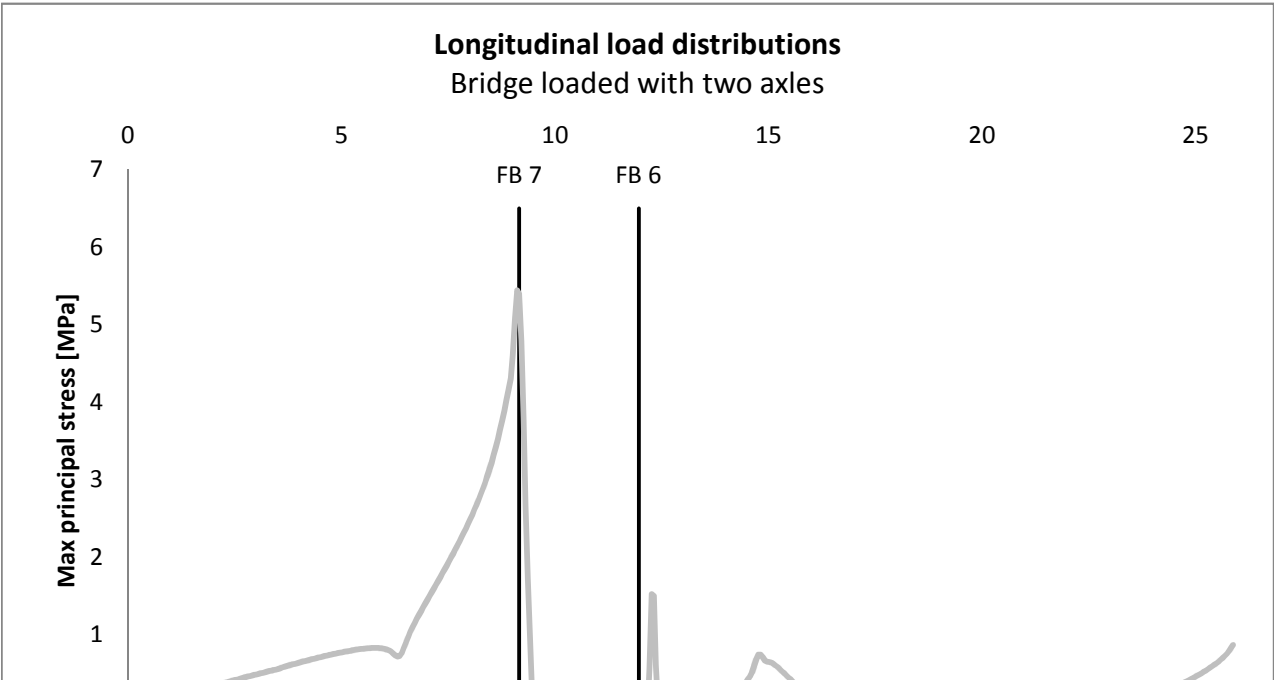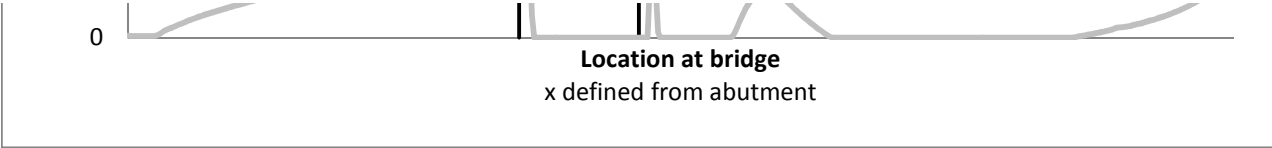
Bridge loaded with four axles

Minimum principla stress in the longitudinal direction

Longitudinal load distributions
Bridge loaded with fouraxles

FB 9   FB 8   FB 7   FB 6

Location at bridge
x defined from abutment

Maximum principla stress in the longitudinal direction

Longitudinal load distributions
Bridge loaded with fouraxles

FB 9   FB 8   FB 7   FB 6

Location at bridge
x defined from abutment
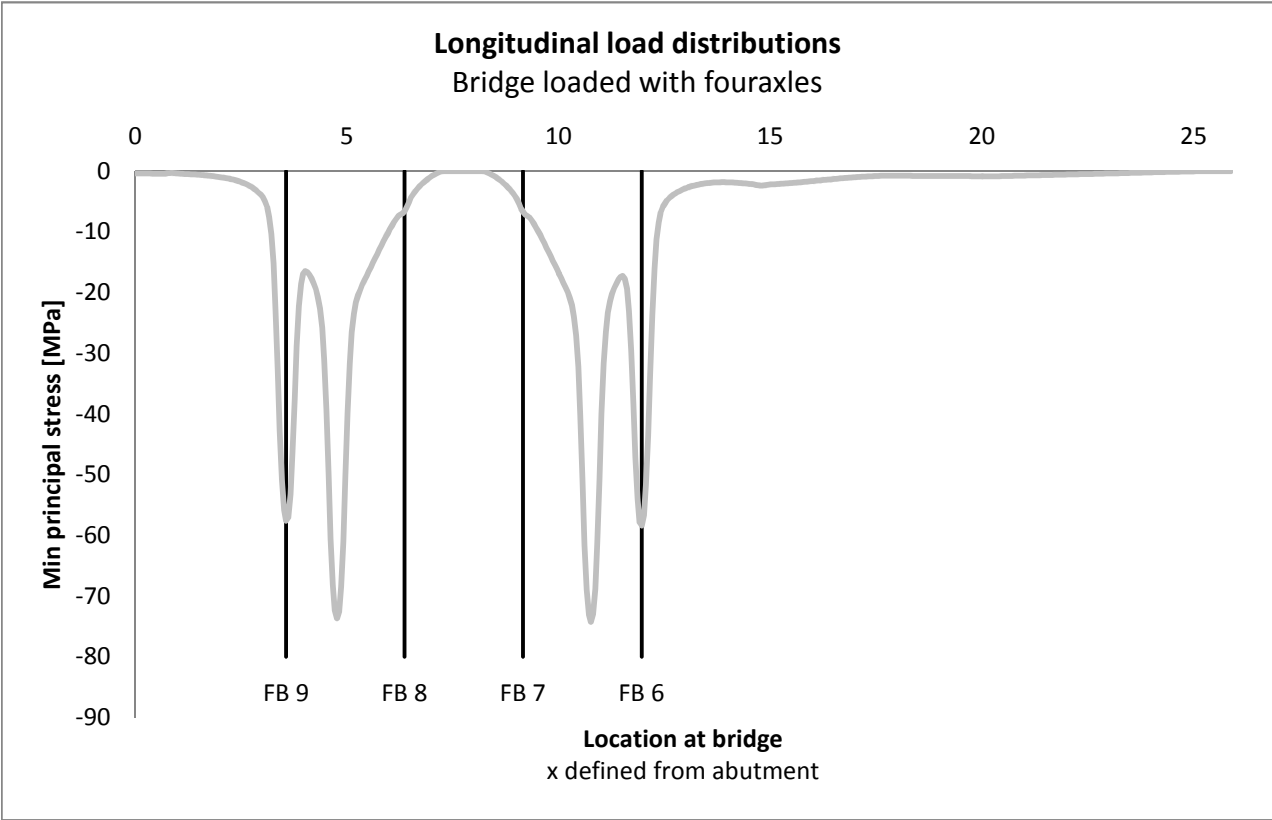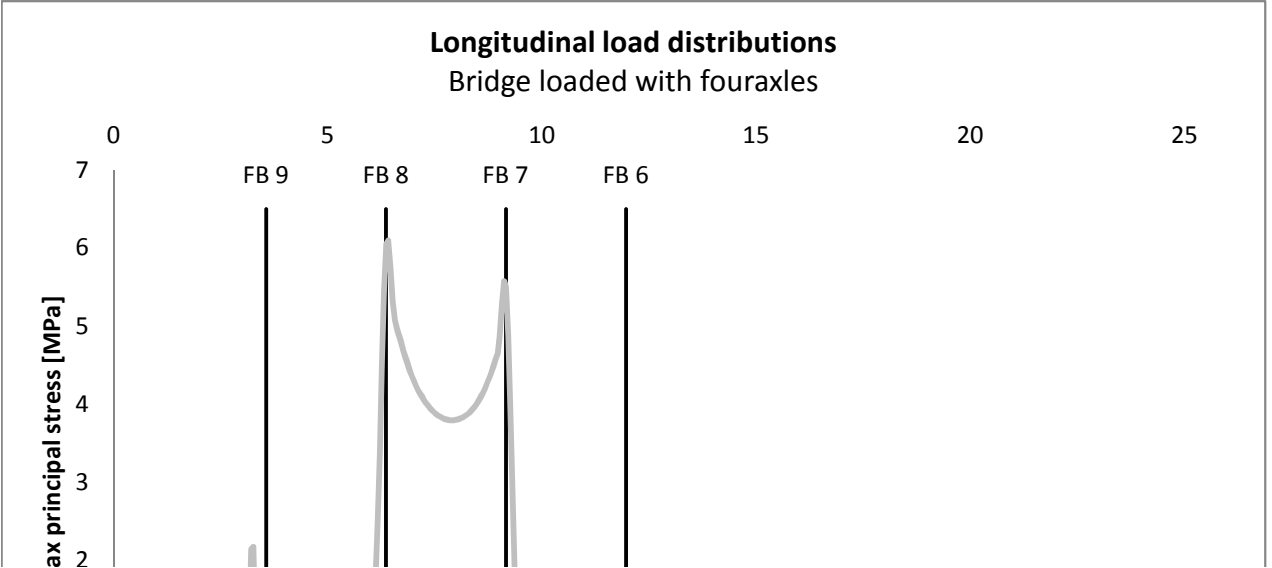
Stresses from Brigade/Plus

Bottom values are used

x	2 load axles		4 load axles		
	σ_p_max	σ_p_min	σ_p_max	σ_p_min	
0,00	24882	-285598	413440	-361688	
0,05	21385	-266853	432879	-365002	
0,10	20097	-244255	449339	-361684	
0,15	20273	-221091	468822	-361153	
0,20	20242	-197984	490016	-364804	
0,25	20151	-175329	511817	-371953	
0,31	20039	-153331	534602	-382341	
0,36	19946	-131957	557937	-394518	
0,41	19891	-111291	581502	-407205	
0,46	19818	-91362	605161	-419526	
0,51	19819	-72352	627340	-430087	
0,56	19871	-54272	648886	-440492	
0,61	20600	-37212	666304	-450554	
0,66	25283	-23805	660223	-442635	
0,71	36887	-15923	614260	-401497	
0,76	54497	-11924	544727	-344091	FB10
0,81	74228	-7907	483845	-300563	
0,86	91342	-2599	452099	-292685	
0,91	104060	0	448310	-319055	
0,96	114844	0	450912	-356794	
1,01	126021	0	444729	-389421	
1,06	137536	0	431256	-416172	
1,11	149073	0	413895	-439142	
1,16	160721	0	393119	-459000	
1,21	172408	0	370532	-477355	
1,26	184076	0	346828	-495032	
1,31	195642	0	322745	-512968	
1,36	207030	0	298736	-531674	
1,41	218183	0	275038	-551802	
1,46	229055	0	251748	-573667	
1,51	239626	0	228858	-597697	
1,56	249885	0	206228	-624089	
1,61	259839	0	183656	-653064	

1,66	269500	0	160853	-684722
1,71	278891	0	137476	-719149
1,76	288037	0	113155	-756376
1,81	296970	0	87500	-796444
1,86	305720	0	63815	-839402
1,91	314315	0	45551	-885347
1,96	322782	0	29296	-934425
2,01	331146	0	11462	-986874
2,06	339427	0	1049	-1042980
2,11	347640	0	0	-1103150
2,16	355798	0	0	-1167880
2,21	363910	0	0	-1237830
2,26	371980	0	0	-1313800
2,31	380010	0	0	-1396780
2,36	387998	0	0	-1487900
2,41	395938	0	0	-1588530
2,46	403827	0	0	-1700050
2,51	411656	0	0	-1824120
2,56	419419	0	0	-1962280
2,61	427112	0	0	-2116400
2,66	434728	0	0	-2288140
2,71	442263	0	0	-2479750
2,76	449713	0	0	-2693430
2,81	457078	0	0	-2932710
2,86	464356	0	0	-3202490
2,91	471547	0	0	-3511450
2,96	478655	0	0	-3877300
3,01	485681	0	0	-4334420
3,06	492634	0	44635	-4963180
3,11	499533	0	399320	-5916010
3,16	506385	0	1212600	-7520490
3,21	513269	0	2139870	-10327300
3,26	520208	0	2171520	-15178700
3,31	527298	0	889566	-22884300
3,36	534148	0	0	-32939100
3,41	540450	0	0	-42824700
3,46	546740	0	0	-50843000
3,51	554137	0	0	-55857000
3,56	562970	0	0	-57620900	FB 9
3,61	573100	0	0	-57054000
3,66	583358	0	0	-53225200
3,71	592304	-910	0	-46382300
3,76	600207	-10980	0	-37673600
3,81	607411	-30275	0	-28795200
3,86	614577	-50795	0	-22267600
3,91	621997	-71736	0	-18586900
3,96	629507	-93016	0	-16934600
4,01	637066	-114634	0	-16461300
4,06	644576	-136619	0	-16614700
4,11	652026	-158959	0	-17079100
4,16	659410	-181628	0	-17718700

4,21	666712	-204596	0	-18490800
4,26	673937	-227818	0	-19438000
4,31	681075	-251254	0	-20707400
4,36	688124	-274855	0	-22621100
4,41	695081	-298578	0	-25780300
4,46	701940	-322373	0	-31052100
4,51	708702	-346194	0	-39319800
4,56	715360	-369991	0	-50137300
4,61	721917	-393716	0	-60687600
4,66	728365	-417316	0	-68227900
4,71	734707	-440742	0	-72345000
4,76	740937	-463940	0	-73667500
4,81	747055	-486856	0	-72464400
4,86	753057	-509435	0	-68462300
4,91	758942	-531619	0	-61032700
4,96	764704	-553349	0	-50594200
5,01	770339	-574566	0	-39890500
5,06	775839	-595206	0	-31731400
5,11	781193	-615205	0	-26558800
5,16	786390	-634495	0	-23485700
5,21	791414	-653007	0	-21640800
5,26	796246	-670669	0	-20420000
5,31	800864	-687406	0	-19494000
5,36	805241	-703141	0	-18699100
5,41	809342	-717795	0	-17958600
5,46	813130	-731276	0	-17238100
5,51	816567	-743503	0	-16523000
5,56	819607	-754381	0	-15808300
5,61	822198	-763824	0	-15092700
5,66	824259	-771728	0	-14376800
5,71	825707	-778001	0	-13662700
5,76	826421	-782516	0	-12952400
5,81	826299	-785181	0	-12249000
5,86	825180	-785832	0	-11555400
5,91	822902	-784390	0	-10875400
5,96	819203	-780653	0	-10213000
6,01	813726	-774688	291058	-9573210
6,06	805744	-766259	962553	-8960010
6,11	794659	-755896	1724300	-8387710
6,16	778174	-743670	2480820	-7844050
6,21	754276	-729724	3381410	-7390700
6,26	728657	-712839	4463800	-7160570
6,31	714108	-693242	5459340	-6943920
6,36	723655	-672130	6051320	-6522730	FB8
6,41	765190	-646780	6097970	-5925320
6,46	829958	-618291	5753490	-5127140
6,51	902481	-585105	5319460	-4346130
6,56	972859	-547794	5074490	-3785890
6,61	1035800	-509644	4974610	-3322020
6,66	1093760	-470469	4874370	-2890800
6,71	1148850	-430259	4778330	-2506200

6,76	1201570	-388715	4684810	-2154860
6,81	1252760	-346284	4594560	-1834190
6,86	1302850	-303094	4509620	-1540180
6,91	1352180	-259539	4430660	-1269980
6,96	1400970	-215875	4358030	-1021460
7,01	1449440	-172456	4291260	-793183
7,06	1497720	-129569	4230190	-583864
7,11	1545970	-87538	4174280	-392785
7,16	1594270	-46660	4123230	-219017
7,21	1642730	-13275	4076700	-77027
7,26	1691420	0	4034360	-8757
7,31	1740420	0	3996020	0
7,36	1789770	0	3961410	0
7,41	1839520	0	3930390	0
7,46	1889720	0	3902780	0
7,51	1940410	0	3878480	0
7,56	1991640	0	3857360	0
7,61	2043440	0	3839340	0
7,66	2095870	0	3824350	0
7,71	2148990	0	3812310	0
7,76	2202870	0	3803190	0
7,81	2257600	0	3796940	0
7,86	2313270	0	3793520	0
7,91	2370010	0	3792940	0
7,96	2427970	0	3795180	0
8,01	2487320	0	3800280	0
8,06	2548250	0	3808270	0
8,11	2611000	-3963	3819250	0
8,16	2675830	-35459	3833290	0
8,21	2743030	-103815	3850560	-4035
8,26	2812940	-191597	3871210	-67010
8,31	2885940	-292429	3895490	-205950
8,36	2962440	-407150	3923630	-373672
8,41	3042900	-536871	3955950	-557774
8,46	3127890	-682504	3992810	-758759
8,51	3217860	-845338	4034540	-977558
8,56	3313610	-1026510	4081720	-1214920
8,61	3415490	-1227630	4134510	-1472110
8,66	3524270	-1450560	4193450	-1750570
8,71	3639910	-1697680	4258220	-2052390
8,76	3762240	-1972360	4328290	-2380460
8,81	3889570	-2278540	4401680	-2738540
8,86	4022480	-2619590	4478070	-3129400
8,91	4162380	-3007720	4558830	-3565710
8,96	4308400	-3430610	4640830	-4034750
9,01	4604810	-3949520	4865590	-4598380
9,06	5078680	-4679490	5269180	-5372300
9,11	5444360	-5420050	5576110	-6156720
9,16	5400270	-5966300	5494410	-6743720	FB7
9,21	4792800	-6351390	4875990	-7161560
9,26	3771320	-6546580	3862800	-7385330

9,31	2659950	-6766010	2768430	-7629470
9,36	1733490	-7213640	1856050	-8097570
9,41	957773	-7753470	1086690	-8655540
9,46	284372	-8323420	349583	-9241460
9,51	0	-8935890	0	-9867520
9,56	0	-9577010	0	-10519500
9,61	0	-10242800	0	-11193600
9,66	0	-10928200	0	-11884900
9,71	0	-11629200	0	-12589600
9,76	0	-12341600	0	-13303700
9,81	0	-13062700	0	-14024500
9,86	0	-13789600	0	-14749400
9,91	0	-14520200	0	-15476300
9,96	0	-15252300	0	-16203100
10,01	0	-15985500	0	-16929600
10,06	0	-16720500	0	-17656600
10,11	0	-17462800	0	-18389700
10,16	0	-18226700	0	-19143100
10,21	0	-19045900	0	-19950700
10,26	0	-19997300	0	-20889100
10,31	0	-21244700	0	-22121700
10,36	0	-23117800	0	-23977800
10,41	0	-26221100	0	-27061800
10,46	0	-31425200	0	-32245800
10,51	0	-39615700	0	-40416700
10,56	0	-50350000	0	-51132900
10,61	0	-60814600	0	-61582600
10,66	0	-68268200	0	-69022300
10,71	0	-72297100	0	-73035100
10,76	0	-73530200	0	-74249900
10,81	0	-72240000	0	-72940300
10,86	0	-68157900	0	-68837700
10,91	0	-60654700	0	-61312800
10,96	0	-50139200	0	-50776400
11,01	0	-39353400	0	-39971700
11,06	0	-31117400	0	-31718900
11,11	0	-25879000	0	-26465300
11,16	0	-22755000	0	-23326800
11,21	0	-20877400	0	-21434100
11,26	0	-19643500	0	-20184000
11,31	0	-18730000	0	-19253100
11,36	0	-17989500	0	-18494500
11,41	0	-17379300	0	-17865200
11,46	0	-16942500	0	-17408000
11,51	0	-16814400	0	-17257900
11,56	0	-17311800	0	-17731400
11,61	0	-18986900	0	-19381500
11,66	0	-22691500	0	-23061500
11,71	0	-29242100	0	-29589600
11,76	0	-38144400	0	-38472100
11,81	0	-46873100	0	-47181200

11,86	0	-53738700	0	-54023100	
11,91	0	-57590800	0	-57851200	
11,96	0	-58174400	0	-58415800	FB6
12,01	0	-56434200	0	-56661300	
12,06	0	-51437400	0	-51655400	
12,11	0	-43439300	0	-43650400	
12,16	0	-33580300	0	-33784700	
12,21	562840	-23549400	364264	-23746700	
12,26	1520690	-15867100	1121110	-16056000	
12,31	1494700	-11036100	1090160	-11215500	
12,36	603065	-8248890	333316	-8418030	
12,41	66220	-6661680	0	-6820760	
12,46	0	-5724840	0	-5874950	
12,51	0	-5110480	0	-5252900	
12,56	0	-4666710	0	-4802740	
12,61	0	-4313100	0	-4443800	
12,66	0	-4015270	0	-4141550	
12,71	0	-3755340	0	-3878030	
12,76	0	-3524450	0	-3644330	
12,81	0	-3317590	0	-3435430	
12,86	0	-3131160	0	-3247700	
12,91	0	-2962990	0	-3078880	
12,96	0	-2810960	0	-2926740	
13,01	0	-2673640	0	-2789670	
13,06	0	-2549500	0	-2665950	
13,11	0	-2437450	0	-2554260	
13,16	0	-2336350	0	-2453210	
13,21	0	-2245350	0	-2361750	
13,26	0	-2163620	0	-2278860	
13,31	0	-2090580	0	-2203830	
13,36	0	-2025670	0	-2136070	
13,41	0	-1968520	0	-2075220	
13,46	0	-1918780	0	-2021030	
13,51	0	-1876200	0	-1973420	
13,56	0	-1840550	0	-1932350	
13,61	0	-1811590	0	-1897820	
13,66	0	-1789080	0	-1869820	
13,71	0	-1772740	0	-1848270	
13,76	0	-1762270	0	-1832980	
13,81	0	-1757310	0	-1823720	
13,86	0	-1757460	0	-1820100	
13,91	0	-1762330	0	-1821710	
13,96	0	-1771460	0	-1828070	
14,01	0	-1784430	0	-1838700	
14,06	0	-1800790	0	-1853080	
14,11	0	-1820130	0	-1870740	
14,16	18306	-1841980	0	-1891160	
14,21	68618	-1866090	0	-1914000	
14,26	132548	-1892050	0	-1938840	
14,31	195943	-1919870	0	-1965580	
14,36	257966	-1949440	0	-1994050	

14,41	317070	-1981370	0	-2024760	
14,46	371222	-2015440	0	-2057380	
14,51	419532	-2054430	0	-2094490	
14,56	457521	-2095080	220	-2133050	
14,61	509921	-2148450	31548	-2183650	
14,66	595307	-2235000	107695	-2264080	
14,71	683957	-2317540	190213	-2339970	
14,76	739029	-2356060	242560	-2375610	FB5
14,81	741996	-2348150	248791	-2368360	
14,86	705373	-2291830	219004	-2316600	
14,91	663384	-2225300	183347	-2254410	
14,96	648459	-2187160	171334	-2217290	
15,01	647019	-2161050	171061	-2191360	
15,06	636692	-2136400	162674	-2166690	
15,11	620828	-2115100	149143	-2144910	
15,16	600546	-2094180	131458	-2123260	
15,21	577363	-2073350	111021	-2101510	
15,26	552584	-2051730	89016	-2078880	
15,31	526840	-2029130	66055	-2055200	
15,36	500630	-2005300	42614	-2030290	
15,41	474180	-1980310	19051	-2004180	
15,46	447708	-1954140	3655	-1976910	
15,51	421333	-1926920	0	-1948580	
15,56	395162	-1898710	0	-1919260	
15,61	369280	-1869610	0	-1889070	
15,66	343740	-1839700	0	-1858070	
15,71	318604	-1809070	0	-1826370	
15,76	293896	-1777790	0	-1794020	
15,81	269656	-1745950	0	-1761140	
15,86	245893	-1713610	0	-1727780	
15,91	222628	-1680850	0	-1694020	
15,96	199861	-1647740	0	-1659940	
16,01	177602	-1614330	0	-1625600	
16,06	155846	-1580700	0	-1591070	
16,11	134597	-1546910	0	-1556420	
16,16	113849	-1513010	0	-1521710	
16,21	93599	-1479060	0	-1487010	
16,26	73840	-1445110	0	-1452370	
16,31	54561	-1411220	0	-1417860	
16,36	35756	-1377440	0	-1383530	
16,41	17409	-1343810	0	-1349450	
16,46	4185	-1310380	0	-1315670	
16,51	0	-1277190	0	-1282250	
16,56	0	-1244300	0	-1249250	
16,61	0	-1211730	0	-1216740	
16,66	0	-1179520	0	-1184770	
16,71	0	-1147730	0	-1153430	
16,76	0	-1116380	0	-1122770	
16,81	0	-1085510	0	-1092900	
16,86	0	-1055160	0	-1063880	
16,91	0	-1025370	0	-1035840	

16,96	0	-996169	0	-1008870	
17,01	0	-967583	0	-983105	
17,06	0	-939609	0	-958658	
17,11	0	-912236	0	-935638	
17,16	0	-885386	0	-914150	
17,21	0	-858923	0	-894132	
17,26	0	-832746	0	-875716	
17,31	0	-807019	0	-858713	
17,36	0	-782258	0	-844009	
17,41	0	-760070	0	-833174	
17,46	0	-737885	0	-820268	
17,51	0	-711222	0	-800463	
17,56	0	-680924	0	-776447	FB4
17,61	0	-650693	0	-753860	
17,66	0	-625096	0	-740522	
17,71	0	-606319	0	-737703	
17,76	0	-593087	0	-740553	
17,81	0	-581657	0	-744644	
17,86	0	-570590	0	-747994	
17,91	0	-560195	0	-750679	
17,96	0	-550164	0	-752957	
18,01	0	-540851	0	-755040	
18,06	0	-532381	0	-757148	
18,11	0	-524924	0	-759272	
18,16	0	-518542	0	-761437	
18,21	0	-513285	0	-763623	
18,26	0	-509119	0	-765810	
18,31	0	-506011	0	-767994	
18,36	0	-503865	0	-770158	
18,41	0	-502599	0	-772305	
18,46	0	-502096	0	-774425	
18,51	0	-502258	0	-776521	
18,56	0	-502982	0	-778592	
18,61	0	-504180	0	-780640	
18,66	0	-505773	0	-782663	
18,71	0	-507693	0	-784663	
18,76	0	-509882	0	-786637	
18,81	0	-512296	0	-788586	
18,86	0	-514894	0	-790510	
18,91	0	-517647	0	-792410	
18,96	0	-520531	0	-794288	
19,01	0	-523524	0	-796144	
19,06	0	-526611	0	-797982	
19,11	0	-529777	0	-799802	
19,16	0	-533012	0	-801605	
19,21	0	-536308	0	-803394	
19,26	0	-539655	0	-805169	
19,31	0	-543050	0	-806933	
19,36	0	-546489	0	-808689	
19,41	0	-549969	0	-810440	
19,46	0	-553490	0	-812188	

19,51	0	-557050	0	-813936
19,56	0	-560648	0	-815688
19,61	0	-564285	0	-817445
19,66	0	-567961	0	-819210
19,71	0	-571678	0	-820986
19,76	0	-575439	0	-822777
19,81	0	-579248	0	-824587
19,86	0	-583109	0	-826419
19,91	0	-587002	0	-828245
19,96	0	-590917	0	-830040
20,01	0	-594674	0	-831571
20,06	0	-598179	0	-832664
20,11	0	-601112	0	-832957
20,16	0	-603298	0	-831963
20,21	0	-607694	0	-833957
20,26	0	-614126	0	-840300
20,31	0	-618539	0	-846025
20,36	0	-617474	0	-845465	FB3
20,41	0	-609612	0	-835867
20,46	0	-598161	0	-821060
20,51	0	-587193	0	-806689
20,56	0	-580021	0	-797633
20,61	0	-575023	0	-791551
20,66	0	-569230	0	-784228
20,71	0	-562968	0	-776220
20,76	0	-556412	0	-767757
20,81	0	-549695	0	-759032
20,86	0	-542973	0	-750266
20,91	0	-536261	0	-741483
20,96	0	-529593	0	-732733
21,01	0	-522960	0	-724008
21,06	0	-516363	0	-715311
21,11	0	-509798	0	-706642
21,16	0	-503261	0	-697997
21,21	0	-496752	0	-689377
21,26	0	-490266	0	-680778
21,31	0	-483802	0	-672201
21,36	0	-477358	0	-663642
21,41	0	-470932	0	-655100
21,46	0	-464522	0	-646574
21,51	0	-458126	0	-638062
21,56	0	-451742	0	-629562
21,61	0	-445370	0	-621074
21,66	0	-439007	0	-612595
21,71	0	-432652	0	-604126
21,76	0	-426305	362	-595664
21,81	0	-419964	3169	-587209
21,86	0	-413628	8165	-578760
21,91	0	-407297	13292	-570317
21,96	0	-400969	18468	-561878
22,01	0	-394644	23694	-553444

22,06	0	-388321	28969	-545012
22,11	1127	-381999	34295	-536584
22,16	4785	-375679	39672	-528158
22,21	9864	-369360	45100	-519734
22,26	14974	-363040	50578	-511312
22,31	20117	-356720	56110	-502890
22,36	25290	-350399	61693	-494468
22,41	30496	-344076	67329	-486044
22,46	35732	-337748	73015	-477617
22,51	40999	-331417	78754	-469184
22,56	46294	-325077	84540	-460740
22,61	51621	-318728	90379	-452284
22,66	56977	-312365	96269	-443806
22,71	62382	-305975	102236	-435286
22,76	67846	-299542	108298	-426697
22,81	73447	-292975	114558	-417912
22,86	79188	-286188	121029	-408806
22,91	85302	-279082	128040	-399254
22,96	91587	-271302	135301	-388760
23,01	98721	-264867	143814	-380287
23,06	108738	-261361	156471	-376031
23,11	119052	-258839	169386	-372947
23,16	126543	-254402	178024	-366739	FB2
23,21	131515	-246611	182928	-355354
23,26	133449	-236570	183500	-340633
23,31	135152	-226612	183987	-326240
23,36	139637	-219387	188694	-316015
23,41	145193	-213673	194955	-308042
23,46	150983	-207355	201526	-299202
23,51	157201	-200780	208709	-289996
23,56	163627	-193983	216184	-280463
23,61	170267	-187059	223960	-270739
23,66	177068	-180109	231964	-260969
23,71	184039	-173155	240204	-251185
23,76	191165	-166230	248661	-241437
23,81	198465	-159342	257361	-231735
23,86	205940	-152499	266304	-222095
23,90	213610	-145711	275517	-212527
23,95	221479	-138981	285007	-203038
24,00	229564	-132317	294795	-193639
24,05	237873	-125722	304893	-184335
24,10	246421	-119203	315319	-175134
24,15	255217	-112764	326088	-166044
24,20	264274	-106411	337218	-157070
24,25	273604	-100148	348722	-148220
24,30	283219	-93980	360619	-139500
24,35	293131	-87909	372924	-130912
24,40	303353	-81948	385656	-122475
24,45	313902	-76114	398837	-114216
24,50	324778	-70407	412467	-106134
24,55	335982	-64833	426543	-98240

24,60	347535	-59390	441095	-90527
24,65	359450	-54071	456145	-82981
24,70	371755	-48893	471730	-75625
24,75	384476	-43861	487894	-68471
24,79	397599	-38970	504609	-61508
24,84	411121	-34224	521868	-54743
24,89	425069	-29639	539710	-48199
24,94	439448	-25227	558144	-41893
24,99	454273	-20989	577187	-35828
25,04	469550	-16933	596848	-30012
25,09	485293	-13061	617148	-24449
25,14	501509	-9383	638095	-19152
25,19	518213	-5903	659709	-14127
25,24	535417	-2634	682005	-9391
25,29	553139	-531	705007	-4960
25,34	571408	0	728755	-1407
25,39	590257	0	753288	0
25,44	609767	0	778714	0
25,49	630023	0	805141	0
25,54	651223	0	832828	0
25,59	673629	0	862114	0
25,64	697657	0	893541	0
25,68	724193	0	928269	0
25,69	724228	0	928314	-1
25,73	753899	-425	967173	-982
25,78	788187	-4770	1012100	-7221
25,83	825958	-10816	1061650	-15001
25,88	865232	-18171	1113220	-23920

Positions of floor beams

Floor beam	x		
FB 10	0,76	0	0
FB 10	0,76	-80000000	6500000
FB 9	3,56	0	0
FB 9	3,56	-80000000	6500000
FB 8	6,36	0	0
FB 8	6,36	-80000000	6500000
FB 7	9,16	0	0
FB 7	9,16	-80000000	6500000
FB 6	11,96	0	0
FB 6	11,96	-80000000	6500000
FB 5	14,76	0	0
FB 5	14,76	-80000000	6500000
FB 4	17,56	0	0
FB 4	17,56	-80000000	6500000
FB 3	20,36	0	0
FB 3	20,36	-80000000	6500000
FB 2	23,16	0	0

FB 2	23,16	-80000000	6500000
FB 1	25,96	0	0
FB 1	25,96	-80000000	6500000

Appendix IV

Determination of most adverse load position for cracks

1. Local transverse load location

Area loads placed at four location in relation to the rib, (A, B, C, D). They are placed directly above the floor beam and in mid span. Total of 8 area load locations. One axis with two wheels are applied as the load, the distance between the centreline of the wheels is 2 m.
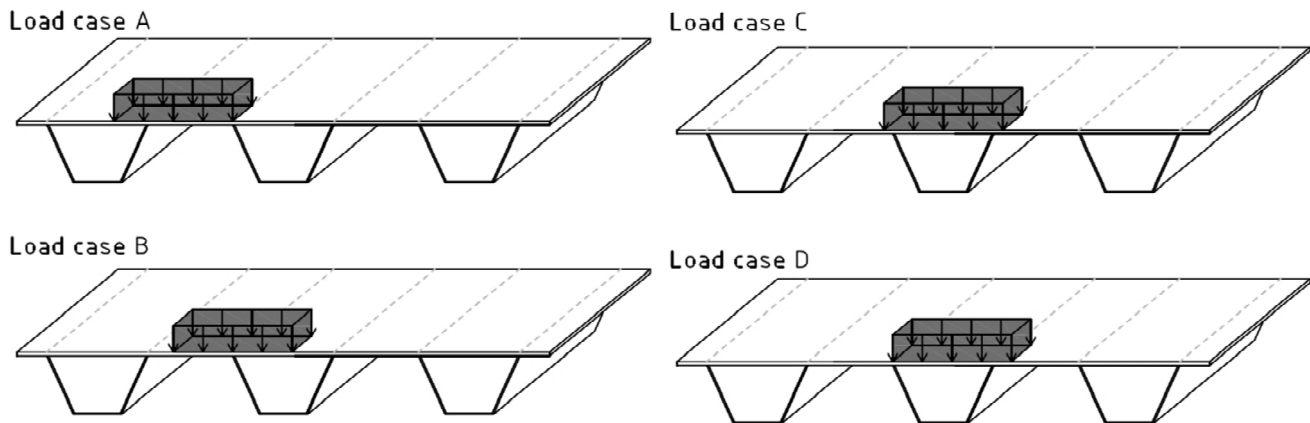
The ribs in the figure is Rib 6, 7 and 8 counted from the right.

C is the location most common used in simplified calculations. The results from this position will be compared to the moste adverse result to see the difference if more localised effects are considered. Load case A and D are simillar except that load A is directed towards the free span between the ribs and load D towards the closed span inside the rib walls.

From the load positions shown above it is possibe to extrapolate the response for rib wall 7.1 or 7.2 to get a full influence line, this will be done as following:

Extrapolated values			
7.1		7.2	
A		A	
B		B	
C		C	
D		D	
E	= B(7.2)	E	= B(7.1)
F	= A(7.2)	F	= A(7.1)

Where E approximately represent the load respone for rib wall 7.2 as i would have been if the load was placed as the position A in relation to 7.1

Stresses in the analysis:

The stresses are hot spot stresses and calculated from the principal stresses. Only the principal stresses which have an angle of 60 degrees or less from the perpendicular direction of the qweld are included. These values are marked with blue and if the angle of the principla stress excceds 60 degrees tha values are marked with red and disregarded.

Hot spot stress:

The stresses are calculated as hot spot stresses from the equation below. The included stress values are taken as nodal values at the given distancens which is ensured with the use of partitions at these locations.

$$\sigma_{hs} = 1.67 \cdot \sigma_{0.4 \cdot t} - 0.67 \cdot \sigma_{1.0 \cdot t}$$

Only the toe crack are investigated since root cracks can not be evaluated by hot-spot stress method. Because of the many stress singularities neither nominal stress can be used to analyze the root cracks.

Rib-DP Crack I

Toe crack propagating in the deck plate. Hot spot stresses in the deck plate are extracted from the FE-analysis with principal stresses from nodal values. First is the load responce checked in rib 7.1 (wall toward the left main girder), then the load responce is checked for rib 7.2 (wall toward the middle of the bridge). For this crack all loads are placed in the span. When the loads are placed above floor beam no effect is shown in a visual check and this is not investigated further.
For cack I in the deck plate the bottom values are the ones to be used since theses are the values at the lower side of the deck plate, at the weld. The top values are checked to investigate the amount of membran stresses in the deck.

Crack I - Load response in deck plate above rib wall 7.1:

	Bottom		Top		Final			Without σ_mem	
							Load placed in at A (span, 7.1):		
x (m)	σ_p_max	σ_p_min	σ_p_max	σ_p_min	Bottom	Top	σ_mem	Bottom	Top
0,006	0	-4,52	0	-6,11	0,0	0,0	0	0,0	0,0
0,014	0	-4,5	0	-6,02					
	σ_hs_max	σ_hs_min	σ_hs_max	σ_hs_min					
	0,0	-4,5	0,0	-6,2					

	Bottom		Top		Final			Without σ_mem	
				Load placed at B (span, 7.1):					
x (m)	σ_p_max	σ_p_min	σ_p_max	σ_p_min	Bottom	Top	σ_mem	Bottom	Top
0,006	0	-24,8	20,02	-2,88	-25,4	20,7	-2,3532	-23,0	23,0
0,014	0	-23,9	19,01	-2,74					
	σ_hs_max	σ_hs_min	σ_hs_max	σ_hs_min					
	0,0	-25,4	20,7	-3,0					

	Bottom		Top		Final			Without σ_mem	
				Load placed in at C (span, 7.1):					
x (m)	σ_p_max	σ_p_min	σ_p_max	σ_p_min	Bottom	Top	σ_mem	Bottom	Top
0,006	0	-25,45	22,09	-6,66	-28,5	25,3	-1,6164	-26,9	26,9
0,014	0	-20,89	17,34	-7,45					
	σ_hs_max	σ_hs_min	σ_hs_max	σ_hs_min					
	0,0	-28,5	25,3	-6,1					

	Bottom		Top		Final			Without σ_mem	
				Load placed in at D (span, 7.1):					
x (m)	σ_p_max	σ_p_min	σ_p_max	σ_p_min	Bottom	Top	σ_mem	Bottom	Top
0,006	0	-31,26	28,16	-6,42	-36,5	33,6	-1,4763	-35,1	35,1
0,014	0	-23,37	20,05	-8,15					
	σ_hs_max	σ_hs_min	σ_hs_max	σ_hs_min					
	0,0	-36,5	33,6	-5,3					

Crack I - Load response in deck plate above rib wall 7.2:

Load placed in at A (span, 7.2):

x (m)	Bottom σ_p_max	Bottom σ_p_min	Top σ_p_max	Top σ_p_min	Final Bottom	Final Top	σ_mem	Without σ_mem Bottom	Without σ_mem Top
0,006	0	-28,5	23,02	-4,61	-35,2	29,8	-2,7166	-32,5	32,5
0,014	0	-18,47	12,92	-7,96					
	σ_hs_max	σ_hs_min	σ_hs_max	σ_hs_min					
	0,0	-35,2	29,8	-2,4					

Load placed at B (span, 7.2):

x (m)	Bottom σ_p_max	Bottom σ_p_min	Top σ_p_max	Top σ_p_min	Final Bottom	Final Top	σ_mem	Without σ_mem Bottom	Without σ_mem Top
0,006	0	-36,57	33,24	-5,57	-43,5	40,3	-1,6014	-41,9	41,9
0,014	0	-26,24	22,72	-8,46					
	σ_hs_max	σ_hs_min	σ_hs_max	σ_hs_min					
	0,0	*-43,5*	40,3	-3,6					

Load placed in at C (span, 7.2):

x (m)	Bottom σ_p_max	Bottom σ_p_min	Top σ_p_max	Top σ_p_min	Final Bottom	Final Top	σ_mem	Without σ_mem Bottom	Without σ_mem Top
0,006	0	-24,58	21,5	-6,78	-27,6	24,7	-1,4763	-26,1	26,1
0,014	0	-20,06	16,79	-7,55					
	σ_hs_max	σ_hs_min	σ_hs_max	σ_hs_min					
	0,0	-27,6	24,7	-6,3					

Load placed in at D (span, 7.2):

x (m)	Bottom σ_p_max	Bottom σ_p_min	Top σ_p_max	Top σ_p_min	Final Bottom	Final Top	σ_mem	Without σ_mem Bottom	Without σ_mem Top
0,006	0	-27,02	23,63	-4,32	-27,7	24,4	-1,6481	-26,1	26,1
0,014	0	-25,96	22,43	-4,04					
	σ_hs_max	σ_hs_min	σ_hs_max	σ_hs_min					
	0,0	-27,7	24,4	-4,5					

Crack I - Summary of results

x	Rib 7.1				Rib 7.2			
	Stresses		*Membrane*		*Stresses*		*Menbrane*	
	Bottom	**Top**	**Stress**	**Without**	**Bottom**	**Top**	**Stress**	**Without**
A	0,0	0,0	0,0	0,0	-35,2	29,8	-2,7	-32,5
B	-25,4	20,7	-2,4	-23,0	*-43,5*	40,3	-1,6	-41,9
C	-28,5	25,3	-1,6	-26,9	-27,6	24,7	-1,5	-26,1
D	-36,5	33,6	-1,5	-35,1	-27,7	24,4	-1,6	-26,1
Delta	36,5				*43,5*			

Comparison between resposne in B and C for deck plate above rib wall 7.2:

x	Bottom stresses
B	-43,5
C	-27,6
Diff:	*58%*

Extrapolated values for the deck plate above rib wall 7.2

x	Bottom stresses
A	-35,2
B	-43,5
C	-27,6
D	-27,7
E	-25,4
F	0,0

Crack I
Bottom values for stresses in deck plate for transversal positions

Crack I
Influence line for deck plate above rib wall 7.2

Crack I
Effect of membrane stresses above rib wall 7.2
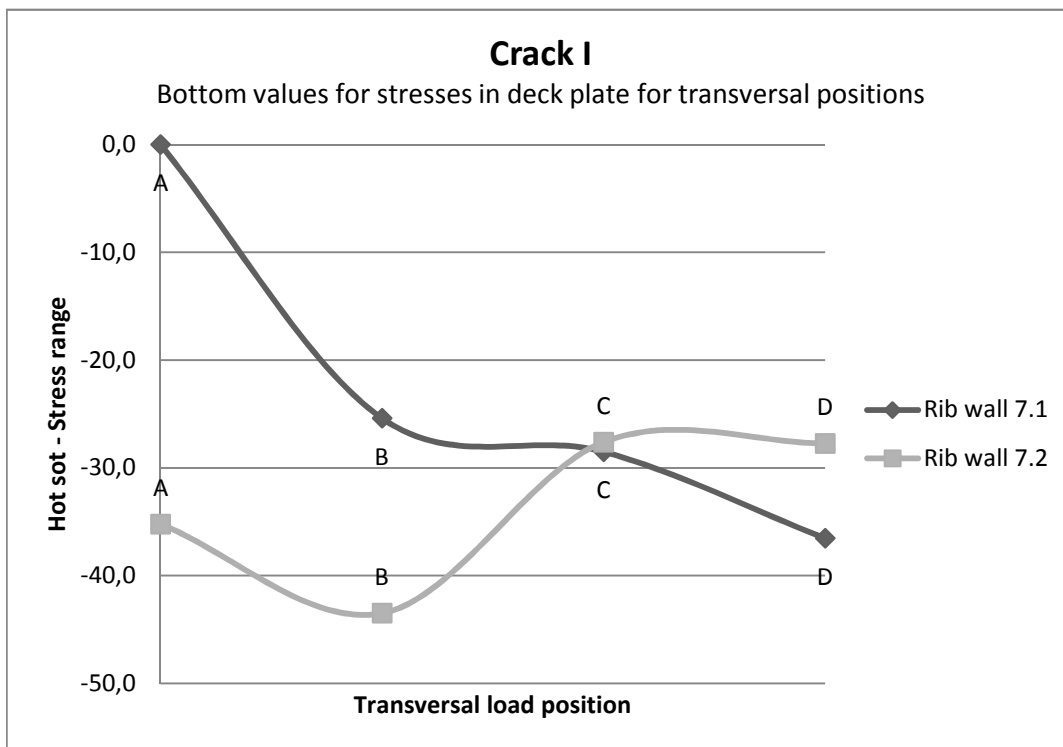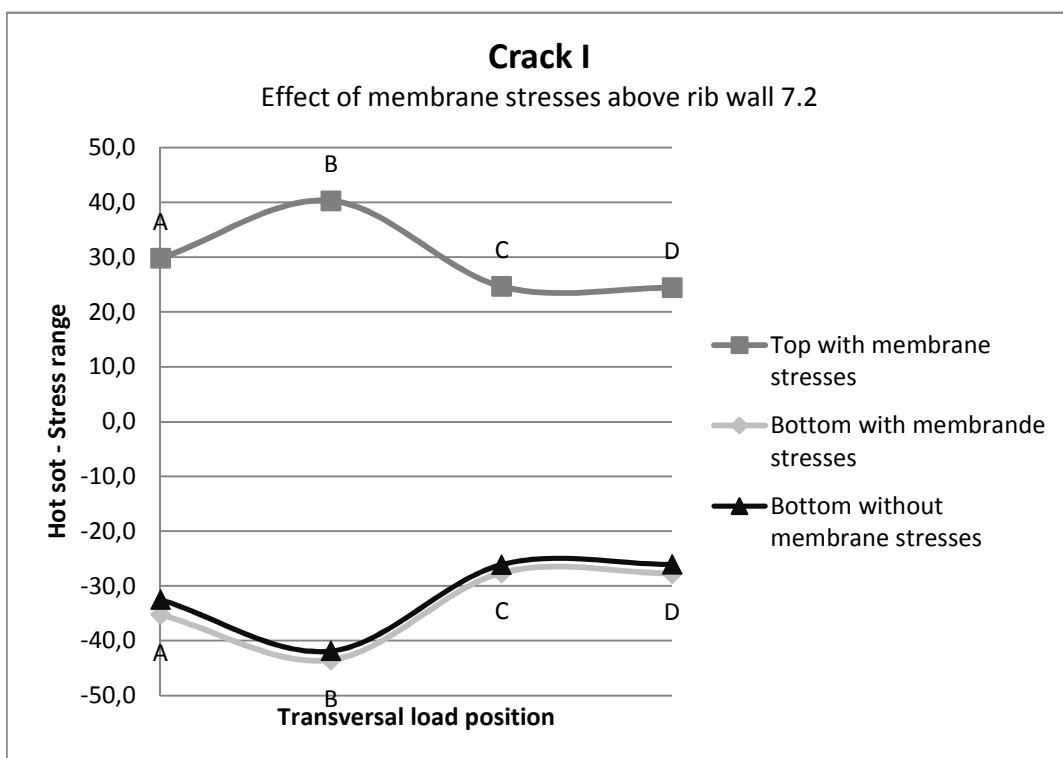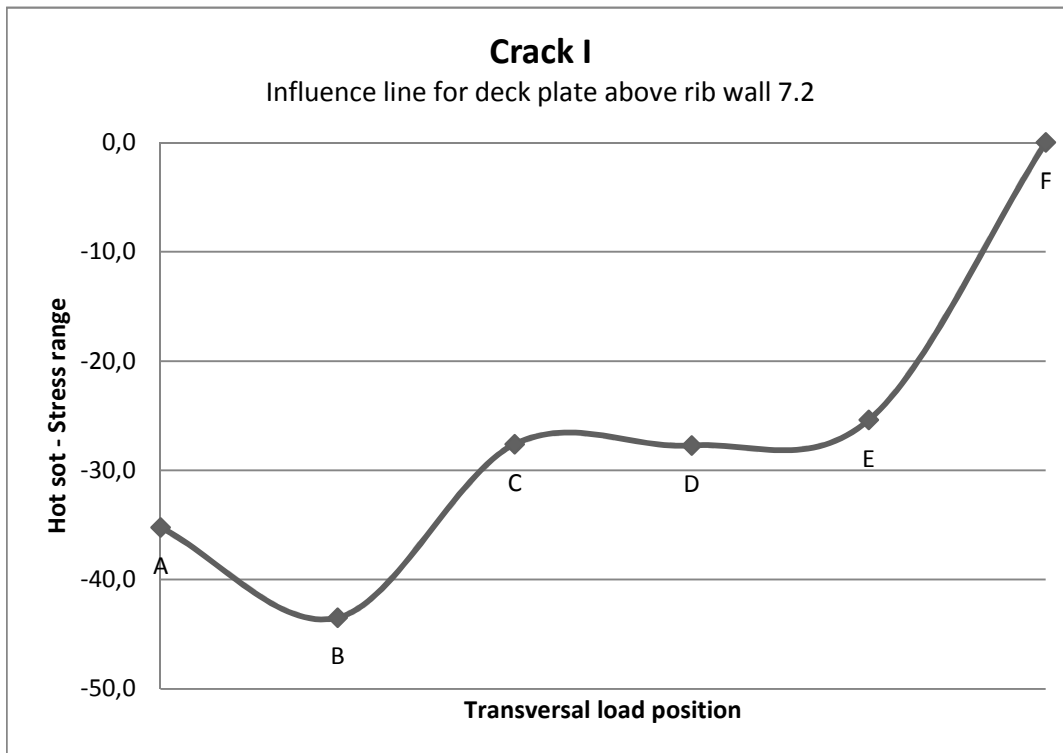
For Crack I the membrane stresses are small in comparisson to the bending stresses, which governs the crack initiatopn and propagation

Rib-DP Crack II

Toe crack propagating in the rib wall. Hot spot stresses in the rib wall are extracted from the FE-analysis with principal stresses from nodal values. All loads area placed in span.
For cack II the bottom values are the ones to be used since theses are the values at the out side of the rib wall, at the weld. The top values are checked to investigate the amount of membran stresses in the deck.

Crack II - Load response in rib wall 7.1:

	Bottom		Top		Final			Without σ_mem	
			Load placed at A (span):						
x (m)	σ_p_max	σ_p_min	σ_p_max	σ_p_min	Bottom	Top	σ_mem	Bottom	Top
0,002	26,61	0	0	-25,67	27,5	-26,5	0,48005	27,0	-27,0
0,006	25,33	0	0	-24,42					
	σ_hs_max	σ_hs_min	σ_hs_max	σ_hs_min					
	27,5	0,0	0,0	-26,5					

	Bottom		Top		Final			Without σ_mem	
			Load placed at B (span):						
x (m)	σ_p_max	σ_p_min	σ_p_max	σ_p_min	Bottom	Top	σ_mem	Bottom	Top
0,002	43,14	0	0	-52,6	44,4	-54,0	-4,8037	49,2	-49,2
0,006	41,29	0	0	-50,53					
	σ_hs_max	σ_hs_min	σ_hs_max	σ_hs_min					
	44,4	0,0	0,0	-54,0					

	Bottom		Top		Final			Without σ_mem	
			Load placed in at C (span):						
x (m)	σ_p_max	σ_p_min	σ_p_max	σ_p_min	Bottom	Top	σ_mem	Bottom	Top
0,002	17,26	-4,67	0	-42,17	17,7	-43,0	-12,646	30,3	-30,3
0,006	16,62	-3,25	0	-40,96					
	σ_hs_max	σ_hs_min	σ_hs_max	σ_hs_min					
	17,7	-5,6	0,0	-43,0					

	Bottom		Top		Final			Without σ_mem	
			Load placed in at D (span):						
x (m)	σ_p_max	σ_p_min	σ_p_max	σ_p_min	Bottom	Top	σ_mem	Bottom	Top
0,002	0	-11,95	0	-25,59	0,0	-25,9	-12,932	12,9	-12,9
0,006	0	-10,11	0	-25,18					
	σ_hs_max	σ_hs_min	σ_hs_max	σ_hs_min					
	0,0	-13,2	0,0	-25,9					

Crack II - Load response in rib wall 7.2:

	Bottom		Top		Final			Without σ_mem	
	Load placed in at A (span):								
x (m)	σ_p_max	σ_p_min	σ_p_max	σ_p_min	Bottom	Top	σ_mem	Bottom	Top
0,002	0	-57,69	40,71	0	-59,3	42,0	-8,6173	-50,6	50,6
0,006	0	-55,35	38,75	0					
	σ_hs_max	σ_hs_min	σ_hs_max	σ_hs_min					
	0,0	**-59,3**	42,0	0,0					

	Bottom		Top		Final			Without σ_mem	
	Load placed at B (span):								
x (m)	σ_p_max	σ_p_min	σ_p_max	σ_p_min	Bottom	Top	σ_mem	Bottom	Top
0,002	0	-31,16	0	-11,9	-32,1	0,0	-16,042	-16,0	16,0
0,006	0	-29,78	0	-10,33					
	σ_hs_max	σ_hs_min	σ_hs_max	σ_hs_min					
	0,0	-32,1	0,0	-13,0					

	Bottom		Top		Final			Without σ_mem	
	Load placed in at C (span):								
x (m)	σ_p_max	σ_p_min	σ_p_max	σ_p_min	Bottom	Top	σ_mem	Bottom	Top
0,002	19,48	-3,92	0	-44,91	20,0	-46,2	-13,11	33,1	-33,1
0,006	18,75	-2,52	0	-43					
	σ_hs_max	σ_hs_min	σ_hs_max	σ_hs_min					
	20,0	-4,9	0,0	-46,2					

	Bottom		Top		Final			Without σ_mem	
	Load placed in at D (span):								
x (m)	σ_p_max	σ_p_min	σ_p_max	σ_p_min	Bottom	Top	σ_mem	Bottom	Top
0,002	36,78	0	0	-55,26	37,8	-56,5	-9,384	47,2	-47,2
0,006	35,29	0	0	-53,34					
	σ_hs_max	σ_hs_min	σ_hs_max	σ_hs_min					
	37,8	0,0	0,0	-56,5					

Crack II - Summary of results

x	Rib 7.1 Stresses Bottom	Top	Membrane Stress	Without	Rib 7.2 Stresses Bottom	Top	Membrane Stress	Without
A	27,5	-26,5	27,0	0,0	*-59,3*	42,0	-8,6	-50,6
B	44,4	-54,0	49,2	0,0	-32,1	0,0	-16,0	-16,0
C	17,7	-43,0	30,3	0,0	20,0	-46,2	-13,1	33,1
D	0,0	-25,9	12,9	0,0	37,8	-56,5	-9,4	47,2
Delta	44,4				*59,3*			

Comparison between resposne in A and C for deck plate in rib wall 7.2:

x	Bottom stresses
B	59,3
C	20,0
Diff:	*197%*

Extrapolated values for the deck plate above rib wall 7.2

x	Bottom stresses
A	-59,3
B	-32,1
C	20,0
D	37,8
E	44,4
F	27,5

Crack II
Bottom values for stresses in rib walls for transversal positions

Crack II

Influence line for rib wall 7.2

Crack II

Effect of membrane stresses above rib wall 7.2
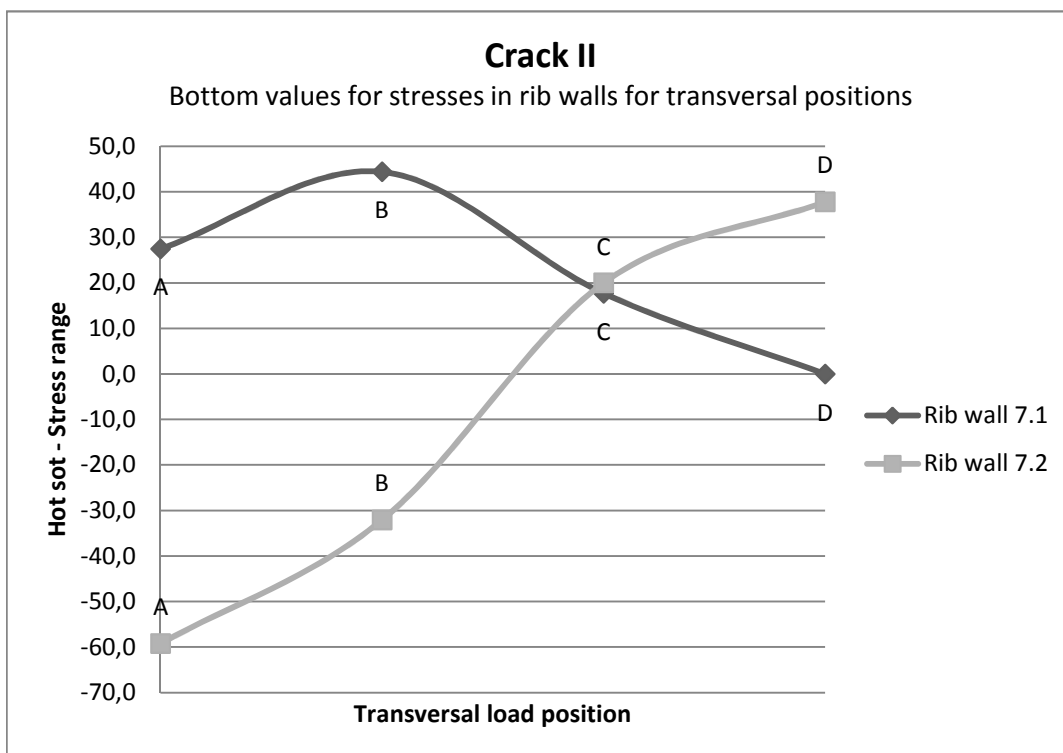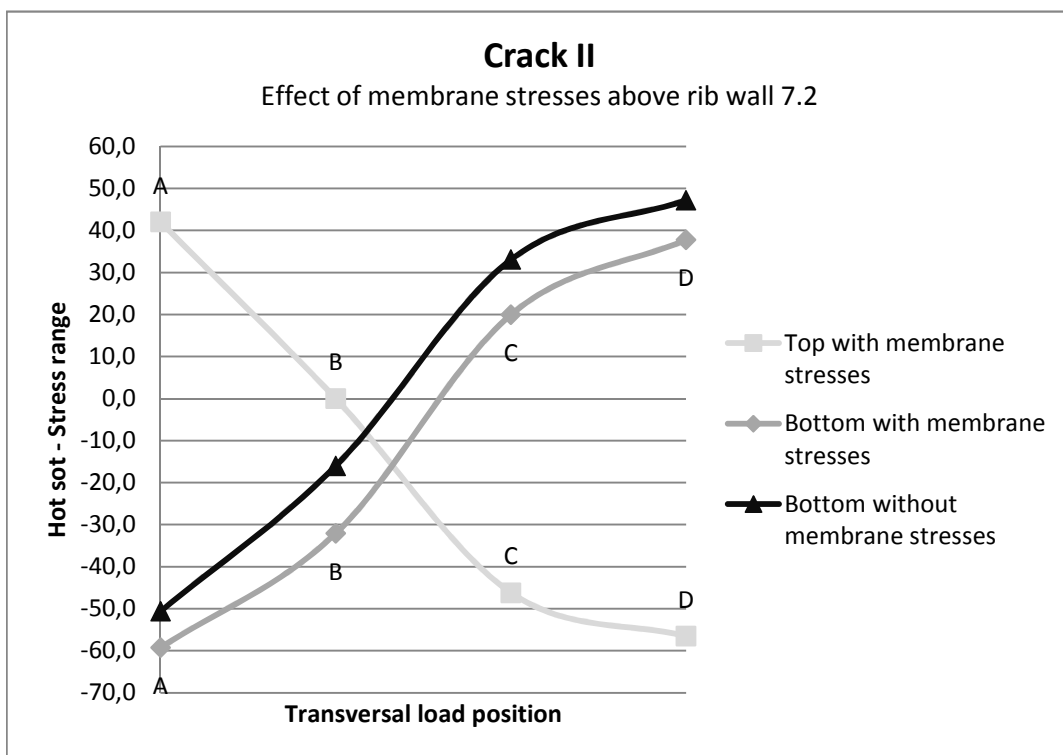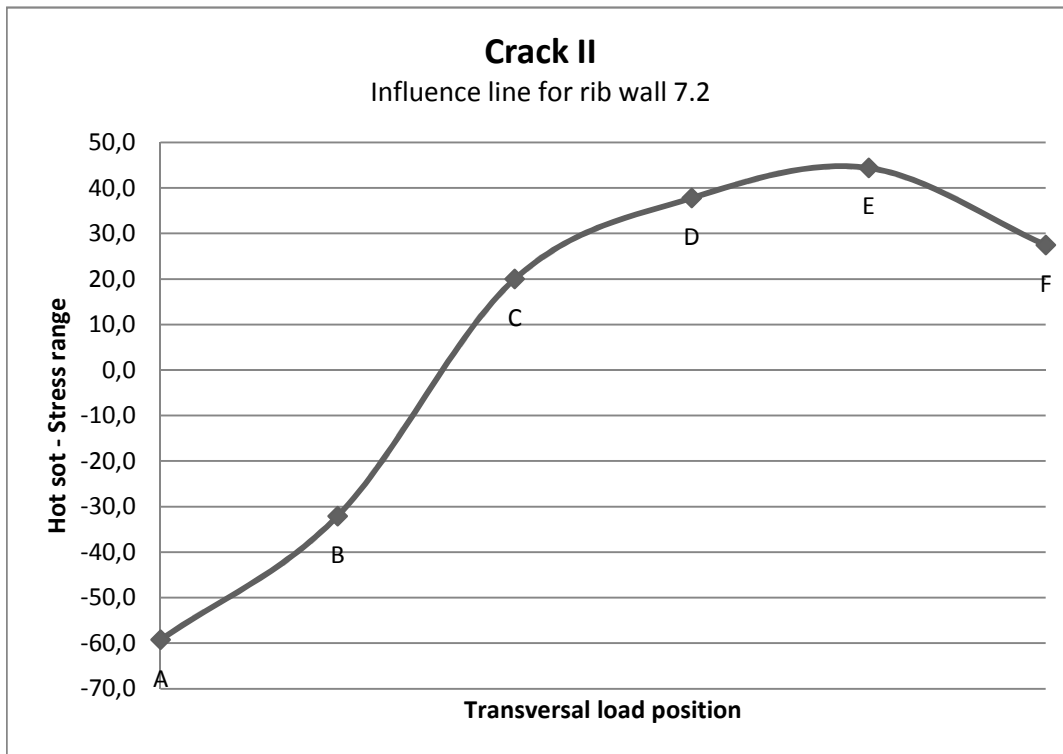
For Crack II the membrane stresses have a larger influence then for Crack I

Rib-FB Crack III

The crack starts in the toe of the weld and propagate in the floor beam. The crack propagation direction will follow the main direction of the highest principal stress. In the report we assume the crack to propagate from the middle of the rib radius and with an inclination of 45 degrees. The stresses are therefore extracted in a perpendicular direction to this. Hot spot stresses in the floor beam web are extracted from the FE-analysis with principal stresses from nodal values.
For cack III it doesen't matter if the top or bottom values are choosen since there is a weld on both sides of the floor beam web. Hence, the highest value of the top and bottom stresses will be the governing stress.

Crack III - Load response ABOVE rib wall 7.1:

Load placed at A (FB):

x (m)	Bottom σ_p_max	σ_p_min	Top σ_p_max	σ_p_min	Bottom	Top	σ_mem	Without σ_mem Bottom	Top
						Final		**Without σ_mem**	
0,004	8,04	0	8,2	0	0,0	9,1	4,5355	-4,5	4,5
0,01	6,75	0	6,9	0					
	σ_hs_max	σ_hs_min	σ_hs_max	σ_hs_min					
	8,9	0,0	9,1	0,0					

Load placed at B (FB):

x (m)	Bottom σ_p_max	σ_p_min	Top σ_p_max	σ_p_min	Bottom	Top	σ_mem	Without σ_mem Bottom	Top
0,004	3,34	-5,82	3,3	-5,62	3,7	-6,2	-1,2573	4,9	-4,9
0,01	2,82	-4,94	2,77	-4,75					
	σ_hs_max	σ_hs_min	σ_hs_max	σ_hs_min					
	3,7	-6,4	3,7	-6,2					

Load placed at C (FB)

x (m)	Bottom σ_p_max	σ_p_min	Top σ_p_max	σ_p_min	Bottom	Top	σ_mem	Without σ_mem Bottom	Top
0,004	0	-33,33	0	-33,15	0,0	-37,0	-18,491	18,5	-18,5
0,01	0	-27,61	0	-27,43					
	σ_hs_max	σ_hs_min	σ_hs_max	σ_hs_min					
	0,0	-37,2	0,0	-37,0					

Load placed at D (FB)

x (m)	Bottom σ_p_max	σ_p_min	Top σ_p_max	σ_p_min	Bottom	Top	σ_mem	Without σ_mem Bottom	Top
0,004	0	-43,11	0	-42,96	0,0	***-48,1***	-24,033	24,0	-24,0
0,01	0	-35,49	0	-35,34					
	σ_hs_max	σ_hs_min	σ_hs_max	σ_hs_min					
	0,0	-48,2	0,0	-48,1					

Crack III - Load response ABOVE rib wall 7.2:

	Load placed at A (FB):								
	Bottom		*Top*		**Final**			**Without σ_mem**	
x (m)	σ_p_max	σ_p_min	σ_p_max	σ_p_min	Bottom	Top	σ_mem	Bottom	Top
0,004	0	-12,25	0	-11,93	0,0	0,0	0	0,0	0,0
0,01	0	-9,65	0	-9,35					
	σ_hs_max	σ_hs_min	σ_hs_max	σ_hs_min					
	0,0	-14,0	0,0	-13,7					

	Load placed at B (FB):								
	Bottom		*Top*		**Final**			**Without σ_mem**	
x (m)	σ_p_max	σ_p_min	σ_p_max	σ_p_min	Bottom	Top	σ_mem	Bottom	Top
0,004	0,49	-24,93	0,23	-24,49	0,6	0,3	0,4136	0,1	-0,1
0,01	0,4	-21,09	0,16	-20,7					
	σ_hs_max	σ_hs_min	σ_hs_max	σ_hs_min					
	0,6	-27,5	0,3	-27,0					

	Load placed at C (FB):								
	Bottom		*Top*		**Final**			**Without σ_mem**	
x (m)	σ_p_max	σ_p_min	σ_p_max	σ_p_min	Bottom	Top	σ_mem	Bottom	Top
0,004	10,09	-8,47	10,47	-8	-9,1	11,6	1,29145	-10,4	10,4
0,01	8,42	-7,59	8,72	-7,18					
	σ_hs_max	σ_hs_min	σ_hs_max	σ_hs_min					
	11,2	-9,1	11,6	-8,5					

	Load placed at D (FB)								
	Bottom		*Top*		**Final**			**Without σ_mem**	
x (m)	σ_p_max	σ_p_min	σ_p_max	σ_p_min	Bottom	Top	σ_mem	Bottom	Top
0,004	14,99	-0,78	15,36	0	-1,2	17,4	8,07725	-9,3	9,3
0,01	12,05	-0,12	12,35	0					
	σ_hs_max	σ_hs_min	σ_hs_max	σ_hs_min					
	17,0	-1,2	17,4	0,0					

Crack III - Summary of results

x	Rib 7.1 Stresses Bottom	Top	Membrane Stress	Without	Rib 7.2 Stresses Bottom	Top	Menbrane Stress	Without
A	0,0	9,1	4,5	4,5	0,0	0,0	0,0	0,0
B	3,7	-6,2	-1,3	-4,9	0,6	0,3	0,4	-0,1
C	0,0	-37,0	-18,5	-18,5	-9,1	11,6	1,3	10,4
D	0,0	*-48,1*	-24,0	-24,0	-1,2	17,4	8,1	9,3
Delta		48,1			0,0			

Comparison between resposne in D and C for deck plate in rib wall 7.1:

x	Top stresses
D	-48,1
C	-37,0
Diff:	*30%*

Extrapolated values for the deck plate above rib wall 7.1:

x	Top stresses
A	9,1
B	-6,2
C	-37,0
D	-48,1
E	0,3
F	0,0

Crack III — Top valuess in floor beam web for transversal position

Crack III

Influence line for floor beam web at rib wall 7.1

Hot sot - Stress range

Transversal load position

Crack III

Effect of membrane stresses in floor beam at rib wall 7.1

Hot sot - Stress range

Transversal load position

- Bottom with membrane stresses
- Top with membrane stresses
- Top without membrane stresses

Summary:

	Load position	Rib wall	Location	Δσ_p_hs_max [MPa]	Δσ_p_hs_C [MPa]
R-DP Crack I	**B**	2	span	43,5	28,5
R-DP Crack II	**A**	2	span	59,3	20,0
R-FB Crack III	**D**	1	FB	48,1	37,0

Increase of stress between worst local load position and load location C:
C is the position which is commonly used in simplified analysis

R-DP Crack I	**53%**
R-DP Crack II	**197%**
R-FB Crack III	**30%**

To find the worst global load loaction, i.e. Which rib that has the highes load effects, the three positions A, B respective D are tried for each weld at each rib and the results are as a first step analysed visually. The position with the highest compressive stresse will be included even if this is not the position generating the highest total respons, this due to the fact that fatigue cracks arise from compressiv stresses, if no compressive stresses are present no crack will arise.

2. Global transverse load location

In step 2 of the method the goal is to determine at which rib intersection the stresses are highest. The stresses one node from the shell intersections is compared to each other at the different ribs. The highest stress will determine which rib that have the highest load response. To find the worst global load loaction,which rib that has the highes load effects, the critical postions for each weld are loaded at each rib. The influence of the second wheel in the load axle is also investigated. If the load responce is very local, the second wheel may be disregarded.
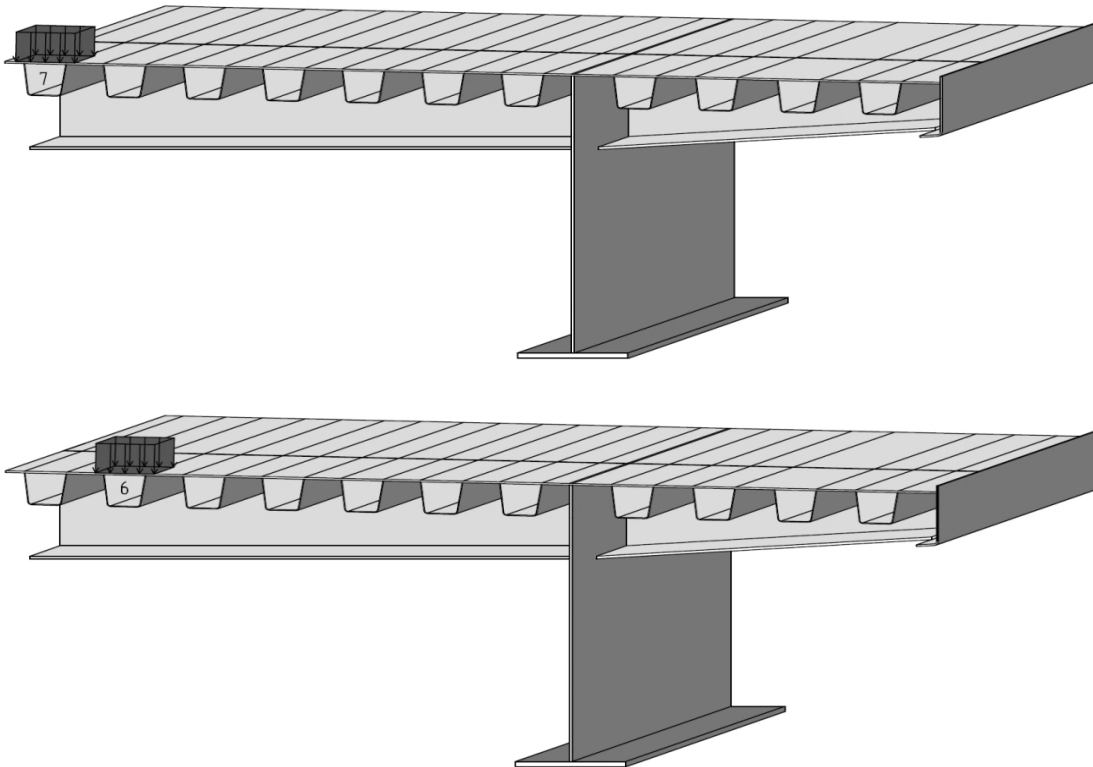
Simplifications:
The stresses in this analysis are not hot spot stresses due to the extra time required with partitioning the model and meshing. The stresses are instead nodal values taken one node away from the connection to avoid singularites. These values cannot be used for fatugue evaluation but are valied for comparison of which rib that have the most adverse load response.
Only one axis is modelled to save modelling effort. On this axis one wheel is modelled for all ribs, and for the ribs generating the highest stress range two wheels are modelled to see the impact of the second wheel of the axis.

Rib-DP Crack I

Load response with one wheel in span 6-7

	Bottom		Top		Membran	Without membrane	
x (m)	σ_p_max	σ_p_min	σ_p_max	σ_p_min		Bottom	Top
7.2	0	-31,04	30,10	-6,06	-0,47	-30,57	30,57
6.2	0	-31,06	30,25	-6,00	-0,40	-30,66	30,66
5.2	0	-31,03	30,48	-5,91	-0,28	-30,76	30,76
4.2	0	-30,95	30,78	-5,76	-0,08	-30,87	30,87
3.2	0	-30,79	31,17	-5,56	0,19	-30,98	30,98
2.2	0	-30,62	31,62	-5,29	0,50	-31,12	31,12
1.2	0	-30,06	31,64	-4,41	0,79	-30,85	30,85

Load placed at B (span, 7.2):

Load response with two wheels in span 6-7

	Bottom		Top		Membran	Without membrane	
x (m)	σ_p_max	σ_p_min	σ_p_max	σ_p_min		Bottom	Top
7.2	0	-31,69	28,48	-6,96	-1,61	-30,09	30,09
6.2	0	-31,65	28,92	-6,74	-1,37	-30,29	30,29
5.2	0	-31,48	29,54	-6,46	-0,97	-30,51	30,51
4.2	0	-31,07	30,51	-6,10	-0,28	-30,79	30,79
3.2					0	0	0
2.2					0	0	0
1.2					0	0	0

Load placed at B (span, 7.2):

The membrane stresses are low, hence the dominating stresses for Crack I are the bending stresses. The membrane stresses increases when the second wheel is applied compared to when only one wheel is used. Accorindingly, a larger part of the stresses in the section consists of membrane stresses.
The difference in stresses between one and two wheels increases the furter toward the middle of the span between the main girders the load is positioned. Accoringdingly, the global deflection have an influence on the stress state for Crack I.

Influence of second wheel: 2,0%

Rib-DP Crack II

Load response with one wheel in span 6-7

	Bottom		**Top**		**Membran**	**Without membrane**	
			Load placed at A in span				
x (m)	σ_p_max	σ_p_min	σ_p_max	σ_p_min		**Bottom**	**Top**
7.2	0	-56,06	39,53	0	-8,27	-47,80	47,80
6.2	0	-56,32	39,77	0	-8,28	-48,05	48,05
5.2	0	-56,59	40,02	0	-8,29	-48,31	48,31
4.2	0	-56,90	40,32	0	-8,29	-48,61	48,61
3.2	0	-57,21	40,61	0	-8,30	-48,91	48,91
2.2	0	-57,48	40,87	0	-8,31	-49,18	49,18
1.2	0	-59,49	42,87	0	-8,31	-51,18	51,18

Load response with two wheels in span 6-7

	Bottom		**Top**		**Membran**	**Without membrane**	
			Load placed at A in span				
x (m)	σ_p_max	σ_p_min	σ_p_max	σ_p_min		**Bottom**	**Top**
7.2	0	-54,76	38,29	0	-8,24	-46,53	46,53
6.2	0	-55,28	38,78	0	-8,25	-47,03	47,03
5.2	0	-55,84	39,31	0	-8,27	-47,58	47,58
4.2	0	-58,54	41,87	0	-8,34	-50,21	50,21
3.2	0	-59,13	42,44	0	-8,35	-50,79	50,79
2.2	0	-59,63	42,9	0	-8,37	-51,27	51,27
1.2	0	-61,7	44,94	0	-8,37	-53,31	53,31

For rib 1, 2, 3 and 4 the secon wheel is placed towards the middle of the span
For rib 5, 6 and 7 the secon wheel is placed towards the main girder

For Crack II the membrane stresses is a larger part of the total stress state. In the tables it can be seen that membranse stress is very similar between one and two wheels.
It can also be seen in the tables that the stress state for one and two wheels differ if the loads are placed near the main girders or in the middle of the span. Accorindly, it is important to include the second wheel to mirror a realistic behaviour.
Since the worst stresses are found in rib wall 1.2 it is interesting to investigate the responce in rib wall 1.1 to ensure where the stresses are highest. But this investigation would place a load on rib wall 1.1 corresponding to load case A for rib 1.2. The load on wall 1.1 is therefore very simillar to load place D. Load case A and D are simillar except that load A is directed towards the free span between the ribs and load D towards the closed span inside the rib walls. The responce from D is less than for A and therefore the highest stress will be found in rib wall 1.2.

Influence of second wheel: 3,7%

Rib-FB Crack III

Load response with one wheel above floor beam 6

	Load placed in D at floor beam						
	Bottom		**Top**		**Membran**	**Without membrane**	
x (m)	**σ_p_max**	**σ_p_min**	**σ_p_max**	**σ_p_min**		**Bottom**	**Top**
7.1	0	-30,80	0	-30,70	-30,75	-0,05	0,05
6.1	0	-26,18	0	-26,07	-26,13	-0,05	0,05
5.1	0	-22,96	0	-22,82	-22,89	-0,07	0,07
4.1	0	-19,07	########	-18,90	-18,99	-0,09	0,09
3.1	0,61	-14,62	0,64	-14,41	-14,52	-0,10	0,11
2.1	4,44	-11,49	4,51	-11,23	-11,36	-0,13	0,13
1.1	12,15	-16,91	12,54	-16,42	-16,67	-0,25	0,24

Load response with two wheels above floor beam 6

	Load placed in D at floor beam						
	Bottom		**Top**		**Membran**	**Without membrane**	
x (m)	**σ_p_max**	**σ_p_min**	**σ_p_max**	**σ_p_min**		**Bottom**	**Top**
7.1	0	-42,25	0	-42,10	-42,18	-0,08	0,07
6.1	0	-33,95	0	-33,77	-33,86	-0,09	0,09
5.1	0	-26,76	0	-26,53	-26,65	-0,11	0,12
4.1							
3.1							
2.1							
1.1							

The response in the floor beam web, crack III, is much worse when the load is placed in mid-span between the main girders. The results from the loadcase with 2 wheels also shows that the effect of the 2nd wheel is much higher for load in middle than out towards the main girders. Therefore, the worst load situation for the rib-fb weld is with two wheel loads and one of the wheels placed in centre span. It is important to include the second wheel in the analysis.
The membrane stresses are significantly higher for two wheels compared to one wheel
All principal stresses have a high angle, up to 60 degrees

Influence of second wheel: 37,2%

Summary:

Results from previous analyses:

	Load position	Rib wall	Location
R-DP Crack I	**B**	2	span
R-DP Crack II	**A**	2	span
R-FB Crack III	**D**	1	FB

Results from "Worst global transverse location" analysis:

	Worst rib	Influence of 2nd wheel
R-DP Crack I	7	2,0%
R-DP Crack II	1	3,7%
R-FB Crack III	7	37,2%

3. Local longitudinal load location

The load is placed at three different locations in longitudinal direction in relations to the floor beam to find the most adverse local longitudinal positions for each crack
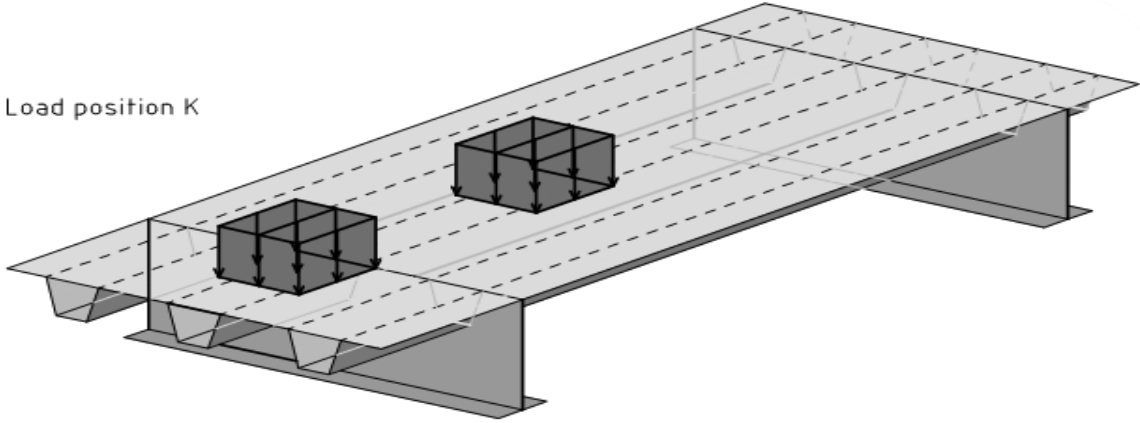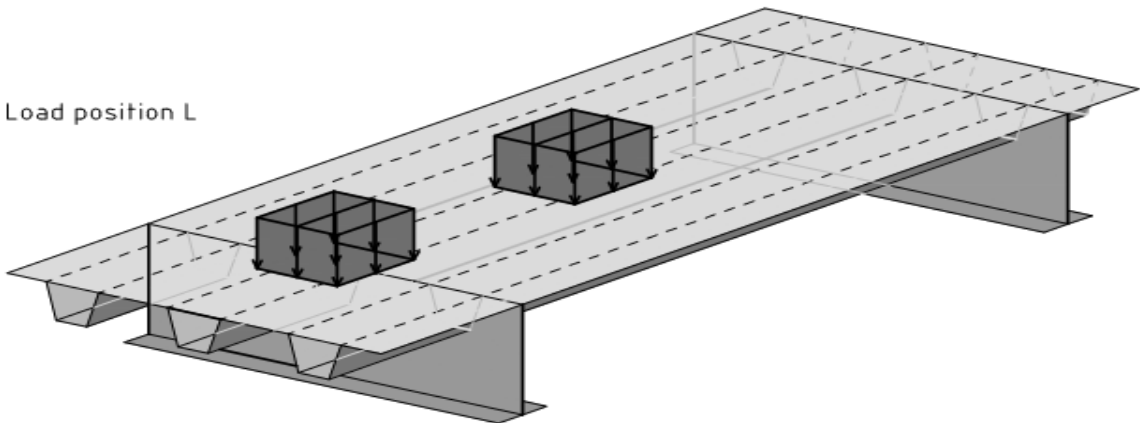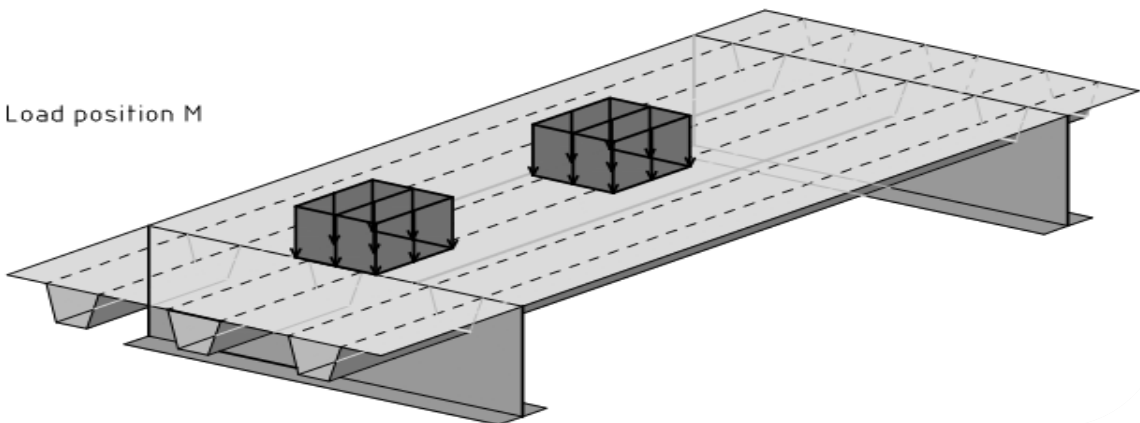
Rib-DP Crack I

The highest stresses are found below the wheel load. It has previously been shown that only one wheel per load axle contribute to the stress. Worst stress response in deck plate close to rib wall 7.2 for load placed at location B. At this step of the analysis is the second load axles contribution investigated.

Load case B

One load axle (one wheel)

	Bottom		Top		Sammanställning			Without σ_mem	
			Load placed at K (FB in transvers D):						
x (m)	σ_p_max	σ_p_min	σ_p_max	σ_p_min	Bottom	Top	σ_mem	Bottom	Top
0,0056	0	-35256300	34296400	-4889880	-42,9	42,1	-0,4037	-42,5	42,5
0,014	0	-23789200	22601700	-8057500					
	σ_hs_max	σ_hs_min	σ_hs_max	σ_hs_min					
[MPa]	0,0	-42,9	42,1	-2,8					

Two load axles (one wheel/axle)

	Bottom		Top		Sammanställning			Without σ_mem	
			Load placed at K (FB in transvers D):						
x (m)	σ_p_max	σ_p_min	σ_p_max	σ_p_min	Bottom	Top	σ_mem	Bottom	Top
0,0056	0	-32557100	29089400	-7782100	-40,1	36,8	-1,6576	-38,4	38,4
0,014	0	-21295900	17600700	-10899600					
	σ_hs_max	σ_hs_min	σ_hs_max	σ_hs_min					
[MPa]	0,0	-40,1	36,8	-5,7					

It can be noted that the hot-spot stress in this analysis is 0.6MPa lower than it was in analysis 1. The reason for this is mainly the disregard of the second wheel in analysis 3. This simplification lower the stresses with 2% which corresponds to 0.88MPa. The remaining difference can be explained with the quality of the mesh. In analysis 1, the mesh is less dense and some regions close to the stress extraction has an unsymmetric distribution.

Influence of second load axle: -6,6%

Rib-DP Crack II

Load case A
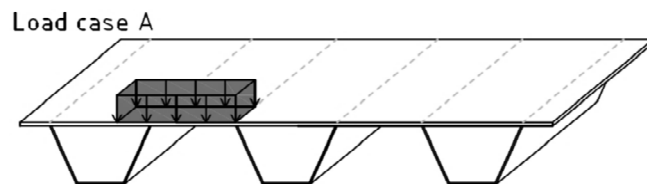
One load axle (one wheel)

Load placed at K (FB in transvers D):									
	Bottom		*Top*		**Sammanställning**			**Without σ_mem**	
x (m)	σ_p_max	σ_p_min	σ_p_max	σ_p_min	Bottom	Top	σ_mem	Bottom	Top
0,0024	0	-63121100	45992200	0	-64,4	47,1	-8,6552	-55,7	55,7
0,0061	0	-61253300	44395200	0					
	σ_hs_max	σ_hs_min	σ_hs_max	σ_hs_min					
[MPa]	0,0	-64,4	47,1	0,0					

Two load axles (one wheel/axle)

Load placed at K (FB in transvers D):									
	Bottom		*Top*		**Sammanställning**			**Without σ_mem**	
x (m)	σ_p_max	σ_p_min	σ_p_max	σ_p_min	Bottom	Top	σ_mem	Bottom	Top
0,0024	0	-69947100	52660800	0	-71,3	53,9	-8,7297	-62,6	62,6
0,0061	0	-67874200	50846400	0					
	σ_hs_max	σ_hs_min	σ_hs_max	σ_hs_min					
[MPa]	0,0	-71,3	53,9	0,0					

Influence of second load axle: 10,8%

Rib-FB Crack III

Load case D
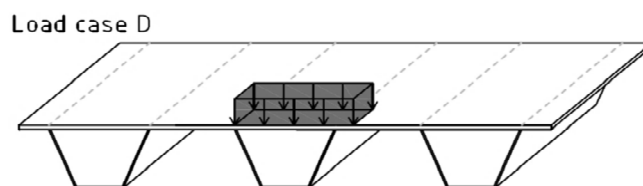
One axis (two wheels)

Load placed at K (FB in transvers D):									
	Bottom		*Top*		**Sammanställning**			**Without σ_mem**	
x (m)	**σ_p_max**	**σ_p_min**	**σ_p_max**	**σ_p_min**	**Bottom**	**Top**	**σ_mem**	**Bottom**	**Top**
0,004	0	-43,44	0	-43,2	-48,0	-47,8	-47,926	-0,1	0,1
0,01	0	-36,57	0	-36,32					
	σ_hs_max	**σ_hs_min**	**σ_hs_max**	**σ_hs_min**					
	0,0	-48,0	0,0	-47,8					

Load placed at L (FB in transvers D):									
	Bottom		*Top*		**Sammanställning**			**Without σ_mem**	
x (m)	**σ_p_max**	**σ_p_min**	**σ_p_max**	**σ_p_min**	**Bottom**	**Top**	**σ_mem**	**Bottom**	**Top**
0,004	0	-50,22	0	-37,02	-55,4	-41,3	-48,33	-7,1	7,1
0,01	0	-42,5	0	-30,68					
	σ_hs_max	**σ_hs_min**	**σ_hs_max**	**σ_hs_min**					
	0,0	-55,4	0,0	-41,3					

Load placed at M (FB in transvers D):									
	Bottom		*Top*		**Sammanställning**			**Without σ_mem**	
x (m)	**σ_p_max**	**σ_p_min**	**σ_p_max**	**σ_p_min**	**Bottom**	**Top**	**σ_mem**	**Bottom**	**Top**
0,004	0	-37,26	0	-49,97	-41,5	-55,1	-48,325	6,8	-6,8
0,01	0	-30,93	0	-42,24					
	σ_hs_max	**σ_hs_min**	**σ_hs_max**	**σ_hs_min**					
	0,0	-41,5	0,0	-55,1					

Comparison for Rib wall 7.1

With membrane stresses

x	Bottom	Top
K	-48,0	-47,8
L	-55,4	-41,3
M	-41,5	-55,1

Without membrane stresses

x	Bottom	Top
K	-0,1	0,1
L	-7,1	7,1
M	6,8	-6,8

Two axles (four wheels)

Load placed at K (FB in transvers D):

x (m)	Bottom σ_p_max	σ_p_min	Top σ_p_max	σ_p_min	Sammanställning Bottom	Top	σ_mem	Without σ_mem Bottom	Top
0,004	0	-59,19	0	-82,17	-66,1	-90,5	-78,305	12,2	-12,2
0,01	0	-48,84	0	-69,76					
	σ_hs_max	σ_hs_min	σ_hs_max	σ_hs_min					
	0,0	-66,1	0,0	-90,5					

Load placed at L (FB in transvers D):

x (m)	Bottom σ_p_max	σ_p_min	Top σ_p_max	σ_p_min	Sammanställning Bottom	Top	σ_mem	Without σ_mem Bottom	Top
0,004	0	-69,01	0	-80,31	-76,8	-88,7	-82,74	5,9	-5,9
0,01	0	-57,39	0	-67,81					
	σ_hs_max	σ_hs_min	σ_hs_max	σ_hs_min					
	0,0	-76,8	0,0	-88,7					

Load placed at M (FB in transvers D):

x (m)	Bottom σ_p_max	σ_p_min	Top σ_p_max	σ_p_min	Sammanställning Bottom	Top	σ_mem	Without σ_mem Bottom	Top
0,004	0,41	-50,36	0	-84,41	-56,6	-92,8	-74,732	18,1	-18,1
0,01	0,18	-41,01	0	-71,83					
	σ_hs_max	σ_hs_min	σ_hs_max	σ_hs_min					
	0,6	-56,6	0,0	-92,8					

Comparison for Rib wall 7.2

With membrane stresses				*Without membrane stresses*		
x	Bottom	Top		x	Bottom	Top
K	-66,1	-90,5		K	12,2	-12,2
L	-76,8	-88,7		L	5,9	-5,9
M	-56,6	-92,8		M	18,1	-18,1

All stresses from the analysis are below, but very close to 60 degrees. The local longitudinal position is of smaller significance but M gives the higest responce as expected

Influence of second axle :   67,60%

Summary

Results from previous analyses:

	Load position	Rib wall	Location	Worst rib	Influence of the 2nd wheel
R-DP Crack I	**B**	2	span	7	2,0%
R-DP Crack II	**A**	2	span	1	3,7%
R-FB Crack III	**D**	1	FB	7	37,2%

Results from "Worst local longitudinal location" analysis:

	Load position	Influence of the 2nd load axle	$\Delta\sigma\_p\_hs$ [MPa]
R-DP Crack I	M	-6,6%	42,9
R-DP Crack II	M	10,8%	71,3
R-FB Crack III	M	67,6%	92,8

4.Final load position

	Rib wall	Transversal position	Longitudinal position	No. Wheels /axle	No. Axles
R-DP Crack I	7.2	B	M (span)	1	1
R-DP Crack II	1.2	A	M (span)	1	2
R-FB Crack III	7.1	D	M (FB)	2	2

Increase of stress between the total worst local load position and the commonly used position (C) in simplified analysis:

		$\Delta\sigma$_FEM [MPa]	$\Delta\sigma$_hand [MPa]
R-DP Crack I	51%	42,9	28,5
R-DP Crack II	257%	71,3	20,0
R-FB Crack III	151%	92,8	37,0

1. Local transversal position

	Load position	Rib wall	Location	$\Delta\sigma$_p_hs_max [MPa]	$\Delta\sigma$_p_hs_C [MPa]
R-DP Crack I	B	7.2	span	43,5	28,5
R-DP Crack II	A	7.2	span	59,3	20,0
R-FB Crack III	D	7.1	FB	48,1	37,0

Increase of stress between worst local load position and load location C, which is commonly used in simplified analysis:

R-DP Crack I	53%
R-DP Crack II	197%
R-FB Crack III	30%

2. Global transversal position

	Worst rib	Influence of 2nd wheel
R-DP Crack I	7	2%
R-DP Crack II	1	4%
R-FB Crack III	7	37%

3. Local longitudinal position

	Load position	Influence of 2nd load axle	$\Delta\sigma$_p_hs [MPa]
R-DP Crack I	M	-6,6%	42,9
R-DP Crack II	M	10,8%	71,3
R-FB Crack III	M	67,6%	92,8

Appendix V

Stressrange in rib wall for moving traffic load

Stress range in different rib walls

7.2 - S22   7.1 - S22   8.1 - S22

Stress range in rib wall 8.1

8.1 - S22

Stress range in rib wall for moving traffic load
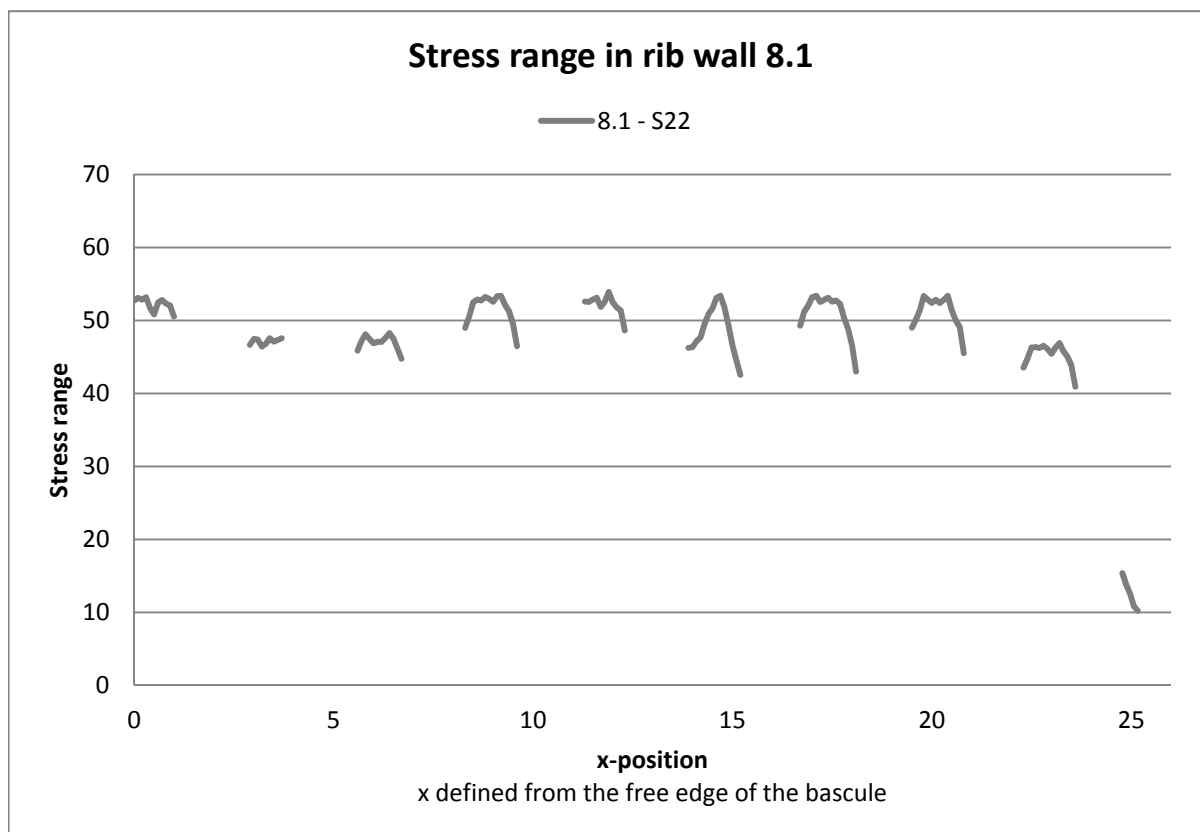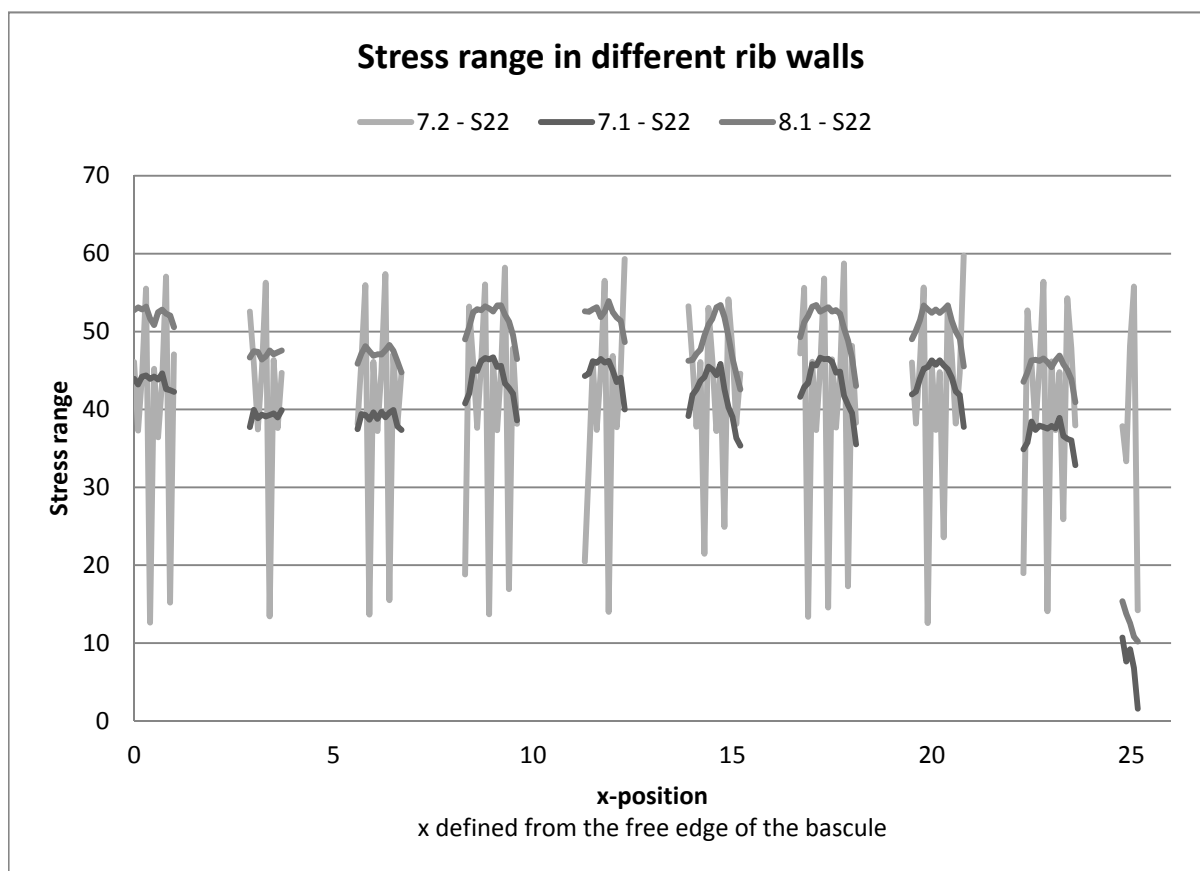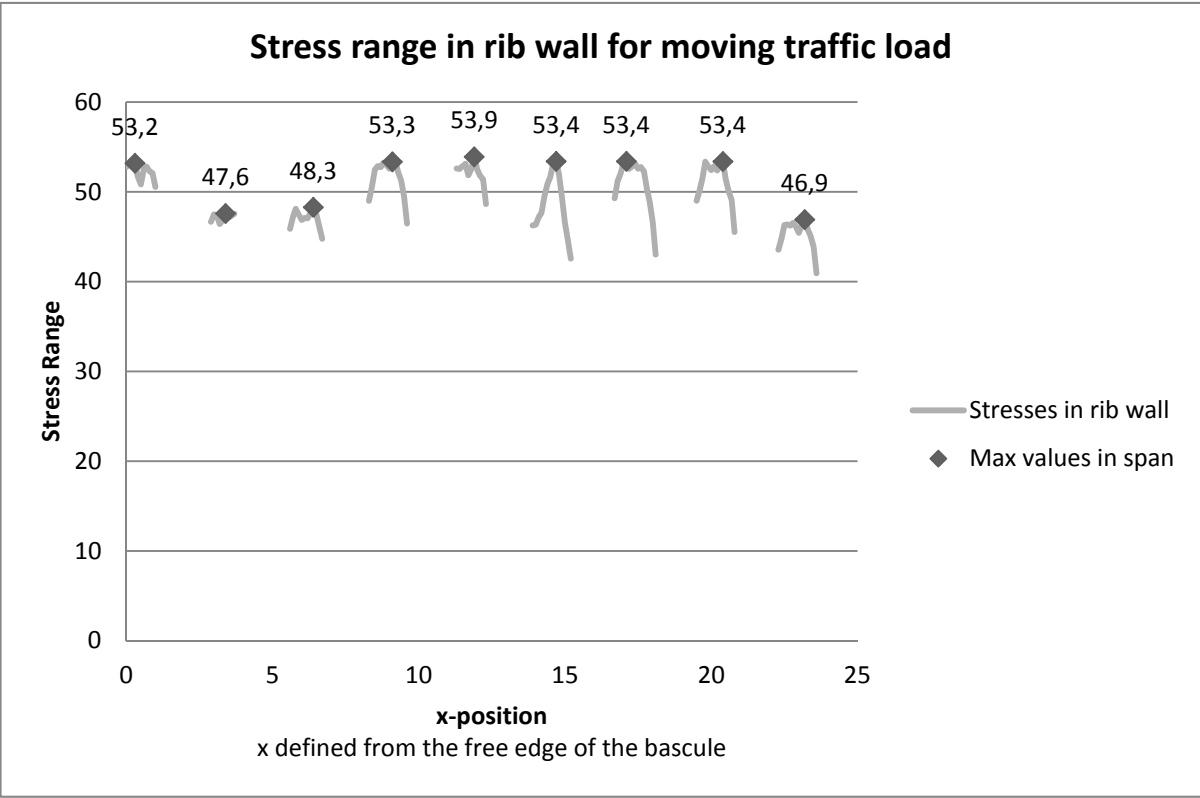
	7.1 S22	7.2 S22	8.1 S22		
x	**Delta_P**	**Delta_P**	**Delta_P**	**x**	
0,00	43,93	46,09	52,75	0,00	
0,10	43,20	37,30	53,10	0,10	
0,20	44,22	44,51	52,86	0,20	
0,30	**44,35**	**55,50**	**53,19**	**0,30**	**53,2**
0,40	43,93	12,63	51,68	0,40	
0,50	44,22	45,21	50,84	0,50	
0,60	43,85	36,42	52,47	0,60	
0,70	44,63	43,58	52,80	0,70	
0,80	42,61	57,05	52,29	0,80	
0,90	42,46	15,20	52,06	0,90	
1,00	42,27	47,05	50,56	1,00	
1,10				1,10	
1,20				1,20	
1,30				1,30	
1,40				1,40	
1,50				1,50	
1,60				1,60	
1,70				1,70	
1,80				1,80	
1,90				1,90	
2,00				2,00	

2,10				2,10	
2,20				2,20	
2,30				2,30	
2,40				2,40	
2,50				2,50	
2,60				2,60	
2,70				2,70	
2,80				2,80	
2,90	37,73	52,57	46,67	2,90	
3,00	39,93	45,86	47,48	3,00	
3,10	38,87	37,43	47,40	3,10	
3,20	39,33	45,08	46,42	3,20	
3,30	39,11	56,27	46,82	3,30	
3,40	39,29	13,44	**47,57**	3,40	**47,6**
3,50	39,50	46,32	47,10	3,50	
3,60	38,97	37,61	47,33	3,60	
3,70	39,90	44,68	47,56	3,70	
3,80				3,80	
3,90				3,90	
4,00				4,00	
4,10				4,10	
4,20				4,20	
4,30				4,30	
4,40				4,40	
4,50				4,50	
4,60				4,60	
4,70				4,70	
4,80				4,80	
4,90				4,90	
5,00				5,00	
5,10				5,10	
5,20				5,20	
5,30				5,30	
5,40				5,40	
5,50				5,50	
5,60	37,47	38,18	45,88	5,60	
5,70	39,40	46,43	47,18	5,70	
5,80	39,28	55,95	48,11	5,80	
5,90	38,69	13,66	47,48	5,90	
6,00	39,62	46,09	46,89	6,00	
6,10	38,78	37,23	47,07	6,10	
6,20	39,68	45,04	47,06	6,20	
6,30	38,99	57,36	47,60	6,30	
6,40	39,59	15,51	**48,27**	**6,40**	**48,3**
6,50	39,93	47,14	47,53	6,50	
6,60	37,83	37,97	46,17	6,60	
6,70	37,38	44,71	44,77	6,70	
6,80				6,80	

6,90				6,90	
7,00				7,00	
7,10				7,10	
7,20				7,20	
7,30				7,30	
7,40				7,40	
7,50				7,50	
7,60				7,60	
7,70				7,70	
7,80				7,80	
7,90				7,90	
8,00				8,00	
8,10				8,10	
8,20				8,20	
8,30	40,79	18,81	49,00	8,30	
8,40	42,04	53,20	50,52	8,40	
8,50	45,16	46,10	52,47	8,50	
8,60	44,95	37,64	52,87	8,60	
8,70	46,22	45,91	52,74	8,70	
8,80	46,59	56,03	53,24	8,80	
8,90	46,43	13,71	52,97	8,90	
9,00	46,68	46,25	52,58	9,00	
9,10	45,47	37,33	**53,34**	**9,10**	**53,3**
9,20	45,59	45,05	53,37	9,20	
9,30	43,33	58,20	52,16	9,30	
9,40	42,75	16,93	51,28	9,40	
9,50	42,01	47,84	49,54	9,50	
9,60	38,61	38,14	46,47	9,60	
9,70				9,70	
9,80				9,80	
9,90				9,90	
10,00				10,00	
10,10				10,10	
10,20				10,20	
10,30				10,30	
10,40				10,40	
10,50				10,50	
10,60				10,60	
10,70				10,70	
10,80				10,80	
10,90				10,90	
11,00				11,00	
11,10				11,10	
11,20				11,20	
11,30	44,31	20,46	52,60	11,30	
11,40	44,61	32,70	52,54	11,40	
11,50	46,18	45,81	52,87	11,50	
11,60	45,98	37,38	53,11	11,60	

11,70	46,48	44,97	51,86	11,70	
11,80	46,03	56,50	52,58	11,80	
11,90	46,23	14,01	**53,90**	**11,90**	**53,9**
12,00	45,00	46,84	52,50	12,00	
12,10	43,51	37,72	51,80	12,10	
12,20	44,06	44,98	51,38	12,20	
12,30	40,01	59,30	48,64	12,30	
12,40				12,40	
12,50				12,50	
12,60				12,60	
12,70				12,70	
12,80				12,80	
12,90				12,90	
13,00				13,00	
13,10				13,10	
13,20				13,20	
13,30				13,30	
13,40				13,40	
13,50				13,50	
13,60				13,60	
13,70				13,70	
13,80				13,80	
13,90	39,15	53,24	46,25	13,90	
14,00	41,88	46,15	46,35	14,00	
14,10	42,56	37,79	47,16	14,10	
14,20	43,66	46,07	47,69	14,20	
14,30	44,16	21,47	49,48	14,30	
14,40	45,48	53,03	50,87	14,40	
14,50	45,12	46,22	51,67	14,50	
14,60	44,41	37,23	53,11	14,60	
14,70	45,85	44,95	**53,40**	**14,70**	**53,4**
14,80	42,57	24,91	51,83	14,80	
14,90	40,26	54,12	49,36	14,90	
15,00	39,04	47,69	46,58	15,00	
15,10	36,32	38,14	44,56	15,10	
15,20	35,35	44,59	42,57	15,20	
15,30				15,30	
15,40				15,40	
15,50				15,50	
15,60				15,60	
15,70				15,70	
15,80				15,80	
15,90				15,90	
16,00				16,00	
16,10				16,10	
16,20				16,20	
16,30				16,30	
16,40				16,40	

16,50				16,50	
16,60				16,60	
16,70	41,64	47,19	49,29	16,70	
16,80	42,87	55,60	51,18	16,80	
16,90	43,42	13,36	52,03	16,90	
17,00	45,80	46,11	53,20	17,00	
17,10	45,66	37,35	**53,40**	**17,10**	**53,4**
17,20	46,63	45,41	52,56	17,20	
17,30	46,45	56,79	52,83	17,30	
17,40	46,49	14,56	53,12	17,40	
17,50	46,12	46,41	52,59	17,50	
17,60	44,72	37,68	52,74	17,60	
17,70	44,85	44,73	52,29	17,70	
17,80	41,75	58,72	50,37	17,80	
17,90	40,55	17,29	48,86	17,90	
18,00	39,56	48,15	46,61	18,00	
18,10	35,53	38,29	43,01	18,10	
18,20				18,20	
18,30				18,30	
18,40				18,40	
18,50				18,50	
18,60				18,60	
18,70				18,70	
18,80				18,80	
18,90				18,90	
19,00				19,00	
19,10				19,10	
19,20				19,20	
19,30				19,30	
19,40				19,40	
19,50	41,93	46,03	49,02	19,50	
19,60	42,29	38,20	50,11	19,60	
19,70	43,95	46,14	51,46	19,70	
19,80	45,23	55,64	53,35	19,80	
19,90	45,44	12,57	52,85	19,90	
20,00	46,28	45,92	52,42	20,00	
20,10	45,74	37,38	52,82	20,10	
20,20	46,30	44,76	52,39	20,20	
20,30	45,66	23,58	52,83	20,30	
20,40	45,17	53,25	**53,37**	**20,40**	**53,4**
20,50	44,06	47,09	51,38	20,50	
20,60	42,32	38,19	50,00	20,60	
20,70	41,86	44,68	49,09	20,70	
20,80	37,76	59,73	45,53	20,80	
20,90				20,90	
21,00				21,00	
21,10				21,10	
21,20				21,20	

21,30				21,30	
21,40				21,40	
21,50				21,50	
21,60				21,60	
21,70				21,70	
21,80				21,80	
21,90				21,90	
22,00				22,00	
22,10				22,10	
22,20				22,20	
22,30	34,88	18,99	43,56	22,30	
22,40	35,76	52,71	44,78	22,40	
22,50	38,44	45,97	46,29	22,50	
22,60	37,36	37,62	46,37	22,60	
22,70	37,90	45,64	46,23	22,70	
22,80	37,75	56,38	46,53	22,80	
22,90	37,54	14,09	46,09	22,90	
23,00	37,88	46,14	45,43	23,00	
23,10	37,58	37,35	46,30	23,10	
23,20	38,92	44,78	**46,91**	**23,20**	**46,9**
23,30	36,59	25,91	45,81	23,30	
23,40	36,21	54,27	45,08	23,40	
23,50	36,03	47,86	43,86	23,50	
23,60	32,84	37,96	40,93	23,60	
23,70				23,70	
23,80				23,80	
23,90				23,90	
24,00				24,00	
24,10				24,10	
24,20				24,20	
24,30				24,30	
24,40				24,40	
24,50				24,50	
24,60				24,60	
24,70				24,70	
24,78	10,69	37,85	**15,37**	**24,78**	**15,4**
24,88	7,64	33,33	13,77	24,88	
24,97	9,20	48,15	12,55	24,97	
25,07	6,80	55,77	10,83	25,07	
25,17	1,57	14,22	10,21	25,17	

Appendix VI

Input calculations for properties required in GoBeam

In this document the sectional properties of the ribs and sprig stiffness of the floor beams are calculated. These are transferred to a GoBeam model and from this model the moments and forces received are converted into stresses and a fatigue evaluation is performed. The fatigue ratio is compared to the fatigue ratio received from the evaluation based on the FE-model and the hot spot approach

Models of the interesting part:

The spring stiffens should vary along the direction of the floor beam depending on the distance from the main girders. The closer to the main girder, the stiffer behaviour. The weakest spring is located at mid-span and this is the spring used in the model. This is a simplification.
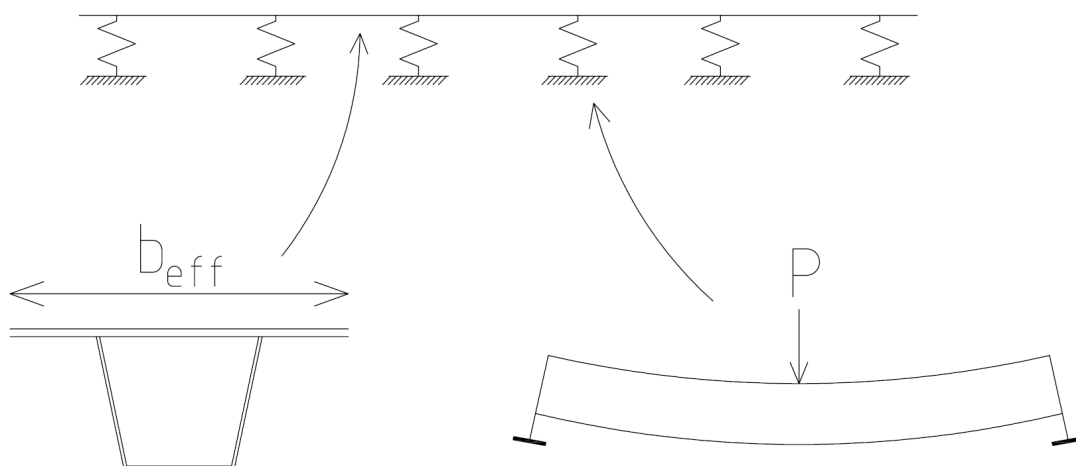
The rib together with the effective part of the deck plate acts as a beam
The floor beams are represented by springs

The spring stiffness of the floor beams is calculated by the model in the figure above, but to represent the actual behavior more realistically springs should have been inserted at the bottom of the main girders to represent the stiffness they have from bending out.

Materials

Deck plate, S420
Rib, S420

$$f_{yk} := 420 \text{MPa}$$

Floor beams, S355

$$f_{yk.fb} := 355 \text{MPa}$$

End plate, S275

$$f_{yk.endplate} := 275 \text{MPa}$$

$$\gamma_{M0} := 1$$

$$f_{yd} := \frac{f_{yk}}{\gamma_{M0}} = 420 \cdot \text{MPa}$$
$$\varepsilon_{420} := 0.75$$

$$f_{yd.fb} := \frac{f_{yk.fb}}{\gamma_{M0}} = 355 \cdot \text{MPa}$$
$$\varepsilon_{FB} := 0.81$$

$$f_{yd.endplate} := \frac{f_{yk.endplate}}{\gamma_{M0}} = 275 \cdot \text{MPa}$$
$$\varepsilon_{endplate} := 0.92$$

$$E := 210 \text{GPa}$$

Ribs - Sectional properties

Geometry for the ribs:

Indata:

$t_{dp} := 14\,mm$ Thickness of deck plate

$t_r := 6\,mm$ Thickness of rib

$b_{bf} := 220\,mm$ Width of bottom flange

$h_{web} := 237\,mm$ Height of web

$b_{dp.inner} := 284\,mm$ The width of the deck plate part inbetween the rib walls

$b_{dp.outer} := 256\,mm$ The width of the deck plate part between the ribs
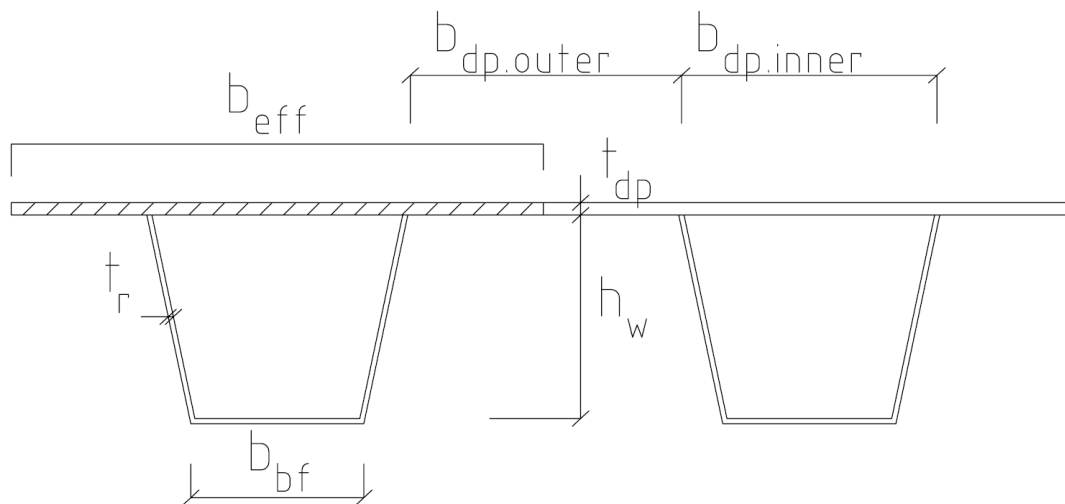
Calculation of participating part of the rib section

In the calculations the inclination of the ribs will be disragarded, the effect is small enough to be neglected.

With regard to fatigue the effective section of the rib can be set to the full section if the reduction factor ρ for ULS is 0.5 or more. The calculations are done according to EN-1993-1-5 4.4 for each separate part. From this follow that it is enough to calculate the part with the most adverse response.

All parts of the rib are seen as internal sections:

$k_\sigma := 4$ Buckling factor (Table 4.2 EN-1993-1-5)

$\psi := 1$ Stress relation, section in compression (4.1 EN-1993-1-5)

Calculate the reduction factor for the internal section of the deck plate between the rib wall of one rib

$$\lambda_{p.dp.inner} := \frac{\dfrac{b_{dp.inner}}{t_{dp}}}{28.4 \cdot \varepsilon_{420} \cdot \sqrt{k_\sigma}} = 0.476$$

$$\rho_{dp.inner} := min\left[1, \; \left| \begin{array}{l} 1 \quad \text{if} \; \lambda_{p.dp.inner} \le 0.673 \\[2mm] \dfrac{\lambda_{p.dp.inner} - 0.055 \cdot (3 + \psi)}{\lambda_{p.dp.inner}^2} \quad \text{otherwise} \end{array} \right. \right] = 1$$

$$b_{dp.inner.eff} := \left| \begin{array}{l} b_{dp.inner} \quad \text{if} \; \rho_{dp.inner} \ge 0.5 \qquad = 0.284\,m \\[2mm] b_{dp.inner} \cdot \rho_{dp.inner} \quad \text{otherwise} \end{array} \right.$$

It is not nessessary to calculate the reduction factor for the deck plate between two ribs as this width is smaller than the width between two rib walls, hence the reduction factor will be 1 here as well.

Calculate the reduction factor for the web of the rib

$$\lambda_{p.r.web} := \frac{\dfrac{h_{web}}{t_r}}{28.4 \cdot \varepsilon_{420} \cdot \sqrt{k_\sigma}} = 0.927$$

$$\rho_{r.web} := min\left[1, \; \left| \begin{array}{l} 1 \quad \text{if} \; \lambda_{p.r.web} \le 0.673 \\[2mm] \dfrac{\lambda_{p.r.web} - 0.055 \cdot (3 + \psi)}{\lambda_{p.r.web}^2} \quad \text{otherwise} \end{array} \right. \right] = 0.823$$

$$h_{w.eff} := \left| \begin{array}{l} h_{web} \quad \text{if} \; \rho_{r.web} \ge 0.5 \qquad = 0.237\,m \\[2mm] h_{web} \cdot \rho_{r.web} \quad \text{otherwise} \end{array} \right.$$

With the same argument as for the deck plate part between two ribs it is not nessessary to calculate the effective part of the bottom flange.

Effective width of deck plate acting as top flange for rib
According to above the full section of the rib is effective and will be used in the calculations of the sectional properties

$$b_{eff.rib} := b_{dp.inner} + 2 \cdot \frac{b_{dp.outer}}{2} = 0.54\,m \qquad \text{Effective width for a rib placed in span between main girders}$$

Sectional properties for a rib in the center of the span between main girders

One rib, with the full cross-section and the effective part of the deck plate, is seen as box beam
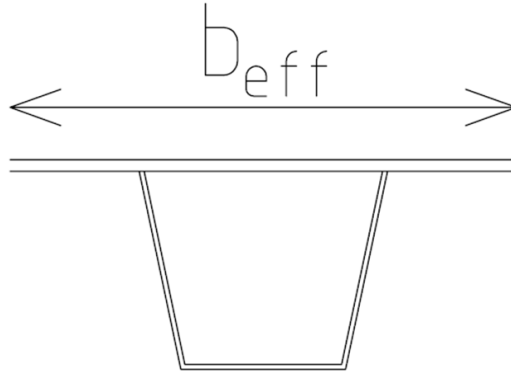
$$A_{rib} := 2 \cdot h_{web} \cdot t_r + t_r \cdot b_{bf} + b_{eff.rib} \cdot t_{dp} = 0.012\,m^2$$

$$z_{rib} := \frac{2t_r \cdot \dfrac{h_{web}^2}{2} + \dfrac{t_r^2}{2} \cdot b_{bf} + b_{eff.rib} \cdot t_{dp} \cdot \left(h_{web} + \dfrac{t_{dp}}{2}\right)}{A_{rib}} = 0.186\,m$$

The neutral axis, z, is defined from the bottom of the cross-section.

$$I_{rib} := \frac{b_{bf} \cdot t_r^3}{12} + b_{bf} \cdot t_r \left(z_{rib} - \frac{t_r}{2}\right)^2 + 2\left[\frac{t_r \cdot h_{web}^3}{12} + t_r \cdot h_{web} \cdot \left(z_{rib} - \frac{h_{web}}{2}\right)^2\right] \dots$$
$$+ \frac{b_{eff.rib} \cdot t_{dp}^3}{12} + b_{eff.rib} \cdot t_{dp} \cdot \left(h_{web} + \frac{t_{dp}}{2} - z_{rib}\right)^2$$

$$I_{rib} = 9.603 \times 10^{-5}\,m^4$$

Calculation of spring stiffness for floor beams

Model for calcultation of spring stiffness of floor beams

In the structural system the ribs will be resting on floor beam which are represented with springs, see figure below. The floor beam closes to the edge of the bascule, FB1, is stiffened by the locking mechanism, this will be simulated with a higher spring stiffness. Floor beam 2 to 9 have the similar dimensions and will be simplified to have the same spring stiffness. Floor beam 10 is much stiffer due to the K-joint. The end plate, closes to the abutment, have a lower stiffness.

FB1 FB2	FB3	FB4	FB5	FB6	FB7	FB8	FB9	FB10	FB11 FB12
F_2	F_3	F_3	F_3	F_3	F_3	F_3	F_3	F_3	F_4 F_5

FB1	--> F.2
FB2-9	--> F.3
FB10	--> F.4
End plate	--> F.5

The spring stiffness for each floor beam will be calculated with the model seen in the structural model below.

The floor beams are seen as beams resting on pinned supports and loaded with a unit load, P. The span length is the same as the span length between the main girders. The cantilivering parts of the floor beams are disregarded.
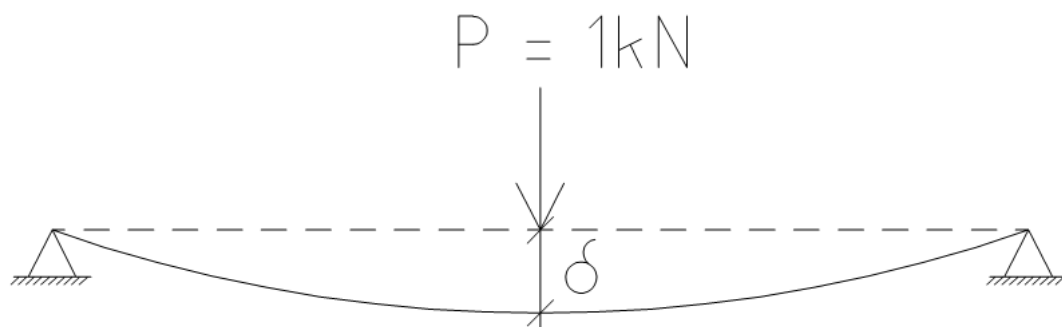
$$P = 1kN$$

$P := 1\text{kN}$

$l_{fb} := 7.7\text{m}$ Span length of floor beams. (Between main girders)

The spring stiffness will be calculated separetly for the representative floor beam. To calculate the spring stiffness the participating part of the floor beams needs to be calculated and the sectional properties with this taken into account. The effective width participating in the floor beam stiffness is calculated according to EN-1993-1-5 4.4. The ribs are not included as they do not give an increased stiffness in the transversal directions.
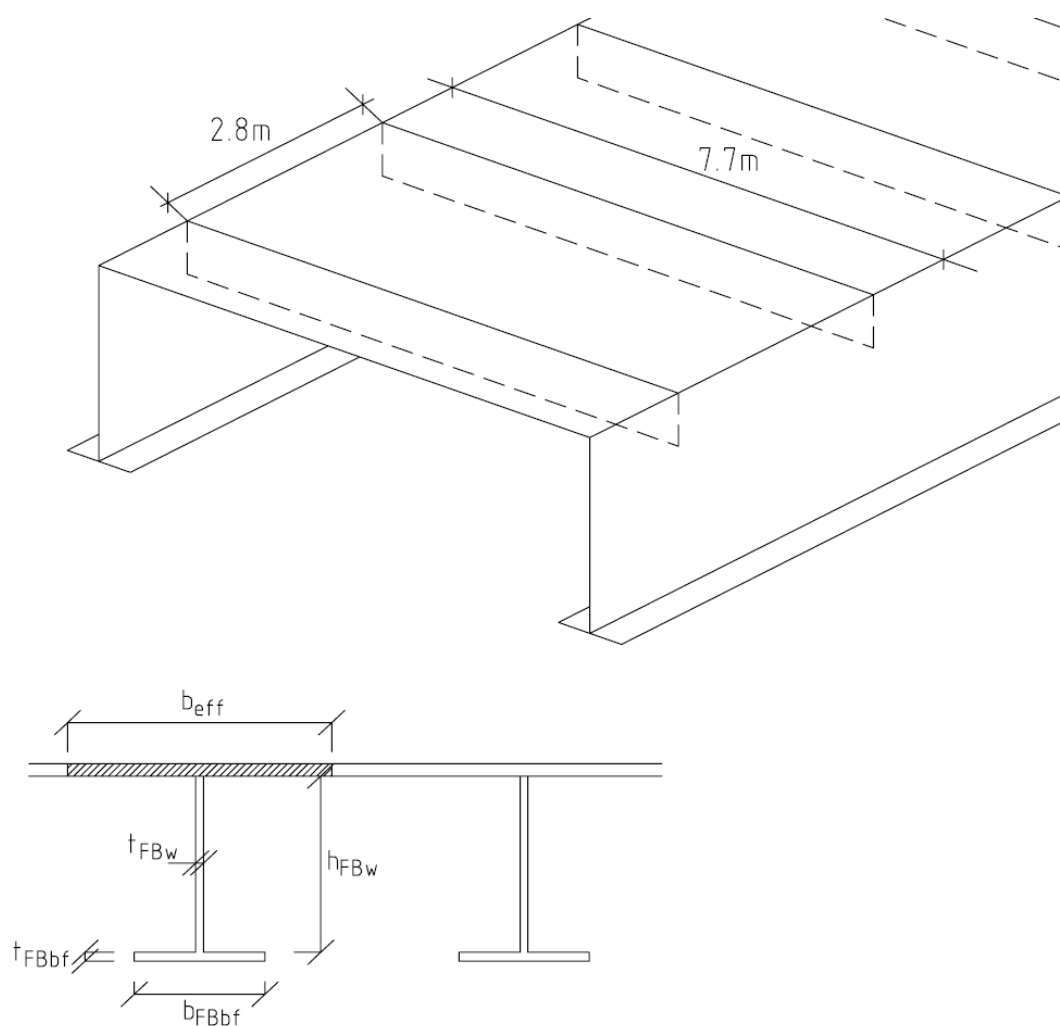
$t_{FBw} := 10mm$

$t_{FBbf} := 20mm$

$b_{FBbf} := 250mm$

$s_{FB} := 2800mm$

Calculations for floor beam 1 --> F.2

Floor beam 1 is located at the moment free joint connecting the two bascules to each other. This joint transfere shear force but no moment or normal force. As a consequened of this the floor beam stiffness will be calculated as usual but the spring stiffness will be multiplied with two, to account for the added stiffness of the second bascule.

$$h_{2FBw} := 650mm$$

Claculate the reduction factor for the web of the floor beam

$$\lambda_{2FBw} := \frac{\dfrac{h_{2FBw}}{t_{FBw}}}{28.4 \cdot \varepsilon_{FB} \cdot \sqrt{k_\sigma}} = 1.413$$

$$\rho_{2FBw} := \min\left[1, \; \left| \begin{array}{l} 1 \quad \text{if } \lambda_{2FBw} \le 0.673 \\[2mm] \dfrac{\lambda_{2FBw} - 0.055 \cdot (3 + \psi)}{\lambda_{2FBw}^2} \quad \text{otherwise} \end{array} \right. \right] = 0.598$$

$$h_{2FBw.eff} := \left| \begin{array}{l} h_{2FBw} \quad \text{if } \rho_{2FBw} \ge 0.5 \\[2mm] h_{2FBw} \cdot \rho_{2FBw} \quad \text{otherwise} \end{array} \right. = 650 \cdot mm$$

Claculate the reduction factor for the bottom flange of the floor beam

The bottom flange is a free edge and the conditions for a free edge when calculating rho are different

$$\lambda_{2FBbf} := \frac{\dfrac{b_{FBbf}}{t_{FBbf}}}{28.4 \cdot \varepsilon_{FB} \cdot \sqrt{k_\sigma}} = 0.272$$

$$\rho_{2FBbf} := \min\left(1, \; \left| \begin{array}{l} 1 \quad \text{if } \lambda_{2FBbf} \le 0.748 \\[2mm] \dfrac{\lambda_{2FBbf} - 0.188}{\lambda_{2FBbf}^2} \quad \text{otherwise} \end{array} \right. \right) = 1$$

$$b_{2FBbf.eff} := \left| \begin{array}{l} b_{FBbf} \quad \text{if } \rho_{2FBbf} \ge 0.5 \\[2mm] b_{FBbf} \cdot \rho_{2FBbf} \quad \text{otherwise} \end{array} \right. = 250 \cdot mm$$

Claculate the reduction factor for the effective part of the deck plate:

$$s_{edge} := 165\,mm$$

$$s_{FB1} := \frac{s_{FB}}{2} + s_{edge} = 1.565\,m$$

$$\lambda_{2FBdp} := \frac{\dfrac{s_{FB1}}{t_{dp}}}{28.4 \cdot \varepsilon_{420} \cdot \sqrt{k_\sigma}} = 2.624$$

$$\rho_{2FBdp} := \min\left(1,\ \left|\begin{array}{l} 1 \quad \text{if } \lambda_{2FBdp} \le 0.748 \\[2mm] \dfrac{\lambda_{2FBdp} - 0.188}{\lambda_{2FBdp}^{2}} \quad \text{otherwise} \end{array}\right.\right) = 0.354$$

$$b_{2eff} := \left|\begin{array}{l} s_{FB} \quad \text{if } \rho_{2FBdp} \ge 0.5 \\[2mm] s_{FB} \cdot \rho_{2FBdp} \quad \text{otherwise} \end{array}\right. = 990.594 \cdot mm$$

Calculate sectional properties for the effective section of the floor beam

$$A_{2FB} := t_{dp} \cdot b_{2eff} + t_{FBw} \cdot h_{2FBw} + t_{FBbf} \cdot b_{FBbf} = 0.02537\,m^{2}$$

$$z_{2FB} := \frac{\left[t_{dp} \cdot b_{2eff} \cdot \left(t_{FBbf} + h_{2FBw} + 0.5 \cdot t_{dp} \right) + t_{FBw} \cdot h_{2FBw} \cdot \left(t_{FBbf} + \dfrac{h_{2FBw}}{2} \right) + b_{FBbf} \cdot \dfrac{t_{FBbf}^{2}}{2} \right]}{A_{2FB}}$$

$$z_{2FB} = 0.46\,m$$

The neutral axis, z, is defined from the bottom of the cross-section.

$$\begin{aligned} I_{2FB} := {} & \frac{t_{FBw} \cdot h_{2FBw}^{3}}{12} + t_{dp} \cdot b_{2eff} \cdot \left(z_{2FB} - \frac{t_{dp}}{2} - h_{2FBw} - t_{FBbf} \right)^{2} \dots = 2.209 \times 10^{-3}\,m^{4} \\[2mm] & + \frac{t_{FBw} \cdot h_{2FBw}^{3}}{12} + t_{FBw} \cdot h_{2FBw} \cdot \left(z_{2FB} - \frac{h_{2FBw}}{2} - t_{FBbf} \right)^{2} \dots \\[2mm] & + \frac{b_{FBbf} \cdot t_{FBbf}^{3}}{12} + t_{FBbf} \cdot b_{FBbf} \cdot \left(z_{2FB} - \frac{t_{FBbf}}{2} \right)^{2} \end{aligned}$$

Calculate the spring stiffness of the floor beam

For floor beam 1 the spring stiffness will be multipied with 2 to account for the resistance of the second basculed of the bridge

$$F_{2FB} := \frac{P \cdot l_{fb}^{3}}{2 \cdot 48 \cdot E \cdot I_{2FB}} \cdot \frac{1}{kN} = 1.025 \times 10^{-5} \cdot \frac{m}{kN}$$

Calculations for floor beam 2 to 9 --> F.3

The heigth of the floor beams are varying between 600-740 mm. Also, the floor beam web has a loss of cross-section where the rib intersects. When calculating the spring stiffnesses for respective floor beam, an approximate height of the floor beam cross section is assumed to 650mm for floor beam 2-9.

$$h_{3FBw} := 650mm$$

Claculate the reduction factor for the web of the floor beam

$$\lambda_{3FBw} := \frac{\dfrac{h_{3FBw}}{t_{FBw}}}{28.4 \cdot \varepsilon_{FB} \cdot \sqrt{k_{\sigma}}} = 1.413$$

$$\rho_{3FBw} := \min\left[1, \; \begin{vmatrix} 1 & \text{if } \lambda_{3FBw} \le 0.673 \\ \dfrac{\lambda_{3FBw} - 0.055 \cdot (3 + \psi)}{\lambda_{3FBw}^{2}} & \text{otherwise} \end{vmatrix}\right] = 0.598$$

$$h_{3FBw.eff} := \begin{vmatrix} h_{3FBw} & \text{if } \rho_{3FBw} \ge 0.5 \\ h_{3FBw} \cdot \rho_{3FBw} & \text{otherwise} \end{vmatrix} = 650 \cdot mm$$

Calculate the reduction factor for the bottom flange of the floor beam

$$\lambda_{3FBbf} := \dfrac{\dfrac{b_{FBbf}}{t_{FBbf}}}{28.4 \cdot \varepsilon_{FB} \cdot \sqrt{k_\sigma}} = 0.272$$

$$\rho_{3FBbf} := \min\left(1, \begin{array}{|ll} 1 & \text{if } \lambda_{3FBbf} \le 0.748 \\[2mm] \dfrac{\lambda_{3FBbf} - 0.188}{\lambda_{3FBbf}^2} & \text{otherwise} \end{array}\right) = 1$$

$$b_{3FBbf.eff} := \begin{array}{|ll} b_{FBbf} & \text{if } \rho_{3FBbf} \ge 0.5 \\[2mm] b_{FBbf} \cdot \rho_{3FBbf} & \text{otherwise} \end{array} \quad = 250 \cdot mm$$

Calculate the reduction factor for the effective part of the deck plate:

$$\lambda_{3FBdp} := \dfrac{\dfrac{s_{FB}}{t_{dp}}}{28.4 \cdot \varepsilon_{420} \cdot \sqrt{k_\sigma}} = 4.695$$

$$\rho_{3FBdp} := \min\left[1, \begin{array}{|ll} 1 & \text{if } \lambda_{3FBdp} \le 0.673 \\[2mm] \dfrac{\lambda_{3FBdp} - 0.055 \cdot (3 + \psi)}{\lambda_{3FBdp}^2} & \text{otherwise} \end{array}\right] = 0.203$$

$$b_{3eff} := \begin{array}{|ll} s_{FB} & \text{if } \rho_{3FBdp} \ge 0.5 \\[2mm] s_{FB} \cdot \rho_{3FBdp} & \text{otherwise} \end{array} \quad = 568.453 \cdot mm$$

Calculate sectional properties for the effective section of the floor beam

$$A_{3FB} := t_{dp} \cdot b_{3eff} + t_{FBw} \cdot h_{3FBw} + t_{FBbf} \cdot b_{FBbf} = 0.01946 \, m^2$$

z defined from bottom of section:

$$z_{3FB} := \frac{\left[t_{dp} \cdot b_{3eff} \cdot \left(t_{FBbf} + h_{3FBw} + 0.5 \cdot t_{dp} \right) + t_{FBw} \cdot h_{3FBw} \cdot \left(t_{FBbf} + \frac{h_{3FBw}}{2} \right) + b_{FBbf} \cdot \frac{t_{FBbf}^2}{2} \right]}{A_{3FB}}$$

$$z_{3FB} = 0.395 \, m$$

$$
\begin{aligned}
I_{3FB} := \ & \frac{t_{FBw} \cdot h_{3FBw}^3}{12} + t_{dp} \cdot b_{3eff} \cdot \left(z_{3FB} - \frac{t_{dp}}{2} - h_{3FBw} - t_{FBbf} \right)^2 \ \dots = 1.848 \times 10^{-3} \, m^4 \\
& + \frac{t_{FBw} \cdot h_{3FBw}^3}{12} + t_{FBw} \cdot h_{3FBw} \cdot \left(z_{3FB} - \frac{h_{3FBw}}{2} - t_{FBbf} \right)^2 \ \dots \\
& + \frac{b_{FBbf} \cdot t_{FBbf}^3}{12} + t_{FBbf} \cdot b_{FBbf} \cdot \left(z_{3FB} - \frac{t_{FBbf}}{2} \right)^2
\end{aligned}
$$

Calculate the spring stiffness of the floor beam

$$F_{3FB} := \frac{P \cdot l_{fb}^3}{48 \cdot E \cdot I_{3FB}} \cdot \frac{1}{kN} = 2.451 \times 10^{-5} \cdot \frac{m}{kN}$$

Calculations for floor beam 10 --> F.4

The K-joint located at floor beam 10 and accordingly this section very stiff. The spring is therefore modelled as an undeformable support.

$$F_{4FB} := 0 \, \frac{m}{kN}$$

Calculations for end plate --> F.5

The end plate have a different section than the other floor beams. No bottom flange and it is located at the end of the deck which means it only has the deck plate as top flange on one side of the web.

$$t_{5FBw} := 12mm$$

$$h_{5FBw} := 400mm$$

$$s_{endplate} := \frac{s_{FB}}{2} = 1.4\,m$$

Claculate the reduction factor for the web of the end plate

$$\lambda_{5FBw} := \frac{\dfrac{h_{5FBw}}{t_{5FBw}}}{28.4 \cdot \varepsilon_{FB} \cdot \sqrt{k_\sigma}} = 0.725$$

$$\rho_{5FBw} := \min\left(1, \; \left| \begin{array}{l} 1 \quad \text{if } \lambda_{5FBw} \le 0.748 \\[2mm] \dfrac{\lambda_{5FBw} - 0.188}{\lambda_{5FBw}{}^2} \quad \text{otherwise} \end{array} \right. \right) = 1$$

$$h_{5FBw.eff} := \left| \begin{array}{l} h_{5FBw} \quad \text{if } \rho_{5FBw} \ge 0.5 \qquad = 400 \cdot mm \\[2mm] h_{5FBw} \cdot \rho_{5FBw} \quad \text{otherwise} \end{array} \right.$$

Claculate the reduction factor for the effective part of the deck plate:

$$\lambda_{5FBdp} := \frac{\dfrac{s_{endplate}}{t_{dp}}}{28.4 \cdot \varepsilon_{420} \cdot \sqrt{k_\sigma}} = 2.347$$

$$\rho_{5FBdp} := \min\left(1, \; \left| \begin{array}{l} 1 \quad \text{if } \lambda_{5FBdp} \le 0.748 \\[2mm] \dfrac{\lambda_{5FBdp} - 0.188}{\lambda_{5FBdp}{}^2} \quad \text{otherwise} \end{array} \right. \right) = 0.392$$

$$b_{5eff} := \left| \begin{array}{l} s_{endplate} \quad \text{if } \rho_{5FBdp} \ge 0.5 \qquad = 548.636 \cdot mm \\[2mm] s_{endplate} \cdot \rho_{5FBdp} \quad \text{otherwise} \end{array} \right.$$

Calculate sectional properties for the effective section of the floor beam

$$A_{5FB} := t_{dp} \cdot b_{5eff} + t_{5FBw} \cdot h_{5FBw} = 0.01248 \, m^2$$

$$z_{5FB} := \frac{t_{dp} \cdot b_{3eff} \cdot \left(h_{5FBw} + 0.5 \cdot t_{dp}\right) + t_{5FBw} \cdot h_{5FBw} \cdot \dfrac{h_{5FBw}}{2}}{A_{5FB}} = 0.336 \, m$$

$$\begin{aligned}I_{5FB} := &\frac{t_{5FBw} \cdot h_{5FBw}^{3}}{12} + t_{5FBw} \cdot h_{5FBw} \cdot \left(z_{5FB} - \frac{h_{5FBw}}{2}\right)^2 \, \ldots = 1.917 \times 10^{-4} \, m^4 \\ &+ \frac{b_{5eff} \cdot t_{dp}^{3}}{12} + t_{dp} \cdot b_{5eff} \cdot \left(z_{5FB} - \frac{t_{dp}}{2} - h_{5FBw}\right)^2\end{aligned}$$

Calculate the spring stiffness of the floor beam

$$F_{5FB} := \frac{P \cdot l_{fb}^{3}}{48 \cdot E \cdot I_{5FB}} \cdot \frac{1}{kN} = 2.362 \times 10^{-4} \cdot \frac{m}{kN}$$

Calculation of spring constants to use in GoBeam

$$F_{2FB} = 1.025 \times 10^{-5} \cdot \frac{m}{kN}$$

$$K_2 := \frac{1}{F_{2FB}} = 9.756 \times 10^4 \cdot \frac{N}{mm}$$

$$F_{3FB} = 2.451 \times 10^{-5} \cdot \frac{m}{kN}$$

$$K_3 := \frac{1}{F_{3FB}} = 4.081 \times 10^4 \cdot \frac{N}{mm}$$

$$F_{4FB} = 0$$

$$K_4 \qquad \text{Infinite}$$

$$F_{5FB} = 2.362 \times 10^{-4} \cdot \frac{m}{kN}$$

$$K_5 := \frac{1}{F_{5FB}} = 4.233 \times 10^3 \cdot \frac{N}{mm}$$

Modulus of elasticity, E

Beam: 21000 MPa
Columns: 21000 MPa

Beam end restraints _____

Left End	Right
Support ▼	Free ▼

Sway frame: ☐

Span №	1	2	3	4	5	6	6	6	6	6
Length, mm	865	2800	2800	2800	2800	2800	2800	2800	2800	2800
Moment of Inertia, mm⁴	9,60E+07	9,60E+07	9,60E+07	9,60E+07	9,60E+07	9,60E+07	9,60E+07	9,60E+07	9,60E+07	9,60E+07

Support №	1	2	3	4	5	6	7	7	7	7
Support coordinate, mm	0	865	3665	6465	9265	12065	14865	17665	20465	23265
Vertical spring constant, N/mm	4,23E+03		4,08E+04	4,08E+04	4,08E+04	4,08E+04	4,08E+04	4,08E+04	4,08E+04	4,08E+04
Support type or hinge	Roller	Roller	Roller	Roller	Roller	Roller	Roller	Roller	Roller	Roller
Column under Length, mm										
Moment of Inertia, mm⁴										
Column above Length, mm										
Moment of Inertia, mm⁴										
Induced support displacements, mm										

Positive loads: ↑ ↺

Load case: **Moving loads: OL-1**

Comment	Load Type	WA N or N/mm	WB N/mm	LA mm	LB mm
	P	-60000		12065	
	P	-60000		10865	

Moment, N-mm

-27538093

42317821

Type of Analysis: Force Envelope

Notes:

F:\Andrea\EXJOBB\,Rapport\,Main report\Appendix\Färdiga - ska namnges\6 - Comparison of response from hand calculations and FEM\2 - Hand_Calculation_GoBEAM.xlsb

Appendix 303

Load placed in span

Load placed in the span, one wheel in the centre of the span and one wheel 1.2m closer to the floor beam, position N in figure below. The stress values from Brigade/Plus and GoBeam are taken at in the centre of the span between floor beam 6 and 7. Linear stress distribution in the cross-section is assumed

Corss-sectional constants:

Here the cross-section is represented by one rib with the effective width of the deck plate as the top flange. The dimensions and constants are calculated in the hand calculations, MathCad. The hight of the cross-section is defined from the middle of the deck plate since it is the membrane stresses that are of interest

h =	0,247	m
I =	0,00009603	m^4
z =	0,065	m (from top)

Summary

	From Brigade/Plus	From GoBeam	
	4 Wheel loads	*2 point loads*	*2 lineloads (0.4m)*
Moment in section:	-	31,9 kNm	29,1 kNm
Shear force in section	-17,3 kN	-34,0 kN	-4,0 kN
Stresses at top flange	-12,1 MPa	-21,6 MPa	-19,7 MPa
Stresses at bottom	58,3 MPa	60,5 MPa	55,2 MPa
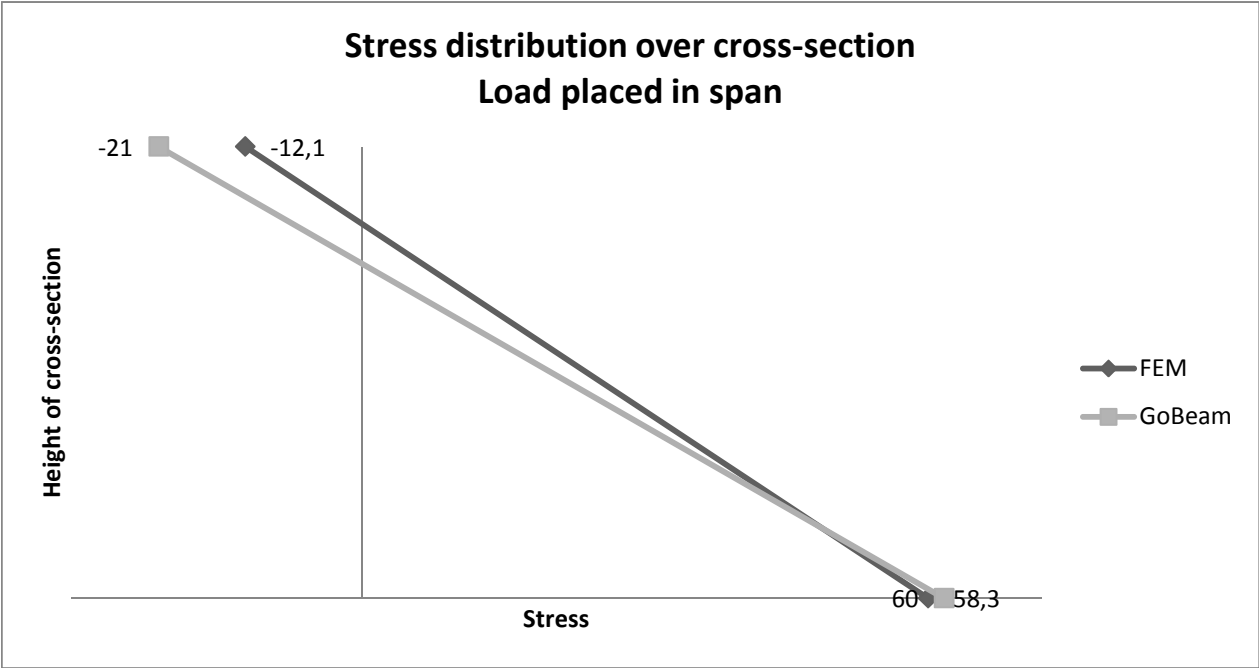
Calculations of normal stresses in top and bottom flange

Top flange:

x [m]	Bottom [Pa]	Top [Pa]	Membrane [Mpa]
0,000	-12001000	-8094480	-10,05
0,008	-11951400	-8447790	-10,20
0,016	-11905200	-8808830	-10,36
0,024	-11862100	-9178470	-10,52
0,032	-11821500	-9557680	-10,69
0,040	-11782900	-9947550	-10,87
0,048	-11745600	-10349300	-11,05
0,056	-11708900	-10764300	-11,24
0,063	-11671700	-11193800	-11,43
0,071	-11662200	-11615400	-11,64
0,080	-11767400	-11947600	-11,86
0,088	-12075300	-12098700	-12,09
0,096	-12614700	-12035700	-12,33
0,105	-13384200	-11760400	-12,57
0,113	-14382900	-11273700	-12,83
0,121	-15611900	-10574200	-13,09
0,129	-16483700	-9856520	-13,17
0,129	-3825140	-25550100	-14,69
0,162	-3183440	-22247200	-12,72
0,170	166085	-25404200	-12,62
0,178	3278700	-28340400	-12,53
0,186	6149790	-31051200	-12,45
0,202	11149700	-35778400	-12,31
0,211	13270200	-37786000	-12,26
0,219	15132700	-39551300	-12,21
0,259	20475600	-44636300	-12,08
0,267	20736600	-44890800	-12,08
0,275	20726100	-44888700	-12,08
0,284	20444200	-44630100	-12,09
0,292	19891200	-44115400	-12,11
0,300	19068300	-43345700	-12,14
0,308	17976900	-42322600	-12,17
0,316	16618900	-41048100	-12,21
0,324	14996800	-39524800	-12,26
0,332	13113500	-37755700	-12,32
0,340	10972200	-35744200	-12,39
0,348	8576690	-33494100	-12,46
0,357	5930930	-31009600	-12,54
0,365	3039230	-28295300	-12,63
0,373	-93946	-25355600	-12,72
0,381	-3463940	-22195400	-12,83
0,389	-7066140	-18819400	-12,94
0,397	-10896300	-15231900	-13,06
0,405	-14951200	-11433000	-13,19

Bottom flange:

x [m]	Bottom [Pa]	Top [Pa]	Membrane [Mpa]
0,000	5,81E+07	6,08E+07	59,47
0,008	5,77E+07	6,07E+07	59,23
0,016	5,73E+07	6,04E+07	58,86
0,024	5,69E+07	6,02E+07	58,53
0,033	5,66E+07	5,99E+07	58,24
0,041	5,63E+07	5,97E+07	58,00
0,049	5,60E+07	5,96E+07	57,80
0,057	5,58E+07	5,95E+07	57,64
0,065	5,56E+07	5,94E+07	57,53
0,074	5,55E+07	5,94E+07	57,46
0,082	5,55E+07	5,94E+07	57,42
0,090	5,54E+07	5,94E+07	57,43
0,098	5,54E+07	5,95E+07	57,48
0,106	5,55E+07	5,96E+07	57,57
0,114	5,56E+07	5,98E+07	57,70
0,123	5,58E+07	6,00E+07	57,87
0,131	5,59E+07	6,02E+07	58,09
0,139	5,62E+07	6,05E+07	58,34
0,147	5,65E+07	6,08E+07	58,64
0,155	5,68E+07	6,12E+07	58,98
0,163	5,72E+07	6,16E+07	59,37
0,172	5,76E+07	6,20E+07	59,80
0,180	5,80E+07	6,22E+07	60,09
σ_mean			58,33

0,413	-16941200	-9701900	-13,32
0,413	-5066380	-24591900	-14,83
0,422	-16164900	-10345200	-13,26
0,430	-14914800	-11080600	-13,00
0,438	-13895100	-11603200	-12,75
0,446	-13104400	-11914700	-12,51
0,455	-12543800	-12014000	-12,28
0,463	-12214600	-11899300	-12,06
0,471	-12088200	-11603200	-11,85
0,479	-12077100	-11217100	-11,65
0,487	-12093800	-10822600	-11,46
0,495	-12110100	-10442900	-11,28
0,503	-12126900	-10076400	-11,10
0,511	-12145100	-9721960	-10,93
0,519	-12165200	-9378200	-10,77
0,527	-12188000	-9044080	-10,62
0,535	-12213800	-8718620	-10,47
0,543	-12243000	-8400940	-10,32
σ_mean			-12,07

Stresses in top flange over the effective width
Load placed in span

Stresses in bottom flange
Load placed in the span

Stresses in bottom flange
Load placed in the span
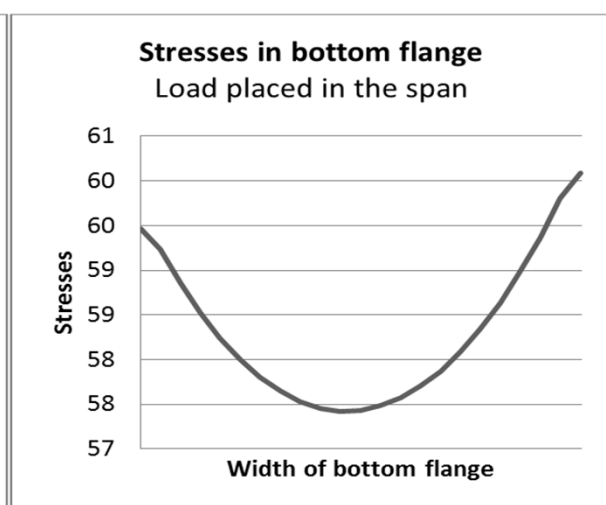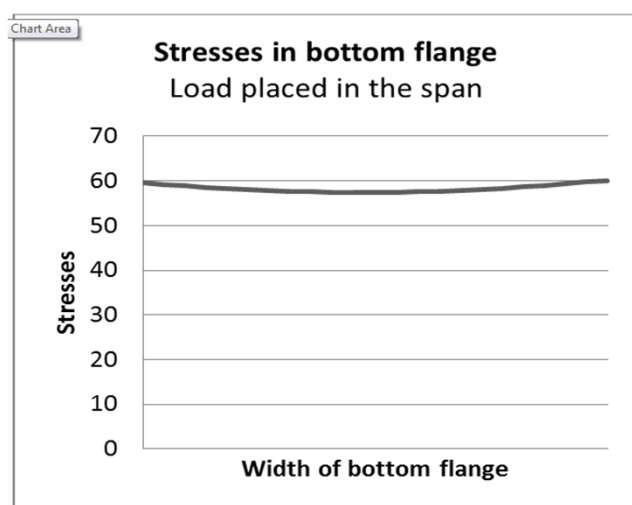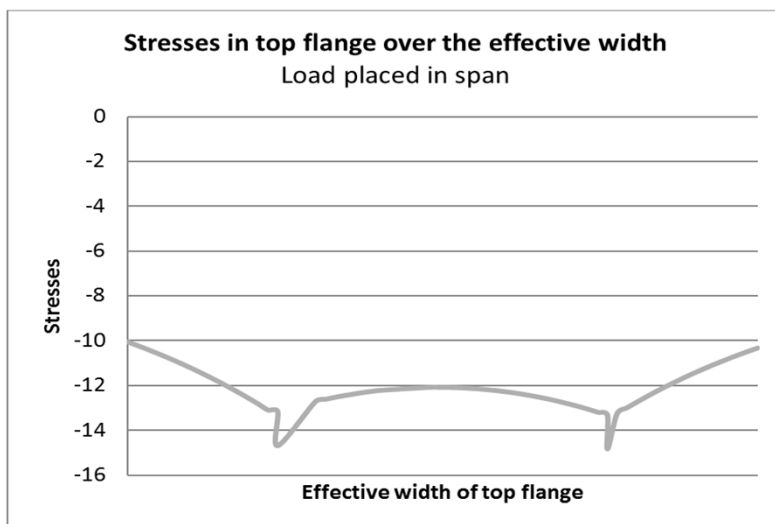
Calculations of shear force in top and bottom flange

For the shear stresses the S22 stress component is used in a path in each rib wall in the centre of the span, directly beneath the load

t_rib=   0,006 m

Rib wall 7.1

y [m]	Bottom [Pa]	Top [Pa]	Membrane	F_element
0	2,30E+07	-4,74E+07	-12161750	-591,0
0,0081	2,24E+07	-4,63E+07	-11954600	-580,9
0,0162	2,12E+07	-4,42E+07	-11534750	-560,5
0,0243	1,99E+07	-4,21E+07	-11105800	-539,6
0,0324	1,88E+07	-4,01E+07	-10669250	-518,4
0,0405	1,76E+07	-3,81E+07	-10225300	-496,9
0,0486	1,65E+07	-3,61E+07	-9774300	-474,9
0,0567	1,54E+07	-3,41E+07	-9316800	-452,7
0,0648	1,44E+07	-3,21E+07	-8853600	-430,2
0,0729	1,34E+07	-3,02E+07	-8385650	-407,5
0,081	1,24E+07	-2,83E+07	-7914150	-384,6
0,0891	1,15E+07	-2,64E+07	-7440150	-361,5
0,0972	1,06E+07	-2,45E+07	-6965050	-338,5
0,1053	9,67E+06	-2,26E+07	-6490200	-315,3
0,1134	8,79E+06	-2,08E+07	-6016975	-292,4
0,1215	7,92E+06	-1,90E+07	-5546820	-269,5
0,1296	7,07E+06	-1,72E+07	-5081130	-246,9
0,1377	6,24E+06	-1,55E+07	-4621315	-224,6
0,1458	5,41E+06	-1,37E+07	-4168845	-202,6
0,1539	4,58E+06	-1,20E+07	-3725125	-181,0
0,162	3,76E+06	-1,03E+07	-3291630	-159,9
0,1701	2,95E+06	-8,68E+06	-2869690	-139,4
0,1782	2,13E+06	-7,05E+06	-2460820	-119,6
0,1863	1,31E+06	-5,44E+06	-2066440	-100,4
0,1944	478228	-3,85E+06	-1688001	-82,0
0,2025	-356927	-2,30E+06	-1326988,5	-64,5
0,2106	-1,21E+06	-7,63E+05	-984778,5	-47,9
0,2187	-2,36E+06	1,09E+06	-634760	-30,8
0,2268			**Tot**	**-8614,1**

Rib wall 7.2

y [m]	Bottom [Pa]	Top [Pa]	Membrane	F_element
0	1,93E+07	-4,38E+07	-12252950	-595,4
0,0081	1,88E+07	-4,29E+07	-12044900	-585,3
0,0162	1,78E+07	-4,10E+07	-11623450	-564,8
0,0243	1,68E+07	-3,92E+07	-11192800	-543,9
0,0324	1,59E+07	-3,74E+07	-10754600	-522,6
0,0405	1,50E+07	-3,56E+07	-10308950	-500,9
0,0486	1,41E+07	-3,38E+07	-9856200	-478,9
0,0567	1,33E+07	-3,21E+07	-9396900	-456,6
0,0648	1,25E+07	-3,04E+07	-8931900	-434,0
0,0729	1,17E+07	-2,86E+07	-8462150	-411,2
0,081	1,10E+07	-2,70E+07	-7988700	-388,2
0,0891	1,03E+07	-2,53E+07	-7512850	-365,1
0,0972	9,60E+06	-2,37E+07	-7035860	-341,9
0,1053	8,94E+06	-2,21E+07	-6559090	-318,7
0,1134	8,30E+06	-2,05E+07	-6083900	-295,6
0,1215	7,68E+06	-1,89E+07	-5611730	-272,7
0,1296	7,07E+06	-1,74E+07	-5144000	-250,0
0,1377	6,47E+06	-1,58E+07	-4682125	-227,5
0,1458	5,88E+06	-1,43E+07	-4227585	-205,4
0,1539	5,30E+06	-1,29E+07	-3781785	-183,8
0,162	4,72E+06	-1,14E+07	-3346135	-162,6
0,1701	4,14E+06	-9,99E+06	-2922040	-142,0
0,1782	3,56E+06	-8,59E+06	-2510985	-122,0
0,1863	2,98E+06	-7,21E+06	-2114395	-102,7
0,1944	2,39E+06	-5,86E+06	-1733725	-84,2
0,2025	1,80E+06	-4,54E+06	-1370455	-66,6
0,2106	1,19E+06	-3,24E+06	-1025970	-49,8
0,2187			**Tot**	**-8672,4**

Shear stresses in rib walls
Load placed in span

Rib wall 7.1
Rib wall 7.2
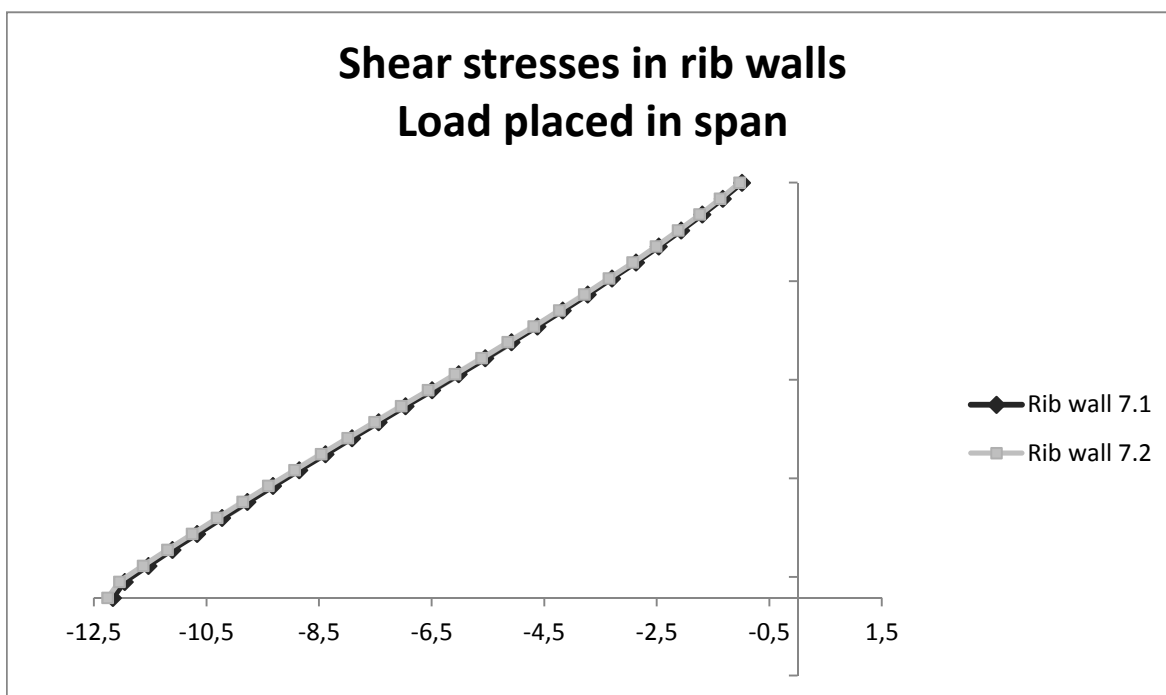
Stress distribution in top flange for one wheel load in span

Path in deck plate. First x-value is one node away from the right main girder and the last one node from the left main girder.
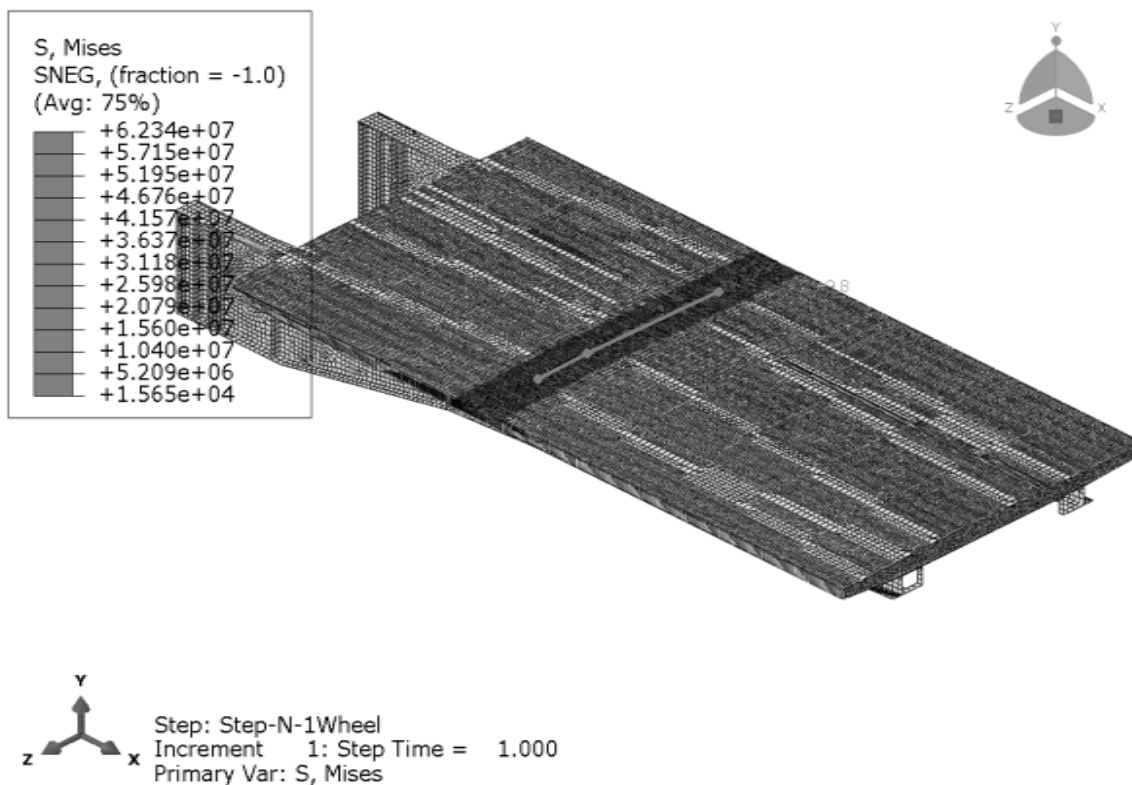
Note: The second axle is included
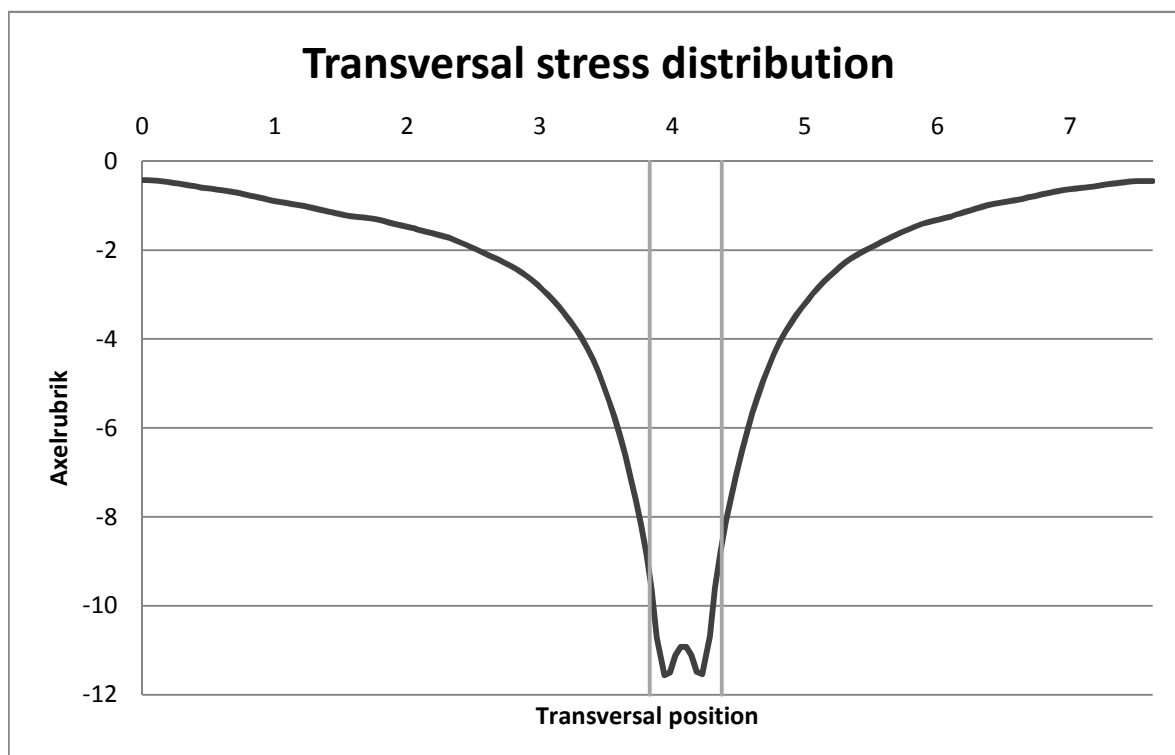
Span - Top Flange - One wheel

x	S11-Bottom	S11-Top	Membrane, [Mpa]
0,000	-665042	-181423	-0,42
0,039	-556492	-301165	-0,43
0,116	-342342	-542277	-0,44
0,155	-339884	-568502	-0,45
0,195	-418151	-522350	-0,47
0,236	-474352	-500563	-0,49
0,276	-531879	-479248	-0,51
0,317	-590317	-459087	-0,52
0,357	-648982	-440419	-0,54
0,398	-707727	-423551	-0,57
0,438	-799194	-376431	-0,59
0,481	-807968	-404631	-0,61
0,524	-703722	-540756	-0,62
0,567	-600066	-678146	-0,64
0,609	-497432	-816408	-0,66
0,652	-396569	-954413	-0,68
0,695	-423697	-972274	-0,70
0,735	-542957	-904750	-0,72
0,776	-626313	-871988	-0,75
0,816	-711087	-839154	-0,78
0,857	-796866	-806443	-0,80
0,898	-882684	-775357	-0,83
0,938	-968175	-745693	-0,86
0,979	-1088890	-682625	-0,89
1,021	-1107790	-712371	-0,91
1,064	-990945	-869895	-0,93
1,107	-874173	-1028460	-0,95
1,149	-757521	-1187240	-0,97
1,192	-641548	-1345670	-0,99
1,235	-662015	-1374760	-1,02
1,275	-781241	-1312240	-1,05
1,316	-861514	-1286380	-1,07
1,357	-942401	-1259180	-1,10
1,397	-1024080	-1231390	-1,13
1,438	-1105130	-1203840	-1,15
1,478	-1185500	-1176990	-1,18
1,519	-1296700	-1119740	-1,21
1,562	-1305050	-1153730	-1,23
1,604	-1180770	-1311080	-1,25
1,647	-1056010	-1467980	-1,26
1,690	-930825	-1624170	-1,28
1,732	-805673	-1778850	-1,29
1,775	-808134	-1816610	-1,31
1,816	-974408	-1709320	-1,34
1,856	-1174570	-1570370	-1,37

1,897	-1374580	-1429930	-1,40
1,937	-1574210	-1288670	-1,43
1,978	-1771940	-1147700	-1,46
2,018	-1967730	-1008370	-1,49
2,059	-2187000	-836031	-1,51
2,062	-2255150	-803546	-1,53
2,148	-1842620	-1334160	-1,59
2,191	-1601850	-1642660	-1,62
2,234	-1360770	-1951420	-1,66
2,277	-1120500	-2259070	-1,69
2,320	-1114440	-2347740	-1,73
2,361	-1296720	-2264800	-1,78
2,401	-1433800	-2227680	-1,83
2,442	-1572960	-2190160	-1,88
2,483	-1714690	-2153410	-1,93
2,523	-1857350	-2118760	-1,99
2,564	-2001840	-2087120	-2,04
2,604	-2206980	-2002550	-2,10
2,647	-2280160	-2046150	-2,16
2,690	-2165020	-2274470	-2,22
2,732	-2053460	-2507860	-2,28
2,775	-1946000	-2745900	-2,35
2,818	-1845100	-2988740	-2,42
2,860	-1940620	-3055710	-2,50
2,901	-2169590	-3005800	-2,59
2,942	-2342980	-3020690	-2,68
2,982	-2524280	-3041220	-2,78
3,023	-2713440	-3069790	-2,89
3,063	-2910970	-3108100	-3,01
3,104	-3117150	-3157760	-3,14
3,144	-3396250	-3163110	-3,28
3,187	-3549680	-3318440	-3,43
3,230	-3515320	-3683850	-3,60
3,272	-3495020	-4068100	-3,78
3,315	-3490390	-4473610	-3,98
3,358	-3502190	-4902110	-4,20
3,401	-4136240	-4781190	-4,46
3,441	-5163880	-4331230	-4,75
3,482	-5977220	-4132250	-5,05
3,522	-6814220	-3967780	-5,39
3,563	-7681020	-3840630	-5,76
3,603	-8586620	-3748760	-6,17
3,644	-9542180	-3692680	-6,62
3,685	-10945100	-3282400	-7,11
3,724	-11624000	-3635170	-7,63
3,764	-11223600	-5141790	-8,18
3,803	-10944600	-6733190	-8,84
3,843	-10752700	-8500020	-9,63

3,883	-11971000	-9464070	-10,72
3,941	-10661600	-12470100	-11,57
3,981	13819	-23028600	-11,51
4,022	13068000	-35305500	-11,12
4,062	19739100	-41585400	-10,92
4,103	19734700	-41576200	-10,92
4,144	13065300	-35287000	-11,11
4,184	23973	-23010100	-11,49
4,225	-10621000	-12464000	-11,54
4,283	-11900600	-9469220	-10,68
4,322	-10676100	-8495900	-9,59
4,362	-10870700	-6715430	-8,79
4,402	-11158900	-5107120	-8,13
4,441	-11569800	-3582370	-7,58
4,481	-10897300	-3214310	-7,06
4,522	-9483810	-3619390	-6,55
4,562	-8507060	-3679140	-6,09
4,603	-7580370	-3772840	-5,68
4,643	-6691560	-3902460	-5,30
4,684	-5835320	-4066400	-4,95
4,724	-5003370	-4265450	-4,63
4,765	-3962880	-4713200	-4,34
4,808	-3329280	-4819220	-4,07
4,850	-3327990	-4368550	-3,85
4,893	-3344380	-3941070	-3,64
4,936	-3375610	-3534340	-3,45
4,978	-3421420	-3145990	-3,28
5,021	-3262900	-2983610	-3,12
5,062	-2965050	-2981760	-2,97
5,102	-2745670	-2929410	-2,84
5,143	-2535300	-2886910	-2,71
5,183	-2332230	-2852730	-2,59
5,224	-2137960	-2825860	-2,48
5,264	-1951100	-2805170	-2,38
5,305	-1701440	-2855730	-2,28
5,348	-1598280	-2781850	-2,19
5,390	-1707610	-2516480	-2,11
5,433	-1822190	-2256020	-2,04
5,476	-1942300	-2000730	-1,97
5,519	-2065610	-1751170	-1,91
5,561	-2004940	-1684340	-1,84
5,602	-1808780	-1750280	-1,78
5,642	-1664880	-1773330	-1,72
5,683	-1522410	-1800620	-1,66
5,724	-1381740	-1831290	-1,61
5,764	-1243850	-1864390	-1,55
5,805	-1109170	-1898680	-1,50
5,845	-920064	-1991220	-1,46

5,883	-866611	-1961220	-1,41
5,926	-1011440	-1743930	-1,38
5,970	-1165220	-1519870	-1,34
6,014	-1320270	-1297810	-1,31
6,058	-1476500	-1078900	-1,28
6,101	-1453170	-1033630	-1,24
6,138	-1296600	-1115180	-1,21
6,174	-1190290	-1152820	-1,17
6,210	-1084460	-1191960	-1,14
6,246	-979105	-1232860	-1,11
6,283	-876144	-1273760	-1,07
6,317	-777279	-1314020	-1,05
6,351	-681481	-1353340	-1,02
6,385	-530990	-1442550	-0,99
6,428	-503853	-1414690	-0,96
6,471	-654008	-1217890	-0,94
6,514	-805616	-1021300	-0,91
6,556	-958341	-825826	-0,89
6,599	-1111490	-632067	-0,87
6,642	-1091380	-603045	-0,85
6,682	-946814	-688559	-0,82
6,723	-852316	-727061	-0,79
6,763	-757705	-768091	-0,76
6,804	-662833	-810827	-0,74
6,844	-569675	-854526	-0,71
6,885	-478337	-897769	-0,69
6,926	-334982	-990658	-0,66
6,968	-304374	-979662	-0,64
7,011	-437457	-814096	-0,63
7,054	-572849	-648889	-0,61
7,096	-709219	-484942	-0,60
7,139	-846474	-322862	-0,58
7,182	-841162	-296354	-0,57
7,222	-733413	-363685	-0,55
7,263	-668715	-391171	-0,53
7,303	-604028	-420822	-0,51
7,344	-539776	-452770	-0,50
7,385	-476752	-485923	-0,48
7,425	-415036	-520109	-0,47
7,466	-325599	-583838	-0,45
7,505	-338797	-556344	-0,45
7,545	-482858	-408921	-0,45
7,585	-628247	-262691	-0,45
7,624	-775475	-116914	-0,45

Stress distribution in top flange for two wheels placed in span

Path in deck plate. First x-value is one node away from the right main girder and the last one node from the left main girder.
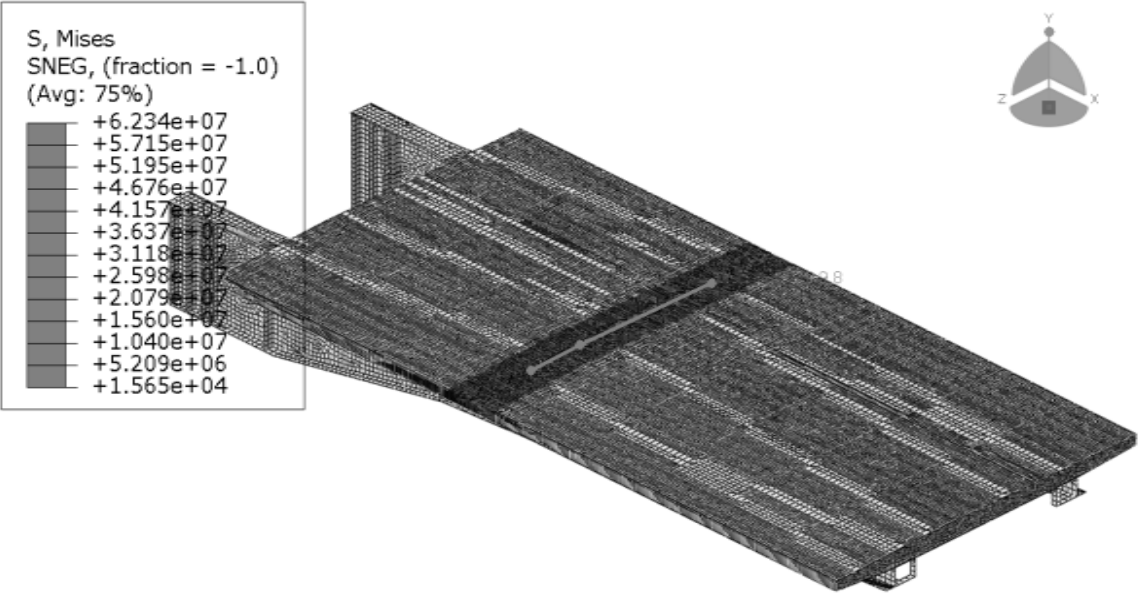
Note: The second axle is included
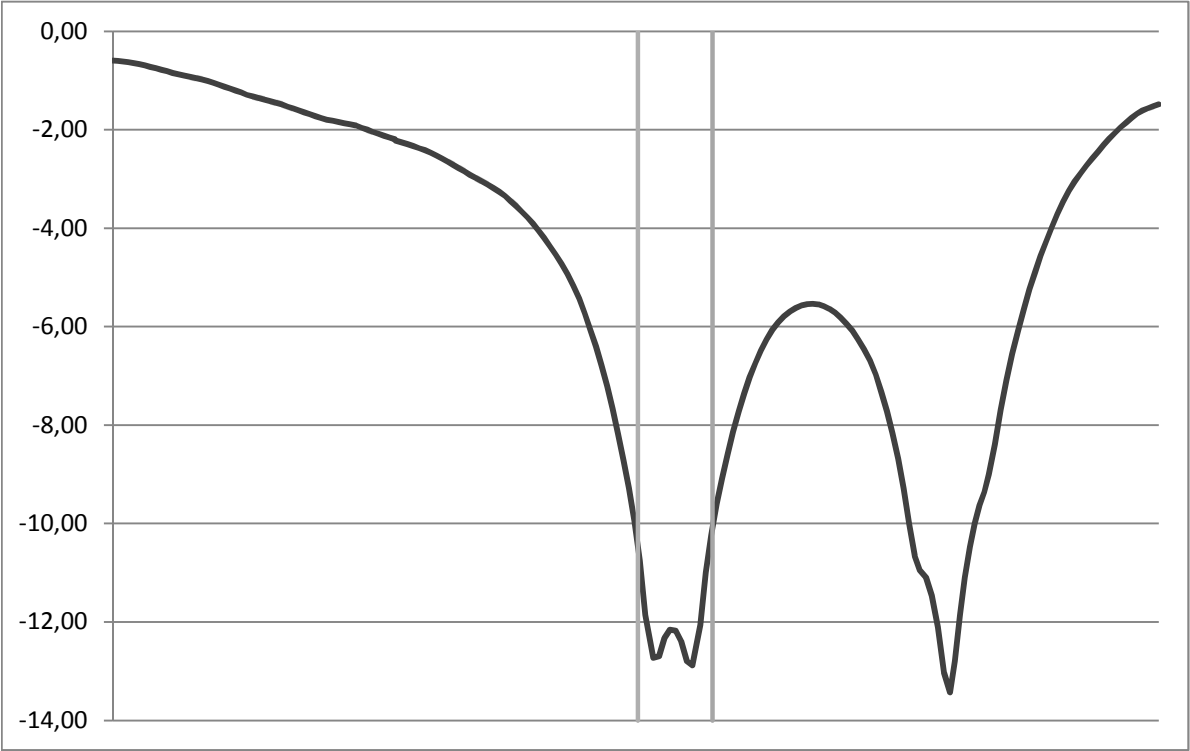
Span - Top Flange - Two wheels

x	S11-Bottom	S11-Top	Membrane, [Mpa]
0,000	-922298	-264309	-0,59
0,039	-774694	-431481	-0,60
0,116	-483497	-768079	-0,63
0,155	-482739	-805863	-0,64
0,195	-594488	-743073	-0,67
0,236	-676319	-713520	-0,69
0,276	-759988	-684658	-0,72
0,317	-844958	-657415	-0,75
0,357	-930255	-632247	-0,78
0,398	-1015700	-609575	-0,81
0,438	-1145540	-545831	-0,85
0,481	-1158640	-588407	-0,87
0,524	-1013900	-781630	-0,90
0,567	-870004	-976623	-0,92
0,609	-727549	-1172840	-0,95
0,652	-587537	-1368720	-0,98
0,695	-626614	-1396570	-1,01
0,735	-795381	-1304360	-1,05
0,776	-914688	-1260120	-1,09
0,816	-1035960	-1215830	-1,13
0,857	-1158640	-1171740	-1,17
0,898	-1281350	-1129890	-1,21
0,938	-1403610	-1090010	-1,25
0,979	-1574520	-1003920	-1,29
1,021	-1602130	-1048420	-1,33
1,064	-1439580	-1271890	-1,36
1,107	-1277090	-1496760	-1,39
1,149	-1114730	-1721900	-1,42
1,192	-953270	-1946490	-1,45
1,235	-983298	-1989580	-1,49
1,275	-1152880	-1903260	-1,53
1,316	-1268730	-1867520	-1,57
1,357	-1385390	-1829880	-1,61
1,397	-1503070	-1791380	-1,65
1,438	-1619830	-1753160	-1,69
1,478	-1735540	-1715820	-1,73
1,519	-1893670	-1636380	-1,77
1,562	-1905870	-1686180	-1,80
1,604	-1731140	-1909550	-1,82
1,647	-1555600	-2132170	-1,84
1,690	-1379340	-2353660	-1,87
1,732	-1202930	-2572910	-1,89
1,775	-1206220	-2627070	-1,92
1,816	-1437890	-2478680	-1,96
1,856	-1714810	-2287720	-2,00

1,897	-1991350	-2094540	-2,04
1,937	-2267160	-1899990	-2,08
1,978	-2540130	-1705600	-2,12
2,018	-2810180	-1513180	-2,16
2,059	-3113840	-1273930	-2,19
2,062	-3207790	-1226860	-2,22
2,148	-2630590	-1950930	-2,29
2,191	-2293440	-2371290	-2,33
2,234	-1955430	-2791510	-2,37
2,277	-1618020	-3209690	-2,41
2,320	-1602990	-3325580	-2,46
2,361	-1847940	-3203730	-2,53
2,401	-2030860	-3143720	-2,59
2,442	-2215950	-3082430	-2,65
2,483	-2403790	-3021410	-2,71
2,523	-2592070	-2962440	-2,78
2,564	-2781940	-2906670	-2,84
2,604	-3052520	-2778070	-2,92
2,647	-3137450	-2825860	-2,98
2,690	-2961050	-3126590	-3,04
2,732	-2788120	-3432740	-3,11
2,775	-2619250	-3743540	-3,18
2,818	-2457690	-4059070	-3,26
2,860	-2561470	-4133970	-3,35
2,901	-2849250	-4044410	-3,45
2,942	-3063810	-4036810	-3,55
2,982	-3286910	-4034510	-3,66
3,023	-3518140	-4040490	-3,78
3,063	-3757930	-4057050	-3,91
3,104	-4006200	-4086100	-4,05
3,144	-4343620	-4055660	-4,20
3,187	-4504010	-4222270	-4,36
3,230	-4409250	-4662670	-4,54
3,272	-4328440	-5122860	-4,73
3,315	-4264010	-5604890	-4,93
3,358	-4216390	-6110410	-5,16
3,401	-4866400	-5995300	-5,43
3,441	-5962440	-5503390	-5,73
3,482	-6819500	-5286010	-6,05
3,522	-7700900	-5103500	-6,40
3,563	-8613030	-4958620	-6,79
3,603	-9564410	-4850000	-7,21
3,644	-10566000	-4778410	-7,67
3,685	-12038900	-4330210	-8,18
3,724	-12734800	-4694510	-8,71
3,764	-12274700	-6285320	-9,28
3,803	-11936900	-7961730	-9,95
3,843	-11687100	-9814610	-10,75

3,883	-12842100	-10875600	-11,86
3,941	-11548500	-13909900	-12,73
3,981	-951773	-24436900	-12,69
4,022	12046000	-36701800	-12,33
4,062	18659600	-42970400	-12,16
4,103	18595900	-42950600	-12,18
4,144	11866600	-36652700	-12,39
4,184	-1236030	-24369000	-12,80
4,225	-11964800	-13803200	-12,88
4,283	-13263900	-10856400	-12,06
4,322	-11981000	-10002100	-10,99
4,362	-12125400	-8331430	-10,23
4,402	-12365300	-6834710	-9,60
4,441	-12730600	-5423700	-9,08
4,481	-12108400	-5083480	-8,60
4,522	-10808800	-5461710	-8,14
4,562	-9916420	-5528710	-7,72
4,603	-9077980	-5632550	-7,36
4,643	-8280900	-5776100	-7,03
4,684	-7520160	-5958800	-6,74
4,724	-6787030	-6182300	-6,48
4,765	-5877480	-6634740	-6,26
4,808	-5309630	-6818870	-6,06
4,850	-5281020	-6547190	-5,91
4,893	-5276050	-6306390	-5,79
4,936	-5293140	-6093420	-5,69
4,978	-5332860	-5905670	-5,62
5,021	-5341330	-5796080	-5,57
5,062	-5343930	-5739840	-5,54
5,102	-5393120	-5681550	-5,54
5,143	-5461080	-5643500	-5,55
5,183	-5547030	-5626900	-5,59
5,224	-5651020	-5633600	-5,64
5,264	-5771220	-5665950	-5,72
5,305	-5880830	-5752550	-5,82
5,348	-5908300	-5968740	-5,94
5,390	-5880320	-6288390	-6,08
5,433	-5877930	-6635920	-6,26
5,476	-5912660	-7001870	-6,46
5,519	-5998480	-7373270	-6,69
5,561	-7081530	-6869900	-6,98
5,602	-8757570	-5895710	-7,33
5,642	-10092800	-5344000	-7,72
5,683	-11478800	-4850330	-8,16
5,724	-12882000	-4480030	-8,68
5,764	-14253200	-4317880	-9,29
5,805	-15541900	-4455270	-10,00
5,845	-14597300	-6722120	-10,66

5,883	-6865880	-15040000	-10,95
5,926	3223030	-25413900	-11,10
5,970	7286600	-30219200	-11,47
6,014	3817920	-28019700	-12,10
6,058	-6947790	-19101700	-13,02
6,101	-13752500	-13109100	-13,43
6,138	-7040810	-18539700	-12,79
6,174	3341420	-27060500	-11,86
6,210	8895800	-31084800	-11,09
6,246	9391800	-30348100	-10,48
6,283	5441820	-25429900	-9,99
6,317	-1037360	-18219400	-9,63
6,351	-8245440	-10471700	-9,36
6,385	-11924900	-6074200	-9,00
6,428	-11754000	-5023160	-8,39
6,471	-11277500	-4115240	-7,70
6,514	-10726900	-3452660	-7,09
6,556	-10163600	-2943570	-6,55
6,599	-9631370	-2513820	-6,07
6,642	-8463030	-2799490	-5,63
6,682	-7142140	-3328150	-5,24
6,723	-6354880	-3415780	-4,89
6,763	-5605000	-3514970	-4,56
6,804	-4879130	-3633450	-4,26
6,844	-4177800	-3772280	-3,98
6,885	-3494940	-3930760	-3,71
6,926	-2641690	-4283260	-3,46
6,968	-2237430	-4248550	-3,24
7,011	-2461040	-3649410	-3,06
7,054	-2700160	-3067160	-2,88
7,096	-2951030	-2502110	-2,73
7,139	-3214050	-1952760	-2,58
7,182	-3088150	-1796730	-2,44
7,222	-2705940	-1900960	-2,30
7,263	-2471020	-1885260	-2,18
7,303	-2242370	-1880580	-2,06
7,344	-2020100	-1886640	-1,95
7,385	-1806170	-1900660	-1,85
7,425	-1600210	-1921680	-1,76
7,466	-1306790	-2043290	-1,68
7,505	-1309530	-1909740	-1,61
7,545	-1700460	-1425870	-1,56
7,585	-2097540	-948055	-1,52
7,624	-2501970	-474182	-1,49

Load placed above Floor beam

One axis placed centred above the floor beam, the second axis 1.2m out in the span, see figure below. The stress values from Brigade/Plus are taken at the intersection with the floor beam. The moment and shear force are at floor beam 6 for both the GoBeam analysis and the results from Brigade/Plus. It is assumed that the distribution between top and bottom moment is linear.

Corss-sectional constants:

Here the cross-section is represented by one rib with the effective width of the deck plate as the top flange. The dimensions and constants are calculated in the hand calculations, MathCad. The hight of the cross-section is defined from the middle of the deck plate since it is the membrane stresses that are of interest

$h =$ 0,247   m
$I =$ 0,00009603   m^4
$z =$ 0,065   m (from top)

Summary

	From Brigade/Plus		From GoBeam	
	4 Wheel loads		*2 point loads*	*2 lineloads (0.4m)*
Moment in section:	-	-	-11,9 kNm	-14,5 kNm
Shear force in section	-28,8	kN	-34,0 kN	-63,9 kN
Stresses at top	1,1	MPa	8,0 MPa	9,8 MPa
Stresses at bottom	-8,8	MPa	-22,5 MPa	-27,5 MPa

Stress distribution over cross-section
Load placed above floor beam

Height of cross-section

1,1 8

-22 -8,8

Stress

FEM
GoBeam
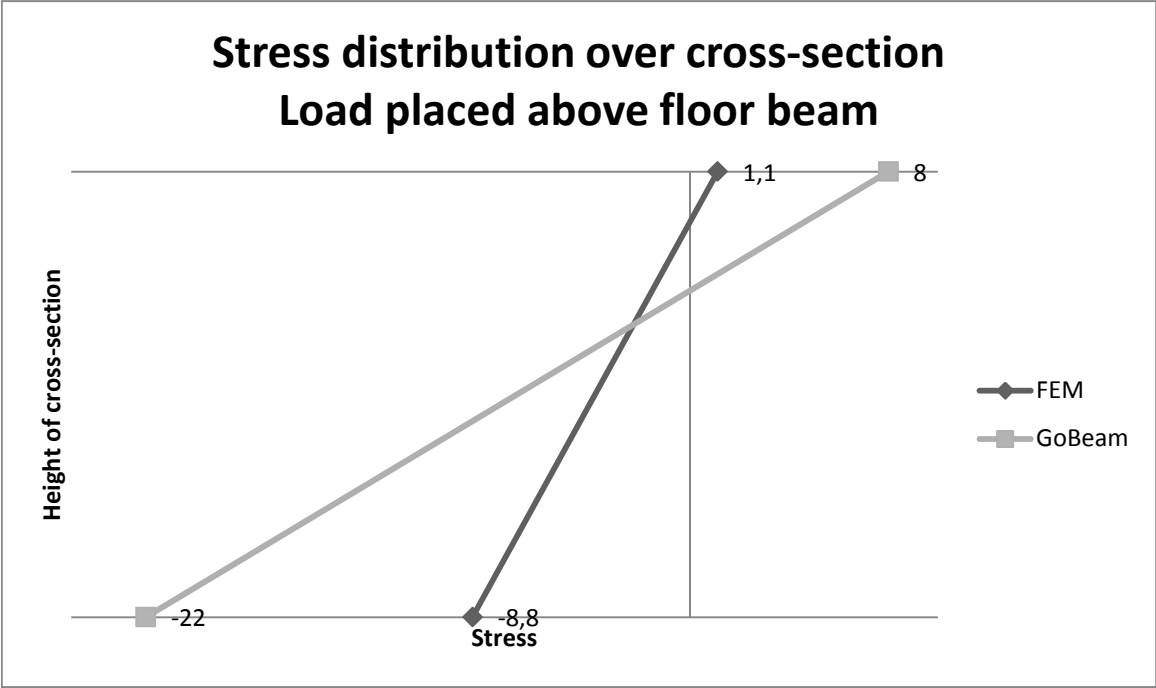
Calculations of forces in top and bottom flange

Top flange:

x [m]	Bottom [Pa]	Top [Pa]	Membrane [Mpa]
0,000	865893	-6115920	-2,63
0,008	1335620	-6330260	-2,50
0,016	1835930	-6552160	-2,36
0,024	2366660	-6778870	-2,21
0,032	2903210	-6982850	-2,04
0,040	3426840	-7137140	-1,86
0,048	3942350	-7241990	-1,65
0,056	4414430	-7249480	-1,42
0,063	4792000	-3867440	0,46
0,071	5012550	-3857840	0,58
0,080	4849970	-4010910	0,42
0,088	3935630	-3926800	0,00
0,096	-3548080	-481119	-2,01
0,105	-4441600	5444360	0,50
0,113	-9987750	15171800	2,59
0,121	-18865000	29465700	5,30
0,129	-26895600	40955300	7,03
0,138	-26754700	38615000	5,93
0,146	-20145300	29061100	4,46
0,154	-14984700	21760800	3,39
0,162	-10301600	15683000	2,69
0,170	-6200870	10519600	2,16
0,178	-2512120	6038630	1,76
0,186	775353	2122910	1,45
0,194	3717440	-1308630	1,20
0,202	6323750	-4306460	1,01
0,211	8615310	-6904420	0,86
0,219	10597100	-9126170	0,74
0,227	12277600	-10987300	0,65
0,235	13658900	-12499200	0,58
0,243	14744200	-13668900	0,54
0,251	15534100	-14501800	0,52
0,259	16029500	-15000400	0,51
0,267	16230100	-15166000	0,53
0,275	16135600	-14998600	0,57
0,284	15745100	-14496500	0,62
0,292	15057200	-13656700	0,70
0,324	9281020	-6791270	1,24
0,332	7057950	-4139590	1,46
0,340	4503460	-1073530	1,71
0,357	-1662530	6461270	2,40
0,365	-5324390	11055900	2,87

Bottom flange:

x [m]	Bottom [Pa]	Top [Pa]	Membrane [Mpa]
0,000	-6733040	-20596100	-13,66
0,008	-8029380	-17849800	-12,94
0,016	-6983220	-13385200	-10,18
0,024	-5466650	-9697730	-7,58
0,033	-4342990	-7363360	-5,85
0,041	-15182900	2388000	-6,40
0,057	-10622900	-834863	-5,73
0,065	-1351970	-2842820	-2,10
0,074	-977972	-2354000	-1,67
0,082	-7880110	-3499060	-5,69
0,090	-7550430	-4166050	-5,86
0,098	-7415570	-4807480	-6,11
0,106	-7478030	-5431820	-6,45
0,114	-7774710	-6015300	-6,90
0,123	-8314650	-6595780	-7,46
0,131	-9143880	-7166400	-8,16
0,139	-10343100	-7713320	-9,03
0,147	-12023800	-8236970	-10,13
0,155	-14436900	-8678890	-11,56
0,163	-18111000	-8896890	-13,50
0,172	-23847900	-9107000	-16,48
0,180	-30778400	-9573890	-20,18

σ_mean [MPa] = -8,80

0,373	-9460270	16343600	3,44
0,381	-14092700	22499400	4,20
0,413	-24714100	54185700	14,74
0,422	-20223600	39937500	9,86
0,430	-12814300	22009700	4,60
0,438	-3535930	9678430	3,07
0,446	-7746970	2005460	-2,87
0,455	4991740	-2572560	1,21
0,463	6384740	-5177150	0,60
0,471	6783500	-6546580	0,12
0,479	6604140	-6764210	-0,08
0,487	6140530	-6406630	-0,13
0,495	5543080	-5950220	-0,20
0,503	4848000	-5598750	-0,38
0,511	4097820	-7067540	-1,48
0,519	3354570	-6799020	-1,72
0,527	2594560	-6478050	-1,94
0,535	1847750	-6145010	-2,15
0,543	1127120	-5811740	-2,34

σ_mean [Mpa] =		**1,10**

Top flange:

Bottom flange:
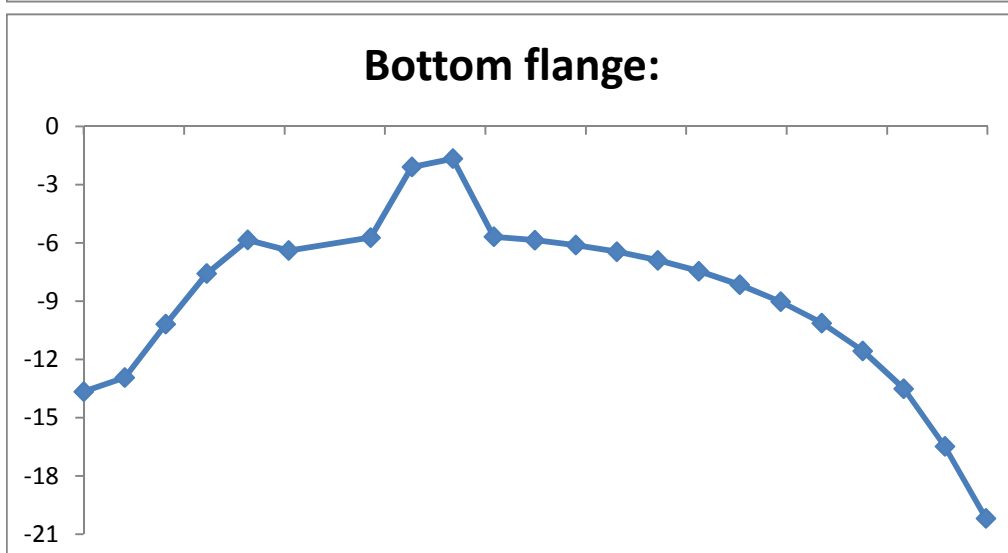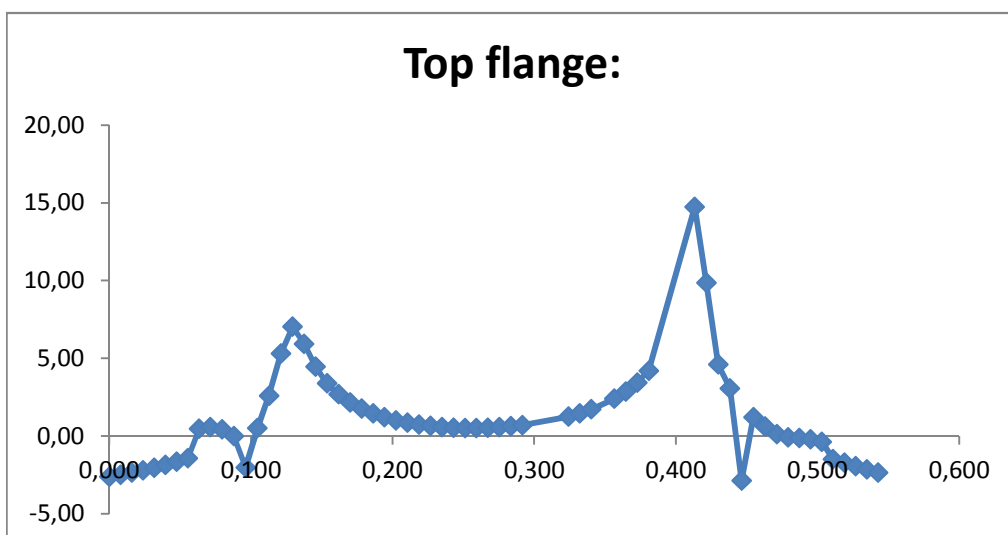
Calculations of shear force in rib walls

For the shear stresses the S22 stress component is used in a path in each rib wall in the centre of the span, directly beneath the load

t_rib=   0,006 m

Shear force in rib walls

Rib wall 7.1

y [m]	Bottom [Pa]	Top [Pa]	Membrane	F_element
0	5,50E+07	-1,19E+08	-31897200	-1549,9
0,008	1,66E+07	-1,44E+07	1121400	54,5
0,016	-2,42E+07	-5,31E+06	-14771285	-717,8
0,024	-2,42E+07	4,60E+06	-9784435	-475,4
0,032	-1,95E+07	5,46E+06	-7036065	-341,9
0,04	-1,59E+07	4,95E+06	-5474705	-266,0
0,049	-1,33E+07	4,37E+06	-4472275	-217,3
0,057	-1,15E+07	3,84E+06	-3807855	-185,0
0,065	-1,01E+07	3,30E+06	-3399340	-165,2
0,073	-9,07E+06	2,81E+06	-3130850	-152,1
0,081	-8,27E+06	2,34E+06	-2964585	-144,1
0,089	-7,62E+06	1,89E+06	-2868255	-139,4
0,097	-7,09E+06	1,46E+06	-2816240	-136,9
0,105	-6,68E+06	1,07E+06	-2803940	-136,2
0,113	-6,40E+06	7,38E+05	-2831511	-137,6
0,121	-6,17E+06	3,56E+05	-2907381	-141,3
0,13	-5,98E+06	-8,76E+04	-3031749	-147,3
0,138	-5,97E+06	-4,11E+05	-3189755	-155,0
0,146	-6,04E+06	-7,65E+05	-3404215	-165,4
0,154	-5,99E+06	-1,41E+06	-3700995	-179,8
0,162	-6,10E+06	-2,00E+06	-4051460	-196,9
0,17	-6,45E+06	-2,48E+06	-4463965	-216,9
0,178	-6,83E+06	-3,12E+06	-4975655	-241,8
0,186	-7,29E+06	-3,90E+06	-5594890	-271,8
0,194	-7,78E+06	-4,87E+06	-6327190	-307,5
0,202	-8,13E+06	-6,39E+06	-7264285	-353,0
0,211	-7,74E+06	-8,67E+06	-8208615	-398,9
0,219	-6,90E+06	-8,52E+06	-7710470	-374,7
0,227				
			Tot:	**-7860,6**

Rib wall 7.2

y [m]	Bottom [Pa]	Top [Pa]	Membran	F_element
0	3,92E+07	-9,40E+07	-27440000	-1333,4
0,008	1,02E+07	-5,50E+07	-22391650	-1088,0
0,016	-2,11E+07	-9,15E+06	-15139715	-735,7
0,024	-2,21E+07	-1,36E+06	-11737615	-570,3
0,032	-1,94E+07	-9,33E+05	-10183327	-494,8
0,04	-1,73E+07	-1,84E+06	-9578645	-465,4
0,049	-1,59E+07	-2,75E+06	-9325210	-453,1
0,057	-1,49E+07	-3,70E+06	-9305825	-452,2
0,065	-1,43E+07	-4,40E+06	-9323030	-453,0
0,073	-1,40E+07	-5,00E+06	-9492370	-461,2
0,081	-1,39E+07	-5,72E+06	-9809295	-476,6
0,089	-1,40E+07	-6,39E+06	-10206240	-495,9
0,097	-1,43E+07	-7,04E+06	-10652820	-517,7
0,105	-1,45E+07	-7,83E+06	-11179175	-543,2
0,113	-1,51E+07	-8,46E+06	-11801995	-573,5
0,121	-1,57E+07	-9,08E+06	-12410990	-603,0
0,13	-1,62E+07	-9,87E+06	-13037065	-633,5
0,138	-1,69E+07	-1,06E+07	-13781250	-669,7
0,146	-1,79E+07	-1,14E+07	-14651150	-711,9
0,154	-1,92E+07	-1,21E+07	-15677700	-761,8
0,162	-2,08E+07	-1,28E+07	-16822250	-817,4
0,17	-2,26E+07	-1,37E+07	-18166600	-882,8
0,178	-2,51E+07	-1,49E+07	-19993700	-971,5
0,186	-2,89E+07	-1,58E+07	-22367450	-1086,9
0,194	-3,43E+07	-1,74E+07	-25865500	-1256,9
0,202	-4,17E+07	-2,14E+07	-31506950	-1530,9
0,211	-4,63E+07	-3,13E+07	-38793150	-1885,3
0,219				
			Tot:	**-20925,8**

Stress distribution in top flange for one wheel load placed above floor beam

Path in deck plate. First x-value is one node away from the right main girder and the last one node from the left main girder. All stresses are extracted one node away from the floor beam intersection.

S, S11
SNEG, (fraction = -1.0)
(Avg: 75%)
+3.286e+07
+2.572e+07
+1.858e+07
+1.144e+07
+4.303e+06
-2.836e+06
-9.976e+06
-1.712e+07
-2.426e+07
-3.140e+07
-3.854e+07
-4.567e+07
-5.281e+07

Step: FB-K-1wheel
Increment   1: Step Time =   1.000
Primary Var: S, S11

Note: The second axle is included

Stress distribution in deck plate at floor beam intersection
Load applied above floor beam, one wheel

Stresses in deck plate

Position in the deck between the main girders
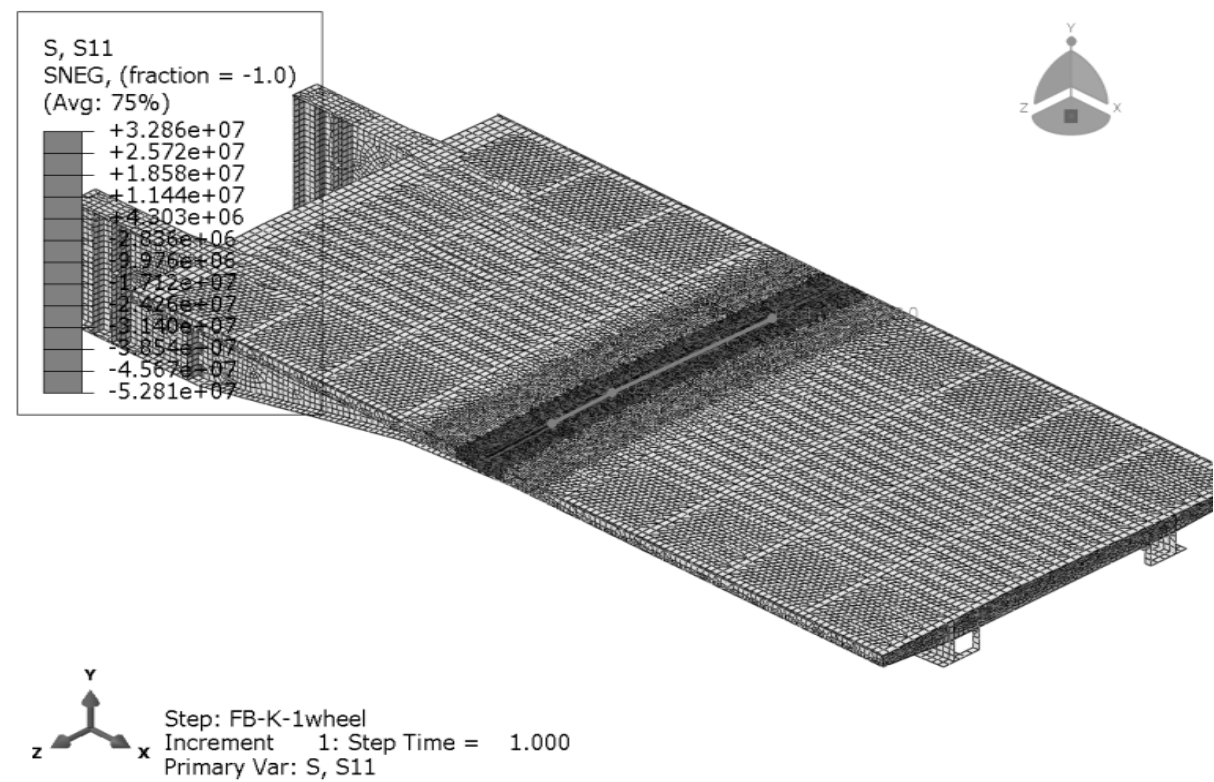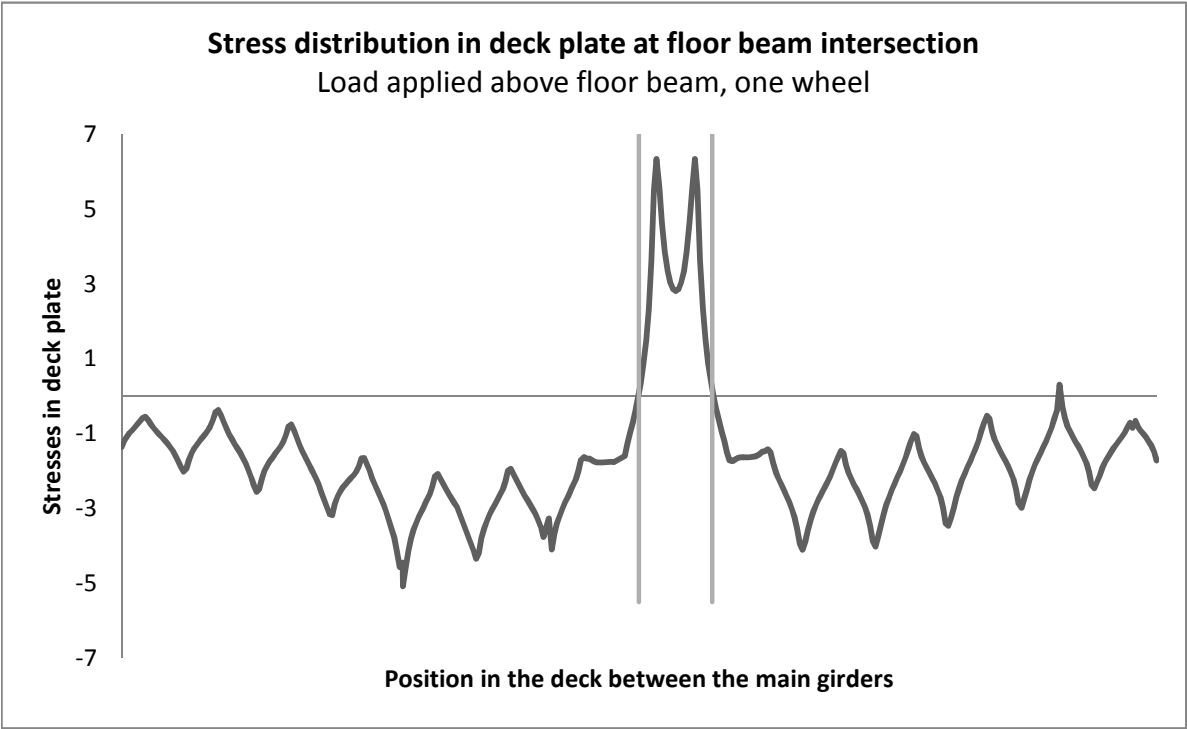
FB - Top Flange - One wheel

x	S11-Bottom	S11-Top	Membrane, [Mpa]
0,000	-1151930	-1562660	-1,36
0,019	-392135	-1979670	-1,19
0,058	51050	-2014150	-0,98
0,077	47618	-1864500	-0,91
0,155	-1256210	99367	-0,58
0,174	-1957420	867609	-0,54
0,194	-2200790	942961	-0,63
0,214	-1962650	485712	-0,74
0,235	-1735010	50224	-0,84
0,275	-1338710	-688172	-1,01
0,296	-1156510	-1028520	-1,09
0,316	-974547	-1370460	-1,17
0,336	-783146	-1728740	-1,26
0,356	-576235	-2120150	-1,35
0,377	-331823	-2571740	-1,45
0,397	-34507	-3122120	-1,58
0,417	355547	-3827920	-1,74
0,438	852709	-4613110	-1,88
0,458	604659	-4635310	-2,02
0,478	-117750	-3778550	-1,95
0,497	-558475	-2829700	-1,69
0,517	-887319	-2150980	-1,52
0,537	-978118	-1814680	-1,40
0,556	-921782	-1658420	-1,29
0,576	-801793	-1592560	-1,20
0,596	-664133	-1549440	-1,11
0,615	-560603	-1474750	-1,02
0,635	-546569	-1292890	-0,92
0,655	-725982	-891662	-0,81
0,675	-1233210	-67991	-0,65
0,694	-2018190	1177960	-0,42
0,714	-3086320	2358500	-0,36
0,734	-3451550	2423450	-0,51
0,755	-2928970	1557220	-0,69
0,775	-2484490	753692	-0,87
0,795	-2117680	85976	-1,02
0,815	-1796900	-497996	-1,15
0,836	-1506780	-1035980	-1,27
0,856	-1226530	-1557690	-1,39
0,876	-943835	-2086440	-1,52
0,897	-647446	-2646340	-1,65
0,917	-312201	-3271430	-1,79
0,937	80202	-4007700	-1,96
0,957	571642	-4920590	-2,17
0,978	1169620	-5925300	-2,38

0,998	814571	-5930470	-2,56
1,018	-217411	-4745220	-2,48
1,037	-923241	-3454210	-2,19
1,057	-1410450	-2569500	-1,99
1,077	-1559880	-2146500	-1,85
1,097	-1503220	-1971480	-1,74
1,116	-1353890	-1919140	-1,64
1,136	-1176790	-1901770	-1,54
1,156	-1036090	-1852600	-1,44
1,175	-994841	-1685450	-1,34
1,195	-1170530	-1274240	-1,22
1,215	-1714260	-388543	-1,05
1,234	-2565510	965189	-0,80
1,254	-3769420	2268710	-0,75
1,274	-4183810	2349500	-0,92
1,295	-3570030	1376430	-1,10
1,315	-3059660	468373	-1,30
1,335	-2646270	-283475	-1,46
1,396	-1666760	-2123660	-1,90
1,416	-1362570	-2713430	-2,04
1,437	-1045590	-3336690	-2,19
1,457	-689441	-4030390	-2,36
1,477	-274294	-4843970	-2,56
1,538	-5056370	-1249770	-3,15
1,558	-653113	-5711800	-3,18
1,578	-1443610	-4313550	-2,88
1,597	-1992630	-3365520	-2,68
1,617	-2171040	-2922850	-2,55
1,637	-2123470	-2755610	-2,44
1,656	-1972340	-2728280	-2,35
1,676	-1786360	-2748690	-2,27
1,696	-1633410	-2748250	-2,19
1,716	-1580800	-2634110	-2,11
1,735	-1763470	-2268390	-2,02
1,755	-2357600	-1395760	-1,88
1,775	-3299730	-22017	-1,66
1,794	-4610570	1317490	-1,65
1,835	-4392290	416432	-1,99
1,855	-3851180	-533540	-2,19
1,876	-3417050	-1333420	-2,38
1,896	-3045600	-2042050	-2,54
1,916	-2718440	-2705020	-2,71
1,936	-2408730	-3357740	-2,88
1,957	-2103980	-4029000	-3,07
2,017	-1041850	-6523340	-3,78
2,038	-554242	-7729070	-4,14
2,058	-12451	-9120240	-4,57
2,078	-6425910	-2466850	-4,45

2,081	-1146870	-9006400	-5,08
2,101	-1725830	-7508060	-4,62
2,121	-2382790	-5886350	-4,13
2,141	-2753990	-4864540	-3,81
2,161	-2795610	-4351050	-3,57
2,181	-2643620	-4113930	-3,38
2,201	-2404390	-4016850	-3,21
2,220	-2147530	-3967470	-3,06
2,240	-1940720	-3889000	-2,91
2,260	-1862600	-3678150	-2,77
2,280	-2054380	-3183910	-2,62
2,300	-2710370	-2124160	-2,42
2,320	-3795200	-484409	-2,14
2,340	-5303810	1147540	-2,08
2,400	-4353610	-593647	-2,47
2,421	-3816620	-1401200	-2,61
2,461	-2925280	-2763310	-2,84
2,482	-2520960	-3402380	-2,96
2,603	668605	-8893510	-4,11
2,624	235334	-8913820	-4,34
2,643	-1063570	-7340480	-4,20
2,663	-1994380	-5602940	-3,80
2,683	-2628830	-4436660	-3,53
2,702	-2791830	-3888500	-3,34
2,722	-2676540	-3672340	-3,17
2,742	-2445940	-3618330	-3,03
2,761	-2179410	-3612860	-2,90
2,781	-1953530	-3580860	-2,77
2,801	-1854570	-3414190	-2,63
2,821	-2046450	-2933090	-2,49
2,840	-2713140	-1851000	-2,28
2,860	-3792800	-189035	-1,99
2,880	-5356690	1475960	-1,94
2,900	-5864770	1703300	-2,08
2,981	-3255360	-2022620	-2,64
3,001	-2814760	-2703980	-2,76
3,042	-1978830	-4030980	-3,00
3,062	-1551960	-4737560	-3,14
3,083	-1085650	-5525280	-3,31
3,103	-557073	-6449370	-3,50
3,123	74917	-7591290	-3,76
3,164	-5358940	-1166380	-3,26
3,183	-919785	-7265140	-4,09
3,203	-1869820	-5497330	-3,68
3,223	-2491670	-4304330	-3,40
3,243	-2653340	-3722720	-3,19
3,262	-2534010	-3478440	-3,01
3,282	-2284480	-3406480	-2,85

3,302	-1991750	-3390550	-2,69
3,321	-1738860	-3346660	-2,54
3,341	-1604540	-3170210	-2,39
3,361	-1730400	-2712750	-2,22
3,381	-2302100	-1694540	-2,00
3,400	-3269300	-138671	-1,70
3,420	-4689810	1438810	-1,63
3,440	-5080560	1746170	-1,67
3,461	-4180040	853427	-1,66
3,501	-2843210	-667440	-1,76
3,521	-2317000	-1217890	-1,77
3,542	-1846360	-1695040	-1,77
3,562	-1399550	-2131840	-1,77
3,623	-84686	-3416960	-1,75
3,643	399976	-3922140	-1,76
3,724	669390	-3858520	-1,59
3,743	5423	-2557800	-1,28
3,763	-201197	-1778900	-0,99
3,783	78505	-1491220	-0,71
3,803	656374	-1449800	-0,40
3,823	1385820	-1485920	-0,05
3,843	2172080	-1451050	0,36
3,862	2858890	-1154160	0,85
3,882	3205890	-225203	1,49
3,902	2405470	2236500	2,32
3,921	-1082620	8294650	3,61
3,941	-8103860	19121500	5,51
3,960	-15825000	28509300	6,34
3,980	-14105100	25279200	5,59
4,001	-4466550	13716900	4,63
4,021	3689210	4010800	3,85
4,041	10009700	-3326690	3,34
4,061	14546300	-8477990	3,03
4,082	17245900	-11529400	2,86
4,102	18172600	-12557800	2,81
4,122	17275200	-11555900	2,86
4,143	14605400	-8532240	3,04
4,163	10101100	-3411030	3,35
4,183	3813940	3892050	3,85
4,203	-4305210	13560300	4,63
4,224	-13914200	25086200	5,59
4,244	-15643300	28325700	6,34
4,263	-7996250	19034100	5,52
4,283	-1066790	8319010	3,63
4,302	2380610	2314760	2,35
4,322	3185810	-136333	1,52
4,342	2855180	-1069060	0,89
4,362	2182190	-1366780	0,41

4,381	1410270	-1399910	0,01
4,401	697447	-1369390	-0,34
4,421	138857	-1419350	-0,64
4,441	-131353	-1706410	-0,92
4,461	65732	-2461730	-1,20
4,480	705780	-3718700	-1,51
4,500	1468250	-4887100	-1,71
4,521	1525980	-4997840	-1,74
4,541	951083	-4339270	-1,69
4,561	445805	-3748790	-1,65
4,581	-15701	-3253870	-1,63
4,602	-445002	-2813300	-1,63
4,622	-861038	-2396530	-1,63
4,642	-1277090	-1979470	-1,63
4,663	-1709100	-1541800	-1,63
4,683	-2165960	-1061420	-1,61
4,703	-2680140	-504747	-1,59
4,723	-3273510	177039	-1,55
4,744	-4002760	1047310	-1,48
4,764	-4906610	1969200	-1,47
4,784	-4530990	1699360	-1,42
4,804	-3155440	163064	-1,50
4,824	-2231070	-1369010	-1,80
4,843	-1662900	-2396540	-2,03
4,863	-1526290	-2872760	-2,20
4,883	-1654970	-3057200	-2,36
4,902	-1907180	-3107400	-2,51
4,922	-2195220	-3135030	-2,67
4,942	-2434070	-3225270	-2,83
4,962	-2539410	-3492240	-3,02
4,981	-2355370	-4106720	-3,23
5,001	-1689030	-5364750	-3,53
5,021	-664746	-7235040	-3,95
5,040	735579	-8941900	-4,10
5,061	1199210	-8943190	-3,87
5,081	442097	-7589770	-3,57
5,101	-213063	-6374870	-3,29
5,122	-761405	-5387330	-3,07
5,142	-1244710	-4541790	-2,89
5,162	-1686900	-3780400	-2,73
5,182	-2117110	-3058170	-2,59
5,203	-2553470	-2342380	-2,45
5,223	-3011520	-1600080	-2,31
5,243	-3527090	-787569	-2,16
5,264	-4124640	152992	-1,99
5,284	-4864700	1298330	-1,78
5,304	-5768660	2508350	-1,63
5,324	-5237800	2312390	-1,46

5,344	-3597160	558939	-1,52
5,364	-2463840	-1214030	-1,84
5,383	-1762060	-2365190	-2,06
5,403	-1560990	-2880230	-2,22
5,423	-1653480	-3073870	-2,36
5,443	-1879200	-3117420	-2,50
5,462	-2150920	-3127450	-2,64
5,482	-2379130	-3196830	-2,79
5,502	-2470210	-3451120	-2,96
5,521	-2257560	-4071700	-3,16
5,541	-1540630	-5372480	-3,46
5,561	-466716	-7303700	-3,89
5,581	1044160	-9078350	-4,02
5,601	1558780	-9074300	-3,76
5,621	728411	-7617940	-3,44
5,641	26298	-6303190	-3,14
5,662	-548173	-5238110	-2,89
5,682	-1047350	-4329740	-2,69
5,702	-1497240	-3514190	-2,51
5,723	-1931550	-2742710	-2,34
5,743	-2368390	-1980410	-2,17
5,763	-2825110	-1192570	-2,01
5,783	-3336750	-334230	-1,84
5,804	-3928180	653696	-1,64
5,824	-4657250	1850030	-1,40
5,844	-5538780	3122840	-1,21
5,865	-5008560	2990980	-1,01
5,883	-3391500	1272940	-1,06
5,902	-2240750	-523151	-1,38
5,922	-1475840	-1752570	-1,61
5,942	-1218420	-2336470	-1,78
5,962	-1287760	-2555660	-1,92
5,982	-1508870	-2600280	-2,05
6,001	-1781440	-2602290	-2,19
6,021	-2012500	-2658980	-2,34
6,041	-2109370	-2894080	-2,50
6,061	-1908410	-3485240	-2,70
6,081	-1209150	-4747580	-2,98
6,101	-151845	-6634800	-3,39
6,121	-5949590	-974596	-3,46
6,141	1885710	-8417980	-3,27
6,161	1048050	-7003070	-2,98
6,181	347435	-5715700	-2,68
6,201	-221418	-4671870	-2,45
6,221	-712826	-3782210	-2,25
6,242	-1152310	-2983840	-2,07
6,262	-1573950	-2229020	-1,90
6,282	-1994990	-1483760	-1,74

6,302	-2434500	-710796	-1,57
6,323	-2927920	137987	-1,39
6,343	-3498140	1117810	-1,19
6,364	-4197610	2305630	-0,95
6,384	-5037600	3583290	-0,73
6,405	-4515130	3470630	-0,52
6,424	-2932270	1741890	-0,60
6,444	-1805360	-51252	-0,93
6,464	-1088320	-1225550	-1,16
6,484	-865568	-1770380	-1,32
6,503	-938158	-1983690	-1,46
6,523	-1149020	-2035480	-1,59
6,543	-1408810	-2046120	-1,73
6,562	-1626460	-2107550	-1,87
6,582	-1714210	-2339380	-2,03
6,602	-1518320	-2910070	-2,21
6,622	-857531	-4109860	-2,48
6,641	126566	-5878230	-2,88
6,661	1564080	-7527030	-2,98
6,681	2051020	-7560320	-2,75
6,702	1224760	-6223620	-2,50
6,722	542554	-5004130	-2,23
6,742	-6351	-4019450	-2,01
6,762	-477890	-3182760	-1,83
6,783	-896848	-2432840	-1,66
6,803	-1297290	-1723990	-1,51
6,823	-1694570	-1023800	-1,36
6,843	-2105570	-300879	-1,20
6,864	-2558680	485150	-1,04
6,884	-3075240	1385350	-0,84
6,904	-3698270	2470660	-0,61
6,925	-4429060	3640720	-0,39
6,945	2396050	-1774990	0,31
6,965	-2466390	1904560	-0,28
6,984	-1387080	201400	-0,59
7,004	-702782	-912181	-0,81
7,024	-464053	-1457190	-0,96
7,043	-489661	-1703190	-1,10
7,063	-649545	-1787900	-1,22
7,083	-860400	-1827060	-1,34
7,103	-1042160	-1903650	-1,47
7,122	-1125870	-2112100	-1,62
7,142	-997954	-2577370	-1,79
7,162	-534989	-3521380	-2,03
7,181	110466	-4854030	-2,37
7,201	1158360	-6084080	-2,46
7,221	1510840	-6092300	-2,29
7,242	804552	-5024160	-2,11

7,262	246646	-4058820	-1,91
7,282	-183410	-3304440	-1,74
7,343	-1128160	-1655180	-1,39
7,363	-1397840	-1185800	-1,29
7,384	-1667500	-719130	-1,19
7,404	-1948130	-234720	-1,09
7,424	-2248880	289518	-0,98
7,444	-2578240	880443	-0,85
7,465	-2919800	1497530	-0,71
7,485	108506	-1804750	-0,85
7,505	-1552610	243282	-0,65
7,525	-664358	-949752	-0,81
7,544	-89398	-1744690	-0,92
7,564	188834	-2200080	-1,01
7,584	292350	-2486020	-1,10
7,604	283377	-2678940	-1,20
7,624	126263	-2766550	-1,32
7,643	-335447	-2627870	-1,48
7,663	-1398120	-2045120	-1,72

Stress distribution in top flange for two wheels placed above the floor beam

Path in deck plate. First x-value is one node away from the right main girder and the last one node from the left main girder. All stresses are extracted one node away from the floor beam intersection.
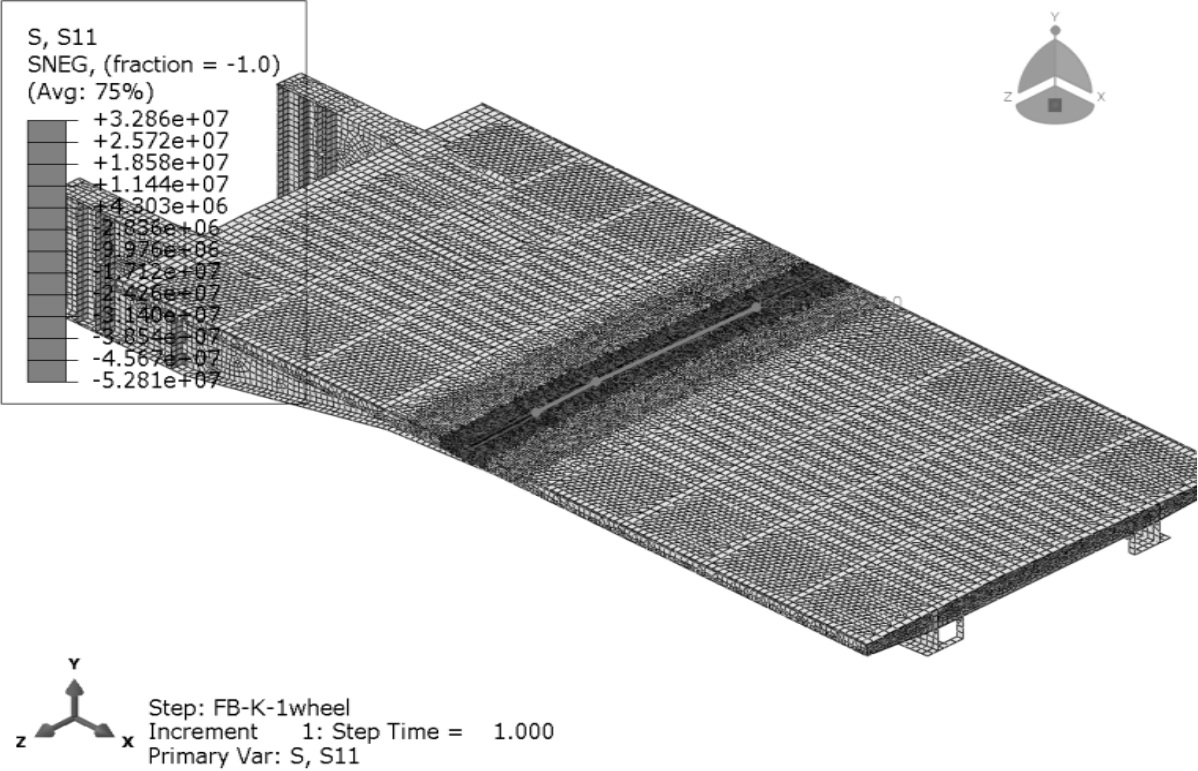
Note: The second axle is included
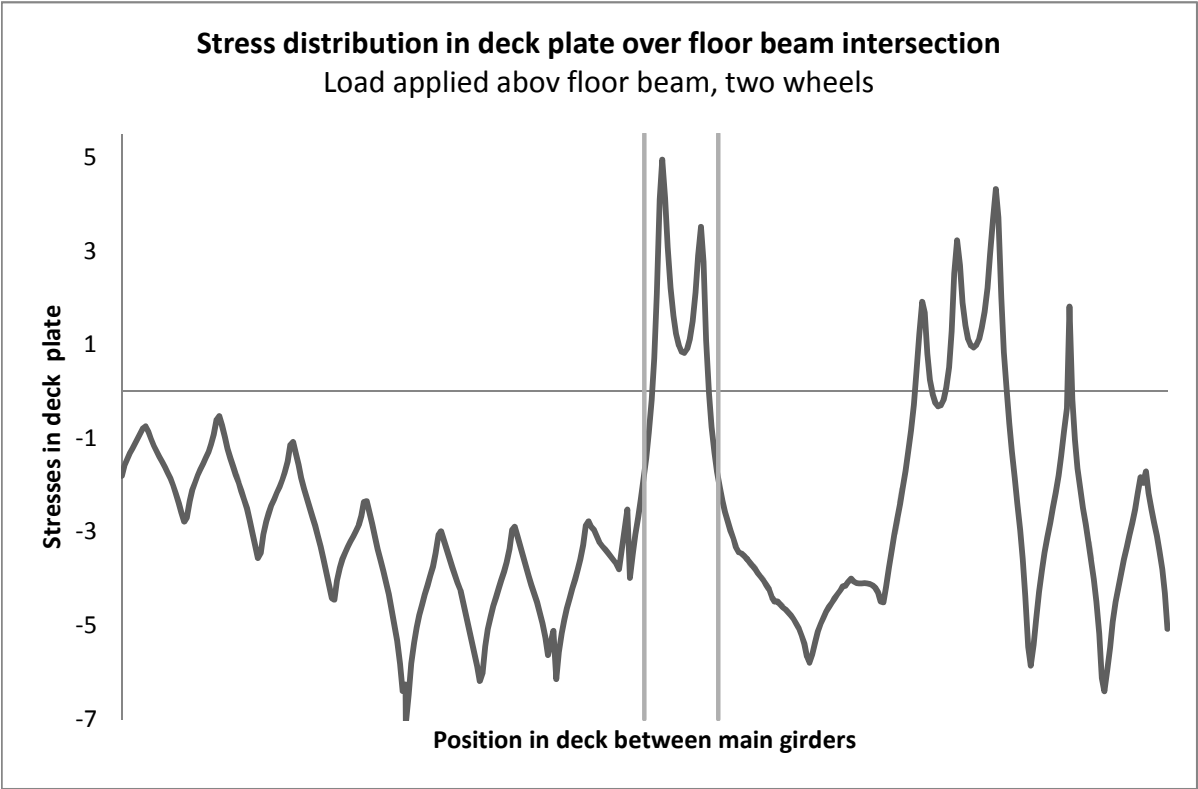
FB - Top Flange - Two wheels

x	S11-Bottom	S11-Top	Membrane, [Mpa]
0,000	-1549270	-2066550	-1,81
0,019	-564190	-2607980	-1,59
0,058	13252	-2654980	-1,32
0,077	10096	-2461880	-1,23
0,155	-1682080	110115	-0,79
0,174	-2606510	1122680	-0,74
0,194	-2937750	1216320	-0,86
0,214	-2633200	603178	-1,02
0,235	-2338490	19663	-1,16
0,275	-1824040	-970882	-1,40
0,296	-1586760	-1428220	-1,51
0,316	-1349230	-1888110	-1,62
0,336	-1098450	-2370410	-1,73
0,356	-826439	-2897780	-1,86
0,377	-503348	-3506930	-2,01
0,397	-108637	-4250050	-2,18
0,417	412303	-5204560	-2,40
0,438	1077210	-6266540	-2,59
0,458	737356	-6300570	-2,78
0,478	-226397	-5156410	-2,69
0,497	-800035	-3889280	-2,34
0,517	-1232870	-2978770	-2,11
0,537	-1353460	-2524060	-1,94
0,556	-1279140	-2309110	-1,79
0,576	-1120620	-2214680	-1,67
0,596	-938739	-2150310	-1,54
0,615	-802740	-2043100	-1,42
0,635	-786677	-1791350	-1,29
0,655	-1030230	-1243900	-1,14
0,675	-1711970	-126990	-0,92
0,694	-2764810	1560070	-0,60
0,714	-4209410	3158710	-0,53
0,734	-4712920	3243380	-0,73
0,755	-4012730	2063240	-0,97
0,775	-3415600	968991	-1,22
0,795	-2923580	60236	-1,43
0,815	-2493510	-734534	-1,61
0,836	-2104880	-1466510	-1,79
0,856	-1729470	-2176210	-1,95
0,876	-1350610	-2895360	-2,12
0,897	-953093	-3656770	-2,30
0,917	-502637	-4506860	-2,50
0,937	25335	-5508050	-2,74
0,957	688372	-6750000	-3,03
0,978	1494660	-8116200	-3,31

0,998	1005680	-8124830	-3,56
1,018	-390549	-6521950	-3,46
1,037	-1334950	-4776970	-3,06
1,057	-1989440	-3578570	-2,78
1,077	-2192090	-3002680	-2,60
1,097	-2117570	-2760990	-2,44
1,116	-1918480	-2684670	-2,30
1,136	-1681850	-2655390	-2,17
1,156	-1494090	-2582970	-2,04
1,175	-1439830	-2351010	-1,90
1,195	-1677330	-1789250	-1,73
1,215	-2408030	-586288	-1,50
1,234	-3549800	1249570	-1,15
1,254	-5179140	3016810	-1,08
1,274	-5749910	3120980	-1,31
1,295	-4924650	1791130	-1,57
1,315	-4237320	551090	-1,84
1,335	-3681690	-474829	-2,08
1,396	-2367460	-2984170	-2,68
1,416	-1959430	-3787800	-2,87
1,437	-1533940	-4636800	-3,09
1,457	-1054970	-5581660	-3,32
1,477	-495825	-6689560	-3,59
1,538	-6996110	-1840440	-4,42
1,558	-1021980	-7885260	-4,45
1,578	-2082510	-5994000	-4,04
1,597	-2822340	-4708900	-3,77
1,617	-3065300	-4106160	-3,59
1,637	-3003760	-3875270	-3,44
1,656	-2802650	-3833340	-3,32
1,676	-2554350	-3855810	-3,21
1,696	-2350370	-3849880	-3,10
1,716	-2281220	-3690010	-2,99
1,735	-2529110	-3189670	-2,86
1,755	-3329640	-2003380	-2,67
1,775	-4597030	-137786	-2,37
1,794	-6374880	1681030	-2,35
1,835	-6096960	438211	-2,83
1,855	-5367720	-862520	-3,12
1,876	-4783820	-1957180	-3,37
1,896	-4284690	-2926950	-3,61
1,916	-3845610	-3834000	-3,84
1,936	-3430070	-4726840	-4,08
1,957	-3021000	-5644870	-4,33
2,017	-1590480	-9055620	-5,32
2,038	-929944	-10705000	-5,82
2,058	-195952	-12607100	-6,40
2,078	-8956710	-3563870	-6,26

2,081	-1755650	-12456700	-7,11
2,101	-2528710	-10424400	-6,48
2,121	-3409930	-8220360	-5,82
2,141	-3910490	-6828570	-5,37
2,161	-3967220	-6126320	-5,05
2,181	-3762420	-5798820	-4,78
2,201	-3439690	-5661330	-4,55
2,220	-3093160	-5588360	-4,34
2,240	-2814510	-5475490	-4,15
2,260	-2710390	-5182120	-3,95
2,280	-2972760	-4502490	-3,74
2,300	-3864140	-3052150	-3,46
2,320	-5336990	-808936	-3,07
2,340	-7396560	1422390	-2,99
2,400	-6126960	-990382	-3,56
2,421	-5399530	-2103830	-3,75
2,461	-4192310	-3983420	-4,09
2,482	-3644550	-4865690	-4,26
2,603	715233	-12459200	-5,87
2,624	111129	-12493200	-6,19
2,643	-1669870	-10341400	-6,01
2,663	-2929780	-7966020	-5,45
2,683	-3794120	-6367880	-5,08
2,702	-4017370	-5616330	-4,82
2,722	-3860440	-5319800	-4,59
2,742	-3546270	-5245540	-4,40
2,762	-3183410	-5237360	-4,21
2,781	-2877430	-5191510	-4,03
2,801	-2747460	-4957980	-3,85
2,821	-3021800	-4286200	-3,65
2,840	-3955860	-2777800	-3,37
2,860	-5466250	-455765	-2,96
2,880	-7653480	1868350	-2,89
2,900	-8379800	2171720	-3,10
2,981	-4800510	-3100500	-3,95
3,001	-4194510	-4072160	-4,13
3,042	-3041640	-5971640	-4,51
3,062	-2450050	-6986400	-4,72
3,083	-1799240	-8120290	-4,96
3,103	-1056440	-9453780	-5,26
3,123	-158150	-11106000	-5,63
3,164	-8176300	-2052540	-5,11
3,183	-1581720	-10716100	-6,15
3,203	-2907830	-8231140	-5,57
3,223	-3790590	-6549530	-5,17
3,243	-4027290	-5736150	-4,88
3,262	-3866720	-5402860	-4,63
3,282	-3522980	-5314930	-4,42

3,302	-3120300	-5305860	-4,21
3,321	-2778580	-5254120	-4,02
3,341	-2612660	-5007050	-3,81
3,361	-2832140	-4344450	-3,59
3,381	-3711490	-2854260	-3,28
3,400	-5184820	-551678	-2,87
3,420	-7327820	1777740	-2,78
3,440	-7968400	2180460	-2,89
3,461	-6711610	788215	-2,96
3,501	-4833030	-1614740	-3,22
3,521	-4095040	-2519710	-3,31
3,542	-3434780	-3326320	-3,38
3,562	-2806160	-4085610	-3,45
3,623	-910183	-6449500	-3,68
3,643	-180669	-7423840	-3,80
3,704	-4841270	-206516	-2,52
3,724	-110634	-7862900	-3,99
3,743	-1211650	-5734420	-3,47
3,763	-1713430	-4400890	-3,06
3,783	-1511640	-3858090	-2,68
3,803	-880478	-3722630	-2,30
3,823	-40261	-3745820	-1,89
3,843	872999	-3724000	-1,43
3,862	1661340	-3422910	-0,88
3,882	2040320	-2415030	-0,19
3,902	1123730	282678	0,70
3,921	-2724850	6877380	2,08
3,941	-10330400	18543000	4,11
3,960	-18874400	28775600	4,95
3,980	-17432800	25659400	4,11
4,001	-7384040	13542400	3,08
4,021	1115190	3300560	2,21
4,041	7715920	-4487220	1,61
4,061	12496800	-10036100	1,23
4,082	15415300	-13457800	0,98
4,102	16551900	-14849400	0,85
4,122	15863700	-14219800	0,82
4,143	13411100	-11594300	0,91
4,163	9148850	-6921730	1,11
4,183	3141760	-149914	1,50
4,203	-4631870	8855280	2,11
4,224	-13833700	19638700	2,90
4,244	-15818500	22854900	3,52
4,263	-8891690	14418200	2,76
4,283	-2456770	4637930	1,09
4,302	652117	-730027	-0,04
4,322	1359140	-2877150	-0,76
4,342	1080220	-3689640	-1,30

4,362	528922	-3964860	-1,72
4,381	-97252	-4013090	-2,06
4,401	-688628	-3983990	-2,34
4,421	-1199720	-3957220	-2,58
4,441	-1583650	-3998150	-2,79
4,461	-1776970	-4169460	-2,97
4,480	-1789090	-4492070	-3,14
4,500	-1956150	-4703880	-3,33
4,521	-2209740	-4666190	-3,44
4,541	-2314990	-4607720	-3,46
4,561	-2429100	-4599910	-3,51
4,581	-2571810	-4593480	-3,58
4,602	-2723300	-4582790	-3,65
4,622	-2890870	-4565350	-3,73
4,642	-3069250	-4539210	-3,80
4,663	-3265610	-4501530	-3,88
4,683	-3479300	-4448240	-3,96
4,703	-3725180	-4371620	-4,05
4,723	-4011780	-4256860	-4,13
4,744	-4368160	-4091870	-4,23
4,764	-4840130	-3961970	-4,40
4,784	-4735710	-4249780	-4,49
4,804	-4139160	-4834520	-4,49
4,824	-3769310	-5320760	-4,55
4,843	-3579730	-5635570	-4,61
4,863	-3551190	-5766610	-4,66
4,883	-3615480	-5819430	-4,72
4,902	-3725390	-5844490	-4,78
4,922	-3848720	-5880410	-4,86
4,942	-3951060	-5962980	-4,96
4,962	-3994080	-6144710	-5,07
4,981	-3907210	-6507460	-5,21
5,001	-3609750	-7179160	-5,39
5,021	-3206390	-8128190	-5,67
5,040	-2718240	-8881880	-5,80
5,061	-2538590	-8703480	-5,62
5,081	-2779580	-7913420	-5,35
5,101	-3011570	-7247090	-5,13
5,122	-3215160	-6709420	-4,96
5,142	-3397970	-6251230	-4,82
5,162	-3571410	-5843150	-4,71
5,182	-3744960	-5461760	-4,60
5,203	-3929490	-5090350	-4,51
5,223	-4130870	-4711580	-4,42
5,243	-4372340	-4303260	-4,34
5,264	-4667450	-3833790	-4,25
5,284	-5061960	-3267080	-4,16
5,304	-5589160	-2707080	-4,15

5,324	-5277960	-2857000	-4,07
5,344	-4361340	-3636380	-4,00
5,364	-3811360	-4318330	-4,06
5,383	-3492740	-4703020	-4,10
5,403	-3422710	-4776710	-4,10
5,423	-3497010	-4701800	-4,10
5,443	-3635160	-4561070	-4,10
5,462	-3790160	-4416800	-4,10
5,482	-3902140	-4329150	-4,12
5,502	-3893460	-4393150	-4,14
5,521	-3617660	-4765870	-4,19
5,541	-2872430	-5708920	-4,29
5,561	-1709540	-7265410	-4,49
5,581	-347835	-8664640	-4,51
5,601	118622	-8485660	-4,18
5,621	-387677	-7148180	-3,77
5,641	-855735	-5921440	-3,39
5,662	-1251580	-4844470	-3,05
5,682	-1584280	-3861980	-2,72
5,702	-1863100	-2934930	-2,40
5,723	-2096110	-2029050	-2,06
5,743	-2294940	-1112040	-1,70
5,763	-2462970	-141231	-1,30
5,783	-2648320	960596	-0,84
5,804	-2890180	2320430	-0,28
5,824	-3355500	4190160	0,42
5,844	-4176650	6633230	1,23
5,865	-5174920	9003740	1,91
5,883	-8270230	11619800	1,67
5,902	-13115700	14733900	0,81
5,922	-17473000	17972100	0,25
5,942	-21290400	21154300	-0,07
5,962	-24093300	23594900	-0,25
5,982	-25473100	24831500	-0,32
6,001	-25240900	24641400	-0,30
6,021	-23407300	23052300	-0,18
6,041	-20200600	20355300	0,08
6,061	-16227100	17250400	0,51
6,081	-12500800	15065700	1,28
6,101	-10110000	15151300	2,52
6,121	-8413560	14863000	3,22
6,141	-3890500	9285570	2,70
6,161	2672400	1122780	1,90
6,181	7869080	-5053910	1,41
6,201	11523500	-9284490	1,12
6,221	13657800	-11703800	0,98
6,242	14207900	-12335200	0,94
6,262	13175600	-11195700	0,99

6,282	10498300	-8251070	1,12
6,302	6338430	-3621200	1,36
6,323	1095880	2303720	1,70
6,343	-4691120	9110490	2,21
6,364	-10944500	16812000	2,93
6,384	-17476300	24801500	3,66
6,405	-16162400	24811200	4,32
6,424	-7364920	14794600	3,71
6,444	-243262	4277770	2,02
6,464	3683490	-2021110	0,83
6,484	4691150	-4669180	0,01
6,503	4121200	-5481720	-0,68
6,523	2892940	-5448240	-1,28
6,543	1450790	-5140380	-1,84
6,562	131252	-4911210	-2,39
6,582	-804510	-5117930	-2,96
6,602	-943225	-6217380	-3,58
6,622	201874	-8965430	-4,38
6,641	2330290	-13261300	-5,47
6,661	5604060	-17319900	-5,86
6,681	6581060	-17405800	-5,41
6,702	4453580	-14171000	-4,86
6,722	2677810	-11234200	-4,28
6,742	1212700	-8857270	-3,82
6,762	-69754	-6826500	-3,45
6,783	-1233500	-4992070	-3,11
6,803	-2359040	-3241570	-2,80
6,823	-3487950	-1493390	-2,49
6,843	-4661350	332654	-2,16
6,864	-5957600	2343020	-1,81
6,884	-7435520	4675820	-1,38
6,904	-9215740	7521610	-0,85
6,925	-11322300	10593700	-0,36
6,945	7541710	-3918380	1,81
6,965	-6108720	5773960	-0,17
6,984	-3225030	1154490	-1,04
7,004	-1416060	-1877440	-1,65
7,024	-826698	-3354580	-2,09
7,043	-960073	-4014100	-2,49
7,063	-1459570	-4233300	-2,85
7,083	-2095100	-4331150	-3,21
7,103	-2642390	-4538060	-3,59
7,122	-2903540	-5121340	-4,01
7,142	-2549770	-6440690	-4,50
7,162	-1211660	-9134740	-5,17
7,181	720008	-12987100	-6,13
7,201	3752450	-16566000	-6,41
7,221	4748640	-16654400	-5,95

7,242	2759960	-13696300	-5,47
7,262	1166760	-11018900	-4,93
7,282	-82087	-8916940	-4,50
7,343	-2894200	-4280770	-3,59
7,363	-3714380	-2948660	-3,33
7,384	-4539540	-1617420	-3,08
7,404	-5404990	-227053	-2,82
7,424	-6338690	1288960	-2,52
7,444	-7372490	3010490	-2,18
7,465	-8467550	4800800	-1,83
7,485	1024240	-4929980	-1,95
7,505	-4366430	941957	-1,71
7,525	-1695720	-2654330	-2,18
7,544	46118	-5078400	-2,52
7,564	894668	-6486170	-2,80
7,584	1213920	-7387730	-3,09
7,604	1185810	-8006730	-3,41
7,624	692707	-8297600	-3,80
7,643	-751480	-7878130	-4,31
7,663	-4072320	-6077610	-5,07

Modulus of elasticity, E

Beam:	21000	MPa
Columns:	21000	MPa

Left End: Support

Right: Support

Sway frame: ☐

Span №	1	2	3	4	5
Length, m	1,2	1,45	1,2	1,925	1,925
Moment of Inertia, m⁴	1,43E-03	1,43E-03	1,43E-03	1,43E-03	1,43E-03

Support №	1	2	3	4	5	6
Support coordinate, m	0	1,2	2,65	3,85	5,775	7,7
Vertical spring constant, N/m		0,00E+00	0,00E+00	0,00E+00	0,00E+00	
Support type or hinge	Roller	Roller	Roller	Roller	Roller	Roller
Column under Length, m						
Moment of Inertia, m⁴						
Column above Length, m						
Moment of Inertia, m⁴						
Induced support displacements, m						

Positive loads: ↑ ↺	Load case:	**Moving loads: OL-1**			
Comment	Load Type	WA N or N/m	WB N/m	LA m	LB m
	P	-90000		3,85	
	P	-90000		2,65	

Moment, N-m

292500

Modulus of elasticity, E

Beam: 21000 MPa

Columns: 21000 MPa

Beam end restraints

Left End: Support

Right: Support

Sway frame: ☐

Span №	1	2	3	4	5
Length, m	1,2	1,45	1,2	1,925	1,925
Moment of Inertia, m⁴	1,43E-03	1,43E-03	1,43E-03	1,43E-03	1,43E-03

Support №	1	2	3	4	5	6
Support coordinate, m	0	1,2	2,65	3,85	5,775	7,7
Vertical spring constant, N/m		0,00E+00	0,00E+00	0,00E+00	0,00E+00	
Support type or hinge	Roller	Roller	Roller	Roller	Roller	Roller
Column under Length, m						
Moment of Inertia, m⁴						
Column above Length, m						
Moment of Inertia, m⁴						
Induced support displacements, m						

Positive loads: ↑ ↺	Load case:	**Moving loads: OL-1**			
Comment	Load Type	WA N or N/m	WB N/m	LA m	LB m
	P	-90000		1,2	
	P	-90000		0	

Shear, N
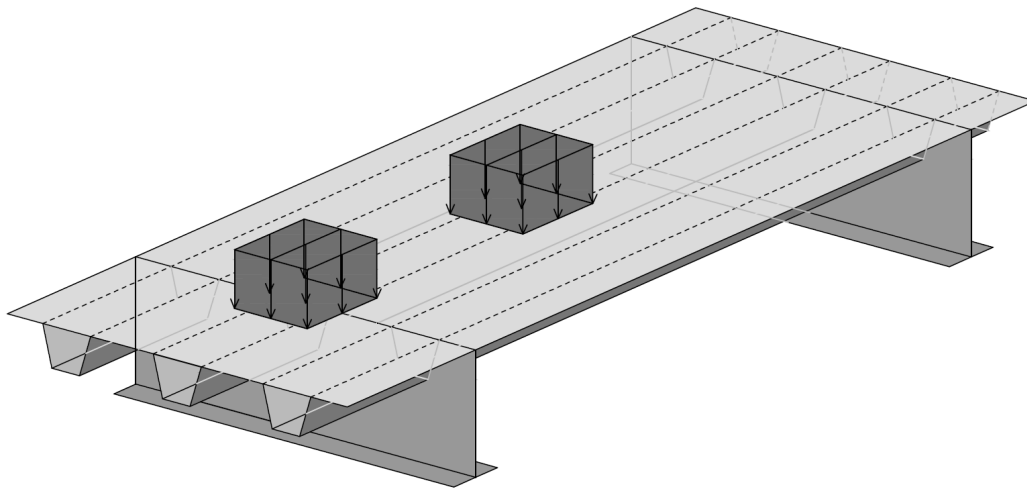
Hand calculations - Fatigue, Crack I-III

$kNm := kN \cdot m$

Crack III:

System:

The floor beam is resting on the main girders, represented by a pinned and a roller supports in the models. The floor beam is loaded with one axle with two wheels directly above the floor beam ad one axle 1.2m out in the span.

Two load axles are included in the analysis. The second load axle is simplified to distribute half its load to the present floor beam. Each wheel load is 60 kN.

$$P := \left(60 + \frac{60}{2}\right)kN = 90 \cdot kN \qquad\qquad L_{tot} := 7.7m$$
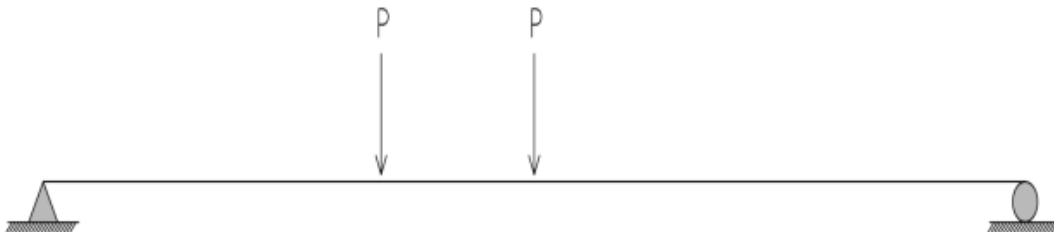
Two load cases are present:

Load case 1
Only P_v is acting on the beam. This corresponds to the highest shear stress

Load case 2
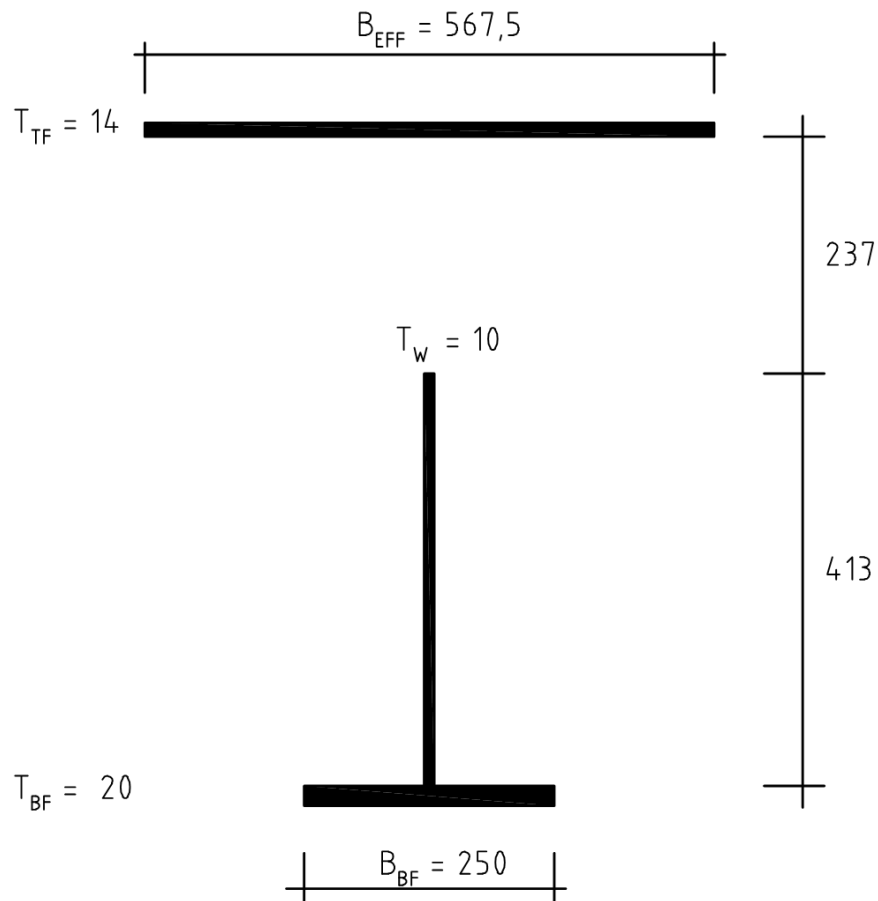Only P_m is acting on the beam. This corresponds to the highest bending stress

Sectional properties:

$E := 210 \text{GPa}$

Effective sectional properties - Reduced web due to rib intersection:

$B_{EFF} = 567,5$

$T_{TF} = 14$

$T_W = 10$

237

413

$T_{BF} = 20$

$B_{BF} = 250$

$A_{eff} := 17089 \text{mm}^2$

$z_{NA.eff} := 311.03 \text{mm}$ From top

$z_{III.eff} := z_{NA.eff} - 237 \text{mm} = 74.03 \cdot \text{mm}$ z - coordinate for the region where the crack initiate.

$S_{NAeff} := 2.42 \cdot 10^{-3} \text{m}^3$
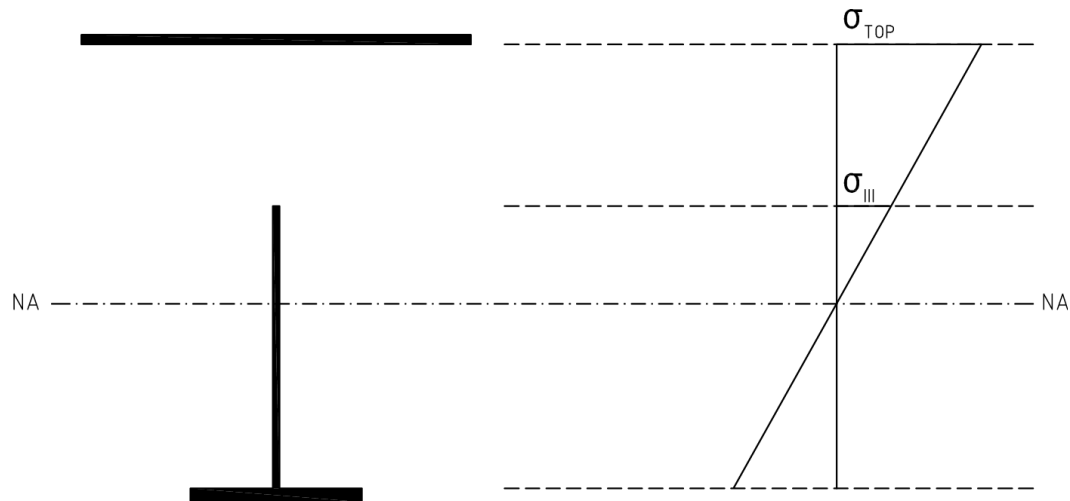
$I_{eff} := 1.428 \cdot 10^{-3} \text{m}^4$

$t_{web} := 10 \text{mm}$

Loads:
By use of GoBEAM, the following maximum moment and shear force are given:

$M := 292.5 \text{kNm}$ Based on P_M (GoBeam)

$V := 76 \text{kN}$ Based on P_V (GoBeam)

Stress calculations:

Stresses in the floor beam web at the rib radius:

$$\sigma_T := \frac{M}{I_{eff}} \cdot z_{III.eff} = 15.164 \cdot \text{MPa}$$

$$\tau_T := \frac{V \cdot S_{NAeff}}{I_{eff} \cdot t_{web}} = 12.88 \cdot \text{MPa}$$

Stresses in the floor beam web at the deck plate and rib connection:

$$\sigma_{T.top} := \frac{M}{I_{eff}} \cdot z_{NA.eff} = 63.709 \cdot \text{MPa}$$

$$\tau_{T.top} := \frac{V \cdot S_{NAeff}}{I_{eff} \cdot t_{web}} = 12.88 \cdot \text{MPa}$$

Fatigue analysis at rib radius:

$\Delta\sigma := \sigma_T$

$\Delta\tau := \tau_T$

$\gamma_{Mf} := 1.35$ 1993-1-9, 3.1,

$\gamma_{Ff} := 1.0$ 1993-2, 9.3

$\Delta\sigma_C := 80 MPa$ EN1993-1-9 Table 8.8, Detail 2, (t=10mm < 12mm)

$\Delta\tau_C := 100 MPa$ 1993-1-9, figur 7.2

$\Delta\sigma_E := \gamma_{Ff} \cdot \Delta\sigma = 15.164 \cdot MPa$

$\Delta\tau_E := \gamma_{Ff} \cdot \Delta\tau = 12.88 \cdot MPa$

Fatigue controll for bending stress: Fatigue controll for shear stress:

$$\frac{\Delta\sigma_E}{\left(\dfrac{\Delta\sigma_C}{\gamma_{Mf}}\right)} = 0.256 \qquad < 1 \ \ OK \qquad\qquad \frac{\Delta\tau_E}{\left(\dfrac{\Delta\tau_C}{\gamma_{Mf}}\right)} = 0.174 \qquad < 1 \ \ OK$$

Fatigue analysis at top:

$\Delta\sigma := \sigma_{T.top}$

$\Delta\tau := \tau_{T.top}$

$\Delta\sigma_C := 71 MPa$ EN1993-1-9 Table 8.8, Detail 2, (t=10mm < 12mm)
                                    The detail category is lowered with one step due to intersecting welds

$\Delta\sigma_E := \gamma_{Ff} \cdot \Delta\sigma = 63.709 \cdot MPa$

$\Delta\tau_E := \gamma_{Ff} \cdot \Delta\tau = 12.88 \cdot MPa$

Fatigue controll for bending stress: Fatigue controll for shear stress:

$$\frac{\Delta\sigma_E}{\left(\dfrac{\Delta\sigma_C}{\gamma_{Mf}}\right)} = 1.211 \qquad > 1 \ \ not\ OK \qquad\qquad \frac{\Delta\tau_E}{\left(\dfrac{\Delta\tau_C}{\gamma_{Mf}}\right)} = 0.174 \qquad < 1 \ \ OK$$

Fatigue calculation Crack I:

$V_{max} := 4kN$ — Shear force is very small, therefore no control of the the shear driven fatigue is done.

$\sigma_T := 19.72MPa$ — Bending stress from hand calculations (GoBEAM shown above).

$\Delta\sigma := \sigma_T$

$\Delta\sigma_C := 50MPa$ — EN1993-1-9 Table 8.8, Detail 8

$\Delta\sigma_E := \gamma_{Ff} \cdot \Delta\sigma = 19.72 \cdot MPa$

Fatigue controll for bending stress:

$$\frac{\Delta\sigma_E}{\left(\dfrac{\Delta\sigma_C}{\gamma_{Mf}}\right)} = 0.532 \qquad < 1 \;\; OK$$

Fatigue calculation Crack II:

$V_{max} := 4kN$ — Shear force is very small, therefore no control of the the shear driven fatigue is done.

$\sigma_T := 19.72MPa$ — Bending stress from hand calculations (GoBEAM shown above).

$\Delta\sigma := \sigma_T$

$\Delta\sigma_C := 50MPa$ — EN1993-1-9 Table 8.8, Detail 8.

$\Delta\sigma_E := \gamma_{Ff} \cdot \Delta\sigma = 19.72 \cdot MPa$

Fatigue controll for bending stress:

$$\frac{\Delta\sigma_E}{\left(\dfrac{\Delta\sigma_C}{\gamma_{Mf}}\right)} = 0.532 \qquad < 1 \;\; OK$$

Summary of the cracks utilization ratios:

Crack I: $u_I := 53.2\%$

Crack II: $u_{II} := 53.2\%$

Crack III: $u_{III} := 25.5\%$

Fatigue analysis with hot spot stresses from FE-analysis

$kNm := kN \cdot m$

$\gamma_{Mf} := 1.35$ 1993-1-9, 3.1,

$\gamma_{Ff} := 1.0$ 1993-2, 9.3

Crack I:

$\Delta\sigma := 42.9 MPa$ From FE-analysis

$\Delta\sigma_C := 90 MPa$ EN1993-1-9 Table B.1, Detail 7

$\Delta\sigma_E := \gamma_{Ff} \cdot \Delta\sigma = 42.9 \cdot MPa$

$$\frac{\Delta\sigma_E}{\left(\dfrac{\Delta\sigma_C}{\gamma_{Mf}}\right)} = 0.644 \qquad < 1 \ \ OK$$

Crack II:

$\Delta\sigma := 71.3 MPa$ From FE-analysis

$\Delta\sigma_C := 90 MPa$ EN1993-1-9 Table B.1, Detail 7

$\Delta\sigma_E := \gamma_{Ff} \cdot \Delta\sigma = 71.3 \cdot MPa$

$$\frac{\Delta\sigma_E}{\left(\dfrac{\Delta\sigma_C}{\gamma_{Mf}}\right)} = 1.07 \qquad > 1 \ \ NOT \ OK$$

Crack III:

$\Delta\sigma := 92.8 MPa$ From FE-analysis

$\Delta\sigma_C := 100 MPa$ EN1993-1-9 Table B.1, Detail 4

$\Delta\sigma_E := \gamma_{Ff} \cdot \Delta\sigma = 92.8 \cdot MPa$

$$\frac{\Delta\sigma_E}{\left(\dfrac{\Delta\sigma_C}{\gamma_{Mf}}\right)} = 1.253 \qquad > 1 \ \ NOT \ OK$$